UNIVERSIDADE D
COIMBRA

Cláudio Miguel de Oliveira Martins

HOT BOX APPARATUS DESIGN AND CONSTRUCTION FOR THE DETERMINATION OF THE THERMAL PERFORMANCE OF BUILDING ELEMENTS

PhD thesis in Steel and Composite Construction supervised by Professor Luís Alberto Proença Simões da Silva, Professor Paulo Fernando Antunes dos Santos and submitted to the Department of Civil Engineering, Faculty of Sciences and Technology of the University of Coimbra.

July of 2020

PREFACE

This thesis is the outcome of the research work developed within the research unit ISISE - Institute for Sustainability and Innovation in Structural Engineering, at the Civil Engineering Department of the University of Coimbra.

It is hoped that this work may contribute to the improvement of scientific knowledge in this area within the research centre and provided a hi-tech apparatus for the laboratory.

Cláudio Martins

Coimbra, June 2020

This work was partly financed by FEDER funds through the Competitiveness Factors Operational Programme - COMPETE and by national funds through FCT –Foundation for Science and Technology within the scope of the project CENTRO-01-0145-FEDER-000006 and PTDC/ECI-EGC/32061/2017.

ACKNOWLEDGEMENTS

I express my gratitude to my supervisors Professor Luís Simões da Silva and Professor Paulo Santos, for their valuable guidance, dedication and supervision, which gave a significant contribution to this work. A very special thanks to Professor Luís Simões da Silva for his teachings in the various areas that we work along these years.

A word of gratitude for all my friends, colleagues, lab technicians, and outsourcing companies' technicians, who accompanied my work closely.

I am deeply grateful to my family for their encouragement, patience, and support. I would like to dedicate this work to my daughters.

RESUMO

A melhoria do desempenho térmico dos edifícios é essencial para garantir a eficiência energética dos edifícios. Um dos componentes mais importantes em termos de perdas de calor num edifício são as paredes externas, devido à sua significante área exposta. O desempenho térmico adequado da envolvente do edifício é crucial para proporcionar um bom comportamento térmico e obter alta eficiência energética, permitindo uma redução na energia operacional do edifício.

A caracterização experimental do coeficiente de transmissão térmica global (valor U) dos elementos do edifício, por exemplo, paredes, janelas e portas, com novas geometrias, configurações ou materiais, é crucial para a previsão do seu desempenho térmico. Também é essencial medir o valor U das paredes com novos materiais e configurações mais complexas, uma vez que a estimativa correta desse valor é um requisito crítico ao executar modelos de simulação energética de edifícios ou auditoria energética.

Os elementos não homogéneos de edifícios, com por exemplo as estruturas leves em aço enformado a frio (LSF), são um desafio na determinação da transmissão térmica dos elementos, especialmente quando os perfis de aço são colocados em mais do que uma direção.

A determinação das propriedades de transmissão térmica dos elementos de construção pode ser feita por várias abordagens, sendo a metodologia mais precisa o método *Hot Box* (HB). Este método permite realizar a determinação do desempenho térmico dos elementos de um edifício, no estado estacionário, medindo o fluxo de calor que passa através dos componentes do edifício e as correspondentes diferenças de temperatura no elemento. Este método pode testar amostras homogêneas ou não-homogêneas, em um ambiente de laboratório, e aplica-se a estruturas de edifícios ou conjuntos compostos, como por exemplo paredes com janelas ou portas.

O método da *Hot Box* foi feito, principalmente, para a realização de medições em laboratório de grandes amostras heterogéneas, permitindo também testar elementos homogêneos. Devido ao crescimento de novos processos construtivos nas últimas décadas, com o uso de, por exemplo, paredes com elementos de aço no seu interior, e devido às necessidades de investimento em investigação científica de novos sistemas construtivos mais sustentáveis, é imprescindível um laboratório ter uma *Hot box*, para poder realizar o estudo e caracterização destes componentes.

Esta tese de doutorado apresenta a construção de uma *Hot Box* (HB) que permita o estudo de paredes fortemente heterogéneas, como por exemplo paredes LSF, com o potencial de permitir fazer vários outros tipos de estudos futuros, de diferentes tipos de elementos verticais. Isso é possível devido à elevada gama de mediação da condutância térmica (0,1 a 15 W/m².K), grande área de medição e possibilidade de testar amostras com espessuras consideráveis. Para a realização deste objetivo, o equipamento deve ser versátil e permitir diferentes configurações, sendo em simultâneo uma *Guarded* e *Calibrated Hot Box*. Assim, para realização destes objetivos, são abordados os seguintes pontos: (*i*) revisão do estado da arte; (*ii*) apresentação dos princípios e requisitos de desenho da HB; (*iii*) solução do projeto, construção e calibração da HB; e (*v*) estudos experimentais e numéricos de paredes com estrutura LSF.

Palavras-Chave: Hot Box apparatus, Guarded Hot Box, Calibrated Hot Box, Paredes LSF, Desempenho térmico, Transmitância térmica, Condutância térmica, valor de U.

ABSTRACT

The improvement of the thermal performance of buildings envelope is essential to ensure the energy efficiency of buildings. One of the critical components regarding heat losses in a building is the external walls, due to its significant exposed area. Proper thermal performance of building envelope is crucial to provide good thermal behaviour and to obtain high energy efficiency, allowing a reduction in the buildings operating energy.

The experimental characterisation of the overall thermal transmittance (U-value) of building elements, e.g., walls, windows and doors, with new geometries, configurations or materials, is crucial for predicting their thermal performance. It is also essential to measure the *U*-value of walls with new materials and with more elaborate designs since the correct estimation of this value is a critical requirement when performing building energy simulations models or energy audit.

Inhomogeneous buildings elements, e.g. Lightweight Steel Framing (LSF) structures, represents a challenge to determining the thermal transmittance of the components, especially when placing the steel profiles in more than one direction.

The determination of the thermal transmission properties of building elements can be done in several approaches, being the most accurate methodology the Hot Box (HB) method. This method allows performing the determination of the thermal performance of building elements, at steady state, by measuring the heat flux through the building components and the corresponding temperature differences across it. This method can test homogeneous or nonhomogeneous specimens, in a laboratory environment, and applies to building structures or composite assemblies, like e.g. walls with windows or doors.

The Hot Box method was primarily planned for laboratory measurements of large nonhomogeneous specimens, allowing also testing homogeneous elements. Due to the growth of new construction processes in the last decades, with the use of, for example, walls with steel elements inside, and due to the investment needs in scientific research of new and more sustainable building systems, it is essential for that a laboratory has a Hot Box apparatus, to be able to carry out the study and characterisation of these components.

This PhD thesis presents the construction of a Hot Box (HB) apparatus that allows the study heavily heterogeneous walls, e.g. LSF walls, with the potential of enabling to make several other future researches

of different types of vertical elements. This is possible due to the high thermal conductance range of possible measurements (0.1 to 15 W/m².K), large measurement area and the possibility of testing samples with considerable thicknesses. For archiving this goal, the equipment is versatile and allow different configurations, being simultaneously a Guarded and Calibrated Hot Box. Thus, to accomplish these objectives, the following points are addressed: (*i*) review state of the art; (*ii*) presentation of the HB design principles, requirements and test procedures; (*iii*) design solution, construction and calibration of the HB; (*iv*) LSF walls experimental and numerical studies.

Keywords: Hot Box apparatus, Guarded Hot Box, Calibrated Hot Box, LSF walls, Thermal performance, Thermal transmittance, Thermal conductance, U-value.

CONTENTS

LIST OF FIGURES

LIST OF TABLES

NOTATION

LOWERCASE LETTERS

q	-	Heat flux [W/m²]
λ	-	Thermal conductivity [W/(m.K)]

UPPERCASE LETTERS

A_c	-	Fractions of the total heat flow area for the air-cores
A_i	-	Area of assembly "*i*" [m²]
A_w	-	Fractions of the total heat flow area for the webs and air-cores
Cav	-	Width of the zone defined in Figure 2.5 [m]
D	-	Distance from panel surface to metal [m]
D_d	-	Thickness of section *d* [m]
D_i	-	Thickness of the material layer in section *a* [m]
D_i	-	Thickness of section *i* [m]
D_i	-	Thickness of the material layer in section *a* [m]
D_{ii}	-	Thickness of section *ii* [m]
D_j	-	Thickness of the material layer in section *b* [m]
L	-	Stud flange size [m]
L_{2d}	-	Thermal coupling coefficient obtained from a 2D calculation
L_{3d}	-	Thermal coupling coefficient
M	-	Width or diameter of metal heat path terminal [m]
Q	-	Heat flow [W]
$\dot{Q}$	-	Heat transfer [W]
R	-	Thermal resistance [m².K/W]
R	-	Ratio of thermal resistivity
R_1, r_2, r_n	-	Design thermal resistance of each layer[m².K/W]
$R_{air\text{-}to\text{-}air}$	-	Air-to-air thermal resistance [m².K/W]

R_c	-	Thermal resistance for the space between faces for all air-filled cores [m².K/W]
$R_{conv,1}$	-	Convection resistance side 1 [K/W]
$R_{conv,2}$	-	Convection resistance side 2 [K/W]
R_e	-	Exterior air-film resistances [m².K/W]
R_{eff}	-	Effective thermal resistance [m².K/W]
R_{fe}	-	Exterior face resistances [m².K/W]
R_{fi}	-	Interior face resistances [m².K/W]
R_i	-	Interior air-film resistances [m².K/W]
R_i	-	Thermal resistivity of the material layer in section *a* [m.K/W]
R_{ins}	-	Thermal resistivity of insulation in the cavity between studs [m.K/W]
$R_{insulation}$	-	Thermal resistivity of cavity insulation [m.K/W]
R_j	-	Thermal resistivity of the material layer in section *b* [m.K/W]
R_{layer}		Thermal resistivity of the layers [m.K/W]
R_{se}	-	External thermal surface resistance[m².K/W]
$R_{sheathing}$	-	Thermal resistivity of the sheathing layer on the [m.K/W]
R_{si}	-	Internal surface thermal resistance [m².K/W]
R_{ste}	-	Thermal resistivity of steel studs [m.K/W]
R_{ti}	-	Thermal resistance for assembly "*i*" [m².K/W]
R_{tot}	-	Total thermal resistance [m².K/W]
R_{total}	-	Total thermal resistance [K/W]
R-value	-	Thermal resistance [m².K/W]
R_w	-	Thermal resistance for the space between faces for all webs[m².K/W]
$R_{wall,1}$	-	Thermal resistance wall 1 [K/W]
$R_{wall,2}$	-	Thermal resistance wall 2 [K/W]
S	-	Distance between studs [m]
$T_{\infty 1}$	-	Ambient temperature side 1 [° C]
$T_{\infty 2}$	-	Ambient temperature side 2 [° C]
U	-	Thermal transmittance – [W/(m².K)]
U_i	-	Heat transmission coefficient for assembly "*i*" [W/(m².K)]
U-value	-	Thermal transmittance [W/(m².K)]
W	-	Width of the area of influence originated by the steel profiles [m]
W	-	Width of the area of influence originated by the steel profiles [m]
Z_f	-	Zone factor
Δu_f	-	Correction for mechanical fastener
Δu_g	-	Correction for air voids
X	-	Point thermal transmittance due to one fastener
Ψ	-	Linear thermal transmittances obtained from a 3D calculation

ABBREVIATIONS

€	-	Euros
1D	-	One-dimensional
2D	-	Two-dimensional
3D	-	Three-dimensional
ASHRAE	-	American Society of Heating Refrigerating and Air-conditioning Engineers
ASTM	-	American Society for Testing and Materials
BS	-	British standards institution

CF	-	Cold flux side
CFD	-	Computational fluid dynamics
CHB	-	Calibrated hot box
CO_2	-	Carbon dioxide
CT	-	Cold thermocouple
DSC	-	Differential scanning calorimeter
EPS	-	Expanded polystyrene
ETICS	-	External thermal insulation composite systems
EU	-	European union
FEM	-	Finite element method
FSS	-	From standard subsection
GHB	-	Guarded hot box
GHP	-	Guarded hot plate
GOST	-	State Standard of the Soviet Union
HB	-	Hot box
HF	-	Hot flux side
HFM	-	Heat flow meter
HT	-	Hot thermocouple
HVAC	-	Heating, ventilation, and air conditioning
IR	-	Infrared
IRT	-	Infrared thermography
ISO	-	International standard organisation
k€	-	Thousand euros
LSF	-	Lightweight steel framing
M€	-	Millions of euros
OSB	-	Oriented strand board
PCM	-	Phase change material
PCMs	-	Phase change materials
PhD	-	*Philosophiae* doctor
RPM	-	Representative points method
SLS_HF	-	Sum of Least Square of the error between the measured and the calculated Heat Flux
SLS_TIN	-	Sum of Least Square of the error between the measured and the calculated Internal Temperature
VIPs	-	Vacuum insulation panels
WAM	-	Weighted area method
ISISE	-	Institute for Sustainability and Innovation in Structural Engineering

1. INTRODUCTION

1.1. RESEARCH BACKGROUND

The Earth climate is changing dramatically. Global climate change and global warming is a reality nowadays days. The building sector is crucial for reducing the carbon footprint. Making better buildings more energy-efficient, finding new technologic solutions is essential for improving our lives.

The demand to reduce the energy consumption in buildings and to use recyclable materials has increased in the last few decades, as a result of the need to make a more sustainable environment. In Europe, buildings are responsible for 40 % of the energy consumption and 36 % of CO_2 emissions, with the space conditioning, heating and cooling systems, taking a significant share, which also depends on the climate [1–3]. Given the high energy consumption of buildings, the European Union established several objectives in the Energy Performance Building Directive (European Parliament Directive 2010/31/EU [2], recast in 2018 by Directive 2018/844 [4]) regarding "nearly zero-energy buildings" for the year 2020. The directive defined that not only the contribution of renewable energy sources must increase, but also the improvement of buildings energy efficiency should improve.

On November 30, 2016, the European Commission presented a package of measures to keep the European Union (EU) competitive as the clean energy transition changes global energy markets. For this reason, the EU has committed to cut CO_2 emissions by at least 40 % by 2030. The proposals have three primary goals: putting energy efficiency first, achieving global leadership in renewable energies and providing a fair deal for consumers [5].

On January 15, 2020, the European Parliament approved the European Green Deal, which aims the net-zero greenhouse gas emissions objective, making the EU climate-neutral by 2050, in line with the Paris Agreement.

Today, around 75 % of the building stock is energy inefficient. At the current 1 % annual renovation rate, it would take around a century to decarbonise the building stock to modern, low-carbon levels [6].

Looking ahead, it is essential to work on principles and rules for the sustainable design of buildings to generate less construction, demolition waste and facilitate materials recycling. These initiatives will help to reduce energy consumption and costs related to construction materials.

In buildings, the ambient conditioning inside, space heating and cooling are an increasing trend, given people growing needs regarding comfort. One of the most crucial components regarding heat losses in a building are the external walls, due to their very significant exposed area. To ensure the energy efficiency of buildings is essential to improve the thermal performance of the building envelope.

For a nearly zero-energy building, it is essential to develop new solutions for external walls that improve thermal performance. In recent years, alternatives to traditional structural systems for buildings have emerged, e.g.: (*i*) the use of Lightweight Steel Framing (LSF) systems [7,8], and (*ii*) alveolar bricks [9], among others. Furthermore, other related influencing parameters were analysed: (*i*) the number of wall panes [10]; (*ii*) the amount, relative position and thickness of the insulation layers [11]; and (*iii*) the adoption of an air-gap, and the ventilation level of the latter [12].

The thermal transmittance (*U*-value) of the building envelope plays a crucial role in the overall thermal performance of a building, in both the thermal comfort and the energy saving throughout its operational phase. In fact, as suggested by Sassine [13], evaluating how much lost heat energy through the building envelope is a vital requirement for building energy simulation and audit, and it is also needed to support decision making during design, construction and refurbishment.

During the design phase, the thermal transmittance of the elements must be correctly estimated and optimised considering the climate conditions, the construction typology, and the final use of the building. In this context, the level of insulation is one of the main features that influence the *U*-value of the opaque elements [14], and it takes a critical role in energy saving by reducing the rate of heat transfer through the building envelope [15]. The literature suggests that the level of insulation should increase in colder climates to reduce the energy demand for heating and decrease in warmer climates (while the ventilation and free cooling strategies should be improved) to reduce the energy demand for cooling [16].

The improvement of the thermal performance of external walls using different strategies is essential, e.g.: (*i*) improving the thermal transmittance coefficient or U-value; (*ii*) increasing the thermal mass or thermal inertia; and (*iii*) correcting thermal bridges.

Due to the growing importance of energy conservation, there is the need of having reliable data on the thermal transmission properties of insulants and insulated structures. For this purpose, a reliable equipment is essential, such as a hot box apparatus, which is required for: (*i*) making a rigorous experimental determination of the thermal performance of building envelopes; (*ii*) research into the performance of materials and constructions new solutions; (*iii*) verification of simulation models; (*iv*) judging compliance with regulations and specifications; and (*v*) for design guidance creation.

The design, construction, and operation of the hot box apparatus is a complicated subject. It is essential that the designer and user of such equipment have a thorough background knowledge of heat transfer, and experience with precision measurement techniques [17].

Making individual tests by the standards by an accredited laboratory can cost between 2 500 € and 10 000 € per sample. There are not many labs with this type of equipment, and for those that have, the waiting list is several months. The cost of conducting multiple tests to optimise, evaluate and research for new solutions can reach a prohibitive price. A commercial hot box apparatus can cost between 0.5 M€ and 1 M€, which is a considerable amount of money for small laboratories, especially the ones that are in a starting phase. For this reason, at ISISE laboratory research centre, it was decided to develop internally such equipment, with the dual objective of building internally high-level expertise and at the same time to save a significant amount of money.

The next chapters will describe the research work for creating a hot box apparatus, its standards requirements and details, the construction process and calibration.

1.2. HOT BOX APPARATUS PRINCIPLE

The basis of the hot box method is the measurement, at steady state, of the heat flux through the building components and the corresponding temperature differences across it. This test method is used for homogeneous or nonhomogeneous specimens and applies to building structures or composite assemblies of building materials (e.g., walls with windows or with doors). For which it is also possible to build a representative specimen that fits the test apparatus.

There are two types of hot box apparatus: Guarded Hot Box (GHB) and Calibrated Hot Box (CHB). Both types of equipment are suitable for vertical specimens, such as walls, and horizontal specimens, such as ceilings and floors. The apparatus can be sufficiently large to study full-scale components.

The guarded hot box apparatus is shown schematically in Figure 1.1a and consists of three principal objects: guard box, metering box and cold box. The test specimen is placed, in a support frame, between the guarded/metering box and the cold box.

The calibrated hot box apparatus is shown schematically in Figure 1.1b and consists of two principal objects: a metering box and cold box. The test specimen is placed, in a support frame, between the metering box and the cold box.

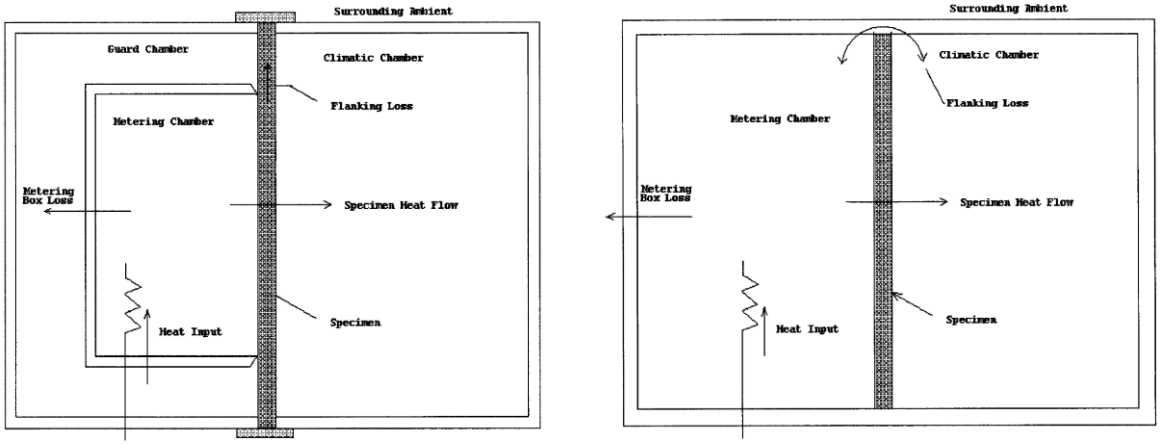

a) Guarded Hot Box **b) Calibrated Hot Box**

Figure 1.1 – Schematic of typicals apparatus [18].

The hot box methods use a hot (guarded and metering chamber) and a cold box, which are both five-sided boxes, between which a test specimen is placed. The basis of the hot box method is to determine the heat flow through a specific area of the test element, and the temperature difference across it. Measurements are made at steady-state conditions, for the test to be valid, of air and surface temperatures, and the power input to the hot side metering chamber. From these measurements are calculated the specimen thermal transfer properties.

The calibrated and guarded hot box apparatus differ by the mode in which the metering box is surrounded. The first is the self-masking, which has a controlled "guard" chamber surrounding the metering chamber. The second configuration is the masked hot box. In this configuration, the guarded chamber is the surrounding ambient. The calibrated hot box surrounding ambient needs to be a temperature-controlled space, which does not necessarily need to be at the same air temperature as that inside the metering box.

1.3. OBJECTIVES

The primary goal of the PhD work is to provide means for quantifying the thermal transmittance of building elements, with a focus on vertical elements.

In a research made before to heterogeneous buildings vertical elements, with high conductivity materials, e.g. LSF framed walls, has felt the need for a rigorous methodology that can test different solutions with a high degree of accuracy. For achieving this objective, this work performs a research study that evaluates the various approaches, analytical, experimental and numerical solutions. The research will show that the most reliable and rigorous methodology that allows achieving what is desired is the hot box method, which is a standardised approach. For that purpose, this research work has the objective of making a hot box apparatus that follows the standards.

For achieve the purpose of the design and construct a hot box apparatus, the main tasks are:

- Study existing types of equipment;
- Analysis of the standards that define the apparatus;
- Design;
- Construction;
- Numerical FEM simulation;
- Thermal bridges verification, with infrared thermographic cameras;
- Study of the repeatability;
- Calibration.

The secondary objective is to study a new constructive solution, such as:

- Thermal performance of lightweight steel-framed wall using two experimental approaches: hot box method and heat flow meter methodology;
- Thermal performance of lightweight steel-framed walls with phase change materials (PCMs);

1.4. THESIS LAYOUT

This thesis is based on the design and construction of a hot box apparatus for the determination of the thermal performance of building elements.

The thesis is organised into six chapters, as follows:

Chapter 1: This chapter intends to present the theme, its importance and the PhD work objectives.

Chapter 2: This chapter presents state of the art, which has three subsections: (i) methods for determining the thermal transmittance of buildings envelope, (ii) hot box historical development, and (iii) lightweight construction systems. The first subsection presents a literature review of the methods, analytical, experimental and numerical, for measurement of the overall thermal transmittance of nonhomogeneous elements, with a particular focus in LSF walls. It also shows the advantages and drawbacks of each one. The second subsection, presents the history of the hot box apparatus, being this part important, due to the quantity of relevant information collected, which provides relevant information for the apparatus design process, e.g. advantages and problems of each typology, problems that can arise and best design solutions depending on the type of specimen intended to be tested. The third part presents the literature review of lightweight steel construction systems, its advantages, problems and new materials than can improve this constructive system.

Chapter 3: The third chapter summarises the standards design principles and requirements for constructing a hot box apparatus. This chapter gives the principal information used in the next chapter for planning the

equipment solution. The last subsection of the chapter presents the test procedures, which are essential to the goal of archiving excellent and reliable results.

Chapter 4: The fourth chapter presents the design solution for the apparatus and its construction, which will operate in both modes, i.e. as a Guarded Hot Box (GHB) and as a Calibrated Hot Box (CHB). Next is presented the experimental characterisation work of the thermal properties of the materials used in the construction of the equipment. After are performed several numerical studies to characterise the flanking losses of the equipment entirely. The numerical models are essential for the next subsection, where is performed a full calibration and verification of the proper operation of the equipment.

Chapter 5: The fifth chapter presents experimental and numerical studies performed to LSF framed walls. Next is made a parametric study to mitigate the thermal bridges and improve the thermal behaviour of the wall.

Chapter 6: The last chapter presents the final considerations on the thesis and summarises the work accomplished.

Throughout the document, the presentation of the values of the quantities are not always following the respective standards. For example, the value of thermal transmission and thermal conductance has one more decimal place, three instead of two as it is normative, and the same happens with the thermal conductivity in which it is sometimes presented with four, instead of the three decimal places. This change aims to increase the accuracy of the comparison analysis. Otherwise, similar values after rounding can lead to significant percentage differences and in other cases, the existence of differences is not noticeable.

2. STATE OF THE ART

The estimation of the overall thermal transmittance of buildings envelope components is crucial when performing a building energy simulation, to optimise the design and the configuration of the construction elements, and to reduce the energy demand for air-conditioning during the operational phase. The estimation is usually carried out by considering the opaque component regarding its different successive layers and considering the thickness and the thermal conductivity (λ) of each layer. In a straightforward approach, calculating the *U*-value can then be done by finding the reciprocal of the sum of the thermal resistance (*R*) of each layer of the construction element.

However, the layer-by-layer approach does not account for thermal bridges caused by metal framing crossing insulation layers in lightweight steel-framed (LSF) construction, or mortar joints in heavyweight walls, air gaps around insulation and cavities with air movements, and moisture. Moreover, as stated by Lucchi [19], the calculation of the *U*-value of construction elements composed by plane, parallel and uniform layers, in which the heat flow is unidirectional, is more theoretical than real. Some standards cover calculation methods to estimate the thermal transmittance of different construction elements, including some of the features listed before (e.g., references ISO 7345, 1987; Anderson, 2006; ISO 10077-1, 2017; ISO 10077-2, 2017; ISO 10211, 2017; ISO 13370, 2017; ISO 13786, 2017; ISO 6946, 2017 [20–27]. However, the overall thermal transmittance of some nonhomogeneous opaque elements cannot be calculated using these standards.

The development of laboratory equipment that allows measuring the *U*-value has been a subject of great interest during the last decades. The results of the experimental approach are crucial for the validation of numerical or analytical models to determine the *U*-value of more complex configurations, and to support new standard procedures.

This chapter aims to provide a literature review of the primary methods for determining the thermal transmittance of the buildings envelope. The first subsection presents the following methods: analytical, experimental, and numerical. The second part summarises the history of the development, along the years, of the hot box apparatus. The third part describes a literary review of the lightweight construction systems and new materials that can improve the thermal performance of these components.

2.1. METHODS FOR DETERMINING THE THERMAL TRANSMITTANCE OF THE BUILDINGS ENVELOPE

Heat is lost from buildings by two distinct processes, first by infiltration or air leakages, and second, by conduction through the walls [28].

The precise characterisation of the thermal performance of building envelopes is crucial to correctly predict, at the design stage, its thermal behaviour, and energy efficiency. As said before, the most important parameters are the thermal transmittance (*U*-value), which allows to calculate the thermal transfer of the constructive elements and knowing the heat balance, thus allowing to estimate the energy needs for heating or cooling the spaces.

This work dedicates particular attention to the measurement of the overall thermal transmittance of LSF walls, by including the effects of thermal bridges caused by steel framing components. In many studies, several methods are considered together to perform comparative analyses between results obtained by different experimental methodologies and to compare experimental measurements with standard and analytical procedures. Given the higher heterogeneity of the thermal properties (e.g., conductivity) between the steel frames and other materials, the accurate quantification of the thermal transmittance in LSF structures is even more complicated than with traditional-construction like brick walls [29]. The *U*-value can be determined using different approaches, which have different levels of accuracy/reliability, including analytical calculations, experimental assessments, and numerical computational models, presented in the next subsections.

The LSF construction elements (e.g. walls) can be classified into three types, depending on the position of the insulation materials, which affects the choice of the method for determining the thermal resistance element. Figure 2.1 shows examples of cold, hybrid and warm frame construction. The presented examples differ in the position of the wall materials: gypsum; lightweight steel frame; stone wool; oriented strand board (OSB); expanded polystyrene (EPS); and external thermal insulation composite systems (ETICS).

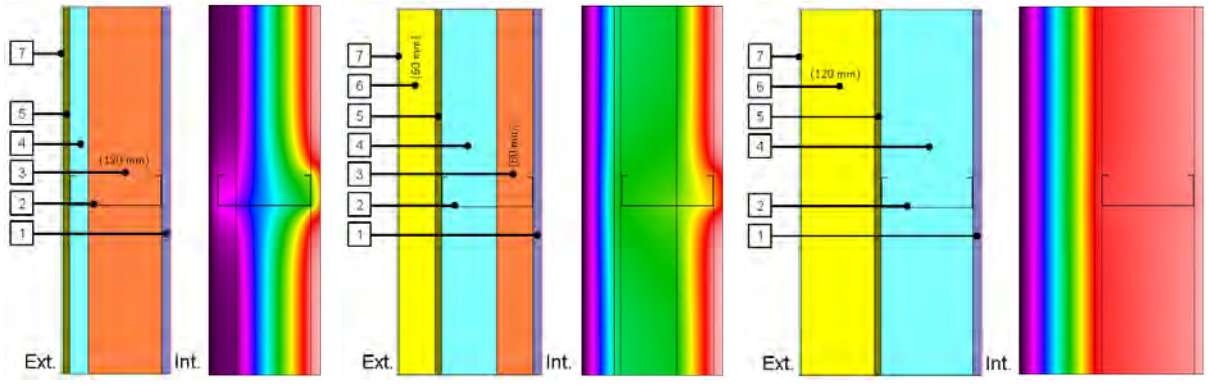

a) Cold frame construction $U = 0.5255$ W/(m².K)

b) Hybrid construction $U = 0.3856$ W/(m².K)

c) Warm frame construction $U = 0.2828$ W/(m².K)

Materials:

1 - Gypsum	4 - Air gap	7 - ETICS
2 - LSF	5 - OSB	
3 - Stone wool	6 - EPS	

Figure 2.1 – Classification of LSF constructions, depending on the position of insulation materials and horizontal cross-section temperature distribution. [3].

The cold frame construction includes all the insulation within the thickness of the steel, being the insulation layer crossed by the steel studs. This type of construction, illustrated in Figure 2.1a, is not suitable for cold climates, given the lower temperature inside the wall, there is a higher risk of interstitial condensation

occurring, especially in the steel studs and their vicinity. Figure 2.1b shows an example of hybrid construction, which places the insulation between the steel frames. The thickness of external continuous thermal insulation when maximised allows better thermal bridge mitigation. In the third type, warm frame construction (Figure 2.1c), places all the insulation outside of the steel framing. This approach is the best option, reducing the risk of interstitial condensation and maximising the thermal mass of the building envelope, as shown in the temperature distribution of Figure 2.1.

2.1.1. Analytical methods

Analytical methods for the calculation of the thermal behaviour of buildings elements is a complicated subject, especially in nonhomogeneous elements. There are many methodologies for determining the thermal performance of building envelopes, and the proper method depends on the types of construction and thermal insulation. These methods allow determining the *R*-values and *U*-values for assemblies with one- or two-dimensional heat transfer.

2.1.1.1. Homogeneous multilayer plane walls

For homogeneous multilayer plane walls, the thermal resistance concept can be used to determine the rate of heat transfer, at steady state, through composite walls. This determination is done by basically saying that the conduction resistance of each wall is $L/k.A$ (where: L is the thickness, A the area, and k the thermal conductivity) connected in series and using the electrical analogy. That is, by dividing the temperature difference between two surfaces at known temperatures by the total thermal resistance between them.

For a plane wall, as illustrated in Figure 2.2, with two layers, the rate of heat transfer ($\dot{Q}$), at steady-state, through this two-layer composite wall can be given by:

$$\dot{Q} = \frac{T_{\infty 1} - T_{\infty 2}}{R_{total}} \ [W] \tag{1}$$

where: $T_{\infty 1}$ ambient temperature side 1, $T_{\infty 2}$ ambient temperature side 2, and R_{total} is the total thermal resistance, expressed as:

$$R_{total} = R_{conv,1} + R_{wall,1} + R_{wall,2} + R_{conv,2} \ [K/W] \tag{2}$$

where: $R_{conv,1}$ convection resistance side 1, $R_{wall,1}$ thermal resistance wall 1, $R_{wall,2}$ thermal resistance wall 2, and $R_{conv,2}$ convection resistance side 2.

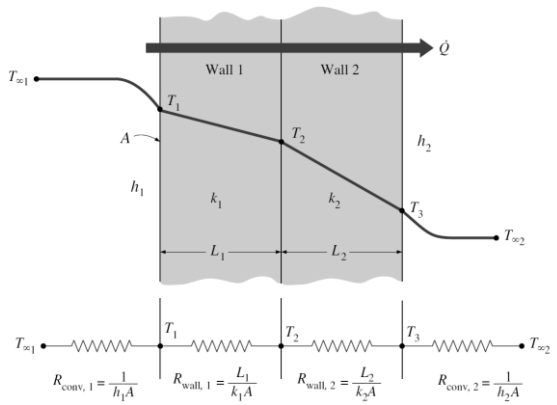

Figure 2.2 – Thermal resistance network for heat transfer through a two-layer plane wall subjected to convection on both sides [30]

The thermal resistance network for heat transfer through multiple layers can be obtained by:

$$R_{total} = R_{conv,1} + \sum_{i=1}^{n} R_{wall,i} + R_{conv,2} \ [K/W] \quad (3)$$

where: i is the element number and n the total number of layers.

2.1.1.2. Parallel path method

The parallel path method assumes that heat flows independently through zones that are in parallel, and there is no heat exchange between zones, as illustrated in Figure 2.3.

The parallel-path calculations yield relatively accurate results for one-dimensional heat transfer, where there is little or no heat exchange between the "parallel" paths in the actual assembly [31].

The heat flow (Q) through a defined area with multiple adjacent assemblies can be determined by:

$$Q = (A_1/R_{T1} + A_2/R_{T2} + A_3/R_{T3} + \cdots)\Delta T \ [W] \quad (4)$$

or alternatively:

$$Q = (U_1.A_1 + U_2.A_2 + U_3.A_3 + \cdots)\Delta T \ [W] \quad (5)$$

where: A_i is the area of assembly "i", in m², R_{Ti} is the thermal resistance in m².K/W for assembly "i", obtained by summing the resistance of each layer of material in the assembly including inner and outer air films, ΔT is the difference between the indoor and outdoor air temperatures, and U_i is the heat transmission coefficient in W/(m².K) for assembly "i" including the effect of the interior and exterior surface films.

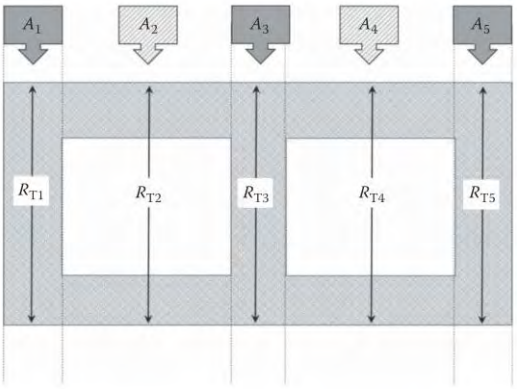

Figure 2.3 –Schematic for the parallel path method [31].

The effective R-value and U-value for this method can be calculated using the following equation:

$$R_{eff} = 1/U = (A_1/R_{T1} + A_2/R_{T2} + A_3/R_{T3} + \cdots)/A_{total} \ [\mathrm{m^2.K/W}] \quad (6)$$

2.1.1.3. Isothermal planes (series-parallel path) method

In buildings with highly conductive structural members or other components made for example of concrete, steel, aluminium, or glass, the assumption of parallel heat flow is not likely to provide reliable results [31]. For these situations, the isothermal planes method provides an alternate procedure for calculating the *U*-value.

The isothermal planes method assumes a uniform temperature (isothermal) for the highly conductive planes, separating less conductive layers. This method is used, for example, to analyse heat flow through wood-framed assemblies or masonry walls [31].

The method divides the construction assembly into a series of layers, as shown in Figure 2.4 for the example of hollow masonry units. The webs, which are solid, connecting the face shells are more conductive compared to the air spaces in the hollow cores, and the face shells conduct heat laterally. In Figure 2.4 example, the layer containing the webs and cores is treated with a parallel-path calculation to achieve an average *R*-value of the layer, being added to the *R*-values of the two face shells in series.

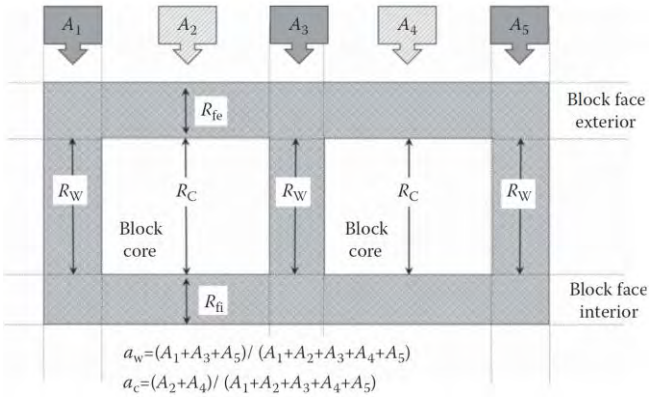

Figure 2.4 –Schematic for the isothermal plane method [31].

The air-to-air *R*-value is computed using the following equation:

$$R_{air-to-air} = \frac{1}{U} = R_e + R_{fe} + \frac{a_w}{R_w} + \frac{a_c}{R_c} + R_{fi} + R_i \ \ [\mathrm{m^2.K/W}] \tag{7}$$

where: R_e and R_i are exterior and interior air-film resistances, R_{fe} and R_{fi} are exterior and interior face resistances, a_w and a_c are fractions of the total heat flow area for the webs and air-cores, and R_w and R_c are *R*-values calculated for the space between faces, for all webs and air-filled cores.

2.1.1.4. Zone method

For structures with widely spaced metal members of substantial cross-sectional area, calculation by the isothermal planes method can result in thermal resistance values that are too low [32]. Heat flow through construction assemblies with metal framing is more complicated and requires special consideration.

To overcome this problem and to provide a simplified method, one of the first methods to be developed was the ASHRAE zone method [33] for calculating the U for walls with cold-formed steel profiles. This method allows calculating the value of the thermal resistance (*R*) of a constructional member, e.g., wall type, when it contains elements of high thermal conductivity, such as steel profiles, in cross-section. This

methodology is a modification of the parallel path method, in which the wall is divided into several parallel paths, from heat flow paths with different conductance's, from the surface to surface, and a wall area weighting factor applied with a thermal bridge originated by the steel profile. The width of the area of influence arise by the steel profiles can be estimated by:

$$W = m + 2 \times d \ \ [m] \tag{8}$$

where: W = width of the area of influence originated by the steel profiles [m]; m = width or diameter of metal heat path terminal [m]; and d = distance from panel surface to metal [m]. Figure 2.5 illustrates d and m.

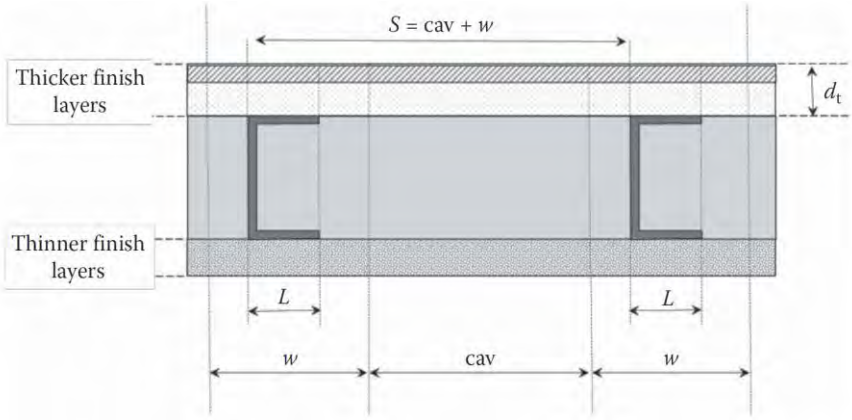

Figure 2.5 – ASHRAE zone method [31].

The ASHRAE zone method has the limitation that it can only be applied to walls and slabs with metallic profiles assembled in one direction. It is not applicable in situations with steel profiles perpendicular to each other.

For walls with steel profiles and empty cavities, the accuracy of Zone Method R-value calculations is not sensitive to changes of the area of thermal bridge zone in this cases the zone method overestimates *R*-values by 4 to 14% [29]. The errors are even more significant for walls without exterior insulation. Kosny *et al.* [29] suggest that the application of the ASHRAE zone method should be limited to cases of metal-frame walls containing a cavity filled with insulation.

For the zones marked as in Figure 2.6, calculating the partial resistances R_A, R_B, R_I, and R_{II} is done as follows:

for section *A*:

$$R_A = \sum_{i=1}^{n} (r_i . d_i) \ \ [\mathrm{m^2.K/W}] \tag{9}$$

where: r_i is the thermal resistivity, and d_i is thickness, of the material layer in section *A*.

for section *B*:

$$R_B = \sum_{j=1}^{m} (r_j . d_j) \ \ [\mathrm{m^2.K/W}] \tag{10}$$

where: r_j is the thermal resistivity, and d_j is thickness, of the material layer in section *B*.

for a section *I*:

$$R_I = \frac{R_{ste}^I . R_{ins}^I . w}{d_{II} . \left(R_{ins}^I - R_{ste}^I\right) + w . R_{ste}^I} \ [\mathrm{m^2.K/W}] \tag{11}$$

where: d_{II} is the thickness of section *II* (also steel stud thickness), and:

$$R_{ste}^I = r_{ste} . d_I \ [\mathrm{m^2.K/W}] \tag{12}$$

$$R_{ins}^I = r_{ins} . d_I \ [\mathrm{m^2.K/W}] \tag{13}$$

where: r_{ste} is the thermal resistivity of steel studs, r_{ins} is the thermal resistivity of insulation in the cavity between studs, and d_I is the thickness of section *I*.

for section *II*:

$$R_{II} = \frac{R_{ste}^{II} . R_{ins}^{II} . w}{L . \left(R_{ins}^{II} - R_{ste}^{II}\right) + w . R_{ste}^{II}} \ [\mathrm{m^2.K/W}] \tag{14}$$

where: d_D is the thickness of section *D* (also steel stud thickness), and:

$$R_{ste}^{II} = r_{ste} . d_{II} \ [\mathrm{m^2.K/W}] \tag{15}$$

$$R_{ins}^{II} = r_{ins} . d_{II} \ [\mathrm{m^2.K/W}] \tag{16}$$

where: r_{ste} is the thermal resistivity of steel studs, r_{ins} is the thermal resistivity of insulation in the cavity between studs, and d_{II} is the thickness of section *II*.

For calculating the total *R*-value is as a parallel sum of resistances of the zones *w* and *cav* using the following equation:

$$\frac{1}{R_{tot}} = \frac{\frac{w}{\sum R_w} + \frac{cav}{\sum R_{cav}}}{s} \ [\mathrm{m^2.K/W}] \tag{17}$$

where: *cav* is the width of the zone defined in Figure 2.5 that can be calculated by:

$$cav = s - w \ [m] \tag{18}$$

where: *s* is the distance between studs.

By simplification, the total *R*-value is calculated by equation (19):

$$R_{tot} = \frac{\sum R_w . \sum R_{cav} . s}{w . (\sum R_{cav} - \sum R_w) + s . \sum R_w} \ [\mathrm{m^2.K/W}] \tag{19}$$

where:

$$\sum R_{cav} = R_A + R_B + R_{ins}^{I} + 2.R_{ins}^{II} \ [\mathrm{m^2.K/W}] \tag{20}$$

$$\sum R_w = R_A + R_B + R_I + 2.R_{II} \ [\mathrm{m^2.K/W}] \tag{21}$$

In the case of walls without insulation in the cavity, the thermal resistance R_{II} must be omitted, and the thermal resistance R_{ins}^{I} must be replaced in equations (10) and (11) by the thermal resistance of an airspace. Nevertheless, [29] do not recommend the use of this methodology for walls with an air cavity between steel profiles.

Walls with internal steel structure attached on one or both sides to a metal skin or covering presents problems of lateral heat flow, not covered in the zone method.

2.1.1.5. Modified zone method

Based on ASHRAE zone method, Jan Kośny developed the modified zone method for metal stud walls with insulated cavities [29,34], which differs from the previous approach in the way that the metal stud thermal bridge zone of influence is estimated, leading to more reliable results. The modified zone method was, for the first time, recommended in the 1997 ASHRAE Handbook of Fundamentals [35] and following editions. The modified zone method improves the accuracy of *R*-value calculations for light steel framed walls with insulated cavities containing steel *C*-shape studs with solid webs [31,36].

In the modified zone method, the zone width depends on the following three parameters: the ratio between the thermal resistivity of sheathing material and cavity insulation; size (depth) of the stud; and thickness of sheathing material.

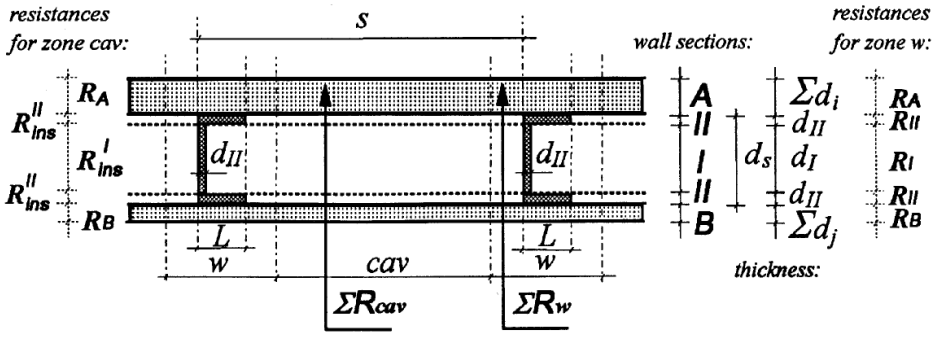

Figure 2.6 – Modified zone method [32].

In the modified zone method, the width of the area of influence arise by the steel profiles can be estimated by the following equation:

$$w = L + z_f \sum_{i=1}^{n} d_i \ [m] \tag{22}$$

where: w is the width of the area of influence originated by the steel profiles [m]; L is the stud flange size [m]; d_i the thickness of the material layer in section A [m]; z_f is the zone factor.

The determination of the zone factor arises from simulations of different steel-stud walls configurations. It depends on the ratio between the thermal resistivity of the finishing material and cavity insulation, depth of stud, and thickness of finish material layers, Figure 2.7 shows how to obtain the zone factor.

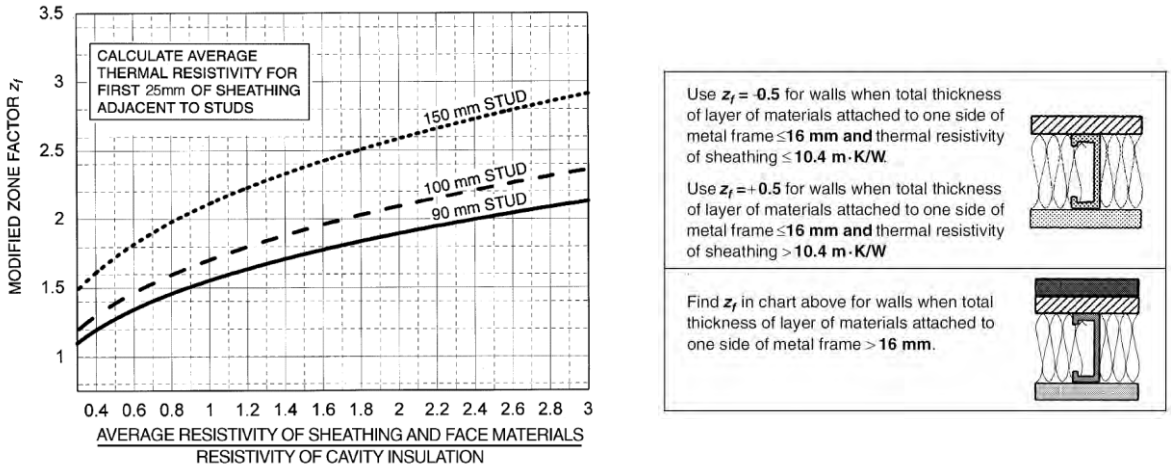

Figure 2.7 – Modified zone factor for calculating *R*-value of metal stud walls with cavity insulation [32].

For obtaining the zone factor, retrieved from the abacus of Figure 2.7, it is necessary the thermal resistance and profile width. For achieving the thermal resistivity needs to divide the resistance of the coating layers and the thermal resistance of the cavity compartment, given by equation (23):

$$r = \frac{r_{sheathing}}{r_{insulation}} \tag{23}$$

where: r is the ratio of thermal resistivity; $r_{\text{sheathing}}$ is the thermal resistivity of the sheathing layer on the [m.K/W]; and $r_{insulation}$ is the thermal resistivity of cavity insulation [m.K/W];

The thermal resistivity of the layers is done by equation (24):

$$r_{layer} = \frac{1}{\lambda}\ [m.K/W] \tag{24}$$

where: λ is the thermal conductivity [W/(m.K)].

The calculation of the total *R*-value is done by the same procedure presented in the previous subsection, from equation (9) to (21).

Kosny and Desjarlais [37] verified the precision of the modified zone method, by finite-difference modelling, for over than 200 simulated cases of metal frame walls with insulated cavities. The modified zone method considered the discrepancy between results within ±2 %, of the results of the three-dimensional finite-difference evaluations.

ASHRAE Handbook of Fundamentals [35] performed the comparison between hot box measured R-values for 15 metal stud walls tested by [29], with results obtained by [34] and [38], concluding that the modified zone method is a more accurate method for estimating the *R*-value of LSF walls with insulated cavities.

2.1.1.6. ISO 6946 method

ISO 6946 [26] presents an analytical method to calculate *R*-values and *U*-value of building elements, including thermally homogeneous and thermally inhomogeneous layers parallel to the surface. This method is not applicable for many LSF elements (other than full warm frame construction) in which metallic elements bridged the insulation layers.

For steel-frame constructions in which metal parts do not penetrate the insulation, i.e. for wholly warm frame constructions, the method given in ISO 6946 [26] may be used [39].

The total thermal resistance, R_T, is given by equation (25):

$$R_T = \frac{R_{max} + R_{min}}{2} \; [m^2.K/W] \tag{25}$$

where: R_{max} is the upper limit of the total thermal resistance and R_{min} is the lower limit of the total thermal resistance.

The calculation of the upper and lower limits of the total thermal resistance can be carried out by considering the component split into sections and layers, as shown in Figure 2.8. The component is divided into parts that are thermally homogeneous.

The upper limit of the total thermal resistance, R_{max}, is determined by assuming one-dimensional heat flow perpendicular to the surfaces of the component, which is given by the following expression:

$$\frac{1}{R_{max}} = \frac{f_a}{R_{Ta}} + \frac{f_b}{R_{Tb}} + \cdots + \frac{f_q}{R_{Tq}} \tag{26}$$

where: f_a, f_b, ..., f_q are the fractional areas of each section; and R_{Ta}, R_{Tb}, ..., R_{Tq} are the total thermal resistance from the environment to environment for each section, calculated using equation (27):

$$R_{T\,a,b\ldots q} = R_{si} + R_1 + R_2 + \cdots R_n + R_{se} \; [m^2.K/W] \tag{27}$$

where: R_{si} is the internal surface resistance; R_1, R_2, ... R_n are the design thermal resistance of each layer; and R_{se} is the external surface resistance.

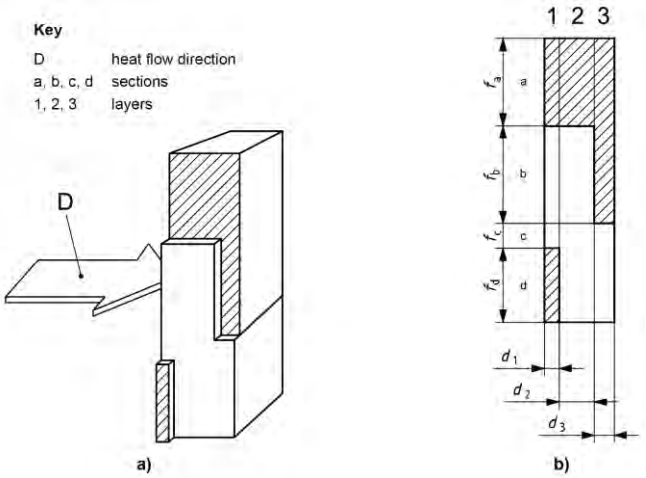

Figure 2.8 – Sections and layers of a thermally inhomogeneous component [26].

The lower limit of the total thermal resistance, R_{min}, is determined by assuming that all planes parallel to the surfaces of the component are isothermal surfaces, given by equation (28):

$$R_{min} = R_{si} + R_1 + R_2 + \cdots R_n + R_{se}\ [m^2.K/W] \tag{28}$$

where: R_{si} is the internal surface resistance; R_{se} is the external surface resistance; and R_1, R_2, ... R_n are given by:

$$\frac{1}{R_j} = \frac{f_a}{R_{aj}} + \frac{f_b}{R_{bj}} + \cdots + \frac{f_q}{R_{qj}} \tag{29}$$

where: R_j is the equivalent thermal resistance for each thermally inhomogeneous layer; and f_a, f_b, ..., f_q are the fractional areas of each section.

The thermal transmittance is given by:

$$U = \frac{1}{R_T} + \Delta U_g + \Delta U_f \tag{30}$$

where: ΔU_g is the correction for air voids; ΔU_f is the correction for mechanical fasteners, and R_T is the total thermal resistance.

The corrections ΔU_g and ΔU_f can be ignored if they together are less than 3 % of $1/R_T$., and the correction for air voids, ΔU_g, is adjusted by equation (31):

$$\Delta U_g = \Delta U''.\left(\frac{R_1}{R_{T,h}}\right)^2 \tag{31}$$

where: R_1 is the thermal resistance of the layer containing gaps, obtained by equation (32); $R_{T,h}$ is the total thermal resistance of the component ignoring any thermal bridging, obtained by equation (27); and $\Delta U''$ is given by Table 2.1.

$$R = \frac{d}{\lambda}\ [m^2.K/W] \tag{32}$$

where: d is the thickness of the material layer in the component, and λ is the design thermal conductivity of the material.

Table 2.1 – Corrections for air voids, $\Delta U''$ [26]

Level	Description	$\Delta U''$ [W/(m²·K)]
0	No air voids within the insulation, or where only minor air voids are present that have no significant effect on the thermal transmittance.	0.00
1	Air gaps bridging between the hot and cold side of the insulation, but not causing air circulation between the warm and cold side of the insulation.	0.01
2	Air gaps bridging between the hot and cold side of the insulation, combined with cavities resulting in free air circulation between the warm and cold sides of the insulation.	0.04

The correction for mechanical fasteners, ΔU_f, is adjusted by the equation:

$$\Delta U_f = n_f . \chi \tag{33}$$

where: n_f is the number of fasteners per square metre, and χ is the point thermal transmittance due to one fastener, that can be obtained from ISO 10211 [27], by equation (34):

$$\chi = L_{3D} - \sum_{i=1}^{N_i} U_i . A_i - \sum_{j=1}^{N_j} \Psi_j . l_j \tag{34}$$

where: L_{3D} is the thermal coupling coefficient, obtained from a 3D calculation; U_i is the thermal transmittance of the 1D component i separating the two environments; A_i is the area over which the value U_i applies; Ψ_j is the linear thermal transmittances calculated using equation (35); l_j is the length over which the value Ψ_j applies; N_j is the number of 2D components; and N_i is the number of 1D components.

$$\Psi = L_{2D} - \sum_{j=1}^{N_j} U_j . l_j \tag{35}$$

where: L_{2D} is the thermal coupling coefficient obtained from a 2D calculation of the component separating the two environments being considered; U_j is the thermal transmittance of the 1D component, j, separating the two environments being considered; and l_j is the length over which the value U_j applies.

2.1.1.7. Simplified method of calculating U-values in light steel framing

Doran and Gorgolewski [39] suggested a simplified method to estimate the U-value of LSF assemblies. This method is an adaptation of the approach established in ISO 10211 [27] that includes various additional parameters (e.g., flange width, stud spacing, and depth) to account for the overall thermal behaviour of the steel-framed element. As shown by the author, with this method, the mean error of prediction (compared with finite-element numerical modelling) is less than 3 % with a maximum error of 8 % for a range of 52 constructions assessed [40]. Additional details about this method can be found in Doran and Gorgolewski [39], including some examples regarding the calculation of U-values of hybrid and cold frame LSF assemblies.

The simplified method sets out the same methodology suggested in ISO 6946 [26] for warm frame constructions. For cold frame and hybrid constructions, Doran and Gorgolewski [39] set out a similar methodology in which the total thermal resistance, R_T, is given by the equation:

$$R_T = p \, . \, R_{max} + \, (1 - p) \, . \, R_{min} \; [m^2.K/W] \tag{36}$$

where the factor p can be obtained through the equation (37):

$$p = 0.8 \; \frac{R_{min}}{R_{max}} + 0.44 - 0.1 \; \frac{w}{40 \; mm} - 0.2 \; \frac{600 \; mm}{s} - 0.04 \; \frac{d}{100 \; mm} \tag{37}$$

where: w is the width of the flange of the steel profile [mm]; s is the spacing between steel profiles [mm]; d is the web width [mm]; R_{max} is the upper limit of the total thermal resistance; and R_{min} is the lower limit of the total thermal resistance. R_{max} and R_{min} can be obtained from equations (26) and (28).

The thermal transmittance is given by equation (38):

$$U = \frac{1}{R_T} + \Delta U \tag{38}$$

where: R_T is the total thermal resistance; and ΔU is a correction to the U-value, that have in account the effects of the thermal bridge of the metal fixings and air gaps influence, being ΔU given by:

$$\Delta U = \Delta U_g + \Delta U_f \tag{39}$$

where: ΔU_g is the correction for air voids, obtained by equation (31); and ΔU_f is the correction for mechanical fasteners, obtained by:

$$\Delta U_f = \alpha . \lambda_f . A_f . n_f . (R_i / R_T)^2 / d_i \tag{40}$$

where: the value of a is 0.8 for warm frame construction and 1.6 for hybrid construction; λ_f is the thermal conductivity of the fixing; A_f is the cross-sectional area of the fixing; n_f is the number of fixings per square metre of the area; R_i is the thermal resistance of the insulation layer penetrated by the fixings, obtain by equation (32); R_T is the total thermal resistance of the element (taking account of the bridging by the steel studs and noggings), as calculated in equation (36); and d_i is the thickness of insulation penetrated by the fixings.

This method has the same limitations of applicability as the previous ones, as it only applies to walls with metallic profiles applied in one direction. It has the advantage of giving more rigorous values than the previous ones.

2.1.1.8. Methods remarks

Table 2.2 resumes the principal advantages and drawbacks of the analytical methods.

Table 2.2 – Analytical methods: advantages and drawbacks.

Method	Advantages	Drawbacks
Homogeneous multilayer plane walls	- Simple to use;	- Homogeneous multilayer plane walls; - Only steady-state analyses.
Parallel path method	- More complete than the previous; - Allows calculating heat flows independently through zones that are in parallel.	- Only for one-dimensional heat transfer; - Only steady-state analyses; - For highly conductive structural members is not likely to provide reliable results.
Isothermal planes (series-parallel path) method	- More complete than the previous for structures nonhomogeneous;	- For structures with widely spaced metal members of the substantial cross-sectional area, can give thermal resistance values too low.

Method	Advantages	Drawbacks
	- Allows to calculate heat flows highly conductive structural members.	
Zone method	- For structures with widely spaced metal members of substantial cross-sectional is more accurate than all methods above.	- Only applicable to walls and slabs with metallic profiles assembled in one direction; - Limited to cases of metal-frame walls containing a cavity filled with insulation.
Modified zone method	- More reliable results than zone method; - More accurate method for estimating the R-value of LSF walls with insulated cavities comparatively to the previous ones.	- Only for metal stud walls with insulated cavities.
ISO 6946 method	- For homogeneous and thermally inhomogeneous layers parallel to the surface.	- Only for full warm frame construction.
Simplified method of calculating *U*-values in light steel framing	- More rigorous values than the previous ones.	- The method has the same limitations of applicability as the previous ones, only applies to walls with metallic profiles applied in one direction.

2.1.2. Experimental methods

The experimental evaluation is crucial for the validation of numerical or analytical models to determine the *U*-value of more complex configurations and to support new standard procedures.

The development of new laboratory experiments and innovative non-destructive *in-situ* methods to measure the *U*-value of non-homogeneous walls has been a subject of great interest during the last years. Non-destructive *in-situ* measurements to determine the overall thermal transmittance of existing walls is very important for an energy audit or retrofitting actions. In fact, as suggested by Sassine [13], when dealing with existing buildings, it is more complicated to perform the thermal characterisation of the construction elements, since the properties of materials are usually unknown, components are often degraded over time, and the experiments should be simple, fast, and non-destructive. Most of the methodologies described in the literature concern measurements of samples in laboratory conditions with well-known environmental conditions, geometries, configurations and materials. Therefore, there is a lack of reliable methodologies for *in-situ* measurement of the *U*-value of existing walls in real buildings, particularly for existing LSF walls.

As stated by Gori *et al.* [41], the precise evaluation of the thermophysical properties of building elements based on *in-situ* measurements can enable their performance to be assessed for qualitative assurance and correct decision in policy making, building design, construction and refurbishment.

This subsection aims to provide a literature review of the primary experimental methods for determining the thermal transmittance of buildings envelope, namely: (*i*) the heat flow meter (HFM); (*ii*) the guarded hot plate (GHP); the hot box (HB), considering (*iii*) the guarded HB (GHB) and (*iv*) the calibrated HB (CHB); and at last, (*v*) the infrared thermography (IRT).

2.1.2.1. Heat flow meter (HFM)

The HFM method is the most widely used technique for determining the thermal transmittance of a building element. According to greenTEG [42], this method is also the only procedure that provides reliable quantitative information about a building envelope. It consists in establishing a temperature difference between the two surfaces of the element and analysing the heat flux across the specimen (from the "hot" to the "cold" side). Indeed, ISO 9869-1 [43] describes the measurement of the environmental temperature of both "hot" and "cold" sides for the *U*-value determination. For achieving good results, the wall shall not have any significant lateral heat flux, i.e., there must be a representative unidirectional heat flow. The predominant heat transfer mechanism in this method is conduction. Convection and radiation effects (boundary conditions) can be simplified, taken together and treated as an ambient temperature, which should be adequately measured. The HFM method can be applied in laboratory-controlled environmental conditions or *in-situ* measurements.

Table 2.3 summarises the main advantages and drawbacks of the HFM method. The ASTM standards cover most issues related to the HFM method. Moreover, the ISO standards are more general, although they contain all the necessary information for the application of this method.

Table 2.3 – HFM method: advantages and drawbacks.

Advantages	Drawbacks
- Non-invasive method [44]; - The higher the temperature gradient, the more reliable the results are [44]; - Internationally recognised and most widely used [45]; - Lightweight and easy to carry equipment [46]; - Can be used in controlled laboratory conditions or *in-situ* measurements [43].	- The measurement is local (does not consider the entire surface of the element) [47]; - Time-consuming method that requires direct contact [43]; - Long measuring time (more than three days) [43]; - Only completely adapted for homogeneous walls [43,48]; - Lightweight construction elements and the presence of multi-layered air spaces lead to questionable results [49]; - Highly dependent on the calibration and error of the equipment, outdoor and indoor thermal environment, thermal bridges, humidity and partial adhesion of sensors [47,49–51]; - The degree of precision depends on temperature variations within the space and differences between air and radiant temperatures [47]; - Dependent on the accuracy of the data logging system [43]; - Difficulties in dealing with internal heat sources, *e.g.*, walls with internal pipes inside which hot/cold water flows [44]; - It is relatively expensive, and it leaves marks and damages the surface of the building element [52].

Table 2.4 summarises the primary standards that prescribe the essential procedures that should be considered, matching the contents of the ASTM and ISO standards.

Table 2.4 – Main standards in the field of the HFM method.

ASTM	ISO
Principles for the use of the method and calculation of thermal properties	
- ASTM C1155-95 [48], "Standard practice for determining thermal resistance of building envelope components from the in-situ data". - ASTM C1046-95 [53], "Standard practice for in-situ measurement of heat flux and temperature on building envelope components".	- ISO 9869-1 [43], "Thermal insulation - Building elements - In-situ measurement of thermal resistance and thermal transmittance - Part 1: Heat flow meter method".
Steady-state thermal properties	
- ASTM C518-17 [54], "Standard test method for steady-state thermal transmission properties by means of the heat flow meter apparatus".	- ISO 8301 [55], "Thermal insulation - Determination of steady-state thermal resistance and related properties - Heat flow meter apparatus".
Thermal transmittance in glass	
	- ISO 10293 [56], "Glass in building - Determination of steady-state U values (thermal transmittance) of multiple glazing - Heat flow meter method".
Thermal storage properties in phase change materials and products	
- ASTM C1784-14 [57], "Standard test method for using a heat flow meter apparatus for measuring thermal storage properties of phase change materials and products".	
Thermal transmission properties of vacuum insulation panels	
- ASTM C1667-15 [58], "Standard test method for using heat flow meter apparatus to measure the centre-of-panel thermal transmission properties of vacuum insulation panels".	

For measuring the *U*-value of walls, the HFM method requires heat flux meters, thermocouples, and data acquisition systems. Figure 2.9 shows a sketch of an HFM laboratory apparatus and an example of an instrumented wall. According to ISO 9869-1 [43], the data collected by the heat flux meter and the temperature sensors shall be recorded continuously or at fixed intervals over a period of full days. It should be pointed out that this standard was developed for *in-situ* measurement-cycles of 24 hours under outdoor environmental conditions. The maximum period between two records and the minimum duration of the test depends on the nature of the element (*e.g.*, heavy- or light-weight construction, the insulation position, etc.), the indoor and outdoor temperatures (mean temperature and temperature fluctuations, before and during measurements) and the method used for the data analysis. The minimum duration for the measurements is 72 hours, if the temperature is kept stable around the heat flux meter. Otherwise, the test may have to last over seven days. The duration of experiments shall be determined by applying criteria to the values obtained during the test. According to the ASTM C1155-95 [48], the data of each sensor should be monitored at least every 5 minutes. With this, the average values of temperature and heat flow must be calculated and recorded in intervals of 60 minutes or less. The experiment should last three or more

multiples of 24 h (24 h is a dominant temperature cycle). However, since temperatures on both sides are controlled (if/when in the laboratory), the test duration must be adapted considering the temperature stability.

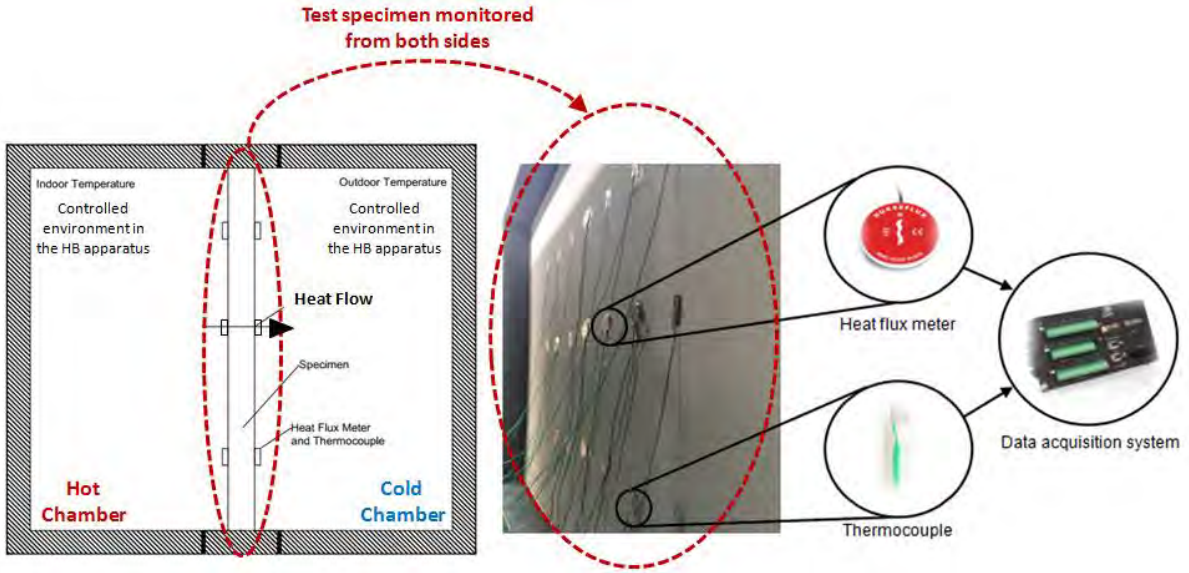

Figure 2.9 – The instrumented outer surface of an LSF wall (test sample): a sketch of the application of the HFM method in a laboratory-controlled environment [59].

To evaluate the *U*-value in steady-state conditions, ISO 9869-1 [43] proposes the simple average method. The average method is very used because, despite leading to a more extended test duration, it makes the calculation process simpler. Also, it considers that the heat transfer process does not achieve a steady-state (which is what happens), considering the variation over time of the heat flux and the ambient temperatures. The average method indicated in this standard also proposes an alternative methodology for data correction, considering the effects of thermal storage (applicable to constructive elements with high thermal inertia).

ASTM C1155-95 [48] indicates the sum of the least squares method (rather a complicated method) and the summation technique (similar to the average method), requiring a significant difference between surface temperatures for fast convergence (the surface temperatures are required for the thermal resistance measurement). Since the procedure does not consider thermal storage, the method is sensitive to a gradual increase or decrease of temperature differences.

For evaluation of the *U*-value in a dynamic state, ISO 9869-1 [43] presents another method with varying temperature and heat flow, to obtain the steady-state properties of a building element. The implementation of the dynamic method requires: (*i*) measuring the density of the heat flow rate and the temperatures at the indoor and outdoor surfaces, taken at several time intervals; (*ii*) computing the derivative of the indoor and outdoor surface temperatures; (*iii*) selecting the time intervals; (*iv*) computing the exponential functions of time constants; (*v*) forming the heat flow matrix; (*vi*) estimating heat flow vectors; (*vii*) estimating total square deviation, and (*viii*) considering that the best time constant set is the one giving the smallest square deviation, which will provide the best estimate of the heat flow vector that allows in turn to estimate the thermal conductance.

The average and the summation methods are similar to each other, and they can be considered the most widely used methods due to their simplicity and rapid achievement of results. However, the accuracy of the results can be strongly influenced by the measuring conditions. On the other hand, as stated by Atsonios *et al.* [60], the dynamic and the sum of the least squares methods are more likely to provide reliable results

regardless of the measuring conditions. Nevertheless, they are less commonly used because of their complexity (e.g., they require the use of complex algorithms and computational tools).

Atsonios *et al.* [60] carried out a comparative assessment of the four standardized methods described in ISO 9869-1 [43] and ASTM C1155-95 [48] for the *in-situ* measurement of the thermal resistance of three different walls (drywall, rubble and brick walls): the average, the summation, the dynamic and two different approaches of the sum of the least squares method (SLS_HF and SLS_TIN methods). Since the main limitations of the standardized methods are the duration of the measuring period and the dependence of the accuracy of the results on the measuring conditions, the authors evaluated the measuring period required for the experiments and the variability of the results of each method. They concluded that the average and the summation methods require a higher temperature difference between indoor and outdoor conditions to achieve reliable *R*-values in a short measuring period. Therefore, these methods should not be used when the temperature difference between the hot and the cold surfaces of the wall is too low. This conclusion is in agreement with the results provided by Desogus, Mura, and Ricciu [46] in a study to evaluate the use of the average method for different measuring conditions (with a temperature difference of 10° C and 7° C). As pointed out by these authors, the reliability of this method depends on the temperatures difference between the two environments separated by the building envelope, and the smaller the temperature difference, the less precise the results obtained.

On the other hand, Atsonios *et al.* [60] concluded that for the dynamic and SLS_TIN methods, the results appear to be independent of the measuring conditions. However, the results are significantly affected by the direction of the heat flow, and present low variability (up to 6 %) only if the heat flow direction is kept stable during the measurements. Regarding the SLS_HF method, it is not affected by the measuring conditions, providing fast and reliable results in all cases [60].

Gaspar, Casals, and Gangolells [61] and Deconinck and Roels [62] carried out comparative studies on the use of the average and dynamic methods based on different measuring conditions. They concluded that in case of low difference of hot-to-cold surface temperatures of the wall, only the dynamic method leads to reliable results. Flanders, Desjarlais, and Kunz [63] compared the summation and the sum of least squares methods to estimate the R-value of construction elements of different buildings under in-situ winter conditions (high internal and external temperature difference). The results suggested that the latter method provides slightly lower *R*-values than the former and that both methods can be used for temperature regimes encountered and for construction with the range of thermal mass and insulation levels evaluated. For these authors, each method has its intrinsic advantages: the summation technique is more straightforward (against its recognised random error), and the sum of least squares provides more information about the *R*-value sensitivity to temperature and better statistical report (against the complexity of the technique).

More methods for the *U*-value measurement based on the HFM approach can be found in the literature, such as the RC networks [64] and the system identification tools [65].

2.1.2.2. Guarded hot plate (GHP)

The GHP method is suitable for determining the thermal conductivity in steady-state conditions, of materials or construction elements. While the HFM method can be applied to large-scale specimens (e.g., full-size walls), the GHP methods are used for middle-scale or small specimens. Table 2.5 shows the main advantages and disadvantages of this method. The GHP apparatus is usually composed of two cold plates, and a heated (measuring) plate bordered by a guard heating system (guard ring), as shown in Figure 2.10 and Figure 2.11. An electric system heats the hot plate up, and a group of coolers or liquid-cooled heat sinks cools the cold plates down [66].

Table 2.5 – GHP method: advantages and drawbacks.

Advantages	Drawbacks
- Use of various elements and materials [67]; - High accuracy [68]; - Allows the control of the heat flux through the material [68]; - The simplicity of design and reduced cost [69]; - Most accurate technique for determining the thermal conductivity [70].	- Long measuring time [68]; - Limited to low conductivity materials [68]; - Test on small-scale elements (such as 300 × 300 mm) [66].

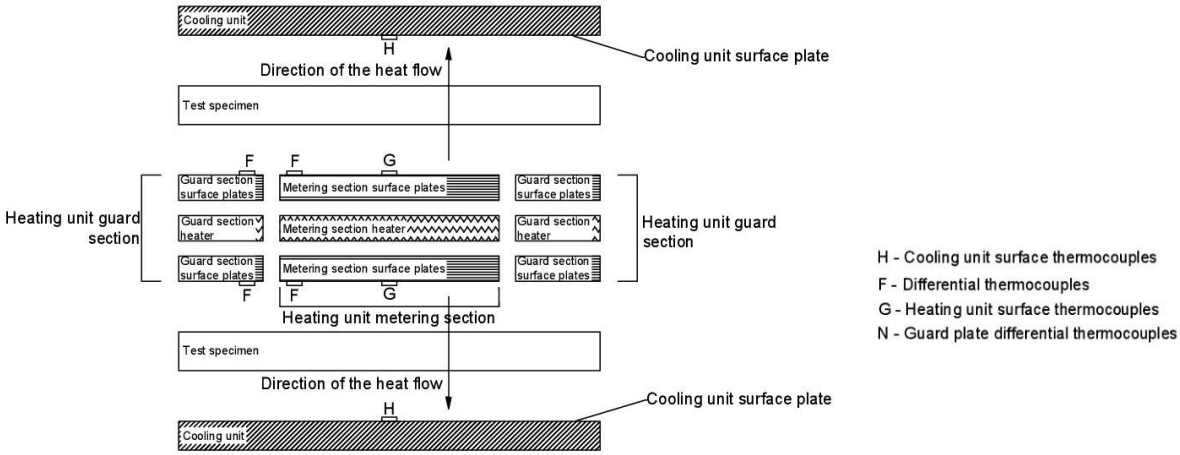

Figure 2.10 – GHP two-specimen apparatus functioning sketch. Adapted from ref. ISO 8302 [71].

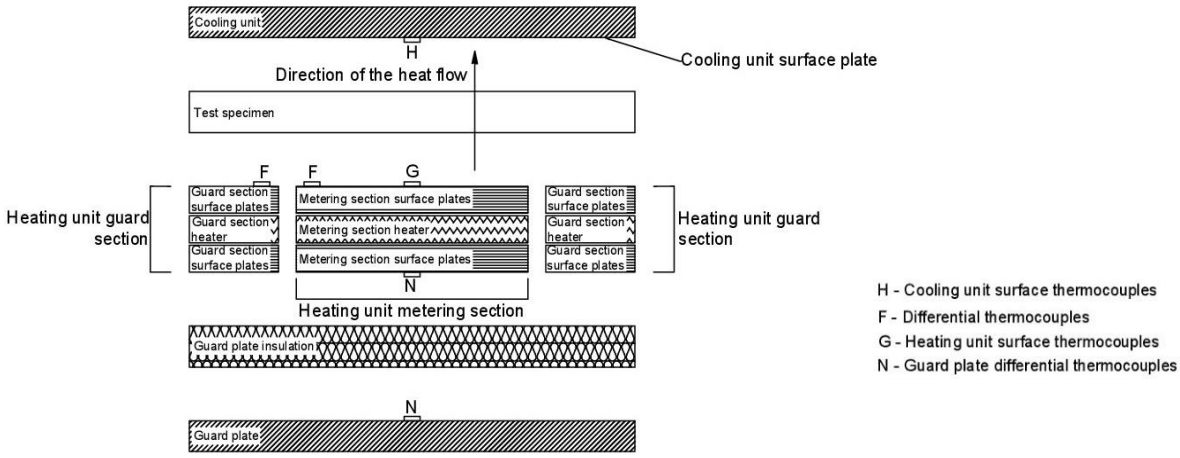

Figure 2.11 – GHP single-specimen apparatus functioning sketch. Adapted from ref. ISO 8302 [71].

The operating principle of this method is very similar to that described for the HFM method. The heat flux is applied from the hot plate to the cold plate(s) in a direction perpendicular to the sample(s) surfaces, and the apparent thermal conductivity of the sample(s) is determined from the heat flux estimated after the heat input, the temperature difference measured between the plates and the thickness of the sample(s). In ideal conditions, the plates are in perfect contact with the sample, and the unidirectional heat flux is constant in time, while the border sector heated in a controlled way (so that its temperature equals that of the heated measuring plate) acts as an insulating guard, thus ensuring an adiabatic border [72]. Indeed, as remarked by

Zarr [73], the GHP method establishes one-dimensional heat flow through the specimens by reducing undesired lateral heat flows to negligible and controlled proportions. Table 2.6 presents the primary standards in the field of the GHP method.

To ensure the reliability of the results and the correct implementation of the method for steady-state conditions, it is necessary to assume some considerations. Salmon [70] says that the plates of the appliance should be identical in geometry and material and as flat as possible, must have high emissivity surfaces and should be made of highly conductive material so that there is an excellent uniformity of temperature. Temperatures in the guard ring and measuring zone should be as similar as possible, and the width of the shield should be at least 0.25 times the width of the measurement area and not less than the thickness of the sample to ensure unidirectional flow. Moreover, there must be an excellent thermal contact between the thermocouples and the plates. These plates should be placed parallel to the surfaces in an isothermal region to limit the flow of heat along with them and minimise the error in the measured temperature.

Table 2.6 – Main standards in the field of the GHP method.

ASTM	ISO
Principles for the use of the method and calculation of thermal properties	
- ASTM C177-13 [67], "Standard test method for steady-state heat flux measurements and thermal transmission properties by means of the guarded-hot-plate apparatus".	- ISO 8302 [71], "Thermal insulation – Determination of steady-state thermal resistance and related properties – Guarded hot plate apparatus".
Steady-state thermal properties in glass	
	- ISO 10291 [74], "Glass in building – Determination of steady-state U values (thermal transmittance) of multiple glazing – Guarded hot plate method".

Finally, ASTM C177-13 [67] indicates that the measurement should run for at least four 30 minutes intervals or four longer system time constants. With this method, it is possible to obtain the *U*-value of the element or material indirectly. To do this, the equations given in ISO 6946 (2017) [26] should be considered. This standard provides a methodology for calculating the thermal resistance and thermal transmittance of building components and some building elements (consisting of thermally homogeneous layers), based on the appropriate design thermal conductivities or design thermal resistances of the materials and products. It also provides an approximate method that can be used for elements containing inhomogeneous layers. However, in cases, where insulation is bridged by metal, are considered outside of the scope of this standard.

Labudová and Vozárová [75] studied the thermophysical properties of a material in the GHP apparatus, in a dynamic state. A mathematical formulation was adapted to calculate the temperature variation in the hot plate sensor, which is determined by measuring the voltage change through the source. It depends on the electric current of heating, the initial resistance of the hot plate and a temperature coefficient of the nickel resistivity (flat heat source). It was concluded that perfect thermal contact between the source of the plate and the sample is hardly guaranteed and that the thermal contact resistance can cause a possible thermal barrier between the sample and the heat sink, which leads to significant errors. Heat losses from the side surfaces of the sample(s) cannot be neglected. During the initial seconds of the test, there is an influence of the thermal inertia of the heat exchanger and the thermal contact resistance between plate and sample(s).

Thomas and Zarr [76] presented a mathematical model to measure the thermal conductivity of insulation

materials in a GHP apparatus. The main steps of the study were: (*i*) to describe and confirm the incremental control algorithm and to determine satisfactory gain configurations using a mathematical model that simulates tests in seconds (not in days); (*ii*) to create and validate a model that responds by heating rates in the various components and interactions with their environments; (*iii*) simulating the performance and dynamic control with the model and determining the configurations of the controllers. The determination of the temperature response is necessary to know the thermal storage capacities and the conductance values for all heat flow paths. With this, and by applying first-order differential equations governed by the energy balance, the dynamic system can be computed.

2.1.2.3. Hot box (HB)

The basis of the HB method is the measurement, at steady-state conditions, of the heat flux through the building components and the corresponding temperature differences across it. This method can be applied for the thermal characterisation of homogeneous or non-homogeneous specimens and building structures or composite assemblies (*e.g.*, walls with windows, doors, etc.).

There are two types of HB apparatus: the Guarded HB (GHB) and the Calibrated HB (CHB). Both methods are suitable for vertical and horizontal specimens (such as walls, ceilings and floors). The apparatus can be sufficiently large to study full-scale components. Figure 2.12a show, respectively. A sketch of the GHB apparatus. It consists of three main objects: the guard box, the metering box, and the cold box. The test specimen is placed between the guard/metering box and the cold box. A sketch of the CHB apparatus is shown in Figure 2.12b. It consists of two main objects: the metering box and the cold box. The test specimen is placed between the metering box and the cold box.

The GHB and the CHB apparatus differ from the mode in which the metering box is surrounded. The first one is the self-masking, which has a controlled "guard" chamber surrounding the metering chamber. The second configuration is the masked hot box. In this configuration, the guarded chamber is the surrounding ambient. The CHB surrounding ambient needs to be a temperature-controlled space, which does not necessarily need to be at the same air temperature as that inside the metering box. In the GHB method, the temperatures in the boxes are controlled in such a way that, as far as possible, the temperatures in the guard and in the metering boxes are the same. This is fundamental to ensure that the total heat supplied to the metering box passes through the test element in a perpendicular direction to its faces.

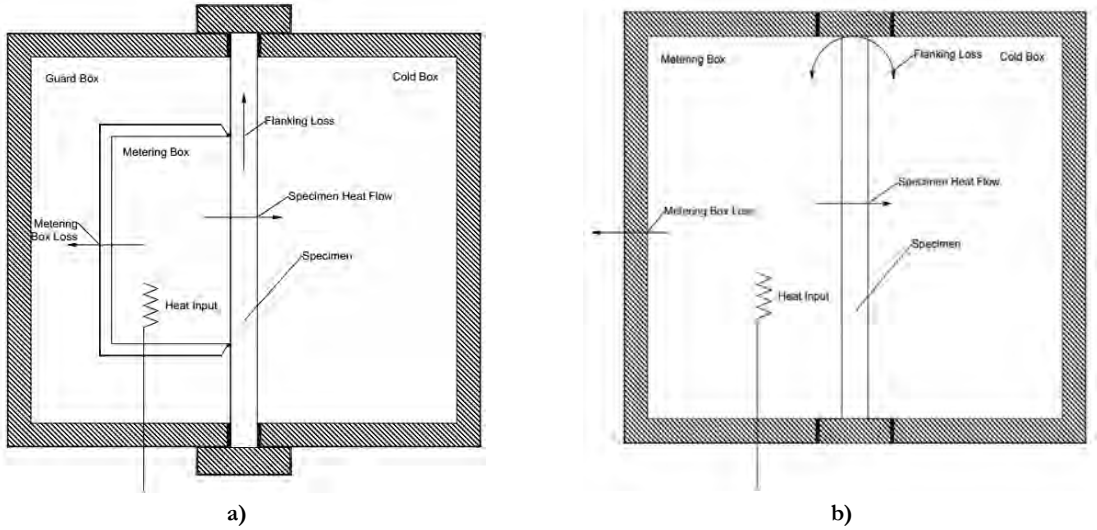

a) **b)**

Figure 2.12 — Sketch of a typical: a) GHB, adapted from ref. [18,77]; b) CHB, adapted from ref. [18,77].

In the CHB method, the heat flow that passes through the sample is determined from the total power supplied to the measuring box, correcting for losses or gains through the metering box walls and the flanking loss to the cold box occurring around the perimeter of the sample. These corrections are performed through calibration measurements, carried out before the test, using specimens of known thermal properties. Table 2.7 shows the main advantages and disadvantages of the HB method. Table 2.8 presents the primary standards that contain all the necessary procedures in the field of the HB method.

Table 2.7 – HB method: advantages and drawbacks.

Advantages	Drawbacks
Hot Box (HB)	
- The HB methodology is an accurate and reliable method for obtaining thermal resistance values on large-scale systems [78,79]; - Can test homogeneous or non-homogeneous specimens [18]; - The inside surface conductance provided by the box are similar to those that occur in practice under natural convection conditions, and realistic outside surface conductance can be provided in the cold room [80]; - The possibility of measurements under both winter and summer outdoor temperatures without removing the sample [81]; - HB large scale better simulates real phenomena, because the small-scale test does not adequately simulate the thermal performance when the specimen is under natural convection [82].	- Very expensive equipment [83]; - Long measuring time [17]; - Regular periodic calibration [84]; - Does not give the distribution of surface temperatures for locations of strong thermal bridges [85]; - Requires an operator very specialized in the equipment and thermal phenomena [18].
Guarded Hot Box (GHB)	
- Does not need to have a calibration factor for the flanking loss of the metering box, due to the existence of the guard box [17]; - More simple to calibrate than the CHB [17].	- The measuring area is limited to the size of the metering box [17]; - More challenging to analyse inhomogeneous specimens due to the size of the metering box [17]; - The metering box interferes with the convection over the test wall [86]; - It is challenging to produce equal coefficients for the metering area and the guard area [86];
Calibrated Hot Box (CHB)	
- CHB apparatus is simpler in design and operation than the GHB [87]; - Allows testing of larger specimens [17].	- Flanking loss between the metering chamber and the climatic chamber through the specimen frame [88]; - The laboratory temperature must be controlled to avoid corrections in the calibration factor [87].

The HB apparatus requires a set of verifications, which must be carried out to establish its adequate operation and accuracy [87]. Tests are performed by simulating end-use application, considering the effect of testing conditions. For this purpose, the interior (hot chamber) and exterior temperatures (cold chamber), and air velocity must be reproduced. The ISO 8990 [17] suggests a difference of at least 20° C between chambers. The time required to reach stability for steady-state measurements depends on the apparatus. The ISO 8990 [17] requires measurements for *R*- and *U*-values from two successive measuring periods of at least 3 hours after the equipment has reached the stability or near-stability. For specimens with a high thermal resistance, the test period must be extended. The HB apparatus can also perform dynamic tests to compute the thermal performance of a wall specimen. Burch *et al.* [89] proposed a dynamic test method for determining transfer function coefficients for a wall specimen using a CHB. The dynamic method predicted with a good agreement the diurnal performance of a masonry wall specimen, as determined empirically. To carry out the dynamic tests, it is necessary to know the response of the measuring equipment to temperature changes. The dynamic test is made by modifying the exterior air temperature, usually changing the cold box temperature in a sinusoidal cycle amplitude in a time interval within the capacity of the dynamic response of the equipment.

Table 2.8 – Main standards in the field of HB method.

ASTM	ISO
Determination of thermal properties	
- ASTM C1363-11 [18], "Standard test method for thermal performance of building materials and envelope assemblies by means of a hot box apparatus".	- ISO 8990 [17], "Thermal insulation – Determination of steady-state thermal transmission properties - Calibrated and guarded hot box".
Determination of thermal transmittance of windows and doors	
- ASTM C1199-14 [90], "Standard test method for measuring the steady-state thermal transmittance of fenestration systems using hot box methods".	- ISO 12567-1 [91], "Thermal performance of windows and doors – Determination of thermal transmittance by the hot-box method - Part 1: Complete windows and doors". - ISO 12567-2 [92], "Thermal performance of windows and doors – Determination of thermal transmittance by the hot-box method - Part 2: Roof windows and other projecting windows".

The HB apparatus is used in several studies to evaluate the *U*-value of different construction elements that are described in subsection 2.2 (hot box historical development).

2.1.2.4. Infrared thermography (IRT)

In the literature, the IRT technique can be divided into qualitative and quantitative IRT. The former is considered many times as a support for HFM measurements. Quantitative IRT can be used for assessing the *U*-value of construction elements.

Over the last years, the use of IRT technique has increased in building energy audit. In a recent paper, Lucchi [93] presents a critical review on the use of this technique, describing: (*i*) the main passive and active

approaches, (*ii*) well-established and emerging techniques, (*iii*) general procedures, (*iv*) types of infrared (IR) cameras, (*v*) technical issues, (*vi*) main limitations of the IRT and potential sources of errors, (*vii*) main advantages of the technology, and (*viii*) future trends in the use of IRT for an energy audit. The author also pointed out the potential of IRT for: (*i*) thermal characterization of buildings, (*ii*) detection of thermal bridging, insulation level, air leakage and moisture, and (*iii*) assessment of thermal comfort. Balaras and Argiriou [94] also pointed out that the use of IRT is a valuable tool for building diagnostics. It can be used for inspecting and performing non-destructive testing of building elements in order to detect where and how energy is leaking from the envelope of the building, to evaluate operation conditions of HVAC systems, and to identify problems with electrical and mechanical installations. Taylor, Counsell, and Gill [95] added that IRT can be used as a qualitative tool during the different stages of the construction process to improve the final thermal performance of the building envelope.

The IRT is a technique widely used in building construction because it allows the measurement of surface characteristics involving all possible heat transfer phenomena [96]. The basic principle of IRT is that all objects emit thermal radiation, which depends on their temperature and emissivity. Emissivity comes from the relation between the energy emitted by the surface of an object and the energy of a black body (the ideal, perfect emitter). IRT allows to capture and analyze the IR radiation from an object, with or without illumination. Still, since the amount of radiation emitted by an object increases with (the fourth power of) the surface temperature, IRT allows perceiving the spatial temperature distribution. Table 2.9 summarizes the main advantages and disadvantages of this technique.

Table 2.9 – IRT method: advantages and drawbacks.

Advantages	Drawbacks
- Non-destructive method [97]; - Large number of applications [96]; - It can be used as support to justify the choice of the measurement zones [98]; - Requires no direct contact with the element and can be used over long distances [93,99]; - Lightweight and easy to carry equipment [99]; - Allows to evaluate extensive areas in a short period, and in real-time [100]; - Allows to determine the overall transmittance of an envelope in a short time especially in comparison with HFM method [101]; - It is not a punctual measurement (it considers all the surfaces of the element) [102]; - It can detect several pathologies of the element [100]; - The IRT camera may calibrates automatically.	- Very high price for the equipment [103]; - Qualified person to analyse the results [103] and to operate the IR camera; - Highly dependent on climatic conditions [99]; - Pollution and smokes with high emissivity may influence the results [94]; - Misreading information is taken by the camera when temperatures have a very close range [100].

The IR cameras capture the radiation emitted by the surface converting it into electrical signals, and then creating an image with the distribution of the surface temperatures of the bodies, by applying the Stefan-Boltzmann law [104]. Although the image shows an approximation of the temperature at which the object is operating, the camera is using various data sources based on the areas surrounding the object to determine that value instead of detecting the actual temperature [100]. Figure 2.13 presents an example of the application of this technique in the inspection of buildings (note that the heat flux through the wall is the result of thermal stimulation by artificial sources − a hot chamber). Figure 2.13a and Figure 2.13b show, respectively, a digital photograph and an IRT image with the temperature distribution of the outer surface

of an LSF wall with an external thermal insulation composite system (ETICS). By analyzing the IRT image, it is possible to identify the location of the plastic wall plugs of the ETICS system. In fact, as suggested by O'Grady, Lechowska, and Harte [105], the IRT can be beneficial to define the correct locations for HFM sensors, since these sensors must be located in a place without any inhomogeneities or defects that may lead to incorrect results of the overall *U*-value of the construction element. Other authors have used IRT as a qualitative tool to select the right place for the location of HFM sensors, such as Asdrubali *et al.* [106], Evangelisti *et al.* [107] and Asdrubali *et al.* [108].

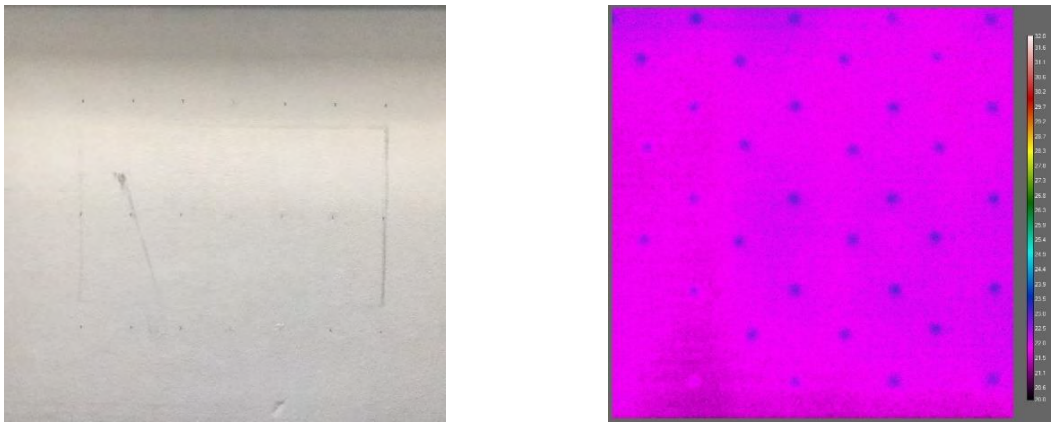

a) **b)**

Figure 2.13 – Outer surface of an LSF wall with ETICS: a) digital photograph; b) IRT image.

Table 2.10 presents the primary standards that contain the necessary procedures that should be considered to render a correct use of the IRT methodology, matching the contents of the ASTM and ISO standards. It should be remarked that a new standard, [109], is under development concerning the *in-situ* measurement of the thermal transmittance of frame structures employing the IRT technique.

Table 2.10 – Main standards in the field of IRT technique.

ASTM	ISO
Principles for the use of the method and calculation of thermal properties	
	- ISO 9869-2 [109] (under development), "Thermal insulation - Building elements - In-situ measurement of thermal resistance and thermal transmittance - Part 2: Infrared method for frame structure dwelling".
Detecting thermal irregularities in building envelopes	
- ASTM C1060-11a [110], "Standard practice for thermographic inspection of insulation installations in envelope cavities of frame buildings".	- ISO 6781 [111], "Thermal insulation - Qualitative detection of thermal irregularities in building envelopes - Infrared method".
Non-destructive testing terminology	
- ASTM E1316-18a [112], "Standard terminology for non-destructive examinations".	- ISO 10878 (2013) [113], "Non-destructive testing - Infrared thermography – Vocabulary".
General principles	
	- ISO 10880 (2017) [114], "Non-destructive testing - Infrared thermographic testing - General principles".

ASTM	ISO
Determination of the minimum resolvable and detectable temperature differences	
- ASTM E1213-14 (2014) [115], "Standard practice for minimum resolvable temperature difference for thermal imaging systems". - ASTM E1311-14 (2014) [116], "Standard practice for minimum detectable temperature difference for thermal imaging systems".	
System and equipment components and their characteristics	
	- ISO 18251-1 [117], "Non-destructive testing - Infrared thermography - Part 1: Characteristics of system and equipment".
Procedures for measuring and compensating for reflected temperature and emissivity	
- ASTM E1862-14 [118], "Standard practice for measuring and compensating for reflected temperature using infrared imaging radiometers". - ASTM E1933-14 [119], "Standard practice for measuring and compensating for emissivity using infrared imaging radiometers".	

Albatici and Tonelli [120] proposed an alternative methodology for the *in-situ* estimation of the *U*-value of opaque construction elements by means of IR thermovision. The authors stated that the proposed methodology can only be used during winter. Because of the difference between the estimated and the theoretical *U*-values, the authors suggested further research on several case studies to establish an average correlation between the results of the measurements and the theoretical values obtained from technical standards. To provide a robust procedure for the use of quantitative thermography and to validate this *in-situ* methodology, Albatici, Tonelli, and Chiogna [121] performed a parametric study on the thermal performance of different light- and heavy-weight walls for over three years. The authors defined some parameters of significance for the accuracy of the results, evaluated the influence of weather conditions on the results, and provided a comparison between values achieved through IR thermovision, international standards approach and HFM method. The methodology provides excellent results for heavyweight construction, while further studies are needed for lightweight and super-insulated walls. In fact, the *U*-values measured for heavyweight walls showed absolute deviations of 8-20 % and 10-18 %, compared to the ones given by the HFM method and the standards approach, respectively.

Nardi, Paoletti, *et al.* [122] tested the previous methodology in a controlled environment provided by the GHB apparatus. The *U*-value of a large heavyweight sample-wall was determined by means of IRT, HFM method, and standards-based calculation. The IRT results show good agreement with the results of the other two approaches. Mainly, the difference between the results obtained from the IRT and the HFM methods was about 3.2-12.9 %.

Tejedor *et al.* [123] proposed a method for determining *in-situ U*-values using quantitative IRT with a deviation of 1-2 % for single-leaf walls and 3-4 % for multi-leaf walls. This method takes 2-3 hours, which is a great advantage in comparison to the typical 72 hours required for the execution of the HFM method in steady-state conditions.

O'Grady, Lechowska, and Harte [124] evaluated the application of the quantitative IRT technique to evaluate the heat lost via multiple thermal bridges and windows. The methodology was validated against experimental measurements carried out in an HB device.

Bianchi *et al.* [125] also proposed an IRT quantitative methodology to assess building envelope thermal

losses due to thermal bridges and Asdrubali *et al.* [104] proposed a methodology to perform a quantitative analysis of some sorts of thermal bridges through simple thermographic surveys and subsequent analytical processing. The IRT was also used by Ascione *et al.* [126] as part of an experimental apparatus to evaluate thermal bridging effects under dynamic conditions. In fact, the evaluation of the multidimensional and dynamic aspects of thermal bridges is very challenging, and it should not be neglected when performing dynamic simulations using building energy simulation programs [127].

In another study, Nardi, Ambrosini, *et al.* [101] performed *in-situ* measurements based on the HFM and IRT methodologies to evaluate the thermal performance of three different walls (historical stone masonry, a heavyweight wall made of hollow brick and concrete blocks, and a lightweight wall made of cement-wood brick insulated by the interior) in real environment conditions. The results showed good agreement between the *U*-value obtained from the HFM and IRT methods for the heavyweight walls (up to 2.56 %). For the lightweight wall, a discrepancy of about 47.62 % was recorded.

Fokaides and Kalogirou [96] used the IRT to estimate the overall thermal transmittance of different building envelope elements (wall, roof, glazing) in five dwellings within two seasons, during August 2009 and February 2010. According to these authors, the *U*-value can be determined by using the following equation:

$$U = \frac{\varepsilon_v \sigma\left(T_{s,out}^4 - T_{out}^4\right) + 3.8054 v\left(T_{s,out} - T_{out}\right)}{T_{int} - T_{out}} \tag{41}$$

where: ε_v is the wall spectral emissivity; σ is the Stefan–Bolzmann constant [W/m²K⁴]; $T_{s,out}$ is the outer surface temperature [K]; T_{out} is the outdoor ambient temperature [K]; v is the wind speed [m/s]; and T_{int} is the indoor ambient temperature [K].

All parameters can be measured using the same IRT camera to minimize systematic measurement errors (except for v, which must be measured by means of an anemometer). The value of emissivity must be measured because it depends not only on the surface materials, but also on actual surface conditions that suffer from pollution, moisture, etc.. The measurement of the ε-value can be achieved by two methods: comparison with a reference material (*e.g.*, special adhesive tapes with known emissivity) or direct measurement of the reflected brightness of the material. The absolute percentage deviations between the theoretical prediction and the measured *U*-values using IRT were found to be at an acceptable level, in the range of 10-20 %.

Aversa *et al.* [128] proposed an innovative experimental procedure to investigate the thermal dynamic behaviour of two prototype walls (an empty wall and a hemp fiber-filled wall) regarding decrement factor and time lag. For the correct implementation of the method, it is necessary to ensure: (*i*) thermal stimulation by means of a heat source, focused in the centre of the wall of the prototype; (*ii*) conditioning of the test room over the duration of the test to ensure a constant indoor temperature; (*iii*) application of a periodic square wave signal for three cycles − for this purpose, the lamps were turned on for 4 hours and turned off for another 4 hours (the total duration of the wall stimulation was 24 hours); (*iv*) simultaneous acquisition on the two wall surfaces, through two infrared cameras; (*v*) analysis of the thermographic data. The results were compared with those obtained with numerical simulation and standard procedures. Comparing the experimental and the numerical simulation results, some minor differences were found, demonstrating the best result for the simulation concerning measurements (lower decrement factor and higher time lag). On the other hand, very different results were obtained using ISO 13786 [21], concerning those obtained with experimental and numerical approaches. Output parameters of the new procedure are the same of standard one, but they were obtained with a different set-up. All the results related to the three approaches showed an improvement in the thermal dynamic behaviour of the fiber-filled wall, concerning the empty one (lower decrement factor and higher time lag).

2.1.2.5. Transient Plane Source (TPS)

The Transient Plane Source (TPS) method is a technique for studying thermal transport properties. It is a technique that gives information on thermal conductivity, thermal diffusivity, as well specific heat per unit volume, of the sample under study. The TPS method approach was invented by Gustafsson in 1981 [129] and was made an international standard based on this method, the ISO 22007-2 [130]. This standard is about the determination of thermal conductivity and thermal diffusivity of plastics. The methodology is suitable for testing homogeneous and isotropic materials [131], as well as anisotropic materials with a uniaxial structure [132–136].

The experimental setup can have an arrangement that matches different specimen sizes. Measurements can also be made in gaseous and in vacuum environments. The tests can be performed at a different range of temperatures and pressures. It is suitable for specimens with thermal conductivity in the range of 0.010 to 500 W/(m.K), values of thermal diffusivity in the range of 5×10^{-8} to 10^{-4} m^2/s, and temperatures in the range of 50 K to 1000 K [130]. New equipments in the market, like the Hot Disk of Thermtest Inc. [137], have a thermal conductivity range of 0.005 to 1800 W/mK and temperature range of -160 to 1000° C.

The TPS method uses a transiently heated plane sensor, which consists of an electrically conducting pattern with the shape of a double spiral, which is etched to a thin metal foil of nickel. The equipment's operating mode consists of placing the sensor between two identical samples and applied a current to the sensor, which generates heat, being monitored the temperature vs time. Figure 4.14a illustrates the schematic diagram of the apparatus, and Figure 4.14b shows a typical ho-disc probe.

The equipment can be used for analysing a large number of different materials such as metals, alloys, minerals, ceramics, glasses, powders, plastics, building materials, biomaterials in vivo or in vitro, and liquids [138]. The sample size is typically between 1 and 10 cm^3.

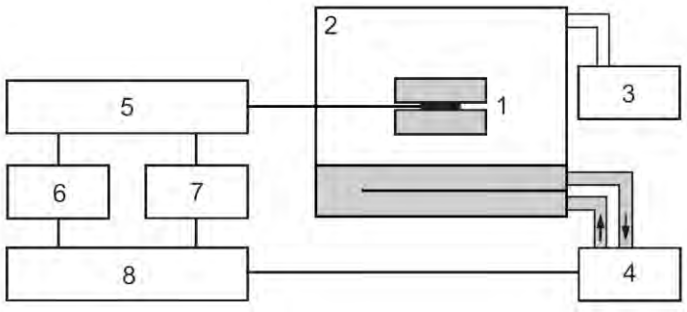

Key

1	specimen with probe	5	bridge circuit
2	chamber	6	voltmeter
3	vacuum pump	7	voltage source
4	thermostat	8	personal computer

a)

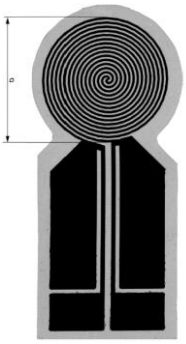

b)

Figure 2.14 –Thermal constants analyser: a) schematic diagram of the apparatus; and b) typical hot-disc probe [130].

Table 2.12 summarises the main advantages and drawbacks of the TPS method. The only standard about this method is the ISO 22007-2 [130].

Table 2.11 – TPS method: advantages and drawbacks.

Advantages	Drawbacks
- Can perform tests at high temperature [130,138]; - Allows to obtain thermal conductivity, thermal diffusivity, and specific heat simultaneously [130,138,139]; -The methodology permits measuring the properties of inhomogeneous and/or anisotropic materials [139]; - Ability to measure small samples [139]; - The measurements are in general fast [139].	- Measurements with standard steady-state technique at around room temperature have accuracy for thermal conductivity at the range of 2% to 5% and diffusivity at 5 % to 10 % [130]. - The results obtained by the transient method are approximately 20% higher than those given by the standard method [139]; - Test only small-scale elements.

Li *et al.* [140] proposed an improved model of the TPS methodology that can improve the measurement precision about 1.8-2.3% as evaluated by the relative standard deviation.

Zhang *et al.* [136] performed a study about the accuracy of anisotropic thermal conductivity determined by the TPS method that discusses the influence of the theoretical assumptions on the accuracy obtained. They concluded that the method could be used for measuring in-plane and through-plane thermal conductivities precisely when neglecting the sensor thickness. In other work, Zheng *et al.* [141] presented a numerical and experimental study that identifies the error sources in hot disk TPS measurements of low-k materials.

2.1.2.6. Methods remarks

Table 2.12 resumes the principal advantages and drawbacks of the experimental methods.

Table 2.12 – Experimental methods: advantages and drawbacks.

Method	Advantages	Drawbacks
Heat flow meter	- Allows *in-situ* measurements; - Allows calculating heat flows independently; - Non-invasive method; - Cheapest methodology.	- The measurement does not consider the entire surface of the element, is local; - *In-situ* measurements take Long measuring time (more than 3 days).
Guarded hot plate	- For laboratory use; - High accuracy, being the most accurate technique for determining the thermal conductivity of small elements.	- Test only small-scale elements.
Hot box	- For laboratory use; - Accurate and reliable method for large-scale systems; - Can test homogeneous or non-homogeneous specimens.	- More expensive equipment than the other methods equipments; - Requires an operator very specialized.
Infrared thermography	- Allows *in-situ* measurements; - Non-invasive method; - Faster methodology.	- Can have misreading information.
Transient Plane Source	- For laboratory use; - Fast results.	- Test only small-scale elements

2.1.3. Numerical Methods

Numerous advanced numerical computational methods are available, such as finite element analysis (FEA) and computational fluid dynamics (CFD). With these advanced numerical methods, it is possible to produce highly detailed models of building components and provide more accurate and reliable values for their thermal properties (e.g. thermal resistance). In contrast to the experimental approach, these sophisticated numerical models, when validated, have the advantage of being less expensive regarding time and money, allowing the rationalisation of resources and optimisation of the constructive elements. Obviously, the accuracy of these advanced numerical algorithms must be verified. To this end, ISO 10211 [27] establishes the specifications to be followed, during the modelling of thermal bridges in buildings and test cases, to evaluate the precision of the numerical algorithms and to validate the calculation method, verifying the calculation of the heat fluxes and surface temperatures.

In the next subsections, the capacity of using the software is demonstrated and its accuracy, for two-dimensional (2D) and three-dimensional (3D) finite element method (FEM) software.

2.1.3.1. Two-dimensional numerical models

Two-dimensional numerical modelling has as objectives: (*i*) to assess the reliability of the results of 2D models, knowing that the steel structure gives rise to 3D effects that are not possible to analyze in 2D rigorously; (*ii*) to evaluate the importance of the absence of the horizontal and diagonal metallic structure, compared to 3D models; and (*iii*) to verify the accuracy of the software by making comparisons with the analytical results.

For the validation of the 2D software, ISO 10211 [27] establishes specifications and test cases, which include the geometric limits and subdivisions of the model, the boundary conditions, temperature and the relationships to be used. For 2D analyses, THERM [142] software is used, which has been validated [143]. However, the validation procedures specified in ISO 10211 [27] can be used to validating the good use of the software. This standard establishes that for the calculation software algorithm to be classified as a high two-dimensional precision method in steady-state, it should give results corresponding to those of the test cases of reference 1 and 2. Figure 2.15 presents the test case number 1 performed in THERM. It aims to calculate the temperatures at 28 equidistant points, considering the calculation algorithm to be validated, in case that the difference between the temperatures calculated by the software and the standard do not exceed 0.1° C. In this test case the software achieved exactly the same values as the standard, which are placed in the matrix of Figure 2.15.

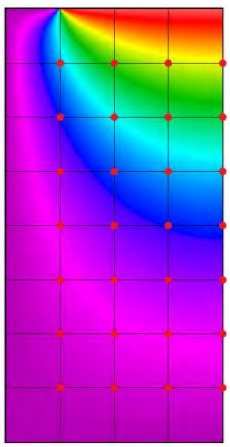

Matrix of temperatures at the marked points [° C]			
9.7	13.4	14.7	15.1
5.3	8.6	10.3	10.8
3.2	5.6	7.0	7.5
2.0	3.6	4.7	5.0
1.3	2.3	3.0	3.2
0.7	1.4	1.8	1.9
0.3	0.6	0.8	0.9

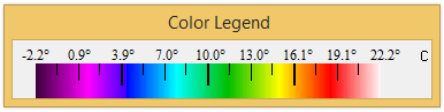

Figure 2.15 – Test case number 1 in THERM.

Figure 2.16 shows the fulfilment of the requirements of test case 2, with the same temperatures being reached, which are shown in Table 2.13. The calculated total heat flow rate differs by 0.0079 W / m from the standard, less than the required 0.1 W/m.

It is concluded that THERM is correctly used, having verified the requirements established in ISO 10211 (2007) for the two-dimensional steady-state high precision method.

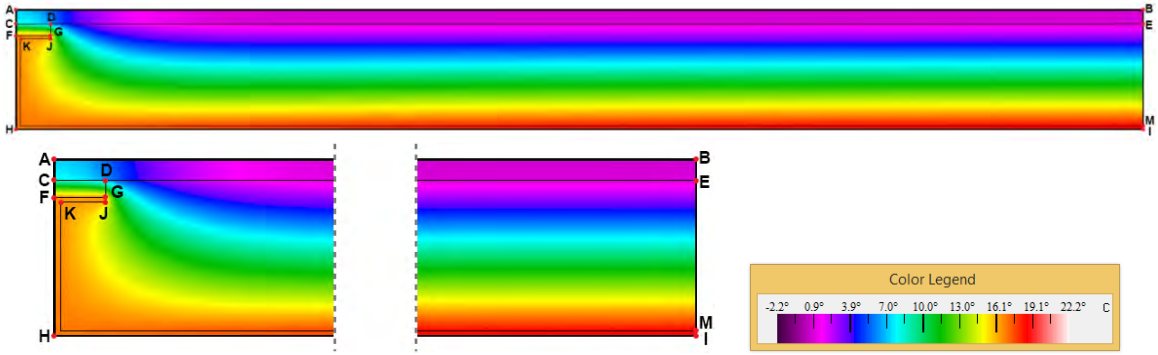

Figure 2.16 – Test case number 2 in THERM.

Table 2.13 – Results of test case number 2 modelled in THERM.

Points	A	B	C	D	E	F	G	H	I
Temperature [° C]	7.1	0.8	7.9	6.3	0.8	16.4	16.3	16.8	18.3
Total heat flow rate: 9.492 W/m									

2.1.3.2. 3D numerical models

ISO 10211 [27] establishes that that for the software calculation algorithm to be classified as a three-dimensional steady-state high precision method, it should give results corresponding to reference test cases 1, 2, 3 and 4.

Figure 2.17 presents the test case number 1 performed in Ansys [144], in which two analyses were performed.

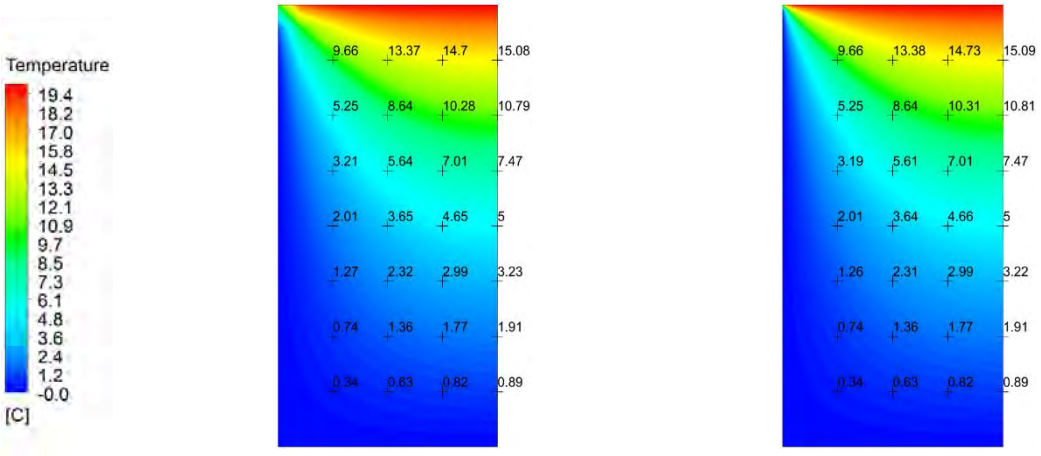

a) 924 nodes. **b) 72114 nodes.**

Figure 2.17 – Test case number 1 in Ansys.

In the model of Figure 2.18a, 924 nodes were used, and in Figure 2.18b, 72 114 nodes were used, obtaining the maximum difference of 0.05° C. Although not evident, this software is more rigorous than the previous one, because in THERM it is only possible to obtain temperatures with a decimal precision, which motivates not having differences on the results with the test case.

It is possible to conclude that the values obtained in Ansys have a difference of less than 0.1° C compared to the standard.

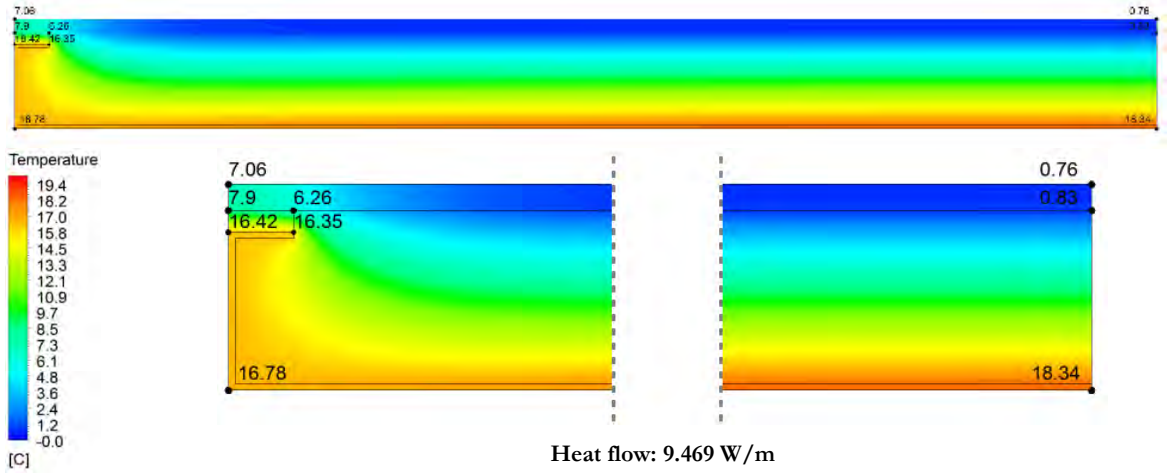

Figure 2.18 – Test case number 2 in Ansys.

Figure 2.19 illustrates test case number 3 and Table 2.14 shows the results, highlighting that the software meets the criteria required in the standard for this test, evidencing high precision.

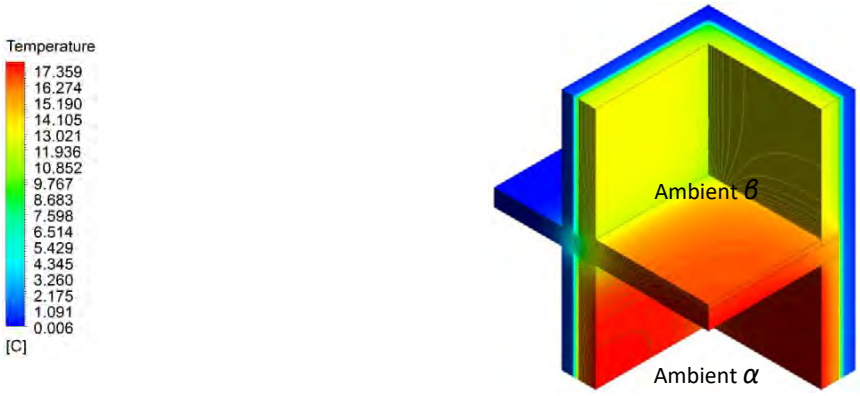

Figure 2.19 – Test case number 3 in Ansys.

Table 2.14 – Comparison between the values defined in ISO 10211 and software Ansys, for test case number 3.

Measured parameter	Expected value	Ansys value	Difference	Difference limit
Minimum ambient temperature *a*	11.32° C	11.276° C	0.044° C	< 0.1° C Ok
Minimum ambient temperature *β*	11.11° C	11.127° C	0.017° C	< 0.1° C Ok
Heat flow *a*	25.15 W	25.139 W	0.04 %	< 1 % Ok
Heat flow *β*	34.83 W	34.532 W	0.02 %	< 1 % Ok

The test case of number 4, illustrated in Figure 2.20, verifies the prescribed in ISO 10211 [27], as shown in Table 2.15 the obtained results, which demonstrates the high precision of the software.

The results allow to conclude that Ansys is correctly used, having verified the requirements established in ISO 10211 [27] for the three-dimensional steady-state high precision method.

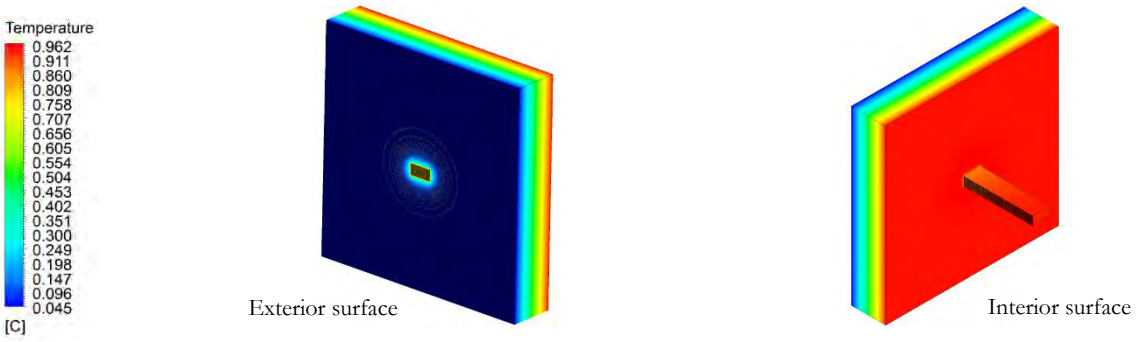

Figure 2.20 – Test case number 4 in Ansys.

Table 2.15 – Comparison between the values defined in ISO 10211 and software Ansys, for test case number 4.

Measured parameter	Expected value	Ansys value	Difference	Difference limit
Maximum temperature on exterior surface	0.805° C	0.809° C	0.003° C	< 0.005 Ok
Heat flow	0.540 W	0.537 W	0.61 %	< 1 % Ok

2.2. HOT BOX HISTORICAL DEVELOPMENT

The scope of this sub-section is to present a literature review about hot box apparatus, limited to building applications, and the more relevant case studies about the present work. The sources of material considered in this review are limited to published literature. This limitation can be severe, having in consideration that in this technical area, the private sector is active, and, for obvious motives, does not share such data.

The HB historical review is organised by decades and presents a resumed description of each equipment and its testing objectives.

The 1920s

One of the first works performed with the hot box was done by Rowley [28], which had the object of development and improvement of the methods for testing insulating and building materials. Usually, there were two hot box methods: a cubic box without one side (Figure 2.21a), where is placed the specimen; and the second was a cubical box made of the material intended to be studied (Figure 2.21b).

The methodology with the test box open in one side, Figure 2.21a, was to have the material placed on the open face and the temperature T_1 maintained higher than T_0. The drawbacks of this method are: (*i*) it is challenging to make a precise calibration of the box; (*ii*) the lines of heat flow are not all perpendicular to the surface; (*iii*) the exact area of the surface under test cannot be determined for thick walls as this surface

should be higher than the inner surface and not so large as the outer surface; and (*iv*) the average might lead to unreasonable errors.

The other methodology, Figure 2.21b, is a box constructed entirely with the material that is intended to test. This method does not require calibration, as all the losses occur through the material under test. The drawbacks are: (*i*) the same uncertainty as to what would constitute the exact area of the test specimen; (*ii*) also the condition of heat passing through the material in lines which are not all normal to the surface; and (*iii*) the difficulties increase as the thickness of the material are higher in proportion to the size of the box.

a) b)

Figure 2.21 – Hot Box method: a) testing over one open side; b) testing a complete cubical of the material [28].

To overcome the difficulties stated in the previous methodologies, Rowley [28] suggested a double or guard ring box. Figure 2.22a shows the cross-section view, where both boxes are well insulated, and each box has the same temperature. The test specimen is placed across the open faces of the two boxes, and the test area is the portion of the material over the inner box. In this method, the heat flow is normal to the surface, and by maintaining the same temperature on both sides of the inner box, the only heat loss from the internal box is the one passing through the test area. Figure 2.22b shows a schematic drawing of the boxes and instrumentation. Rowley [28] used the HB with a double box to study the insulating properties of building materials.

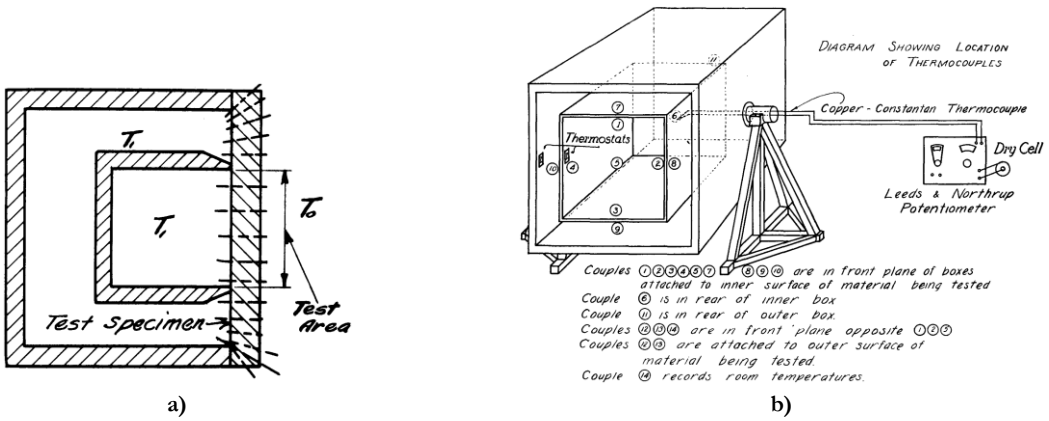

a) b)

Figure 2.22 – Improved hot box method using double box: a) cross-section view; b) instrumentation location [28].

The 1930s

Van Dusen and Finck [145] developed a HB apparatus based on the hot plate method, which consists of two insulated chambers, each open on one side, with the wall panel placed between them. Figure 2.23a shows a sketch of the cross-section of the apparatus. The chambers have steel rods, clamped against the test panel with considerable pressure, and sealed with felt gaskets. The right box is kept at the lower temperature, the left at high temperature, and fans make the air circulation and temperature distribution.

With this method for measuring the thermal resistance of building wall sections under laboratory conditions 17 walls with 0.8 by 0.8 [m²] were tested. Figure 2.23a shows an image of the apparatus partly disassembled to be possible to see the systems installed in the interior.

a) **b)**

Figure 2.23 – Apparatus: a) cross-section sketch view; b) partly disassembled [145].

Rowley and Algren [146] improved the equipment previously presented by Rowley [28], by adding a cold box to the apparatus. The improvement consisted of adding on the other side of the testing wall a cold storage room and maintaining the double box on the warm side, illustrated in Figure 2.24. Since the air temperatures on both sides of the boxes, on the warm side, are equal, the heat supplied to the inner box can only pass through the test specimen to the cold box. The apparatus works with automatic control, maintaining temperatures at the range up to 65.5° C on the hot side and -37.2° C on the cold side. All the heat supplied to the test boxes is done by electric heating elements and in the inner box is accurately metered. The area of the tested wall that is possible to analyse in the apparatus is 1.52 by 1.52 m². The objectives of this work were: (*i*) to develop and build an apparatus for determining the thermal conductivity of insulating materials and the overall heat transmission coefficients of built-up wall constructions; (*ii*) to determine the thermal coefficients for air space inside and at the surface of the materials; (*iii*) to compare the experimental results with analytical to determine the accuracy of the apparatus; and (*iv*) to determine the feasibility of using other materials and other types of construction.

Rowley and Algren [147] completed the work performed in 1932, presenting new results and completing the previous work leading to the analysis of 92 different types of wall sections by the hot box method to determine the overall coefficient of thermal conductivity. The walls types include frame, brick, tile, stone, concrete, and cinder blocks with several unique types of construction.

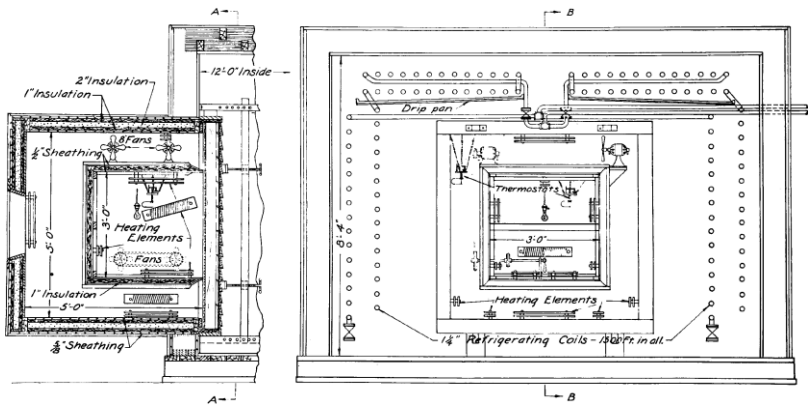

a) **b)**

Figure 2.24 – Hot box: a) sectional view of the double box and wall in place; b) sectional view of the cold room, by looking into the open end of test room [146].

The 1940s

Whittemore *et al.* [148] made a study on the structural and heat-transfer properties of constructions intended for low-cost houses and apartments, with a focus on prefabricated sheet-steel constructions for walls, partitions, and roofs. For determining the heat transfer coefficients, they used a shielded hot box apparatus, but no details of the apparatus are given in the report.

Later, Whittemore *et al.* [149] made a study on the structural and heat-transfer properties of constructions intended for low-cost houses and apartments, with focus on multiple box-girder plywood panels for walls, floors, and roofs. They used a shielded hot box apparatus, shown in Figure 2.25, with a temperature range of - 17.7° C, on the cold box, to 21.1° C, on the metering and guard boxes. The heat transfer measurement area of the equipment is 0.838 m wide by 1.549 m high, centrally located on the face of the specimen.

The 1950s

Robinson and Powlitch [150] constructed during 1948 a GHB apparatus, suitable for determining the heat transfer coefficients of air spaces of buildings. After being used for other purposes, the apparatus became available in 1950 for conducting the tests required for the above purpose. The heat transfer tests were made in panels with 1.54 by 2.44 m². Figure 2.26 shows a photograph of the apparatus, where the boxes are held using long bolts engaging lugs around the periphery of the join. The contact between the metering box and the specimen is made with a rubber gasket, which maintains a substantially airtight, defining is zone, the periphery of the metering area, a rectangle with 1.52 m high by 0.81 m wide.

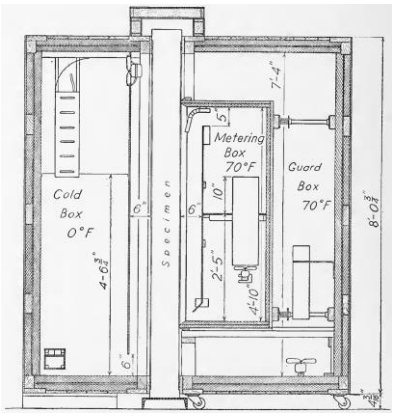

Figure 2.25 – Longitudinal section of a shielded hot box apparatus [149].

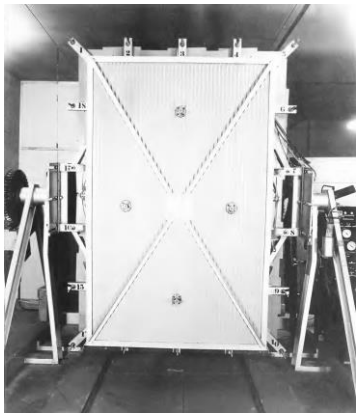

Figure 2.26 – Guarded hoy box apparatus [150].

Solvason [86] constructed an apparatus to measure at steady-state the heat flow through 2.44 m² wall sections. Figure 2.27a shows a sketch and Figure 2.27b a photo of the apparatus, which consists of two boxes open on one side, with 2.44 m high by 1.22 m wide between which are the test walls placed, and 1.22 m depth. The temperature range variation is from -37.2° C to 10° C on the cold side, and 18.3° C to 23.9° C on the warm side. The constructed equipment is one of the first types of calibrated hot box apparatus. To prevent heat transfer in the walls of the guard box the outer panel, the surrounding room is maintained at the same temperature as the inner panel of the warm side.

The 1960s

Brown *et al.* [80] created a unique guarded hot box, Figure 2.28, to measure the heat transmission coefficients of building sections with 1.22 m wide and 2.44 m high, a property of the Division of Building Research, National Research Council, Ottawa, Ontario, Canada. The intended testing wall is placed in the room, creating two compartments, the smaller compartment, a warm room, and the other a cold room.

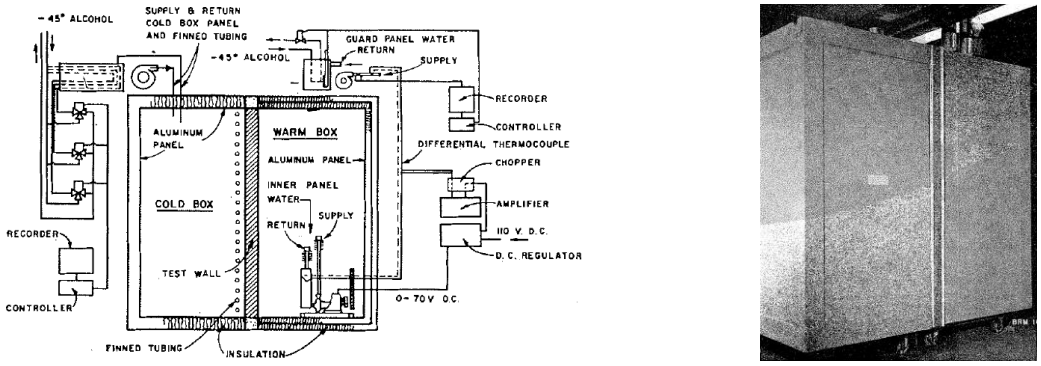

Figure 2.27 – Calibrated hot box: a) Cross-section sketch view; b) Photography of the equipment [86].

The temperature range variation is from -51.1° C to 4.4° C on the cold side, and 18.3° C to 23.9° C on the warm side. The guarded hot box is positioned against the warm side of the specimen, illustrated in Figure 2.28a and Figure 2.28b. The apparatus was used for the measurement of heat transmission coefficients on numerous metal skinned curtain walls [80].

Christensen, Brown and Wilson [151] made measurements of inside surface temperatures on a basic double window arrangement, with two sheets of glass surrounded by insulated construction, using the same equipment, as shown in Figure 2.28b.

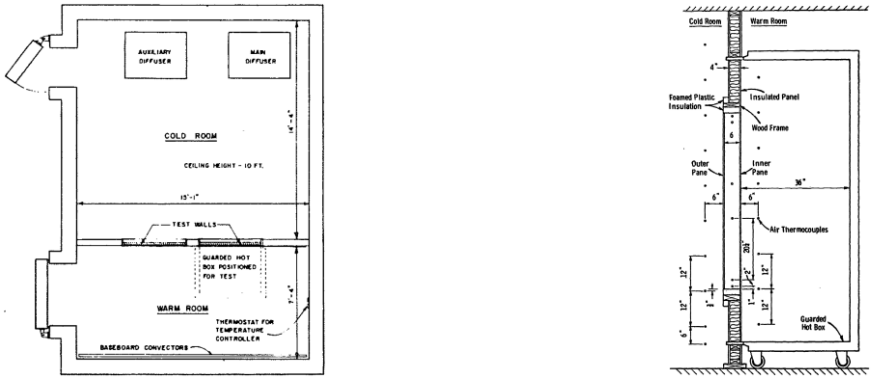

Figure 2.28 – Guard hot box: a) plant view of the equipment [80]**; b) schematic cross section** [151]**.**

Lorentzen *et al.* [152] constructed a special guarded hot box apparatus, Figure 2.29, for measuring the heat leakage of a wall with irregular convection pattern. The test specimen area of the equipment is 1.7 by 2.2 m^2. The equipment can reach temperature differences up to about 70° C.

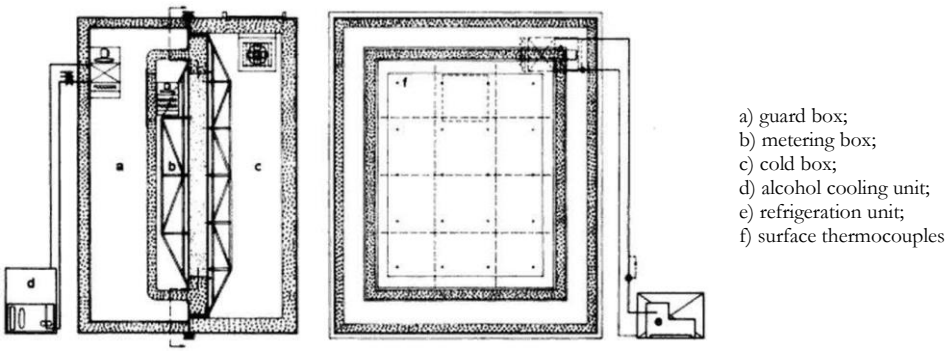

Figure 2.29 – Guarded hot box apparatus design [152]**.**

The 1970s

Bondi *et al.* [153] constructed an apparatus to measure the thermal transmittance of walls from 3 by 1 m² up to 3 by 3 m². The equipment consists of a steel frame entirely covered by an insulating material, with two rails that hold the two specimens that provide a hot room in the central zone of the apparatus and have two cold rooms on each side of the hot room, as illustrated in Figure 2.30. The apparatus is different from standard hot box apparatus, as it does not have unidirectional heat flow from the hot chamber, protected by a peripherical guard box, to a single cold side but actuates bi-directionally, with symmetrical distribution. The thermal flow is transmitted from a central hot box through two identical specimens to two external rooms symmetrical to the warm chamber.

Di Filippo *et al.* [154] used an apparatus, an ASTM type with a calorimetric chamber and a guard chamber, which has been modified to determine the parameters of total coefficients of heat transfer and their response times under standard conditions of the walls surface resistances. Figure 2.31 shows a scheme of the apparatus.

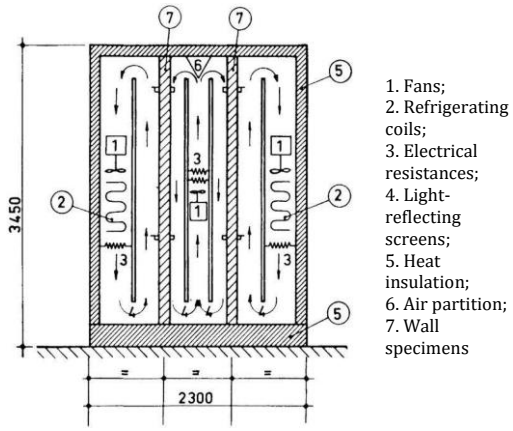

Figure 2.30 – Scheme of the apparatus: [153].

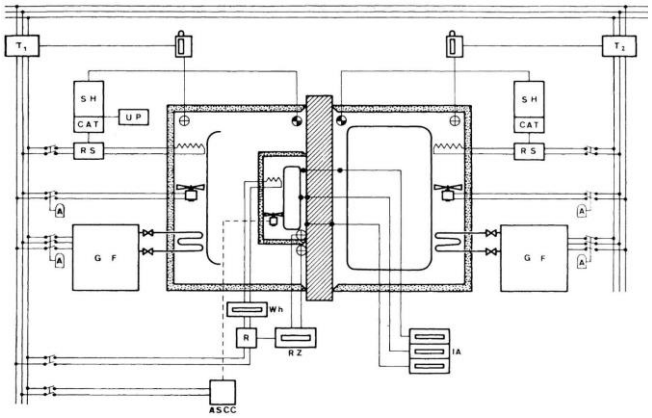

Figure 2.31 – Scheme of the apparatus [154].

Mumaw [155] constructed a big calibrated hot box apparatus, using highly thermal resistant walls, allowing to carry out fast and accurate thermal conductance measurements for large vertical sections. The apparatus is at Product Testing Laboratories, of Owens-Corning Fiberglas Corporation, in Granville, Ohio. The test wall specimens nominal section has 2.7 by 4.2 m² and are placed between the two chambers, which are maintained at different temperatures. The hot side chamber temperature range is 0° to 60° C and the cold side chamber - 40° to +20° C. Figure 2.32 shows details of the equipment.

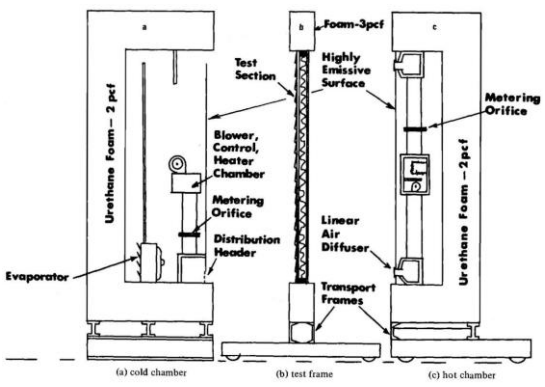

a)

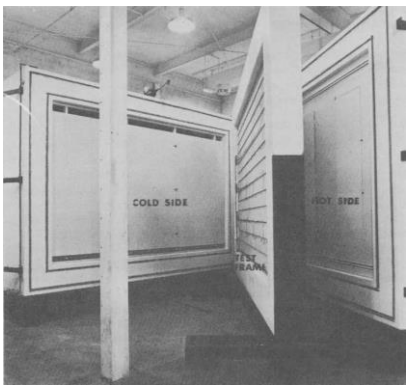

b)

Figure 2.32 – Calibrated hot box apparatus: a) schematic vertical section; b) equipment before closing [155].

Brendeng *et al.* [156] presented a guarded hot box, shown in Figure 2.33, that is an improved version of the apparatus constructed by Lorentzen *et al.* [152], which permit testing insulation systems at cold temperatures of -162° C. The specimen measuring area is 1.7 by 2.2 m², with a thickness of 0.2 m. The goal of the study is testing wall sections insulated with fibrous materials and expanded ebonite.

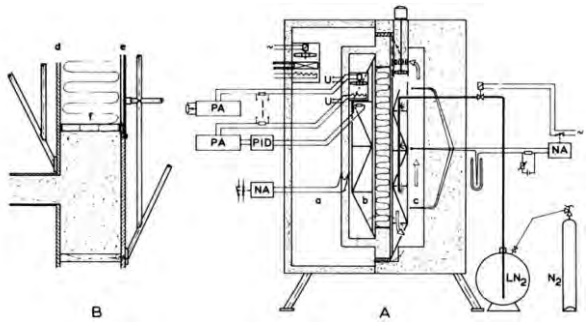

Figure 2.33 – Scheme of the guard hot box apparatus: a) guard box; b) metering box; and c) cold box [156].

Hunley [157] presented the construction and design description of the large-scale climate simulator GHB type has been completed at Oak Ridge National Laboratory. This new facility allows horizontal testing elements, e.g. roofs and slabs, under static and dynamic conditions. The apparatus can test specimens weighing up to 10 tons and maximum dimensions of 3.8 by 3.8 m under a range of temperatures of -40 to 65° C. Additionally they can simulate humidity, sunlight, and wind conditions.

a) **b)**

Figure 2.34 – Large-scale climate simulator GHB: a) exterior view [158]**; b) interior view** [158].

Sabine *et al.* [159] made laboratory tests of thermal transmittance in the apparatus created by Mumaw [155], previously presented. The objective was to study full-scale walls, 2.7 by 1.3 m², of typical residential exterior wall constructions, unbroken and penetrated by a door or window. A total of 48 thermal tests were performed, and the results compared with literature. Figure 2.35 shows some tested walls.

a) **b)** **c)**

Figure 2.35 – Walls specimens tested on the calibrated hot box apparatus: a) plastic-coated wood wall with window; b) plastic-coated wood wall with sliding glass door; c) brick veneer wall with the opening cut for window [159].

Miller *et al.* [78] made a series of studies with a hot box test facility, that could operate as guarded, with a metering area of 1.8 by 1.8 m², or calibrated apparatus, with test specimen area dimensions of 2.4 by 2.4 m². Independent tests made in other laboratories allowed to correlate results with guarded hot plate tests, as well as with itself in guarded and calibrated modes. The objective is to determine more accurately the heat loss factors for the calibrated mode since this approach can have higher measurement test areas of samples. The apparatus manufacturer is Wiss, Janney, Elstner and Associates for Jim Walter Research Corp. The apparatus comprises of a separate hot box, metered box, both with a temperature range from 2 to 71° C, specimen frames, and cold box, with a temperature range from 27 to -46° C. The hot and cold boxes insulation is polyurethane low-density foam, with a thickness of 30.5 cm. The equipment can be also assembled for testing vertical elements, e.g. walls are shown in Figure 2.36a, and horizontal elements, e.g. floors are shown in Figure 2.36b, providing upward, downward, or horizontal heat flow. The boxes have a ventilation system that can provide variable air velocities parallel to the specimens, with an air velocity range of 0.8 to 24 km/h.

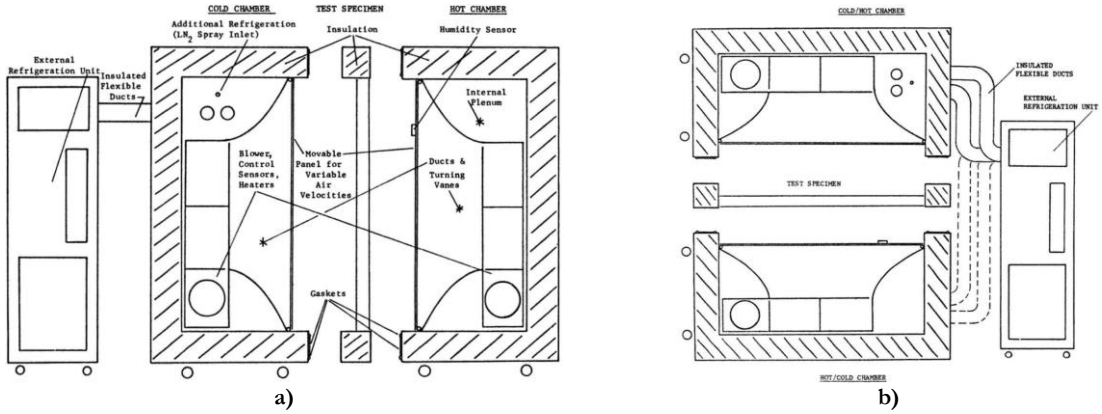

Figure 2.36 – CHB apparatus schematic: a) in horizontal heat flow mode; b) in vertical heat flow mode [78].

Lauvray [160] presents a special calibrated hot box for measuring heat transfer, at steady state, through the walls of air duct systems under operating conditions and configurations. The box is 3.0 m long by 0.91 m² interior, and the walls are constructed with 12.7 mm plywood, insulated with 152 mm of urethane foam. Figure 2.37 shows a drawing of the apparatus.

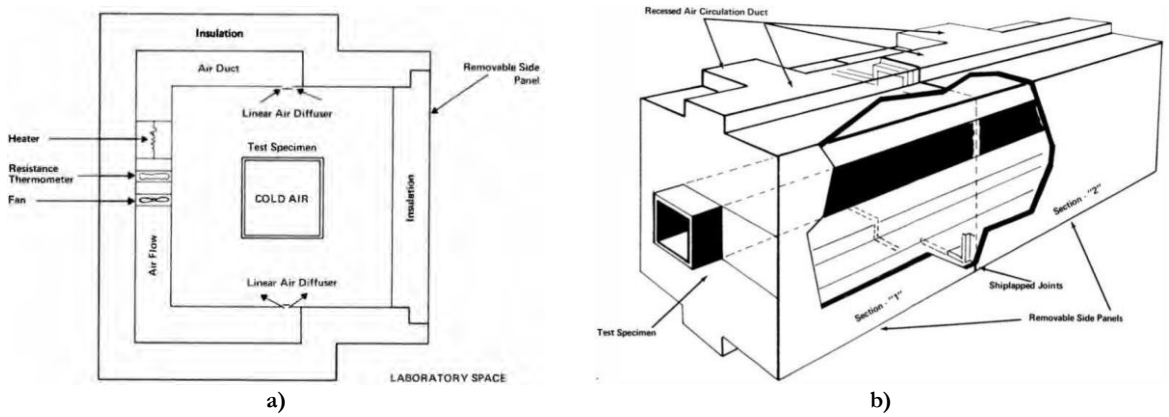

Figure 2.37 – Calibrated hot box apparatus schematic: a) vertical cross-section; b) with the installed specimen [160].

Wahle *et al.* [161] presented a modified high temperature guarded hot box constructed for testing reflective insulation panels. The modified guarded hot-box facility, shown in Figure 2.38, consists primarily of only have the hot side of the typical facility. The measurement test area is 914 mm2 and can test panels up to

203 mm thick. The equipment temperature hot surface can reach up to 538° C, and the other temperature is the one of the surrounding room. It can be rotated to test horizontal or vertical elements and was verified for testing both homogeneous and nonhomogeneous insulations.

Klems [162] built, at the Building Technology Laboratory, a small calibrated hot box, with an opening of 0.9 by 1.2 m², for studying methods of improving windows thermal performance. Figure 2.39 shows the vertical section of the apparatus, which is composed of two boxes of 15 cm rigid polyurethane foam insulation with a plywood outer skin. The interior of the equipment is painted black for radiation purposes and is fully covered with an aluminium sheet of 2 mm thick to ensure uniform surface temperatures. The hot side works at the temperature of the surrounding room, at 22° C, and the cold side can reach -18.5° C.

Figure 2.38 – High-temperature guarded hot box: a) vertical cross-section; b) facility photography [161].

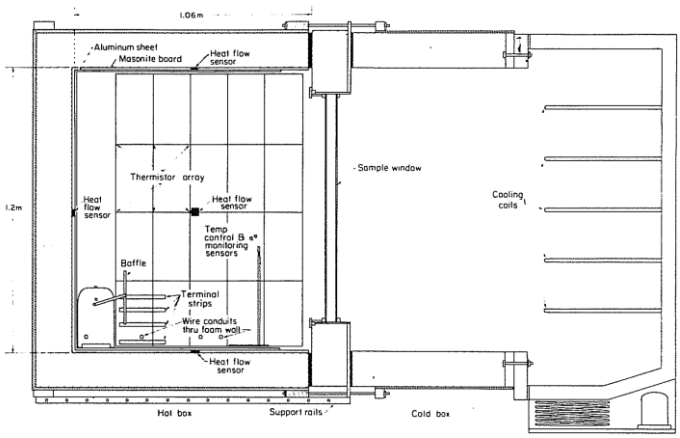

Figure 2.39 – Calibrated hot box vertical section [162].

Rucker and Mumaw [163] describe a large-scale horizontal calibrated hot box, constructed in the Owens-Corning Fiberglas Thermal Research Facility, Granville, Ohio. The goal of the work is to achieve an accurate calibration of the metering chamber and the overall systems of the hot box apparatus. The research facility incorporates a below-ground metering chamber with a 4.3 by 6 m opening into the floor that is inside of a room with 10.7 by 21.3 by 7.6 m, assigned as the primary environmental chamber. The test samples are placed over the metering chamber, shown in Figure 2.40. The temperature range in the primary chamber is from -46 to 66° C, within the control of 0.3° C and the temperature range in the metering chamber is from -9.5 to 66° C, within the control of 0.1° C.

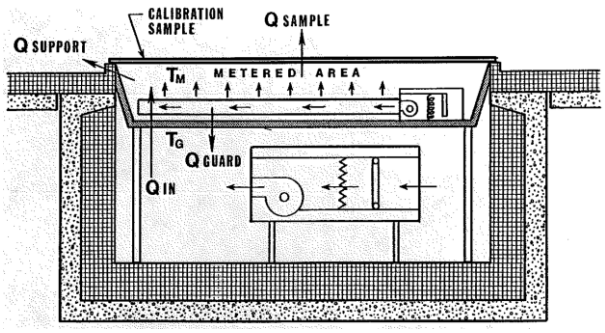

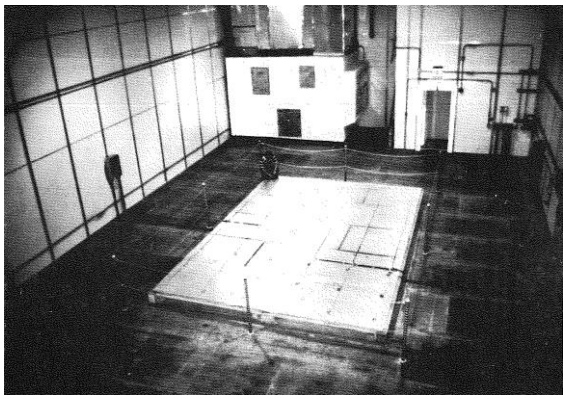

a) **b)**

Figure 2.40 – Large-scale horizontal calibrated hot box: a) metering chamber schematic; b) room facility shown the calibration sample installed over the metering chamber [163].

Rucker *et al.* [163] presented the design of a large calibrated hot box for measuring the heat, air and moisture transfer of composite building walls. The apparatus was constructed at the National Bureau of Standards to support the development of standard procedures for measuring the heat, air and moisture transfer of room-size, with 3.0 by 4.5 m², exterior wall specimens allowing to simulate the climatic conditions. The apparatus works in the steady and dynamic state. Figure 2.41 shows the schematic of the apparatus. The temperature range in the metering chamber is from 10 to 65° C, and the environmental chamber is from -40 to 65° C.

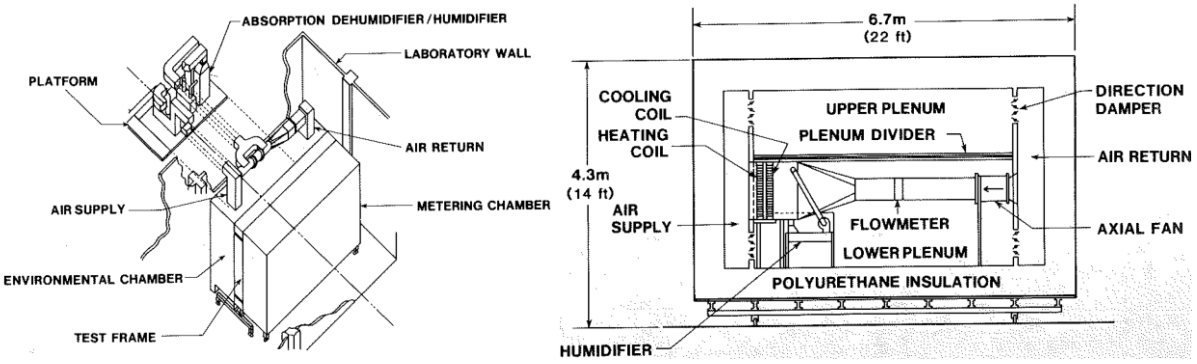

a) **b)**

Figure 2.41 – Calibrated hot box apparatus schematic: a) axonometric view; b) metering chamber section [163].

Fiorato [79] presented a calibrated hot box test facility to evaluate the steady-state and dynamic thermal performance of wall assemblies constructed in the Construction Technology Laboratories, A Division of the Portland Cement Association, Illinois. The overall dimensions of the test wall are 2.62 by 2.62 m². The temperature range in the metering chamber is from 18 to 27° C, and the cold chamber is from -29 to 49° C. The maximum air velocity parallel to the specimen in both chambers is 0.3 m/s.

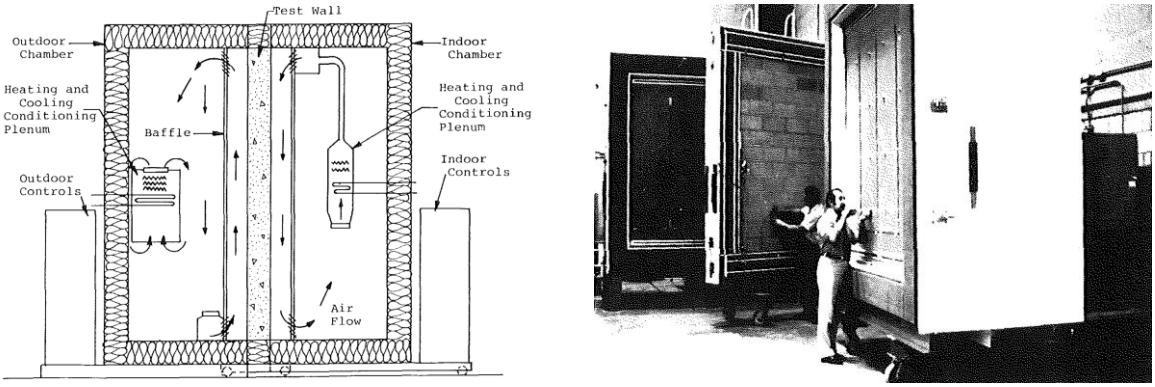

a) **b)**

Figure 2.42 – Calibrated hot box apparatus: a) vertical cross-section; b) photography with the apparatus open [79].

Perrine *et al.* [164] presented a calibrated/guarded hot box apparatus fabricated by Wiss, Janney, Elstner and Associates for the Construction Products Division of W. R. Grace & Company. The equipment is similar to the one presented by Miller *et al.* [78]. The apparatus allows testing horizontal and vertical specimens, under steady or dynamic state conditions. The facility has two environmental boxes when testing 2.44 by 2.44 m² the environmental and calibrated boxes have the same size, as shown in Figure 2.43a. When testing 1.83 by 1.83 m² both test frame and the environmental box have 1.83 by 1.83 m² apertures, and calibrated box has 2.44 by 2.44 m², as shown in Figure 2.43b. The temperature range in the calibrated chamber is from 10 to 49° C, and the environmental chamber is from -34.4 to 71.1° C.

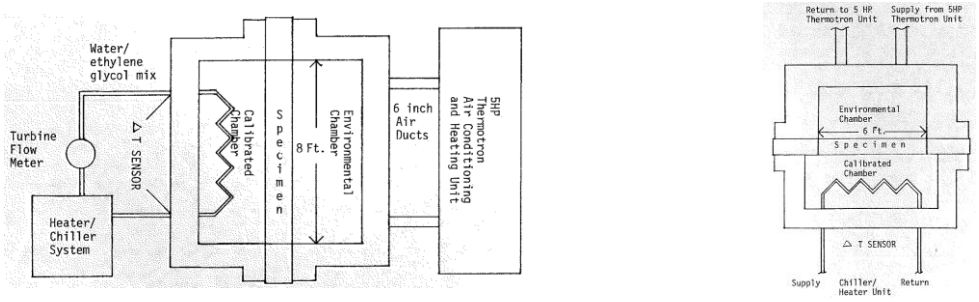

a) **b)**

Figure 2.43 – Hot box apparatus: a) schematic of a measuring area of 2.44 by 2.44 m²; b) schematic of a measuring area of 1.83 by 1.83 m² [164].

The 1980s

Palfey [165] studied the thermal performance of low emittance building sheathing. For that purpose, he used a calibrated hot box that is in a controlled environment room, located at Dow Chemical USA, Granville, Ohio. The test specimens measuring 3.0 by 4.0 m², are placed in portable frames that are positioned and sealed between the hot and cold chambers. The facility can rotate 90° for use either for test walls or floors/ceilings. The operating temperature range for the metering chamber is 0 to 60° C and 25 to -40° C for the climatic chamber. Figure 2.44 shows the schematics of the equipment.

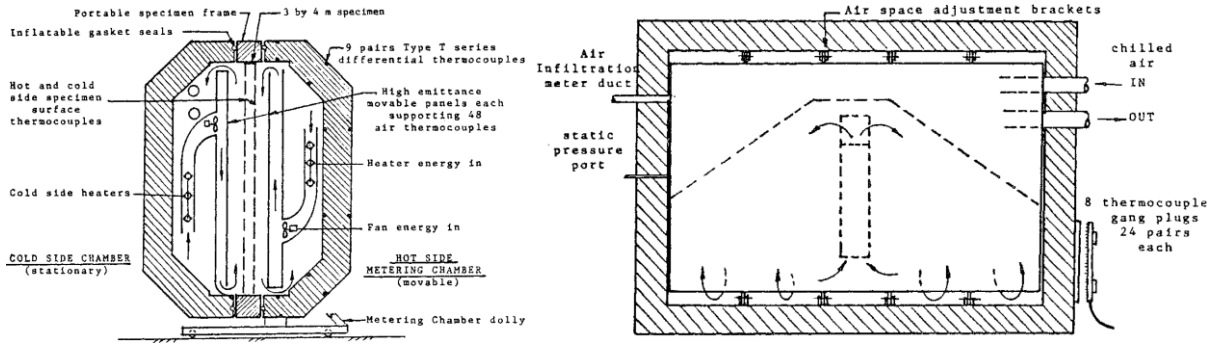

a) **b)**

Figure 2.44 – Calibrated hot box apparatus: a) side cross-section; b) cold side frontal cross section [165].

Mumaw [166] describes the design considerations and construction details required to build the facility using state-of-the-art technology for measurements and control, of the large-scale horizontal calibrated hot box of Rucker and Mumaw [163], previous presented. Figure 2.45 gives a new illustration of the facility.

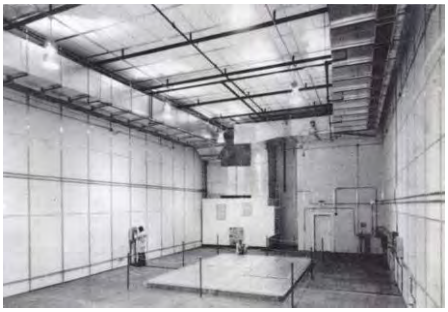

Figure 2.45 – Calibrated hot box apparatus interior of Thermal Research Facility [166].

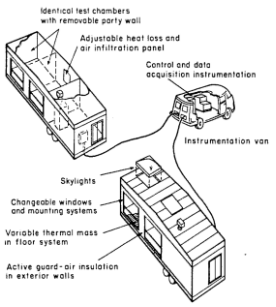

Figure 2.46 – MoWitt GHB apparatus [167].

Klems et al. [167] developed a mobile field test facility, named MoWitt, to directly measure the thermal transmittance, solar heat gain and overall thermal performance of fenestration systems under solar irradiation. The apparatus belongs to the Lawrence Berkeley National Laboratory, USA, and each module contains two-rooms, with 2.4 by 3.l by 2.4 m3, and is a guarded hot box. The MoWitt facility provides good agreement results, comparing with commercial test laboratory, for the thermal performance of the windows [168]. The drawback of the apparatus was an operating cost of 1 300 € a week, which limited its use [169]. Figure 2.46 illustrates the apparatus.

Goss and Olpak [170] described the design of a large rotatable calibrated hot box type test facility located at the University of Massachusetts at Amherst. The facility test specimen dimensions have 2.4 by 2.4 m^2 and can be rotated 90°, to a vertical position or through a horizontal position. The operating temperature range for the hot side is 20 to 65° C, and an air velocity of 0.0 to 5.4 m/s. The operating temperature range for the cold side is -32 to 10° C and an air velocity of 0.0 to 5.4 m/s. The walls of each chamber are made of eleven 2.5 cm polyisocyanurate sheets glued together and highly thermal resistant. These walls, with 27.5 cm thickness, are attached to internal wooden frame support made from standard, which provides the necessary strength and rigidity to the chambers. Figure 2.47 shows the schematics of the equipment.

Orlandi *et al.* [171] made the development of a testing procedure for a guarded hot box facility of the W. R. Grace & Company, Cambridge, Massachusetts, previously presented by Perrine *et al.* [164]. This apparatus, as shown before, can have both configurations GHB and CHB. In this study configuration, the GHB has the schematic configuration presented in Figure 2.48. The objective of the developed method is to determine the thermopile electromotive force set point that corresponds to negligible average heat flow across the metering walls. The procedure quantifies the net heat flow rate across the metering box walls as a function of the thermopile measurements and when the net heat flow rate across the metering box walls is zero the thermopile electromotive force set point is then obtained.

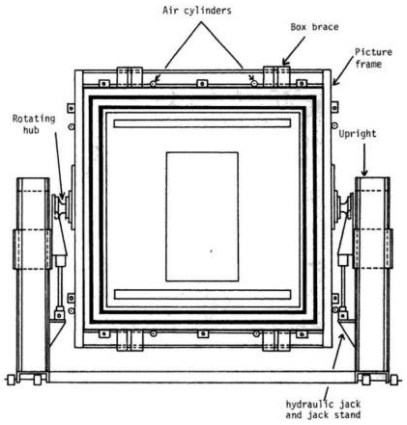

Figure 2.47 – Calibrated hot box apparatus schematic of rotatable cold side chamber [170].

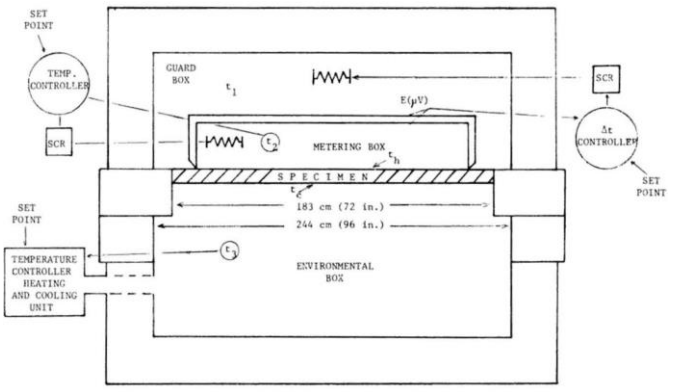

Figure 2.48 – Schematic of the W. R. Grace company GHB [171].

Lavine *et al.* [88] studied the flanking loss calibration for a calibrated hot box. For this purpose, they used the calibrated hot box of Mumaw [155], from Owens-Corning Fiberglas Corporation. The calibrated hot boxes energy input to the metering chamber needs corrections for extraneous losses. Initially, it was assumed that the losses occurred only through the chamber walls. However, events demonstrated that significant heat flow also occurs in the zone of the specimen frame, as illustrated in Figure 2.49. The calibration factor must account for this additional flanking loss that must be added to the walls loss of the chamber to achieve highly accurate results. The work presented by Lavine *et al.* [88] gives the procedures for obtaining the flanking loss calibration for the existing CHB.

Bowen and National Research Council Canada [172] report discusses the problems with testing windows; the current standard hot box techniques for determining the thermal conductance of walls are not adequate for windows. The work presents the Division of Building Research window calorimeter designed to reduce the errors associated with determining calorimeter enclosure air and surface temperatures. For achieving a constant and uniform temperature on the baffle, an evaporating condensing panel was designed. The constant temperature baffle and convection heater were mounted in the new calorimeter box, as shown in Figure 2.50.

Onega and Burns [173] presented work about thermal flanking loss calculations for the National Bureau of Standards (NBS) calibrated hot box. The work consists of the development of a computer code called FLANK, which computes the flanking loss for the NBS calibrated hot box. The software is a two-dimensional finite-difference dynamic thermal simulation of the test frame and specimen when subjected to steady or dynamic state conditions. Although the code has designed explicitly for the NBS-CHB, it can be used with any CHB.

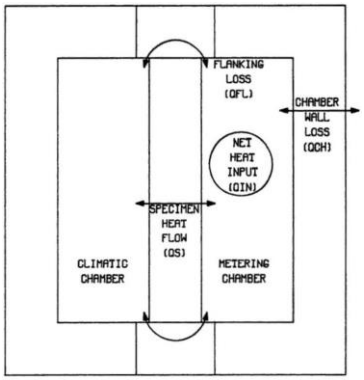

Figure 2.49 – Heat flow paths in the CHB [88].

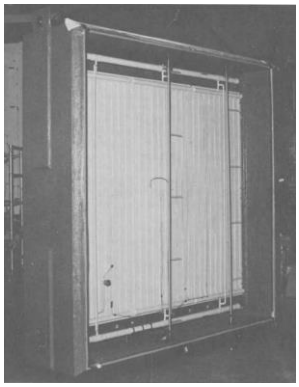

Figure 2.50 – Division of Building Research wind machine window calorimeter [172,174].

Zarr *et al.* [175] presented a study about thermal resistance measurements of a well-insulated residential wall, conducted using NBS calibrated hot box, under winter and summer climatic conditions. The wall comprises two insulated wood-frame sections with a thermal resistance of 4.8 m^2.K/W. The experimental thermal data was compared with predictions, using the ASHRAE parallel-path and isothermal-plane method and a finite difference model, archiving a good agreement between measured and predicted values.

Guy and Nixon [176] carried out a verification procedure for a guarded hot box facility, Figure 2.51, installed at Pilkington Brothers, Research and Development Laboratories, United Kingdom. The hot box can operate either in calibrated or guarded mode and manufactured by Wiss, Janney, Elstner, and Associates. The study analysed, the various energy flows in the GHB, gives the procedures for application of various correction measures, including the zeroing of any out-of-balance flux through the metering box walls and, in the specimen, across the metering box periphery.

Geem [177] tested block-brick cavity walls in the CHB facility at the Construction Technology Laboratories, a division of the Portland Cement Association, illustrated in Figure 2.52. The experimental test results provide a database for evaluation of building envelope performance where cavity walls are used and also provide information on the effectiveness of expanded perlite as a cavity fill material.

De Ponte [178] made a paper about design considerations on guarded and calibrated hot box apparatus. The goal is to supply some practical tips for better understanding the apparatus performance. States that after building new equipment, the temperatures and velocities must be checked, and a performance check is mandatory to allowing evaluate the sources errors.

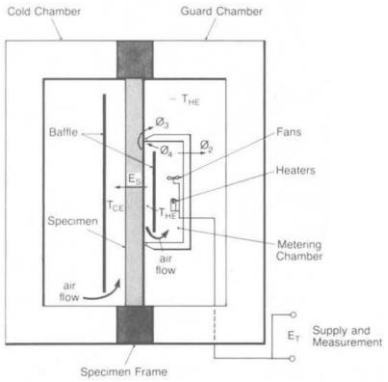

Figure 2.51 – GHB facility of Pilkington Brothers, Research and Development Laboratories schematic [176].

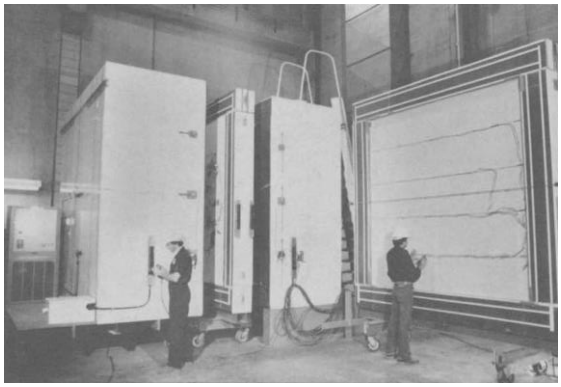

Figure 2.52 – CHB facility of Construction Technology Laboratories, Portland Cement Association [177].

Elmahdy and Bowen [179] tested heat transmission of insulated glazed units, in the GHB of the Institute for Research in Construction, National Research Council Canada, presented previously [172,174]. Figure 2.53a shows the sketch of the specimen placed in the calorimeter box. The work compares the thermal characteristics of various types of glazing units, as shown in Figure 2.53b. The tests provide *U*-values for the glazing units, which are essential information for window designers and manufacturers, and allows to update data in design guides.

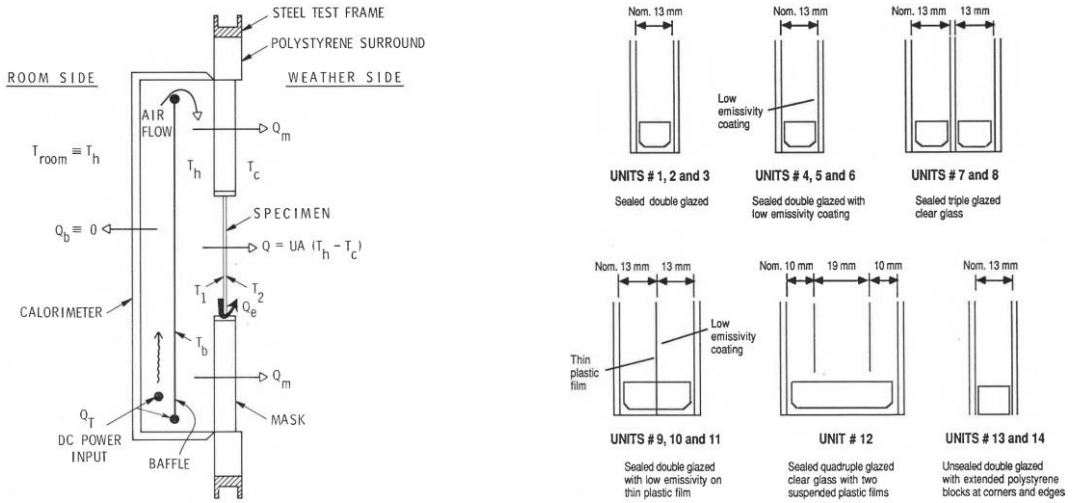

a) **b)**

Figure 2.53 – Glazing units: a) sketch of the specimen in the calorimeter box; b) diagram showing cross-section of the tested types [179].

Stephenson *et al.* [180] developed a ramp test method for GHB to determine transfer function coefficients for a wall specimen. The GHB facility of the Institute for Research in Construction National Research Council Canada, Ottawa, Ontario, is shown schematically in Figure 2.54. This method places the specimen between the climatic and metering chambers of a GHB, and a slow ramp excitation function is generated in the climatic chamber. The metering chamber works as a calorimeter and is kept at indoor conditions. The wall specimen inside surface transient heat transfer rate is determined from the energy balance of the metering chamber. The limits and points of the analytical ramp solution are determined by analysing the measured heat transfer response of the wall specimen.

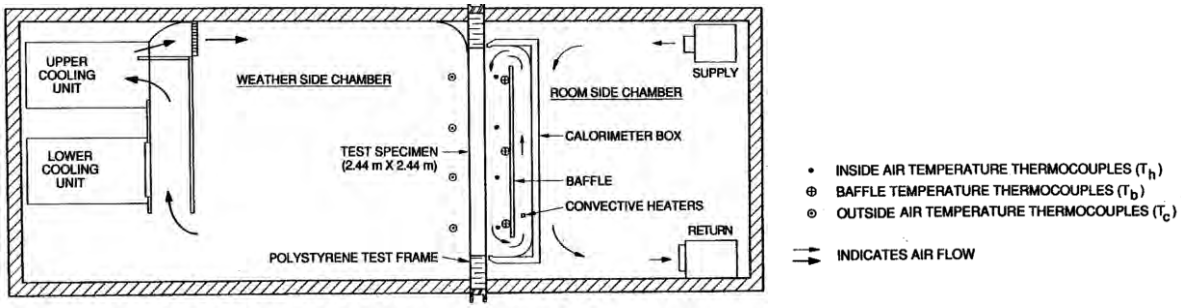

Figure 2.54 – Institute for Research in Construction GHB facility [180].

The 1990s

Burch *et al.* [89] describe a dynamic test method for determining transfer function coefficients of a wall using a CHB. In the study is used CHB facility of the National Institute of Standards and Technology, in Gaithersburg, shown the schematic cross-section in Figure 2.55a and Figure 2.55b the energy balance of the metering chamber under dynamic conditions. In this method, a wall specimen is installed between the climatic and metering chambers of a CHB. After the specimen heat transfer rate is steady, the air temperature in the climatic chamber is rapidly ramped from to another temperature level linearly. The final temperature level is maintained until the specimen reaches a new steady heat transfer rate. The methodology is similar to the one presented by Stephenson *et al.* [180].

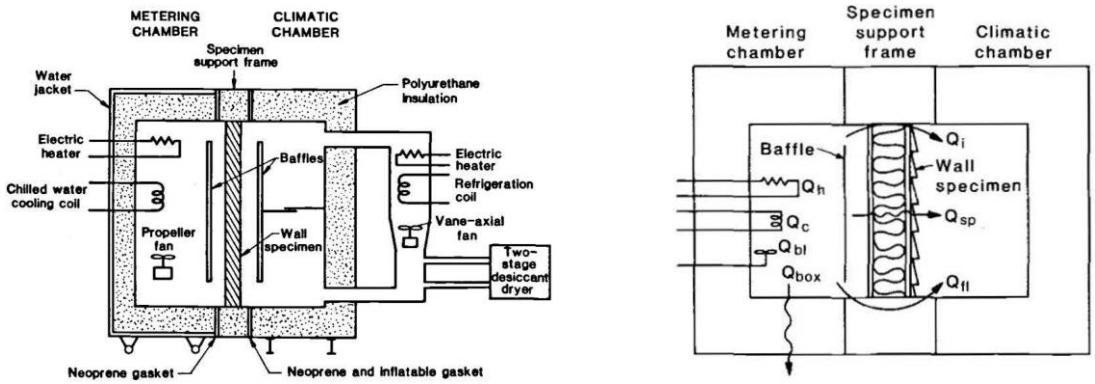

Figure 2.55 – CHB facility of the National Institute of Standards and Technology: a) schematic cross-section; b) energy balance of metering chamber under dynamic conditions [89].

Hagan *et al.* [181] present the results of two experimental studies, conducted at the GHB facility of the Jim Walter Research Corporation. The first study was a continuation of a 5-year ageing study on foil-faced polyisocyanurate thermal insulation boards. These boards were retested and characterise 11-year old data. The second was a correlation study between the large-scale GHB and small-scale heat flow meter tests using permeable faced polyisocyanurate foam thermal insulation boards. The results show that there is good agreement between both methods.

Wilkes *et al.* [82] conducted a series of experiments on one commonly available loose-fill fibreglass attic insulation. The tests were performed using the GHB of the large-scale climate simulator at the Oak Ridge National Laboratory, presented [157] and illustrated schematically in Figure 2.56a. The tests were made to an attic test module, illustrated in Figure 2.56b, to simulate typical residential construction. A series of additional tests were also performed with various materials laid on top of the existent insulation, to study possible optimisations of the construction system.

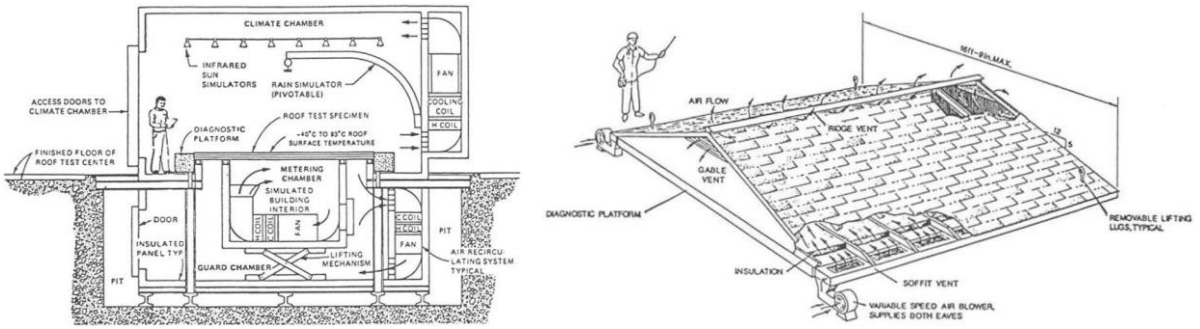

a) **b)**

Figure 2.56 – GHB: a) Cross-section of the large-scale climate simulator; b) Schematic of the attic test module, built to simulate characteristics residential roofs [82]**.**

Brown and Stephenson [182] presented one of the first methodologies for measuring the dynamic heat transfer characteristics of a full-scale homogeneous specimen using the GHB facility, at the Institute for Research in Construction National Research Council Canada, Ottawa, Ontario, illustrated schematically in Figure 2.54. For these tests, the first step is the dynamic calibration of the facility. This calibration is based on the thermal characteristics of a specific specimen, which had been determined from measurements of material properties. The procedure consists in making a series of measurements of the response of the facility and test specimen, to sinusoidal variations of exterior temperature and interior power.

Brown and Stephenson [183] continued the work above, presented a development of the previous methodology, for measuring the dynamic heat transfer characteristics of full-scale non-homogeneous specimens. The study shows that the dynamic response of a wall system is quite sensitive to the magnitude of the interior and exterior surface convection coefficients.

Adam and Jones [184] measured the thermal conductivity of lime/cement stabilised hollow and plain earth blocks, using a GHB of the University of Wales College of Cardiff, U.K., which is illustrated schematically in Figure 2.57.

Gatland *et al.* [185] designed a unique guarded hot box for thermal testing of fenestration products that incorporates several new design concepts retrieved from guarded hot plates, namely wall and edge guards. Figure 2.58 presents a sketch of the vertical cross-section.

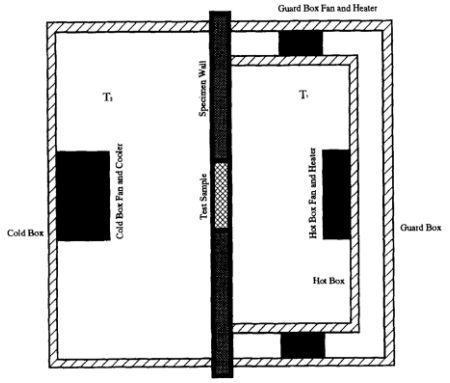

Figure 2.57 – GHB schematic top view [184].

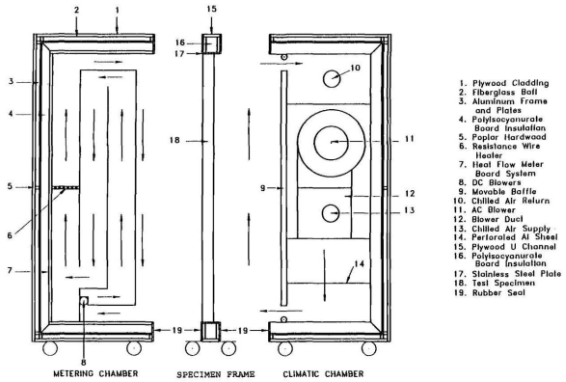

Figure 2.58 – Fenestration hot box construction details [185]**.**

Gatland, Goss, and Curcija [186] designed a second-generation research calibrated hot box, constructed at the University of Massachusetts's, at the Building Energy Research Laboratory. The innovation on this hot box is the capability of simulating both parallel and perpendicular wind directions on the specimens,

including fenestration systems, e.g. windows and doors, illustrated in Figure 2.59. The cold box temperature range is -23.3 to 60° C, and the hot side is 21.1 to 60° C.

Derome *et al.* [187] present results from a series of tests performed on wood stud wall assemblies in an environmental chamber, a GHB and CHB facility, located on the Centre for Building Studies, of Concordia University, Montreal. The facility allows the study of the hygrothermal, e.g. air, moisture and heat flow, and aspects of building envelope performance simultaneously. The environmental chamber in CHB mode can enclose between the cold and hot box wall specimens with 4.1 by 7.2 m². Also, it can be a GHB by adding a 2.4 by 2.4 m² large metering box, shown in Figure 2.60. The equipment has the advantage of permitting measuring large specimens dimensions wide sections of walls, reducing the effect of local dissimilarities. The facility also allows test rooms, with a maximum size of 3.2 by 5 by 6 m³ high, by joining the cold and hot box together. This arrangement permits also testing roofs and walls, up to two storeys high.

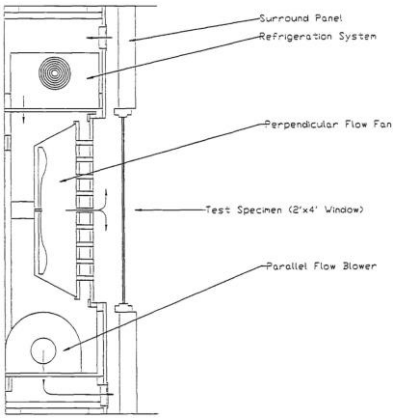

Figure 2.59 – CHB University of Massachusetts's: a) hot chamber front view; b) cold chamber side view [186].

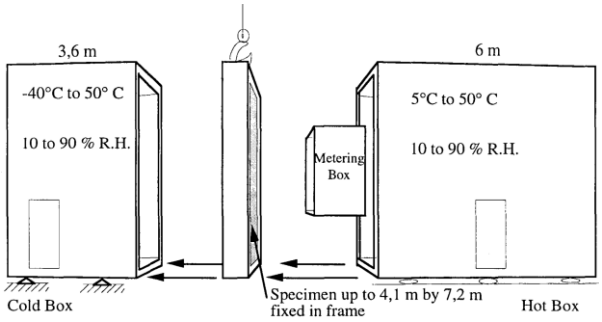

Figure 2.60 – Schematic representation of the environmental chamber [187].

The 2000s

Elmahdy and Haddad [188] presented a laboratory test procedure in a guarded hot box facility to determine the thermal transmission coefficient of skylights. The details about the hot box facility, of Division of Building Research, National Research Council, Ottawa, Ontario, Canada, can be found in the work of [80]. Skylights need to be tested at an inclination angle between 20 to 90° from the horizontal. Figure 2.61 illustrates the setup for testing skylights.

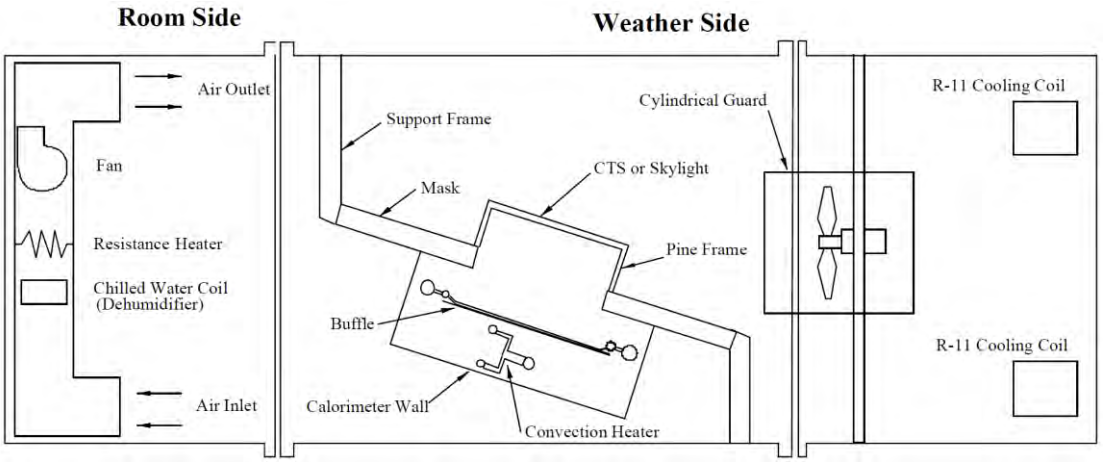

Figure 2.61 – Schematic of the hot box facility for inclined skylight testing [188].

Kosny and Childs [189] present a study of the thermal performance wall system, called Rastra. The experimental tests were made at the rotatable GHB of Oak Ridge National Laboratory (ORNL) Buildings Technology Center, shown in Figure 2.62. The test wall assemblies were installed in the specimen frame which has an aperture of 4 by 3 m. The hot box tests were compared with and finite difference computer modelling, Heating 7.2 Simulations, for validation.

a) b)

Figure 2.62 – ORNL facility: a) unfinished Rastra wall on the hot box test support frame [189]**; b) GHB** [158]**.**

Aviram *et al.* [190] carry out an experimental investigation of heat transfer through a variable aspect ratio cavity wall. The tests were performed in a GHB of Faculty of Technology, School of Civil Engineering, Kingston University, UK. The temperature range of the equipment is -50 to 50° C. The walls tests contemplate blocks and bricks cavity walls measuring 1.2 by 1.2 m², with cavity depths of 78, 60 and 40 mm. The tests results show that by increasing aspect ratio, low size falls, the circulation strength decreases and the air cavity thermal resistance increase. Figure 2.63 illustrates the GHB apparatus.

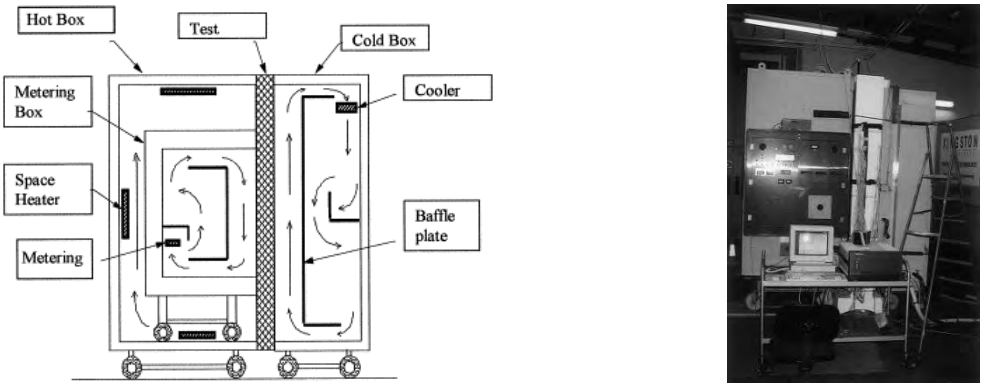

a) b)

Figure 2.63 – GHB apparatus: a) schematic vertical cross-section view; b) side view and variable cavity wall [190]**.**

Kosny *et al.* [85] developed a new procedure for increasing the accuracy of hot box testing method for walls containing strong thermal bridges. The traditional HB analysis method described standards is relatively accurate for testing conventional wood framed walls. Nevertheless, this methodology is much less accurate for heavily thermally bridged walls, e.g. steel-framed walls, since steel is around one thousand times more conductive than wood. These structures are containing strong thermal bridges that need a new procedure methodology to achieve accurate results. Kosny *et al.* [85] proposed a new method, where three sources of inaccuracies were identified for steel stud assemblies: the zone of influence for the thermally bridged areas; distribution of surface temperatures for locations of higher thermal bridges; and thermal conductivity of foam used in the surround panel.

Yuan *et al.* [191] studied the importance of a complete calibration on any guarded or calibrated hot box. They concluded that the calibration is critical for improving the precision of the measurement of fenestration products. All heat transfer that does not occur directly through the test specimen must be determined from the detailed calibration experiments results. Figure 2.64 details the possible heat transfer paths in a CHB. Yuan *et al.* [191] do for this work several calibration procedures using the University of Massachusetts Research CHB by the ASTM and ISO test methods. Yuan *et al.* [191] paper describe in detail the calibration procedures necessary for fenestration products. Yuan, Russell and Goss [192] state that for achieving accurate *U*-value measurements, the unreliability of the specimen flanking loses on heat transfer calibration should be kept below 5 %.

Petrie *et al.* [193] performed experimental tests at the large-scale climate simulator at the Oak Ridge National Laboratory's Buildings Technology Center, illustrated in Figure 2.56. The experiments intended to assess the impact of light steel framing (LSF) on the thermal performance of attic/ceiling assemblies. The study provides some basis for changes in codes and standards, which reflect the thermal performance effects of LSF in attic/ceiling assemblies and discourage LSF to extend beyond the insulation in the assemblies.

Wakili and Tanner [194] studied the *U*-value of a dry wall made of vertically perforated porous clay bricks. The thermal properties were obtained by an experimental method according to ISO 8990:1994 [17] and by two numerical methods, according to EN 1745. The experimental work was performed in a CHB of the Section of Applied Physics in Building, Swiss Federal Laboratories for Materials Testing and Research, Duebendorf, Switzerland. The apparatus is illustrated schematically in Figure 2.65, in which it is possible to see that the cold and hot side boxes are inside of a bigger one. Wakili and Tanner [194] study results lead to a proposal for the refinement of the model chosen for the numerical analysis.

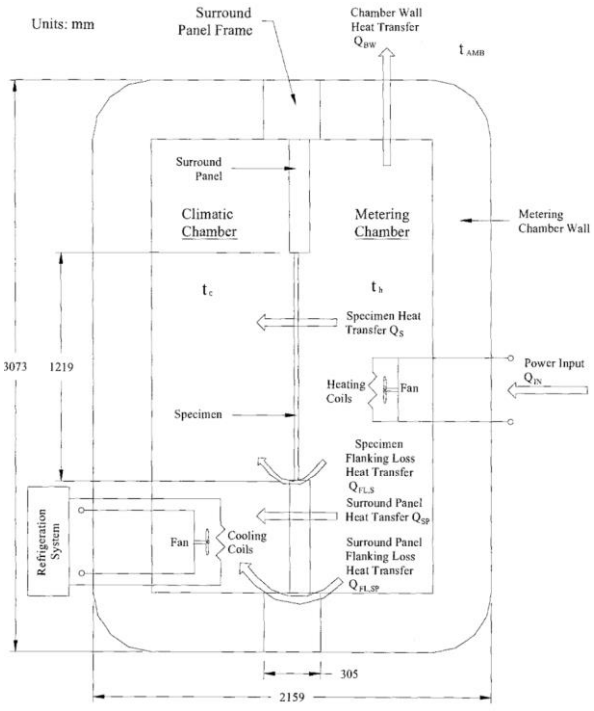

Figure 2.64 – Heat transfer in the CHB [191]

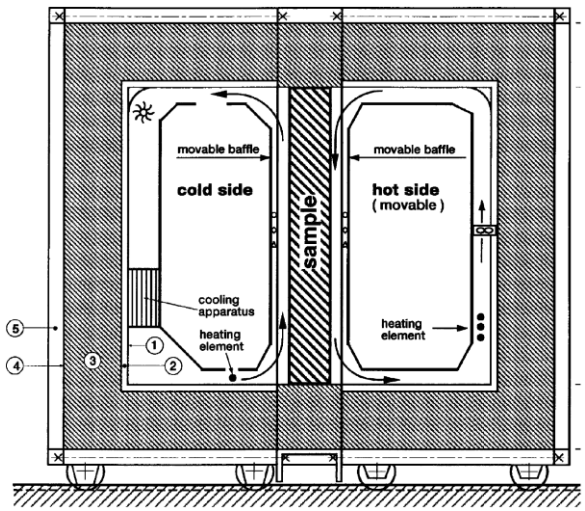

Figure 2.65 – Schematic cross-section of the CHB [194].

NAHB Research Center [195] reviewed and evaluated possible optimisations of LSF walls. The experimental study was made in the rotatable GHB of the Oak Ridge National Laboratory, shown in Figure 2.62 and Figure 2.66. The studied test thermally efficient LSF studs, thermally efficient, which have a slip web. The results showed that the prototype slit web studs performed 17 % better than the solid-web studs.

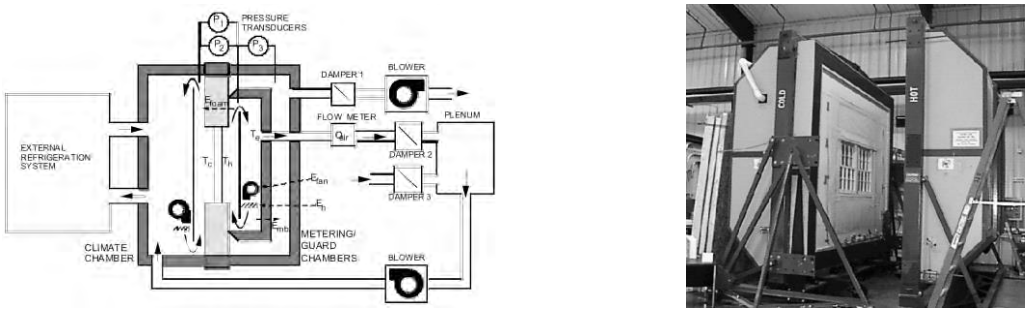

a) **b)**

Figure 2.66 – Rotatable GHB: a) schematic vertical cross-section; b) side view [195].

Gao *et al.* [196] compared the results of numerical models with experimental tests performed in a CHB, Thermal Sciences Center, Building Physics, National Institute of Applied Sciences Lyon, France, shown in Figure 2.67. The classical one-dimensional heat flow computations do not accurately determine the heat loss under dynamic conditions for building envelopes made of hollow blocks. Due to the complex three-dimensional heat transfers analyses, computational models are complex with high-order matrixes, which requires intensive computation time. The solution is using model size reduction techniques, based on Moore's balanced method, which decreases the computation time, and if it is good implemented will not have significant losses of precision. The confrontations of results show that the proposed reduced models provide an excellent prediction of hollow blocks thermal behaviour.

Rose and Svendsen [197] made a series of experimental test in typical lightweight walls containing different types of linear thermal bridges, using a GHB, shown in Figure 2.68, with a measuring area of 1.2 by 1.8 m², at Department of Buildings and Energy, Lyngby, Denmark. The experimental results were compared with the numerical calculation done using two simulation programs, HEAT2 [198] and HEAT3 [199]. Both software's are validated according to ISO 10211-1 [200]. The validation has proven very successful with deviations range from approximately 1 to 5 %.

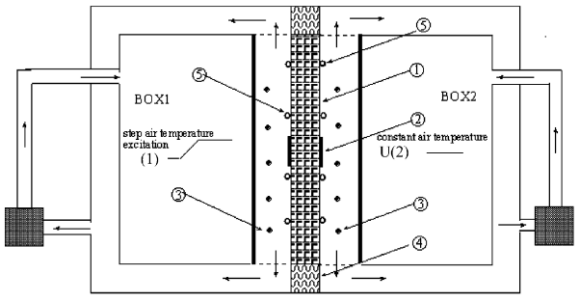

Figure 2.67 – Schematic cross-section of the CHB [196].

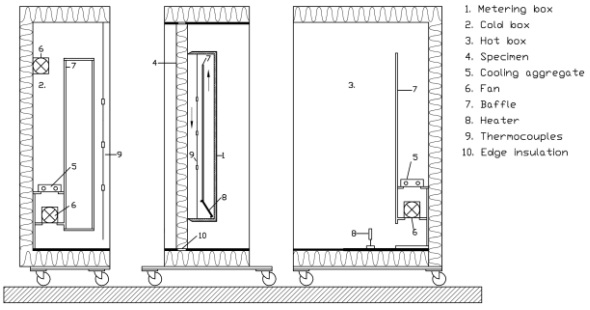

Figure 2.68 – GHB vertical cross-section [197].

Nussbaumer *et al.* [201] tested experimentally and numerically a concrete wall, externally insulated with six expanded polystyrene boards, each containing three vacuum insulation panels. The primary goal is determining the thermal performance of vacuum insulation panels. The experimental test was performed in a GHB facility at Laboratory for Applied Physics in Building, Swiss Federal Laboratories for Materials Testing and Research, Duebendorf, Switzerland, shown in Figure 2.69. The study shows a thermal improvement of over 95 % was for a wall with 40 mm thick VIPs.

Sala *et al.* [202] performed a study in which explains the procedure for the dynamic test in a CHB. The apparatus is at the Thermal Engineering Department, University of the Basque Country, Bilbao, Spain, shown in Figure 2.70. The study consists of an experimental static and dynamic thermal characterisation of

a hollow brick wall, which was compared with numerical models, using a CFD code, namely FLUENT version 6.0. The study concluded that the error committed may be appreciable, even when the heterogeneities are not excessive.

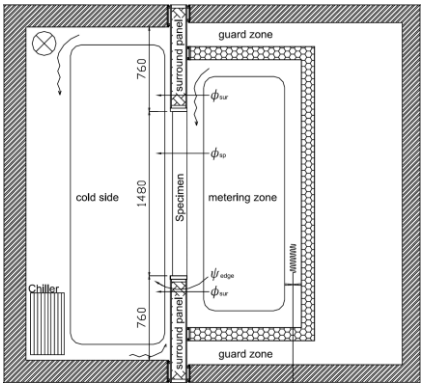

Figure 2.69 – GHB vertical cross section [201].

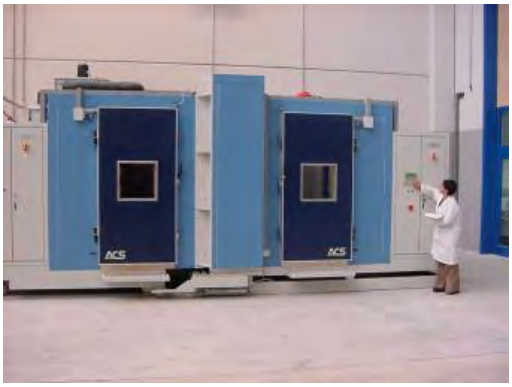

Figure 2.70 – Guarded/calibrated hot box [202].

Baker [203] carry out a series of thermal performance tests on traditional windows. The tests were made at the National Physical Laboratory, UK, using a guarded hot box, shown in Figure 2.71. The study contemplates several optimisation solutions, which concludes that the individual solution of secondary glazing was the most effective option by reducing 63 % of the heat loss through the window.

Geoola *et al.* (2009) designed and constructed a laboratory hot box to investigate the overall heat transfer coefficient of some greenhouse polyethylene plastic films with or without thermal screens. The constructed hot box is, by the authors, partially based on ASTM standards. It is a small setup with a cross-section of 60 by 60 cm² with 60 cm height, with 10 cm thick polyurethane walls. Figure 2.72 shows the equipment, a simple solution, with simple components and cheaper. The study concluded that using a thermal screen would reduce the *U*-value by about 30 %, an energy saving of about 30 %.

Figure 2.71 – Guarded hot box [203].

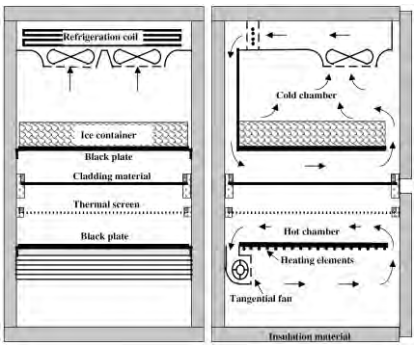

Figure 2.72 – Hot box [204].

The 2010s

Asdrubali *et al.* [205] made a study comparing two different systems for thermal conductivity measurement, respectively CHB and guarded hot plate methods. The CHB as constructed at the Department of Industrial Engineering of the University of Perugia, Perugia, Italy, as shown in Figure 2.73. The test campaign concluded that for specimens with different thermal conductivity and thickness, both methods are equivalents and that the hot box system gives more accurate results for low thermal resistance systems. [206] use the same CHB evaluation of the thermal insulation properties of low emittance surfaces.

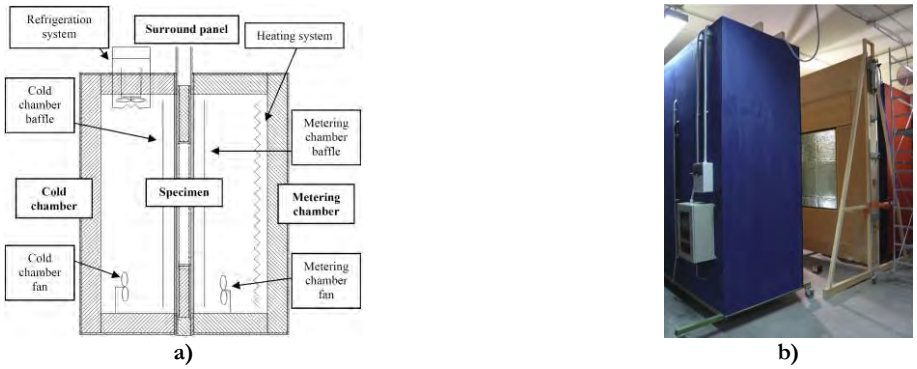

a) b)

Figure 2.73 – CHB: a) Schematic vertical cross section [205]**; b) Side view** [206]**.**

Cao *et al.* [207] proposed a methodology to evaluate the impact of a phase change materials (PCM) enhanced wall on the indoor air and wall temperature using the GHB apparatus, shown in Figure 2.74. The results showed that the inclusion of the PCM layer in the wall reduces the interior air and wall temperatures up to 2° C in comparison to the wall without PCM.

Asdrubali *et al.* [77] performed the calibration of a CHB, at the Department of Industrial Engineering of the University of Perugia, presented previously, shown in Figure 2.73. The calibration and experimental procedures were performed by three standards: ISO 8990 [17]; ASTM C1363-05 [208]; and GOST 26602.1-99 [209]. The experimental tests highlighted that the ASTM and ISO standards are similar, and for achieving more accurate results, the ideal procedure must also include the Russian method.

Martin *et al.* [210] performed a study about the dynamic uncertainty behaviour of thermal bridges. For that, they made numerical simulations and carried out a series of tests in a GHB facility, at University of the Basque Country, shown in Figure 2.70, and Figure 2.74 is an example of a sample being assemble with a thermal bridge, a concrete column. The experimental tests show the limitations of the GHB test for characterisation of heterogeneous samples. The fact is that the metering box does not cover a sufficiently representative area of the thermal bridge, not allowing to achieve reliable results. Still, the total thermal resistance value does not diverge by more than 8 % compared with the calculation according to ISO 10211.

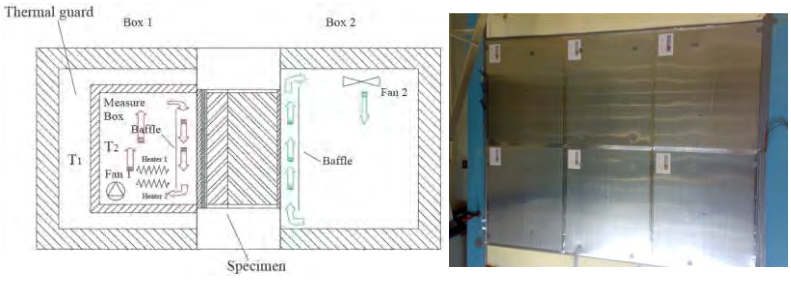

a) b)

Figure 2.75 – GHB: a) Schematic vertical cross-section; b) Wall specimen with PCM assembled in the frame [207]**.**

Figure 2.74 – GHB: wall specimen being assembled in the frame [210]**.**

Choudhary *et al.* [211] investigated heat transfer in two metal building walls insulation assemblies. To compute the *U*-value were made numerical models, which were compared with measurements from calibrated hot boxes. The predicted and measured *U*-values were in 93.3 % agreement for one of the wall assemblies and 95.5 % agreement for others.

Kus *et al.* [212] conducted to study the hygrothermal performance of pumice aggregate concrete block walls using a CHB method. The test concluded that the hygrothermal behaviour change at the lower and the

upper courses depending on the indoor and outdoor climate test conditions. The heterogeneous of the material, the block surface roughness and the block wet construction type are the most problematic subjects, which make measurements and assessments difficult.

Chen *et al.* [213] present a series of experimental tests for measuring the solar heat gain coefficient of thin-film semi-transparent photovoltaic glazing. The tests were performed in a GHB at the Solar Energy Research Institute of Singapore, being used only half of the apparatus, i.e. the guard and metering boxes, and solar simulator, shown in Figure 2.76. The results show that the solar heat gain coefficient is sensitive to the incident angle of solar radiation, particularly for angles above 45° and reduces significantly for angles of 0°.

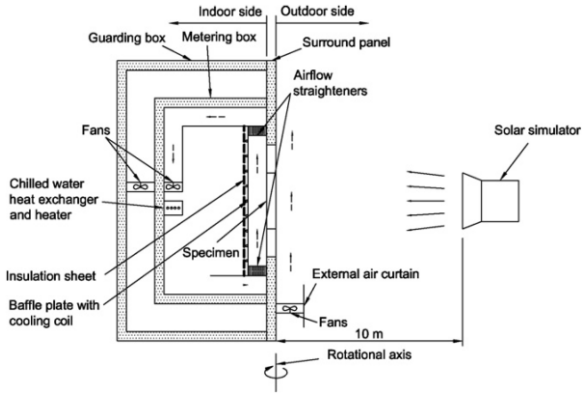

Figure 2.76 – Schematics of the GHB and solar simulator [213].

Chen and Wittkopf [1] presented a study of summer condition thermal transmittance measurement of fenestration systems using a GHB with advanced measurement methodology and numerical approach. The details of the GHB, located at the Solar Energy Research Institute of Singapore, Singapore, are shown in Figure 2.77. The experimental results were compared with simulation results obtained with THERM [142] and WINDOW [214] software, revealed a difference of less than 5 %.

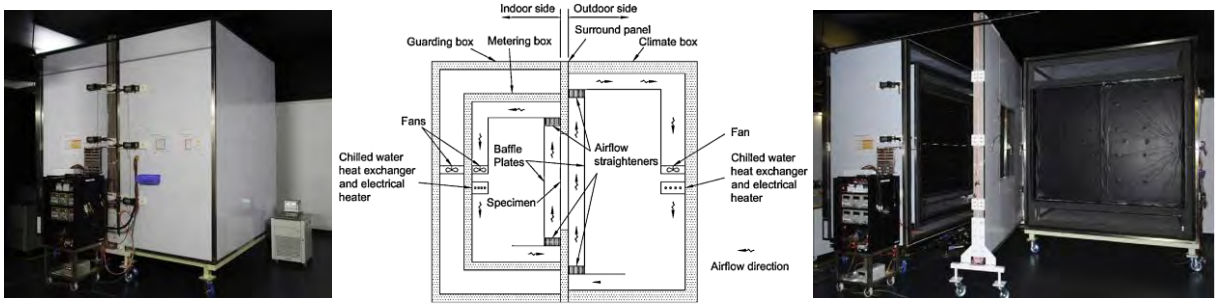

a) **b)** **c)**

Figure 2.77 – GHB: a) side view; b) schematics vertical cross section; c) side view with the apparatus open [1].

Schumacher *et al.* [81] developed a new hot box apparatus designed to measure the true thermal performance of modern wall assemblies accurately. The equipment is an approach based on ASTM C1363-05 [208], constructed at Building Science Consulting Inc., Waterloo, Ontario, Canada. The new apparatus has several improvements: systems to simulate heat and cold climates without removing specimen; a large-double-guarded meter box, shown in Figure 2.78; a closed-loop air system that induces and measures air pressure differences across and through the assembly; a tracer gas system to measure induced airflows; and the ability to measure with better precision. These improvements allow a better quantification of wall assemblies performance comparatively to others hot box apparatus.

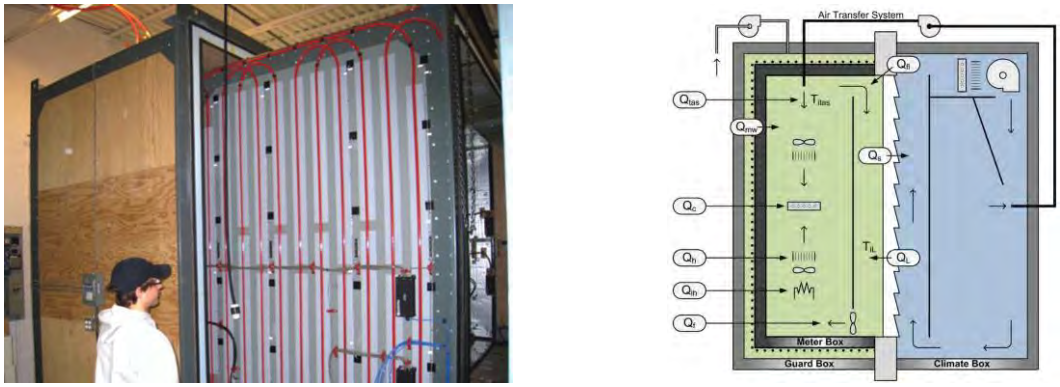

a) b)

Figure 2.78 – Hot box: a) view illustrating the double-guarded concept; b) energy balance diagram [81].

Ghosh *et al.* [215] presented work about three different types of software-based temperature control strategies for controlling a GHB apparatus boxes inside temperatures. In the first two strategies, on-off control was implemented, and in the third strategy, proportional control was implemented. The first two strategies experimental data revealed that they give similar performances, obtaining temperatures satisfactorily according to the standards, i.e. less than 1 % fluctuations. The third approach did not give good results, presenting temperatures fluctuations that are not acceptable by the standards.

Holstein and Bohnhoff [216] presented a rotatable GHB apparatus that was designed and constructed on the University of Wisconsin-Madison campus, illustrated in Figure 2.79, for large-scale thermal tests of building envelopes. The apparatus can test a wall or roof, can rotate 360 degrees about its horizontal axis, test specimens up to 2.9 by 3.8 m² and apply static pressure differential across the specimen, for simulating the effects of air infiltration.

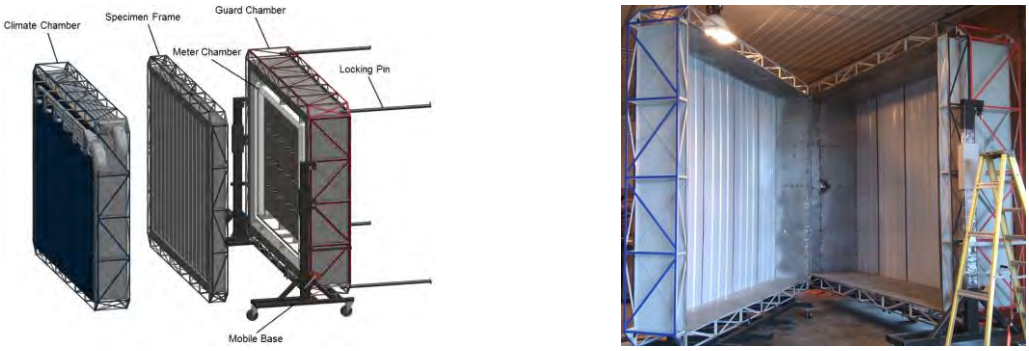

a) b)

Figure 2.79 – Rotatable GHB: a) sketch; b) boxes of apparatus in the construction phase [216].

Shrestha *et al.* [217] performed a study for evaluates various attic radiant barrier systems under summer daytime and night conditions or winter daytime low solar gain conditions. To quantify, the thermal performance of the attic was used the GHB of the large-scale climate simulator at the Oak Ridge National Laboratory, presented by Hunley [157]. The results of the four attic study configurations show that the systems with radiant barriers had lower heat flows during the summer daytime condition.

Amundarain *et al.* [218] present study evaluates and develops LSF structures design. The primary objective is to establish a methodology of design that leads to better thermal performance. Both, computational and experimental work has carried out, being used a GHB with a 1.2 by 1.2 m² metering box and 2.4 by 2.4 m² guard box area, shown in Figure 2.80.

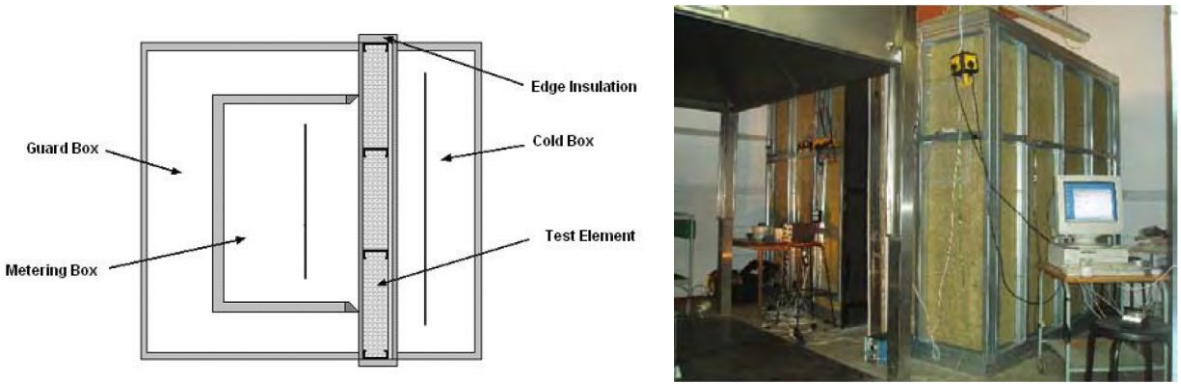

a) b)

Figure 2.80 –GHB: a) schematic; b) apparatus [218].

Shrestha *et al.* [219] made a study that the objective is to evaluate the thermal performance of walls with gas-filled insulation panels. For that purpose, were made thermal performance tests in the rotatable GHB at the Oak Ridge National Laboratory, illustrated in Figure 2.66. The test result shows that *R*-value of the wall with two layers of gas-filled insulation panels decreases sharply as the temperature of the panels increases, the R-value of the wall with only one layer fairly remains steady.

Baldwin *et al.* [220] compare experimental thermal resistance results obtained using both methods in-situ testing and steady-state testing in a GHB facility, of a wall assembly incorporating vacuum insulation panels (VIPs). The GHB as constructed for the test, which Figure 2.81 shows the schematic. The GHB method achieves more accurate results, not agreeing with computer simulations an *in-situ* measurements. The *in-situ* methodology does not is less precise due to the thermal bridges between panels. In the numerical model VIPs, thermal resistance across the whole panel layer was assumed as constant, which in reality is not, due to the non-homogeneous nature of a VIP layer. The results allowing to concluded that GHB results are more precise, and it is a recommended method for experimentally evaluated VIP panels contain numerous small thermal bridges.

Seitz and Macdougall [83] made the design and construction of a small-scale, affordable hot box apparatus, for testing of straw bale and other non-conventional building panels, illustrated in Figure 2.82. The apparatus was built at Department of Civil Engineering, Queen's University, Kingston. The authors emphasise that the first reason for the self-construction was the cost of a commercial hot box apparatus, 660 k€, being the cost of the self-made apparatus of 20 k€. The second reason is the price of the test conducted by the standard by an accredited laboratory, in which an individual test can cost between 4 k€ and 13 k€ per sample and many labs have waitlists of several months.

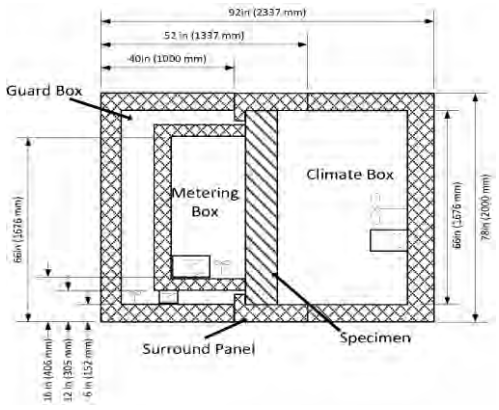

Figure 2.81 – GHB schematics cross section [220].

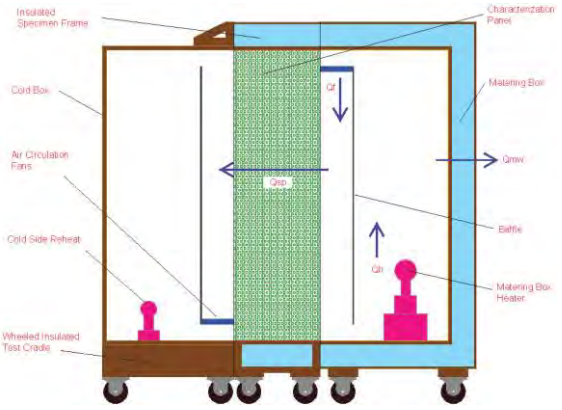

Figure 2.82 – HB schematics vertical cross section [83].

Meng *et al.* [221] propose a simple hot box-heat flow meter method for *in-situ* wall thermal transmittance measurement. The equipment is quite simple, was constructed at Sichuan University, Chengdu, China and Figure 2.83 illustrates the setup. The experimental results show an error of -5.97 % relative to the design value.

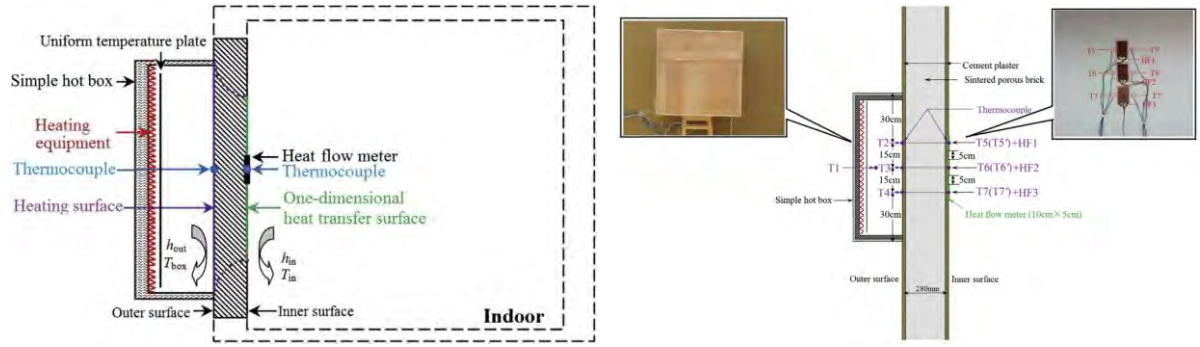

a) **b)**

Figure 2.83 – Simple hot box-heat flow meter: a) schematic; b) measurement equipment arrangement diagram [221].

Buratti *et al.* [222] proposed a new method, the so-called small hot box apparatus, Figure 2.84, to evaluate the thermal properties of small specimens, 0.3 by 0.3 m². The equipment was constructed in the University of Perugia, Italy. Different samples with known thermal properties were analysed, e.g. polistyrol, foam polyurethane, polystyrene, wood, plasterboard, and cement insulating blocks. Following these authors, the proposed method can be a possible alternative system to be used instead of the conventional GHP apparatus.

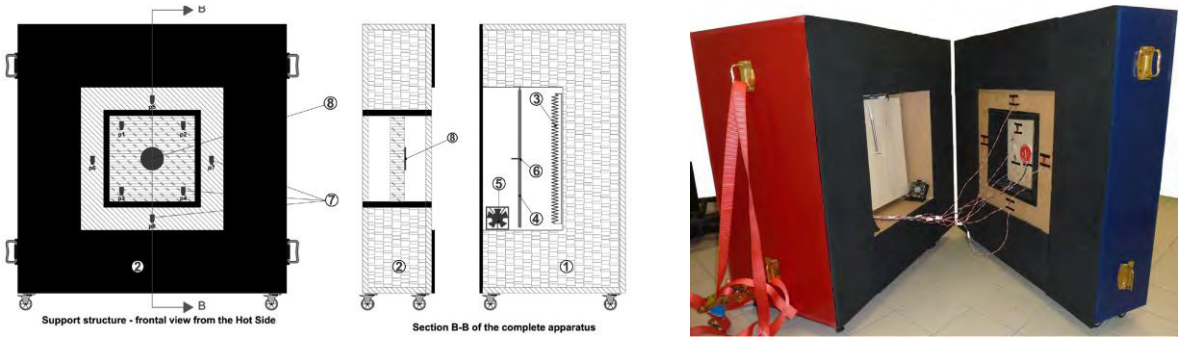

a) **b)**

Figure 2.84 –Small hot box apparatus: a) schematic; b) general view [222,223].

Nardi *et al.* [224] study the validity of thermographic methods by using a GHB. For that purpose, was used a GHB of the Department of Industrial and Information Engineering and Economics of the University of L'Aquila, Italy. The results comparison relative uncertainties agree with the minimum deviations with a range between 5 and 10 %.

Modi *et al.* [225] proposed a mini-scale hot box apparatus to evaluate the thermal performance of an insulation building block. The apparatus as constructed at Université de Strasbourg, Strasbourg Cedex, France, illustrated in Figure 2.85. The experimental thermal resistance value measured relative error with the manufacturer's value was close to 5.6 %.

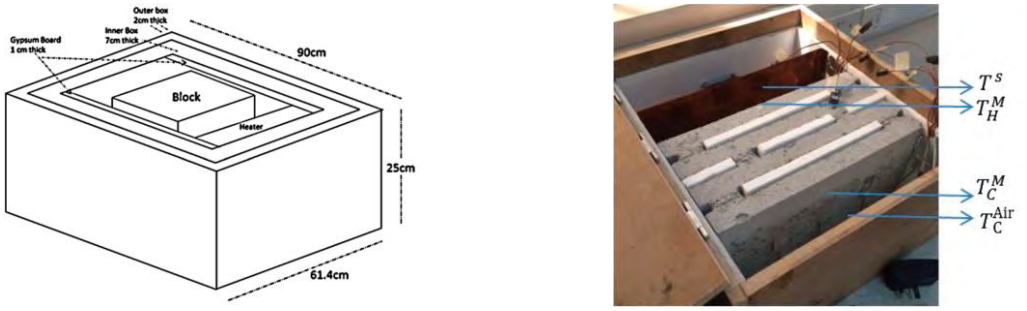

a) **b)**

Figure 2.85 – Mini-scale hot box apparatus: a) schematic; b) final manufactured experimental set-up [225].

Lucchi *et al.* [226] presented a procedure for testing the thermal performance of inhomogeneous specimens, in steady-state, on the HB apparatus of EURAC's Lab [227]. This work suggested complementing procedures for the standard, for moderate inhomogeneous specimens [228].

a) **b)**

Figure 2.86 – Guarded hot box test: a) apparatus [229]**; b) specimen** [230].

Chowdhury and Neogi [231] performed tests in a GHB for the thermal performance evaluation of traditional walls and roof used in a tropical climate. The apparatus is on the Building Energy Laboratory, School of Energy Studies, Jadavpur University. The construction material is simple, being used panels of XPS, illustrated in Figure 2.87. They test burnt clay brick-based wall and reinforced cement concrete wall. From the test was concluded that heat transfer through these building components is dependent on the sample configuration (plaster vs non-plastered, painted vs non-painted) and temperature differentials.

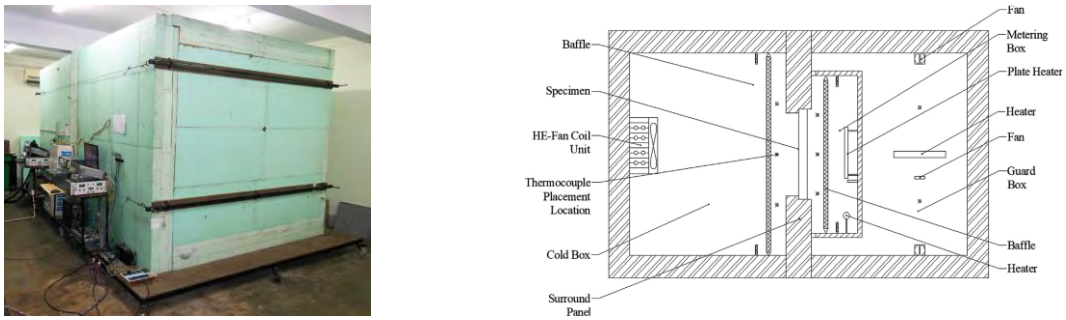

a) **b)**

Figure 2.87 – Guarded hot box: a) apparatus; b) schematic representation [231].

Zhao *et al.* [232] developed a reduced-scale hot box system, for testing small scale specimens, illustrated in Figure 2.88. The equipment tested window insulation materials and was validated by testing commercial

material with which were compared the obtained values.

a) b)

Figure 2.88 – Reduced-scale hot box system: a) schematic; b) snapshot of the assembled setup [232].

Trgala *et al.* [233] study the energy performance of five different building envelope structures, using a modified Guarded Hot Box apparatus, illustrated in Figure 2.89a. The presented solution was the adaptation of a GHB that was transformed into a CHB for performing the dynamic test.

Pourghorban and Kari [234] study the evaluation of reflective insulation systems in walls, using a guarded hot box apparatus of Energy Laboratory of Road, Housing and Urban Development Research Center (BHRC)., illustrated in Figure 2.89b. The overall dimension of the BHRC guarded hot box apparatus is 3.0 by 3.0 m by 1.2 m^3.

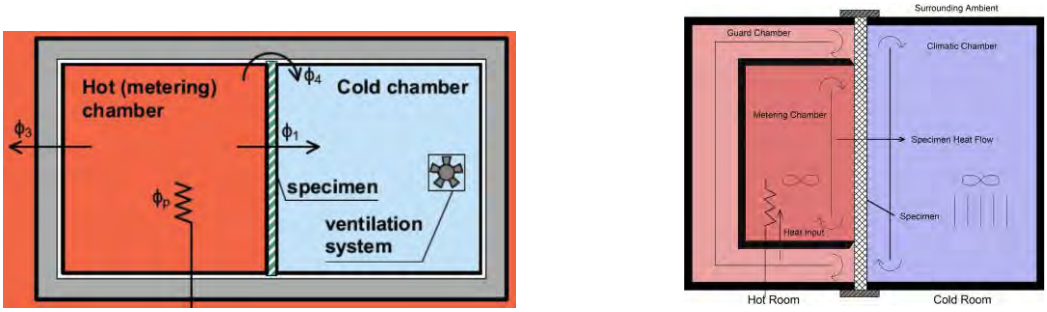

a) b)

Figure 2.89 – Guarded hot box apparatus: a) schematic [233]; b) schematic of the BHRC GHB [234].

Andreotti *et al.* [235] created an *in situ* hot box to measure and analyse different insulation solutions applied to a real historic wall, to quantify the hygrothermal performance of a masonry building. The box size is 2.50 by 2.50 by 4.01 m^3, built with walls composed OSB, timber structure made and stone wool as insulation. Figure 2.90 illustrates the apparatus and shows the schematic representation.

a) b)

Figure 2.90 – *In situ* hot box: a) apparatus; b) drawing of the metering box horizontal plan and vertical section [235].

2.3. LIGHTWEIGHT CONSTRUCTION SYSTEMS

LSF is a dry construction system consisting of three main types of materials that are used in walls and slabs: cold-formed steel studs for load-bearing, interior and exterior sheathing panels and insulation materials. Soares *et al.* [236] provided an extensive review of this type of construction, pointing out the main features related to its energy efficiency and thermal performance. Regarding thermal behaviour, LSF elements are typically classified according to the location of the thermal insulation layers as a cold frame, hybrid and warm frame construction, as previously explained and illustrated in Figure 2.1.

As suggested by Soares *et al.* [236], LSF construction can play an essential role in the development of a more sustainable built environment as it shows great potential for recycling and reuse, lower water consumption, high architectural flexibility for retrofitting purposes, high seismic performance, easy prefabrication allowing modular construction, small weight, economy in transportation and handling, reduced disruption onsite and speed of construction. However, the high thermal conductivity of the metal structure can lead to significant thermal bridges, which can affect the thermal performance of LSF assemblies. Moreover, the steel skeleton crossing insulation layers make the prediction of the thermal performance of the LSF assemblies difficult during the design phase and during the dynamic simulation of the energy in buildings. Also, the *in-situ* measurement of the overall thermal transmittance of LSF walls is very challenging due to the presence of non-homogeneous layers and thermal bridges. However, the *in-situ* characterisation is very important for the post-evaluation of the thermal performance of LSF assemblies, and for an energy audit.

It should be reminded that the existing standardised methods described in standards ISO 9869-1 [43] and ASTM C1155-95 [48] for the *in-situ* measurement of the overall thermal transmittance of construction elements only concern homogeneous walls. In fact, a standardised method for the *in-situ* measurement of the *U*-value of existing LSF walls is still missing.

Regarding laboratory conditions, the ISO 8990 [17] and the ASTM C1363-11 [18] can be used for the experimental assessment of the overall thermal transmittance of LSF walls using the HB apparatus. For the calculation of the overall thermal transmittance of construction elements, the ISO 6946 [26] is only applicable for construction elements with thermally homogeneous layers. In fact, this analytical method is not applicable for many LSF elements (other than full warm frame construction) in which metallic elements bridge insulation layers. In recent years, many studies have been carried out in the scope of the experimental calculation of the *U*-value of LSF walls in laboratory conditions combined with analytical and numerical simulations. Few studies were however devoted to the development of new *in-situ* measurements.

One of the first methods to determine the theoretical *U*-value of walls with cold-formed steel profiles was the ASHRAE zone method [33], presented in subsection 2.1.1.4. Based on the ASHRAE zone method, Kosny *et al.* [237] developed the modified zone method for metal stud walls with insulated cavities, which differs from the previous approach in the way that the zone of influence of the metal stud thermal bridging is estimated, leading to more reliable results, presented in subsection 2.1.1.5. Gorgolewski [40] suggested a simplified method to estimate the theoretical *U*-value of cold and hybrid LSF assemblies, presented in subsection 2.1.1.7. The methodology proposed by Gorgolewski [40] was used in several studies to estimate the thermal behaviour of LSF assemblies, which is required to evaluate the overall thermal behaviour of LSF buildings [16,238]. For example, Soares *et al.* [238] proposed a multi-dimensional optimisation model combining EnergyPlus and GenOpt tools for the annual optimisation of the incorporation of PCM-drywalls in air-conditioned LSF residential buildings in different European climates. In another study, Rodrigues *et al.* [16] proposed an integrated energy performance-driven generative design methodology to foster modular LSF residential buildings in hot climates.

Many research works have been carried out to find some ways to reduce or avoid thermal bridges in LSF buildings, and to improve the thermal performance of LSF assemblies. In this context, the following design

strategies can be listed according to refs. [3,47,50,236,239]: (*i*) keeping the facade geometry as simple as possible; (*ii*) avoiding interruption of the insulation layer and placing a continuous insulation layer on the external side of the steel framing; (*iii*) using materials with the lowest thermal conductivity possible where the interruption of the insulation layer is unavoidable; (*iv*) attaching the studs to the external insulation layer using fixings with low thermal conductivity; (*v*) attaching the insulation layers to the overall width, at the joints of building elements; (*vi*) installing doors and windows in contact with the insulation layer.

Martins *et al.* [50] studied several strategies for the mitigation of thermal bridges and they presented the following guidelines: (*i*) introducing at least one-third of continuous thermal insulation; (*ii*) if the previous condition is verified, then some mitigation strategies could be very much reduced or even irrelevant (*e.g.*, male or female studs, thin rubber strips, fixing bolts instead of steel plate connections and slotted steel profiles, illustrated in Figure 2.91); (*iii*) when selecting or designing thermal profiles, choose the ones with a higher number of narrow slots since they are more efficient than the ones with larger slots; (*iv*) whenever possible, try to use two layers of perpendicular steel studs, avoiding trespassing the entire wall cross-section with two parallel steel profiles.

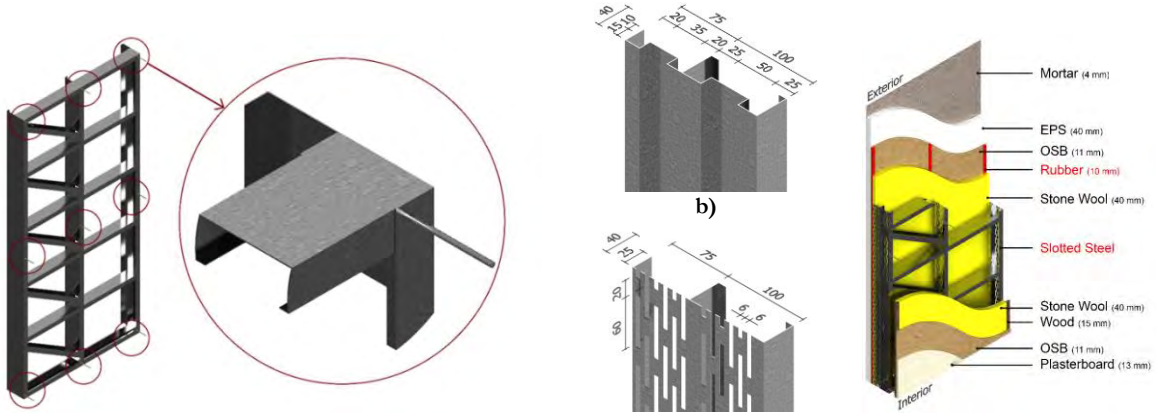

Figure 2.91 – Strategies for the mitigation of thermal bridges: a) fixing bolts instead of steel plate connections; b) male or female studs; c) slotted steel profiles; and d) thin rubber strips [50].

Kosny and Christian [240] also showed that the use of continuous external thermal insulation is an efficient way to improve the thermal performance of LSF walls. Moreover, they showed that increasing the space between the steel profiles allows increasing the thermal resistance of the walls. Höglund *et al.* [241] studied an efficient way to reduce the heat flux through the wall by increasing the heat flux path and decreasing the area of the steel profile (by inserting grooves in the profile web). A similar study was carried out by Blomberg and Claesson [242], who have also concluded that one of the most effective strategies to reduce heat flux is to use perforated steel profiles. The study showed that: (*i*) the thickness of a standard steel profile has to decrease sixfold to achieve the equivalent thermal properties of a metal profile with slots; (*ii*) the heat flux through a steel profile decreases as the number of slots increases.

Zalewski *et al.* [243] proposed a 3D numerical method for the assessment of the effect of thermal bridges in prefabricated lightweight building walls with a steel framework. The numerical method was validated using experimental results carried out in a controlled laboratory environment, as shown in Figure 2.92. In the first part of the study, the authors used IRT for the qualitative assessment of the thermal behaviour of the sample, *i.e.*, to visualise thermal bridges. Then, surface temperature measurements with thermocouples were compared with those provided by IRT to evaluate the evolution of the outside surface temperature during the experiment. In the second part of the study, the authors used local and non-destructive heat flux measurements to show the importance of thermal bridges in the thermal performance of the wall. In the end, the experimental results were used to validate the simulation model.

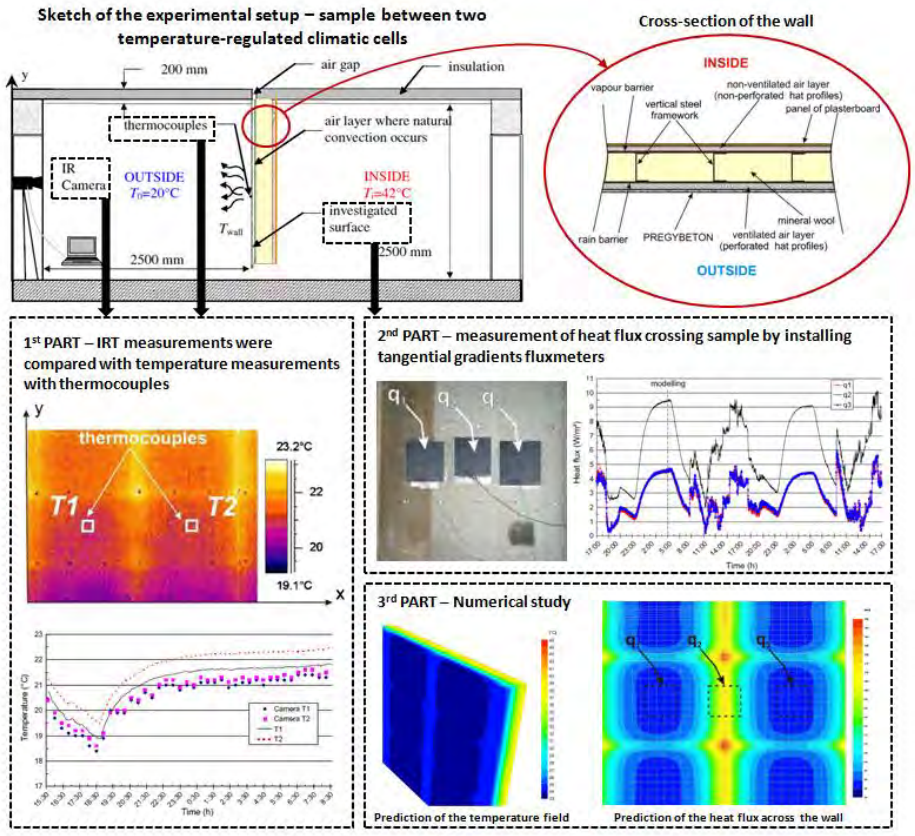

Figure 2.92 – Methodology proposed by Zalewski et al. [243] **for the experimental and numerical characterisation of thermal bridges in a prefabricated lightweight building wall with a steel framework** [244]**.**

Kosny *et al.* [237] used the CHB apparatus to measure the thermal performance of 23 steel-framed wall samples, considering a set of stud frame configurations, insulation sheathing and fiberglass batt insulations. The experimental results were compared to the R-value estimated using the parallel path method, the isothermal planes method and the ASHRAE zone method, showing that these methods do not adequately account for the 3D effects created by steel framing, often underestimating the R-value of the walls when insulation sheathing is used.

Mayer *et al.* [245] used the GHB apparatus to evaluate the thermal performance of different wall assemblies and to provide experimental results to validate a developed 3D finite-element analysis thermal modelling approach.

Other studies that have highlighted the potential of the GHB apparatus to estimate the overall thermal transmittance of LSF assemblies can be found in literature, for instance, the works carried out by Soret *et al.* [246] and Amundarain [247]. The IRT method described by O'Grady *et al.* [248] can also be used for the *U*-value measurement of LSF walls.

In a recent paper, Atsonios *et al.* [249] have proposed two new methods for the *in-situ* measurement of the overall thermal transmittance of existing cold frame LSF walls, which take into account the effect of thermal bridging due to the metal structure: the representative points method (RPM) and the weighted area method (WAM). The first method considers that the heat flow on specific points at the internal surface of the wall is always equal to the averaged heat flow of the whole surface. The WAM method is based on the zone method concept. According to the authors, the two methods comprise five general steps: (*i*) IRT of the internal surface of the wall; (*ii*) assessment of IR images to estimate the temperature profile; (*iii*) analysis of temperature profile according to each method; (*iv*) recording of outdoor/indoor air temperature and heat flux values at the locations which are indicated by each method; and (*v*) calculation of the overall thermal

transmittance of the wall. The methods were numerically validated for both cold frame and hybrid LSF walls and experimentally validated on a well-known cold frame LSF wall. The numerical results showed that the methods could be applied to both typologies of LSF walls. Moreover, the results based on the *in-situ* measurements were in good agreement with the theoretical results obtained according to ISO 10211 [27].

Li *et al.* [250] carried out an experimental and numerical study to evaluate the thermal performance of a lightweight steel-bamboo wall. A testing room was built using this new LSF assembly, and in-situ measurements were performed to determine the heat transfer coefficient, time lag and decrement factor of the wall. The behaviour of two commonly used walls was taken for comparison purposes: a reinforced concrete wall and an aerated concrete blocks wall. The experimental apparatus was a combination of the HFM and HB methods, in order to take advantage of the two methods and to overcome some of their drawbacks − the HFM should not be used in summer conditions; dynamic data analysis requires long-period measurements and complex calculations; the HB procedure is not suitable for in field measurements. Surface temperature sensors and heat flow meters were used to record internal and external surface temperatures and the average heat flux through the wall. These values were then used to estimate the *U*-value of the wall. The results showed that the steel-bamboo wall has a high thermal performance with an improvement of the *U*-value by up to 26.1-48.4 % in comparison to the other two walls.

For achieving better thermal performance in the lightweight construction system, many alternatives may be considered, e.g., other insulation systems, placing more insulation, or insulation materials with higher thermal performance. In the next subsections are presented new or non-conventional insulation materials and PCM-enhanced elements.

2.3.1. New or non-conventional insulation materials

The use of new and more efficient insulation materials can improve the thermal performance of construction elements, dealing with lower thicknesses of the insulation layers [236].

Aerogel insulation blankets may be seen as one of the most promising thermal insulation materials as they have a thermal conductivity 2 to 2.5 times lower than that of conventional mineral wool [251].

Lakatos [252] used different methods for the experimental evaluation of the thermal transmittance of walls with an opaque aerogel insulation layer. A Holometrix type HFM was used to measure the thermal conductivity of insulation materials with different thicknesses. Then, two different steady-state methods were used for measuring the thermal resistance of walls: the calibrated chamber method and heat flux measurements by Hukseflux apparatus. The authors have also used IRT to visualise the impact of adding aerogel. The results showed that by using a 0.013 m thick opaque aerogel insulation layer on a 0.25 m brick wall, the retardation time could be increased from 13 to 17 h.

Wakili *et al.* [253] evaluated the potential of aerogel for retrofitting purposes. The authors carried out *in-situ* measurement of the *U*-value of a retrofitted stone wall of a building situated in the city of Zurich, Switzerland, dating from 1877. IRT was also performed during the cold weather period when there was a large temperature difference between indoor and outdoor environments. The results showed that thin additional insolation layers could be added to the existing external wall to improve the overall thermal performance of the wall without changing the overall appearance of the building.

Walker and Pavía [254] evaluated the *in-situ* thermal performance of seven internal insulation alternatives on a historic brick wall with a traditional lime plaster finish, using heat flux sensors for *U*-value measurement, thermal imaging survey and internal wall temperature. The thermal insulation options evaluated were: aerogel, thermal paint, cork lime, hemp-lime, calcium silicate board, timber fiber board and PIR board. The

results showed that all these internal insulations could be used to reduce the *U*-value of the wall (between 34–61 %) except for thermal paint which had no effect. Aerogel also showed good potential for insulating historic structures as its thickness is almost half the other insulation materials, minimising the adverse visual impact of insulating historic buildings.

Another promising insulation technology is the use of vacuum insulation panels (VIPs), which have a thermal resistance 5 to 8 times higher than other conventional insulation materials [255].

In the study conducted by Ghazi Wakili *et al.* [256], the GHP method was used to determine the thermal conductivity at the centre-of-panel and the edge effect, *i.e.*, the linear thermal transmittance due to the thermal conductivity of the barrier envelope. The results showed that VIPs with a low perimeter-to-surface ratio have a lower effective thermal conductivity.

Nussbaumer, Ghazi Wakili, *et al.* [257] studied the behaviour of a system of VIPs embedded in an expanded polystyrene foam forming insulation boards mounted on a concrete wall. The thermal transmittance measurements were carried out using a GHB apparatus, and IRT was used as an inspecting tool to recognise damaged VIPs in winter conditions.

Capozzoli *et al.* [258] evaluated the equivalent thermal conductivity of VIPs and their performance degradation caused by vacuum loss. The guarded heat flux meter apparatus was used for the experiments.

Baldwin *et al.* [220] used a GHB apparatus to determine the effective thermal resistance of a wall assembly incorporating VIPs. The authors pointed out that this method allows a more accurate representation of all thermal bridges, including those between panels.

Mandilaras *et al.* [259] carried out a comparative study of conventional and VIP based ETICS utilizing both experimental and theoretical/numerical techniques. A mockup two-storey LSF building located in Athens, Greece, was considered in the experiments. A drywall construction envelope based on a cavity wall system incorporating ETICS was also considered. Two types of ETICS were installed on the walls of the mockup: a conventional system using EPS as insulation material and a VIP system incorporating a composite insulation component consisting of two layers of mineral wool and one layer of VIP. The results showed that the thermal resistance of the VIP wall was 123 % higher than the thermal resistance of the EPS wall. They also showed that there was a significant difference between the anticipated and the achieved thermal performance of the VIP ETICS as the *in-situ* measurements of thermal resistance were considerably lower than expected.

Some non-conventional insolation materials that show low environmental impact can also be found in the literature. Mavromatidis *et al.* [260] experimentally evaluated the thermal behaviour of two different multilayer fibrous insulations for building applications. A GHB apparatus was used to measure the heat transfer through the samples. Afterwards, the experimental results were used for numerical validation purposes.

Ye *et al.* [261] have also used a GHB apparatus to measure the thermal resistance of sheep-wool insulation and wool-hemp mixtures, both in the form of bonded insulation batts.

Shea *et al.* [262] claimed that the presentation of robust data regarding the main thermal properties of straw bales are very important for the development of projects employing this natural fiber insulation material. The authors carried out an experimental study to evaluate the thermal performance of an innovative prefabricated natural plant fiber building system. The FOX 800 HFM was used to evaluate the thermal conductivity of straw bales of different densities. The thermal transmittance of a prefabricated straw-bale panel was also evaluated using a GHB apparatus. In the end, an IRT survey was undertaken on a prototype straw-bale house to identify thermal anomalies, thermal bridging, air infiltration and other weaknesses in the building fabric.

In a recent paper, Lee *et al.* [263] provided an overall survey on reflective thermal insulation systems with radiant barriers and reflective insulations. The authors stated that although many studies have been carried out on reflective insulation, there are still uncertainties in predicting the correct thermal resistance improvement due to the application of these materials. For these authors, the most commonly used method to measure the thermal resistance value is the GHB apparatus, which can simulate large-scale assemblies that are closer to real conditions. The HFM method can be used to test smaller specimens.

Escudero *et al.* [264] carried out an experimental study to evaluate the thermal resistance of radiant barriers for building insulation. The HFM method was used to characterize the insulation layer itself, while the GHB was used to determine the total thermal resistance of a building component, including a radiant barrier.

2.3.2. PCM-enhanced elements

PCMs undergo melting and solidification at a nearly constant temperature, becoming very suitable for thermal management and thermal energy storage applications. As reviewed by. Soares *et al.* [265], a vast number of studies have been developed to improve the thermal performance of building envelope solutions by including PCMs in their configurations. However, the prediction and measurement of the overall thermal transmittance of non-homogeneous assemblies incorporating PCMs is still very challenging. This is mainly caused by the intrinsic physics of these materials (namely the variation of the main thermophysical properties with temperature), and the non-linear nature of the phenomenon, *i.e.*, the presence of different stages during a complete phase change cycle − solid, liquid and mushy zone phases.

The experimental methods to measure the *U*-value of construction elements are typically based on reaching steady-state conditions. Therefore, the overall thermal transmittance of construction elements with PCMs cannot be measured during phase change processes, as heat is absorbed or released by the PCM (the material acts like an "energy source" or an "energy sink"). It can only be measured somehow when the PCM is completely melted or solidified. At these stages, PCMs can be treated as "normal" materials, with known thermophysical properties. The development of experimental approaches and standard procedures to measure the overall thermal transmittance of real-scale PCM-enhanced elements in conditions similar to those experimented in real buildings is exceptionally challenging, and it can be seen as a hot research area for the next decade.

As pointed out by Cabeza *et al.* [266], the appropriate characterisation of the PCM itself is essential to foster the technology. However, it is not always possible to carry it out with conventional equipment, mainly due to the size of the samples. In this context, the authors provided an extensive survey on the main unconventional, experimental technologies available for the characterisation of the main thermophysical properties of PCMs.

Dutil *et al.* [267] have also highlighted the importance of the characterisation of PCMs for model validation purposes. Also, they stated that it is unclear whether the measurements of the thermophysical properties of PCMs done on small samples are representative of the macroscopic thermal behaviour of the final building application. Several studies have been carried out to evaluate the thermal performance of PCM-enhanced elements by considering different scales of the samples. For instance, a transient GHP method based on heat flux and temperature measurements were used by Lachheb *et al.* [268] for the experimental assessment of the thermal behaviour of a plaster composite containing a microencapsulated PCM.

Amaral *et al.* [269] evaluated the thermal conductivity of rigid polyurethane (RPU) foams, with and without PCMs, based on steady-state and transient methods (Figure 2.93). Three different approaches were used: the transient plane source approach (small-scale specimen), the guarded hot plate (middle-scale specimen), and the heat flux meter method in an HB setup (large-scale specimen).

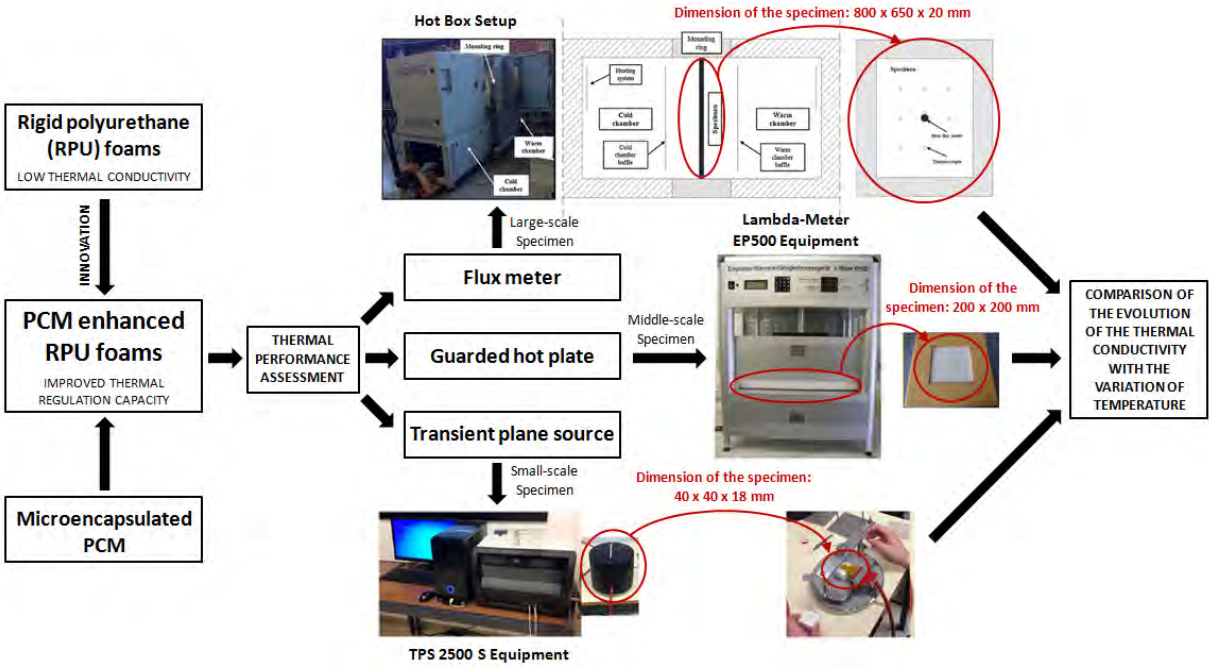

Figure 2.93 – Methodology proposed by Amaral et al. [269] **for the experimental evaluation of the thermal conductivity of RPU foams with and without the incorporation of PCMs based on steady-state and transient methods** [244].

Shukla *et al.* [270] proposed a novel dynamic HFM apparatus to measure the dynamic thermal properties of a PCM impregnated gypsum board. The results were later compared to those obtained through differential scanning calorimeter (DSC) measurements.

Kosny *et al.* [271] have also used a dynamic HFM apparatus for the thermal performance analysis of fiber insulations containing bio-based PCMs. Additionally, an HFM apparatus operating in dynamic mode was used by Mandilaras *et al.* [272] for the determination of the effective heat capacity of PCM-enhanced building components.

Finally, Principi and Fioretti [273] carried out an experimental study based on the HFM method to evaluate the improvement of the thermal performance of hollow bricks through the insertion of a PCM inside the enclosures of the bricks.

Silva *et al.* [274] and Vicente and Silva [275] have also experimentally evaluated the thermal behaviour of PCM-enhanced brick masonry walls.

Few studies using the HB method for measuring the thermal performance of PCM-enhanced assemblies are found in the literature. Indeed, further work has to be developed in the future to establish reliable dynamic methods to measure the overall thermal transmittance of non-homogeneous assemblies with PCMs. In the literature, there is also a lack of reliable large-scale experimental results that can be used for validating numerical simulation approaches.

Figure 2.94 shows a sketch of the methodology proposed by Cao *et al.* [207] to evaluate the impact of a PCM-enhanced wall on the indoor air and wall temperature using the GHB apparatus. The results showed that the inclusion of the PCM layer in the wall reduces the interior air and wall temperatures up to 2° C in comparison to the wall without PCM.

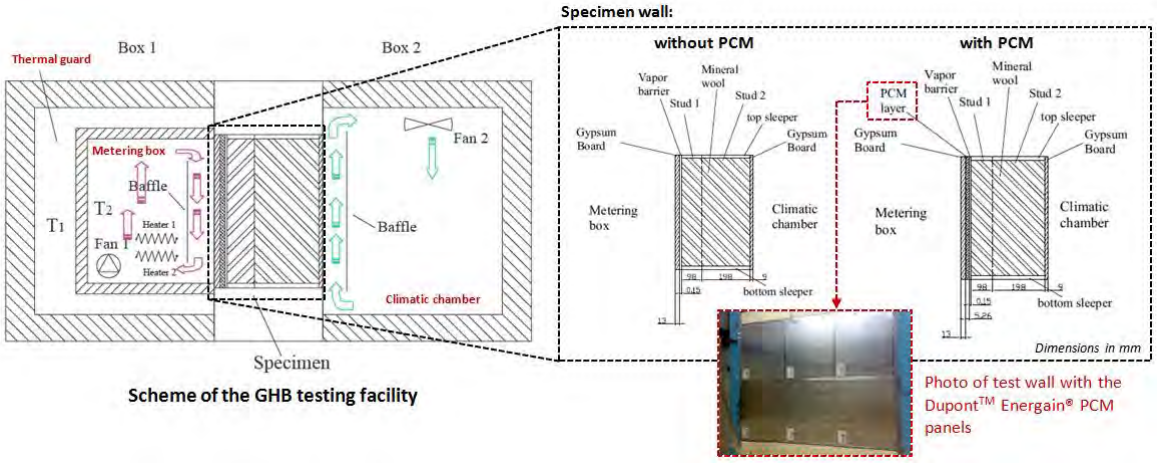

Figure 2.94 – Methodology proposed by Cao et al. [207] **to evaluate the impact of a PCM-enhanced wall on the indoor air and wall temperature using the GHB apparatus** [244]**.**

3. HOT BOX APPARATUS: DESIGN PRINCIPLES AND REQUIREMENTS, AND TEST PROCEDURE

3.1. INTRODUCTION

The determination of the thermal transmission properties with hot box (HB) methodology of large building elements such as parts or sections of walls, roofs, floors, is a complex combination of conduction, convection and radiation. The HB methods measure the total quantity of heat transferred on the specimen from one side to the other, for a specific temperature difference, regardless of the individual modes of heat transfer, and the test results can, therefore, be applied to situations when that is the property required [17].

The HB method is primarily intended for laboratory measurements of large and inhomogeneous specimens. Although homogeneous specimens can also be tested, and these can provide the calibration and validation of the apparatus. ISO 8990 [17] considers that when testing homogeneous elements, it is expected to reach an accuracy of ± 5 %.

The design and operation of the guarded or calibrated hot box is a complex subject and must be noted that the thermal transmission properties of a specimen depend on; (*i*) itself; (*ii*) boundary conditions; (*iii*) specimen dimensions; (*iv*) direction of heat transfer; (*v*) temperature differences; (*vi*) air velocities; and (*vii*) relative humidity. It is also essential that conditions replicate the conditions for those is intended the application of the element. Otherwise, the result will be inaccurate.

There are many different designs of the calibrated and the guarded hot box existing worldwide, depending on structures to be tested and requirements for test conditions. In consequence, there are several arrangements of apparatus, being not practical to mandate a specific size or design of apparatus.

In order to determine suitable design principles and requirements for constructing a hot box apparatus, in the next sections are reviewed the following standards: (*i*) ISO 8990:1994 [17]; (*ii*) ASTM C1363-11 [18]; (*iii*) GOST 26602.1-99 [209] and GOST 26254-84 [276]; (*iv*) BS 874-3.1:1987 [277]; and (*v*) BS 874-3.2:1990 [87].

Although the ISO 8990 [17] is the last revision, being the more recently published standard that replaces the BS 874-3.1 [277] and BS 874-3.2 [87], it is less specific as it by combining the two parts of standard 874 into a summary document. Due to the higher amount of detail and specifications, are also used these standards in this work.

This chapter presents the design principles and requirements for both types of the GHB and CHB apparatus, to achieve a combination of specifications that will allow the design of an HB apparatus that can have both configurations and that is in accordance with all the above-mentioned standards.

The chapter is divided into two groups, passive components and active components. The passive components are: (*i*) the chambers of the apparatus, namely the guard, metering and cold boxes; (*ii*) the specimen frame; and (*iii*) the baffles. The active components are meant to describe: (*i*) air circulation, heating and refrigeration system; (*ii*) measurement of temperatures, heat flow, air velocity, pressure and power; (*iii*) control; and (*iv*) data logging system.

3.2. REQUIREMENTS OF PASSIVE COMPONENTS

This section establishes the principles for the design of the passive components of both types of HB apparatus and the minimum requirements for thermal performance determination of building assemblies under controlled laboratory conditions.

The GHB, illustrated in Figure 3.1a and Figure 3.2a, comprises five passive components, namely: (*i*) guard box; (*ii*)metering box; (*iii*) specimen frame; (*iv*) cold box; and (*v*) baffles. The CHB has one less component, the small chamber that exists inside of the GHB. It comprises four passive components, namely: (*i*)metering box; (*ii*) specimen frame; (*iii*) cold box; and (*iv*) baffles; as shown in Figure 3.1b and Figure 3.2b.

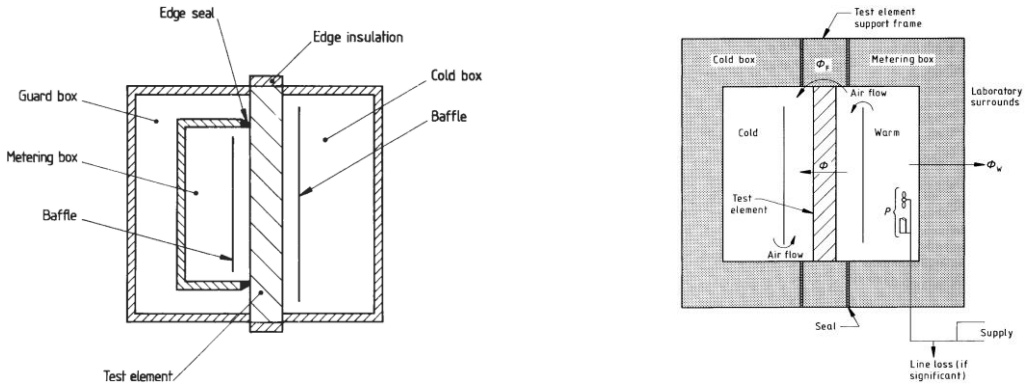

a) **b)**

Figure 3.1 – Sketch of a typical: a) GHB BS 874-3.1 [277]**; b) CHB BS 874-3.2** [87]**.**

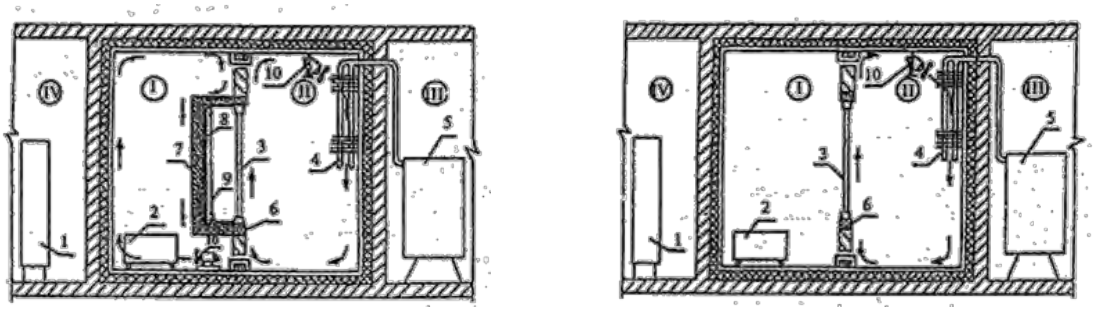

a) **b)**

Figure 3.2 – GOST 26602.1-99 schematic of a typical: a) GHB; b) CHB [209]**.**

3.2.1. Guard box

The guard hot box has the purpose of establishing air temperature and surface coefficients around the metering box and heat flow through the metering box walls, and imbalance heat flow in the surface of the specimen from metered to guard area is minimised. The guard box is a GHB component that does not exist in CHB, as illustrated in Figure 3.1.

Next, are presented the requirements for the guard box obtained from each standard:

I. ISO 8990 (1994):

i) For the homogeneous specimens with maximum expected resistance and thickness, which for the apparatus is design, the peripheral heat loss predicted error on specimen should be smaller than 0.5 %. To avoid this shall have a correct relationship between the metering area size and the guard area size and edge insulation. From standard subsection (FSS) 2.4;

ii) The apparatus shall be designed and operated in such a way as to obtain optimum heat flow balance, the apparatus geometry and guard air space and airflow speed, so that heat flow through the metering box walls does not exceed 10 % of total power input (FSS 1.6.1.1).

II. ASTM C1363-11 (2011):

i) The overall apparatus sized shall match the test specimens type intended to be tested (FSS 6.3);

ii) For building assemblies, it shall have appropriated size to accommodate representative sections (FSS 6.3).

iii) BS 874-3.1 (1987):

iv) The width of the guard space, measured between outside metering box walls and inside guard box walls, is dependent upon the thickness of the test element and upon the insulation, if any, around the outer edges of the test element. If the test specimen outer edges are insulated with the material thermal resistance of at least 1 m^2.K/W, then the guard space shall be at least as wide as the thickness of the test element (FSS 4.3.3);

v) If the test element edges are uninsulated then the guard space width shall be at least 1.5 times the thickness of the test specimen (FSS 4.3.3);

vi) In no case any part of the guard space be less than 150 mm wide (FSS 4.3.3);

vii) The previous requirements are based upon the assumption that the laboratory temperature during the tests, is always between the metering and cold boxes temperatures. If is not, then additional insulation of thermal resistance of at least 1 m^2.K/W shall be required on the test element edges (FSS 4.3.3);

viii) To achieve accurate results the guard space environment needs to be as similar as possible to that in the metering box (FSS 4.3.6);

ix) Internal surfaces in direct radiation exchange with the test element surface shall be matt black (FSS 4.3.6);

x) It is advantageous to have insulation in the guard box walls, to reduce the heat exchange by radiation between the metering box outer surfaces and the guard box inner surfaces and to make the two surface temperatures closer to one another (FSS 4.3.6);

xi) An air-tight seal between the guard box and the test element surface shall be placed. Usually is satisfactory a compressible foam rubber in conjunction with a clamping device (FSS 4.3.6).

3.2.2. Metering box

The metering area is defined: (*i*) for a GHB can assume two areas, if the specimen is thicker or equal to the nose width, then is the area measured from centre-nose to centre-nose, or if the specimen is thinner than

the nose width, as the inner periphery of the nose; (*ii*) for a CHB, as the inner periphery of the metering box [17].

Next, are presented the requirements for the metering box prescribed by each standard:

I. ISO 8990 (1994):

i) The minimum size of the metered area: (i) for GHB is 3 times specimen thickness or 1 by 1 m^2, whichever is the higher; (ii) For the CHB, minimum specimen size is 1.5 m by 1.5 m^2 (FSS 1.6.1.2);
ii) The HB methods of measurement errors in testing are partial related to the length of the metering area perimeter. The relative influence diminishes as the metering area is increased (FSS 1.6.1.2);
iii) To provide a representative test area the metered area shall be big enough (FSS 2.2);
iv) For modular components the metered area should, if possible, span exactly an integral number of modules (FSS 2.2);
v) The depth of the metering box should not be greater than that strictly essential to preserve desired boundary conditions and to accommodate equipment (FSS 2.2);
vi) The box wall insulation shall be chosen considering the intended range of specimen resistance and temperature difference, so that, an error in the metering box losses assessment does not affect the specimen heat flow determination by more than 0.5 % (FSS 2.3.1);
vii) The metering box walls shall be thermally uniform (FSS 2.3.1);
viii) The box walls can be made from panels of suitable insulating material, e.g. a sandwich with a core of cellular plastic and a suitable facing (FSS 2.3.1);
ix) The box walls perimeter seal and specimen shall form an air- and water-vapour-tight enclosure to avoid error due to air and moisture transfer (FSS 2.3.1);
x) In GHB the metering box is held against the specimen to provide an airtight joint. The width of the gasket on the nose of the box shall not exceed 2 % of the metering width or 20 mm (FSS 2.3.1);
xi) Hot spots, e.g. heaters, fans, etc., can disturb the uniformity of the temperatures inside the box, due to their local radiative exchanges with the box walls (FSS 2.3.1).

II. ASTM C1363-11 (2011):

i) For CHB minimum metering area size is 1.5 m^2, which is less than the required by ISO 8990 (2.25 m^2) (FSS 6.5.1);
ii) The metering box wall must be as low as 1 or 2 % of the heat transfer through the specimen. The metering box wall loss shall never be more significant than 10 % of the specimen heat transfer. In any case, the minimum metering chamber walls thermal resistance shall be greater than 0.83 m^2.K/W (FSS 6.5.3.2);
iii) Structural members with highly conductivity shall not be within the insulation (FSS 6.5.3.4.

III. BS 874-3.1 (1987) and BS 874-3.2 (1990):

i) A sandwich construction of two metal or plywood skins with insulating material between them has been found satisfactory for the wall of the metering. From BS 874-3.1 (1987) subsection 4.2 and BS 874-3.2 (1990) subsection 4.2.1;
ii) All surfaces in the metering box that can radiate to the surface of the test element shall be of matt black finish and shall have an emissivity of at least 0.9. From BS 874-3.1 (1987) subsection 4.2 and BS 874-3.2 (1990) subsection 4.2.1;
iii) Recommended a minimum thermal resistance of the walls of 1 m^2.K/W for the metering box of the GHB. BS 874-3.1 (1987) subsection 4.2;
iv) Recommended a minimum thermal resistance of the walls of 2.5 m^2.K/W for the metering box of the CHB. BS 874-3.2 (1990) subsection 4.2.1.

IV. GOST 26254-84 (1984):

The length and width of the test fragment of the enclosing structure shall not be less than four times its thickness and be not less than 1500 by 1000 mm (FSS 2.2.

3.2.3. Specimen frame

The specimen frame as the functional purpose of positioning and providing support to the specimen, and ensure peripheral insulation. There must be a compromise between load-carrying capacity and high thermal resistance.

In the CHB apparatus, the specimen frame is a critical component due to the heat flanking losses, which should be kept at a minimum for achieving higher accuracy.

Next, are presented the requirements for the specimen frame prescribed by each standard:

I. ISO 8990 (1994):

i) The facing towards the specimen should have a low thermal transmission. Figure 3.3 illustrates the heat flow path in the specimen and frame and isothermal lines (FSS 2.5);
ii) In GHB typical configuration, the specimen frame is neglected, and edge insulation minimises the lateral heat flow (FSS 2.5);
iii) Specimen frame must minimise lateral heat flow (FSS 2.5);
iv) For the CHB, the specimen frame is a critical component due to the flanking losses, which for high accuracy, should be kept at a minimum (FSS 2.5).

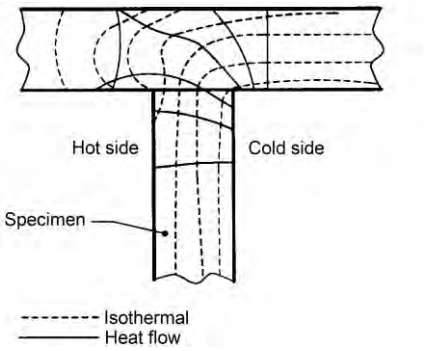

Figure 3.3 – Heat flow path in specimen and frame [17].

II. ASTM C1363-11 (2011):

i) The frame opening must have at least the metering box opening dimensions (FSS 6.7.1;
ii) In the direction of heat flow, the frame shall be at least as thick as the thickest of the specimen (FSS 6.7.1);
iii) In the outward direction perpendicular to the normal energy flow direction, the specimen frame wall thickness shall be at least equal to that of the metering chamber walls or 100 mm, either is greater (FSS 6.7.1);
iv) Must be taken care in the design and construction of specimen frames so that flanking losses are minimised (FSS 6.7.2);
v) Flanking paths should not have conductive plates, fasteners or structural members (FSS 6.7.2);
vi) Must limit the thickness and conductance of the wall skin, to minimize the flanking loss potential (FSS 6.7.2).

III. BS 874-3.2 (1990):

i) Consideration shall be given to providing a well-insulated support frame to house the test element (FSS 4.4.2);

ii) The support frame should not be narrower than the thickest test specimen (FSS 4.4.2);

iii) For CHB is recommended that the thermal resistance of the support frame insulation around the test area edges be at least 2.5 m^2.K/W (FSS 4.4.2);

iv) It is more convenient for the metering box, cold box, and test element support frame to have nominally the same cross-sectional dimensions and insulation properties (FSS 4.4.2).

3.2.4. Cold Box

The purpose of the cold box is to provide controlled conditions on the side of the test specimen opposite to the metering chamber. In the usual arrangement, it is a five-sided insulated chamber with internal dimensions matching or higher than the metering chamber opening and with enough depth to contain the equipments.

The cold box requirements expressed in each standard are:

I. ISO 8990 (1994):

i) The size of the cold box is ruled by the size of the metering box in the case of the CHB, or the guard box in the case of the GHB (FSS 2.6);

ii) The chamber walls should be constructed to prevent moisture condensation and reduce the load of the refrigeration equipment (FSS 2.6);

iii) The chamber inside surfaces shall have an emittance by the desired radiative heat exchange, being the same as for the metering box (FSS 2.6).

II. ASTM C1363-11 (2011):

i) An acceptable alternative to the cold box is to utilise a large environmental chamber with an opening identical to the open size of the metering box. Being especially suitable for testing floors or ceilings, due to the large dimensions of these structures (FSS 6.6.1);

ii) The internal surfaces of the climatic chamber shall also meet the criteria of emittance, identical to the other chambers (FSS 6.6.3).

III. BS 874-3.1 (1987) and BS 874-3.2 (1990):

The cold box height and width should not be less than the guard box corresponding dimensions, for the GHB (FSS 4.4);

Between the cold box and test specimen should be an air-tight seal (FSS 4.4).

3.3. REQUIREMENTS OF ACTIVE COMPONENTS

3.3.1. Baffles

Baffles are used to create a parallel flow of air to the specimen surface, by confining the air and creating a uniform channel, thus aiding in maintaining an air curtain with uniform velocity. It is recommended that a baffle is positioned in the metering box and cold box, parallel to the surface of the specimen when forced convection is used.

The requirements for the baffles expressed in each standard are:

I. ISO 8990 (1994):

i) In the metering box when use forced convection is recommended position the baffle parallel to the surface of the specimen (FSS 2.3.2);
ii) The metering and cold box baffles should extend to the full width and have gaps at each end to allow air circulation (FSS 2.3.2);
iii) The baffle may be moveable, perpendicular to its surface, to allowing adjust the air velocity (FSS 2.3.2);
iv) The baffle can also be necessary to shield test specimen surfaces when using natural convection that may occur originated from radiative heat transfer of heaters (FSS 2.3.2);
v) The emissivity of surfaces also applies to the baffle (FSS 2.3.2);
vi) For testing specimens in a vertical position, the circulation resulting from natural convection can be enough to ensure temperature uniformity and the desired surface coefficients. In this case, the distance between specimen and baffle should be larger than the boundary layer thickness or should not be used a baffle (FSS 2.3.2).

II. ASTM C1363-11 (2011):

i) For maintaining a well-mixed and characterised the air curtain, the baffle-to-specimen spacing may provide an adjustable distance and is recommended to have a spacing of 150 to 200 mm (FSS 6.8.9.2);
ii) A baffle thermal resistance of 1 m^2.K/W is recommended (FSS 6.8.9.1);
iii) The baffle surface facing the specimen shall have an emittance greater than 0.8 (FSS 6.8.9.3).

III. BS 874-3.1 (1987) and BS 874-3.2 (1990):

i) For natural convection conditions the distance between the baffle and the test element shall be not less than 150 mm (FSS 4.2);
ii) For higher airspeeds imposed by fans is permitted to reduce the distance between the baffle and the test element, to a minimum of 40 mm for 3 m/s air velocity or greater (FSS 4.2).

3.3.2. Fans

The fans have the purpose of assisting the control of air velocity and reducing the air temperature gradient across the different chambers.

Next, are presented the requirements for the fans expressed in each standard:

I. ISO 8990 (1994):

i) Motors, fans, evaporators and heaters shall be radiation-shielded (FSS 2.6);
ii) Air velocities should be adjustable to meet the test required surface coefficients (FSS 2.6);
iii) For simulating natural conditions at building components, the fans can have a range from 0.1 m/s to 10 m/s (FSS 2.6);
iv) Airflow direction corresponding to natural convection is suggested (FSS 2.6).

II. ASTM C1363-11 (2011):

i) The commonly used velocities to simulate parallel or perpendicular wind conditions on the exterior side are 2.75 m/s for summer conditions and 5.5 m/s for winter conditions (FSS 6.8.8);
ii) Fans are required to maintain air movement in the direction of natural convection, being recommended down direction on the hot side and up on the cold side (FSS 6.8.7).

III. BS 874-3.2 (1990):

The direction of airflow in an HB apparatus is determined by the test design and can be: parallel, that is up or down; or horizontal, that is perpendicular to surface (FSS 4.2.1).

3.3.3. Heating elements

The heating elements are recommended to be installed in the three boxes.

The requirements for the heating elements expressed in each standard are:

I. ISO 8990 (1994):

i) Heat supply and air circulation shall be such that variations in air temperature across the airflow parallel to the specimen surface shall not exceed 2 % of the air-to-air temperature difference from hot to cold side (FSS 2.3.2);
ii) Any air temperature gradients along the airflow shall not exceed 2 K/m, measured outside the boundary layer on a homogeneous test specimen (FSS 2.3.2);
iii) Electric resistance heaters are normally the most suitable, and they shall be shielded by insulated reflective shields, to minimise radiation in chambers walls and the specimen (FSS 2.3.2).

II. ASTM C1363-11 (2011):

i) The methods for providing heated air can be to install open wire, low thermal mass electrical heaters in an insulated, low emittance section of the blower duct or another part of the air circulation system (FSS 6.9.2);
ii) Another method of heater control is to use several individual heaters (FSS 6.9.2);
iii) Another satisfactory method is to use a controller that varies the power to all the heaters (FSS 6.9.2).

3.3.4. Cooling elements

The cooling system is needed mainly in the cold chamber but is also recommended in guard and metering boxes to achieve a stable set point quickly. For cooling the chambers is usually used an operating refrigeration system.

In guard box, an alternative for cooling the space can be done by creating a system that allows inserting controlled mixing of air from the laboratory to the guard place. The drawback is the change of the pressure in the guard box.

Next, are presented the requirements for the cooling elements expressed in each standard:

I. ASTM C1363-11 (2011):

i) When cooling of the metering chamber is necessary measured accurately the heat extracted amount. One way to cool the metering chamber is to circulate a chilled liquid through a heat exchanger located in the air circuit (FSS 6.9.5);
ii) The amount of cooling used in the metering box must be the minimum necessary to overcome any excess of heating loads. Too much cooling will compromise test accuracy, which will be lost if excessive heating is used to compensate for large cooling (FSS 6.9.5);
iii) To avoid heat flow variations in the specimen caused by humidity control-moisture migration, condensation, and freezing, the warm side relative humidity shall be kept below 15 %. Also, the laboratory must verify that the dew point temperature of the metering side air is 2° C less than the minimum metering side surface temperature of the specimen (FSS 6.9.6).

II. BS 874-3.1 (1987) and BS 874-3.2 (1990):

i) Suitable shielding must prevent direct radiation exchange between any cooling element in the cold box and the surface of the test element (FSS 4.4);

ii) If the cold box is to be operated at temperatures approaching or below 0° C, then consideration shall be given to potential problems of condensation and icing (FSS 4.4).

3.3.5. Temperature measurements

The specimen thermal resistances or thermal transmittances are a function of temperature differences across the specimen itself, the reason why care shall be taken in these measurements.

Next are presented the overall requirements for the temperatures measurements expressed in each standard, which are schematically presented in Figure 3.4.

I. ISO 8990 (1994):

i) The sensors for the measurement of air temperature and specimen surface temperature, if possible, should be consistently spaced over the specimen area and located opposite each other on the hot and cold side (FSS 2.7);

ii) Surface temperatures of the equipment "seen" by the specimen, e.g. in baffles surface temperatures sensors, should be used for calculating the mean radiant temperature (FSS 2.7);

iii) The number of sensors for air temperature and surface temperature measurement must be: (i) at least two per square metre; (ii) and not less than nine (FSS 2.7);

iv) Air and surface temperature differences over the specimen and surface temperature differences over the metering box walls can be determined by differential measurement to improve accuracy (FSS 2.7);

v) Temperature differences shall be measured with an accuracy of ± 1 % of air-to-air temperature difference from hot to cold side (FSS 2.8);

vi) It is recommended that the measuring instrument not add uncertainties greater than 0.05 K (FSS 2.8);

vii) Absolute temperature measurement shall be made with an accuracy of ± 5 % of the air-to-air temperature difference (FSS 2.8);

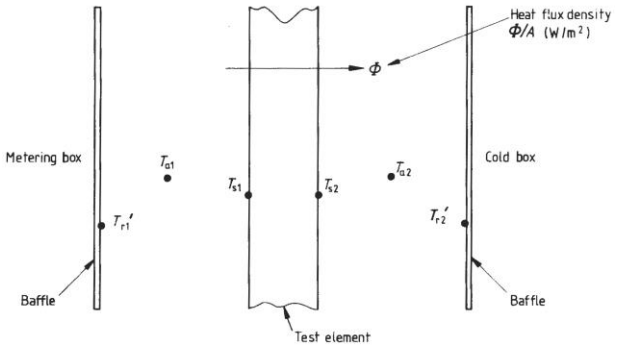

Figure 3.4– Temperature measuring positions on each side of the metering area of the test element [277].

II. ASTM C1363-11 (2011):

i) Is recommended thermocouples with: (i) the wire is no larger in diameter than 0.25 mm; (ii) the wire meets, or is calibrated to, the special limits of error as specified in the ASTM E230 Specification and Temperature-Electromotive Force; (iii) the junctions, not larger than two times the wire

diameter, are twisted and welded or soldered; (iv) 10 mm of adjoining wire is taped, cemented or otherwise held in thermal contact with the surface using materials of emittance close, ± 0.05, to that of the surface; and (v) electrically insulated, or otherwise protected, so that the electrical junction is at the location of the thermocouple bead (FSS 6.10.1);

ii) Metal foil tape painted to make the emittance greater than to 0.80, is an effective means to attach thermocouple sensors to test specimens (FSS 6.10.1).

III. BS 874-3.1 (1987) and BS 874-3.2 (1990):

i) For the measurement of thermal conductance, the mean surface temperature over the metering area on each face of the test element is required (FSS 4.5.1);

ii) Measurement of thermal transmittance requires that air and mean radiant temperatures are measured in the hot and cold boxes, so that the two environmental temperatures may be calculated (FSS 4.5.1);

iii) Thermocouples generally are the most commonly used thermometers for this test method, but the use of other suitable thermometers is not excluded (FSS 4.5.1);

iv) Thermocouples shall be made from a stock of calibrated wire or wire which has been certified by the supplier to comply with BS 4937 to a tolerance of ± 0.4 %. Otherwise, individual thermocouple calibration shall be required (FSS 4.5.1);

v) A potentiometer or digital voltmeter with a resolution of 1 μV or better shall be used to measure the output from the thermocouples (FSS 4.5.1);

vi) The uncertainty in the measurement of the temperature difference between the hot and cold faces of the test element at a point shall not exceed ± 1 % of the temperature difference (FSS 4.5.1);

vii) The uncertainty in the measurement of the voltage output from a thermopile shall not exceed ± 4 μV (FSS 4.5.1).

3.3.5.1. Specimen

Next, are presented the specimen surface temperature sensors requirements, for the temperatures measurements expressed in each standard:

I. ISO 8990 (1994):

i) The temperatures sensors shall choose and applied to the surface in such a way that not change the temperature at the measuring point (FSS 2.7.1);

ii) For fulfilling the previous requirement, can be used thermocouples of wire with less 0.25 mm of diameter, with junctions and adjoining wire of at least 100 mm in thermal contact with the surface, along with the most isothermal path, using cement or tape of emissivity close to that of the surface (FSS 2.7.1);

iii) For nonhomogeneous specimens, the sensors indicated number would not ensure reliable mean surface temperatures (FSS 2.7.1);

iv) For moderately inhomogeneous specimens, additional sensors must be applied to each region of varying temperature. The mean surface temperature of each region shall then be weighted proportionally to the area of that region to obtain the mean surface temperature of the specimen (FSS 2.7.1);

v) For very inhomogeneous specimens, the specimen thermal resistance, cannot be measured. The thermal transmittance can be determinate based on the environmental temperature difference across the specimen (FSS 2.7.1);

vi) As a guideline, if surface temperature caused by inhomogeneities exceeds 20 % of the mean surface-to-surface temperature difference, should be taken as a very inhomogeneous specimen (FSS 2.7.1).

II. ASTM C1363-11 (2011):

Temperature sensors after placed shall not affect the temperature within ± 0.2 K of the reading surface as if the sensor had not been applied (FSS 6.10.1).

III. BS 874-3.1 (1987) and BS 874-3.2 (1990):

i) For homogeneous test elements, there shall be a minimum of nine on each face, uniformly distributed over the test area, illustrated in Figure 3.5 (FSS 4.5.2);

ii) For large test areas, this number shall be increased as necessary such that there is at least one thermocouple per 0.5 m² of the test area (FSS 4.5.2).

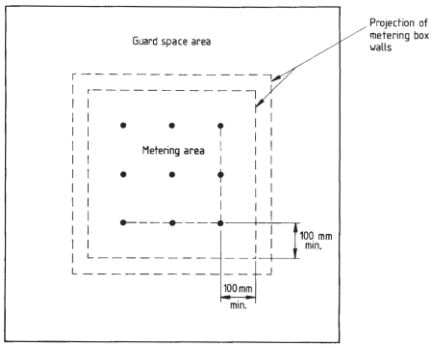

Figure 3.5 – Placement of thermocouples for assessment of specimen surface temperature [277].

3.3.5.2. Air temperature

Next, are presented the air temperature sensors requirements for the chambers ambient temperatures measurements expressed in each standard:

I. ISO 8990 (1994):

i) Air temperature sensors must be radiation-shielded. This requirement can be dismissed if shown that the difference between shielded and unshielded, fulfil accuracy requirements (FSS 2.7.2);

ii) In natural convection, temperature sensors shall be placed outside the boundary layer, and its thickness is a few centimetres in most cases (FSS 2.7.2);

iii) In turbulent flow, the boundary layer thickness can exceed 0.1 m (FSS 2.7.2);

iv) In forced convection, turbulent fully developed flow, sensors shall be placed between the specimen and the baffle to detect bulk air temperatures (FSS 2.7.2).

II. ASTM C1363-11 (2011):

i) The minimum number and locations of sensors used to measure air temperatures shall be that specified for surface temperature sensors (FSS 6.10.3.1);

ii) Sensors shall be small to ensure a fast response to changing temperatures (FSS 6.10.3.1);

iii) The sensors shall be radiation shielded, is a solution for a suitable radiation shield the use of a 12 mm diameter, 75 mm long pieces of thin-walled plastic tubing covered on the outside with aluminium foil tape. The air thermocouple is placed at the centre of the tube to measure the air stream temperature and yet be shielded from radiation sources (FSS 6.10.3.1);

iv) For uniform test results, the maximum point to point air temperature variation across the test specimen, perpendicular to the airflow direction at the centre of the test panels, shall be less than 2 % of the overall air to air temperature difference, or 2 K, whichever is higher (FSS 6.8.6);

v) Thermocouple sensors used for measurement of air temperatures shall meet the requirements expressed for specimen surface temperatures (FSS 6.10.3.3);

vi) The sensors measurements accuracy must be within the range of ± 0.5 K (FSS 6.10.3.3).

III. BS 874-3.1 (1987) and BS 874-3.2 (1990):

i) For the measurement of air temperatures in the metering and cold boxes there shall be a minimum of nine thermocouples in the air spaces on each of the test elements, uniformly distributed in relation to the test area (FSS 4.5.3);

ii) For large test areas, this number shall be increased as necessary such that there is at least one thermocouple per 0.5 m² of the adjacent test area (FSS 4.5.3).

3.3.5.3. Baffles

The temperature of the baffle surfaces, recorded by various thermocouples, is used to deduce the radiation being transmitted to the test element. Next, are presented the baffles surface temperature sensors requirements for the temperatures measurements expressed in each standard:

I. ASTM C1363-11 (2011):

i) The surface temperature of the baffles in the metering and climatic chambers shall be measured by placing sensors on all surfaces seen by the specimen (FSS 6.10.4);

ii) Shall have a minimum area density of three sensors per square meter of baffle area, but not less than one sensor per baffle surface is required (FSS 6.10.4).

i) The data measured by baffle temperature sensors: (*i*) can be used to determine any difference between the baff1e surface and air curtain temperatures; (*ii*) permits corrections to be made to the radiation component of the surface film conductance due to differences in these temperatures; and (*iii*) is a necessary component of the data analysis for specimens such as windows which have a high thermal conductance (FSS 6.10.4).

II. BS 874-3.1 (1987) and BS 874-3.2 (1990):

For the measurement of mean radiant temperatures of surfaces "seen" by the test element in metering and cold boxes, there shall be a minimum of nine thermocouples, appropriately distributed on each surface to take account of its relative radiant influence on the test element (FSS 4.5.2).

3.3.6. Measuring the heat flow

The metering box walls can be used as heat flow transducers by application of many differential thermocouples, connected between the inside and outside surfaces, being this sensor called a thermopile. In GHB must be also be used a secondary thermopile in the zone of the metering box perimeter seal on the surface of the test element. Next, are presented the thermopiles requirements obtained from each standard.

3.3.6.1. Metering box walls

I. ISO 8990 (1994):

i) The heat flow in the walls of the metering box can be monitoring with thermopiles, an arrangement of surface temperature sensors that shall have at least one pair of junctions per 0.25 m² surface. This if the box walls density heat flow rate is uniform (FSS 2.7.3);

ii) A higher number of junctions can be necessary to obtain the required accuracy if there is the presence of heaters or fans, which can affect the uniformity owing to their local radiative exchanges with the box walls (FSS 2.7.3).

II. ASTM C1363-11 (2011):

i) In the metering box walls shall be used a minimum of five differential thermocouple pairs per square meter (FSS 6.5.4.1);

ii) The thermocouple junctions shall be located directly opposite each other and, if possible, located at the centers of almost equal areas (FSS 6.5.4.1);

iii) Small pieces of foil, having surface emittance matching the remainder of the box walls, may be attached to the thermocouples to facilitate the thermal contact with the wall surface (FSS 6.5.4.1);

iv) The junctions and the attached thermocouple wires shall be flush with, and in thermal contact with, the surface of the wall for at least a 100 mm distance from the junctions (FSS 6.5.4.1);

v) The thermocouple pairs are connected in series to form a thermopile in which the individual voltages are summed to give a single output or read out individually in cases where significant differences may occur or be expected in the local heat flow levels (FSS 6.5.4.1).

III. BS 874-3.1 (1987) and BS 874-3.2 (1990):

The thermopile must be made of thermocouples with the arrangement presented in Figure 3.6.

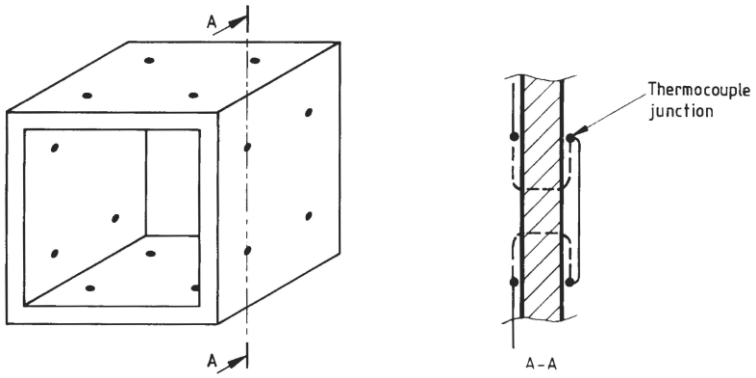

Figure 3.6 – Thermocouple connections to form metering box thermopile [277].

3.3.6.2. Metering box perimeter seal on the surface of the test element

In GHB can occur flanking losses, namely heat transfer between the metering box and the guard or climate chambers around the contact point where the metering box wall touches the specimen, as shown in Figure 3.7. It will usually be impracticable to correct the lateral heat flow in the test element caused by surface temperature differences in the metering and guard box areas. Consequently, it shall be ensured that such surface temperature differences are kept within certain limits by careful control of the guard space environment.

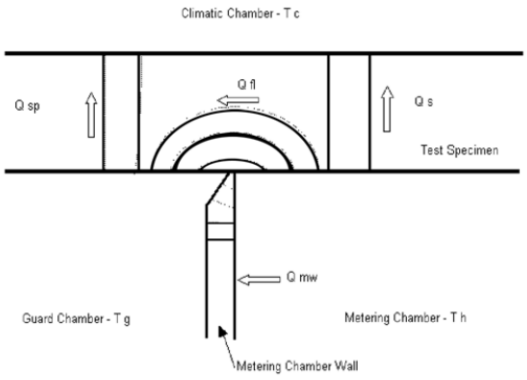

Figure 3.7 – Guard Chamber/Metering Box Interface [18].

Next, are presented the thermopile requirements for the metering box perimeter seal on the surface of the test element, for the GHB, expressed in each standard.

I. ISO 8990 (1994):

i) The thermopile used in the guarded hot box for monitoring imbalance heat flow in the surface of the specimen between metering and guard area shall have at least one pair of junctions per 0.5 m of the perimeter of the metered area (FSS 2.7.3);

ii) The junctions of the thermopile cannot be too close to the nose, due to the surface temperatures are not uniform along the periphery of the metered area, as a consequence of the presence of the nose of the metering box. Nor they can be too distant from the nose, as in the guard area of the specimen surface temperatures are not uniform due to the flanking losses (FSS 2.7.3);

iii) Shall be noted that inhomogeneities could have a severe effect on the reliability of the readings from this thermopile (FSS 2.7.3).

II. BS 874-3.1 (1987) and BS 874-3.2 (1990):

i) The measurements shall be made approximately 50 mm from the projected intersections of the surfaces of the metering box walls with the test element, to be outside the metering box walls influence, shown in Figure 3.8 (FSS 4.3.4);

ii) The average difference in temperature so determined shall not exceed 0.5 K (FSS 4.3.4).

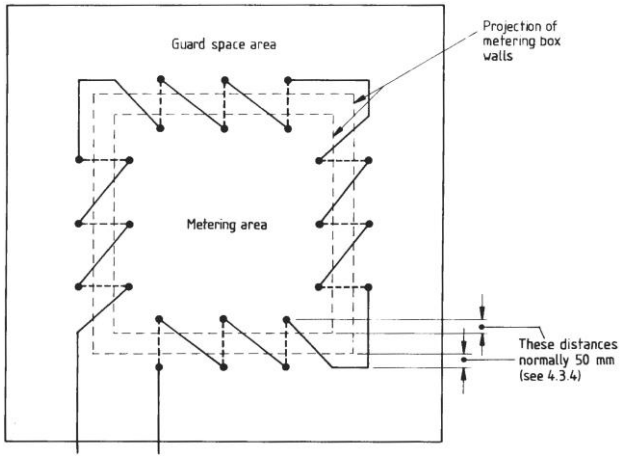

Figure 3.8 – Thermocouple connections to form surface gradient thermopile [277].

3.3.7. Measuring the air velocity

The apparatus design shall provide a way for determining mean air velocity past both the hot and cold faces of the specimen during each test.

The determination of the mean air velocity past both the hot and cold faces of the specimen during each test can be performed, locating velocity sensors directly in the air curtain. For test purpose, wind velocity shall be measured at a fixed location that represents the average free stream condition. For both perpendicular and parallel flow patterns, this location shall be a distance out in the air stream such that the wind velocity sensor is not in the test specimen surface boundary layers.

Next, are presented the air velocity sensors requirements obtained from each standard:

I. ISO 8990 (1994):

When testing homogeneous specimens, the sensors shall provide at least an accuracy within ± 5 % (FSS 1.1).

II. ASTM C1363-11 (2011):

i) One method to compute air velocity is to measure the volumetric airflow in the duct to the inlet distribution header, by using a calibrated orifice or another flow-measuring device. The average baffle space velocity is calculated from the volume flow and the size of the space between the specimen and the parallel baffle. Must be noted that for this technique to work the baffle must be well sealed (FSS 6.8.11.1);

ii) Another method is to calculate the velocity from an energy balance. The rate of loss, or gain, of heat by the air as it moves through the baffle space, as indicated by its temperature change, will match the rate of heat transfer through the metering chamber opening, average values of which can be determined from the test data (FSS 6.8.11.2);

iii) The best method is to locate velocity sensors directly in the air curtain. For test purpose, wind velocity shall be measured at a fixed location that represents the average free stream condition (FSS 6.8.11.3);

iv) For the sensors in the air curtain, for both perpendicular and parallel flow patterns, the location must be a distance out in the air stream, such that the wind speed sensor is not in the test specimen surface boundary layers or wakes (FSS 6.8.11.3);

v) The sensors in the air curtain shall be at a distance out from the test specimen surface of 75 to 150 mm at the center point (FSS 6.8.11.3);

vi) When desired to make tests with natural convection conditions, the air velocity shall be below 0.5 m/s (FSS 6.8.3);

vii) A velocity of approximately 0.3 m/s has proven satisfactory for a wall test apparatus of 3 m height when testing wall systems (FSS 6.8.4);

viii) Velocities commonly used to simulate parallel or perpendicular wind conditions on the exterior side are 3.4 m/s for summer conditions and 6.7 m/s for winter conditions (FSS 6.8.8).

ix) For minimum velocities, the minimum spacing from the specimen surface is 75 mm (FSS 6.10.3.2);

x) At velocities higher than 1 m/s, the required minimum spacing is greater. When forced convection is established, and the flow is fully developed, the sensors shall be located at a distance from the specimen surface corresponding to 2/3 up to 3/4 of the specimen-to-baffle distance (FSS 6.10.3.2);

3.3.8. Measuring Pressure

For testing some specimens, e.g. windows, modular walls, is necessary to establish and measure the air pressure differential between the faces of the test specimen, being particularly important where the airflow resistance between the specimen surfaces is low.

Next, are presented the pressure sensors requirements obtained from each standard:

I. ASTM C1363-11 (2011):

i) When this measurement is required, the specimen test pressure difference is defined as the difference, side to side, in local pressure measured in the direction perpendicular to the specimen surface, at a location at the geographic center of the metered area at a distance 75 mm from the surfaces of the sample (FSS 6.11.1);

ii) Pressure difference measurements shall be accurate to within ± 5 % of reading or ± 1 Pa, whichever is greater (FSS 6.12.1.5).

II. GOST 26602.1-99 (1999):

To measure the air pressure difference, the hose ends of the sensor must be located on both sides of the test structure at 1000 mm from the floor (FSS 4.1.3).

3.3.9. Temperature control system

The temperature control system shall be installed to achieve the following requirements: (*i*) restriction of the temperature gradient across the metering box perimeter seal; (*ii*) heat transfer through the sides and back of the metering box limitation.

The temperature control system requirements obtained from each standard are:

I. ISO 8990 (1994):

i) At steady-state, for the air-to-air temperature difference over the specimen the controllers shall keep any random temperature fluctuations and long-term drifts within 1 %, at least for two consecutive test periods (FSS 2.7.5);

ii) This requirement applies primarily to metering chamber temperature, and in principle to guard and cold chamber temperatures (FSS 2.7.5);

iii) Also, the control system for the guard box temperatures shall not introduce additional errors on imbalance heat flow rate greater than 0.5 % of the heat flow rate through the specimen (FSS 2.7.5).

II. ASTM C1363-11 (2011):

i) The control system shall maintain, and not change during the measurement period, the air entering temperature at air curtains within ± l K of the setpoint temperature, across its width and for steady-state tests (FSS 6.9.1);

ii) Temperature controllers for steady-state tests shall be capable of controlling temperatures constant to within ± 0.25 K (FSS 6.12.1.7).

III. BS 874-3.1 (1987) and BS 874-3.2 (1990):

i) For GHB, in the metering and guard boxes the inside temperatures must be maintained as close to each other as possible so that lateral heat transfer is avoided (FSS 4.3.1);

ii) For GHB, the control system must increase or decrease the temperature in the guard box in order to achieve the same temperature as the metering box (FSS 4.3.1);

iii) On the cold side, the temperature control system must provide an equilibrium of temperatures in the way of obtaining a steady-state (FSS 3).

3.3.10. Power input measurement

At steady-state conditions, the energy transfer through the specimen equals the electrical power to the heaters and blowers minus the cooling energy extraction, corrected for the energy passing through the chamber walls and flanking the specimen. Therefore it must be measured by the power input to the systems.

Next, are presented the power input measurement requirements obtained from each standard:

I. ISO 8990 (1994):

i) Power input to heaters, fans, etc. shall be measured with such accuracy that added error in the measurement of the specimen heat flow, due to instrumentation accuracy shall be smaller than 1.5 % (FSS 2.8);

ii) If the fan motors are installed inside the metering box, then their power consumption shall be measured and added to the consumption of the heaters (FSS 2.3.2);
iii) If only the fans are inside the metering box, the shaft power shall be determined and added to the heater power: this shall be done with an accuracy such that the error on specimen heat flow is less than 0.5 % (FSS 2.3.2).

II. ASTM C1363-11 (2011):

i) The power measuring instruments shall be compatible with the power supplied whether: AC, DC, on-off, proportioning, etc. (FSS 6.12.1.6);
ii) Voltage stabilised power supplies are strongly recommended (FSS 6.12.1.7).

III. BS 874-3.1 (1987) and BS 874-3.2 (1990):

i) The power consumption of the heater shall be measured to an accuracy of ± 0.25 % (FSS 4.2);
ii) The total uncertainty in the determination of the net power input into the metering box due to the heater, fans, power loss in the leads and heat transfer through the sides and back walls shall not exceed ± 1.0 % (FSS 4.2).

3.3.11. Data logging system

All instruments shall be calibrated according to the specified accuracy, by a national standards laboratory, and shall meet the following additional requirements:

I. ISO 8990 (1994):

The output from balancing thermopiles, the power input to heaters, fans, etc., shall be measured with such accuracy that added error in the measurement of the specimen heat flow, due to instrumentation accuracy, will be smaller than 1.5 % (FSS 2.8).

II. ASTM C1363-11 (2011):

i) All data logging instruments and signal conditioning shall be located outside of the apparatus (FSS 6.12.1);
ii) All data logging instrumentation shall have adequate sensor response so that the scanning speed does not affect the measurement results (FSS 6.12.1.1);
iii) Temperatures shall be readable to ±0.05 K (FSS 6.12.1.2);
iv) Air velocity measurement shall have an accuracy of ±5 % of the reading (FSS 6.12.1.4);
v) The data logging of the integrated energy over a specified time period, or total average power, to the metering box shall be accurate to within ±0.5 % of reading under conditions of use (FSS 6.12.1.3).

3.4. TEST PROCEDURE

Laboratory methods for determining the thermal performance of building elements are to create a constant temperature differential on both sides of the test specimen, the measurement of air temperatures and surfaces of the sample areas, thermal power on its creation (or heat flux), passing through the sample under stationary test conditions, and subsequent calculation of the values of thermal resistance and heat transfer resistance.

The element under study should be representative in terms of materials and construction processes regarding the real application. The results of the test measurements need careful analysis, being verified if

the terms conditions of the sample are the same directly applied in practice. Flanking thermal losses may drastically change the measured global thermal transmittance of a building component [47]. Flanking heat loss must be taken into account, not only in laboratory tests or numerical simulations but also in real buildings given the lateral heat exchange with the adjacent construction [47].

3.4.1. Preparation for test

The preparation for experimental determination of the thermal performance of building elements begins with drawing up of the program of tests and a schematic layout of placing the primary thermocouples and heat flux sensors on the surfaces of the test specimen. The test program shall begin with the consideration of technical documentation for the products of a particular type and the preparation of a test program, which takes into account the design features of the product and establish requirements for temperature and air velocity, in the warm and cold compartments of the climatic chamber.

The layout of primary surface temperature thermocouples and heat flux sensors is based on the design solution of the element under test, e.g. joints between panels, and if the element is homogeneous or inhomogeneous. For this purpose, in case of an inhomogeneous element, the sensors must have a location that allows functional characterisation of all zones of the element. Thermal image, using IRT technique, can help to detect heat-supply inclusions and thermally homogeneous zones, their configuration and dimensions.

Next, are presented the requirements of preparation for test obtained from each standard:

I. ISO 8990 (1994):

i) Specimens in which heat flow is affected by the presence of moisture, conditioning shall be reported;
ii) For GHB when surface temperatures are uniform near the metering area periphery, the specimen surface imbalance detection and the evaluation of heat flow through the box are the most accurate solution;
iii) However, for GHB, when inhomogeneities are present near the metering area periphery, air-to-air balance solution can be the only possible solution and imbalance heat flow is an unknown source of error;
iv) When possible, in the GGB, placing the thermal bridges symmetrically on the borderline between metering and guard area is recommended;
v) For testing modular specimen in GHB, the metering box dimensions should be a suitable multiple of the module. The metering box perimeter must either fall in the middle between the module lines or coincide with the module lines;
vi) In the CHB, the effect of thermal bridges at the specimen edges should be considered;
vii) If the specimen surface is uneven, it is necessary to ensure an airtight seal between metering and guard box. The solution is to smooth the specimen at the contact area with the perimeter seal of the metering box with caulking, plaster or other suitable material.

II. ASTM C1363-11 (2011):

i) Tests specimens smaller than the representative specimens shall be avoided;
ii) The standard recommends the installation of additional sensors throughout the interior of the element is important for special investigations of local temperature variations;
iii) Before testing, check the chambers, verify the availability of measuring equipment and instruments, and ensure that the hot and cold compartments are insulated from the outside;
iv) The building element should not be permeable to air. If permeable, the element must be gasketed, caulked, taped, or otherwise sealed in place to prevent air movement around its perimeter;

v) For all specimen, it is necessary to maintain a near-zero lateral energy flow between guard and metering area, which can be achieved by maintaining a near-zero temperature difference on the element surface between the areas;

vi) For the specimens with elements incorporating high lateral conductance, e.g. metal sheet, maintain a near-zero lateral energy flow between guard and metering area, it is necessary to separate the highly conductive element with a thermal break. This can be done by creating a thermal break at the metering chamber boundary, e.g. a narrow gap caused by a saw cut.

III. BS 874-3.1 (1987) and BS 874-3.2 (1990):

The selection of test conditions, airspeeds and temperatures, must be carefully selected for practical applications to the test element. For example, high air velocities may change the thermal transmission properties of some low density. In addition, the thermal properties of some materials are temperature dependent, and thus consideration shall be given to the relevance of the hot and cold face temperatures to practical conditions.

IV. GOST 26602.1-99 (1999):

i) In non-homogeneous elements for determining the heat transfer of a part, uniform on the surface temperature, the temperature thermocouples and heat flux sensors are installed at least in two characteristic sections with the same design solution;

ii) Thermal flux sensors are fixed on the internal and external surfaces of the test element at least two on each surface.

3.4.2. Testing

The operation of the hot box apparatus is a complex matter, requiring the test to be carried out by an experienced operator. When conducting tests, the presence of people and equipment not used in the test inside the climatic chambers during the measurement is not allowed.

There must be a written operating procedure, which details the procedures on the equipment and test parameters to be performed. This document must be available to ensure that tests are done in accordance with the requirements of the test method.

The time required to perform a test is determined by the response speed of the HB apparatus and the response of the sample to changes in its environment. The time controlling factors for testing are: (i) the heating and cooling capacity for the apparatus; (ii) the air circulation patterns and velocity; (iii) the internal heat storage capacity of the test chambers; (iv) the thermal diffusivity and resistance of the materials used to construct the apparatus boxes; (v) the specimen geometry; (vi) the specimen thermal diffusivity and resistance; and (vii) the specimen heat storage capacity [18].

Next, are presented the requirements for testing from each standard:

I. ISO 8990 (1994):

i) Test conditions shall be chosen considering the end-use application, contemplating the effect of testing conditions on accuracy;

ii) Both temperature differences and mean test temperature influence results. The temperature difference of at least 20 °C and mean temperatures of 10 to 20 °C are common in building applications;

iii) Air velocity on both sides of the specimen shall be adjusted according to the purpose of the test;

iv) The temperature in chambers shall be adjusted in such a way that either the imbalance of heat flow rate parallel to specimen or imbalance heat flow rate through metering box walls, or both, are small

or zero;

v) The measurement period required to reach stability for steady-state tests depends upon several factors: performance of the apparatus; thermal resistance and thermal capacity of the specimen; surface coefficients; and presence of mass transfer and/or moisture redistribution within the specimen. Due to these factors, it is impossible to give a single criterion for the steady-state;

vi) If the measurements of thermal resistance, total power input, heating or cooling, and temperatures from two successive measuring periods of at least three hours after near-stability has been reached shall agree within 1%, results shall not change unidirectionally. For specimens with a high mass or high thermal resistance or both, this test period shall be extended.

II. ASTM C1363-11 (2011):

i) The required time to reach stability for a steady-state test and the test period for data acquisition cannot be provided, due to depends upon the properties of the apparatus and the specimen, and upon the test initial and final conditions;

ii) After reach test temperature setpoint, five successive repeated data acquisition sets shall be done with an equal time interval of not less than 30 minutes;

iii) The criteria for test completion is the combination of five data acquisition runs, which constitute a valid test if the datum obtained for each measured variable differs from its mean by no more than the uncertainty of that variable;

iv) If the data obtained changes monotonically with time, the test should be repeated.

III. BS 874-3.1 (1987) and BS 874-3.2 (1990):

i) The recommended minimum difference between the hot and cold air temperatures is 20 K;

ii) The temperature of HB and CB needs to reflect the real conditions of use since the thermal properties of some materials are temperature dependent. For example, masonry samples rich the equilibrium temperatures on the hot and cold faces at 27±3 °C and 10±3 °C;

iii) The criteria for test completion is when the equilibrium has been reached, i.e. once the power supplied, the temperatures and the computed results begin to differ randomly, rather than continuously increasing or decreasing. The test must continue for at least more than 8 h and can terminate if the test averaged measurements of thermal transmittance or conductance differ by less than 1% over at least two successive 4h periods;

iv) The time required for the apparatus to reach equilibrium can vary from some hours to a week. It depends upon the apparatus type and control method and test element.

IV. GOST 26602.1-99 (1999):

i) When measuring the density of heat flux, by means of thermal flux sensors, through the test sample is considered stationary if the results are repeated, at intervals of at least 0.5 h. The temperature measurements on the surfaces of homogeneous areas of the sample in the warm side compartment differ from each other not more than on 0.3 °C, and the values of thermal resistance calculated according to the results of sequential measurements of sensors signals differ from each other not more than by 5%, provided that these values do not increase and do not decrease monotonically;

ii) After establishing a stationary mode of heat transfer, check the correctness of the choice of homogeneous temperature zones on the sample by measuring the density of thermal flows and the temperature of its inner surface. In case of significant deviations of temperature and density of heat flows within the zone, exceeding 10%, adjust the location of temperature sensors and heat fluxes;

iii) At least measure the temperature and density of heat fluxes three times at intervals of at least 1 hour;

iv) Measurements of the surface temperature of the sample, as well as the voltage and current in the electric heater network of the HB, shall be carried out at least three times at intervals of 15 minutes;

v) After setting in the compartments of the climatic chamber of the specified air temperature, measurements are made for enclosing structures with thermal inertia to 1.5, not less than in 1.5 days, with thermal inertia from 1.5 to 4 after 4 days, and thermal inertia from 4 to 7 through 7 days, and with thermal inertia over 7 through 7.5 days;

vi) In the absence of a system of automated collection of experimental data, temperature and density of thermal fluxes are measured around the clock every 3 hours (0; 3; 6; 9; 12; 15; 18; 21 h). Air humidity in the room or compartment of the climatic chamber is measured every 6 hours (0; 6; 12; 18 h);

vii) It can take wind speed and direction according to the nearest weather station.

3.4.3. Processing of test results

Heat is transferred to and from the specimen both by convective heat transfer at the specimen surface, depending on the adjacent air temperature, depending on the mean radiant temperature seen by the test sample. The heat flow through the specimen is therefore influenced by the radiant and air temperatures on both sides.

The heat balance equation at either surface of the specimen is given by:

$$\frac{\emptyset}{A} = Eh_r(T'_r - T_s) + h_c(T_a - T_s) \tag{42}$$

where: $\emptyset/A$ is the heat flow per unit area into the surface, in watts per square metre; E is the emissivity factor; h_r is the radiation coefficient, in watts per square metre kelvin; T'_r is the mean radiant temperature seen by the specimen, in kelvin or degrees Celsius; T_s is the surface temperature of the specimen, in kelvins or degrees Celsius; h_c is the convection coefficient, in watts per square metre kelvin; T_a is the temperature adjacent to specimen, in kelvin or degrees Celsius.

Combining the radiant and air temperatures into a single index, the environmental temperature T_n, which represents the appropriate weighting of air and radiant temperatures for the objective of determining the heat flow to the surface. Writing:

$$\frac{\emptyset}{A} = \frac{1}{R_s}(T_n - T_s) \tag{43}$$

where: R_s is the surface thermal resistance, this is equivalent to equation (42) with:

$$T_n = \frac{Eh_r}{Eh_r + h_c}T'_r + \frac{h_c}{Eh_r + h_c}T_a \tag{44}$$

and

$$R_s = \frac{1}{Eh_r + h_c} \tag{45}$$

The calculation of the thermal transmittance from a test is obtained following the next steps:

i) Mean radiant absolute temperature (T_m), given by:

$$T_m = \frac{T'_r + T_s}{2} \ [K] \tag{46}$$

ii) Environmental temperature (T_n), given by:

$$T_n = \frac{T_a \frac{\emptyset}{A} + E h_r (T_a - T'_r) T_s}{\frac{\emptyset}{A} + E h_r (T_a - T'_r)} \ [°C] \tag{47}$$

where: T_a is the mean air temperature; $\emptyset$ is the heat flow through the metering area (in W), i.e. the rate of heat supplied to the metering box, including power supplied to any fans and corrected where necessary for: (*a*) heat flow through the metering box walls, and (*b*) power loss in the leads to the heater or to the fans in the metering box; A is the test area that normally shall be defined by the centre-line of the perimeter seal, in m². However, if the thickness of the test element is less than the contact width of the seal, the test area shall be taken as the average of those areas defined by the centre-line and the inside edge of the perimeter seal; E is the emissivity factor, which if there is a baffle close to and parallel to the specimen surface the emissivity factor is given by:

$$\frac{1}{E} = \frac{1}{\varepsilon_1} + \frac{1}{\varepsilon_2} - 1 \tag{48}$$

where: ε_1 and ε_2 are the emissivities of the baffle and specimen surfaces, respectively. With the baffle painted matt black ε_1 = 0,97 and for most building materials will give E = 0.9.

The radiation coefficient, h_r, is given by:

$$h_r = \varepsilon_{eff} \, \sigma \, T_m^3 \ [W/(m^2.K)\,] \tag{49}$$

where: σ is the Stefan's constant [5.67x10^{-8} W/(m²·K⁴)], and ε_{eff} is the effective emittance of the specimen surface and surrounding enclosure surface as defined by:

$$\varepsilon_{eff} = \frac{1}{\frac{1}{\varepsilon_s} + \frac{1}{\varepsilon_b} - 1} \tag{50}$$

where: ε_s is the area weighted emittance of the specimen surface; and ε_b is the area weighted emittance of the surrounding enclosure and baffle surfaces as seen by the specimen surface.

iii) The measured thermal transmittance, $U_{measured}$, is given by:

$$U_{measured} = \frac{\emptyset}{A(T_{n1} - T_{n2})} \ [W/(m^2.K)\,] \tag{51}$$

where: T_{n1} is the environmental temperature of the hot side; and T_{n2} is the environmental temperature of the cold side.

iv) The surface thermal resistance for the hot side is:

$$R_{s1} = \frac{A(T_{n1} - T_{s1})}{\emptyset} \ [(m^2.K)/W\,] \tag{52}$$

where: T_{s1} is the surface temperature of the specimen on the hot side.

v) The surface thermal resistance for the cold side is:

$$R_{s2} = \frac{A(T_{n2} - T_{s2})}{\emptyset} \ [(m^2.K)/W\ ] \tag{53}$$

where: T_{s2} is the surface temperature of the specimen on the cold side.

vi) The standard thermal transmittance, $U_{standard}$, is given by:

$$\frac{1}{U_{standard}} = \frac{1}{U_{measured}} - \ (R_{s1} + R_{s2}) + (R_{si} + R_{se}) \tag{54}$$

where: R_{si} is the internal surface resistance; and R_{se} is the external surface resistance. The surface resistance values for normal (high) emissivity materials are given in Table 1 of ISO 6946 [26], which establish for room heat loss horizontal through outside walls R_{si} = 0.13 (m².K)/W and R_{se} = 0.04 (m².K)/W.

Or:

$$\frac{1}{U_{standard}} = \frac{1}{\Lambda} + (R_{si} + R_{se}) \tag{55}$$

where: Λ is thermal conductance, given by:

$$\Lambda = \frac{\emptyset}{A(T_{s1} - T_{s2})} \ [W/(m^2.K)\ ] \tag{56}$$

The calculation of the thermal resistance from a heat flux sensors used in a test is obtained following the next steps, accordingly with the procedures presented in the standards ISO 9869:1994 [278], ASTM C1155-95 [279] and ASTM C1046-95 [280]:

i) To obtain the wall thermal resistance, ASTM C1155-95 [279] establishes a calculation procedure named summation technique. This method uses an accumulation of data on heat flux and differences in surface temperatures over time. It requires a significant difference in temperatures and constant temperature on one side for rapid convergence. The average method defined in ISO 9869 [278] is similar to the summation technique method of ASTM C1155 [279]. The equation is:

$$\mathrm{R} = \frac{\sum_{\mathrm{j=1}}^{\mathrm{n}}(\mathrm{T_{sij}} - \mathrm{T_{sej}})}{\sum_{\mathrm{j=1}}^{\mathrm{n}} \mathrm{q_j}} \ [m^2.K/W] \tag{57}$$

where: R is the thermal resistance [m².K/W]; $\mathrm{T_{si}}$ is the interior surface temperature of the building element [°C]; $\mathrm{T_{se}}$ is the exterior surface temperature [°C]; q is the heat flux [W/m²]; the index *j* enumerates the individual measurements; and *n* is the total number of measurements.

ii) From the values measured during a test, not all can be used, and it is necessary to guarantee a convergence criterium established in the ASTM C1155-95 [279], using the following equation:

$$CR_n = \frac{R_e(t) - R_e(t-n)}{R_e(t)} \tag{58}$$

where: CR_n is the convergence factor; R_e is the estimated thermal resistance [m².K/W]; *t* is the time period [h]; and *n* is the time interval to check the convergence [h].

The values are convergent when the convergence factor CR_n is less than 10%, for at least 3 periods of duration *n*, that is, CR_n<0.10.

iii) To ensure good results, it is also necessary to check the variation of the thermal resistance value, $V(R_e)$, at the various points measured on the wall. The variation can be calculated using the following equation, indicated by ASTM C1155-95 [279]:

$$V(R_e) = [s(R_e)/mean(R_e)] \times (100\%) \tag{59}$$

where: $V(R_e)$ is the variance of the R_e values; $s(R_e)$ is the standard deviation of the estimated thermal resistance; and $mean(R_e)$ is the average value of the estimated thermal resistance.

It should be noted that the variance test must be performed for at least three sensor positions (N ≥ 3). If the variance is less than or equal to 10%, the value to be used for the thermal resistance of the wall can be considered equal to the average value of all R_e that met the requirements presented.

In case of heat flows independently through zones the average weighted thermal resistance of the wall is calculated with the different zones values of the estimated thermal resistance, and the overall value for the wall is weighted accordingly to the area of influence of each sensor, as suggested by the ASTM C 1155:

$$R_m = \frac{\sum_{j=1}^{n} A_j}{\sum_{j=1}^{n} \frac{A_j}{R_{ej}}} \quad [\mathrm{m^2.K/W}] \tag{60}$$

where: R_m is the average thermal resistance; A_j is the area around sensor *j* [m²]; the index *j* enumerates the sensor; and *n* is the total number of sensors.

4. HOT BOX APPARATUS: DESIGN SOLUTION, CONSTRUCTION AND CALIBRATION

4.1. INTRODUCTION

The overall apparatus size must match the type of specimens intended for testing. For building assemblies, the equipment must accommodate representative sections, being essential for maximum accuracy that the specimen size matches the size of the metering box and the cold box much have the same size or bigger. A large apparatus has the advantage of minimising perimeter effects but has the drawback of exhibiting longer equilibrium times. Therefore, it is needed to reach a good size compromise.

For a suitable design, the proposed Hot Box (HB) apparatus operates in both modes, i.e. as a Guarded Hot Box (GHB), and by removing the inner metering box also work as a Calibrated Hot Box (CHB).

The apparatus can test specimens with the size 3600 mm (width) by 2700 mm (height) until a thickness of 800 mm, which are the internal dimensions of the specimen frame. This allows testing LSF modular walls, which have usual standards sizes of 2200-2700 mm height and 600 (6 modules) or 1200 mm (3 modules) width. In GHB mode, the metering test area is 1800 (W) by 1050 (H) mm^2, which allows testing a modular wall. In CHB, the metering test area is 3180 (W) by 2280 (H) mm^2. Figure 4.1a shows a sketch from the design phase of the HB apparatus closed, where it can be seen that the chambers are going into the specimen frame, being this way possible test walls with different thicknesses using the same frame. Figure 4.1b illustrates the actual look of the equipment.

The HB apparatus design specifications are:

- Type: GHB and CHB;
- Specimens type: vertical;
- Temperature range: is 0° C to 50° C, in both main chambers, i.e. guard box and cool box. In CHB the guard box of the GHB configuration assumes the name of the metering box, by the standards;
- Temperature control: steady and dynamic state, and inverse cycles between chambers;

- Air velocity: until 6 m/s. Which allows simulating summer conditions on the exterior side, 2.75 m/s and winter conditions, 5.5 m/s;
- Measurement accuracy: ± 5 %;
- Thermal conductance range: 0.1 W/(m².K) to 15 W/(m².K).

HB apparatus limitations:

- Not possible to test horizontal elements;
- Negative temperatures are not recommended, due not having dehumidifier and the consequent risk of freezing;
- Upper limit temperatures of 50° C, given by the limitation of the upper working range of the active components, e.g. fans systems, air sensors.

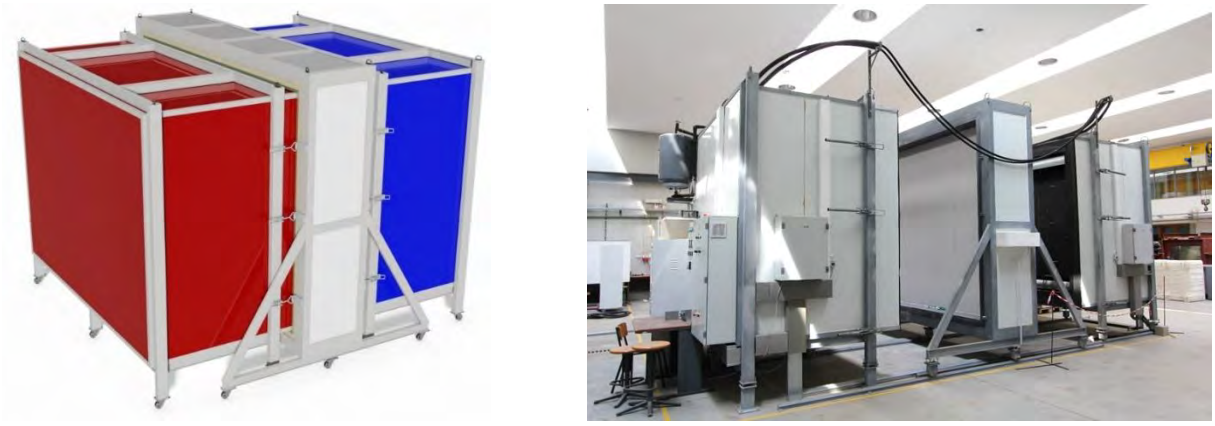

a) b)

Figure 4.1 – Hot box apparatus: a) sketch from the design phase of the equipment closed; b) photography of the equipment open.

Next are presented the design details and the construction of the HB apparatus in accordance with the standards: (*i*) ISO 8990 (1994); (*ii*) ASTM C1363-11 (2011); (*iii*) GOST 26602.1-99 (1999); (*iv*) BS 874-3.1 (1987); and (*v*) BS 874-3.2 (1990) , as previously described in section 3.

The HB apparatus constitutive parts are divided into two groups: (*i*) passive components; and (*ii*) active components. The assembly is divided into three main tasks: (i) structural passive components fabrication and assembly; (ii) sensors, electric systems and heating, ventilation, and refrigeration system; and (iii) control and data logging system, which are detailly described in the next sections.

4.2. PASSIVE COMPONENTS

The equipment, as mentioned before, has two possible configurations, GHB and CHB, which has as the main difference the passive elements to be used. Figure 4.2a and Figure 4.3a illustrates the passive components of the GHB, namely: (*i*) guard box; (*ii*) metering box; (*iii*) specimen frame; and (*iv*) cold box. Figure 4.2b and Figure 4.3b shows the CHB passive components, which are: (*i*) metering box (that corresponds to the guard box of the GHB); (*iii*) specimen frame; and (*iv*) cold box.

The HB apparatus passive components are mainly made of two materials: (i) main structure made of S275 steel profiles with metallization corrosion protection; and (ii) sandwich panels of steel plate at both side and polyurethane in the centre.

In the next sub-sections are present and described the details of each passive component.

a) b)

Figure 4.2 – Apparatus passive components: a) GHB; b) CHB.

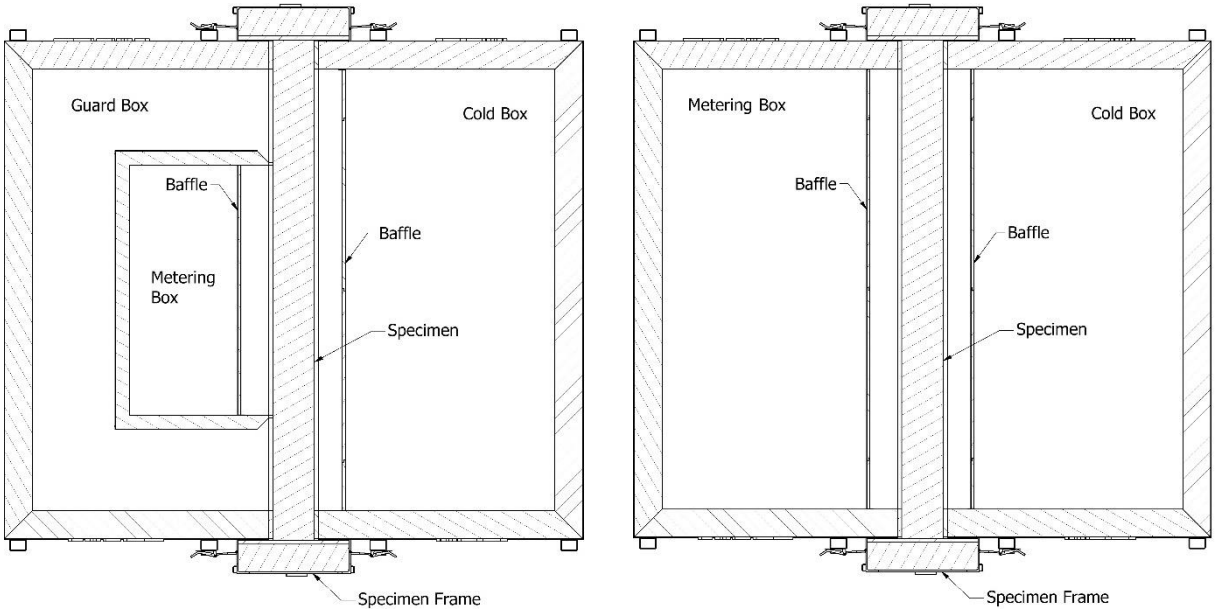

a) b)

Figure 4.3 – Apparatus horizontal cross-section: a) GHB; b) CHB.

4.2.1. Guard and cold box

The guard box and cold box have the same characteristics, with inner dimensions of 3.18 (W) by 2.28 (H) by 1.70 (D) m^3, with 200 mm thick wall of sandwich panels with *U*-value of 0.11 W/(m^2.K). In order to provide air- and water-tightness and mitigate the creation of thermal bridges, the transition between walls is done with a 45° angle and is glued.

In the open side of the boxes, between the box wall and the test element surface, illustrated in Figure 4.4a, is placed an air-tight seal of compressible foam rubber, with a thickness of 32 mm, $\lambda_{0° C} \leq 0.036$ W/(m.K), the working temperature range of -50° to 110° C, and water vapour diffusion resistance ≥ 7 000.

The first task of the construction process is the fabrication of steel structure, Figure 4.4b, followed by the assembly of the sandwich panels. The steel structure is all placed out of the insulation, to avoid any thermal bridge. Figure 4.5 shows the drawings of the guard and cold boxes front and horizontal view.

Figure 4.6 shows the assembly of the sandwich panels walls, with 200 mm thickness, cut with a 45° angle and glued in the transition between walls, to provide air- and water-tightness and mitigate the creation of thermal bridges. Figure 4.7a shows the final assembly result of the chambers, and Figure 4.7b illustrates the cold box interior, being visible the air-tight seal of compressible foam rubber, with a thickness of 32 mm.

a) **b)**

Figure 4.4 – Guard and cold boxes: a) 3D view; b) steel structure.

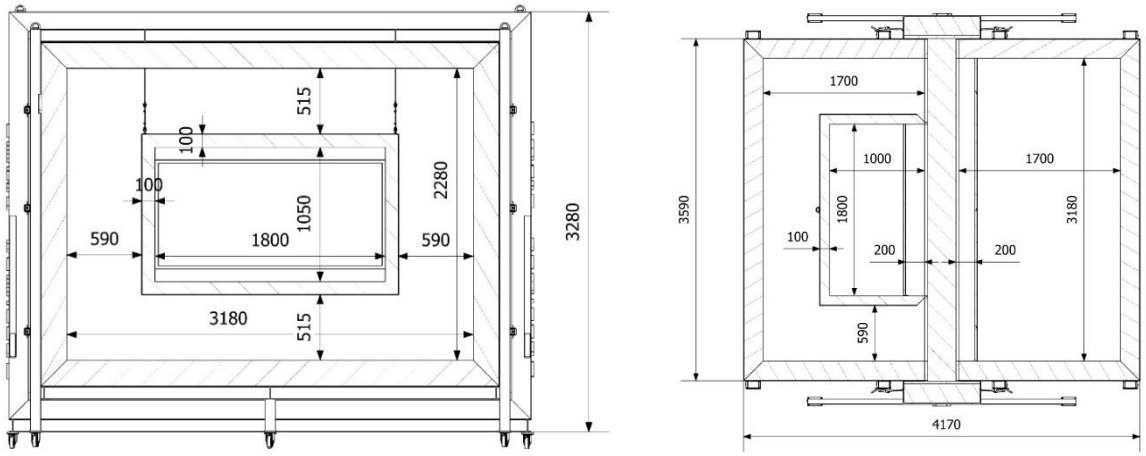

a) **b)**

Figure 4.5 – Guard and cold boxes: a) front view; b) horizontal view.

a) **b)**

Figure 4.6 – HB apparatus sandwich walls panels corners with 45° angle.

a) b)

Figure 4.7 – HB apparatus passive components after assembly.

4.2.2. Metering box of guarded hot box

The metering box has inner dimensions of 1.80 (W) by 1.05 (H) by 1.00 (D) m^3, with 100 mm thick wall of sandwich panels with *U*-value of 0.21 W/(m^2.K). Analogous to the other chambers, the transition between walls is also done with a 45° angle and is glued, to provide air- and water-tightness and avoid the creation of thermal bridges.

Figure 4.5 shows the drawings of the GHC metering box front and horizontal view. In the open side of the box, between the box wall noise and the test element surface, illustrated in Figure 4.8a, is placed an air-tight seal of compressible foam rubber, with a thickness of 19 mm, $\lambda_{0° C} \leq 0.036$ W/(m.K), a working temperature range of -50° to 110° C, and water vapour diffusion resistance ≥ 7 000. Figure 4.8b shows the schematic of the steel structure, all placed out of the insulation, to avoid any thermal bridge.

a) b)

Figure 4.8 – GHB metering box: a) photography; b) steel structure.

4.2.3. Specimen frame

The specimen frame has inner dimensions of 3.60 (W) by 2.70 (H) by 0.80 (D) m^3, with 200 mm thick wall of sandwich panels with *U*-value of 0.21 W/(m^2.K) and 30 mm thick rigid PVC sheets with $\lambda_{20° C}$ of 0.160 W/(m.K), illustrated in Figure 4.9a. The PVC sheets give resistance and durability to the surface of the zone in contact with the specimen. The specimen frame supports heavy specimens, e.g. concrete wall, brick wall, etc. Figure 4.9b shows the schematic of the steel structure, all placed out of the insulation, to avoid any thermal bridge.

a) b)

Figure 4.9 – Specimen frame: a) photography; b) steel structure.

4.3. ACTIVE COMPONENTS

The HB apparatus active components are a complex set of equipment's, sensors and electric systems that require a skilled assembly and configuration. The second main task of the assembly is placing: sensors, electric systems, and heating, ventilation and refrigeration system. Next, are presented the specification of all equipments and sensors placed in the apparatus.

4.3.1. Temperature sensors

The temperature measurements are made with thermocouples are type *K*, made from a stock of wire certified by the supplier that complies with IEC 584-3, with a tolerance of ± 0.4 %. The thermocouples wires had 0.25 mm diameter, twisted and welded on the junction. Table 4.1 list the number of thermocouples sensors.

The surface thermocouples are fixed to the surface with appropriated tape, painted to have low emittance. Air temperature thermocouples are placed inside 12 mm diameter PVC pipes suitable for radiation shield. In the CHB apparatus mode the sensors used in the metering box of the GHB mode are used in the metering box (guard box of the GHB), the reason why both modes are presented in the appendices when needed. Figure 4.10a shows the disposition of sensors in the baffle of the metering box of the GHB, and Figure 4.10b illustrates the cold box sensors in the baffle. Annex A presents schematic drawings of all temperature sensors listed in Table 4.1

Table 4.1 – Number of thermocouples and locations.

Location		N.º of sensors
Specimen surface temperature	Metering box	21
	Cold box	21
Air temperature sensors in the metering box		9
Surface temperature sensors in the baffle of the metering box		9
Surface temperature sensors in the baffle of the cold box		32
Air temperature sensors in the cold box (between specimen and baffles)		12
External air temperature sensors		3
Air temperature sensors inside the guard box		9
Temperature sensors for specimen interior		16
	Total	**132**

a) b)

Figure 4.10 – Sensors a) GHB metering box; b) cold box.

4.3.2. Heat flow sensors

The heat flow is measured with thermopiles applied in the metering box walls and, in the case of the GHB apparatus mode, in the zone of the metering box perimeter seal on the surface of the test element. The thermopiles are made with the same type of thermocouples presented in the previous section. Table 4.2 list the number of thermopiles sensors and surface contacts of the sensors, and Annex B shows the drawings.

Table 4.2 – List of heat flow sensors.

Location	N.º of sensors	N.º of contacts
Thermocouple connections to form surface gradient thermopile for GHB metering box	1	94
Thermocouple connections to form surface gradient thermopile for GHB metering box perimeter seal	1	32
Total	2	

4.3.3. Heat flux sensors

For measuring the local heat flux of elements, particularly important for thermally inhomogeneous components, the apparatus is equipped with twelve heat flux sensors, Hukseflux type HFP01, with a measurement range of -2000 to 2000 W/m², operating temperature range -30 to 70° C and uncertainty of ± 3 %, illustrated in Figure 4.11.

a) b)

Figure 4.11 – Heat flux sensor Hukseflux type HFP01, side: a) positive; and b) negative [281].

4.3.4. Air velocity sensors

The air velocity is measured in all chambers with velocity sensors with the following specifications: work range 0 to 10 m/s; temperature working a range of -40 to 60° C; and uncertainty of ± 1 %, illustrated in Figure 4.12. Table 4.3 list the number of sensors, and Annex C shows the drawings with the location of each sensor.

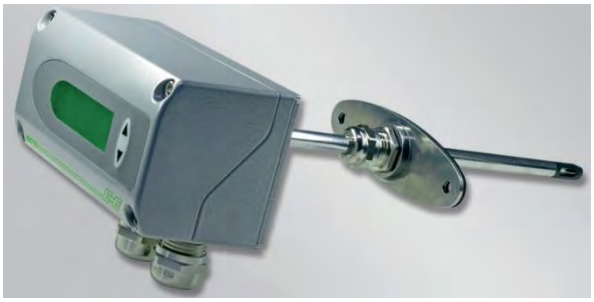

Figure 4.12 – Air velocity sensor E+E model EE75 [282].

Table 4.3 – List of air velocity sensors.

Location	N.º of sensors
Guard box	4
GHB metering box	2
CHB metering box	4*
Cold box	4
Total	10

*Same sensors used in guard box.

4.3.5. Air pressure sensors

For measuring the pressures in each chamber, two air pressures sensors are placed in the guard box (metering box of CHB) and cold box, with the following specifications: work range -200 to 200 Pa; temperature working range of -40 to 100° C; and accuracy of ± 1 %, illustrated in Figure 4.13a.

4.3.6. Air humidity sensors

The air humidity is measure using four sensors, placed in: guard, cold and metring box, and in the exterior of the HB. The equipment has a measuring range of 0 to 100 % RH, the accuracy of ±2.5 % RH from 5 to 95 % at 23 °C, and a resolution of 0.1% RH. Figure 4.13b illustrates the equipment.

a) **b)**

Figure 4.13 – Sensors: a) Air pressure KPLAY model FKC X 22 [283]**; and b) Air Humidity, Comet model T3111-4** [284].

4.3.7. Air circulation, heating and refrigeration

The air circulation, heating and refrigeration system is a group of ducts with: (*i*) tubular axial fans; (*ii*) heating resistors; and (*iii*) cold coils. There are four groups of ducts in the guarded box (metering box of CHB), Figure 4.14a, other four in cold box and two in the metering box of the GHB, Figure 4.14b. In Figure 4.14, it is possible to see that the interior of the chamber is painted matte black, for radiation purposes.

a) b)

Figure 4.14 – Air circulation, heating and refrigeration system duct: a) guard/cold box; and b) GHB metering box.

The tubular axial fans can provide an air velocity of approximately 6 m/s in the guarded (metering of CHB) and cold boxes, and 3 m/s in the metering box of the GHB. Each duct of guarded (metering of CHB) and cold boxes have heating resistors of 1100 W, having each chamber 4400 W, and the metering box of the GHB, 500 W per duct, having a total of 1000 W. All heating resistors are assembled inside a pipe, placed inside of the duct, as a radiation shield.

The cooling of the chambers is provided by a chiller that cools glycine water, which passes by a hydraulics system with coils, which is illustrated in Annex D.

In order to guarantee the homogeneous diffusion of the air, the ducts systems have perforated plates placed both in the insufflation and in return. The air will also pass through deflector blades to ensure that there are no zones without air movement and with uniform air velocities.

4.3.8. Power/Energy meter

The power input for fans and heating resistors is measured to an accuracy of ± 0.1 %. For the fans are used three triphasic electric network analysers, namely for the fans groups of the guard, metering and cold boxes, illustrated in Figure 4.15a. For the heating resistors of the mentioned groups are used three monophasic electric analysers, illustrated in Figure 4.15b.

To measure the amount of energy supplied by the cooling system are installed enthalpy measurement systems, for each chamber, consisting of an electromagnetic flowmeter for temperatures up to - 20° C, illustrated in Figure 4.15c, associated with a heat meter integrator with an accuracy of 0.2 %, illustrated in Figure 4.15d, and two PT100 temperature probes. Annex D shows the location of the equipment in the hydraulic cooling system design schematic.

a) b) c) d)

Figure 4.15 – Electric analysers: a) triphasic Sfere model Diva 11 [285]**; b) Sfere model Diva 5** [286]**; c) Electromagnetic flowmeter; and d) Heat meter integrator.**

4.3.9. Control and data logging system

The control and data logging system are divided into two groups: (*i*) hardware and (*ii*) software, described in the following sub-sections.

4.3.9.1. Hardware

The control of the system is achieved with a complex net of electric systems, e.g. electric protections, speed variators for fans, solid-state relays for on/off systems, thermostat, security measures and controller, illustrated in Figure 4.16.

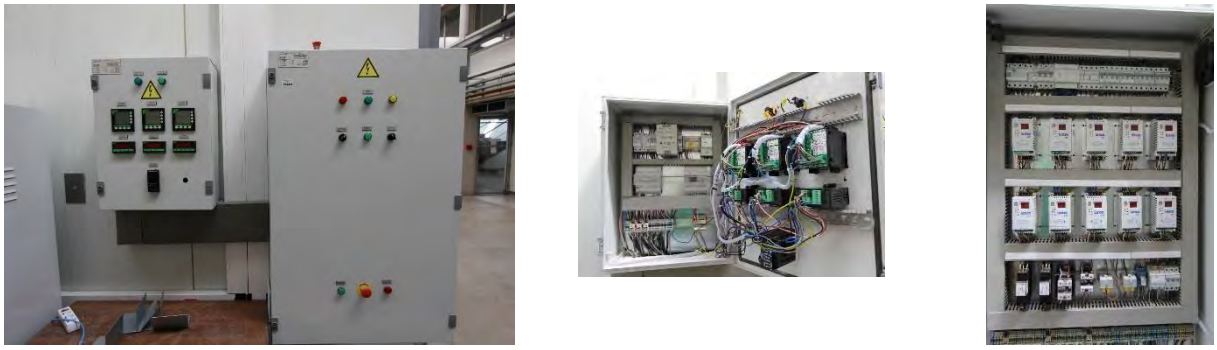

a) **b)** **c)** **d)**

Figure 4.16 – Electric panels: a) secondary panel; b) main control panel; c) interior view of the secondary panel; and d) interior view of the main control panel.

The primary system that controls all system and makes data logging is a National Instruments CompactRIO Controller model cRIO-9074, which have an embedded controller for advanced control and monitoring applications. Linked to this controller are two additional expansion units NI 9144 8-slot, illustrated in Figure 4.17.

a) **b)**

Figure 4.17 – Control and data logging panels: a) main with CompactRIO Controller model cRIO-9074 on the top and the expansion unit NI 9144 8-slot in the bottom; b) secondary with the other expansion unit NI 9144 8-slot.

4.3.9.2. Software

The National Instruments CompactRIO Controller model cRIO-9074 and additional two expansions units NI 9144 8-slot are controlled by the software LabView, which operates in a desktop. For controlling the

apparatus, was implemented a dedicated application that manages all system in the function of several defined parameters and data logging information retrieved in real-time. Figure 4.18 illustrates the software main menu.

The software two main requirements are: (*i*) control the system according to the defined test configurations and specified accuracy, and according to the information measured by the system sensors; and (ii) data logging all the information of the sensors and system configurations.

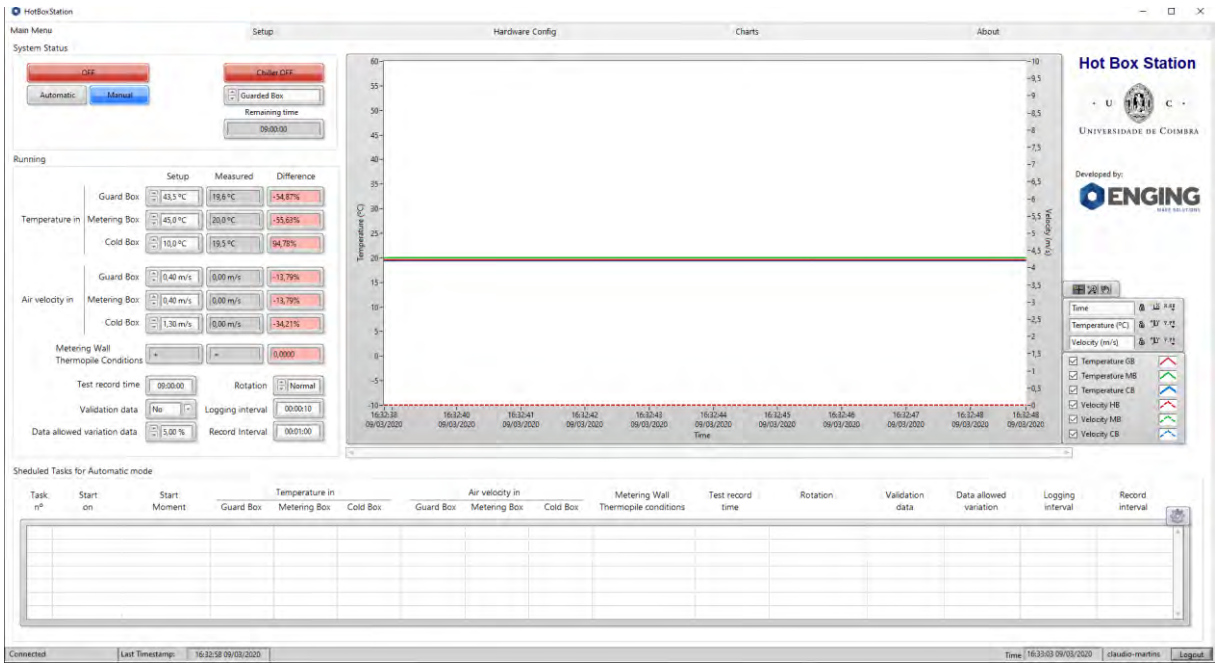

Figure 4.18 – Software Main Menu.

The software was made in collaboration with a outsource company. The software testing and fine-tuning of the proportional–integral–derivative controller (PID) was a hard task, which required several months and conducting many tests and proper functioning checks. The software has four main windows, namely: main menu; setup; hardware configuration; and charts, respectively.

The main menu, Figure 4.18, is the main window of the software where it is possible to define the conditions and test tasks to be performed, namely

The main menu, Figure 4.18, is the principal window of the software where it is possible to define the test conditions and tasks to be performed, namely: (*i*) temperatures of chambers; (*ii*) air velocities in each box; (*iii*) data logging parameters; (*iv*) tasks scheduled menu; (*v*) temperatures chart; (*vi*) velocities chart; and (*vii*) turn on/off the equipment.

In the setup window, Figure 4.19, it is possible to define several configuration parameters, such as: (*i*) predefined values for fields of the main menu; (*ii*) range limits for temperatures and velocities in each chamber; (*iii*) users permissions; and (*iv*) default data folders for output excel files types.

The hardware menu window, Figure 4.20, intends to allow the definition of parameters and settings for each channel of the equipment, e.g. type of signal, signal range, calibration parameter and reading value of the channel on real-time.

The last window shows the chartsof measurements done by the system, Figure 4.21, namely: (*i*) PID's; (*ii*) temperatures; (*iii*) thermopiles; (*iv*) heat flux; (*v*) air velocity; (*vi*) pressure; (*vii*) humidity; and (*viii*) energy consumption.

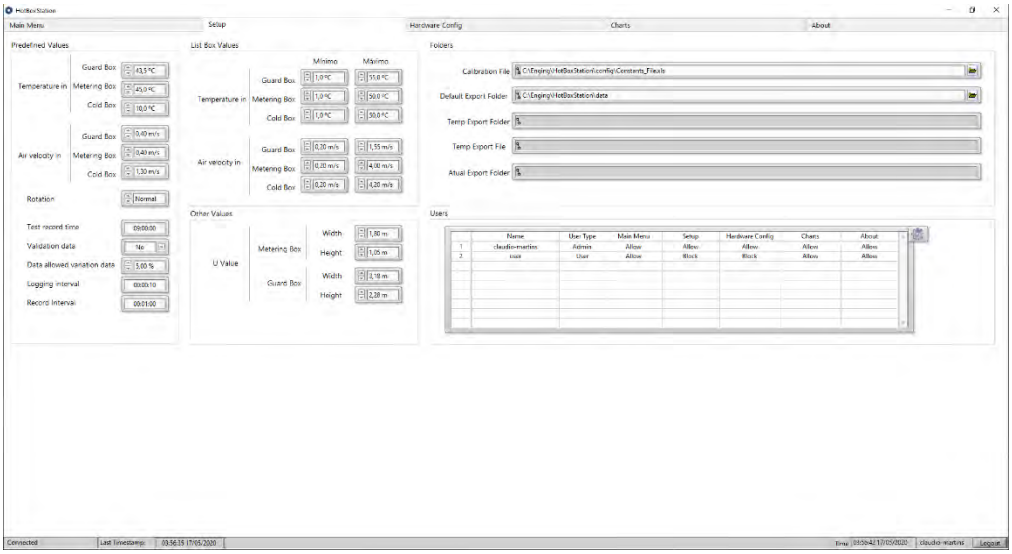

Figure 4.19 – Software Setup.

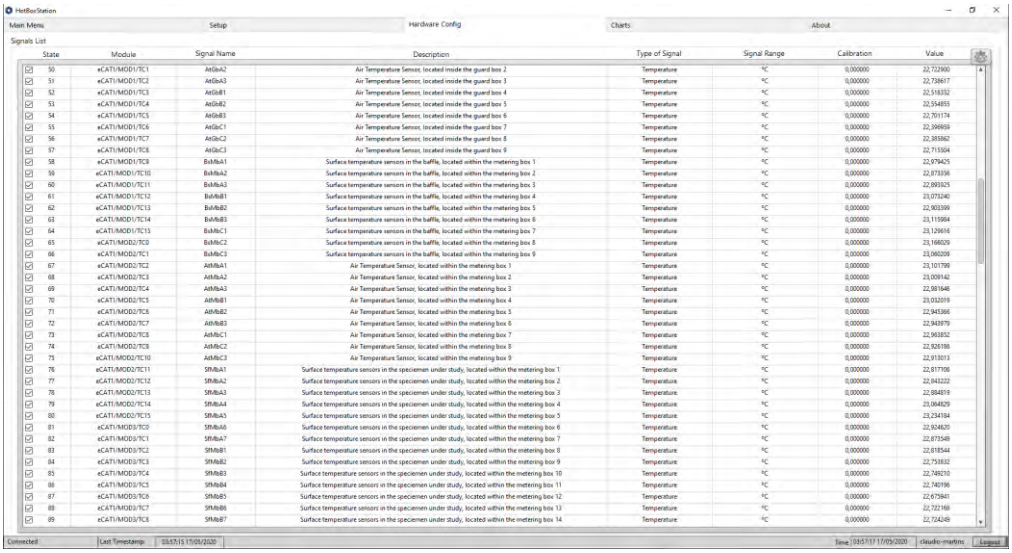

Figure 4.20 – Software Hardware config.

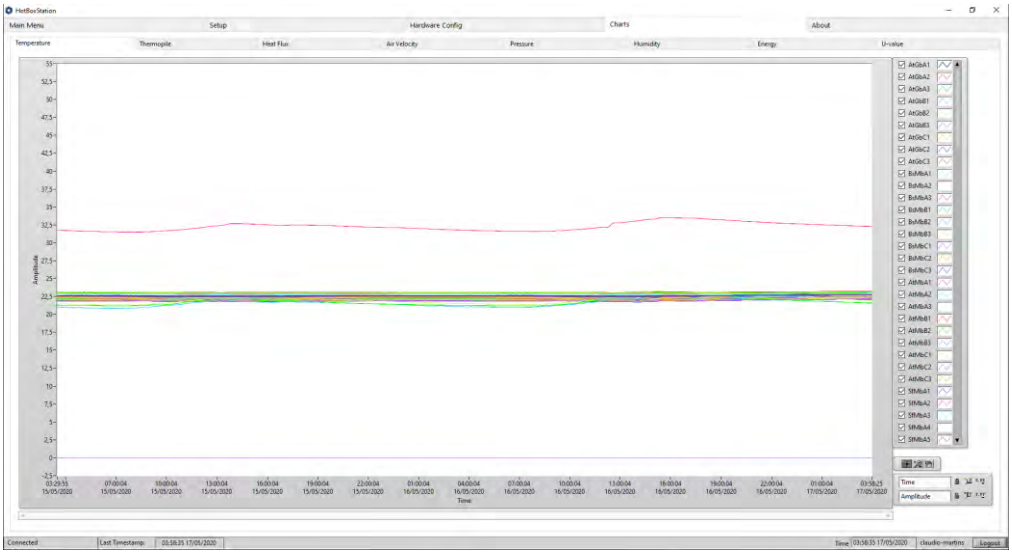

Figure 4.21 – Software Charts.

4.4. EXPERIMENTAL THERMAL PROPERTIES CHARACTERIZATION OF HOT BOX PASSIVE COMPONENTS

For the complete characterization of the equipment, its operating range and flaking losses, it is necessary to have a complete characterization of the materials used in the construction of the apparatus, namely: (*i*) sandwich panels, made of steel plates and polyurethane; (*ii*) foam rubber; and (*iii*) PVC sheets.

Although all materials purchased are certified, being the respective thermal properties defined in the technical datasheets, a campaign of experimental tests was carried out to verify the values of thermal properties. The experimental study uses the transient plane source (TPS) method described in sub-section 2.1.2.5. The apparatus used for the determination of the thermal conductivity, a Hot Disk thermal constants analyser (model: TPS 2500) with an accuracy of ±5%, is shown in Figure 4.22a and Figure 4.22b illustrates the interior of the sample holder with a specimen of polyurethane. Table 4.4 presents the results of the experimental campaign, which tested three pairs of samples for each material and performed five repetitions for each analysis.

a) **b)**

Figure 4.22 – Hot Disk thermal constants analyser: a) Apparatus, sample holder and computer for control; and b) Interior of the sample holder with a specimen of polyurethane.

Table 4.4 – Thermal conductivity of the hot box materials.

Test		Steel	Polyurethane	PVC	Rubber 30	Rubber 20
Sample n.º	**Repetition n.º**					
1	**1**	53,9960	0,0246	0,1691	0,0366	0,0367
	2	54,2470	0,0248	0,1694	0,0368	0,0365
	3	53,9291	0,0257	0,1695	0,0372	0,0366
	4	53,8580	0,0256	0,1695	0,0372	0,0366
	5	54,0395	0,0256	0,1689	0,0370	0,0366
2	**1**	54,6027	0,0255	0,1664	0,0370	0,0367
	2	54,7450	0,0257	0,1652	0,0369	0,0367
	3	54,7370	0,0258	0,1658	0,0368	0,0367
	4	54,8187	0,0258	0,1660	0,0368	0,0368
	5	54,3919	0,0260	0,1661	0,0369	0,0368
3	**1**	54,6138	0,0250	0,1667	0,0370	0,0370
	2	54,7696	0,0252	0,1672	0,0369	0,0371
	3	55,0476	0,0250	0,1673	0,0369	0,0371
	4	54,9964	0,0251	0,1679	0,0369	0,0371
	5	54,6520	0,0252	0,1685	0,0369	0,0372
Average [W/(m.K)]		**54,496** ±5%	**0,025** ±5%	**0,168** ±5%	**0,037** ±5%	**0,037** ±5%
Standard Deviation		0,3797	0,0004	0,0014	0,0001	0,0002

Figure 4.23 presents charts performing the comparison of the thermal conductivity obtained experimentally with the values taken from the products certificates and with theoretical values retrieved from the book of Cengel [30] and ISO 10456 [287].

The sandwich panel of the boxes walls is made with double metal lining and polyurethane insulation in the middle. Figure 4.23a shows the chart of the steel, which compares only the experimental value with theoretical, due to the product certificate does not provide this information. This material does not affect the *U*-value of the element owing to the low thickness of the steel sheet, 1.5mm, when compared with the insulation depth, 200mm of polyurethane. The U-value for the sandwich panel experimentally is 0.12 W/(m².K) and in the product certificate is 0.11 W/(m².K), respectively.

The charts of Figure 4.23b presents the results of the experimental test of the polyurethane, PVC, rubber with 30 mm and rubber with 20 mm, which compare with the product certificates are identical.

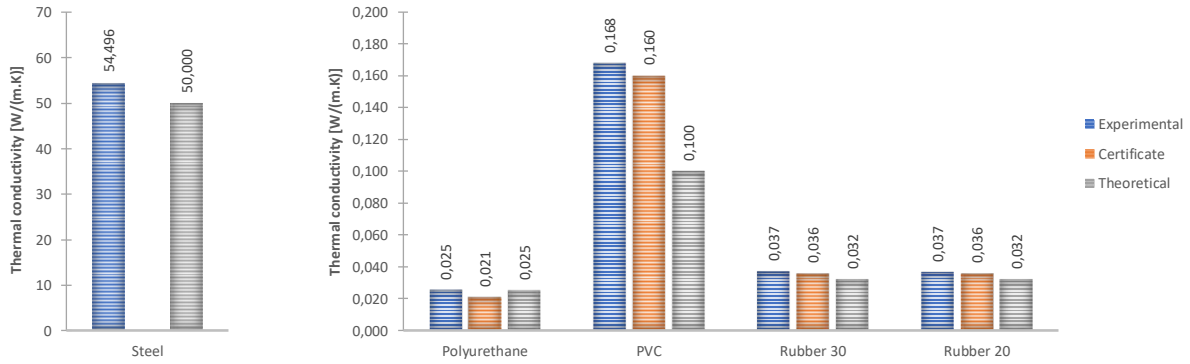

a) **b)**

Figure 4.23 – Thermal conductivity of the hot box materials.

4.5. NUMERICAL VERIFICATIONS OF THE APPARATUS FLANKING LOSSES

The apparatus flanking losses are of two types: (*i*) specimen frame, (*ii*) metering box walls. The flanking loss is for a given part of the equipment a function of specimen thickness and thermal resistance and construction type of the specimen frame and chambers. The determination of the global flanking losses is done with calibration tests, run at steady state on known homogeneous specimens, presented in section 4.6.

For checking the quality of the constructive solution of the specimen frame, in the early sate of project, the alternative to the calibration process suggested by ISO 8990 [17] and ASTM C1363-11 [18] is to use calculation procedures of two-dimensional or three-dimensional finite elements or finite differences, to estimate the flanking losses.

By definition, when there is a thermal bridge, the flow of heat through the element becomes two-dimensional or three-dimensional, rather than one-dimensional. The three-dimensional effect becomes more relevant, due to the lateral heat flow, for example, caused by steel profiles. Therefore, some simplified methods should not be applied because they may give imprecise results.

The specimen frame is the critical component of the HB apparatus, due to the flanking losses that can arise, which for high accuracy should be kept at a minimum.

Next subsections present: (*i*) a two-dimensional numerical verification carried out in the design phase that aims to assess the thermal bridges in the specimen frame, validate and optimize the projected solution and

check the range of operation of the specimen frame; and (*ii*) a three-dimensional numerical simulation that allows determining the total losses in all elements of the equipment, allowing to measure the behaviour of the equipment in various test situations.

4.5.1. Two-dimensional flanking losses verification

In order to investigate the thermal bridges of the specimen frame, numerical studies were carried out for four different types of test specimen placement, namely:

i) Directly on the specimen frame, with 3.60 (W) by 2.70 (H) m², illustrated in Figure 4.24a;
ii) With an additional 100 mm insulation, with 3.40 (W) by 2.50 (H) m², explained in Figure 4.24b;
iii) With extra insulation of 200 mm, with 3.20 (W) by 2.30 (H) m², illustrated in Figure 4.24c;
iv) A reference model without interruption of the continuity of the walls chambers, shown in Figure 4.24d.

The thermal boundary conditions used in the numerical model of the wall were: (*i*) outside ambient temperature of 20° C; (*ii*) inside chambers ambient temperature of 50° C, in both sides of the specimen wall; (*iii*) film coefficient of 7.69 W/(m².K) for all surfaces.

To assess the situations in which it is necessary to place additional insulation, to maintain the precision of the HB apparatus measurements, four walls with 100 mm thickness were considered with different thermal conductance:

i) 15 W/(m².K), which is the maximum thermal conductance range of the HB apparatus;
ii) 1 W/(m².K);
iii) 0.5 W/(m².K);
iv) 0.25 W/(m².K).

The thermal properties of the passive components used for the present study are the conservative values presented in section 4.4, namely: λ_{steel} = 54.496 W/(m.K); $\lambda_{polyurethane}$ = 0.025 W/(m.K); λ_{PVC} = 0.168 W/(m.K); $\lambda_{rubber30}$ = 0.037 W/(m.K); and the additional insulation of polyurethane foam with impermeable facings with λ_{pol_foam} = 0.022 W/(m.K).

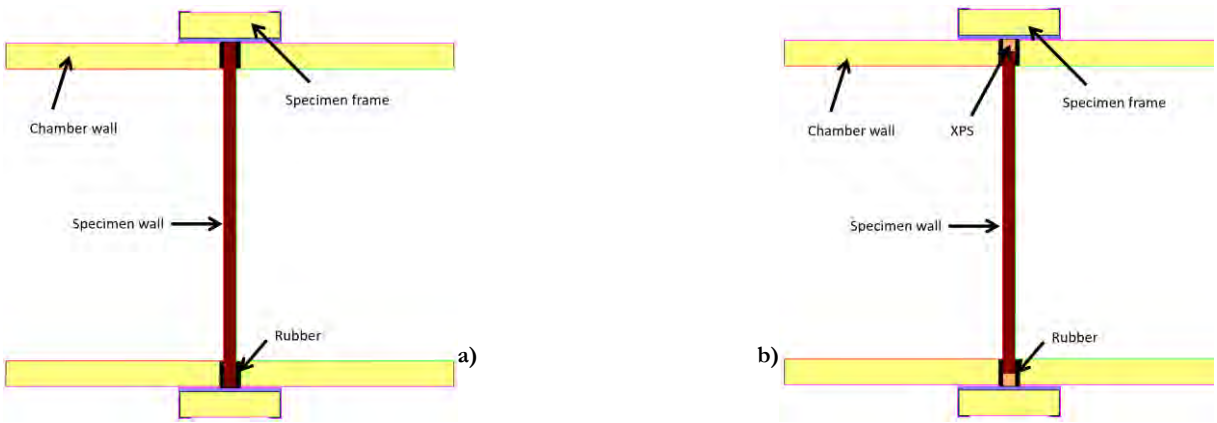

Figure 4.24 – Numerical models of the specimen placed directly: a) on the specimen frame; b) surrounded of insulation with 100 mm.

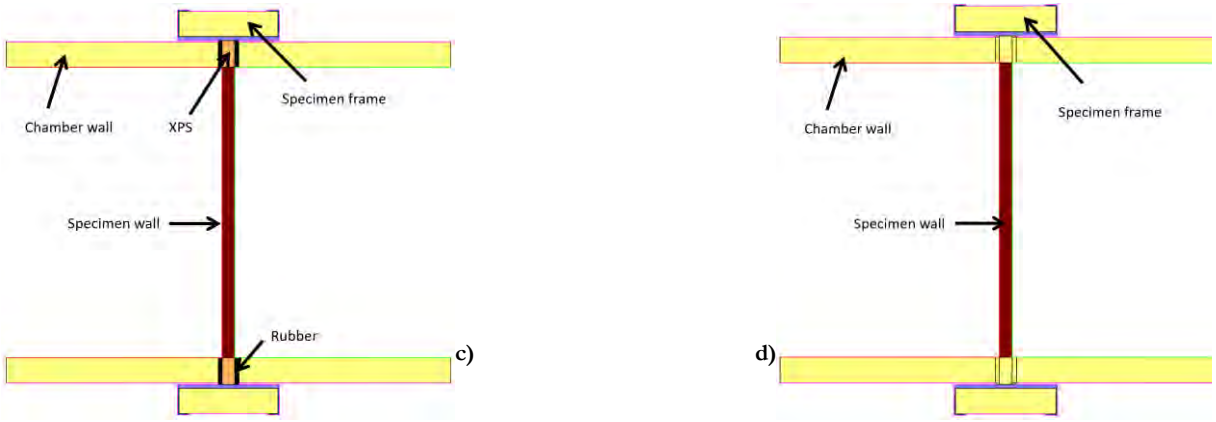

Figure 4.24 – Numerical models of the specimen placed directly: c) surrounded of insulation with 200 mm; d) reference model.

Table 4.5 shows the results of the simulations, presenting the heat flow (Q) and heat flux (q) of the surrounding elements of the apparatus, walls and specimen frame components.

The reference model, Figure 4.24d, allows quantifying the thermal losses that occur through the envelope, or that happen only in the ideal situation. In this numeric model, the losses by the specimen frame are equal to the losses through the boxes walls, i.e. there is continuity of internal insulation. By comparing the reference model with the other models, it is possible to calculate the energy losses that arise from having the specimen frame.

Flanking losses by the specimen frame are easy to measure only when testing homogeneous samples, which is why situations in which losses can be high, that is, non-homogeneous samples with high conductivity elements should be avoided.

Table 4.5 – Heat flow and heat flux of the walls and the specimen frame.

Type	Description specimen condition	Wall with thermal conductance of: [W/(m².K)]			
		15	**1**	**0.5**	**0.25**
1	Reference model	Q: **20.4003** q: **1.9247**	Q: **20.3855** q: **1.9233**	Q: **20.3754** q: **1.9224**	Q: **20.3581** q: **1.9207**
2	Placed directly on the specimen frame	Q: **28.9573** q: **2.7321** (Δ_{12} = 42 %)	Q: **22.1098** q: **2.0860** (Δ_{12} = 8 %)	Q: **21.2307** q: **2.0031** (Δ_{12} = 4 %)	Q: **20.7144** q: **1.9554** (Δ_{12} = 2 %)
3	Insulation of polyurethane foam with 100 mm	Q: **22.0665** q: **2.0819** (Δ_{13} = 8 %)	Q: **21.2132** q: **2.0014** (Δ_{13} = 4 %)	Q: **20.9231** q: **1.9740** (Δ_{13} = 3 %)	Q: **20.6849** q: **1.9516** (Δ_{13} = 2 %)
4	Insulation of polyurethane foam with 200 mm	Q: **20.7013** q: **1.9531** (Δ_{14} = 1 %)	Q: **20.6825** q: **1.9513** (Δ_{14} = 1 %)	Q: **20.6693** q: **1.9501** (Δ_{14} = 1 %)	Q: **20.6519** q: **1.9485** (Δ_{14} = 1 %)

Where: Q is the heat flow [W]; and q is the heat flux [W/m²].

From the results presented in Table 4.5, it is possible to conclude that for the condition of the wall with the thermal conductance of 15 W/(m².K) additional insulation of 200 mm must be used.

This numerical study concluded that to guarantee the accuracy of the measurements performed with HB apparatus, in order to avoid additional parameters in the post-treatment results and to take into account the marginal losses, it is recommended to place, at least, the following additional insulation surrounding for the specimens with the following thermal conductance:

i) between 15 and 1 W/(m².K) – additional insulation of 200 mm;

ii) between 1 and 0.5 W/(m².K) for a specimen with thickness:
- until 400 mm – additional insulation of 100 mm;
- between 400 and 800 mm – additional insulation of 200 mm;

iii) less than 0.5 W/(m².K) for a specimen with thickness:
- until 400 mm – there is no need for additional insulation;
- between 400 and 800 mm – additional insulation of 100 mm.

Figure 4.25 presents the temperature variations occurring in the four assembly situations, for the test specimen with Λ of 15 W/(m².K), being visible that in the condition without insulation, Figure 4.25a, and with less additional insulation, Figure 4.25b, there are flaking losses. Figure 4.26 shows the heat flux that occurs in the same numerical simulations. Is clear that the highest heat flow occurs in the situation where there is less insulation in the specimen frame, Figure 4.26a.

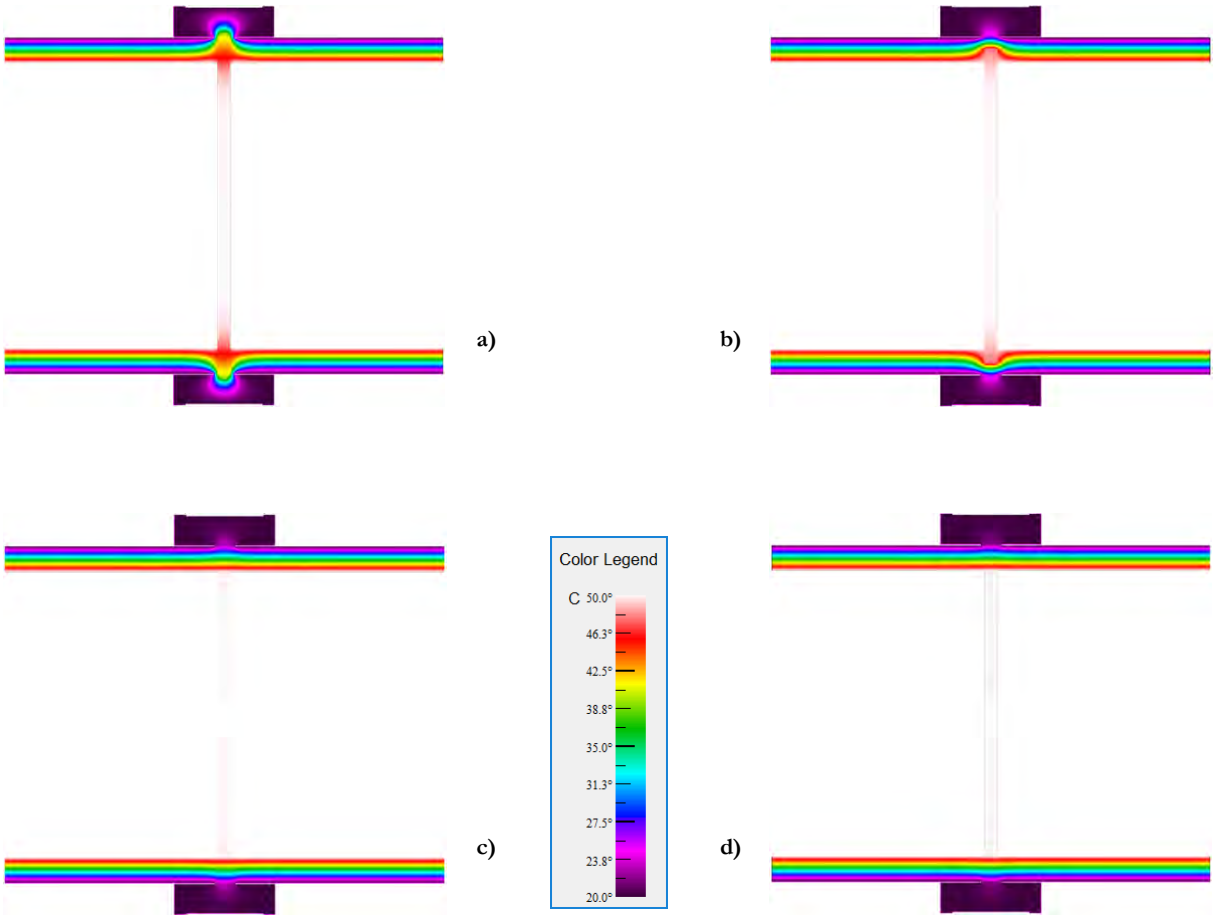

Figure 4.25 – Temperature variation when the specimen is placed directly: a) on the specimen frame; b) surrounded of insulation with 100 mm; c) surrounded of insulation with 200 mm; d) reference model.

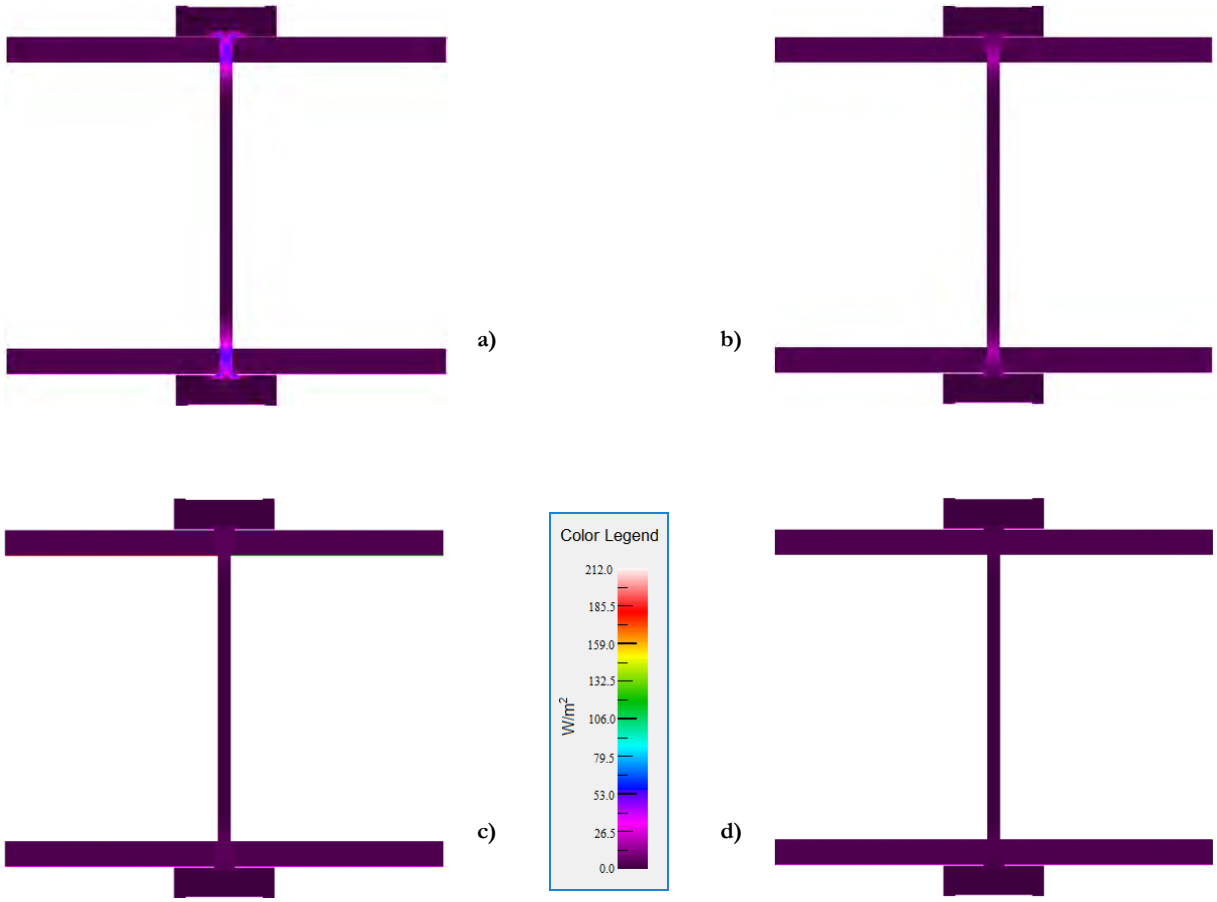

Figure 4.26 – Heat flux when the specimen is placed directly: a) on the specimen frame; b) surrounded of insulation with 100 mm; c) surrounded of insulation with 200 mm; d) reference model.

4.5.2. Three-dimensional flanking losses verification

For performing the calibration of the HB, it is necessary to have a complete characterization of the flanking losses of the equipment. The losses by the envelope are dependent on the thermal resistance of the sample and the test conditions, with the temperature being the most relevant.

The standard ASTM C1363-11 [18] suggests that the easiest way to predict flaking losses is to perform numerical models, which once validated, will allow estimating losses for other ranges of thermal resistances and temperatures. For this purpose, HB was modelled three-dimensionally with the software Ansys [144] software, to predict the losses by MB and specimen frame.

For both operating modes of the equipment, CHB and GHB, modelling runs are studied. Were studied three different thermal conductivities, with the thickness of the specimen ranged from 10 to 300 mm for each, to determine the effect of thickness. The three thermal conductivities used in numerical models are the ones of the materials used in the calibration of the equipment, presented in subsection 4.6. Figure 4.27 shows a slice of the apparatus in both modes with the specimen placed between chambers, namely Figure 4.27a CHB and Figure 4.27b the GHB. Between tests is changed the thickness of the models for the three types of thermal conductivities.

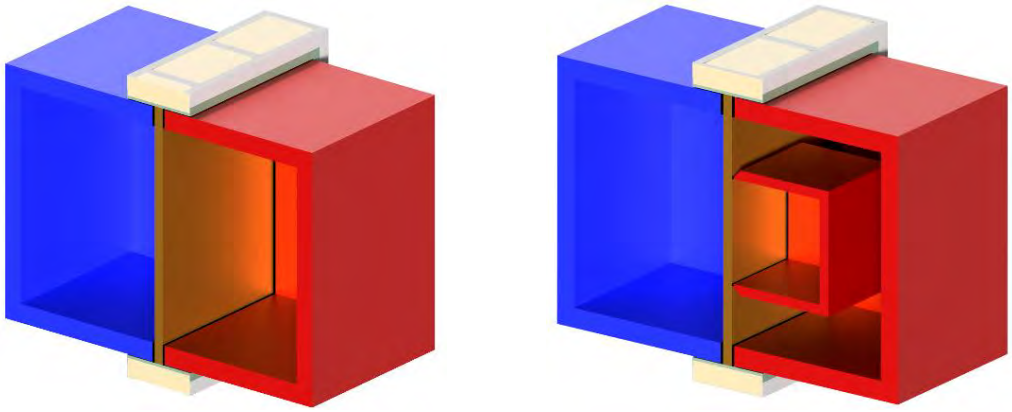

a) b)

Figure 4.27 – Half-section geometry of the HB apparatus for the FEM model, with a 100 mm thick specimen: a) CHB; and b) GHB.

Table 4.6 presents the 324 numerical models performed that allow full characterization of the apparatus for the intended thermal range and temperatures of the calibration. The boundary temperatures conditions used in the numerical models are in Table 4.6 and the film coefficient used is 7.69 W/(m².K) for all surfaces.

Table 4.6 – List of numerical models for obtaining the flanking losses of the equipment.

Numerical model n.º	MB air temperature [°C]	Lab. air temperature [°C]	CB air temperature [°C]	MB wall heat flux	Apparatus mode	λ [W/(m.K)]
1 to 12	27	27	5	0		
13 to 24	35	26	5	+	CHB	0.036
25 to 36	20	26	5	-		
37 to 48	35	35	5	0		
49 to 60	45	45	10	0		
61 to 72	35	20	5	+	GHB	0.036
73 to 84	45	35	10	+		
85 to 96	35	50	5	-		
97 to 108	45	55	10	-		
109 to 120	18	18	5	0		
121 to 132	45	18	5	+	CHB	0.175
133 to 144	10	18	5	-		
145 to 156	35	35	5	0		
157 to 168	45	45	10	0		
169 to 180	35	20	5	+	GHB	0.175
181 to 192	45	35	10	+		
193 to 204	35	50	5	-		
205to 216	45	55	10	-		
217 to 228	18	18	5	0		
229 to 240	45	18	5	+	CHB	0.039
241 to 252	10	18	5	-		
253 to 264	35	35	5	0		
265 to 276	45	45	10	0		
277 to 288	35	20	5	+	GHB	0.039
289 to 300	45	35	10	+		
301 to 312	35	50	5	-		
313 to 324	45	55	10	-		

With 12 models per configuration for obtaining the twelve points of the curve for the following thickness: 300, 200, 150, 90, 80, 60, 50, 40, 30, 20 and 10 mm.

Numeric models (1 to 108) with λ=0.036 W/(m.K):

For the numerical models, 1 to 36, presented in Table 4.6, with the apparatus in the CHB configuration, next are presented the results predicted by the 3D FEM models. Figure 4.28a illustrates the shape of the specimen frame flanking loss per unit temperature difference as a function of specimen thickness. Figure 4.28b shows the shape of the MB walls flanking loss per unit temperature difference as a function of the specimen thickness.

Comparing the charts of Figure 4.28, it is possible to conclude that the specimen thickness affects the flanking losses of the specimen frame less than in the MB walls. The MB walls flanking losses are substantially higher than those of the specimen frame. Figure 4.28b also shows that the best operating mode, which has fewer flaking losses, is where the MB have the same temperatures outside and inside, having heat flow in the walls almost null, as expected.

Figure 4.29 and Table 4.7 shows the relationship of MB walls flanking loss to the specimen thickness, being highlighted in the table the values that will be used in the calibration of specimen 1.

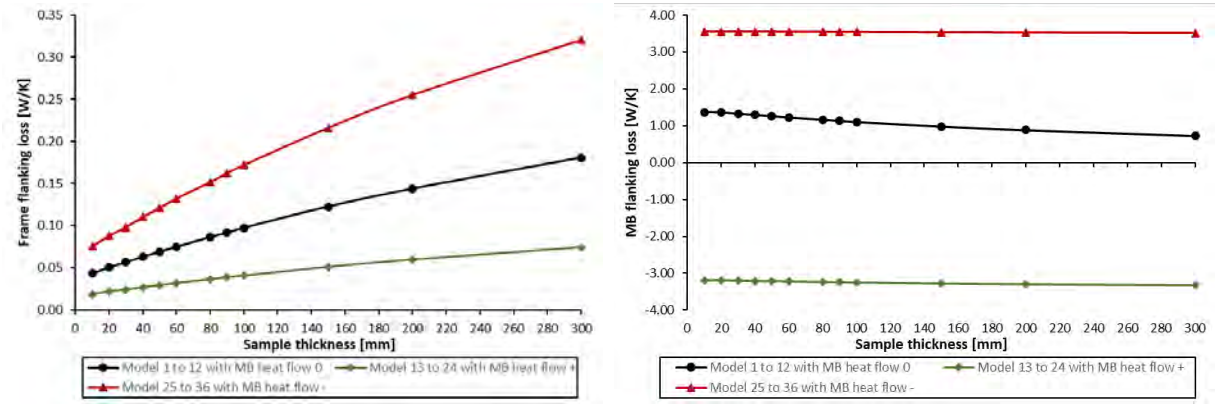

a) b)

Figure 4.28 – Relationship of flanking loss to specimen thickness, estimated with modelling, for models 1 to 36, for CHB of a specimen with specimen λ=0.036 W/(m.K) of: a) Specimen frame; and b) MB walls.

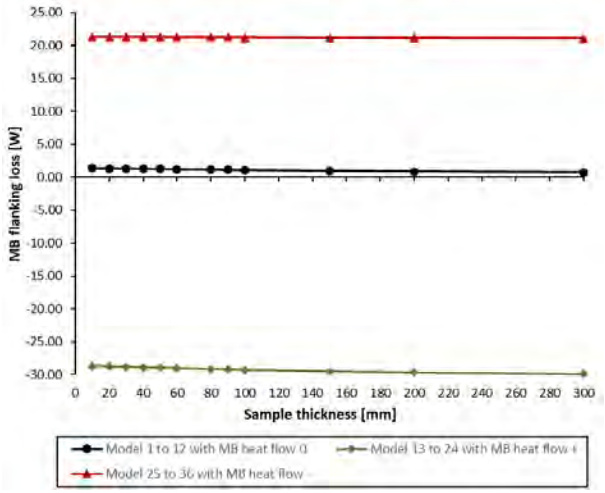

Figure 4.29 – Relationship of MB walls flanking loss to specimen thickness, for models 1 to 36, for CHB of a specimen with specimen λ=0.036 W/(m.K).

Table 4.7 – MB walls flanking loss to specimen thickness, for models 1 to 36, for CHB of a specimen with specimen λ=0.036 W/(m.K).

Thickness [mm]	Heat flow 0 [W]	Heat flow + [W]	Heat flow - [W]
300	0.728	-29.887	21.083
200	0.883	-29.632	21.160
150	0.980	-29.458	21.198
100	1.102	-29.235	21.243
90	1.132	-29.182	21.255
80	1.162	-29.128	21.267
60	1.223	-29.014	21.288
50	1.258	-28.949	21.300
40	1.291	-28.886	21.312
30	1.321	-28.827	21.319
20	1.360	-28.743	21.325
10	1.369	-28.704	21.314

For the numerical models, 37 to 108, presented in Table 4.6, with the apparatus in the GHB configuration are presented next the results predicted with the 3D FEM model. Figure 4.30a illustrates the shape of the specimen frame flanking loss per unit temperature difference as a function of specimen thickness. Figure 4.30b shows the shape of the MB walls flanking loss per unit temperature difference as a function of the specimen thickness.

Comparing the charts of Figure 4.30, it is possible to conclude that the specimen thickness affects less the flanking losses of the specimen frame than the MB walls. This is similar to the previous models, being where also the MB walls flanking losses substantial higher than those of the specimen frame. Figure 4.30b also shows that the best operating mode, having fewer flaking losses, is where the MB have the same temperatures outside and inside, having heat flow in the walls almost null, as expected. Is also visible that in this mode different temperatures, inside and outside of the MB, give almost the same values of flanking losses.

Figure 4.31 and Table 4.8 shows the relationship of MB walls flanking loss to the specimen thickness, being highlighted in the table the values that will be used in the calibration of specimen 1.

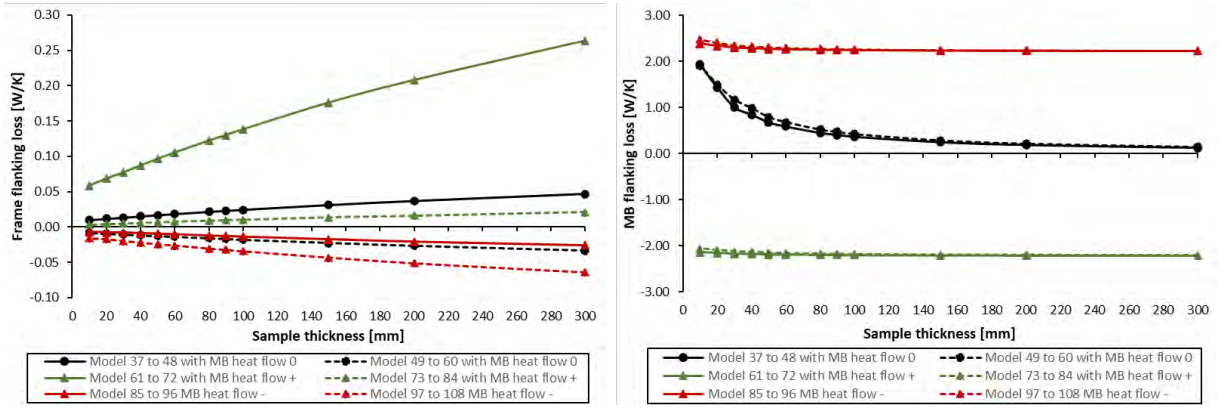

a) b)

Figure 4.30 – Relationship of flanking loss to specimen thickness, estimated with modelling, for models 37 to 108, for GHB of a specimen with specimen λ=0.036 W/(m.K) of: a) Specimen frame; and b) MB walls.

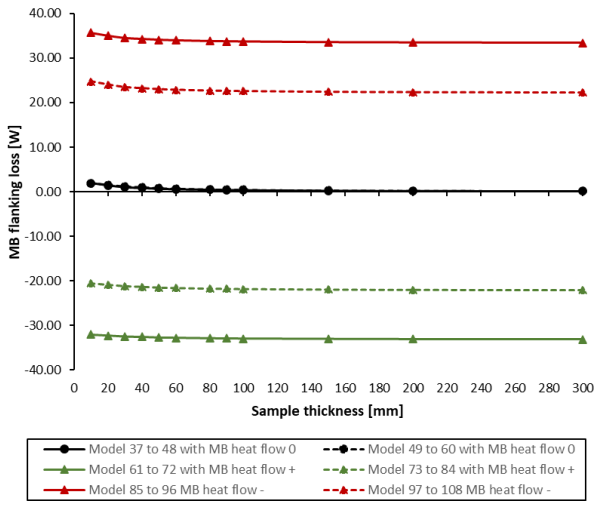

Figure 4.31 – Relationship of MB walls flanking loss to specimen thickness, for models 37 to 108, for GHB of a specimen with specimen λ=0.036 W/(m.K).

Table 4.8 – MB walls flanking loss to specimen thickness, for models 37 to 108, for GHB of a specimen with specimen λ=0.036 W/(m.K).

Thick-ness	Heat flow 0 [W]		Heat flow + [W]		Heat flow - [W]	
[mm]	Model 37 to 48	Model 49 to 60	Model 61 to 72	Model 73 to 84	Model 85 to 96	Model 97 to 108
300	0.125	0.146	-33.128	-22.022	33.379	22.315
200	0.187	0.218	-33.085	-21.963	33.459	22.399
150	0.248	0.289	-33.037	-21.901	33.533	22.479
100	0.364	0.424	-32.954	-21.787	33.682	22.636
90	0.405	0.472	-32.924	-21.747	33.733	22.691
80	0.449	0.524	-32.892	-21.703	33.791	22.752
60	0.586	0.684	-32.784	-21.563	33.956	22.930
50	0.679	0.792	-32.731	-21.481	34.089	23.066
40	0.846	0.988	-32.587	-21.301	34.280	23.277
30	1.003	1.171	-32.499	-21.164	34.506	23.505
20	1.433	1.495	-32.271	-20.873	35.022	24.065
10	1.931	1.907	-32.076	-20.567	35.700	24.765

Figure 4.32 illustrates the temperatures distribution on middle vertical cross-section, retrieved from the FEM model of the HB with approximated null heat flow in the MB walls, for CHB and GHB, respectively.

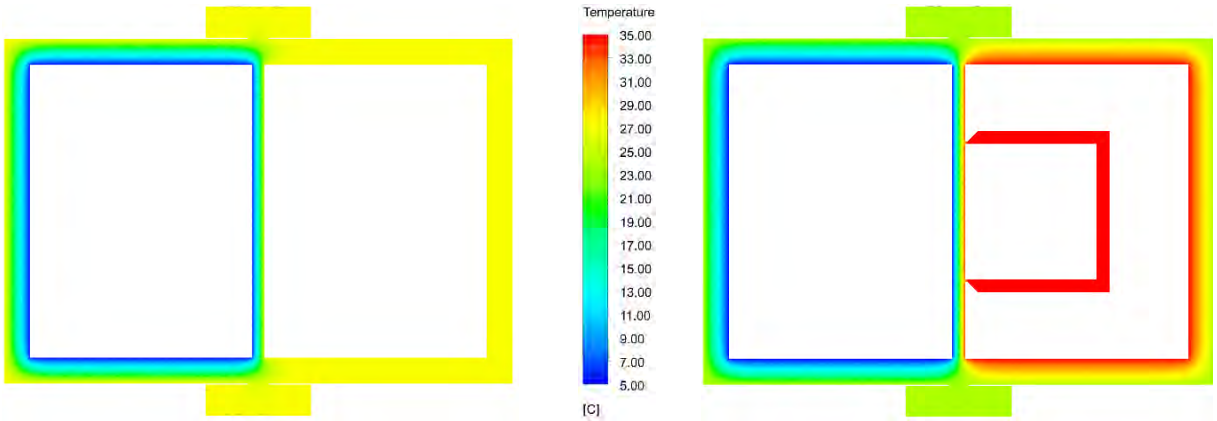

a) b)

Figure 4.32 – Temperatures distribution on middle vertical cross-section, retrieved from the FEM model of the HB with null heat flow in the MB walls of the: a) CHB; and b) GHB; for a specimen with specimen λ=0.036 W/(m.K).

Figure 4.33 illustrates the heat flux in the exterior walls, obtained with the numerical model, for the models where the heat flow in the MB walls is approximately null. It shows that the heat flow is minimal in the specimen frame, as expected, which is essential for achieving good test results.

Figure 4.32a and Figure 4.33a shows good stability in the MB of temperature and heat flux has a result of the boundary conditions in which is intended to have an almost null flow of energy in the walls. Figure 4.32b also shows excellent stability of temperature in the MB, as needed. The heat flux that occurs in the CB is not relevant because this camera is intended only to provide stability to the system, not being important the quantity of energy used for that purpose, in term of results. Being, of course, important minimize this lost for allowing to reduce the energy consumption of the equipment.

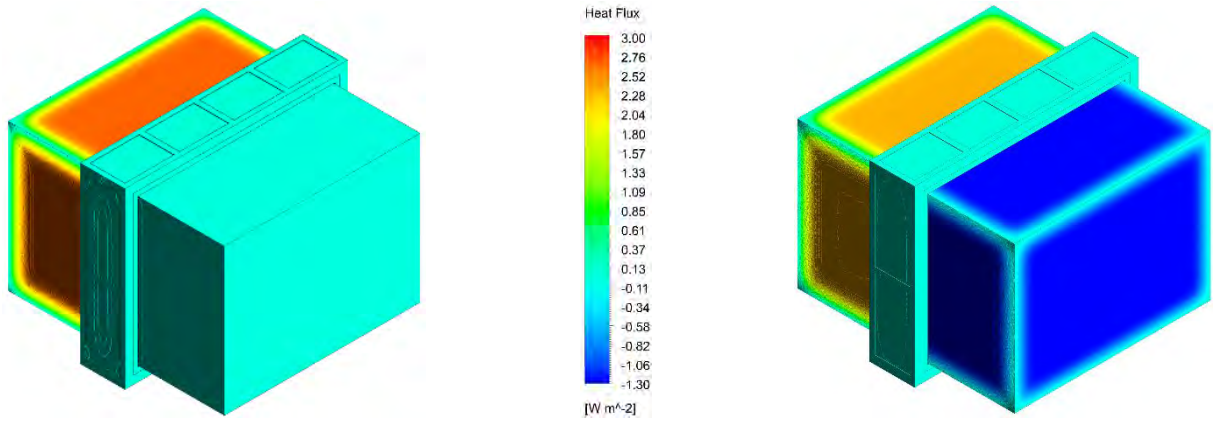

a) b)

Figure 4.33 – Heat Flux distribution exterior walls, retrieved from the FEM model of the HB with approximately null heat flow in the MB walls of the: a) CHB; and b) GHB; for a specimen with specimen λ=0.036 W/(m.K).

Numeric models (109 to 216) with λ=0.175 W/(m.K):

For the numerical models, 109 to 144, presented in Table 4.6, with the apparatus in the CHB configuration are presented next the results as predicted by the 3D FEM model. Figure 4.34a illustrates the shape of the specimen frame flanking loss per unit temperature difference as a function of specimen thickness. Figure 4.34b shows the shape of the MB walls flanking loss per unit temperature difference as a function of the specimen thickness.

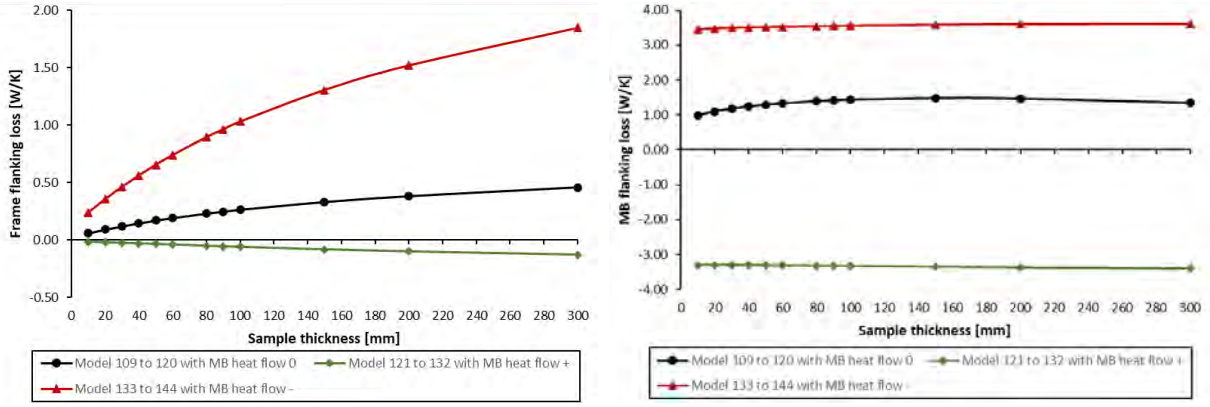

a) b)

Figure 4.34 – Relationship of flanking loss to specimen thickness, estimated with modelling, for models 109 to 144 for CHB of a specimen with specimen λ=0.175 W/(m.K) of: a) Specimen frame; and b) MB walls.

Comparing the charts of Figure 4.34, it is possible to conclude that the specimen thickness affects the flanking losses of the specimen frame less than in the MB walls, being the MB walls flanking losses higher than those of the specimen frame, like the models of the previous thermal conductivity (1 to 108).

Figure 4.35 and Table 4.9 shows the flanking losses of the MB wall, being highlighted the values that, for example, will be used in the calibration of specimen 2.

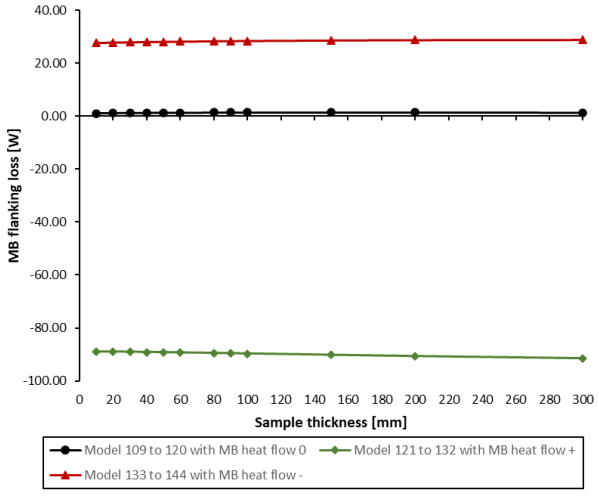

Figure 4.35 – Relationship of MB walls flanking loss to specimen thickness, for models 109 to 144, for CHB of a specimen with specimen λ=0.175 W/(m.K).

Table 4.9 – MB walls flanking loss to specimen thickness, for models 109 to 144, for CHB of a specimen with specimen λ=0.175 W/(m.K).

Thickness [mm]	Heat flow 0 [W]	Heat flow + [W]	Heat flow - [W]
300	1.34459	-91.52757	28.86242
200	1.46730	-90.70145	28.77672
150	1.48138	-90.22274	28.65315
100	1.43692	-89.72347	28.44761
90	1.41931	-89.62580	28.39579
80	1.39563	-89.52703	28.33590
60	1.33183	-89.33728	28.19697
50	1.29126	-89.23604	28.11434
40	1.24207	-89.15283	28.02592
30	1.17939	-89.08283	27.92394
20	1.10046	-88.99619	27.79601
10	0.98678	-89.00605	27.65149

For the numerical models, 145 to 156, presented in Table 4.6, with the apparatus in the GHB configuration, are presented next the results obtained from the numerical model. Figure 4.36a illustrates the shape of the specimen frame flanking loss per unit temperature difference as a function of specimen thickness. Figure

4.36b shows the shape of the MB walls flanking loss per unit temperature difference as a function of the specimen thickness.

Comparing the charts of Figure 4.36, it is possible to conclude that the specimen thickness also affects less the flanking losses of the specimen frame, than the MB walls. This is similar to the previous models being were also the MB walls flanking losses substantial higher than those of the specimen frame. Figure 4.36b shows that in the mode in which the heat flow in the MB walls is almost null, for thickness lower than 80mm, the flaking losses increased substantially. This is because, for this range of thermal conductance, it is recommended to use additional insulation on the periphery, as recommended in sub-section 4.5.1. However, it is possible to carry out tests on the entire area of the sample holder, having to use the corrective value of losses on the periphery here presented.

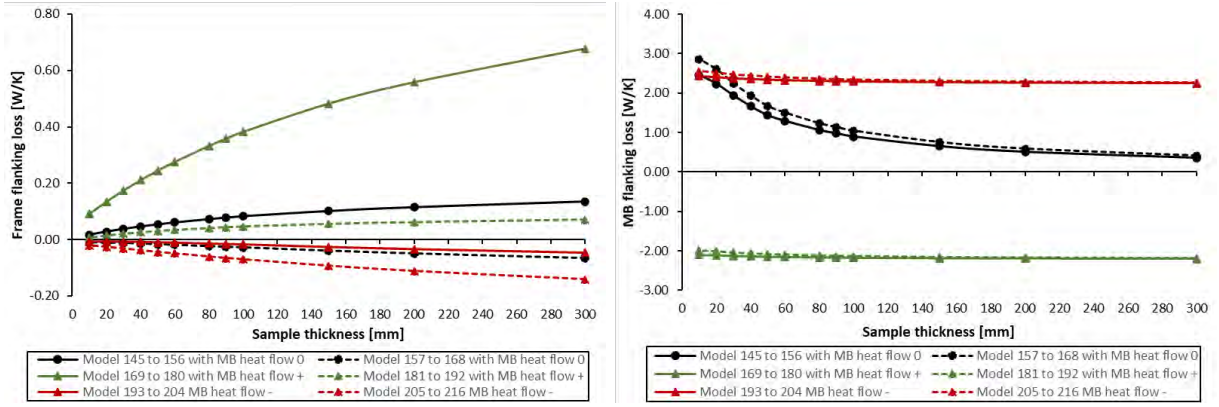

a) b)

Figure 4.36 – Relationship of flanking loss to specimen thickness, estimated with modelling, for models 145 to 216, for GHB of a specimen with specimen λ=0.175 W/(m.K) of: a) Specimen frame; and b) MB walls.

Figure 4.37 and Table 4.10 shows the flanking losses of the MB wall, being highlighted the values that, for example, will be used in the calibration of specimen 3 and 4.

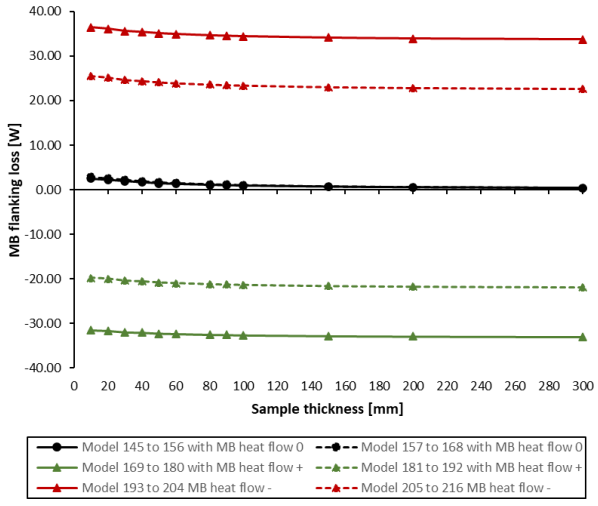

Figure 4.37 – Relationship of MB walls flanking loss to specimen thickness, for models 145 to 216, for GHB of a specimen with specimen λ=0.175 W/(m.K).

Table 4.10 – MB walls flanking loss to specimen thickness, for models 145 to 216, for GHB of a specimen with specimen λ=0.175 W/(m.K).

Thick-ness	Heat flow 0 [W]		Heat flow + [W]		Heat flow - [W]	
[mm]	Model 145 to 156	Model 157 to 168	Model 169 to 180	Model 181 to 192	Model 193 to 204	Model 205 to 216
300	0.353	0.412	-33.044	-21.852	33.749	22.676
200	0.506	0.591	-32.934	-21.703	33.947	22.885
150	0.650	0.758	-32.828	-21.560	34.127	23.076
100	0.896	1.046	-32.649	-21.318	34.441	23.409
90	0.976	1.138	-32.591	-21.240	34.543	23.516
80	1.059	1.236	-32.531	-21.158	34.649	23.629
60	1.292	1.507	-32.352	-20.922	34.935	23.936
50	1.434	1.673	-32.259	-20.789	35.128	24.135
40	1.662	1.939	-32.076	-20.553	35.401	24.432
30	1.936	2.252	-31.973	-20.402	35.626	24.664
20	2.234	2.607	-31.658	-19.988	36.126	25.201
10	2.456	2.865	-31.531	-19.793	36.442	25.522

Figure 4.38 illustrates the temperatures distribution on middle vertical cross-section, retrieved from the FEM model of the HB with positive heat flow in the MB walls, for CHB and GHB.

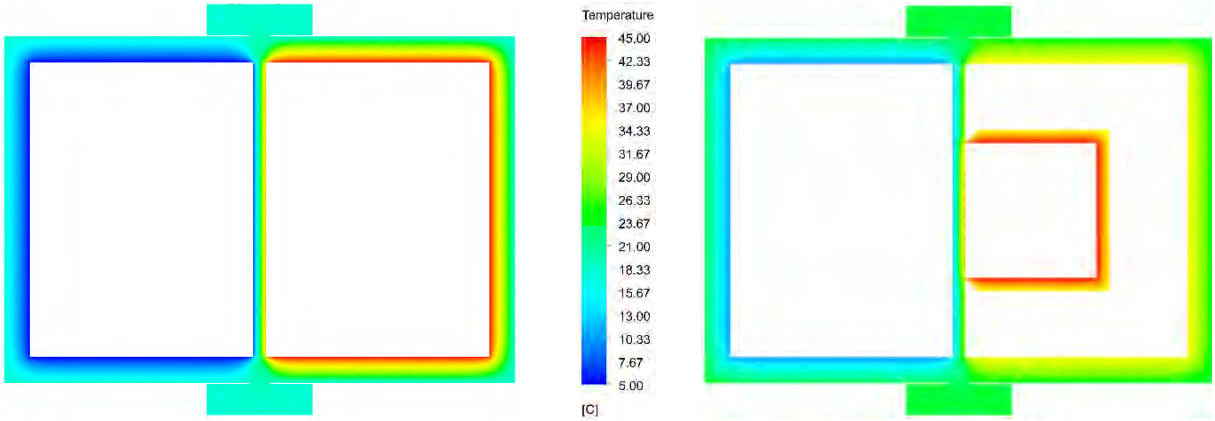

a) b)

Figure 4.38 – Temperatures distribution on middle vertical cross-section, retrieved from the FEM model of the HB with positive heat flow in the MB walls of the: a) CHB; and b) GHB; for a specimen with specimen λ=0.175 W/(m.K).

Figure 4.39 illustrates the heat flux in the exterior walls, obtained with the numerical model, for the models where the heat flow in the MB walls is positive, which means by the standards that the flow of energy is from the interior to the exterior. To be noted that in the legend of the images retrieved from the Ansys, the negative heat flux means that the energy is coming out from that boundary.
Figure 4.39a and Figure 4.39b show a high increase in the heat flux, concerning the previous images of heat flux, due to the operation mode, in which the interior of the MB has a higher temperature than the exterior, which results in a significant increase in flanking losses by walls. The specimen frame continues to show low losses of energy.

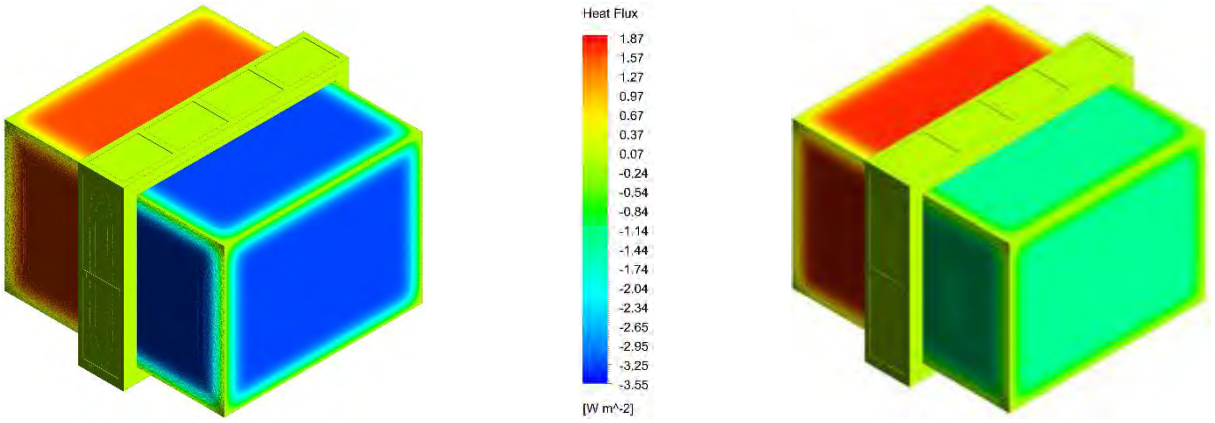

a) b)

Figure 4.39 – Heat Flux distribution exterior walls, retrieved from the FEM model of the HB with positive heat flow in the MB walls of the: a) CHB; and b) GHB; for a specimen with specimen λ=0.175 W/(m.K).

Numeric models (217 to 324) with λ=0.039 W/(m.K):

For the numerical models, 217 to 252, presented in Table 4.6, with the apparatus in the CHB configuration are presented next the results of the numerical models. Figure 4.40a illustrates the shape of the specimen frame flanking loss per unit temperature difference as a function of specimen thickness. Figure 4.40b shows

the shape of the MB walls flanking loss per unit temperature difference as a function of the specimen thickness.

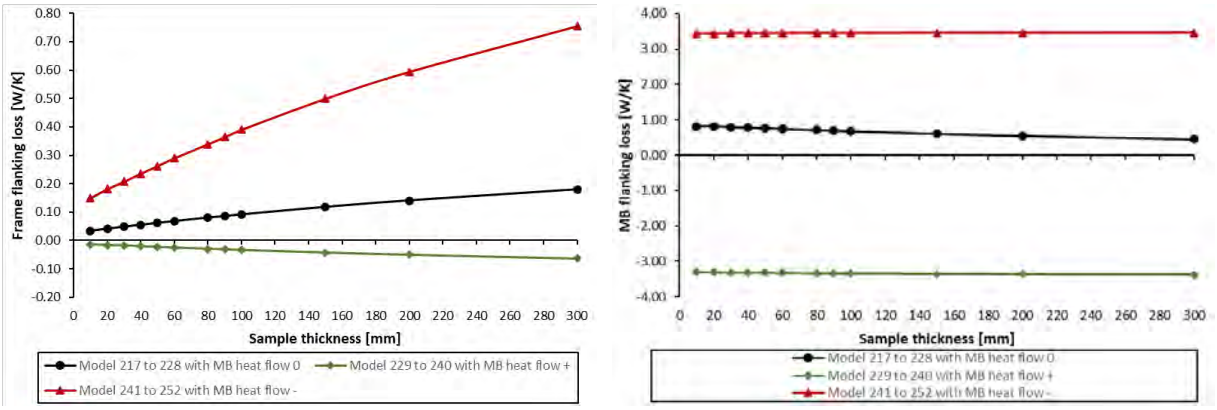

a) b)

Figure 4.40 – Relationship of flanking loss to specimen thickness, estimated with modelling, for models 217 to 228, for CHB of a specimen with specimen λ=0.039 W/(m.K) of: a) Specimen frame; and b) MB walls.

The charts of Figure 4.40b it is similar to the chart of Figure 4.28b due to the similarity of thermal conductivity (0.036 vs 0.039 W/(m.K)). This allows us to conclude that for close conductivity, the variation is small, being able to draw curves of more distant conductivity values and to deduce the values between them by interpolation.

Figure 4.41 and Table 4.11 shows the flanking losses of the MB wall, being highlighted the values that, for example, will be used in the calibration of specimen 3 and 4.

It is interesting to compare the charts in Figure 4.29 with those in Figure 4.41, and the data in Table 4.7 with Table 4.11, in which the values of the models with positive heat flow on the MB walls are very different, however when divided by the difference in temperatures on the walls of which model, they give similar values of flanking losses. This is perceptible when comparing the graphs of Figure 4.28b and Figure 4.40b, which allows concluding that for equal temperature differences it is obtained approximately equal values, the reason why this type of chart is ideal for characterizing the flanking losses of the equipment.

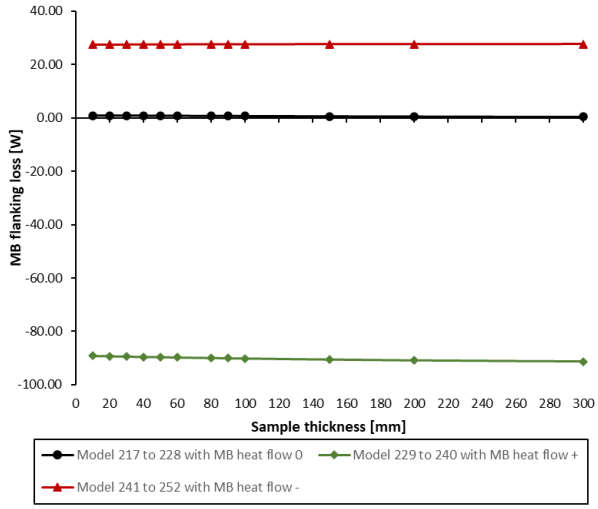

Figure 4.41 – Relationship of MB walls flanking loss to specimen thickness, for models 217 to 252, for CHB of a specimen with specimen λ=0.039 W/(m.K).

Table 4.11 – MB walls flanking loss to specimen thickness, for models 217 to 252, for CHB of a specimen with specimen λ=0.039 W/(m.K).

Thickness [mm]	Heat flow 0 [W]	Heat flow + [W]	Heat flow - [W]
300	0.45864	-91.31813	27.65197
200	0.55219	-90.88659	27.64540
150	0.60898	-90.57445	27.62645
100	0.67827	-90.17621	27.59830
90	0.69457	-90.08450	27.59222
80	0.71122	-89.99023	27.58584
60	0.74415	-89.78908	27.56895
50	0.76247	-89.67405	27.55864
40	0.77967	-89.56623	27.54906
30	0.79412	-89.45847	27.53587
20	0.81325	-89.30159	27.51417
10	0.81461	-89.21155	27.48916

For the numerical models, 253 to 324, presented in Table 4.6, with the apparatus in the GHB configuration are presented next the results, as predicted by the 3D FEM model. Figure 4.42a illustrates the shape of the specimen frame flanking loss per unit temperature difference as a function of specimen thickness. Figure 4.42b shows the shape of the MB walls flanking loss per unit temperature difference as a function of the specimen thickness.

Comparing the charts of Figure 4.42, it is possible to conclude that the specimen thickness also affects less the flanking losses of the specimen frame, than the MB walls, which is similar to the previous models, being where also the MB walls flanking losses substantial higher than those of the specimen frame.

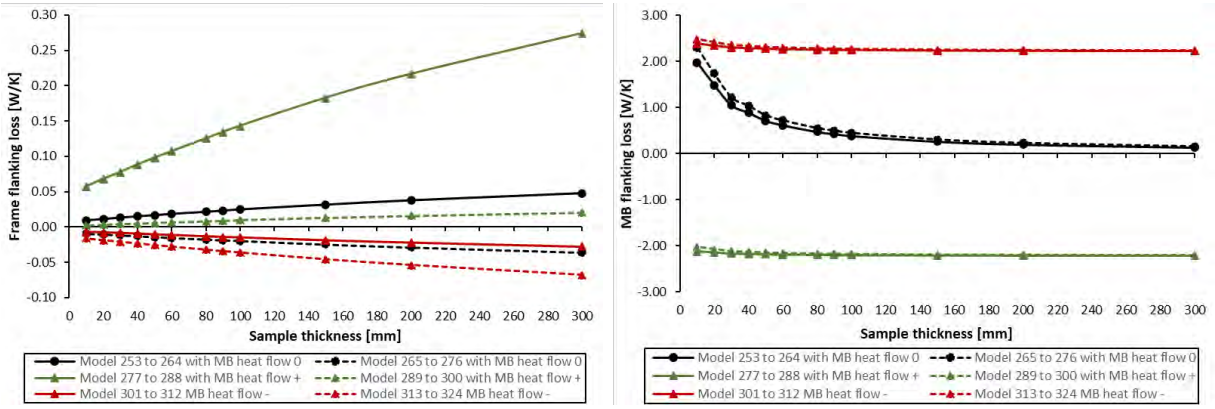

a) b)

Figure 4.42 – Relationship of flanking loss to specimen thickness, estimated with modelling, for models 253 to 324, for GHB of a specimen with specimen λ=0.039 W/(m.K) of: a) Specimen frame; and b) MB walls.

Figure 4.43 and Table 4.12 shows the relationship of MB walls flanking loss to the specimen thickness, being highlighted in the table the values that will be used in the calibration of specimen 3 ad 4.

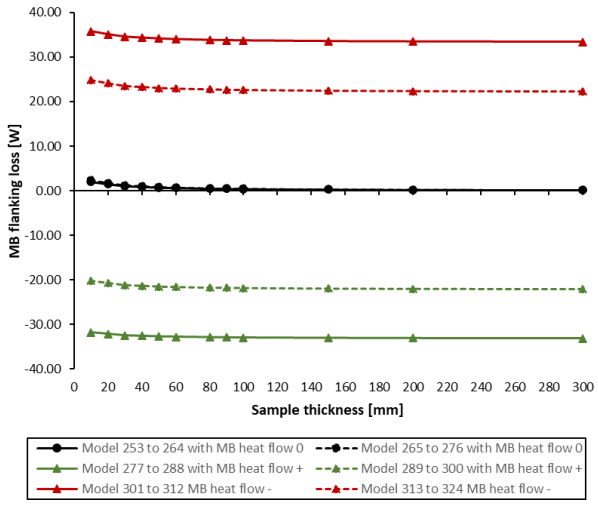

Figure 4.43 – Relationship of MB walls flanking loss to specimen thickness, for models 253 to 324, for GHB of a specimen with specimen λ=0.039 W/(m.K).

Table 4.12 – MB walls flanking loss to specimen thickness, for models 253 to 324, for GHB of a specimen with specimen λ=0.039 W/(m.K).

Thick-ness	Heat flow 0 [W]		Heat flow + [W]		Heat flow - [W]	
	Model 253	Model 265	Model 277	Model 289	Model 301	Model 313
[mm]	to 264	to 276	to 288	to 300	to 312	to 324
300	0.133	0.155	-33.128	-22.019	33.394	22.329
200	0.197	0.230	-33.083	-21.957	33.477	22.417
150	0.262	0.305	-33.033	-21.891	33.556	22.501
100	0.383	0.447	-32.946	-21.772	33.712	22.666
90	0.426	0.497	-32.914	-21.729	33.766	22.724
80	0.473	0.552	-32.881	-21.684	33.826	22.787
60	0.615	0.718	-32.768	-21.537	33.999	22.973
50	0.712	0.831	-32.712	-21.452	34.137	23.114
40	0.886	1.033	-32.564	-21.266	34.335	23.333
30	1.046	1.220	-32.473	-21.126	34.565	23.566
20	1.486	1.733	-32.122	-20.672	35.094	24.139
10	1.974	2.303	-31.813	-20.221	35.761	24.828

Figure 4.44 illustrates the temperatures distribution on middle vertical cross-section, retrieved from the FEM model of the HB with negative heat flow in the MB walls, for CHB and GHB.

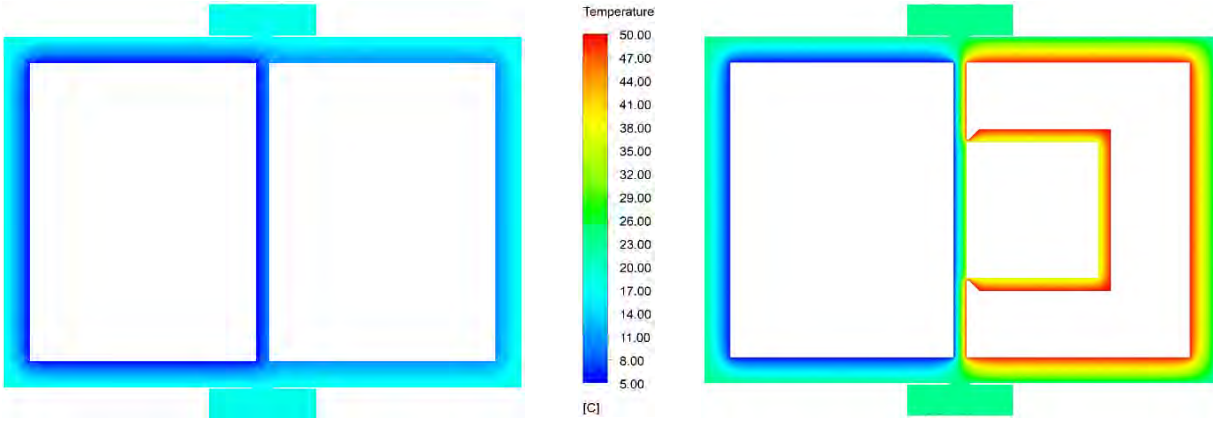

a) b)

Figure 4.44 – Temperatures distribution on middle vertical cross-section, retrieved from the FEM model of the HB with negative heat flow in the MB walls of the: a) CHB; and b) GHB; for a specimen with specimen λ=0.039 W/(m.K).

Figure 4.45 illustrates the heat flux in the exterior walls, obtained with the numerical model, for the models where the heat flow in the MB walls is negative, which means by that the flow of energy is from the exterior to the interior of the chambers. Similarly to the previous heat flux images, there is a significant increase in heat transmission through the walls that in this situation translates into the addition of energy to the MB from the surrounding environment, which has to be accounted in the calculation of the total energy that enters in the camera.

The 324 models made allow characterizing the losses completely and necessarily for understanding the working mode of the apparatus and to perform the equipment calibration. The models show that the ideal test mode is to use the equipment in an approximately zero heat flow mode on the MB walls, thus obtaining results that are close to reality and the corrections of values are very low. The other modes of operation are only interesting for dynamic regimes, which is following the common practice of operation of this type of equipment, allowing these models to have a sense of the magnitude of the error.

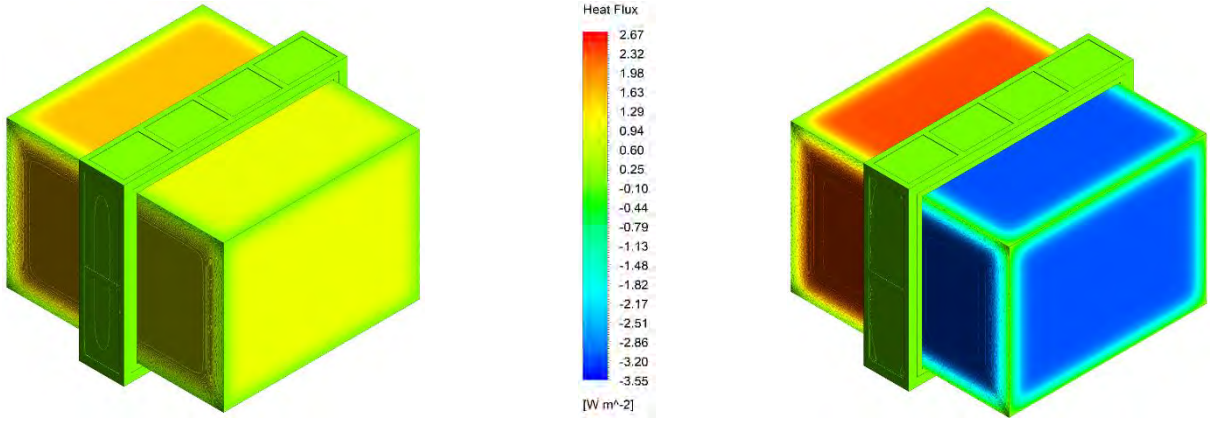

a) b)

Figure 4.45 – Heat Flux distribution exterior walls, retrieved from the FEM model of the HB with negative heat flow in the MB walls of the: a) CHB; and b) GHB; for a specimen with specimen λ=0.039 W/(m.K).

4.6. CALIBRATION AND VERIFICATIONS

The calibration of the hot box apparatus is essential for verifying the performance and is required before testing of products can begin. There is no requirement for GHB to perform the calibration of the equipment by the standards. However, the ISO 8990 [17] and BS 874-3.1:1987 [277] recommended. For CHB, this proceeding is mandatory. ASTM C1363-11 [18] requires the calibration of both types of apparatus, being the standard with more details and verification requirements. The complete apparatus characterization intends to verify the assumptions made during the design phase and to quantify the heat transfer paths of the apparatus.

The outcome expected from the process is to obtain the calibration factor by which the future test results will multiply to get accurate measurements. The calibration factor gives the magnitude of the heat losses and imperfections of the apparatus, being essential to minimize them.

The calibration of the equipment is done using homogeneous specimens, with known thermal resistance that covers the range of use of the desired thermal resistance. The samples must have different thickness and thermal resistance, in a variety of environmental conditions that will allow performing tests similar to the range in which the apparatus will work. The joints between the specimen panels must not form thermal bridges and shall provide on both sides a facing impervious to air and moisture transfer.

ASTM C1363-11 [18] defines that the first step for characterization of the hot box is developing a matrix that identifies all the test conditions and anticipates all specimens for testing. Table 4.13 illustrates ASTM C1363-11 [18] test matrix for calibration, where the apparatus operates at a wide range of temperatures, air velocities, and different specimens thickness.

Table 4.13 – ASTM C1363 Table A6.2 - Test matrix for calibration [18].

Hot box used for general testing at different environmental conditions including multiple air velocities.							
Test No.	Metering Chamber Air Temperature, °C	Guard Chamber[A] Air Temperature, °C	Climate Chamber Air Temperature, °C	Metering Wall Thermopile Output, Volts	Calibration Panel Thickness,[B] mm	Metering Chamber Air Velocity, m/s	Climate Chamber Air Velocity, m/s
1	21.1	21.1	−17.8	0	50	0.2	5.4
2	21.1	18.3	−17.8	+	50	0.2	5.4
3	21.1	23.9	−17.8	−	50	0.2	5.4
4	21.1	21.1	−17.8	0	50	0.4	5.4
5	21.1	18.3	−17.8	+	50	0.4	5.4
6	21.1	23.9	−17.8	−	50	0.4	5.4
7	21.1	21.1	−17.8	0	50	0.2	1.3
8	21.1	18.3	−17.8	+	50	0.2	1.3
9	21.1	21.1	−17.8	−	50	0.2	1.3
10	21.1	21.1	−17.8	0	50	0.4	1.3
11	21.1	18.3	−17.8	+	50	0.4	1.3
12	21.1	23.9	−17.8	−	50	0.4	1.3
13	21.1	21.1	−17.8	0	114	0.2	5.4
14	21.1	18.3	−17.8	+	114	0.2	5.4
15	21.1	23.9	−17.8	−	114	0.2	5.4
16	21.1	21.1	−17.8	0	152	0.2	5.4
17	21.1	18.3	−17.8	+	152	0.2	5.4
18	21.1	23.9	−17.8	−	152	0.2	5.4
Hot box used for wall and fenestration testing at different environmental conditions.							
Test No.	Metering Chamber Air Temperature, °F	Guard Chamber[A] Air Temperature, °F	Climate Chamber Air Temperature, °F	Metering Wall Thermopile Output, Volts	Calibration Panel Thickness,[B] in.	Metering Chamber Air Velocity, mph	Climate Chamber Air Velocity, mph
19	21.1	21.1	−17.8	0	203	0.2	5.4
20	21.1	18.3	−17.8	+	203	0.2	5.4
21	21.1	23.9	−17.8	−	203	0.2	5.4
22	37.8	37.8	10.0	0	50	0.2	1.3
23	37.8	35.0	10.0	+	50	0.2	1.3
24	37.8	40.6	10.0	−	50	0.2	1.3
25	37.8	37.8	10.0	0	50	0.4	1.3
26	37.8	35.0	10.0	+	50	0.4	1.3
27	37.8	40.6	10.0	−	50	0.4	1.3
28	37.8	37.8	10.0	0	114	0.2	1.3
29	37.8	35.0	10.0	+	114	0.2	1.3
30	37.8	40.6	10.0	−	114	0.2	1.3
31	37.8	37.8	10.0	0	152	0.2	1.3
32	37.8	35.0	10.0	+	152	0.2	1.3
33	37.8	40.6	10.0	−	152	0.2	1.3
34	37.8	37.8	10.0	0	203	0.2	1.3
35	37.8	35.0	10.0	+	203	0.2	1.3
36	37.8	40.6	10.0	−	203	0.2	1.3

[A] Guard chamber or surrounding laboratory environment.
[B] Or continuous surround panel.

This case is for a hot box used for testing walls over one set of temperatures and air velocities. The purpose of this matrix is to evaluate the metering chamber heat flow and thermal chamber flanking loss of the apparatus over a wide range of test conditions. The table listed 36 cases, and the completion of all is not necessary if there is no significant variation in the metering wall heat flux and flanking loses coefficients during the testing of the extremes values of each particular environmental condition. ASTM C1363-11 [18] recommends a full characterization of the hot box for research purposes since the equipment is going to perform several different test conditions.

For the matrix of Table 4.13 the ASTM C1363-11 [18] recommends performing: (*i*) a test at each of the environmental conditions in the characterization matrix; (*ii*) a minimum of one test, in the matrix, with the GB temperature above the MB air temperature; (*iii*) a test with GB temperature equal to the MB air temperature; and (*iv*) a test with the GB temperature below the MB air temperature. All tests must be done at steady-state conditions and the other temperatures, and air velocities shall be held constant.
The test results allow identifying which environmental conditions that do not significantly influence on the flanking loss coefficients. The parameters that show no significant changes in the flanking loss coefficients can be removed from the calibration testing matrix.

The tests matrix for calibration also allows a performance check, which helps to ensure compliance with the design requirements. This check should cover the temperature uniformity and stability, air velocity and surface coefficients for hot and cold sides. The repeatability of the data obtained in the experiments is evaluated by comparing the temperature readings obtained in the experiments with identical configurations.

The uncertainty estimation is also important to verify, being dependent on the precision and bias of this method upon the apparatus and operating procedures, and upon the specimen properties and test conditions. The basis for determining uncertainties is an analysis that uses the propagation of errors theory. ASTM C1363-11 [18] suggests an outline procedure for the uncertainty analysis for thermal resistance, which consists of obtaining the individual uncertainty for each item of equation (52) and (53). The estimation is made from instrument and transducer uncertainty or from the results of characterization experiments designed to investigate these uncertainties. ASTM C1363-11 [18] recommends following the propagation of errors theory, which assumes that errors are independent and not systematic, the uncertainties are combined by adding in the square root of the sum of the squares for the absolute uncertainties for sums and the relative uncertainties, fractional or percentage of the variable, for the products or quotients. The guide to the expression of uncertainty in measurement (GUM), of the Bureau International des Poids et Mesures [288] and the document for evaluation of measurement uncertainty in calibration from Portuguese Institute of Accreditation [289] suggests the following equation for the determination of the combined standard uncertainty of uncorrelated input quantities:

$$u_c^2(y) = \sum_{i=1}^{N} \left(\frac{\partial f}{\partial x_i}\right)^2 u^2(x_i) \tag{61}$$

where: $u_c(y)$ is the combined standard uncertainty; f is a functional relationship of measured quantities; and $u(x_i)$ is the standard uncertainty evaluated.

The calculation of the uncertainties is reported next to the results, of the thermal transmittance and conductance, in the following sections.

For the apparatus calibration and verification, a series of hot box tests were run on homogeneous specimens with known thermal characteristics. Four types of walls tested, namely: (*i*) extruded polystyrene (XPS) panels with 100 mm thickness (specimen 1); (*ii*) calcium silicate boards with 24 mm thickness (specimen 2); (*iii*) expanded polystyrene (EPS) panels with 50 mm (specimen 3); and (*iv*) EPS panels with 100 mm (specimen 4). The base decision for the materials was upon the thermal conductivity and the thickness, which is

expected to match those of the test samples range that will be tested in the future. Next subsections present the tests and results.

4.6.1. Specimen 1

For the first set of calibration tests, it was assembled in the specimen frame, a wall composed of seven XPS panels with 600 mm width and 100 mm thickness, that fulfils the 3.60 (W) by 2.70 (H) m² of the frame. This reference material has a thermal conductivity, retrieved from the certificate of the manufacturer, of 0.036 W/(m.° C).
An experimental study was carried out using the TPS method to confirm the values of the thermal conductivity. Table 4.14 presents the results of the experimental campaign, which tested three pairs of samples for each material and performed five repetitions for each analysis. The obtained experimental result is 1.7% different from the certificate value, being used for calibration purposes the value of the certificate.

Table 4.14 – Thermal conductivity of extruded polystyrene [W/(m.K)]

Test repetition n.º	Sample			Average λ	Certificate λ
	1	2	3		
1	0.0363	0.0363	0.0365	**0.0366** ±5% (Standard Deviation: 0.0002)	**0.036** **(Δ_λ=1.7%)**
2	0.0363	0.0363	0.0370		
3	0.0363	0.0363	0.0368		
4	0.0363	0.0363	0.0364		
5	0.0364	0.0364	0.0364		

The next sub-sections present the calibration and verifications for the CHB and GHB method with the XPS specimen.

4.6.1.1. Calibrated Hot Box mode

For the full characterization of the apparatus in CHB mode, Table 4.15 presents the test matrix for the calibration, composed of 18 tests. These tests aim to fully characterize the equipment, having different combinations of temperatures and air velocities for each box of the equipment, namely MB and CB, and temperature variations concerning the surrounding chamber (the room where the device is located) to impose a heat flow through the MB walls. It should be noted that the temperatures of the external environment of the HB are not programmed temperatures, but temperatures recorded during the tests. This is because the laboratory space where is located the equipment is large, being difficult to control the temperature. Due to this situation when the test matrix requires the same temperatures in the metering box and surrounding environment (tests: 1, 4,7, 10, 13 and 16), the temperature of the metering box is adjusted to that of the room.

The sample has the following instrumentation: (*i*) fourth two thermocouples for surface temperature, being twenty-one in each side of the specimen; and (*ii*) twelve heat flux sensors, namely six in each face. With all sensors placed on each side of the wall (hot and cold side) to have symmetry at the measuring points. Figure 4.46 shows the location of all temperature and heat flux sensors placed on the cold side of the XPS wall surface, and shows the limits of the metering area with 3.18 (W) by 2.28 (H) m².

Table 4.15 – Test matrix for calibration of the CHB with XPS panels 100 mm thick.

Test n.º	MB air temperature [°C]	Lab. air temperature [°C]	CB air temperature [°C]	MB wall heat flux	MB air velocity [m/s]	CB air velocity [m/s]
1	27	27	5	0	0.2	4.2
2	35	25	5	+	0.2	4.2
3	20	27	5	-	0.2	4.2
4	26	26	5	0	0.4	4.2
5	35	27	5	+	0.4	4.2
6	20	27	5	-	0.4	4.2
7	27	27	5	0	0.2	1.3
8	35	27	5	+	0.2	1.3
9	20	27	5	-	0.2	1.3
10	27	27	5	0	0.4	1.3
11	35	27	5	+	0.4	1.3
12	20	27	5	-	0.4	1.3
13	27	27	10	0	0.2	1.3
14	45	27	10	+	0.2	1.3
15	20	27	10	-	0.2	1.3
16	27	27	10	0	0.4	1.3
17	45	27	10	+	0.4	1.3
18	20	27	10	-	0.4	1.3

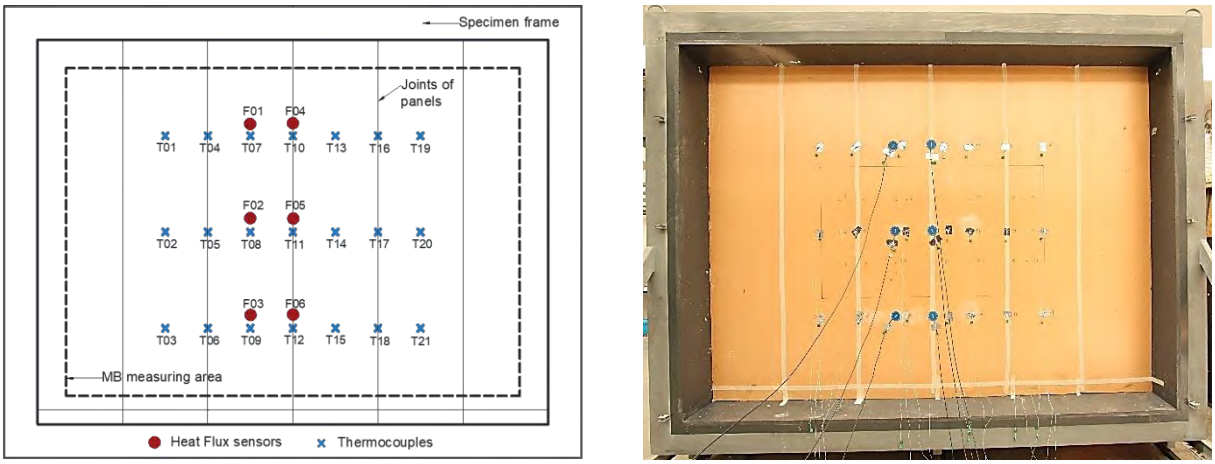

a) **b)**

Figure 4.46 – Location of temperature and heat flux sensors placed on the CHB cold side of the XPS wall surface: a) sketch; b) photo.

The calibration matrix tests were performed according to the requirements presented in section 3.4.2. The test time starts counting from the moment that the setpoints were reached with a difference of less than 1%. All tests had a minimum duration of 8 hours, and the test conditions were achieved on average between one and two hours. Some tests were repeated to verify the repeatability of the equipment, being made 26 tests in total, whose results are shown in Table 4.16. The tests are group by the type, in three groups, namely: (*i*) group "0" for the scenario where the MB wall heat flux in near null; (*ii*) group "+" where the MB temperature is higher than the surrounding room and is losing energy by the walls; and (*iii*) group "-" when the surround room temperature is higher than in the MB, which is winning energy through the walls.

Table 4.16 shows the main results of the tests which allow assessing the thermal conductance and thermal transmittance according to the equations presented in section 3.4.3. The heat flow rate (Φ) is obtained by

correcting the total power imputed to the system by subtracting the flanking losses of the MB, which were obtained numerically in section 4.5.2, chart of Figure 4.29. Next, is obtained the experimental thermal conductance that is multiplied by the calibration factor obtain experimentally, giving the calibrated thermal conductance. Figure 4.47, Figure 4.49 and Figure 4.51 present the relationship of conductance to mean specimen temperature of the three test group cases, from which is obtain the calibration factor.

Table 4.16 shows the difference between thermal conductance obtained experimentally by the CHB method and the reference value. It shows that, as expected, the better results are obtained when the equipment operates in the way the heat flow in the walls of the MB is close to zero. The other test modes are not interesting for tests in steady-state, and calibration has performed in these modes intending to obtain the calibration coefficients for tests in dynamic regime.

Table 4.16 – Test results for calibration of the CHB with XPS panels 100 mm thick.

Test n.º	MB_w	Φ_p [W]	T_{n1} [°C]	$T_{n.out}$ [°C]	T_{n2} [°C]	ΔT_s [°C]	Φ [W]	Λ' [W/(m².K)]	C	Λ [W/(m².K)]	$\Delta\Lambda$	U [W/(m².K)]
M01.C001	0	53.169	27.04	26.19	5.00	20.17	52.067	0.356	1.0018	**0.357** ±0.005	-0.9%	0.336 ±0.004
M01.C002		53.329	27.04	26.06	5.00	20.19	52.227	0.357		**0.357** ±0.005	-0.7%	0.337 ±0.004
M01.C003		53.453	27.05	26.01	5.00	20.19	52.351	0.358		**0.358** ±0.005	-0.5%	0.338 ±0.004
M04.C004		55.846	27.02	26.82	5.00	21.02	54.744	0.359		**0.360** ±0.005	0.0%	0.339 ±0.004
M04.C005		55.987	27.02	25.62	5.00	21.08	54.884	0.359		**0.360** ±0.005	-0.1%	0.339 ±0.004
M04.C006		56.145	27.02	26.20	5.00	21.06	55.042	0.361		**0.361** ±0.005	0.3%	0.340 ±0.004
M07.C007		56.036	27.03	26.26	5.00	21.03	54.934	0.360		**0.361** ±0.005	0.3%	0.340 ±0.004
M10.C008		54.768	27.07	26.09	5.00	20.60	53.666	0.359		**0.360** ±0.005	0.0%	0.339 ±0.004
M13.C009		44.535	27.09	26.14	10.00	17.01	43.433	0.352		**0.353** ±0.006	-2.0%	0.333 ±0.005
M16.C010		44.461	27.10	26.08	10.00	16.97	43.359	0.352		**0.353** ±0.006	-1.9%	0.333 ±0.005
M02.C011	+	101.229	35.10	26.13	5.00	27.30	71.909	0.363	1.0004	**0.363** ±0.005	0.9%	0.342 ±0.004
M02.C012		101.128	35.10	25.45	5.00	27.31	71.808	0.363		**0.363** ±0.005	0.8%	0.342 ±0.004
M02.C013		101.084	35.10	26.51	5.00	27.31	71.764	0.362		**0.363** ±0.005	0.7%	0.342 ±0.004
M05.C014		102.115	35.01	26.03	5.00	27.62	72.795	0.364		**0.364** ±0.005	1.0%	0.343 ±0.004
M08.C015		101.518	35.06	25.94	5.00	27.40	72.198	0.363		**0.364** ±0.005	1.0%	0.342 ±0.004
M11.C016		102.160	35.02	26.42	5.00	27.70	72.840	0.363		**0.363** ±0.005	0.8%	0.342 ±0.004
M14.C017		116.811	45.05	25.59	10.00	33.05	87.491	0.365		**0.365** ±0.006	1.5%	0.344 ±0.005
M17.C018		116.202	45.10	25.45	10.00	32.85	86.882	0.365		**0.365** ±0.006	1.4%	0.344 ±0.005
M03.C019	-	15.224	20.00	25.19	5.00	13.66	36.104	0.365	1.0008	**0.365** ±0.006	1.3%	0.344 ±0.005
M03.C020		15.182	20.00	26.45	5.00	13.68	36.062	0.364		**0.364** ±0.006	1.1%	0.343 ±0.005
M03.C021		15.414	20.01	25.24	5.00	13.67	36.294	0.366		**0.367** ±0.006	1.8%	0.345 ±0.005
M06.C022		15.770	20.15	26.19	5.00	13.89	36.650	0.364		**0.364** ±0.006	1.2%	0.343 ±0.005
M09.C023		14.719	20.30	27.23	5.00	13.41	35.599	0.366		**0.367** ±0.006	1.8%	0.345 ±0.005
M12.C024		15.210	20.06	25.72	5.00	13.66	36.090	0.364		**0.365** ±0.006	1.3%	0.343 ±0.005
M15.C025		2.608	20.20	25.21	10.00	8.80	23.488	0.368		**0.369** ±0.009	2.4%	0.347 ±0.008
M18.C026		3.155	20.05	27.08	10.00	8.98	24.035	0.369		**0.370** ±0.008	2.7%	0.348 ±0.007

Where: MB_w is the MB wall heat flux; Φ_p is de total power input; T_{n1} is the environmental temperature of the hot side; $T_{n.out}$ is the environmental temperature of the room where is the apparatus; T_{n2} is the environmental temperature of the cold side; ΔT_s is the surface temperature difference across the specimen; Φ is the heat flow rate; Λ' is the experimental thermal conductance; C is the calibration factor; Λ is the calibrated thermal conductance; $\Delta\Lambda$ is the thermal conductance difference between the material reference value and the calibrated obtain value; and U is the thermal transmittance

Figure 4.48, Figure 4.50 and Figure 4.52 show charts of ambient temperatures and air velocities in the MB and CB, for a test of each group, during the test period in which the test conditions are fulfilled, and from where the analysis of the results is performed. It is visible that the system has very satisfactory stability.

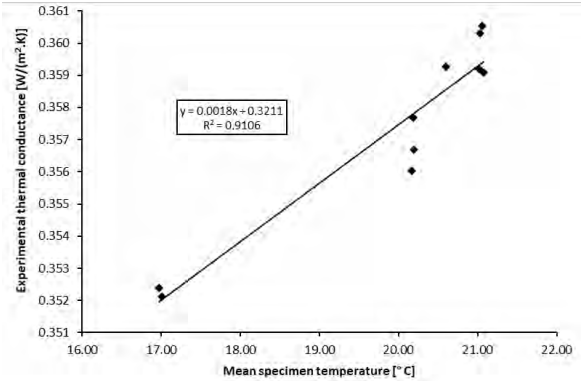

Figure 4.47 – Relationship of conductance to mean specimen temperature of test cases with MB wall heat flux near zero for CHB with XPS panels.

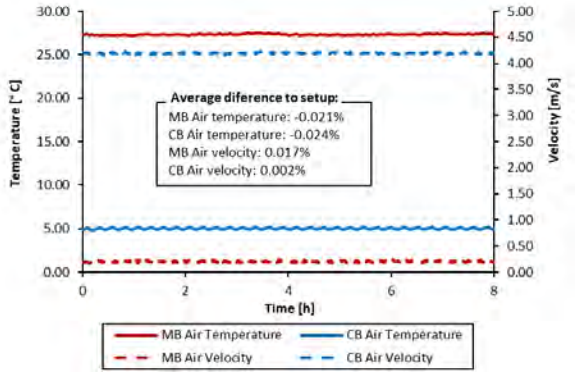

Figure 4.48 – Test M01.C001 air temperature and velocity in chambers for CHB with XPS panels.

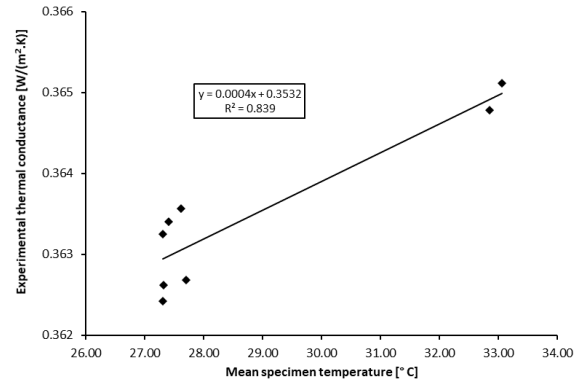

Figure 4.49 – Relationship of conductance to mean specimen temperature of test cases with MB wall heat flux positive for CHB with XPS panels.

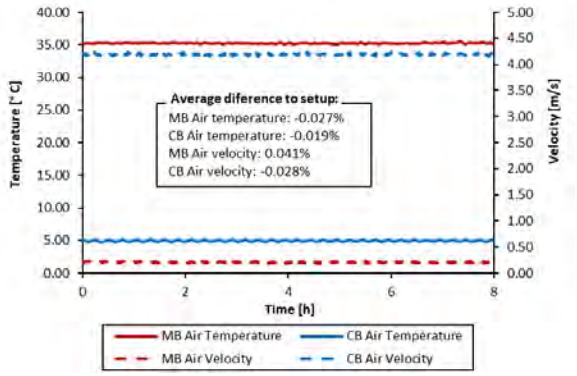

Figure 4.50 – Test M02.C011 air temperature and velocity in chambers for CHB with XPS panels.

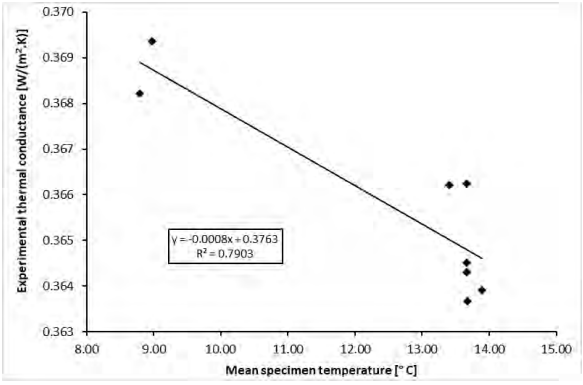

Figure 4.51 – Relationship of conductance to mean specimen temperature of test cases with MB wall heat flux negative for CHB with XPS panels.

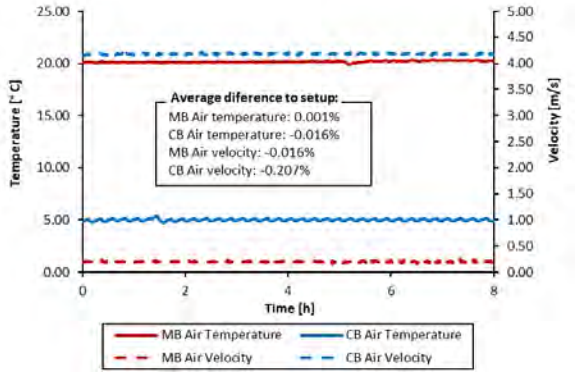

Figure 4.52 – Test M03.C019 air temperature and velocity in chambers for CHB with XPS panels.

Table 4.17 shows a comparison between the CHB and HFM method for the tests performed. It is reminded that the equipment is equipped with 12 heat flux sensors, which allows measuring the thermal conductance simultaneously with the performance of the tests by the other method.

From the results obtained, it is confirmed that the flowmeters method is less rigorous, as expected, compared to the CHB method. However, it can be seen that the average result difference is only 3%, and

the maximum individual difference is 6% in relation to the reference value of the material. These errors are lower than that traditionally obtained, which can reach up to 10% when performed *in situ*, being more accurate in this scenario because the test is performed in a controlled laboratory environment, with known flanking losses.

Comparing methodologies, the maximum difference in results is 6%. Table 4.17 also shows the average difference between the calibrated thermal conductance value obtained by the CHB method and the reference material, giving a low value of only 0.7%, as a result of the technique being more rigorous and the performed calibration.

Table 4.17 – Test results of CHB vs HFM method for XPS panels 100 mm thick.

Test n.º	Λ_{CHB} [W/(m².K)]	Λ_{HFM} [W/(m².K)]	$\Delta\Lambda_{HFM\rightarrow Ref}$	$\Delta\Lambda_{CHB\rightarrow HFM}$	λ_{HFM} [W/(m.K)]	U_{HFM} [W/(m².K)]
M01.C001	**0.357** ±0.005	**0.372** ±0.012	3.2%	4.1%	0.0372	0.350 ±0.011
M01.C002	**0.357** ±0.005	**0.369** ±0.012	2.5%	3.4%	0.0369	0.347 ±0.011
M01.C003	**0.358** ±0.005	**0.370** ±0.012	2.8%	3.4%	0.0370	0.348 ±0.011
M04.C004	**0.360** ±0.005	**0.368** ±0.012	2.2%	2.2%	0.0368	0.346 ±0.011
M04.C005	**0.360** ±0.005	**0.361** ±0.011	0.3%	0.3%	0.0361	0.340 ±0.010
M04.C006	**0.361** ±0.005	**0.368** ±0.012	2.2%	1.9%	0.0368	0.346 ±0.011
M07.C007	**0.361** ±0.005	**0.374** ±0.012	3.8%	3.5%	0.0374	0.351 ±0.011
M10.C008	**0.360** ±0.005	**0.370** ±0.012	2.7%	2.7%	0.0370	0.348 ±0.011
M13.C009	**0.353** ±0.006	**0.374** ±0.012	3.8%	5.8%	0.0374	0.351 ±0.011
M16.C010	**0.353** ±0.006	**0.374** ±0.012	3.9%	6.0%	0.0374	0.352 ±0.011
M02.C011	**0.363** ±0.005	**0.369** ±0.012	2.6%	1.8%	0.0369	0.348 ±0.011
M02.C012	**0.363** ±0.005	**0.371** ±0.012	2.9%	2.1%	0.0371	0.349 ±0.011
M02.C013	**0.363** ±0.005	**0.373** ±0.012	3.7%	2.8%	0.0373	0.351 ±0.011
M05.C014	**0.364** ±0.005	**0.368** ±0.012	2.3%	1.2%	0.0368	0.347 ±0.011
M08.C015	**0.364** ±0.005	**0.372** ±0.012	3.4%	2.3%	0.0372	0.350 ±0.011
M11.C016	**0.363** ±0.005	**0.371** ±0.012	3.0%	2.1%	0.0371	0.349 ±0.011
M14.C017	**0.365** ±0.006	**0.374** ±0.012	3.9%	2.5%	0.0374	0.352 ±0.011
M17.C018	**0.365** ±0.006	**0.378** ±0.012	5.0%	3.6%	0.0378	0.355 ±0.011
M03.C019	**0.365** ±0.006	**0.369** ±0.012	2.5%	1.1%	0.0369	0.347 ±0.011
M03.C020	**0.364** ±0.006	**0.372** ±0.012	3.4%	2.3%	0.0372	0.350 ±0.011
M03.C021	**0.367** ±0.006	**0.369** ±0.012	2.6%	0.6%	0.0369	0.347 ±0.011
M06.C022	**0.364** ±0.006	**0.366** ±0.012	1.8%	0.7%	0.0366	0.345 ±0.011
M09.C023	**0.367** ±0.006	**0.379** ±0.012	5.4%	3.4%	0.0379	0.356 ±0.011
M12.C024	**0.365** ±0.006	**0.371** ±0.012	3.2%	1.7%	0.0371	0.349 ±0.011
M15.C025	**0.369** ±0.009	**0.372** ±0.014	3.4%	0.8%	0.0372	0.350 ±0.012
M18.C026	**0.370** ±0.008	**0.362** ±0.013	0.6%	-2.1%	0.0362	0.341 ±0.012
Average	**0.362** ±0.009	**0.371** ±0.014			0.037	0.349 ±0.012
SD	**0.0042**	**0.0039**			0.0004	0.0035
ΔR	**0.7%**	**3.0%**			3.0%	2.8%

Where: Λ_{CHB} is the calibrated thermal conductance obtain by the CHB method; Λ_{HFM} is the thermal conductance obtained by the difference between the reference material value and the calibrated obtain value; $\Delta\Lambda_{HFM\rightarrow Ref}$ is the thermal conductance difference between HFM method and the reference value of the specimen; $\Delta\Lambda_{CHB\rightarrow HFM}$ is the thermal conductance difference between CHB method and HFM method; λ_{HFM} is the thermal conductivity obtain with HFM method; U_{HFM} is the thermal transmittance obtained with HFM method; SD is the standard deviation; and ΔR is the difference in relation to the reference value

Table 4.18 shows the repeatability of the equipment, namely for thermal conductance, ambient temperatures and air velocities in the chambers. This study is carried out for some of the calibration matrix tests, which

were repeated for this purpose. It is observed that a relative standard deviation percentage is low for all parameters, lower than 1%, which demonstrates an excellent performance of the equipment.

Table 4.18 – Tests repeatability on the CHB with XPS panels 100 mm thick.

Test n.º	Λ_{CHB} [W/(m².K)]	T_{n1} [°C]	T_{n2} [°C]	V_{n1} [m/s]	V_{n2} [m/s]	Test n.º	Λ_{CHB} [W/(m².K)]	T_{n1} [°C]	T_{n2} [°C]	V_{n1} [m/s]	V_{n2} [m/s]
M01.C001	0.357	27.043	4.999	0.201	4.200	M03.C019	0.365	20.002	4.999	0.201	4.186
M01.C002	0.357	27.042	5.000	0.202	4.192	M03.C020	0.364	20.000	4.998	0.201	4.200
M01.C003	0.358	27.046	5.000	0.202	4.194	M03.C021	0.367	20.005	4.999	0.202	4.174
Average	**0.357**	**27.044**	**5.000**	**0.202**	**4.196**	**Average**	**0.365**	**20.002**	**4.999**	**0.201**	**4.187**
SD	**0.0005**	**0.0015**	**0.0006**	**0.0001**	**0.0033**	**SD**	**0.0012**	**0.0021**	**0.0003**	**0.0004**	**0.0110**
RSD%	**0.13%**	**0.01%**	**0.01%**	**0.05%**	**0.08%**	**RSD%**	**0.34%**	**0.01%**	**0.01%**	**0.18%**	**0.26%**
M02.C011	0.363	35.100	4.999	0.205	4.198	M04.C004	0.360	27.017	5.001	0.400	4.173
M02.C012	0.363	35.100	5.000	0.204	4.197	M04.C005	0.360	27.017	5.000	0.400	4.178
M02.C013	0.363	35.097	5.000	0.204	4.195	M04.C006	0.361	27.020	4.999	0.400	4.166
Average	**0.363**	**35.099**	**5.000**	**0.204**	**4.197**	**Average**	**0.360**	**27.018**	**5.000**	**0.400**	**4.172**
SD	**0.0000**	**0.0014**	**0.0005**	**0.0003**	**0.0012**	**SD**	**0.0005**	**0.0013**	**0.0009**	**0.0001**	**0.0048**
RSD%	**0.00%**	**0.00%**	**0.01%**	**0.17%**	**0.03%**	**RSD%**	**0.13%**	**0.00%**	**0.02%**	**0.02%**	**0.12%**

Where: Λ_{CHB} is the calibrated thermal conductance obtain by the CHB method; T_{n1} is the environmental temperature of the hot side; T_{n2} is the environmental temperature of the cold side; V_{n1} is the air velocity in the hot side; V_{n2} is the air velocity in the cold side; SD is the standard deviation; RSD is the relative standard deviation

Furthermore, six tests were performed with a longer duration, 24 hours. The first set of three tests was carried out during the software development phase of the equipment. Due to the software development phase be a time-consuming process, and cannot be done continuously, tests were carried out in CHB mode using an independent alternative data recording system. This approach allows starting to make verifications of the equipment, perform tests of specimens using the HFM methodology and have data obtained with other data logging system. The second set of three tests was a repetition of the previous ones, with the equipment already completed and calibration carried out, using the same test conditions.

The experimental tests were performed in a steady-state regime, with average ambient temperatures of 40° C and 10° C in the hot and cold chambers, respectively, and the air velocity in both chambers was 0.5 m/s. The convergence interval was 24 hours.

For the first set of test the wall was instrumented with: (*i*) sixth thermocouples type K with ± 2.2° C accuracy; (*ii*) twelve heat flux sensors Hukseflux type HFP01 with ± 3 % accuracy; (*iii*) two thermo-hygrometers with ± 3 % accuracy; and (*iv*) two air velocity sensors with ± 1 % accuracy, being the data registered in a data logger. Half of these sensors were placed on each side of the wall (hot and cold side) to have symmetry at the measuring points.

The average thermal conductance (Λ) of the first set obtained experimentally by the heat flow meters method was 0.37 W/(m².K) that gives a thermal conductibility (λ) of 0.037 W/(m.K), which is 2.8 % higher than the reference value. Table 4.19 summarises the results obtained.

The second set of tests, performed after the equipment calibration phase, obtained results identical to those of the first set, for the HFM method. In this set it is possible to compare the difference between methodologies, CHB vs HFM, being 0.5% and 2.8% respectively, which are identical values to the ones

achieved in Table 4.17 of the matrix tests.

Table 4.19 – Results of the 24h test duration of CHB and HFM method for XPS panels.

Test n.º	Λ_{CHB} [W/(m².K)]	Λ_{HFM} [W/(m².K)]	$\Delta\Lambda_{HFM\rightarrow Ref}$	$\Delta\Lambda_{CHB\rightarrow HFM}$
M00.C027		**0.364** ±0.012	1.1%	
M00.C028		**0.375** ±0.012	4.2%	
M00.C029		**0.371** ±0.012	3.1%	
M00.C030	**0.362** ±0.006	**0.370** ±0.012	2.8%	2.2%
M00.C031	**0.361** ±0.006	**0.369** ±0.012	2.5%	2.2%
M00.C032	**0.362** ±0.006	**0.371** ±0.012	3.1%	2.5%
Average	**0.362** ±0.006	**0.370** ±0.012		
SD	**0.0005**	**0.0010**		
ΔR	**0.5%**	**2.8%**		

Where: Λ_{CHB} is the calibrated thermal conductance obtain by the CHB method; Λ_{HFM} is the thermal conductance obtained by the difference between the reference material value and the calibrated obtain value; $\Delta\Lambda_{HFM\rightarrow Ref}$ is the thermal conductance difference between HFM method and the reference value of the specimen; $\Delta\Lambda_{CHB\rightarrow HFM}$ is the thermal conductance difference between CHB method and HFM method; SD is the standard deviation; and ΔR is the difference in relation to the reference value

4.6.1.2. Guarded Hot Box mode

For the full characterization of the apparatus in GHB mode, Table 4.20 presents the tests matrix for the calibration, composed of 18 tests. These tests aim to fully characterize the equipment, having different combinations of temperatures and air velocities for each box of the equipment, namely GB, MB and CB.

Table 4.20 – Test matrix for calibration of the GHB with XPS panels 100 mm thick.

Test n.º	MB air temperature [°C]	HB air temperature [°C]	CB air temperature [°C]	MB wall heat flux	MB air velocity [m/s]	CB air velocity [m/s]
1	35	35	5	0	0.2	4.2
2	35	20	5	+	0.2	4.2
3	35	50	5	-	0.2	4.2
4	35	35	5	0	0.4	4.2
5	35	20	5	+	0.4	4.2
6	35	50	5	-	0.4	4.2
7	35	35	5	0	0.2	1.3
8	35	20	5	+	0.2	1.3
9	35	50	5	-	0.2	1.3
10	35	35	5	0	0.4	1.3
11	35	20	5	+	0.4	1.3
12	35	50	5	-	0.4	1.3
13	45	45	10	0	0.2	1.3
14	45	35	10	+	0.2	1.3
15	45	55	10	-	0.2	1.3
16	45	45	10	0	0.4	1.3
17	45	35	10	+	0.4	1.3
18	45	55	10	-	0.4	1.3

The sample has the following instrumentation: (*i*) fourth two thermocouples for surface temperature, being twenty-one in each side of the specimen; and (*ii*) twelve heat flux sensors, namely six in each face. With all sensors placed on each side of the wall (hot and cold side) to have symmetry at the measuring points. Figure 4.53 shows the location of all temperature and heat flux sensors placed on the cold side of the XPS wall surface, and shows the limits of the metering area with 1.80 (W) by 1.05 (H) m².

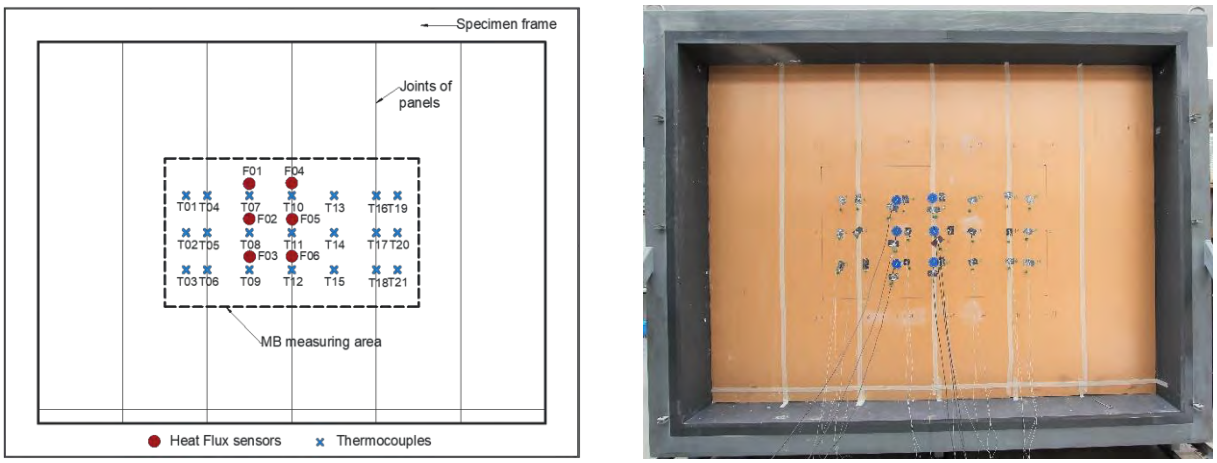

a) **b)**

Figure 4.53 – Location of temperature and heat flux sensors placed on the GHB cold side of the XPS wall surface: a) sketch; b) photo.

The calibration matrix tests were performed according to the requirements presented in section 3.4.2. The test time starts counting from the moment that the setpoints were reached with a difference of less than 1%. All tests had a minimum duration of 8 hours, and the test conditions were achieved on average between one and two hours. Some tests were repeated to verify the repeatability of the equipment, being made 32 tests in total, whose results are shown in Table 4.21.

Table 4.21 shows the main results of the tests which allow assessing the thermal conductance and thermal transmittance according to the equations presented in section 3.4.3. The heat flow rate (Φ) is obtained by using the flanking losses of the MB walls obtain numerically in section 4.5.2, chart of Figure 4.31. Figure 4.54, Figure 4.56 and Figure 4.58 present the relationship of conductance to mean specimen temperature of the three test group cases, from which is obtain the calibration factor.

Table 4.21 shows the difference between thermal conductance obtained experimentally by the GHB method and the reference value. It shows, as expected that the better results are obtained when the equipment operates in the way the heat flow in the walls of the MB is close to zero. The other test modes are not so interesting for steady-state tests, because they have more considerable variability in results than the previous mode. However, it is essential to carry out the calibration in these operating modes, which are used in dynamic regime tests, so it is important to check these calibration coefficients.

Figure 4.55, Figure 4.57 and Figure 4.59 show charts of ambient temperatures and air velocities in the MB and CB, for a test of each group, during the test period in which the test conditions are fulfilled and from where the analysis of the results is performed. It is visible that the system has very satisfactory stability. Additionally, from the equipment tuning tests and calibration tests was achieved average differences of less than 2° C/m and ±5% for the temperatures and velocities values, respectively. In Figure 4.60 it is possible to check the air temperature differences between sensors in the hot and cold camera, being the maximum difference of 1.5° C/m.

Table 4.21 – Test results for calibration of the GHB with XPS panels 100 mm thick.

Test n.º	MB_w	Φ_p [W]	T_{n1} [°C]	$T_{n.out}$ [°C]	T_{n2} [°C]	ΔT_s [°C]	Φ [W]	Λ' [W/(m².K)]	C	Λ [W/(m².K)]	$\Delta\Lambda$	U [W/(m².K)]
M01.C033		20.690	35.01	34.00	5.00	29.91	20.326	0.360		**0.360** ±0.005	-0.1%	0.339 ±0.004
M01.C034		20.620	35.02	34.01	5.00	29.82	20.256	0.359		**0.360** ±0.005	-0.1%	0.339 ±0.004
M01.C035		20.960	35.05	33.91	5.00	30.35	20.596	0.359		**0.359** ±0.005	-0.2%	0.338 ±0.004
M01.C036		20.680	35.09	34.04	5.00	29.91	20.316	0.359		**0.359** ±0.005	-0.1%	0.339 ±0.004
M01.C037		20.660	35.03	34.18	5.00	29.91	20.296	0.359		**0.359** ±0.005	-0.2%	0.338 ±0.004
M04.C038		19.830	35.03	34.01	5.00	28.66	19.466	0.359		**0.359** ±0.005	-0.1%	0.339 ±0.004
M04.C039		20.361	35.02	34.02	5.00	29.46	19.997	0.359		**0.359** ±0.005	-0.2%	0.339 ±0.004
M04.C040		19.970	35.03	34.22	5.00	28.90	19.606	0.359		**0.359** ±0.005	-0.2%	0.338 ±0.004
M07.C041		19.920	35.50	34.45	5.00	28.79	19.556	0.359		**0.360** ±0.005	-0.1%	0.339 ±0.004
M07.C042	0	19.720	35.01	34.12	5.00	28.54	19.356	0.359	1.0004	**0.359** ±0.005	-0.3%	0.338 ±0.004
M07.C043		19.410	35.02	34.72	5.00	28.05	19.046	0.359		**0.359** ±0.005	-0.2%	0.339 ±0.004
M10.C044		19.420	35.04	34.12	5.00	28.01	19.056	0.360		**0.360** ±0.005	0.0%	0.339 ±0.004
M10.C045		19.480	35.08	34.15	5.00	28.17	19.116	0.359		**0.359** ±0.005	-0.2%	0.339 ±0.004
M10.C046		19.680	35.02	34.11	5.00	28.40	19.316	0.360		**0.360** ±0.005	0.0%	0.339 ±0.004
M13.C047		22.730	45.04	44.12	10.00	32.99	22.306	0.358		**0.358** ±0.006	-0.6%	0.337 ±0.005
M13.C048		22.530	45.02	44.02	10.00	32.70	22.106	0.358		**0.358** ±0.006	-0.6%	0.337 ±0.005
M13.C049		22.510	45.05	44.36	10.00	32.66	22.086	0.358		**0.358** ±0.006	-0.6%	0.337 ±0.005
M16.C050		22.290	45.01	44.10	10.00	32.29	21.866	0.358		**0.358** ±0.006	-0.4%	0.338 ±0.005
M16.C051		22.930	45.04	44.23	10.00	33.30	22.506	0.358		**0.358** ±0.006	-0.6%	0.337 ±0.005
M16.C052		22.691	45.04	44.04	10.00	32.91	22.267	0.358		**0.358** ±0.006	-0.5%	0.338 ±0.005
M02.C053		52.340	35.05	20.12	5.00	28.50	19.386	0.360		**0.360** ±0.005	0.0%	0.339 ±0.004
M05.C054		52.390	35.01	20.21	5.00	28.53	19.436	0.360		**0.361** ±0.005	0.2%	0.340 ±0.004
M08.C055	+	52.190	35.02	20.14	5.00	28.28	19.236	0.360	1.0005	**0.360** ±0.005	0.0%	0.339 ±0.004
M11.C056		51.950	35.00	20.10	5.00	27.88	18.996	0.360		**0.361** ±0.005	0.2%	0.340 ±0.004
M14.C057		44.187	45.01	35.02	10.00	32.66	22.400	0.363		**0.360** ±0.006	0.8%	0.339 ±0.005
M17.C058		44.087	45.01	35.10	10.00	32.71	22.300	0.362		**0.361** ±0.006	0.6%	0.340 ±0.005
M03.C059		-14.052	35.01	50.02	5.00	28.74	19.630	0.361		**0.362** ±0.005	0.5%	0.341 ±0.004
M06.C060		-14.232	35.00	50.10	5.00	28.62	19.450	0.360		**0.360** ±0.005	0.0%	0.339 ±0.004
M09.C061	-	-14.282	35.02	50.08	5.00	28.30	19.400	0.363	1.0015	**0.363** ±0.005	0.9%	0.342 ±0.004
M12.C062		-14.082	35.02	50.13	5.00	28.61	19.600	0.363		**0.363** ±0.005	0.9%	0.342 ±0.004
M15.C063		-0.712	45.02	55.03	10.00	32.70	21.924	0.355		**0.355** ±0.006	-1.3%	0.335 ±0.005
M18.C064		-0.660	45.01	55.04	10.00	32.69	21.976	0.356		**0.356** ±0.006	-1.0%	0.336 ±0.005

Where: MB_w is the MB wall heat flux; Φ_p is de total power input; T_{n1} is the environmental temperature of the hot side; $T_{n.out}$ is the environmental temperature of the GB; T_{n2} is the environmental temperature of the cold side; ΔT_s is the surface temperature difference across the specimen; Φ is the heat flow rate; Λ' is the experimental thermal conductance; C is the calibration factor; Λ is the calibrated thermal conductance; $\Delta\Lambda$ is the thermal conductance difference between the material reference value and the calibrated obtain value; and U is the thermal transmittance

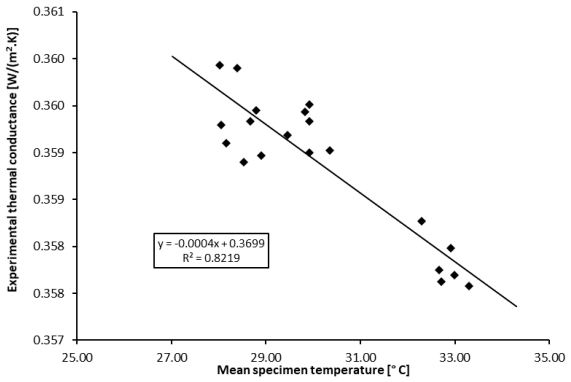

Figure 4.54 – Relationship of conductance to mean specimen temperature of test cases with MB wall heat flux near zero for GHB with XPS panels.

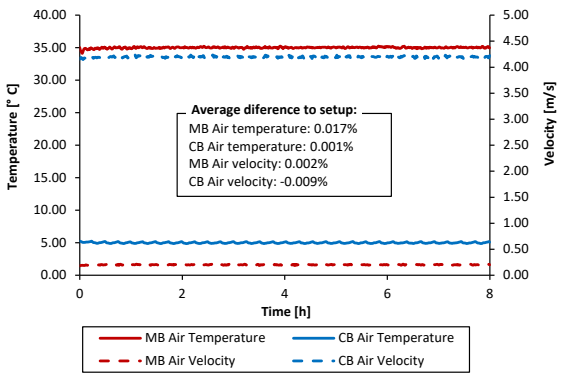

Figure 4.55 – Test M04.C038 air temperature and velocity in chambers for GHB with XPS panels.

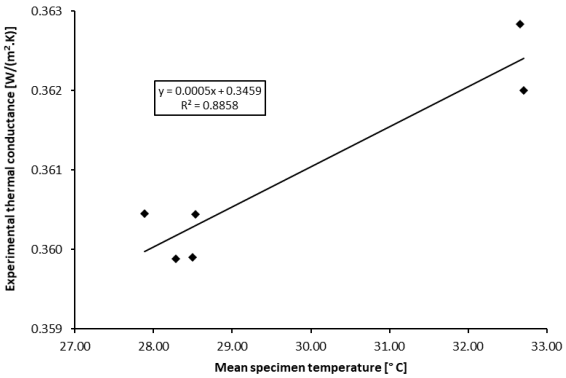

Figure 4.56 – Relationship of conductance to mean specimen temperature of test cases with MB wall heat flux positive for GHB with XPS panels.

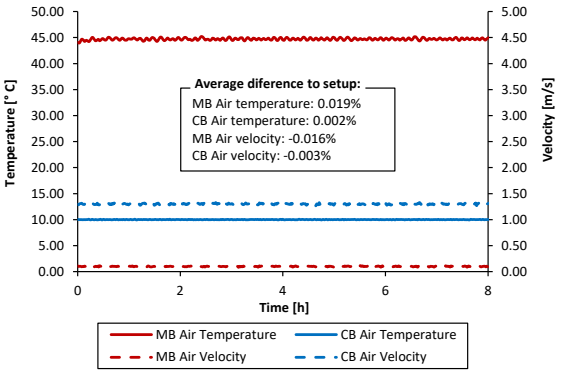

Figure 4.57 – Test M14.C057 air temperature and velocity in chambers for GHB with XPS panels.

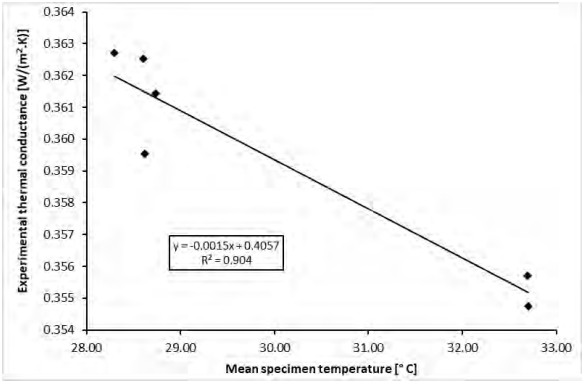

Figure 4.58 – Relationship of conductance to mean specimen temperature of test cases with MB wall heat flux negative for GHB with XPS panels.

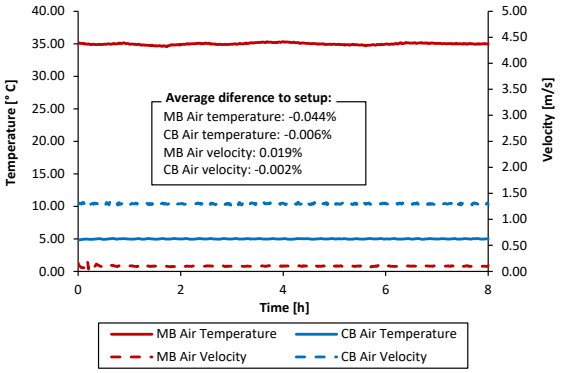

Figure 4.59 – Test M09.C061 air temperature and velocity in chambers for GHB with XPS panels.

Table 4.22 shows a comparison between the GHB and HFM method for the tests performed. From the results obtained, it is confirmed that the flowmeters method is less rigorous, as expected, compared to the GHB method. However, it can be seen that the average result difference is only 3.4%, and the maximum individual difference is 5.1% in relation to the reference value of the material.

Comparing methodologies, the maximum difference in results is 5.7%. Table 4.22 also shows the average difference between the calibrated thermal conductance value obtained by the GHB method and the reference material, giving a low value of only -0.2%, as a result of the technique being more rigorous and the performed calibration.

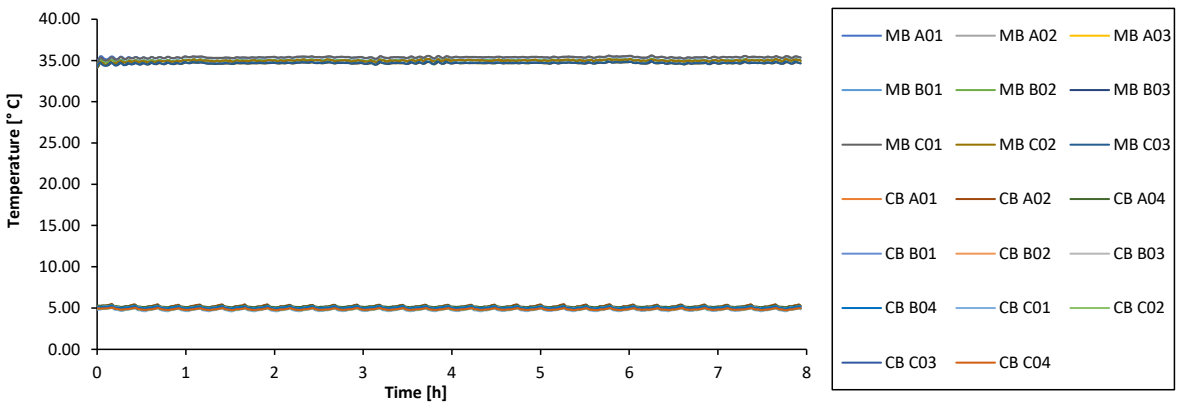

Figure 4.60 – Test M14.C057 air temperatures.

Table 4.22 – Test results of GHB vs HFM method for XPS panels 100 mm thick.

Test n.º	Λ_{CHB} [W/(m².K)]	Λ_{HFM} [W/(m².K)]	$\Delta\Lambda_{HFM\rightarrow Ref}$	$\Delta\Lambda_{CHB\rightarrow HFM}$	λ_{HFM} [W/(m.K)]	U_{HFM} [W/(m².K)]
M01.C033	**0.360** ±0.005	**0.370** ±0.012	2.6%	2.6%	0.0370	0.348 ±0.011
M01.C034	**0.360** ±0.005	**0.373** ±0.012	3.6%	3.6%	0.0373	0.351 ±0.011
M01.C035	**0.359** ±0.005	**0.375** ±0.012	4.0%	4.3%	0.0375	0.352 ±0.011
M01.C036	**0.359** ±0.005	**0.370** ±0.012	2.6%	2.9%	0.0370	0.348 ±0.011
M01.C037	**0.359** ±0.005	**0.369** ±0.012	2.6%	2.9%	0.0369	0.348 ±0.011
M04.C038	**0.359** ±0.005	**0.370** ±0.012	2.8%	3.0%	0.0370	0.348 ±0.011
M04.C039	**0.359** ±0.005	**0.370** ±0.012	2.8%	3.1%	0.0370	0.348 ±0.011
M04.C040	**0.359** ±0.005	**0.369** ±0.012	2.4%	2.7%	0.0369	0.347 ±0.011
M07.C041	**0.360** ±0.005	**0.374** ±0.012	3.9%	3.9%	0.0374	0.352 ±0.011
M07.C042	**0.359** ±0.005	**0.376** ±0.012	4.3%	4.6%	0.0376	0.353 ±0.011
M07.C043	**0.359** ±0.005	**0.373** ±0.012	3.7%	4.0%	0.0373	0.351 ±0.011
M10.C044	**0.360** ±0.005	**0.372** ±0.012	3.3%	3.3%	0.0372	0.350 ±0.011
M10.C045	**0.359** ±0.005	**0.373** ±0.012	3.5%	3.8%	0.0373	0.350 ±0.011
M10.C046	**0.360** ±0.005	**0.374** ±0.012	3.9%	3.9%	0.0374	0.352 ±0.011
M13.C047	**0.358** ±0.005	**0.377** ±0.012	4.6%	5.2%	0.0377	0.354 ±0.011
M13.C048	**0.358** ±0.005	**0.378** ±0.012	5.1%	5.7%	0.0378	0.356 ±0.011
M13.C049	**0.358** ±0.005	**0.377** ±0.012	4.8%	5.4%	0.0377	0.354 ±0.011
M16.C050	**0.358** ±0.005	**0.376** ±0.012	4.6%	5.1%	0.0376	0.354 ±0.011
M16.C051	**0.358** ±0.005	**0.368** ±0.012	2.3%	2.8%	0.0368	0.346 ±0.011
M16.C052	**0.358** ±0.005	**0.367** ±0.012	2.0%	2.6%	0.0367	0.346 ±0.011
M02.C053	**0.360** ±0.005	**0.371** ±0.012	3.1%	3.1%	0.0371	0.349 ±0.011
M05.C054	**0.361** ±0.006	**0.373** ±0.012	3.7%	3.4%	0.0373	0.351 ±0.011
M08.C055	**0.360** ±0.006	**0.374** ±0.012	3.9%	3.9%	0.0374	0.352 ±0.011
M11.C056	**0.361** ±0.006	**0.371** ±0.012	2.9%	2.6%	0.0371	0.349 ±0.011
M14.C057	**0.360** ±0.006	**0.371** ±0.012	3.1%	3.1%	0.0371	0.349 ±0.011
M17.C058	**0.361** ±0.006	**0.371** ±0.012	3.1%	2.8%	0.0371	0.349 ±0.011
M03.C059	**0.362** ±0.006	**0.377** ±0.012	4.7%	4.1%	0.0377	0.354 ±0.011
M06.C060	**0.360** ±0.005	**0.365** ±0.012	1.3%	1.3%	0.0365	0.343 ±0.011
M09.C061	**0.363** ±0.005	**0.374** ±0.012	3.8%	2.9%	0.0374	0.351 ±0.011
M12.C062	**0.363** ±0.005	**0.369** ±0.012	2.5%	1.6%	0.0369	0.347 ±0.011
M15.C063	**0.355** ±0.005	**0.374** ±0.012	4.0%	5.4%	0.0374	0.352 ±0.011
M18.C064	**0.356** ±0.006	**0.372** ±0.012	3.3%	4.5%	0.0372	0.350 ±0.011
Average	**0.359** ±0.006	**0.372** ±0.012			0.037	0.350 ±0.011
SD	**0.0017**	**0.0032**			0.0003	0.0028
ΔR	**-0.2%**	**3.4%**			3.4%	3.2%

Where: Λ_{CHB} is the calibrated thermal conductance obtain by the CHB method; Λ_{HFM} is the thermal conductance obtained by the difference between the reference material value and the calibrated obtain value; $\Delta\Lambda_{HFM\rightarrow Ref}$ is the thermal conductance difference between HFM method and the reference value of the specimen; $\Delta\Lambda_{CHB\rightarrow HFM}$ is the thermal conductance difference between CHB method and HFM method; λ_{HFM} is the thermal conductivity obtain with HFM method; U_{HFM} is the thermal transmittance obtained with HFM method; SD is the standard deviation; and ΔR is the difference in relation to the reference value

Table 4.23 shows the repeatability of the equipment, namely for thermal conductance, ambient temperatures and air velocities in the chambers. This study is carried out for some of the calibration matrix tests, which were repeated for this purpose.

It is observed that a relative standard deviation percentage is low for all parameters, lower than 1%, which demonstrates good performance of the equipment.

Table 4.23 – Tests repeatability on the GHB with XPS panels 100 mm thick.

Test n.º	Λ_{CHB} [W/(m².K)]	T_{n1} [°C]	T_{n2} [°C]	V_{n1} [m/s]	V_{n2} [m/s]	Test n.º	Λ_{CHB} [W/(m².K)]	T_{n1} [°C]	T_{n2} [°C]	V_{n1} [m/s]	V_{n2} [m/s]
M01.C033	0.360	35.010	5.001	0.100	4.200	M10.C044	0.360	35.040	5.001	0.202	1.300
M01.C034	0.360	35.020	5.000	0.100	4.200	M10.C045	0.359	35.080	4.998	0.203	1.300
M01.C035	0.359	35.050	4.999	0.101	4.199	M10.C046	0.360	35.020	5.000	0.202	1.299
M01.C036	0.359	35.090	5.001	0.100	4.200						
M01.C037	0.359	35.025	5.000	0.100	4.200						
Average	**0.359**	**35.039**	**5.000**	**0.100**	**4.200**	**Average**	**0.360**	**35.047**	**4.999**	**0.202**	**1.300**
SD	**0.0005**	**0.0287**	**0.0008**	**0.0003**	**0.0003**	**SD**	**0.0005**	**0.0249**	**0.0013**	**0.0004**	**0.0001**
RSD	**0.0014**	**0.0008**	**0.0002**	**0.0029**	**0.0001**	**RSD**	**0.0013**	**0.0007**	**0.0003**	**0.0020**	**0.0001**
RSD%	**0.14%**	**0.08%**	**0.02%**	**0.29%**	**0.01%**	**RSD%**	**0.13%**	**0.07%**	**0.03%**	**0.20%**	**0.01%**
M04.C038	0.359	35.025	5.000	0.202	4.199	M13.C047	0.358	45.040	10.000	0.101	1.300
M04.C039	0.359	35.024	5.000	0.202	4.200	M13.C048	0.358	45.020	10.001	0.100	1.300
M04.C040	0.359	35.032	4.998	0.201	4.201	M13.C049	0.358	45.050	10.001	0.100	1.300
Average	**0.359**	**35.027**	**5.000**	**0.202**	**4.200**	**Average**	**0.358**	**45.037**	**10.001**	**0.100**	**1.300**
SD	**0.0000**	**0.0036**	**0.0009**	**0.0003**	**0.0007**	**SD**	**0.0000**	**0.0125**	**0.0005**	**0.0001**	**0.0002**
RSD%	**0.00%**	**0.01%**	**0.02%**	**0.15%**	**0.02%**	**RSD%**	**0.00%**	**0.03%**	**0.01%**	**0.14%**	**0.02%**
M07.C041	0.360	35.500	5.000	0.100	1.300	M16.C050	0.358	45.010	10.000	0.204	1.300
M07.C042	0.359	35.010	5.000	0.100	1.300	M16.C051	0.358	45.040	10.000	0.207	1.300
M07.C043	0.359	35.015	5.000	0.101	1.299	M16.C052	0.358	45.040	10.000	0.205	1.300
Average	**0.359**	**35.175**	**5.000**	**0.101**	**1.300**	**Average**	**0.358**	**45.030**	**10.000**	**0.206**	**1.300**
SD	**0.0005**	**0.2298**	**0.0003**	**0.0004**	**0.0002**	**SD**	**0.0000**	**0.0141**	**0.0001**	**0.0012**	**0.0002**
RSD%	**0.13%**	**0.65%**	**0.01%**	**0.39%**	**0.01%**	**RSD%**	**0.00%**	**0.03%**	**0.00%**	**0.60%**	**0.02%**

Where: Λ_{CHB} is the calibrated thermal conductance obtain by the CHB method; T_{n1} is the environmental temperature of the hot side; T_{n2} is the environmental temperature of the cold side; V_{n1} is the air velocity in the hot side; V_{n2} is the air velocity in the cold side; SD is the standard deviation; RSD is the relative standard deviation

4.6.2. Specimen 2

For the second set of calibration tests, it was assembled in the specimen frame, a wall composed of two layers of calcium silicate boards, 12mm thick, totalizing 24 mm of thickness. The boards dimensions are 1.25 (W) by 2.50 (H) m², being added at the base and top an insulating layer of XPS with 0.1 (H) m across the width and the thickness of the plates calcium silicate, which fulfils the 3.60 (W) by 2.70 (H) m² of the frame. This reference material has a thermal conductivity, retrieved from the certificate of the manufacturer, of 0.175 W/(m.° C).

An experimental study was carried out using the TPS method to confirm the values of the thermal conductivity. Table 4.24 presents the results of the experimental campaign, which tested three pairs of samples for each material and performed five repetitions for each analysis. The obtained experimental result is 3.6 % different from the certificate value, being used for calibration purposes the value of the certificate.

Table 4.24 – Thermal conductivity of calcium silicate boards [W/(m.K)]

Test repetition n.º	Sample			Average λ	Certificate λ
	1	2	3		
1	0.1839	0.1791	0.1805		
2	0.1832	0.1796	0.1811	**0.1812** ±5%	**0.175**
3	0.1831	0.1793	0.1818	(Standard Deviation: 0,0018)	**(Δ_λ=3.6%)**
4	0.1832	0.1790	0.1817		
5	0.1835	0.1786	0.1810		

The next sub-sections present the calibration and verifications for the CHB and GHB method with the calcium silicate specimen.

4.6.2.1. Calibrated Hot Box mode

For the full characterization of the apparatus in CHB mode, Table 4.25 presents the test matrix for the calibration, composed of 18 tests. These tests aim to fully characterize the equipment for another range of thermal conductance of the element, having different combinations of temperatures and air velocities for each box of the equipment, namely MB and CB, and temperature variations in relation to the surrounding chamber to impose a heat flow through the MB walls.

Table 4.25 – Test matrix for calibration of the CHB with calcium silicate boards 24 mm thick.

Test n.º	MB air temperature [°C]	Lab. air temperature [°C]	CB air temperature [°C]	MB wall heat flux	MB air velocity [m/s]	CB air velocity [m/s]
1	18	18	5	0	0.2	0.65
2	45	18	5	+	0.2	0.65
3	10	18	5	-	0.2	0.65
4	18	18	5	0	0.4	0.65
5	45	18	5	+	0.4	0.65
6	10	18	5	-	0.4	0.65
7	18	18	5	0	0.2	1.3
8	45	18	5	+	0.2	1.3
9	10	18	5	-	0.2	1.3
10	18	18	5	0	0.4	1.3
11	45	18	5	+	0.4	1.3
12	10	18	5	-	0.4	1.3
13	18	18	10	0	0.2	1.3
14	25	18	10	+	0.2	1.3
15	15	18	10	-	0.2	1.3
16	18	18	10	0	0.4	1.3
17	25	18	10	+	0.4	1.3
18	15	18	10	-	0.4	1.3

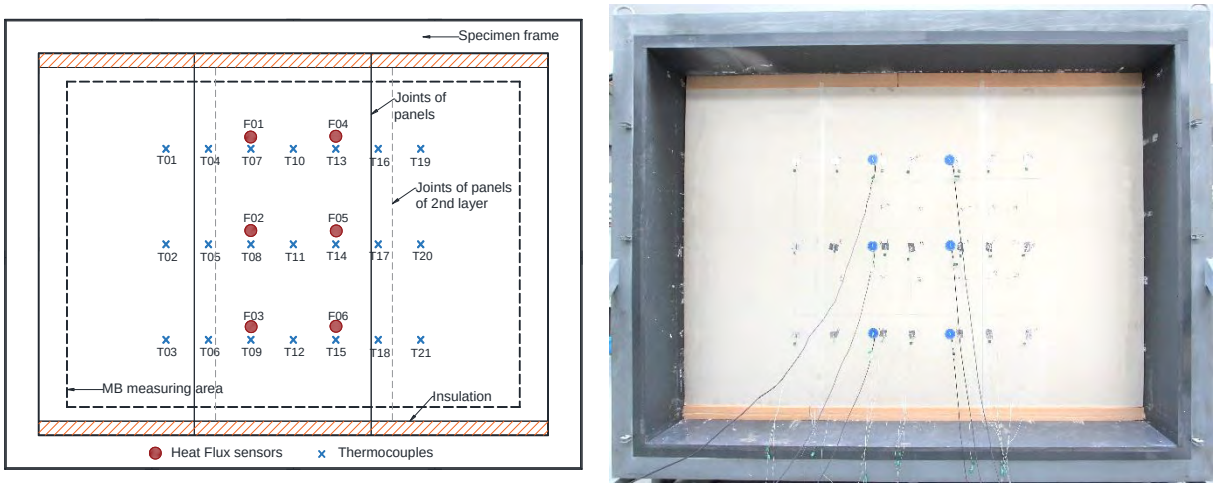

a) b)

Figure 4.61 – Location of temperature and heat flux sensors placed on the CHB cold side of the calcium silicate boards wall surface: a) sketch; b) photo.

The sample has the following instrumentation: (*i*) fourth two thermocouples for surface temperature, being twenty-one in each side of the specimen; and (*ii*) twelve heat flux sensors, namely six in each face. With all sensors placed on each side of the wall (hot and cold side) to have symmetry at the measuring points. Figure 4.61 shows the location of all temperature and heat flux sensors placed on the cold side of the calcium silicate boards, and shows the limits of the metering area with 3.18 (W) by 2.28 (H) m².

The calibration matrix tests were performed according to the requirements presented in section 3.4.2. The test time starts counting from the moment that the setpoints were reached with a difference of less than 1%. All tests had a minimum duration of 8 hours, and the test conditions were achieved on average between one and two hours. Some tests were repeated to verify the repeatability of the equipment, being made 33 tests in total, whose results are shown in Table 4.26.

Table 4.26 – Test results for calibration of the CHB with calcium silicate boards 24 mm thick.

Test n.º	MB_w	Φ_p [W]	T_{n1} [°C]	$T_{n.out}$ [°C]	T_{n2} [°C]	ΔT_s [°C]	Φ [W]	Λ' [W/(m².K)]	C	Λ [W/(m².K)]	$\Delta\Lambda$	U [W/(m².K)]
M01.C065		311.721	18.00	17.70	4.99	5.88	312.854	7.338		**7.273** ±0.203	-0.3%	3.252 ±0.041
M01.C066		312.193	17.99	17.88	5.00	5.88	313.325	7.352		**7.286** ±0.203	-0.1%	3.255 ±0.041
M01.C067		311.614	18.01	17.29	5.00	5.88	312.746	7.333		**7.268** ±0.202	-0.3%	3.251 ±0.04
M04.C068		330.136	17.99	17.34	4.99	6.25	331.268	7.308		**7.243** ±0.192	-0.7%	3.246 ±0.039
M04.C069		334.396	18.01	17.44	5.01	6.29	335.528	7.359		**7.294** ±0.192	0.0%	3.256 ±0.038
M04.C070		331.663	18.01	17.74	4.99	6.26	332.795	7.337		**7.271** ±0.192	-0.3%	3.252 ±0.038
M07.C071		292.275	18.00	17.54	5.00	5.46	293.407	7.408		**7.342** ±0.218	0.7%	3.266 ±0.043
M07.C072		291.687	18.00	17.34	5.00	5.46	292.819	7.399		**7.333** ±0.218	0.6%	3.264 ±0.043
M07.C073		292.211	18.00	17.37	5.00	5.46	293.343	7.414		**7.348** ±0.218	0.8%	3.267 ±0.043
M10.C074		313.896	18.01	17.80	5.00	5.87	315.028	7.397		**7.331** ±0.204	0.5%	3.264 ±0.04
M10.C075	0	313.411	18.00	17.44	5.00	5.87	314.543	7.386	0.9911	**7.320** ±0.204	0.4%	3.261 ±0.04
M10.C076		313.900	18.01	17.89	5.00	5.88	315.032	7.391		**7.325** ±0.204	0.5%	3.262 ±0.04
M13.C077		369.244	17.99	17.80	10.00	7.04	370.376	7.257		**7.192** ±0.187	-1.4%	3.236 ±0.038
M13.C078		369.939	18.00	17.20	10.01	7.04	371.071	7.268		**7.203** ±0.187	-1.2%	3.238 ±0.038
M13.C079		370.493	18.00	17.69	10.00	7.05	371.625	7.275		**7.210** ±0.187	-1.1%	3.239 ±0.038
M13.C080		369.708	18.01	17.80	10.00	7.03	370.840	7.273		**7.208** ±0.188	-1.1%	3.239 ±0.038
M13.C081		369.805	18.00	17.79	10.00	7.02	370.937	7.288		**7.223** ±0.188	-0.9%	3.242 ±0.038
M13.C082		369.144	18.01	17.49	9.99	7.03	370.276	7.267		**7.203** ±0.188	-1.2%	3.238 ±0.038
M16.C083		380.868	17.99	17.81	10.00	7.29	382.000	7.230		**7.166** ±0.181	-1.7%	3.231 ±0.037
M16.C084		380.941	17.99	17.29	10.00	7.29	382.073	7.234		**7.170** ±0.181	-1.7%	3.231 ±0.037
M16.C085		381.214	17.99	17.67	10.00	7.29	382.346	7.238		**7.174** ±0.181	-1.6%	3.232 ±0.037
M02.C086		1417.821	44.89	17.63	4.99	24.80	1328.790	7.390		**7.397** ±0.134	1.4%	3.277 ±0.026
M05.C087		1485.258	45.00	17.74	5.00	26.01	1396.227	7.405		**7.412** ±0.130	1.7%	3.280 ±0.025
M08.C088	+	1354.535	44.90	17.77	5.00	23.59	1265.504	7.398	1.00094	**7.405** ±0.139	1.6%	3.278 ±0.027
M11.C089		1410.653	44.71	17.32	5.00	24.61	1321.622	7.408		**7.412** ±0.135	1.7%	3.280 ±0.026
M14.C090		709.420	25.00	17.44	10.00	11.79	620.389	7.256		**7.405** ±0.154	-0.4%	3.278 ±0.03
M17.C091		739.331	25.00	17.49	10.00	12.28	650.300	7.305		**7.415** ±0.150	0.3%	3.280 ±0.029
M03.C092		-20.089	10.00	17.19	5.00	0.14	7.758	7.541		**7.331** ±0.223	0.5%	3.264 ±0.042
M06.C093		-12.924	10.00	17.28	5.00	0.27	14.923	7.537		**7.327** ±0.224	0.5%	3.263 ±0.042
M09.C094	-	-28.384	10.00	17.48	5.00	-0.01	-0.537	7.552	0.9722	**7.342** ±0.223	0.7%	3.266 ±0.042
M12.C095		-20.112	10.00	17.52	5.00	0.14	7.735	7.529		**7.320** ±0.223	0.4%	3.261 ±0.042
M15.C096		239.115	15.00	17.35	10.00	4.98	266.962	7.401		**7.195** ±0.229	-1.3%	3.236 ±0.046
M18.C097		247.518	15.00	17.79	10.00	5.13	275.366	7.405		**7.200** ±0.223	-1.3%	3.237 ±0.045

Where: MB_w is the MB wall heat flux; Φ_p is de total power input; T_{n1} is the environmental temperature of the hot side; $T_{n.out}$ is the environmental temperature of the room where is the apparatus; T_{n2} is the environmental temperature of the cold side; ΔT_s is the surface temperature difference across the specimen; Φ is the heat flow rate; Λ' is the experimental thermal conductance; C is the calibration factor; Λ is the calibrated thermal conductance; $\Delta\Lambda$ is the thermal conductance difference between the material reference value and the calibrated obtain value; and U is the thermal transmittance

Table 4.26 shows the main results of the tests which allow assessing the thermal conductance and thermal transmittance according to the equations presented in section 3.4.3. The heat flow rate (Φ) is obtained by correcting the total power imputed to the system by subtracting the flanking losses of the MB, which were obtained numerically in section 4.5.2, chart of Figure 4.35. Next, is obtained the experimental thermal conductance that is multiplied by the calibration factor obtain experimentally, giving the calibrated thermal conductance. Figure 4.62, Figure 4.64 and Figure 4.66 present the relationship of conductance to mean specimen temperature of the three test group cases, from which is obtained the calibration factor.

Table 4.26 shows the difference between thermal conductance obtained experimentally by the CHB method and the reference value. It shows that, as expected and similar to the calibration with specimen 1, the better results are obtained when the equipment operates in the way the heat flow in the walls of the MB is close to zero.

Figure 4.63, Figure 4.65 and Figure 4.67 show charts of ambient temperatures and air velocities in the MB and CB, for a test of each group, during the test period in which the test conditions are fulfilled and from where the analysis of the results is performed.

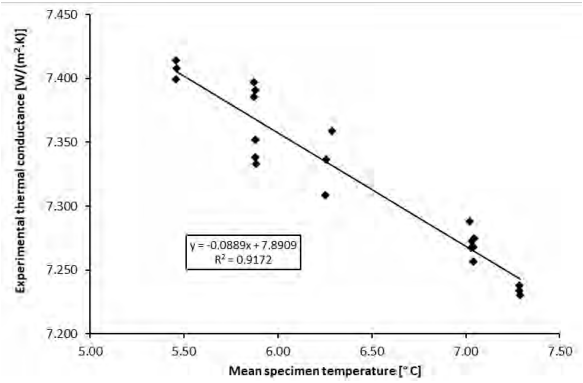

Figure 4.62 – Relationship of conductance to mean specimen temperature of test cases with MB wall heat flux near zero for CHB with calcium silicate boards.

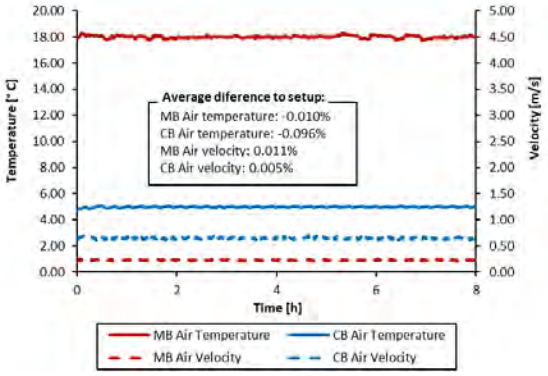

Figure 4.63 – Test M01.C065 air temperature and velocity in chambers for CHB with calcium silicate boards.

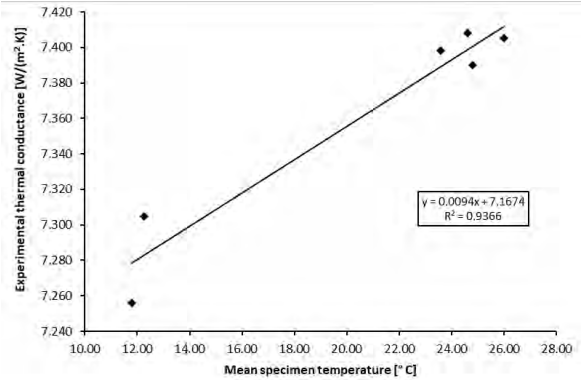

Figure 4.64 – Relationship of conductance to mean specimen temperature of test cases with MB wall heat flux positive for CHB with calcium silicate boards.

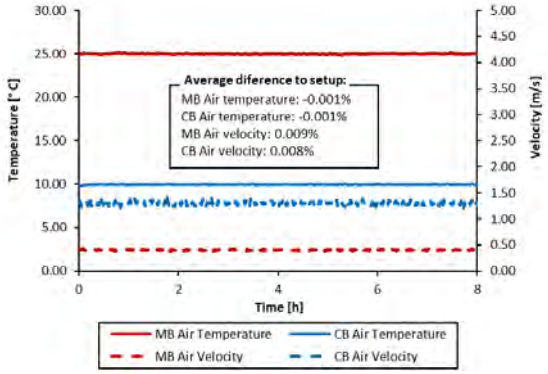

Figure 4.65 – Test M017.C091 air temperature and velocity in chambers for CHB with calcium silicate boards.

Table 4.27 shows a comparison between the CHB and HFM method for the tests performed. From the results obtained, it is confirmed that the flowmeters method is less rigorous. The average result difference is 1.9%, and the maximum individual difference is 4.6% in relation to the reference value of the material.

Comparing methodologies, the maximum difference in results is 5.3%. Table 4.27 also shows the average difference between the calibrated thermal conductance value obtained by the CHB method and the reference material, giving a low value of only -0.03%.

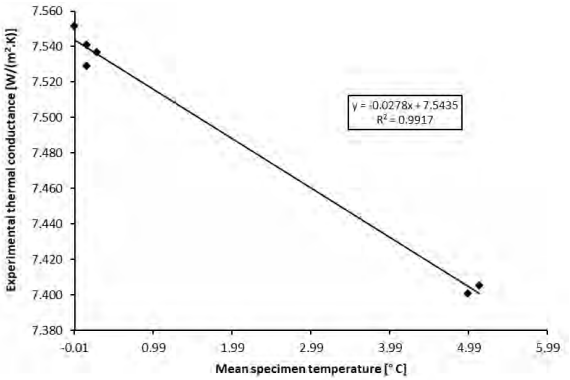

Figure 4.66 – Relationship of conductance to mean specimen temperature of test cases with MB wall heat flux negative for CHB with calcium silicate boards.

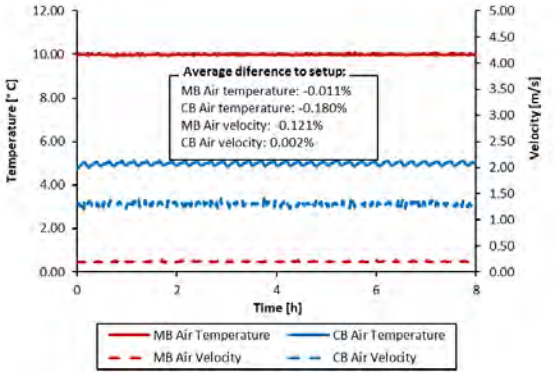

Figure 4.67 – Test M09.C094 air temperature and velocity in chambers for CHB with calcium silicate boards.

Table 4.27 – Test results of CHB vs HFM method for calcium silicate boards 24 mm thick.

Test n.º	Λ_{CHB} [W/(m².K)]	Λ_{HFM} [W/(m².K)]	$\Delta\Lambda_{HFM\rightarrow Ref}$	$\Delta\Lambda_{CHB\rightarrow HFM}$	λ_{HFM} [W/(m.K)]	U_{HFM} [W/(m².K)]
M01.C065	**7.273** ±0.203	**7.437** ±0.292	2.0%	2.3%	0.1785	3.284 ±0.057
M01.C066	**7.286** ±0.203	**7.457** ±0.293	2.3%	2.3%	0.1790	3.288 ±0.057
M01.C067	**7.268** ±0.202	**7.453** ±0.293	2.2%	2.5%	0.1789	3.288 ±0.057
M04.C068	**7.243** ±0.192	**7.389** ±0.283	1.3%	2.0%	0.1773	3.275 ±0.056
M04.C069	**7.294** ±0.192	**7.287** ±0.279	-0.1%	-0.1%	0.1749	3.255 ±0.056
M04.C070	**7.271** ±0.192	**7.330** ±0.281	0.5%	0.8%	0.1759	3.263 ±0.056
M07.C071	**7.342** ±0.218	**7.031** ±0.285	-3.6%	-4.2%	0.1688	3.203 ±0.059
M07.C072	**7.333** ±0.218	**7.035** ±0.286	-3.5%	-4.1%	0.1688	3.204 ±0.059
M07.C073	**7.348** ±0.218	**7.050** ±0.286	-3.3%	-4.1%	0.1692	3.207 ±0.059
M10.C074	**7.331** ±0.204	**7.468** ±0.294	2.4%	1.9%	0.1792	3.290 ±0.057
M10.C075	**7.320** ±0.204	**7.465** ±0.294	2.4%	2.0%	0.1792	3.290 ±0.057
M10.C076	**7.325** ±0.204	**7.420** ±0.292	1.8%	1.3%	0.1781	3.281 ±0.057
M13.C077	**7.192** ±0.187	**7.477** ±0.284	2.5%	4.0%	0.1795	3.292 ±0.055
M13.C078	**7.203** ±0.187	**7.484** ±0.285	2.6%	3.9%	0.1796	3.294 ±0.055
M13.C079	**7.210** ±0.187	**7.487** ±0.285	2.7%	3.8%	0.1797	3.294 ±0.055
M13.C080	**7.208** ±0.188	**7.556** ±0.288	3.6%	4.8%	0.1813	3.307 ±0.055
M13.C081	**7.223** ±0.188	**7.555** ±0.288	3.6%	4.6%	0.1813	3.307 ±0.055
M13.C082	**7.203** ±0.188	**7.582** ±0.289	4.0%	5.3%	0.1820	3.312 ±0.055
M16.C083	**7.166** ±0.181	**7.506** ±0.282	2.9%	4.7%	0.1801	3.298 ±0.054
M16.C084	**7.170** ±0.181	**7.405** ±0.278	1.6%	3.3%	0.1777	3.278 ±0.054
M16.C085	**7.174** ±0.181	**7.490** ±0.281	2.7%	4.4%	0.1798	3.295 ±0.054
M02.C086	**7.397** ±0.134	**7.522** ±0.251	3.2%	1.7%	0.1805	3.301 ±0.048
M05.C087	**7.412** ±0.130	**7.624** ±0.252	4.6%	2.9%	0.1830	3.320 ±0.048
M08.C088	**7.405** ±0.139	**7.472** ±0.252	2.5%	0.9%	0.1793	3.291 ±0.049
M11.C089	**7.412** ±0.135	**7.562** ±0.252	3.7%	2.0%	0.1815	3.309 ±0.048
M14.C090	**7.405** ±0.154	**7.594** ±0.267	4.2%	2.6%	0.1823	3.315 ±0.051
M17.C091	**7.415** ±0.150	**7.402** ±0.257	1.5%	-0.2%	0.1776	3.278 ±0.050
M03.C092	**7.331** ±0.223	**7.459** ±0.301	2.3%	1.7%	0.1790	3.289 ±0.061
M06.C093	**7.327** ±0.224	**7.422** ±0.301	1.8%	1.3%	0.1781	3.282 ±0.062
M09.C094	**7.342** ±0.223	**7.195** ±0.301	-1.3%	-2.0%	0.1727	3.236 ±0.062
M12.C095	**7.320** ±0.223	**7.544** ±0.301	3.5%	3.1%	0.1811	3.305 ±0.062
M15.C096	**7.195** ±0.229	**7.534** ±0.314	3.3%	4.7%	0.1808	3.303 ±0.060
M18.C097	**7.200** ±0.223	**7.524** ±0.309	3.2%	4.5%	0.1806	3.301 ±0.059
Average	**7.289** ±0.229	**7.431** ±0.309			0.178	3.283 ±0.062
SD	**0.0605**	**0.1508**			0.0036	0.0300
ΔR	**-0.03%**	**1.91%**			1.91%	0.83%

Where: Λ_{CHB} is the calibrated thermal conductance obtain by the CHB method; Λ_{HFM} is the thermal conductance obtained by the difference between the reference material value and the calibrated obtain value; $\Delta\Lambda_{HFM\rightarrow Ref}$ is the thermal conductance difference between HFM method and the reference value of the specimen; $\Delta\Lambda_{CHB\rightarrow HFM}$ is the thermal conductance difference between CHB method and HFM method; λ_{HFM} is the thermal conductivity obtain with HFM method; U_{HFM} is the thermal transmittance obtained with HFM method; SD is the standard deviation; and ΔR is the difference in relation to the reference value

Table 4.28 shows the repeatability of the equipment, namely for thermal conductance, ambient temperatures and air velocities in the chambers. This study is carried out for some of the calibration matrix tests, which were repeated for this purpose. It is observed that a relative standard deviation percentage is low for all parameters, lower than 1%, which demonstrates good performance of the equipment.

Table 4.28 – Tests repeatability on the CHB with calcium silicate boards 24 mm thick.

Test n.º	Λ_{CHB} [W/(m².K)]	T_{n1} [°C]	T_{n2} [°C]	V_{n1} [m/s]	V_{n2} [m/s]	Test n.º	Λ_{CHB} [W/(m².K)]	T_{n1} [°C]	T_{n2} [°C]	V_{n1} [m/s]	V_{n2} [m/s]
M01.C065	7.273	17.998	4.991	0.826	0.650	M10.C074	7.331	18.005	5.000	1.025	1.298
M01.C066	7.286	17.995	4.995	0.825	0.650	M10.C075	7.320	18.001	5.000	1.025	1.300
M01.C067	7.268	18.007	5.001	0.825	0.650	M10.C076	7.325	18.006	5.001	1.025	1.300
Average	**7.276**	**18.000**	**4.996**	**0.825**	**0.650**	**Average**	**7.325**	**18.004**	**5.000**	**1.025**	**1.299**
SD	**0.0076**	**0.0051**	**0.0041**	**0.0003**	**0.0002**	**SD**	**0.0045**	**0.0021**	**0.0005**	**0.0001**	**0.0008**
RSD%	**0.10%**	**0.03%**	**0.08%**	**0.04%**	**0.03%**	**RSD%**	**0.06%**	**0.01%**	**0.01%**	**0.01%**	**0.06%**
M04.C068	7.243	17.990	4.991	1.026	0.650	M13.C077	7.192	17.995	9.995	0.825	1.300
M04.C069	7.294	18.006	5.009	1.025	0.650	M13.C078	7.203	18.002	10.010	0.825	1.300
M04.C070	7.271	18.005	4.992	1.026	0.650	M13.C079	7.210	17.998	10.002	0.825	1.301
						M13.C080	7.208	18.010	10.001	0.825	1.301
						M13.C081	7.223	18.000	9.998	0.825	1.299
						M13.C082	7.203	18.012	9.991	0.825	1.301
Average	**7.269**	**18.000**	**4.997**	**1.026**	**0.650**	**Average**	**7.207**	**18.003**	**10.000**	**0.825**	**1.300**
SD	**0.0209**	**0.0076**	**0.0083**	**0.0001**	**0.0003**	**SD**	**0.0093**	**0.0063**	**0.0059**	**0.0002**	**0.0008**
RSD%	**0.29%**	**0.04%**	**0.17%**	**0.01%**	**0.04%**	**RSD%**	**0.13%**	**0.03%**	**0.06%**	**0.03%**	**0.06%**
M07.C071	7.342	18.002	4.995	0.826	1.301	M16.C083	7.166	17.990	10.001	1.025	1.300
M07.C072	7.333	17.998	5.001	0.825	1.300	M16.C084	7.170	17.992	10.001	1.025	1.299
M07.C073	7.348	18.001	5.000	0.825	1.299	M16.C085	7.174	17.992	10.000	1.026	1.302
Average	**7.341**	**18.000**	**4.999**	**0.825**	**1.300**	**Average**	**7.170**	**17.991**	**10.001**	**1.025**	**1.300**
SD	**0.0062**	**0.0019**	**0.0026**	**0.0003**	**0.0006**	**SD**	**0.0028**	**0.0012**	**0.0005**	**0.0003**	**0.0010**
RSD%	**0.08%**	**0.01%**	**0.05%**	**0.04%**	**0.05%**	**RSD%**	**0.04%**	**0.01%**	**0.00%**	**0.03%**	**0.08%**

Where: Λ_{CHB} is the calibrated thermal conductance obtain by the CHB method; T_{n1} is the environmental temperature of the hot side; T_{n2} is the environmental temperature of the cold side; V_{n1} is the air velocity in the hot side; V_{n2} is the air velocity in the cold side; SD is the standard deviation; RSD is the relative standard deviation

4.6.2.2. Guarded Hot Box mode

For the full characterization of the apparatus in GHB mode, Table 4.29 presents the test matrix for the calibration, composed of 18 tests. These tests aim to fully characterize the equipment for another range of thermal conductance of the element, having different combinations of temperatures and air velocities for each box of the equipment.

The sample has the following instrumentation: (*i*) fourth two thermocouples for surface temperature, being twenty-one in each side of the specimen; and (*ii*) twelve heat flux sensors, namely six in each face. With all sensors placed on each side of the wall (hot and cold side) to have symmetry at the measuring points. Figure 4.68 shows the location of all temperature and heat flux sensors placed on the cold side of the calcium silicate boards, and shows the limits of the metering area with 1.80 (W) by 1.05 (H) m².

Table 4.29 – Test matrix for calibration of the GHB with calcium silicate boards 24 mm thick.

Test n.º	MB air temperature [°C]	Lab. air temperature [°C]	CB air temperature [°C]	MB wall heat flux	MB air velocity [m/s]	CB air velocity [m/s]
1	35	35	5	0	0.2	0.65
2	35	20	5	+	0.2	0.65
3	35	50	5	-	0.2	0.65
4	35	35	5	0	0.4	0.65
5	35	20	5	+	0.4	0.65
6	35	50	5	-	0.4	0.65
7	35	35	5	0	0.2	1.3
8	35	20	5	+	0.2	1.3
9	35	50	5	-	0.2	1.3
10	35	35	5	0	0.4	1.3
11	35	20	5	+	0.4	1.3
12	35	50	5	-	0.4	1.3
13	45	45	10	0	0.2	1.3
14	45	35	10	+	0.2	1.3
15	45	55	10	-	0.2	1.3
16	45	45	10	0	0.4	1.3
17	45	35	10	+	0.4	1.3
18	45	55	10	-	0.4	1.3

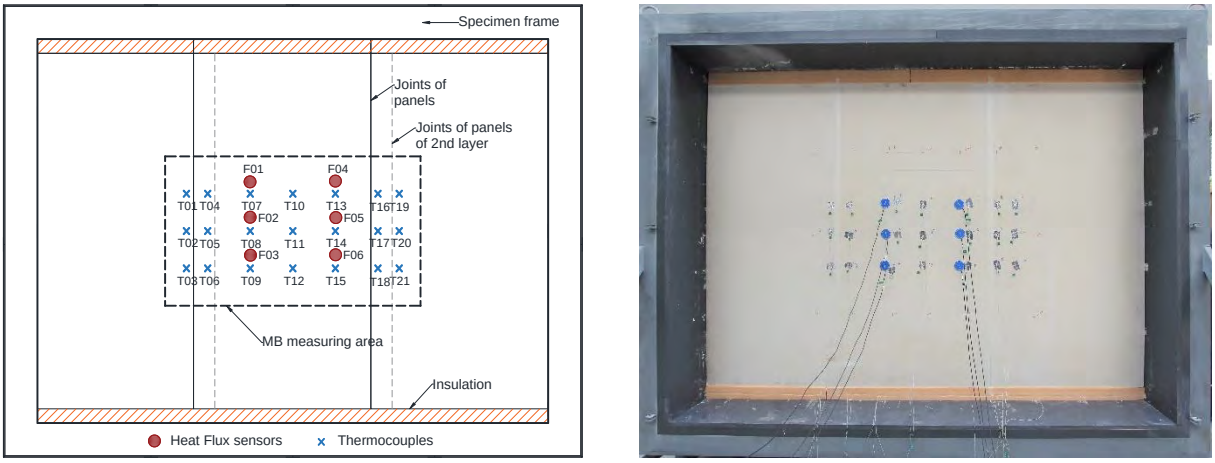

a) b)

Figure 4.68 – Location of temperature and heat flux sensors placed on the GHB cold side of the calcium silicate boards wall surface: a) sketch; b) photo.

The calibration matrix tests were performed according to the requirements presented in section 3.4.2. The test time starts counting from the moment that the setpoints were reached with a difference of less than 1%. All tests had a minimum duration of 8 hours, and the test conditions were achieved on average between one and two hours. Some tests were repeated to verify the repeatability of the equipment, being made 32 tests in total, whose results are shown in Table 4.30.

Table 4.30 shows the main results of the tests which allow assessing the thermal conductance and thermal transmittance according to the equations presented in section 3.4.3. The heat flow rate (Φ) is obtained by correcting the total power imputed to the system by subtracting the flanking losses of the MB, which were obtained numerically in section 4.5.2, chart of Figure 4.37. Next, is obtained the experimental thermal conductance that is multiplied by the calibration factor obtain experimentally, giving the calibrated thermal

conductance. Figure 4.69, Figure 4.71 and Figure 4.73 present the relationship of conductance to mean specimen temperature of the three test group cases, from which is obtain the calibration factor.

Table 4.30 shows the difference between thermal conductance obtained experimentally by the GHB method and the reference value. It reveals that for the range of thermal conductance under analysis, the results obtained in the equipment, when it operates in one of the three different modes of heat flow in the MB walls, similar results are obtained.

Figure 4.70, Figure 4.72 and Figure 4.74 show charts of ambient temperatures and air velocities in the MB and CB, for a test of each group, during the test period in which the test conditions are fulfilled and from where the analysis of the results is performed.

Table 4.30 – Test results for calibration of the GHB with calcium silicate boards 24 mm thick.

Test n.º	MB_w	Φ_p [W]	T_{n1} [°C]	$T_{n.out}$ [°C]	T_{n2} [°C]	ΔT_s [°C]	Φ [W]	Λ' [W/(m².K)]	C	Λ [W/(m².K)]	$\Delta\Lambda$	U [W/(m².K)]
M01.C098		165.890	35.00	34.13	5.00	12.11	168.005	7.338		**7.324** ±0.189	0.5%	3.262 ±0.037
M01.C099		165.920	35.01	34.02	5.00	12.12	168.035	7.338		**7.324** ±0.189	0.4%	3.262 ±0.037
M01.C100		165.045	35.00	34.19	5.00	12.06	167.160	7.336		**7.322** ±0.189	0.4%	3.262 ±0.038
M01.C101		164.875	35.02	34.08	5.00	12.04	166.990	7.340		**7.326** ±0.190	0.5%	3.263 ±0.038
M01.C102		165.007	34.99	34.06	5.00	12.05	167.122	7.337		**7.323** ±0.189	0.4%	3.262 ±0.038
M04.C103		180.361	35.00	34.02	5.00	13.16	182.476	7.336		**7.322** ±0.176	0.4%	3.262 ±0.035
M04.C104		182.521	35.02	34.09	5.00	13.32	184.636	7.333		**7.319** ±0.175	0.4%	3.261 ±0.035
M04.C105		182.540	35.00	34.17	5.00	13.32	184.655	7.336		**7.322** ±0.175	0.4%	3.262 ±0.035
M07.C106		192.599	35.50	34.05	5.00	14.04	194.714	7.337		**7.324** ±0.169	0.4%	3.262 ±0.034
M07.C107	0	192.152	35.01	34.09	5.00	14.01	194.267	7.337	0.9981	**7.323** ±0.168	0.4%	3.262 ±0.033
M07.C108		189.716	33.91	34.10	4.80	13.83	191.831	7.336		**7.322** ±0.165	0.4%	3.262 ±0.033
M10.C109		209.197	35.00	34.14	5.00	15.25	211.312	7.329		**7.316** ±0.157	0.3%	3.261 ±0.031
M10.C110		209.718	35.01	34.04	5.00	15.29	211.833	7.332		**7.318** ±0.157	0.4%	3.261 ±0.031
M10.C111		203.853	34.78	34.01	5.00	14.86	205.968	7.334		**7.321** ±0.160	0.4%	3.262 ±0.032
M13.C112		218.397	45.00	44.02	10.00	15.94	220.861	7.331		**7.317** ±0.187	0.3%	3.261 ±0.037
M13.C113		215.599	44.98	44.11	10.00	15.74	218.064	7.332		**7.318** ±0.189	0.4%	3.261 ±0.038
M13.C114		214.430	45.02	44.16	10.00	15.65	216.895	7.334		**7.320** ±0.190	0.4%	3.262 ±0.038
M16.C115		242.666	45.00	44.17	10.00	17.70	245.131	7.326		**7.312** ±0.172	0.3%	3.260 ±0.034
M16.C116		241.383	45.01	44.04	10.00	17.61	243.847	7.328		**7.314** ±0.173	0.3%	3.260 ±0.034
M16.C117		241.406	45.00	44.11	10.00	17.61	243.871	7.327		**7.313** ±0.173	0.3%	3.260 ±0.034
M02.C118		218.900	35.00	20.00	5.00	13.62	187.116	7.270		**7.281** ±0.170	-0.1%	3.254 ±0.034
M05.C119		237.162	40.00	19.99	5.00	14.92	205.378	7.282		**7.293** ±0.176	0.0%	3.256 ±0.035
M08.C120	+	243.127	40.00	20.00	5.00	15.35	211.343	7.286	1.00156	**7.297** ±0.172	0.1%	3.257 ±0.034
M11.C121		263.937	39.99	20.00	5.00	16.82	232.153	7.301		**7.293** ±0.160	0.3%	3.260 ±0.032
M14.C122		257.029	45.00	35.01	10.00	17.10	236.875	7.330		**7.297** ±0.177	0.7%	3.257 ±0.035
M17.C123		266.991	45.00	35.01	10.00	17.81	246.837	7.332		**7.312** ±0.171	0.7%	3.260 ±0.034
M03.C124		106.107	35.00	50.00	5.00	10.21	142.033	7.359		**7.329** ±0.219	0.5%	3.263 ±0.043
M06.C125		125.882	30.00	50.00	5.00	11.64	161.809	7.357		**7.327** ±0.173	0.5%	3.263 ±0.034
M09.C126	-	120.973	30.01	50.00	5.00	11.29	156.899	7.355	0.9959	**7.325** ±0.177	0.5%	3.262 ±0.035
M12.C127		144.166	30.85	50.00	5.00	12.96	180.092	7.352		**7.322** ±0.162	0.4%	3.262 ±0.032
M15.C128		174.085	40.00	55.01	10.00	14.35	199.072	7.340		**7.309** ±0.186	0.2%	3.259 ±0.037
M18.C129		196.712	42.33	55.00	10.00	15.99	221.699	7.338		**7.308** ±0.178	0.2%	3.259 ±0.035

Where: MB_w is the MB wall heat flux; Φ_p is de total power input; T_{n1} is the environmental temperature of the hot side; $T_{n.out}$ is the environmental temperature of the GB; T_{n2} is the environmental temperature of the cold side; ΔT_s is the surface temperature difference across the specimen; Φ is the heat flow rate; Λ' is the experimental thermal conductance; C is the calibration factor; Λ is the calibrated thermal conductance; $\Delta\Lambda$ is the thermal conductance difference between the material reference value and the calibrated obtain value; and U is the thermal transmittance

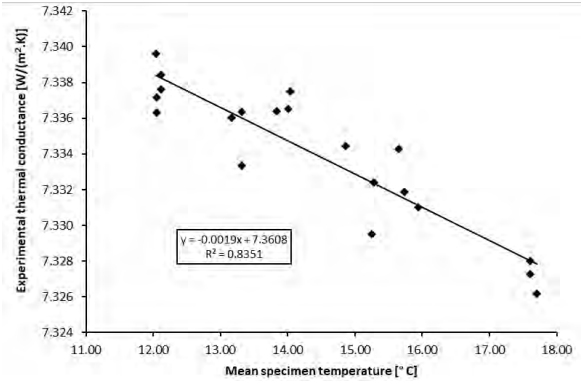

Figure 4.69 – Relationship of conductance to mean specimen temperature of test cases with MB wall heat flux near zero for GHB with calcium silicate boards.

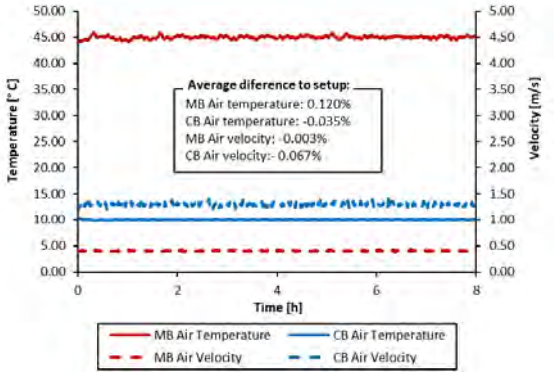

Figure 4.70 – Test M16.C115 air temperature and velocity in chambers for GHB with calcium silicate boards.

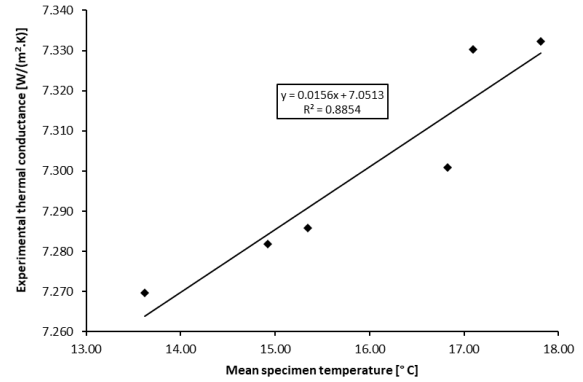

Figure 4.71 – Relationship of conductance to mean specimen temperature of test cases with MB wall heat flux positive for GHB with calcium silicate boards.

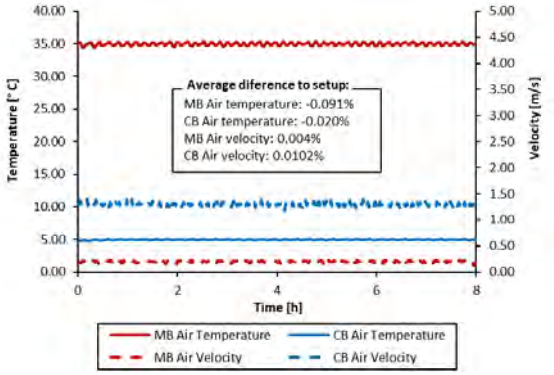

Figure 4.72 – Test M08.C120 air temperature and velocity in chambers for GHB with calcium silicate boards.

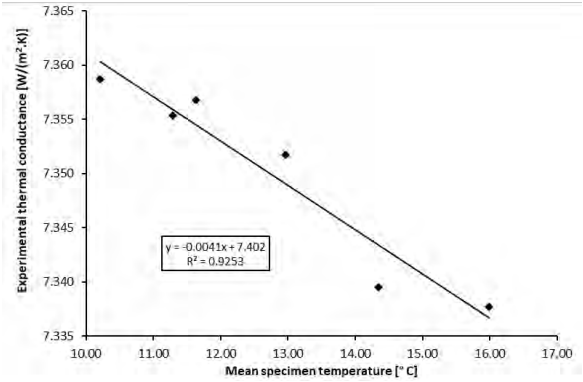

Figure 4.73 – Relationship of conductance to mean specimen temperature of test cases with MB wall heat flux negative for GHB with calcium silicate boards.

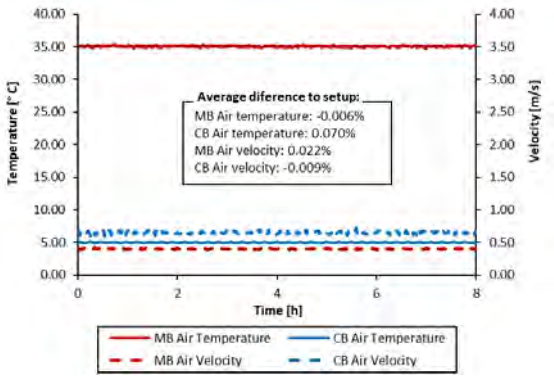

Figure 4.74 – Test M03.C019 air temperature and velocity in chambers for GHB with calcium silicate boards.

Table 4.31 shows a comparison between the GHB and HFM method for the tests performed. From the results obtained, it is confirmed that the flowmeters method is less rigorous. The average result difference is 2.88%, and the maximum individual difference is 3.4% in relation to the reference value of the material.

Comparing methodologies, the maximum difference in results is 3.3%. Table 4.31 also shows the average difference between the calibrated thermal conductance value obtained by the GHB method and the reference material, giving a low value of only 0.33%.

Table 4.31 – Test results of GHB vs HFM method for calcium silicate boards 24 mm thick.

Test n.º	Λ_{CHB} [W/(m².K)]	Λ_{HFM} [W/(m².K)]	$\Delta\Lambda_{HFM\rightarrow Ref}$	$\Delta\Lambda_{CHB\rightarrow HFM}$	λ_{HFM} [W/(m.K)]	U_{HFM} [W/(m².K)]
M01.C098	**7.324** ±0.189	**7.478** ±0.284	2.6%	2.1%	0.1795	3.292 ±0.055
M01.C099	**7.324** ±0.189	**7.534** ±0.286	3.3%	2.9%	0.1808	3.303 ±0.055
M01.C100	**7.322** ±0.189	**7.531** ±0.287	3.3%	2.8%	0.1807	3.303 ±0.055
M01.C101	**7.326** ±0.190	**7.497** ±0.286	2.8%	2.3%	0.1799	3.296 ±0.055
M01.C102	**7.323** ±0.189	**7.475** ±0.285	2.5%	2.1%	0.1794	3.292 ±0.055
M04.C103	**7.322** ±0.176	**7.493** ±0.277	2.8%	2.3%	0.1798	3.295 ±0.054
M04.C104	**7.319** ±0.175	**7.516** ±0.276	3.1%	2.7%	0.1804	3.300 ±0.053
M04.C105	**7.322** ±0.175	**7.522** ±0.276	3.2%	2.7%	0.1805	3.301 ±0.053
M07.C106	**7.324** ±0.169	**7.506** ±0.272	2.9%	2.5%	0.1802	3.298 ±0.053
M07.C107	**7.323** ±0.168	**7.480** ±0.271	2.6%	2.1%	0.1795	3.293 ±0.053
M07.C108	**7.322** ±0.165	**7.505** ±0.270	2.9%	2.5%	0.1801	3.298 ±0.052
M10.C109	**7.316** ±0.157	**7.493** ±0.264	2.8%	2.4%	0.1798	3.295 ±0.051
M10.C110	**7.318** ±0.157	**7.443** ±0.262	2.1%	1.7%	0.1786	3.286 ±0.051
M10.C111	**7.321** ±0.160	**7.482** ±0.265	2.6%	2.2%	0.1796	3.293 ±0.051
M13.C112	**7.317** ±0.187	**7.523** ±0.285	3.2%	2.8%	0.1805	3.301 ±0.055
M13.C113	**7.318** ±0.189	**7.489** ±0.285	2.7%	2.3%	0.1797	3.295 ±0.055
M13.C114	**7.320** ±0.190	**7.513** ±0.287	3.0%	2.6%	0.1803	3.299 ±0.055
M16.C115	**7.312** ±0.172	**7.493** ±0.274	2.8%	2.5%	0.1798	3.295 ±0.053
M16.C116	**7.314** ±0.173	**7.525** ±0.275	3.2%	2.9%	0.1806	3.302 ±0.053
M16.C117	**7.313** ±0.173	**7.505** ±0.275	2.9%	2.6%	0.1801	3.298 ±0.053
M02.C118	**7.281** ±0.170	**7.510** ±0.274	3.0%	3.1%	0.1802	3.299 ±0.053
M05.C119	**7.293** ±0.176	**7.528** ±0.278	3.2%	3.2%	0.1807	3.302 ±0.053
M08.C120	**7.297** ±0.172	**7.496** ±0.275	2.8%	2.7%	0.1799	3.296 ±0.053
M11.C121	**7.293** ±0.160	**7.531** ±0.268	3.3%	3.3%	0.1807	3.303 ±0.052
M14.C122	**7.297** ±0.177	**7.467** ±0.276	2.4%	2.3%	0.1792	3.290 ±0.054
M17.C123	**7.312** ±0.171	**7.489** ±0.273	2.7%	2.4%	0.1797	3.295 ±0.053
M03.C124	**7.329** ±0.219	**7.462** ±0.305	2.3%	1.8%	0.1791	3.289 ±0.059
M06.C125	**7.327** ±0.173	**7.503** ±0.274	2.9%	2.4%	0.1801	3.297 ±0.053
M09.C126	**7.325** ±0.177	**7.501** ±0.277	2.9%	2.4%	0.1800	3.297 ±0.054
M12.C127	**7.322** ±0.162	**7.539** ±0.269	3.4%	3.0%	0.1809	3.304 ±0.052
M15.C128	**7.309** ±0.186	**7.509** ±0.284	3.0%	2.7%	0.1802	3.298 ±0.055
M18.C129	**7.308** ±0.178	**7.510** ±0.278	3.0%	2.8%	0.1802	3.299 ±0.054
Average	**7.315** ±0.219	**7.502** ±0.305			0.180	3.297 ±0.059
SD	**0.0114**	**0.0222**			0.0005	0.0043
ΔR	**0.33%**	**2.88%**			2.88%	1.26%

Where: Λ_{CHB} is the calibrated thermal conductance obtain by the CHB method; Λ_{HFM} is the thermal conductance obtained by the difference between the reference material value and the calibrated obtain value; $\Delta\Lambda_{HFM\rightarrow Ref}$ is the thermal conductance difference between HFM method and the reference value of the specimen; $\Delta\Lambda_{CHB\rightarrow HFM}$ is the thermal conductance difference between CHB method and HFM method; λ_{HFM} is the thermal conductivity obtain with HFM method; U_{HFM} is the thermal transmittance obtained with HFM method; SD is the standard deviation; and ΔR is the difference in relation to the reference value

Table 4.32 shows the repeatability of the equipment, namely for thermal conductance, ambient temperatures and air velocities in the chambers. This study is carried out for some of the calibration matrix tests, which were repeated for this purpose. It is observed that a relative standard deviation percentage is low for all parameters, lower than 1%, which demonstrates good performance of the equipment.

Table 4.32 – Tests repeatability on the GHB with calcium silicate boards 24 mm thick.

Test n.º	Λ_{CHB} [W/(m².K)]	T_{n1} [°C]	T_{n2} [°C]	V_{n1} [m/s]	V_{n2} [m/s]	Test n.º	Λ_{CHB} [W/(m².K)]	T_{n1} [°C]	T_{n2} [°C]	V_{n1} [m/s]	V_{n2} [m/s]
M01.C098	7.324	35.000	4.999	0.101	0.651	M10.C109	7.316	35.000	5.000	0.201	1.297
M01.C099	7.324	35.010	5.001	0.100	0.651	M10.C110	7.318	35.010	5.000	0.201	1.298
M01.C100	7.322	35.000	5.000	0.100	0.649	M10.C111	7.321	34.780	5.001	0.201	1.299
M01.C101	7.326	35.020	4.998	0.100	0.650						
M01.C102	7.323	34.990	4.999	0.100	0.650						
Average	**7.324**	**35.004**	**4.999**	**0.100**	**0.650**	**Average**	**7.318**	**34.930**	**5.000**	**0.201**	**1.298**
SD	**0.0013**	**0.0102**	**0.0011**	**0.0004**	**0.0008**	**SD**	**0.0021**	**0.1061**	**0.0006**	**0.0002**	**0.0007**
RSD%	**0.02%**	**0.03%**	**0.02%**	**0.39%**	**0.13%**	**RSD%**	**0.03%**	**0.30%**	**0.01%**	**0.09%**	**0.05%**
M04.C103	7.322	35.000	5.000	0.201	0.649	M13.C112	7.317	45.000	10.000	0.100	1.299
M04.C104	7.319	35.020	5.000	0.201	0.651	M13.C113	7.318	44.980	9.999	0.100	1.301
M04.C105	7.322	35.000	5.001	0.201	0.650	M13.C114	7.320	45.020	9.998	0.100	1.300
Average	**7.321**	**35.007**	**5.000**	**0.201**	**0.650**	**Average**	**7.318**	**45.000**	**9.999**	**0.100**	**1.300**
SD	**0.0014**	**0.0094**	**0.0005**	**0.0001**	**0.0006**	**SD**	**0.0012**	**0.0163**	**0.0008**	**0.0001**	**0.0007**
RSD%	**0.02%**	**0.03%**	**0.01%**	**0.05%**	**0.09%**	**RSD%**	**0.02%**	**0.04%**	**0.01%**	**0.09%**	**0.05%**
M07.C106	7.324	35.503	5.000	0.100	1.299	M16.C115	7.312	45.000	9.996	0.206	1.297
M07.C107	7.323	35.010	5.000	0.100	1.299	M16.C116	7.314	45.010	10.000	0.206	1.299
M07.C108	7.322	34.990	4.990	0.100	1.301	M16.C117	7.313	45.000	9.999	0.207	1.299
Average	**7.323**	**35.168**	**4.997**	**0.100**	**1.299**	**Average**	**7.313**	**45.003**	**9.998**	**0.206**	**1.299**
SD	**0.0008**	**0.2373**	**0.0047**	**0.0000**	**0.0010**	**SD**	**0.0007**	**0.0047**	**0.0016**	**0.0006**	**0.0009**
RSD%	**0.01%**	**0.67%**	**0.09%**	**0.04%**	**0.08%**	**RSD%**	**0.01%**	**0.01%**	**0.02%**	**0.27%**	**0.07%**

Where: Λ_{CHB} is the calibrated thermal conductance obtain by the CHB method; T_{n1} is the environmental temperature of the hot side; T_{n2} is the environmental temperature of the cold side; V_{n1} is the air velocity in the hot side; V_{n2} is the air velocity in the cold side; SD is the standard deviation; RSD is the relative standard deviation

4.6.3. Specimen 3

For the third set of calibration tests, it was assembled in the specimen frame, a wall composed of expanded polystyrene (EPS) panels with 50 mm thickness, that fulfils the 3.60 (W) by 2.70 (H) m² of the frame. This reference material has a thermal conductivity, retrieved from the certificate of the manufacturer, of 0.039 W/(m.° C).

An experimental study was carried out using the TPS method to confirm the values of the thermal conductivity. Table 4.33 presents the results of the experimental campaign, which tested three pairs of samples for each material and performed five repetitions for each analysis. The obtained experimental result is -0.3% different from the certificate value, being used for calibration purposes the value of the certificate.

Table 4.33 – Thermal conductivity of EPS [W/(m.K)]

Test repetition n.º	Sample 1	Sample 2	Sample 3	Average λ	Certificate λ
1	0.0391	0.0388	0.0391		
2	0.0391	0.0390	0.0390	**0.0389** ±5%	**0.039**
3	0.0388	0.0387	0.0390	(Standard	**(Δ_λ=-0.3%)**
4	0.0388	0.0387	0.0390	Deviation: 0.0001)	
5	0.0388	0.0392	0.0391		

The next sub-sections present the calibration and verifications for the CHB and GHB method with the EPS specimen.

4.6.3.1. Calibrated Hot Box mode

For the full characterization of the apparatus in CHB mode, Table 4.34 presents the test matrix for the calibration, composed of 18 tests. These tests aim to fully characterize the equipment for another range of thermal conductance of the element, having different combinations of temperatures and air velocities for each box of the equipment, namely MB and CB, and temperature variations in relation to the surrounding chamber to impose a heat flow through the MB walls.

The sample has the following instrumentation: (*i*) fourth two thermocouples for surface temperature, being twenty-one in each side of the specimen; and (*ii*) twelve heat flux sensors, namely six in each face. With all sensors placed on each side of the wall (hot and cold side) to have symmetry at the measuring points. Figure 4.75 shows the location of all temperature and heat flux sensors placed on the cold side of the ESP panels, and shows the limits of the metering area with 3.18 (W) by 2.28 (H) m².

Table 4.34 – Test matrix for calibration of the CHB with ESP panels 50 mm thick.

Test n.º	MB air temperature [°C]	Lab. air temperature [°C]	CB air temperature [°C]	MB wall heat flux	MB air velocity [m/s]	CB air velocity [m/s]
1	18	18	5	0	0.2	0.65
2	45	18	5	+	0.2	0.65
3	10	18	5	-	0.2	0.65
4	18	18	5	0	0.4	0.65
5	45	18	5	+	0.4	0.65
6	10	18	5	-	0.4	0.65
7	18	18	5	0	0.2	1.3
8	45	18	5	+	0.2	1.3
9	10	18	5	-	0.2	1.3
10	18	18	5	0	0.4	1.3
11	45	18	5	+	0.4	1.3
12	10	18	5	-	0.4	1.3
13	18	18	10	0	0.2	1.3
14	25	18	10	+	0.2	1.3
15	15	18	10	-	0.2	1.3
16	18	18	10	0	0.4	1.3
17	25	18	10	+	0.4	1.3
18	15	18	10	-	0.4	1.3

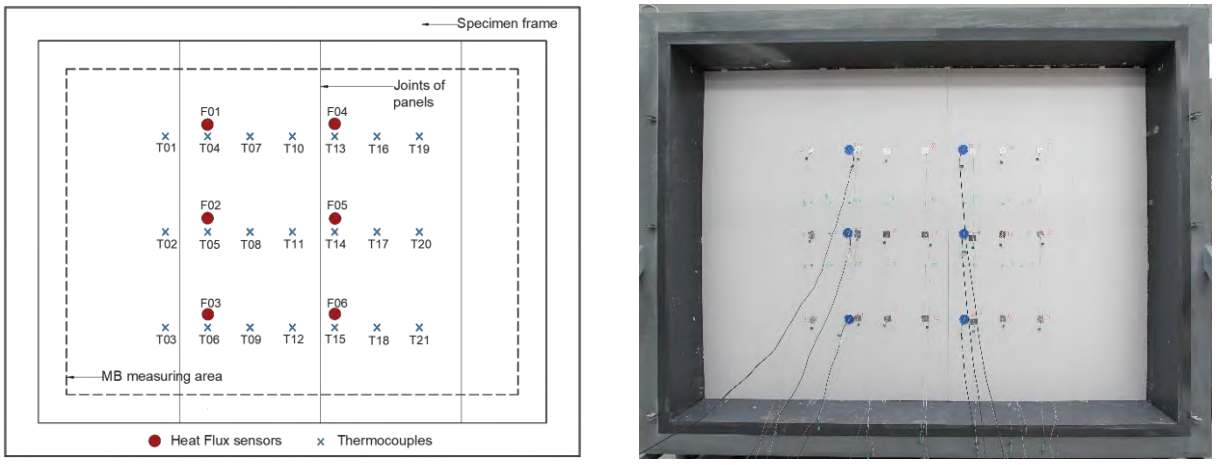

a) b)

Figure 4.75 – Location of temperature and heat flux sensors placed on the CHB cold side of the EPS panels 50 mm thick wall surface: a) sketch; b) photo.

The calibration matrix tests were performed according to the requirements presented in section 3.4.2. The test time starts counting from the moment that the setpoints were reached with a difference of less than 1%. All tests had a minimum duration of 8 hours, and the test conditions were achieved on average between one and two hours. Some tests were repeated to verify the repeatability of the equipment, being made 33 tests in total, whose results are shown in Table 4.35.

Table 4.35 shows the main results of the tests which allow assessing the thermal conductance and thermal transmittance according to the equations presented in section 3.4.3. The heat flow rate (Φ) is obtained by correcting the total power imputed to the system by subtracting the flanking losses of the MB, which were obtained numerically in section 4.5.2, chart of Figure 4.41. Next, is obtained the experimental thermal conductance that is multiplied by the calibration factor obtain experimentally, giving the calibrated thermal conductance. Figure 4.76, Figure 4.78 and Figure 4.80 present the relationship of conductance to mean specimen temperature of the three test group cases, from which is obtain the calibration factor.

Table 4.35 – Test results for calibration of the CHB with EPS panels 50 mm thick.

Test n.º	MB_w	Φ_p [W]	T_{n1} [°C]	$T_{n.out}$ [°C]	T_{n2} [°C]	ΔT_s [°C]	Φ [W]	Λ' [W/(m².K)]	C	Λ [W/(m².K)]	$\Delta\Lambda$	U [W/(m².K)]
M01.C130		49.209	18.00	17.89	5.00	8.75	49.972	0.788		**0.778** ±0.016	-0.2%	0.687 ±0.012
M01.C131		49.229	18.01	17.68	5.00	8.76	49.991	0.787		**0.777** ±0.016	-0.3%	0.687 ±0.012
M01.C132		49.222	18.00	17.42	5.00	8.75	49.984	0.788		**0.778** ±0.016	-0.2%	0.687 ±0.012
M01.C133		49.343	18.00	17.03	5.00	8.75	50.106	0.790		**0.781** ±0.016	0.1%	0.689 ±0.012
M01.C134		49.305	17.99	17.17	5.00	8.75	50.068	0.789		**0.780** ±0.016	0.0%	0.689 ±0.012
M04.C135		50.152	18.00	17.02	5.00	8.93	50.914	0.786		**0.777** ±0.016	-0.4%	0.686 ±0.012
M04.C136		50.272	18.00	17.72	5.00	8.94	51.035	0.787		**0.778** ±0.016	-0.3%	0.687 ±0.012
M04.C137		50.165	18.00	17.21	5.00	8.93	50.928	0.787		**0.777** ±0.016	-0.4%	0.686 ±0.012
M07.C138		49.650	18.00	17.14	5.00	8.82	50.412	0.788		**0.779** ±0.016	-0.2%	0.688 ±0.012
M07.C139	0	49.675	18.01	17.40	5.00	8.82	50.438	0.789	0.9878	**0.779** ±0.016	-0.1%	0.688 ±0.012
M07.C140		49.755	18.01	17.51	5.00	8.84	50.518	0.788		**0.779** ±0.016	-0.2%	0.688 ±0.012
M10.C141		50.207	18.00	17.41	5.00	8.95	50.969	0.785		**0.776** ±0.016	-0.6%	0.685 ±0.012
M10.C142		50.144	17.99	17.63	5.00	8.94	50.906	0.786		**0.776** ±0.016	-0.5%	0.686 ±0.012
M10.C143		50.208	18.01	17.46	5.00	8.96	50.971	0.785		**0.775** ±0.016	-0.6%	0.685 ±0.012
M13.C144		51.288	18.00	17.17	5.00	9.18	52.051	0.782		**0.773** ±0.015	-0.9%	0.683 ±0.012
M13.C145		51.397	18.01	17.80	5.00	9.16	52.160	0.785		**0.776** ±0.015	-0.5%	0.685 ±0.012
M13.C146		51.383	18.01	17.58	5.00	9.17	52.146	0.784		**0.775** ±0.015	-0.7%	0.685 ±0.012
M16.C147		51.507	18.00	17.56	5.00	9.21	52.270	0.783		**0.773** ±0.015	-0.9%	0.683 ±0.012
M16.C148		51.531	18.00	17.95	5.00	9.23	52.293	0.782		**0.772** ±0.015	-1.0%	0.683 ±0.012
M16.C149		51.515	18.00	17.71	5.00	9.20	52.277	0.784		**0.775** ±0.015	-0.7%	0.684 ±0.012
M02.C150		283.328	45.02	17.29	5.00	34.20	193.654	0.781		**0.782** ±0.012	0.2%	0.690 ±0.009
M05.C151		286.661	45.00	17.33	5.00	34.72	196.987	0.782		**0.783** ±0.012	0.4%	0.691 ±0.009
M08.C152	+	283.291	45.00	17.68	5.00	34.46	193.617	0.775	1.0007	**0.776** ±0.012	-0.6%	0.685 ±0.009
M11.C153		285.469	44.99	17.37	5.00	34.80	195.795	0.776		**0.783** ±0.012	-0.4%	0.686 ±0.009
M14.C154		177.698	25.00	17.53	5.00	15.84	88.024	0.767		**0.776** ±0.013	-1.7%	0.685 ±0.010
M17.C155		178.210	25.00	17.64	5.00	15.94	88.536	0.766		**0.777** ±0.013	-1.7%	0.686 ±0.010
M03.C156		-20.991	10.00	17.44	5.00	1.16	6.567	0.784		**0.783** ±0.061	0.4%	0.691 ±0.048
M06.C157		-20.599	10.00	17.50	5.00	1.23	6.960	0.783		**0.782** ±0.058	0.3%	0.690 ±0.045
M09.C158	-	-20.712	10.00	18.09	5.00	1.21	6.846	0.781	0.9987	**0.780** ±0.058	-0.1%	0.688 ±0.045
M12.C159		-20.624	10.00	17.77	5.00	1.23	6.935	0.779		**0.778** ±0.057	-0.3%	0.687 ±0.044
M15.C160		6.709	15.00	17.82	5.00	6.10	34.267	0.775		**0.774** ±0.018	-0.8%	0.684 ±0.014
M18.C161		7.405	15.00	17.51	5.00	6.22	34.964	0.776		**0.775** ±0.018	-0.7%	0.684 ±0.014

Where: MB_w is the MB wall heat flux; Φ_p is de total power input; T_{n1} is the environmental temperature of the hot side; $T_{n.out}$ is the environmental temperature of the room where is the apparatus; T_{n2} is the environmental temperature of the cold side; ΔT_s is the surface temperature difference across the specimen; Φ is the heat flow rate; Λ' is the experimental thermal conductance; C is the calibration factor; Λ is the calibrated thermal conductance; $\Delta\Lambda$ is the thermal conductance difference between the material reference value and the calibrated obtain value; and U is the thermal transmittance

Table 4.26 shows the difference between thermal conductance obtained experimentally by the CHB method and the reference value. It shows that, as expected and similar to the calibration with specimen 1, the better results are obtained when the equipment operates in the way the heat flow in the walls of the MB is close to zero.

Figure 4.77, Figure 4.79 and Figure 4.81 show charts of ambient temperatures and air velocities in the MB and CB, for a test of each group, during the test period in which the test conditions are fulfilled and from where the analysis of the results is performed.

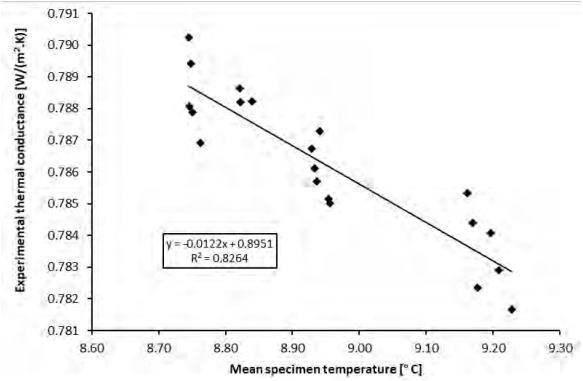

Figure 4.76 – Relationship of conductance to mean specimen temperature of test cases with MB wall heat flux near zero for CHB with EPS panels 50 mm thick.

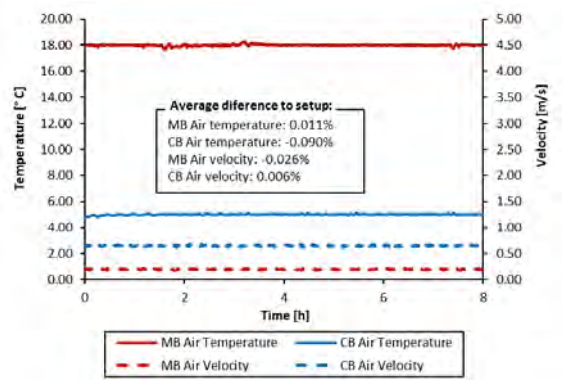

Figure 4.77 – Test M01.C130 air temperature and velocity in chambers for CHB with EPS panels 50 mm thick.

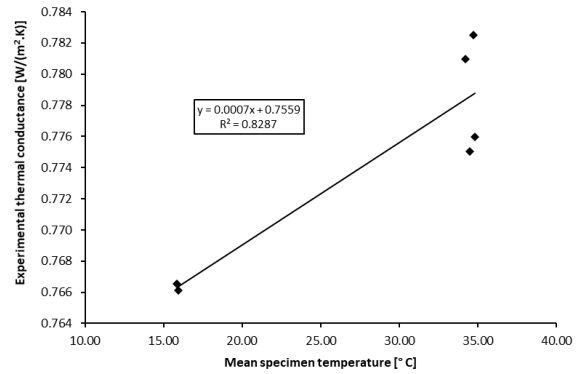

Figure 4.78 – Relationship of conductance to mean specimen temperature of test cases with MB wall heat flux positive for CHB with EPS panels 50 mm thick.

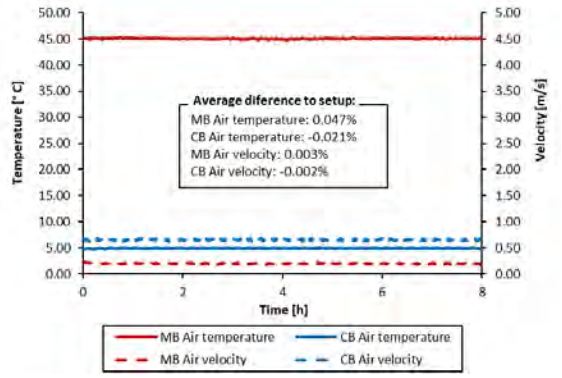

Figure 4.79 – Test M002.C150 air temperature and velocity in chambers for CHB with EPS panels 50 mm thick.

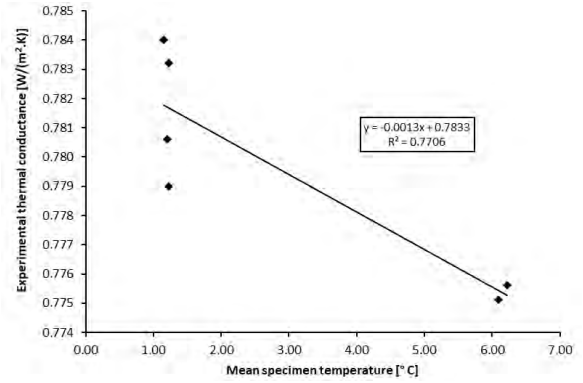

Figure 4.80 – Relationship of conductance to mean specimen temperature of test cases with MB wall heat flux negative for CHB with EPS panels 50 mm thick.

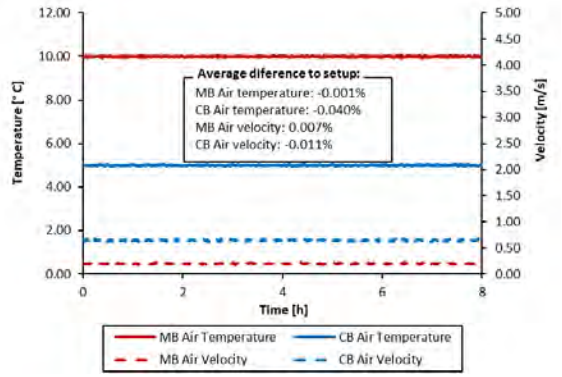

Figure 4.81 – Test M03.C156 air temperature and velocity in chambers for CHB with EPS panels 50 mm thick.

Table 4.36 shows a comparison between the CHB and HFM method for the tests performed. From the results obtained, it is confirmed that the flowmeters method is less rigorous. The average result difference is 2.19%, and the maximum individual difference is 3.1% in relation to the reference value of the material.

Comparing methodologies, the maximum difference in results is 3.6%. Table 4.36 also shows the average difference between the calibrated thermal conductance value obtained by the CHB method and the reference material, giving a low value of only -0.31%.

Table 4.36 – Test results of CHB vs HFM method for EPS panels 50 mm thick.

Test n.º	Λ_{CHB} [W/(m².K)]	Λ_{HFM} [W/(m².K)]	$\Delta\Lambda_{HFM\rightarrow Ref}$	$\Delta\Lambda_{CHB\rightarrow HFM}$	λ_{HFM} [W/(m.K)]	U_{HFM} [W/(m².K)]
M01.C130	**0.778** ±0.016	**0.792** ±0.027	1.6%	1.8%	0.0396	0.698 ±0.021
M01.C131	**0.777** ±0.016	**0.791** ±0.027	1.4%	1.8%	0.0395	0.697 ±0.021
M01.C132	**0.778** ±0.016	**0.790** ±0.027	1.3%	1.6%	0.0395	0.697 ±0.021
M01.C133	**0.781** ±0.016	**0.792** ±0.027	1.5%	1.4%	0.0396	0.698 ±0.021
M01.C134	**0.780** ±0.016	**0.791** ±0.027	1.4%	1.4%	0.0395	0.697 ±0.021
M04.C135	**0.777** ±0.016	**0.798** ±0.027	2.3%	2.7%	0.0399	0.703 ±0.021
M04.C136	**0.778** ±0.016	**0.791** ±0.027	1.3%	1.6%	0.0395	0.697 ±0.021
M04.C137	**0.777** ±0.016	**0.795** ±0.027	1.9%	2.3%	0.0397	0.700 ±0.021
M07.C138	**0.779** ±0.016	**0.799** ±0.028	2.4%	2.6%	0.0399	0.703 ±0.022
M07.C139	**0.779** ±0.016	**0.797** ±0.027	2.2%	2.3%	0.0398	0.702 ±0.021
M07.C140	**0.779** ±0.016	**0.798** ±0.027	2.3%	2.4%	0.0399	0.703 ±0.021
M10.C141	**0.776** ±0.016	**0.793** ±0.027	1.7%	2.2%	0.0396	0.699 ±0.021
M10.C142	**0.776** ±0.016	**0.803** ±0.028	3.0%	3.5%	0.0402	0.707 ±0.022
M10.C143	**0.775** ±0.016	**0.801** ±0.028	2.7%	3.4%	0.0401	0.705 ±0.022
M13.C144	**0.773** ±0.015	**0.797** ±0.027	2.2%	3.1%	0.0398	0.702 ±0.021
M13.C145	**0.776** ±0.015	**0.799** ±0.027	2.5%	3.0%	0.0400	0.704 ±0.021
M13.C146	**0.775** ±0.015	**0.802** ±0.027	2.9%	3.5%	0.0401	0.706 ±0.021
M16.C147	**0.773** ±0.015	**0.800** ±0.027	2.5%	3.5%	0.0400	0.704 ±0.021
M16.C148	**0.772** ±0.015	**0.798** ±0.027	2.3%	3.4%	0.0399	0.703 ±0.021
M16.C149	**0.775** ±0.015	**0.794** ±0.027	1.8%	2.5%	0.0397	0.700 ±0.021
M02.C150	**0.782** ±0.012	**0.800** ±0.025	2.6%	2.3%	0.0400	0.704 ±0.019
M05.C151	**0.783** ±0.012	**0.804** ±0.026	3.1%	2.7%	0.0402	0.707 ±0.020
M08.C152	**0.776** ±0.012	**0.804** ±0.026	3.1%	3.6%	0.0402	0.707 ±0.020
M11.C153	**0.783** ±0.012	**0.795** ±0.025	1.9%	1.5%	0.0397	0.700 ±0.019
M14.C154	**0.776** ±0.013	**0.801** ±0.026	2.7%	3.3%	0.0401	0.705 ±0.020
M17.C155	**0.777** ±0.013	**0.796** ±0.026	2.1%	2.4%	0.0398	0.701 ±0.020
M03.C156	**0.783** ±0.061	**0.802** ±0.067	2.8%	2.4%	0.0401	0.706 ±0.052
M06.C157	**0.782** ±0.058	**0.800** ±0.063	2.6%	2.3%	0.0400	0.704 ±0.049
M09.C158	**0.780** ±0.058	**0.795** ±0.063	1.9%	1.9%	0.0398	0.700 ±0.049
M12.C159	**0.778** ±0.057	**0.793** ±0.062	1.7%	2.0%	0.0397	0.699 ±0.048
M15.C160	**0.774** ±0.018	**0.799** ±0.029	2.5%	3.3%	0.0400	0.704 ±0.022
M18.C161	**0.775** ±0.018	**0.796** ±0.029	2.1%	2.7%	0.0398	0.701 ±0.022
Average	**0.778** ±0.061	**0.797** ±0.067			0.040	0.702 ±0.052
SD	**0.0023**	**0.0041**			0.0002	0.0032
ΔR	**-0.31%**	**2.19%**			2.19%	1.93%

Where: Λ_{CHB} is the calibrated thermal conductance obtain by the CHB method; Λ_{HFM} is the thermal conductance obtained by the difference between the reference material value and the calibrated obtain value; $\Delta\Lambda_{HFM\rightarrow Ref}$ is the thermal conductance difference between HFM method and the reference value of the specimen; $\Delta\Lambda_{CHB\rightarrow HFM}$ is the thermal conductance difference between CHB method and HFM method; λ_{HFM} is the thermal conductivity obtain with HFM method; U_{HFM} is the thermal transmittance obtained with HFM method; SD is the standard deviation; and ΔR is the difference in relation to the reference value

Table 4.37 shows the repeatability of the equipment, namely for thermal conductance, ambient temperatures and air velocities in the chambers. This study is carried out for some of the calibration matrix tests, which were repeated for this purpose. It is observed that a relative standard deviation percentage is low for all parameters, lower than 1%, which demonstrates good performance of the equipment.

Table 4.37 – Tests repeatability on the CHB with EPS panels 50 mm thick.

Test n.º	Λ_{CHB} [W/(m².K)]	T_{n1} [°C]	T_{n2} [°C]	V_{n1} [m/s]	V_{n2} [m/s]	Test n.º	Λ_{CHB} [W/(m².K)]	T_{n1} [°C]	T_{n2} [°C]	V_{n1} [m/s]	V_{n2} [m/s]
M01.C130	0.778	18.002	4.995	0.200	0.650	M10.C141	0.776	18.000	4.995	0.400	1.300
M01.C131	0.777	18.009	4.995	0.200	0.651	M10.C142	0.776	17.993	4.995	0.400	1.301
M01.C132	0.778	18.003	4.995	0.201	0.650	M10.C143	0.775	18.008	4.995	0.400	1.300
M01.C133	0.781	18.000	4.995	0.200	0.651						
M01.C134	0.780	17.995	4.995	0.200	0.651						
Average	**0.779**	**18.002**	**4.995**	**0.200**	**0.651**	**Average**	**0.776**	**18.000**	**4.995**	**0.400**	**1.300**
SD	**0.0015**	**0.0048**	**0.0000**	**0.0004**	**0.0003**	**SD**	**0.0005**	**0.0058**	**0.0000**	**0.0000**	**0.0006**
RSD%	**0.19%**	**0.03%**	**0.00%**	**0.20%**	**0.04%**	**RSD%**	**0.06%**	**0.03%**	**0.00%**	**0.00%**	**0.04%**
M04.C135	0.777	18.000	4.995	0.400	0.651	M13.C144	0.773	18.004	4.995	0.200	1.300
M04.C136	0.778	18.003	4.995	0.400	0.649	M13.C145	0.776	18.007	4.995	0.200	1.300
M04.C137	0.777	18.000	4.995	0.400	0.649	M13.C146	0.775	18.007	4.995	0.200	1.300
Average	**0.777**	**18.001**	**4.995**	**0.400**	**0.650**	**Average**	**0.775**	**18.006**	**4.995**	**0.200**	**1.300**
SD	**0.0005**	**0.0011**	**0.0000**	**0.0000**	**0.0007**	**SD**	**0.0012**	**0.0014**	**0.0000**	**0.0000**	**0.0001**
RSD%	**0.06%**	**0.01%**	**0.00%**	**0.00%**	**0.11%**	**RSD%**	**0.16%**	**0.01%**	**0.00%**	**0.00%**	**0.01%**
M07.C138	0.779	18.000	4.995	0.200	1.299	M16.C147	0.773	18.000	4.995	0.400	1.301
M07.C139	0.779	18.008	4.995	0.200	1.299	M16.C148	0.772	18.001	4.995	0.400	1.299
M07.C140	0.779	18.007	4.995	0.200	1.300	M16.C149	0.775	18.000	4.995	0.402	1.300
Average	**0.779**	**18.005**	**4.995**	**0.200**	**1.299**	**Average**	**0.773**	**18.000**	**4.995**	**0.401**	**1.300**
SD	**0.0000**	**0.0035**	**0.0000**	**0.0000**	**0.0004**	**SD**	**0.0011**	**0.0005**	**0.0000**	**0.0009**	**0.0009**
RSD%	**0.00%**	**0.02%**	**0.00%**	**0.00%**	**0.03%**	**RSD%**	**0.14%**	**0.00%**	**0.00%**	**0.24%**	**0.07%**

Where: Λ_{CHB} is the calibrated thermal conductance obtain by the CHB method; T_{n1} is the environmental temperature of the hot side; T_{n2} is the environmental temperature of the cold side; V_{n1} is the air velocity in the hot side; V_{n2} is the air velocity in the cold side; SD is the standard deviation; RSD is the relative standard deviation

4.6.3.2. Guarded Hot Box mode

For the full characterization of the apparatus in GHB mode, Table 4.38 presents the test matrix for the calibration, composed of 18 tests. These tests aim to fully characterize the equipment for another range of thermal conductance of the element, having different combinations of temperatures and air velocities for each box of the equipment.

The sample has the following instrumentation: (*i*) fourth two thermocouples for surface temperature, being twenty-one in each side of the specimen; and (*ii*) twelve heat flux sensors, namely six in each face. With all sensors placed on each side of the wall (hot and cold side) to have symmetry at the measuring points. Figure 4.82 shows the location of all temperature and heat flux sensors placed on the cold side of the EPS panels, and shows the limits of the metering area with 1.80 (W) by 1.05 (H) m².

Table 4.38 – Test matrix for calibration of the GHB with EPS panels 50 mm thick.

Test n.º	MB air temperature [°C]	Lab. air temperature [°C]	CB air temperature [°C]	MB wall heat flux	MB air velocity [m/s]	CB air velocity [m/s]
1	35	35	5	0	0.2	0.65
2	35	20	5	+	0.2	0.65
3	35	50	5	-	0.2	0.65
4	35	35	5	0	0.4	0.65
5	35	20	5	+	0.4	0.65
6	35	50	5	-	0.4	0.65
7	35	35	5	0	0.2	1.3
8	35	20	5	+	0.2	1.3
9	35	50	5	-	0.2	1.3
10	35	35	5	0	0.4	1.3
11	35	20	5	+	0.4	1.3
12	35	50	5	-	0.4	1.3
13	45	45	10	0	0.2	1.3
14	45	35	10	+	0.2	1.3
15	45	55	10	-	0.2	1.3
16	45	45	10	0	0.4	1.3
17	45	35	10	+	0.4	1.3
18	45	55	10	-	0.4	1.3

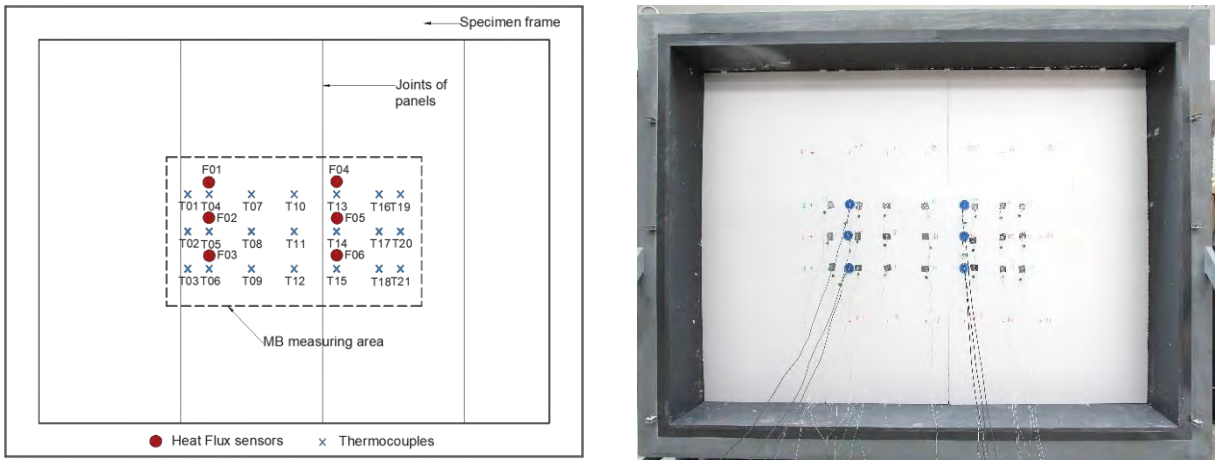

a) **b)**

Figure 4.82 – Location of temperature and heat flux sensors placed on the GHB cold side of the EPS 50 mm thick wall surface: a) sketch; b) photo.

The calibration matrix tests were performed according to the requirements presented in section 3.4.2. The test time starts counting from the moment that the setpoints were reached with a difference of less than 1%. All tests had a minimum duration of 8 hours, and the test conditions were achieved on average between one and two hours. Some tests were repeated to verify the repeatability of the equipment, being made 32 tests in total, whose results are shown in Table 4.39.

Table 4.39 shows the main results of the tests which allow assessing the thermal conductance and thermal transmittance according to the equations presented in section 3.4.3. The heat flow rate (Φ) is obtained by correcting the total power imputed to the system by subtracting the flanking losses of the MB, which were obtained numerically in section 4.5.2, chart of Figure 4.43. Next, is obtained the experimental thermal conductance that is multiplied by the calibration factor obtain experimentally, giving the calibrated thermal

conductance. Figure 4.83, Figure 4.85 and Figure 4.87 present the relationship of conductance to mean specimen temperature of the three test group cases, from which is obtain the calibration factor.

Table 4.39 – Test results for calibration of the GHB with EPS panels 50 mm thick.

Test n.º	MB_w	Φ_p [W]	T_{n1} [°C]	$T_{n.out}$ [°C]	T_{n2} [°C]	ΔT_s [°C]	Φ [W]	Λ' [W/(m².K)]	C	Λ [W/(m².K)]	$\Delta\Lambda$	U [W/(m².K)]
M01.C162		36.349	35.00	34.34	5.09	24.96	37.061	0.786		**0.785** ±0.012	0.6%	0.692 ±0.009
M01.C163		36.277	35.00	34.18	5.00	24.97	36.989	0.784		**0.783** ±0.012	0.4%	0.691 ±0.009
M01.C164		36.228	35.00	34.11	5.00	24.97	36.940	0.783		**0.782** ±0.012	0.2%	0.690 ±0.009
M01.C165		36.225	35.00	34.12	5.00	24.94	36.937	0.784		**0.783** ±0.012	0.3%	0.691 ±0.009
M01.C166		36.213	35.00	34.13	5.00	24.95	36.925	0.783		**0.782** ±0.012	0.3%	0.690 ±0.009
M04.C167		37.326	35.00	34.46	5.00	25.65	38.039	0.785		**0.784** ±0.012	0.5%	0.692 ±0.009
M04.C168		37.392	35.00	34.29	5.00	25.66	38.104	0.786		**0.785** ±0.012	0.6%	0.692 ±0.009
M04.C169		37.359	35.00	34.12	5.00	25.67	38.071	0.785		**0.784** ±0.012	0.5%	0.692 ±0.009
M07.C170		37.326	35.00	34.13	5.00	25.71	38.038	0.783		**0.782** ±0.012	0.2%	0.690 ±0.009
M07.C171	0	37.519	35.00	34.25	5.00	25.75	38.231	0.786	0.9987	**0.785** ±0.012	0.6%	0.692 ±0.009
M07.C172		37.479	35.00	34.47	5.00	25.73	38.191	0.785		**0.784** ±0.012	0.6%	0.692 ±0.009
M10.C173		38.467	35.00	34.32	5.00	26.48	39.179	0.783		**0.782** ±0.012	0.2%	0.690 ±0.009
M10.C174		38.416	35.00	34.20	5.00	26.50	39.128	0.781		**0.780** ±0.012	0.0%	0.689 ±0.009
M10.C175		38.406	35.00	34.36	5.00	26.52	39.118	0.781		**0.780** ±0.012	-0.1%	0.688 ±0.009
M13.C176		42.822	45.00	44.13	10.00	29.66	43.653	0.779		**0.778** ±0.013	-0.3%	0.687 ±0.010
M13.C177		42.880	45.00	44.23	10.00	29.65	43.711	0.780		**0.779** ±0.013	-0.1%	0.688 ±0.010
M13.C178		42.780	45.00	44.22	10.00	29.65	43.611	0.778		**0.777** ±0.013	-0.4%	0.687 ±0.010
M16.C179		44.124	45.00	44.33	10.00	30.63	44.955	0.777		**0.776** ±0.013	-0.6%	0.685 ±0.010
M16.C180		44.089	45.00	44.16	10.00	30.64	44.919	0.776		**0.775** ±0.013	-0.7%	0.685 ±0.010
M16.C181		44.229	45.00	44.40	10.00	30.66	45.059	0.778		**0.777** ±0.013	-0.4%	0.686 ±0.010
M02.C182		74.648	35.00	20.01	5.00	28.40	41.935	0.781		**0.782** ±0.011	0.3%	0.690 ±0.009
M05.C183		75.885	35.00	20.00	5.00	29.16	43.173	0.783		**0.784** ±0.011	0.6%	0.692 ±0.009
M08.C184	+	76.071	35.00	20.00	5.00	29.33	43.358	0.782	1.0013	**0.783** ±0.011	0.4%	0.691 ±0.009
M11.C185		77.280	35.00	20.00	5.00	30.14	44.567	0.782		**0.784** ±0.011	0.4%	0.691 ±0.009
M14.C186		68.955	45.00	35.00	10.00	31.95	47.502	0.787		**0.783** ±0.012	1.0%	0.691 ±0.009
M17.C187		70.413	45.00	35.00	10.00	32.92	48.960	0.787		**0.783** ±0.012	1.0%	0.691 ±0.009
M03.C188		-3.316	35.00	50.00	5.00	20.69	30.821	0.788		**0.786** ±0.014	0.8%	0.693 ±0.011
M06.C189		-1.750	35.00	49.99	5.00	21.67	32.387	0.791		**0.789** ±0.013	1.1%	0.695 ±0.010
M09.C190	-	-2.333	35.00	50.01	5.00	21.32	31.804	0.789	0.9973	**0.787** ±0.013	0.9%	0.694 ±0.010
M12.C191		-1.015	35.00	50.00	5.00	22.15	33.122	0.791		**0.789** ±0.013	1.2%	0.696 ±0.010
M15.C192		15.850	45.00	55.00	10.00	26.60	38.964	0.775		**0.773** ±0.014	-0.9%	0.683 ±0.011
M18.C193		17.341	45.00	55.00	10.00	27.73	40.455	0.772		**0.770** ±0.013	-1.3%	0.681 ±0.010

Where: MB_w is the MB wall heat flux; Φ_p is de total power input; T_{n1} is the environmental temperature of the hot side; $T_{n.out}$ is the environmental temperature of the GB; T_{n2} is the environmental temperature of the cold side; ΔT_s is the surface temperature difference across the specimen; Φ is the heat flow rate; Λ' is the experimental thermal conductance; C is the calibration factor; Λ is the calibrated thermal conductance; $\Delta\Lambda$ is the thermal conductance difference between the material reference value and the calibrated obtain value; and U is the thermal transmittance

Table 4.39 shows the difference between thermal conductance obtained experimentally by the GHB method and the reference value. It reveals that for the range of thermal conductance under analysis, the results obtained in the equipment, when it operates in one of the three different modes of heat flow in the MB walls, similar results are obtained.

Figure 4.84, Figure 4.86 and Figure 4.88 show charts of ambient temperatures and air velocities in the MB and CB, for a test of each group, during the test period in which the test conditions are fulfilled and from where the analysis of the results is performed.

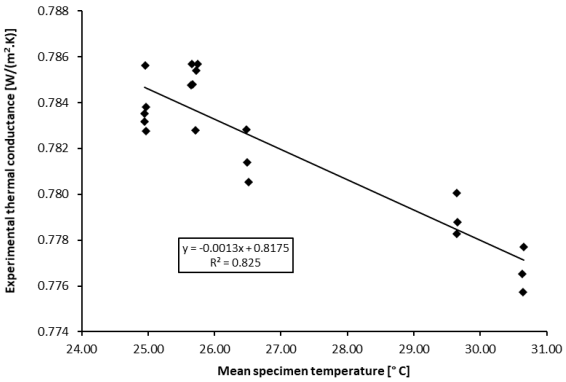

Figure 4.83 – Relationship of conductance to mean specimen temperature of test cases with MB wall heat flux near zero for GHB with EPS panels 50 mm thick.

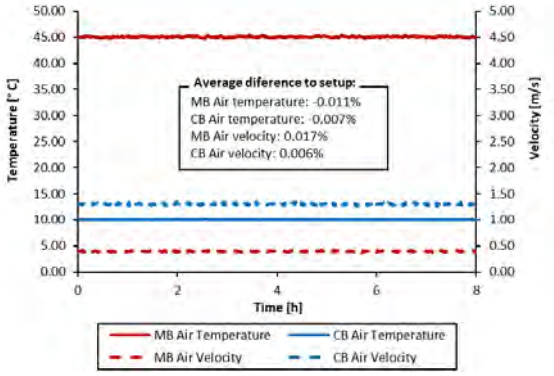

Figure 4.84 – Test M16.C179 air temperature and velocity in chambers for GHB with EPS panels 50 mm thick.

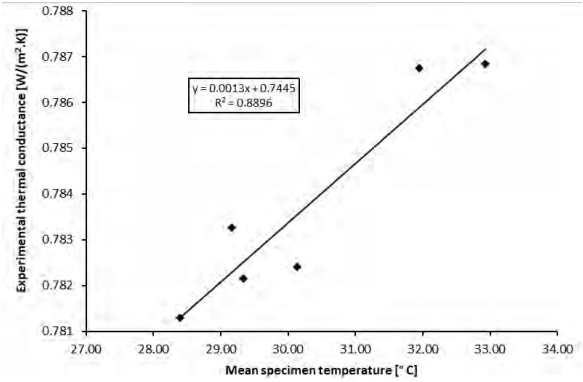

Figure 4.85 – Relationship of conductance to mean specimen temperature of test cases with MB wall heat flux positive for GHB with EPS panels 50 mm thick.

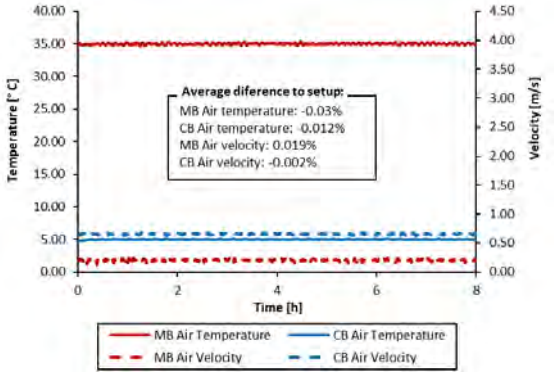

Figure 4.86 – Test M02.C182 air temperature and velocity in chambers for GHB with EPS panels 50 mm thick.

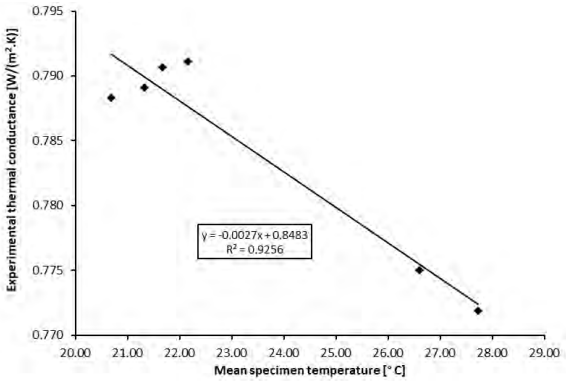

Figure 4.87 – Relationship of conductance to mean specimen temperature of test cases with MB wall heat flux negative for GHB with EPS panels 50 mm thick.

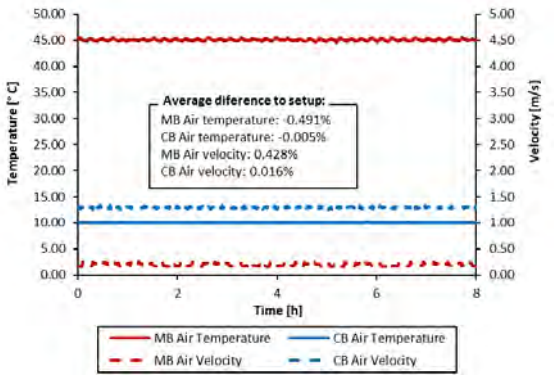

Figure 4.88 – Test M15.C192 air temperature and velocity in chambers for GHB with EPS panels 50 mm thick.

Table 4.40 shows a comparison between the GHB and HFM method for the tests performed. From the results obtained, it is confirmed that the flowmeters method is less rigorous. The average result difference is 1.9%, and the maximum individual difference is 3% in relation to the reference value of the material.

Comparing methodologies, the maximum difference in results is 3.6%. Table 4.40 also shows the average difference between the calibrated thermal conductance value obtained by the GHB method and the reference material, giving a low value of only 0.22%.

Table 4.40 – Test results of GHB vs HFM method for EPS panels 50 mm thick.

Test n.º	Λ_{CHB} [W/(m².K)]	Λ_{HFM} [W/(m².K)]	$\Delta\Lambda_{HFM\rightarrow Ref}$	$\Delta\Lambda_{CHB\rightarrow HFM}$	λ_{HFM} [W/(m.K)]	U_{HFM} [W/(m².K)]
M01.C162	**0.785** ±0.012	**0.798** ±0.026	2.3%	1.6%	0.0399	**0.703** ±0.020
M01.C163	**0.783** ±0.012	**0.798** ±0.026	2.3%	1.9%	0.0399	**0.703** ±0.020
M01.C164	**0.782** ±0.012	**0.797** ±0.026	2.2%	1.9%	0.0399	**0.702** ±0.020
M01.C165	**0.783** ±0.012	**0.800** ±0.026	2.5%	2.1%	0.0400	**0.704** ±0.020
M01.C166	**0.782** ±0.012	**0.801** ±0.026	2.6%	2.4%	0.0400	**0.705** ±0.020
M04.C167	**0.784** ±0.012	**0.793** ±0.025	1.6%	1.1%	0.0396	**0.698** ±0.019
M04.C168	**0.785** ±0.012	**0.792** ±0.025	1.6%	0.9%	0.0396	**0.698** ±0.019
M04.C169	**0.784** ±0.012	**0.795** ±0.025	1.9%	1.4%	0.0398	**0.700** ±0.019
M07.C170	**0.782** ±0.012	**0.793** ±0.025	1.7%	1.4%	0.0397	**0.699** ±0.019
M07.C171	**0.785** ±0.012	**0.792** ±0.025	1.5%	0.9%	0.0396	**0.698** ±0.019
M07.C172	**0.784** ±0.012	**0.792** ±0.025	1.5%	1.0%	0.0396	**0.698** ±0.019
M10.C173	**0.782** ±0.012	**0.785** ±0.025	0.6%	0.4%	0.0392	**0.692** ±0.019
M10.C174	**0.780** ±0.012	**0.784** ±0.025	0.5%	0.5%	0.0392	**0.692** ±0.019
M10.C175	**0.780** ±0.012	**0.783** ±0.025	0.3%	0.3%	0.0391	**0.691** ±0.019
M13.C176	**0.778** ±0.013	**0.803** ±0.026	2.9%	3.2%	0.0401	**0.706** ±0.020
M13.C177	**0.779** ±0.013	**0.801** ±0.026	2.6%	2.8%	0.0400	**0.705** ±0.020
M13.C178	**0.777** ±0.013	**0.803** ±0.026	3.0%	3.4%	0.0402	**0.707** ±0.020
M16.C179	**0.776** ±0.013	**0.798** ±0.026	2.4%	2.9%	0.0399	**0.703** ±0.020
M16.C180	**0.775** ±0.013	**0.800** ±0.026	2.6%	3.3%	0.0400	**0.705** ±0.020
M16.C181	**0.777** ±0.013	**0.802** ±0.026	2.8%	3.2%	0.0401	**0.706** ±0.020
M02.C182	**0.782** ±0.011	**0.801** ±0.025	2.7%	2.4%	0.0400	**0.705** ±0.019
M05.C183	**0.784** ±0.011	**0.797** ±0.025	2.2%	1.7%	0.0399	**0.702** ±0.019
M08.C184	**0.783** ±0.011	**0.797** ±0.025	2.2%	1.8%	0.0399	**0.702** ±0.019
M11.C185	**0.784** ±0.011	**0.786** ±0.025	0.8%	0.3%	0.0393	**0.694** ±0.019
M14.C186	**0.783** ±0.012	**0.803** ±0.026	3.0%	2.6%	0.0402	**0.707** ±0.020
M17.C187	**0.783** ±0.012	**0.799** ±0.026	2.4%	2.0%	0.0399	**0.703** ±0.020
M03.C188	**0.786** ±0.014	**0.791** ±0.026	1.4%	0.7%	0.0396	**0.697** ±0.020
M06.C189	**0.789** ±0.013	**0.782** ±0.026	0.2%	-0.9%	0.0391	**0.690** ±0.020
M09.C190	**0.787** ±0.013	**0.779** ±0.026	-0.1%	-1.0%	0.0390	**0.688** ±0.020
M12.C191	**0.789** ±0.013	**0.794** ±0.026	1.8%	0.7%	0.0397	**0.700** ±0.020
M15.C192	**0.773** ±0.014	**0.798** ±0.026	2.4%	3.3%	0.0399	**0.703** ±0.020
M18.C193	**0.770** ±0.013	**0.798** ±0.026	2.3%	3.6%	0.0399	**0.703** ±0.020
Average	**0.782** ±0.014	**0.795** ±0.026			0.040	**0.700** ±0.020
SD	**0.0031**	**0.0066**			0.0003	0.0051
ΔR	**0.22%**	**1.90%**			1.90%	1.68%

Where: Λ_{CHB} is the calibrated thermal conductance obtain by the CHB method; Λ_{HFM} is the thermal conductance obtained by the difference between the reference material value and the calibrated obtain value; $\Delta\Lambda_{HFM\rightarrow Ref}$ is the thermal conductance difference between HFM method and the reference value of the specimen; $\Delta\Lambda_{CHB\rightarrow HFM}$ is the thermal conductance difference between CHB method and HFM method; λ_{HFM} is the thermal conductivity obtain with HFM method; U_{HFM} is the thermal transmittance obtained with HFM method; SD is the standard deviation; and ΔR is the difference in relation to the reference value

Table 4.41 shows the repeatability of the equipment, namely for thermal conductance, ambient temperatures and air velocities in the chambers. This study is carried out for some of the calibration matrix tests, which were repeated for this purpose. It is observed that a relative standard deviation percentage is low for all parameters, lower than 1%, which demonstrates good performance of the equipment.

Table 4.41 – Tests repeatability on the GHB with EPS panels 50 mm thick.

Test n.º	Λ_{CHB} [W/(m².K)]	T_{n1} [°C]	T_{n2} [°C]	V_{n1} [m/s]	V_{n2} [m/s]	Test n.º	Λ_{CHB} [W/(m².K)]	T_{n1} [°C]	T_{n2} [°C]	V_{n1} [m/s]	V_{n2} [m/s]
M01.C162	0.785	35.001	5.090	0.100	0.650	M10.C173	0.782	35.000	5.000	0.204	1.300
M01.C163	0.783	35.001	4.999	0.100	0.650	M10.C174	0.780	35.000	5.000	0.203	1.301
M01.C164	0.782	35.000	5.000	0.100	0.650	M10.C175	0.780	35.001	4.999	0.203	1.300
M01.C165	0.783	34.999	4.999	0.100	0.650						
M01.C166	0.782	35.000	4.999	0.100	0.651						
Average	**0.783**	**35.000**	**5.018**	**0.100**	**0.650**	**Average**	**0.781**	**35.000**	**5.000**	**0.203**	**1.300**
SD	**0.0011**	**0.0007**	**0.0362**	**0.0001**	**0.0004**	**SD**	**0.0009**	**0.0005**	**0.0005**	**0.0004**	**0.0006**
RSD%	**0.14%**	**0.00%**	**0.72%**	**0.12%**	**0.06%**	**RSD%**	**0.12%**	**0.00%**	**0.01%**	**0.22%**	**0.05%**
M04.C167	0.784	34.999	5.000	0.204	0.651	M13.C176	0.778	44.999	10.000	0.101	1.301
M04.C168	0.785	35.001	4.999	0.203	0.650	M13.C177	0.779	45.001	10.000	0.100	1.299
M04.C169	0.784	35.000	5.000	0.204	0.652	M13.C178	0.777	45.001	10.000	0.100	1.299
Average	**0.784**	**35.000**	**5.000**	**0.204**	**0.651**	**Average**	**0.778**	**45.000**	**10.000**	**0.100**	**1.299**
SD	**0.0005**	**0.0008**	**0.0003**	**0.0005**	**0.0007**	**SD**	**0.0008**	**0.0009**	**0.0000**	**0.0001**	**0.0008**
RSD%	**0.06%**	**0.00%**	**0.01%**	**0.25%**	**0.11%**	**RSD%**	**0.10%**	**0.00%**	**0.00%**	**0.06%**	**0.06%**
M07.C170	0.782	35.001	5.000	0.100	1.299	M16.C179	0.776	45.000	9.999	0.213	1.300
M07.C171	0.785	35.000	5.000	0.100	1.300	M16.C180	0.775	45.001	10.000	0.213	1.300
M07.C172	0.784	34.999	4.999	0.100	1.299	M16.C181	0.777	45.000	10.000	0.212	1.300
Average	**0.784**	**35.000**	**5.000**	**0.100**	**1.299**	**Average**	**0.776**	**45.000**	**10.000**	**0.213**	**1.300**
SD	**0.0012**	**0.0008**	**0.0006**	**0.0002**	**0.0004**	**SD**	**0.0007**	**0.0005**	**0.0004**	**0.0003**	**0.0001**
RSD%	**0.16%**	**0.00%**	**0.01%**	**0.17%**	**0.03%**	**RSD%**	**0.09%**	**0.00%**	**0.00%**	**0.16%**	**0.01%**

Where: Λ_{CHB} is the calibrated thermal conductance obtain by the CHB method; T_{n1} is the environmental temperature of the hot side; T_{n2} is the environmental temperature of the cold side; V_{n1} is the air velocity in the hot side; V_{n2} is the air velocity in the cold side; SD is the standard deviation; RSD is the relative standard deviation

4.6.4. Specimen 4

For the fourth set of calibration tests, it was assembled in the specimen frame, a wall composed of two layers of expanded polystyrene (EPS) panels, 50mm thick, totalizing 100 mm of thickness, that fulfils the 3.60 (W) by 2.70 (H) m² of the frame. This reference material is the same used in the previous section, with thermal conductivity of 0.039 W/(m.° C).
The next sub-sections present the calibration and verifications for the CHB and GHB method with the EPS specimen 100 mm thick.

4.6.4.1. Calibrated Hot Box mode

For the full characterization of the apparatus in CHB mode, Table 4.42 presents the test matrix for the calibration, composed of 18 tests. These tests aim to fully characterize the equipment for another range of thermal conductance of the element, having different combinations of temperatures and air velocities for each box of the equipment, namely MB and CB, and temperature variations in relation to the surrounding chamber to impose a heat flow through the MB walls.

Table 4.42 – Test matrix for calibration of the CHB with ESP panels 100 mm thick.

Test n.º	MB air temperature [°C]	Lab. air temperature [°C]	CB air temperature [°C]	MB wall heat flux	MB air velocity [m/s]	CB air velocity [m/s]
1	18	18	5	0	0.2	0.65
2	45	18	5	+	0.2	0.65
3	10	18	5	-	0.2	0.65
4	18	18	5	0	0.4	0.65
5	45	18	5	+	0.4	0.65
6	10	18	5	-	0.4	0.65
7	18	18	5	0	0.2	1.3
8	45	18	5	+	0.2	1.3
9	10	18	5	-	0.2	1.3
10	18	18	5	0	0.4	1.3
11	45	18	5	+	0.4	1.3
12	10	18	5	-	0.4	1.3
13	18	18	10	0	0.2	1.3
14	25	18	10	+	0.2	1.3
15	15	18	10	-	0.2	1.3
16	18	18	10	0	0.4	1.3
17	25	18	10	+	0.4	1.3
18	15	18	10	-	0.4	1.3

The sample has the following instrumentation: (*i*) fourth two thermocouples for surface temperature, being twenty-one in each side of the specimen; and (*ii*) twelve heat flux sensors, namely six in each face. With all sensors placed on each side of the wall (hot and cold side) to have symmetry at the measuring points. Figure 4.89a shows the location of all temperature and heat flux sensors placed on the cold side of the ESP panels and shows the limits of the metering area with 3.18 (W) by 2.28 (H) m², and Figure 4.89b shows photography of the hot side. The instrumentation is the same presented in specimen 3, differencing the thickness of the element and the new joins of the second layer.

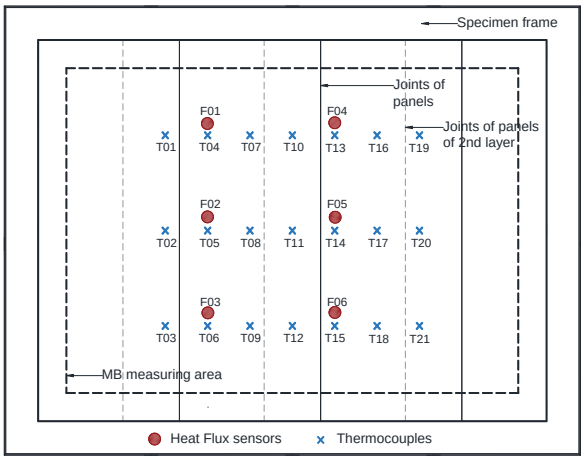

a)

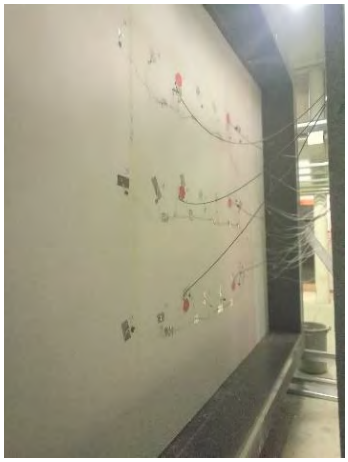

b)

Figure 4.89 – Location of temperature and heat flux sensors placed on the CHB of the EPS panels 100 mm thick wall surface: a) sketch of cold side; b) photo of hot side.

The calibration matrix tests were performed according to the requirements presented in section 3.4.2. The test time starts counting from the moment that the setpoints were reached with a difference of less than 1%. All tests had a minimum duration of 8 hours, and the test conditions were achieved on average between

one and two hours. Some tests were repeated to verify the repeatability of the equipment, being made 33 tests in total, whose results are shown in Table 4.43.

Table 4.43 shows the main results of the tests which allow assessing the thermal conductance and thermal transmittance according to the equations presented in section 3.4.3. The heat flow rate (Φ) is obtained by correcting the total power imputed to the system by subtracting the flanking losses of the MB, which were obtained numerically in section 4.5.2, chart of Figure 4.41. Next, is obtained the experimental thermal conductance that is multiplied by the calibration factor obtain experimentally, giving the calibrated thermal conductance. Figure 4.90, Figure 4.92 and Figure 4.94 present the relationship of conductance to mean specimen temperature of the three test group cases, from which is obtain the calibration factor.

Table 4.43 – Test results for calibration of the CHB with EPS panels 100 mm thick.

Test n.º	MB_w	Φ_p [W]	T_{n1} [°C]	$T_{n.out}$ [°C]	T_{n2} [°C]	ΔT_s [°C]	Φ [W]	Λ' [W/(m².K)]	C	Λ [W/(m².K)]	$\Delta\Lambda$	U [W/(m².K)]
M01.C194		26.177	18.00	17.94	5.00	9.46	26.856	0.391		**0.391** ±0.007	0.3%	0.367 ±0.006
M01.C195		25.691	18.01	18.22	5.00	9.31	26.370	0.390		**0.390** ±0.008	0.1%	0.366 ±0.007
M01.C196		24.737	18.00	18.20	5.00	8.94	25.415	0.392		**0.392** ±0.008	0.5%	0.367 ±0.007
M01.C197		25.163	18.00	17.99	5.00	9.11	25.841	0.391		**0.391** ±0.008	0.3%	0.367 ±0.007
M01.C198		26.714	17.99	17.82	5.00	9.69	27.392	0.390		**0.390** ±0.007	-0.1%	0.365 ±0.006
M04.C199		25.779	18.00	18.07	5.00	9.30	26.458	0.392		**0.392** ±0.008	0.6%	0.368 ±0.007
M04.C200		26.750	18.00	18.04	5.00	9.73	27.429	0.389		**0.389** ±0.007	-0.4%	0.364 ±0.006
M04.C201		25.926	18.00	17.99	5.00	9.41	26.604	0.390		**0.390** ±0.007	-0.1%	0.365 ±0.006
M07.C202		24.688	18.00	18.11	5.00	8.88	25.366	0.394		**0.394** ±0.008	0.9%	0.369 ±0.007
M07.C203	0	27.004	18.01	18.10	5.00	9.79	27.682	0.390	0.9995	**0.390** ±0.007	0.0%	0.366 ±0.006
M07.C204		26.204	18.01	18.02	5.00	9.49	26.882	0.391		**0.390** ±0.007	0.1%	0.366 ±0.006
M10.C205		24.967	18.00	17.83	5.00	9.02	25.646	0.392		**0.392** ±0.008	0.5%	0.368 ±0.007
M10.C206		26.230	17.99	18.10	5.00	9.52	26.908	0.390		**0.390** ±0.007	-0.1%	0.365 ±0.006
M10.C207		26.561	18.01	18.26	5.00	9.68	27.240	0.388		**0.388** ±0.007	-0.5%	0.364 ±0.006
M13.C208		27.459	18.00	18.19	5.00	10.03	28.137	0.387		**0.387** ±0.007	-0.9%	0.363 ±0.006
M13.C209		27.387	18.01	17.90	5.00	10.01	28.065	0.387		**0.387** ±0.007	-0.8%	0.363 ±0.006
M13.C210		26.608	18.01	18.06	5.00	9.66	27.286	0.389		**0.389** ±0.007	-0.2%	0.365 ±0.006
M16.C211		26.386	18.00	18.15	5.00	9.61	27.064	0.388		**0.388** ±0.007	-0.5%	0.364 ±0.006
M16.C212		27.431	18.00	18.19	5.00	9.97	28.109	0.389		**0.389** ±0.007	-0.3%	0.365 ±0.006
M16.C213		27.013	18.00	18.13	5.00	9.87	27.691	0.387		**0.387** ±0.007	-0.8%	0.363 ±0.006
M02.C214		190.331	45.02	16.11	5.00	35.11	100.155	0.393		**0.394** ±0.006	0.9%	0.369 ±0.005
M05.C215		189.002	45.00	17.84	5.00	34.85	98.825	0.391		**0.391** ±0.006	0.3%	0.367 ±0.005
M08.C216	+	190.656	45.00	17.80	5.00	35.35	100.480	0.392	1.0003	**0.392** ±0.006	0.5%	0.368 ±0.005
M11.C217		190.458	44.99	17.81	5.00	35.47	100.282	0.390		**0.391** ±0.006	0.0%	0.366 ±0.005
M14.C218		137.069	25.00	17.84	5.00	16.76	46.893	0.386		**0.392** ±0.006	-1.0%	0.368 ±0.005
M17.C219		137.106	25.00	16.05	5.00	16.75	46.930	0.386		**0.390** ±0.006	-0.9%	0.366 ±0.005
M03.C220		-24.216	10.00	17.80	5.00	1.19	3.382	0.392		**0.392** ±0.030	0.6%	0.368 ±0.026
M06.C221		-22.138	10.00	17.89	5.00	1.92	5.460	0.393		**0.393** ±0.019	0.8%	0.368 ±0.017
M09.C222	-	-21.794	10.00	19.12	5.00	2.05	5.804	0.391	0.9999	**0.391** ±0.018	0.3%	0.367 ±0.016
M12.C223		-22.398	10.00	19.15	5.00	1.83	5.200	0.391		**0.391** ±0.020	0.3%	0.367 ±0.018
M15.C224		-9.494	15.00	16.16	5.00	6.44	18.104	0.388		**0.388** ±0.009	-0.6%	0.364 ±0.008
M18.C225		-8.737	15.00	15.93	5.00	6.75	18.861	0.386		**0.386** ±0.008	-1.1%	0.362 ±0.007

Where: MB_w is the MB wall heat flux; Φ_p is de total power input; T_{n1} is the environmental temperature of the hot side; $T_{n.out}$ is the environmental temperature of the room where is the apparatus; T_{n2} is the environmental temperature of the cold side; ΔT_s is the surface temperature difference across the specimen; Φ is the heat flow rate; Λ' is the experimental thermal conductance; C is the calibration factor; Λ is the calibrated thermal conductance; $\Delta\Lambda$ is the thermal conductance difference between the material reference value and the calibrated obtain value; and U is the thermal transmittance

Table 4.43 shows the difference between thermal conductance obtained experimentally by the CHB method and the reference value. It shows that, as expected and similar to the calibration with specimen 1, the better results are obtained when the equipment operates in the way the heat flow in the walls of the MB is close to zero.

Figure 4.91, Figure 4.93 and Figure 4.95 show charts of ambient temperatures and air velocities in the MB and CB, for a test of each group, during the test period in which the test conditions are fulfilled and from where the analysis of the results is performed.

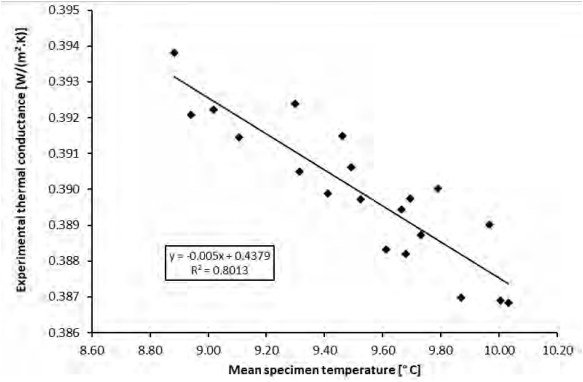

Figure 4.90 – Relationship of conductance to mean specimen temperature of test cases with MB wall heat flux near zero for CHB with EPS panels 100 mm thick.

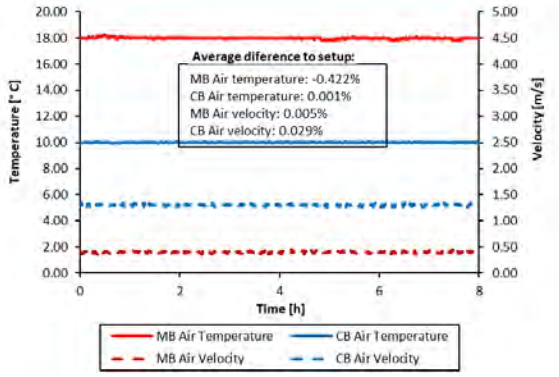

Figure 4.91 – Test M16.C211 air temperature and velocity in chambers of a test cases with MB wall heat flux near zero for CHB with EPS panels 100 mm thick.

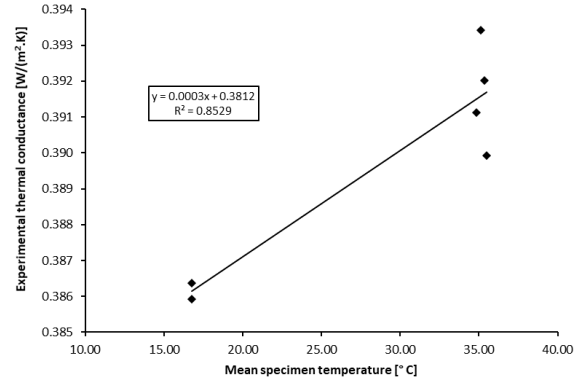

Figure 4.92 – Relationship of conductance to mean specimen temperature of test cases with MB wall heat flux positive for CHB with EPS panels 100 mm thick.

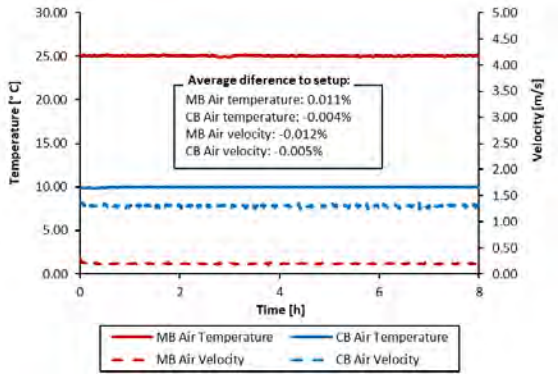

Figure 4.93 – Test M14.C218 air temperature and velocity in chambers of a test cases with MB wall heat flux positive for CHB with EPS panels 100 mm thick.

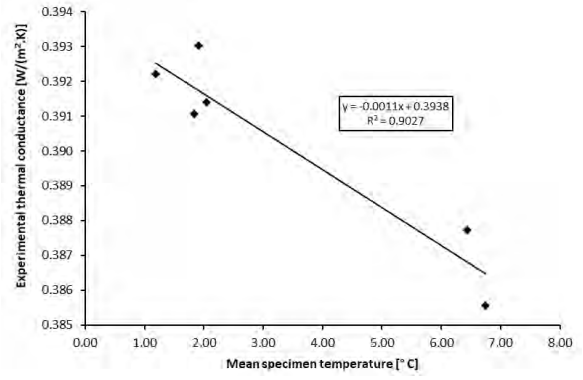

Figure 4.94 – Relationship of conductance to mean specimen temperature of test cases with MB wall heat flux negative for CHB with EPS panels 100 mm thick.

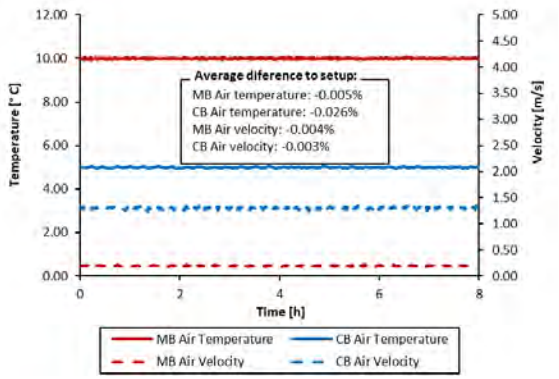

Figure 4.95 – Test M09.C222 air temperature and velocity in chambers of a test cases with MB wall heat flux negative for CHB with EPS panels 100 mm thick.

Table 4.44 shows a comparison between the CHB and HFM method for the tests performed. From the results obtained, it is confirmed that the flowmeters method is less rigorous. The average result difference is 2.11%, and the maximum individual difference is 3.2% in relation to the reference value of the material.

Comparing methodologies, the maximum difference in results is 3.4%. Table 4.44 also shows the average difference between the calibrated thermal conductance value obtained by the CHB method and the reference material, giving a low value of only 0.06%.

Table 4.44 – Test results of CHB vs HFM method for EPS panels 100 mm thick.

Test n.º	Λ_{CHB} [W/(m².K)]	Λ_{HFM} [W/(m².K)]	$\Delta\Lambda_{HFM\rightarrow Ref}$	$\Delta\Lambda_{CHB\rightarrow HFM}$	λ_{HFM} [W/(m.K)]	U_{HFM} [W/(m².K)]
M01.C194	**0.391** ±0.007	**0.395** ±0.013	1.3%	1.1%	0.0395	0.370 ±0.011
M01.C195	**0.390** ±0.008	**0.396** ±0.013	1.6%	1.6%	0.0396	0.371 ±0.011
M01.C196	**0.392** ±0.008	**0.397** ±0.014	1.8%	1.3%	0.0397	0.372 ±0.012
M01.C197	**0.391** ±0.008	**0.396** ±0.014	1.5%	1.3%	0.0396	0.371 ±0.012
M01.C198	**0.390** ±0.007	**0.393** ±0.013	0.9%	0.9%	0.0393	0.369 ±0.011
M04.C199	**0.392** ±0.008	**0.400** ±0.014	2.6%	2.0%	0.0400	0.375 ±0.012
M04.C200	**0.389** ±0.007	**0.396** ±0.013	1.6%	1.9%	0.0396	0.371 ±0.011
M04.C201	**0.390** ±0.007	**0.395** ±0.013	1.4%	1.4%	0.0395	0.370 ±0.011
M07.C202	**0.394** ±0.008	**0.401** ±0.014	2.9%	1.9%	0.0401	0.376 ±0.012
M07.C203	**0.390** ±0.007	**0.397** ±0.013	1.9%	1.9%	0.0397	0.372 ±0.011
M07.C204	**0.390** ±0.007	**0.400** ±0.014	2.5%	2.5%	0.0400	0.374 ±0.012
M10.C205	**0.392** ±0.008	**0.398** ±0.014	2.2%	1.6%	0.0398	0.373 ±0.012
M10.C206	**0.390** ±0.007	**0.403** ±0.014	3.2%	3.2%	0.0403	0.377 ±0.012
M10.C207	**0.388** ±0.007	**0.400** ±0.013	2.5%	3.0%	0.0400	0.374 ±0.011
M13.C208	**0.387** ±0.007	**0.396** ±0.013	1.7%	2.4%	0.0396	0.371 ±0.011
M13.C209	**0.387** ±0.007	**0.400** ±0.013	2.5%	3.3%	0.0400	0.374 ±0.011
M13.C210	**0.389** ±0.007	**0.402** ±0.014	3.1%	3.4%	0.0402	0.376 ±0.012
M16.C211	**0.388** ±0.007	**0.400** ±0.014	2.5%	3.1%	0.0400	0.374 ±0.012
M16.C212	**0.389** ±0.007	**0.399** ±0.013	2.3%	2.6%	0.0399	0.374 ±0.011
M16.C213	**0.387** ±0.007	**0.396** ±0.013	1.6%	2.4%	0.0396	0.371 ±0.011
M02.C214	**0.394** ±0.006	**0.399** ±0.013	2.3%	1.3%	0.0399	0.374 ±0.011
M05.C215	**0.391** ±0.006	**0.400** ±0.013	2.6%	2.3%	0.0400	0.375 ±0.011
M08.C216	**0.392** ±0.006	**0.401** ±0.013	2.8%	2.3%	0.0401	0.375 ±0.011
M11.C217	**0.391** ±0.006	**0.398** ±0.013	2.1%	1.9%	0.0398	0.373 ±0.011
M14.C218	**0.392** ±0.006	**0.401** ±0.013	2.7%	2.2%	0.0401	0.375 ±0.011
M17.C219	**0.390** ±0.006	**0.396** ±0.013	1.5%	1.5%	0.0396	0.371 ±0.011
M03.C220	**0.392** ±0.030	**0.401** ±0.032	2.8%	2.3%	0.0401	0.375 ±0.028
M06.C221	**0.393** ±0.019	**0.398** ±0.022	2.1%	1.3%	0.0398	0.373 ±0.019
M09.C222	**0.391** ±0.018	**0.398** ±0.021	1.9%	1.7%	0.0398	0.372 ±0.018
M12.C223	**0.391** ±0.020	**0.395** ±0.023	1.2%	0.9%	0.0395	0.370 ±0.020
M15.C224	**0.388** ±0.009	**0.398** ±0.014	2.0%	2.5%	0.0398	0.373 ±0.012
M18.C225	**0.386** ±0.008	**0.397** ±0.014	1.8%	2.8%	0.0397	0.372 ±0.012
Average	**0.390** ±0.030	**0.398** ±0.032			0.040	0.373 ±0.028
SD	**0.0018**	**0.0023**			0.0002	0.0020
ΔR	**0.06%**	**2.11%**			2.11%	1.98%

Where: Λ_{CHB} is the calibrated thermal conductance obtain by the CHB method; Λ_{HFM} is the thermal conductance obtained by the difference between the reference material value and the calibrated obtain value; $\Delta\Lambda_{HFM\rightarrow Ref}$ is the thermal conductance difference between HFM method and the reference value of the specimen; $\Delta\Lambda_{CHB\rightarrow HFM}$ is the thermal conductance difference between CHB method and HFM method; λ_{HFM} is the thermal conductivity obtain with HFM method; U_{HFM} is the thermal transmittance obtained with HFM method; SD is the standard deviation; and ΔR is the difference in relation to the reference value

Table 4.45 shows the repeatability of the equipment, namely for thermal conductance, ambient temperatures and air velocities in the chambers. This study is carried out for some of the calibration matrix tests, which were repeated for this purpose. It is observed that a relative standard deviation percentage is low for all parameters, lower than 1%, which demonstrates good performance of the equipment.

Table 4.45 – Tests repeatability on the CHB with EPS panels 100 mm thick.

Test n.º	Λ_{CHB} [W/(m².K)]	T_{n1} [°C]	T_{n2} [°C]	V_{n1} [m/s]	V_{n2} [m/s]	Test n.º	Λ_{CHB} [W/(m².K)]	T_{n1} [°C]	T_{n2} [°C]	V_{n1} [m/s]	V_{n2} [m/s]
M01.C194	0.391	18.002	5.001	0.202	0.651	M10.C205	0.392	17.999	5.000	0.400	1.300
M01.C195	0.390	18.009	5.001	0.200	0.651	M10.C206	0.390	17.993	5.001	0.400	1.301
M01.C196	0.392	18.002	5.001	0.201	0.651	M10.C207	0.388	18.008	4.999	0.400	1.300
M01.C197	0.391	18.001	4.999	0.201	0.651						
M01.C198	0.390	17.994	4.999	0.200	0.651						
Average	**0.391**	**18.002**	**5.000**	**0.201**	**0.651**	**Average**	**0.390**	**18.000**	**5.000**	**0.400**	**1.300**
SD	**0.0007**	**0.0049**	**0.0010**	**0.0006**	**0.0003**	**SD**	**0.0016**	**0.0061**	**0.0008**	**0.0001**	**0.0007**
RSD%	**0.19%**	**0.03%**	**0.02%**	**0.30%**	**0.04%**	**RSD%**	**0.42%**	**0.03%**	**0.02%**	**0.03%**	**0.06%**
M04.C199	0.392	18.001	5.000	0.401	0.651	M13.C208	0.387	18.004	5.001	0.200	1.301
M04.C200	0.389	18.002	4.999	0.400	0.650	M13.C209	0.387	18.007	4.999	0.200	1.300
M04.C201	0.390	18.000	5.000	0.401	0.650	M13.C210	0.389	18.006	5.001	0.200	1.300
Average	**0.390**	**18.001**	**5.000**	**0.401**	**0.650**	**Average**	**0.388**	**18.006**	**5.000**	**0.200**	**1.300**
SD	**0.0012**	**0.0009**	**0.0005**	**0.0002**	**0.0007**	**SD**	**0.0009**	**0.0015**	**0.0009**	**0.0000**	**0.0003**
RSD%	**0.32%**	**0.01%**	**0.01%**	**0.04%**	**0.12%**	**RSD%**	**0.24%**	**0.01%**	**0.02%**	**0.02%**	**0.02%**
M07.C202	0.394	18.000	5.000	0.200	1.299	M16.C211	0.388	18.000	5.001	0.400	1.301
M07.C203	0.390	18.008	4.999	0.201	1.300	M16.C212	0.389	18.001	5.000	0.400	1.299
M07.C204	0.390	18.007	4.999	0.201	1.300	M16.C213	0.387	18.000	5.001	0.400	1.300
Average	**0.391**	**18.005**	**4.999**	**0.201**	**1.300**	**Average**	**0.388**	**18.001**	**5.001**	**0.400**	**1.300**
SD	**0.0019**	**0.0034**	**0.0005**	**0.0002**	**0.0003**	**SD**	**0.0007**	**0.0007**	**0.0005**	**0.0000**	**0.0008**
RSD%	**0.48%**	**0.02%**	**0.01%**	**0.12%**	**0.03%**	**RSD%**	**0.18%**	**0.00%**	**0.01%**	**0.01%**	**0.06%**

Where: Λ_{CHB} is the calibrated thermal conductance obtain by the CHB method; T_{n1} is the environmental temperature of the hot side; T_{n2} is the environmental temperature of the cold side; V_{n1} is the air velocity in the hot side; V_{n2} is the air velocity in the cold side; SD is the standard deviation; RSD is the relative standard deviation

4.6.4.2. Guarded Hot Box mode

For the full characterization of the apparatus in GHB mode, Table 4.46 presents the test matrix for the calibration, composed of 18 tests. These tests aim to fully characterize the equipment for another range of thermal conductance of the element, having different combinations of temperatures and air velocities for each box of the equipment.

The sample has the following instrumentation: (*i*) fourth two thermocouples for surface temperature, being twenty-one in each side of the specimen; and (*ii*) twelve heat flux sensors, namely six in each face. With all sensors placed on each side of the wall (hot and cold side) to have symmetry at the measuring points. Figure 4.96a shows the location of all temperature and heat flux sensors placed on the cold side of the EPS panels and shows the limits of the metering area with 1.80 (W) by 1.05 (H) m², and Figure 4.96b shows photography of the hot side. The instrumentation is the same presented in specimen 3, differencing the thickness of the element and the new joins of the second layer.

Table 4.46 – Test matrix for calibration of the GHB with EPS panels 100 mm thick.

Test n.º	MB air temperature [°C]	Lab. air temperature [°C]	CB air temperature [°C]	MB wall heat flux	MB air velocity [m/s]	CB air velocity [m/s]
1	35	35	5	0	0.2	0.65
2	35	20	5	+	0.2	0.65
3	35	50	5	-	0.2	0.65
4	35	35	5	0	0.4	0.65
5	35	20	5	+	0.4	0.65
6	35	50	5	-	0.4	0.65
7	35	35	5	0	0.2	1.3
8	35	20	5	+	0.2	1.3
9	35	50	5	-	0.2	1.3
10	35	35	5	0	0.4	1.3
11	35	20	5	+	0.4	1.3
12	35	50	5	-	0.4	1.3
13	45	45	10	0	0.2	1.3
14	45	35	10	+	0.2	1.3
15	45	55	10	-	0.2	1.3
16	45	45	10	0	0.4	1.3
17	45	35	10	+	0.4	1.3
18	45	55	10	-	0.4	1.3

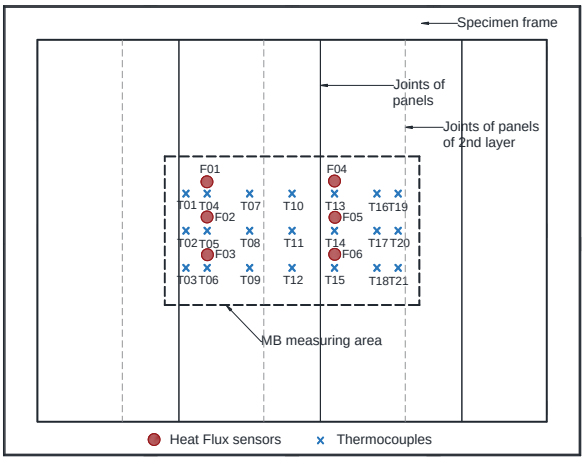

a)

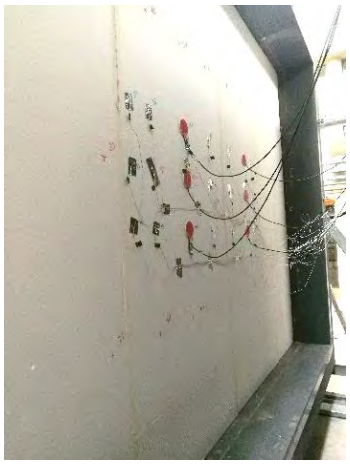

b)

Figure 4.96 – Location of temperature and heat flux sensors placed on the GHB of the EPS 100 mm thick wall surface: a) sketch of cold side; b) photo of hot side.

The calibration matrix tests were performed according to the requirements presented in section 3.4.2. The test time starts counting from the moment that the setpoints were reached with a difference of less than 1%. All tests had a minimum duration of 8 hours, and the test conditions were achieved on average between one and two hours. Some tests were repeated to verify the repeatability of the equipment, being made 32 tests in total, whose results are shown in Table 4.47.

Table 4.47 shows the main results of the tests which allow assessing the thermal conductance and thermal transmittance according to the equations presented in section 3.4.3. The heat flow rate (Φ) is obtained by correcting the total power imputed to the system by subtracting the flanking losses of the MB, which were obtained numerically in section 4.5.2, chart of Figure 4.43. Next, is obtained the experimental thermal conductance that is multiplied by the calibration factor obtain experimentally, giving the calibrated thermal

conductance. Figure 4.97, Figure 4.99 and Figure 4.101 present the relationship of conductance to mean specimen temperature of the three test group cases, from which is obtain the calibration factor.

Table 4.47 – Test results for calibration of the GHB with EPS panels 100 mm thick.

Test n.º	MB_w	Φ_p [W]	T_{n1} [°C]	$T_{n.out}$ [°C]	T_{n2} [°C]	ΔT_s [°C]	Φ [W]	Λ' [W/(m².K)]	C	Λ [W/(m².K)]	$\Delta\Lambda$	U [W/(m².K)]
M01.C226		19.878	35.00	34.26	5.00	27.44	20.261	0.391		**0.390** ±0.006	0.1%	0.366 ±0.005
M01.C227		19.805	35.00	34.12	5.00	27.39	20.189	0.390		**0.390** ±0.006	-0.1%	0.365 ±0.005
M01.C228		20.057	35.00	34.26	5.00	27.66	20.440	0.391		**0.391** ±0.006	0.2%	0.366 ±0.005
M01.C229		19.954	35.00	34.29	5.00	27.43	20.337	0.392		**0.392** ±0.006	0.5%	0.368 ±0.005
M01.C230		19.942	35.00	34.28	5.00	27.43	20.325	0.392		**0.392** ±0.006	0.5%	0.367 ±0.005
M04.C231		19.755	35.00	34.20	5.00	27.15	20.139	0.392		**0.392** ±0.006	0.5%	0.368 ±0.005
M04.C232		20.021	35.00	34.47	5.00	27.56	20.404	0.392		**0.391** ±0.006	0.4%	0.367 ±0.005
M04.C233		19.817	35.00	34.10	5.00	27.28	20.201	0.392		**0.391** ±0.006	0.4%	0.367 ±0.005
M07.C234		19.744	35.00	34.21	5.00	27.25	20.128	0.391		**0.391** ±0.006	0.1%	0.366 ±0.005
M07.C235	0	19.648	35.00	34.29	5.00	27.14	20.031	0.391	0.9993	**0.390** ±0.006	0.1%	0.366 ±0.005
M07.C236		19.508	35.00	34.15	5.00	26.89	19.891	0.391		**0.391** ±0.006	0.3%	0.367 ±0.005
M10.C237		19.696	35.00	34.24	5.00	27.25	20.079	0.390		**0.390** ±0.006	-0.1%	0.365 ±0.005
M10.C238		19.745	35.00	34.20	5.00	27.33	20.128	0.390		**0.389** ±0.006	-0.2%	0.365 ±0.005
M10.C239		19.935	35.00	34.26	5.00	27.46	20.318	0.392		**0.391** ±0.006	0.3%	0.367 ±0.005
M13.C240		22.606	45.00	44.19	10.00	31.33	23.053	0.389		**0.389** ±0.006	-0.2%	0.365 ±0.005
M13.C241		22.414	45.00	44.34	10.00	31.18	22.861	0.388		**0.388** ±0.006	-0.6%	0.364 ±0.005
M13.C242		22.464	45.00	44.28	10.00	31.16	22.911	0.389		**0.389** ±0.006	-0.3%	0.365 ±0.005
M16.C243		22.608	45.00	44.42	10.00	31.46	23.055	0.388		**0.387** ±0.006	-0.7%	0.364 ±0.005
M16.C244		22.972	45.00	44.33	10.00	31.97	23.419	0.388		**0.387** ±0.006	-0.7%	0.363 ±0.005
M16.C245		22.812	45.00	44.19	10.00	31.78	23.259	0.387		**0.387** ±0.006	-0.8%	0.363 ±0.005
M02.C246		53.921	35.00	20.00	5.00	28.45	20.975	0.390		**0.391** ±0.006	0.2%	0.366 ±0.005
M05.C247		54.119	35.00	20.00	5.00	28.85	21.173	0.388		**0.389** ±0.006	-0.3%	0.365 ±0.005
M08.C248	+	54.204	35.00	19.99	5.00	28.81	21.258	0.390	1.0014	**0.391** ±0.006	0.3%	0.367 ±0.005
M11.C249		54.413	35.00	20.01	5.00	29.01	21.467	0.392		**0.389** ±0.006	0.5%	0.368 ±0.005
M14.C250		45.874	45.00	35.00	10.00	32.31	24.102	0.395		**0.391** ±0.006	1.4%	0.367 ±0.005
M17.C251		46.332	45.00	35.01	10.00	32.81	24.560	0.396		**0.392** ±0.006	1.7%	0.368 ±0.005
M03.C252		-15.391	35.00	50.00	5.00	24.71	18.321	0.392		**0.392** ±0.006	0.5%	0.368 ±0.005
M06.C253		-15.125	35.00	50.00	5.00	25.15	18.587	0.391		**0.391** ±0.006	0.2%	0.366 ±0.005
M09.C254	-	-15.408	35.00	50.00	5.00	24.81	18.304	0.390	0.9994	**0.390** ±0.006	0.0%	0.366 ±0.005
M12.C255		-14.991	35.00	50.00	5.00	25.38	18.722	0.390		**0.390** ±0.006	0.0%	0.366 ±0.005
M15.C256		-0.903	45.00	54.99	10.00	29.65	21.764	0.388		**0.388** ±0.006	-0.5%	0.364 ±0.005
M18.C257		-0.511	45.00	55.00	10.00	30.21	22.155	0.388		**0.388** ±0.006	-0.6%	0.364 ±0.005

Where: MB_w is the MB wall heat flux; Φ_p is de total power input; T_{n1} is the environmental temperature of the hot side; $T_{n.out}$ is the environmental temperature of the GB; T_{n2} is the environmental temperature of the cold side; ΔT_s is the surface temperature difference across the specimen; Φ is the heat flow rate; Λ' is the experimental thermal conductance; C is the calibration factor; Λ is the calibrated thermal conductance; $\Delta\Lambda$ is the thermal conductance difference between the material reference value and the calibrated obtain value; and U is the thermal transmittance

Table 4.47 shows the difference between thermal conductance obtained experimentally by the GHB method and the reference value. It reveals that for the range of thermal conductance under analysis, the results obtained in the equipment, when it operates in one of the three different modes of heat flow in the MB walls, similar results are obtained.

Figure 4.98, Figure 4.100 and Figure 4.102 show charts of ambient temperatures and air velocities in the MB and CB, for a test of each group, during the test period in which the test conditions are fulfilled and from where the analysis of the results is performed.

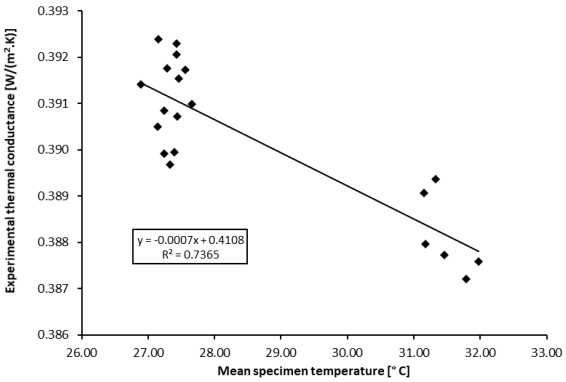

Figure 4.97 – Relationship of conductance to mean specimen temperature of test cases with MB wall heat flux near zero for GHB with EPS panels 100 mm thick.

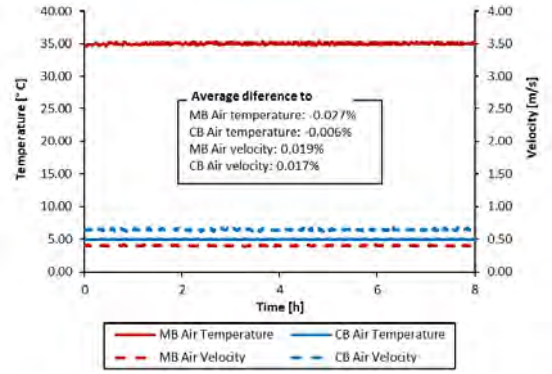

Figure 4.98 – Test M04.C231 air temperature and velocity in chambers of test cases with MB wall heat flux near zero for GHB with EPS panels 100 mm thick.

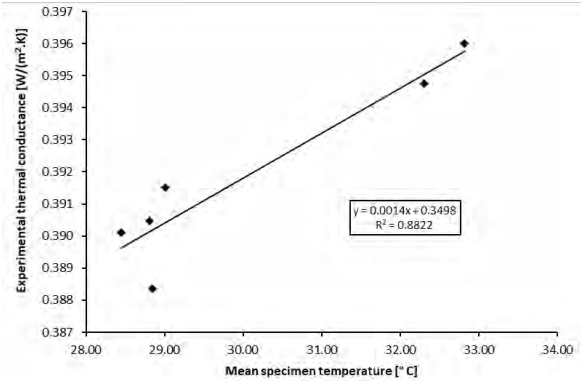

Figure 4.99 – Relationship of conductance to mean specimen temperature of test cases with MB wall heat flux positive for GHB with EPS panels 100 mm thick.

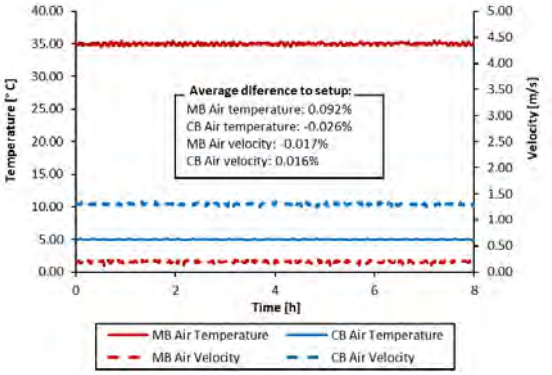

Figure 4.100 – Test M08.C248 air temperature and velocity in chambers of test cases with MB wall heat flux positive for GHB with EPS panels 100 mm thick.

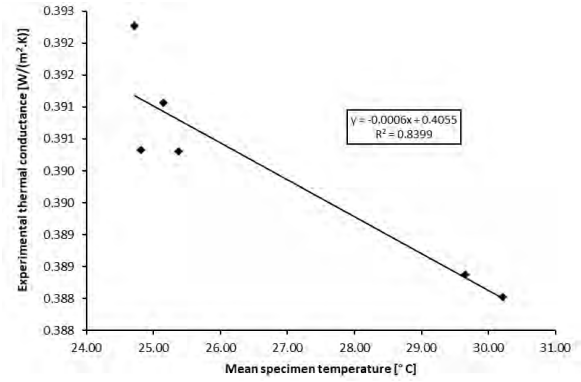

Figure 4.101 – Relationship of conductance to mean specimen temperature of test cases with MB wall heat flux negative for GHB with EPS panels 100 mm thick.

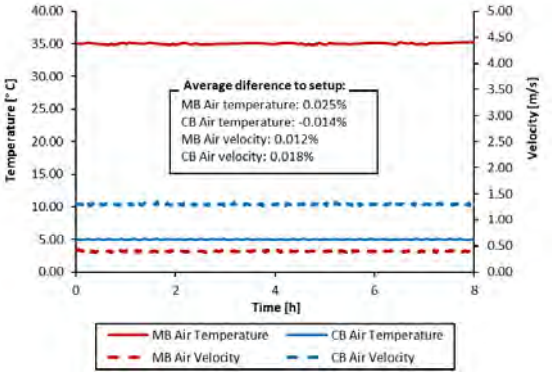

Figure 4.102 – Test M12.C255 air temperature and velocity in chambers of test cases with MB wall heat flux negative for GHB with EPS panels 100 mm thick.

Table 4.48 shows a comparison between the GHB and HFM method for the tests performed. From the results obtained, it is confirmed that the flowmeters method is less rigorous. The average result difference is 2.62%, and the maximum individual difference is 3.1% in relation to the reference value of the material.

Comparing methodologies, the maximum difference in results is 3.7%. Table 4.48 also shows the average difference between the calibrated thermal conductance value obtained by the GHB method and the reference material, giving, in this case, a null difference.

Table 4.48 – Test results of GHB vs HFM method for EPS panels 100 mm thick.

Test n.º	Λ_{CHB} [W/(m².K)]	Λ_{HFM} [W/(m².K)]	$\Delta\Lambda_{HFM\rightarrow Ref}$	$\Delta\Lambda_{CHB\rightarrow HFM}$	λ_{HFM} [W/(m.K)]	U_{HFM} [W/(m².K)]
M01.C226	**0.390** ±0.006	**0.400** ±0.013	2.6%	2.6%	0.0400	0.375 ±0.011
M01.C227	**0.390** ±0.006	**0.398** ±0.013	2.1%	2.1%	0.0398	0.373 ±0.011
M01.C228	**0.391** ±0.006	**0.400** ±0.013	2.4%	2.2%	0.0400	0.374 ±0.011
M01.C229	**0.392** ±0.006	**0.401** ±0.013	2.9%	2.3%	0.0401	0.376 ±0.011
M01.C230	**0.392** ±0.006	**0.400** ±0.013	2.5%	2.0%	0.0400	0.374 ±0.011
M04.C231	**0.392** ±0.006	**0.401** ±0.013	2.8%	2.3%	0.0401	0.375 ±0.011
M04.C232	**0.391** ±0.006	**0.399** ±0.013	2.4%	2.2%	0.0399	0.374 ±0.011
M04.C233	**0.391** ±0.006	**0.400** ±0.013	2.5%	2.3%	0.0400	0.374 ±0.011
M07.C234	**0.391** ±0.006	**0.400** ±0.013	2.6%	2.3%	0.0400	0.375 ±0.011
M07.C235	**0.390** ±0.006	**0.401** ±0.013	2.8%	2.8%	0.0401	0.375 ±0.011
M07.C236	**0.391** ±0.006	**0.398** ±0.013	2.1%	1.8%	0.0398	0.373 ±0.011
M10.C237	**0.390** ±0.006	**0.402** ±0.013	3.1%	3.1%	0.0402	0.376 ±0.011
M10.C238	**0.389** ±0.006	**0.401** ±0.013	2.7%	3.0%	0.0401	0.375 ±0.011
M10.C239	**0.391** ±0.006	**0.401** ±0.013	2.7%	2.5%	0.0401	0.375 ±0.011
M13.C240	**0.389** ±0.006	**0.399** ±0.013	2.3%	2.5%	0.0399	0.374 ±0.011
M13.C241	**0.388** ±0.006	**0.400** ±0.013	2.7%	3.2%	0.0400	0.375 ±0.011
M13.C242	**0.389** ±0.006	**0.400** ±0.013	2.5%	2.7%	0.0400	0.374 ±0.011
M16.C243	**0.387** ±0.006	**0.401** ±0.013	2.9%	3.7%	0.0401	0.376 ±0.011
M16.C244	**0.387** ±0.006	**0.401** ±0.013	2.8%	3.6%	0.0401	0.375 ±0.011
M16.C245	**0.387** ±0.006	**0.401** ±0.013	2.8%	3.6%	0.0401	0.375 ±0.011
M02.C246	**0.391** ±0.006	**0.400** ±0.013	2.7%	2.4%	0.0400	0.375 ±0.011
M05.C247	**0.389** ±0.006	**0.401** ±0.013	2.8%	3.1%	0.0401	0.376 ±0.011
M08.C248	**0.391** ±0.006	**0.399** ±0.013	2.4%	2.2%	0.0399	0.374 ±0.011
M11.C249	**0.389** ±0.006	**0.398** ±0.013	2.2%	2.4%	0.0398	0.373 ±0.011
M14.C250	**0.391** ±0.006	**0.401** ±0.013	2.8%	2.5%	0.0401	0.375 ±0.011
M17.C251	**0.392** ±0.006	**0.399** ±0.013	2.3%	1.7%	0.0399	0.374 ±0.011
M03.C252	**0.392** ±0.006	**0.402** ±0.013	3.0%	2.4%	0.0402	0.376 ±0.011
M06.C253	**0.391** ±0.006	**0.402** ±0.013	3.0%	2.7%	0.0402	0.376 ±0.011
M09.C254	**0.390** ±0.006	**0.399** ±0.013	2.3%	2.3%	0.0399	0.374 ±0.011
M12.C255	**0.390** ±0.006	**0.401** ±0.013	2.8%	2.8%	0.0401	0.375 ±0.011
M15.C256	**0.388** ±0.006	**0.402** ±0.013	3.0%	3.6%	0.0402	0.376 ±0.011
M18.C257	**0.388** ±0.006	**0.399** ±0.013	2.3%	2.8%	0.0399	0.374 ±0.011
Average	**0.390** ±0.006	**0.400** ±0.013			0.040	0.375 ±0.011
SD	**0.0016**	**0.0011**			0.0001	0.0009
ΔR	**0.00%**	**2.62%**			2.62%	2.45%

Where: Λ_{CHB} is the calibrated thermal conductance obtain by the CHB method; Λ_{HFM} is the thermal conductance obtained by the difference between the reference material value and the calibrated obtain value; $\Delta\Lambda_{HFM\rightarrow Ref}$ is the thermal conductance difference between HFM method and the reference value of the specimen; $\Delta\Lambda_{CHB\rightarrow HFM}$ is the thermal conductance difference between CHB method and HFM method; λ_{HFM} is the thermal conductivity obtain with HFM method; U_{HFM} is the thermal transmittance obtained with HFM method; SD is the standard deviation; and ΔR is the difference in relation to the reference value

Table 4.49 shows the repeatability of the equipment, namely for thermal conductance, ambient temperatures and air velocities in the chambers. This study is carried out for some of the calibration matrix tests, which were repeated for this purpose. It is observed that a relative standard deviation percentage is low for all parameters, lower than 1%, which demonstrates good performance of the equipment.

Table 4.49 – Tests repeatability on the GHB with EPS panels 100 mm thick.

Test n.º	Λ_{CHB} [W/(m².K)]	T_{n1} [°C]	T_{n2} [°C]	V_{n1} [m/s]	V_{n2} [m/s]	Test n.º	Λ_{CHB} [W/(m².K)]	T_{n1} [°C]	T_{n2} [°C]	V_{n1} [m/s]	V_{n2} [m/s]
M01.C226	0.390	35.001	5.000	0.100	0.650	M10.C237	0.390	34.999	4.999	0.204	1.300
M01.C227	0.390	35.001	4.999	0.100	0.650	M10.C238	0.389	35.001	4.999	0.203	1.301
M01.C228	0.391	35.001	4.999	0.100	0.650	M10.C239	0.391	35.000	4.998	0.203	1.300
M01.C229	0.392	35.001	5.000	0.100	0.650						
M01.C230	0.392	35.000	5.000	0.100	0.651						
Average	**0.391**	**35.001**	**5.000**	**0.100**	**0.650**	**Average**	**0.390**	**35.000**	**4.999**	**0.203**	**1.300**
SD	**0.0009**	**0.0004**	**0.0006**	**0.0001**	**0.0004**	**SD**	**0.0008**	**0.0008**	**0.0005**	**0.0004**	**0.0006**
RSD%	**0.23%**	**0.00%**	**0.01%**	**0.12%**	**0.06%**	**RSD%**	**0.21%**	**0.00%**	**0.01%**	**0.22%**	**0.05%**
M04.C231	0.392	35.001	5.000	0.204	0.651	M13.C240	0.389	45.000	10.001	0.101	1.301
M04.C232	0.391	35.001	4.998	0.203	0.650	M13.C241	0.388	45.000	10.001	0.100	1.299
M04.C233	0.391	35.000	5.001	0.204	0.652	M13.C242	0.389	45.001	10.000	0.100	1.299
Average	**0.391**	**35.001**	**5.000**	**0.204**	**0.651**	**Average**	**0.389**	**45.000**	**10.001**	**0.100**	**1.299**
SD	**0.0005**	**0.0005**	**0.0013**	**0.0005**	**0.0007**	**SD**	**0.0005**	**0.0005**	**0.0005**	**0.0001**	**0.0008**
RSD%	**0.12%**	**0.00%**	**0.03%**	**0.25%**	**0.11%**	**RSD%**	**0.12%**	**0.00%**	**0.00%**	**0.06%**	**0.06%**
M07.C234	0.391	35.000	5.000	0.100	1.299	M16.C243	0.387	45.001	10.001	0.213	1.300
M07.C235	0.390	34.999	5.000	0.100	1.300	M16.C244	0.387	45.000	10.000	0.213	1.300
M07.C236	0.391	34.999	5.001	0.100	1.299	M16.C245	0.387	44.999	10.001	0.212	1.300
Average	**0.391**	**34.999**	**5.001**	**0.100**	**1.299**	**Average**	**0.387**	**45.000**	**10.001**	**0.213**	**1.300**
SD	**0.0005**	**0.0005**	**0.0006**	**0.0002**	**0.0004**	**SD**	**0.0000**	**0.0008**	**0.0004**	**0.0003**	**0.0001**
RSD%	**0.12%**	**0.00%**	**0.01%**	**0.17%**	**0.03%**	**RSD%**	**0.00%**	**0.00%**	**0.00%**	**0.16%**	**0.01%**

Where: Λ_{CHB} is the calibrated thermal conductance obtain by the CHB method; T_{n1} is the environmental temperature of the hot side; T_{n2} is the environmental temperature of the cold side; V_{n1} is the air velocity in the hot side; V_{n2} is the air velocity in the cold side; SD is the standard deviation; RSD is the relative standard deviation

4.6.5. Infrared thermography verification

During the calibration process, additional checks were carried out on the outside envelope of the equipment using infrared thermography. This system allows for locating thermal bridges and air leakages quickly. This procedure is recommended by the standard ISO 8990:1994 [17]. Figure 4.103 to Figure 4.106 shows the infrared thermographic images of the exterior wall envelop of the HB.

The infrared thermographic images were taken with the HB apparatus in operation mode, in a steady-state regime, with average ambient temperatures of 50° C and 0° C in the hot and cold chambers, respectively, and the air velocity in both chambers was 0.5 m/s. Before taking the images, the apparatus was working in steady-state for 12 hours.

From the analysis carried out, no leaks were found in the equipment. Figure 4.103a shows the release of heat that occurs in the control panel and electrical panel, which are external elements of the chambers, located in the backside of the GB. The heat zone in panels surroundings is caused by the electrical components inside, which emanate heat during their regular operation. The cold part visible in the image, on apparatus left side, is the chambers cooling pipes system, installed in the outside. Figure 4.103b illustrates photography of the presented in the IR image.

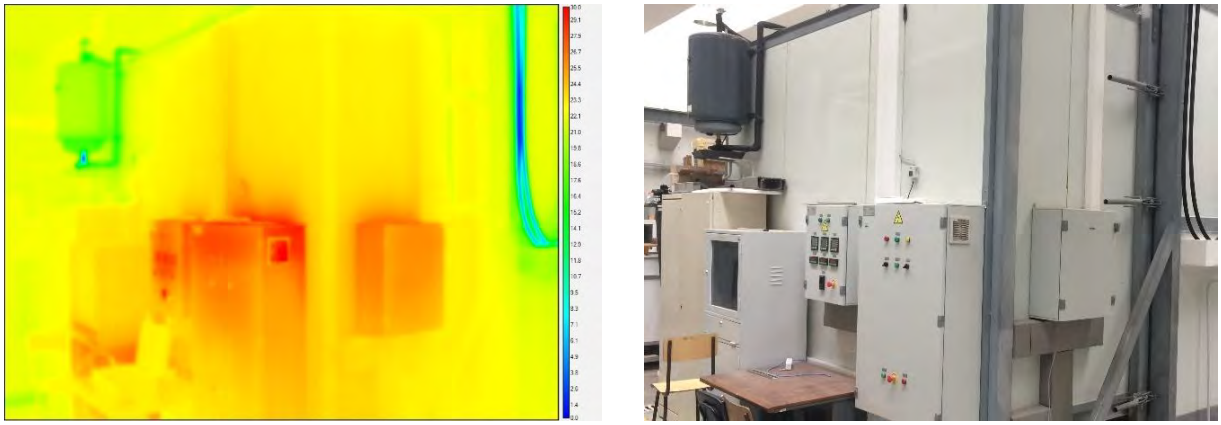

a) b)

Figure 4.103 – HB apparatus exterior wall back and left side: a) infrared thermographic images; and b) photography.

In Figure 4.104a, it is possible to see the pipes that carrying cold fluid to the CB, located on the left side of equipment, reason why it has low temperatures. The middle red spot in top on Figure 4.104a, at the front side of the equipment, is the external light that is turn on when the equipment is working and performing tests. Also visible are the control panels located on the left side of the equipment, which have a heat source originated by the control hardware. Figure 4.104b illustrates a standard view of the observed in the IR image.

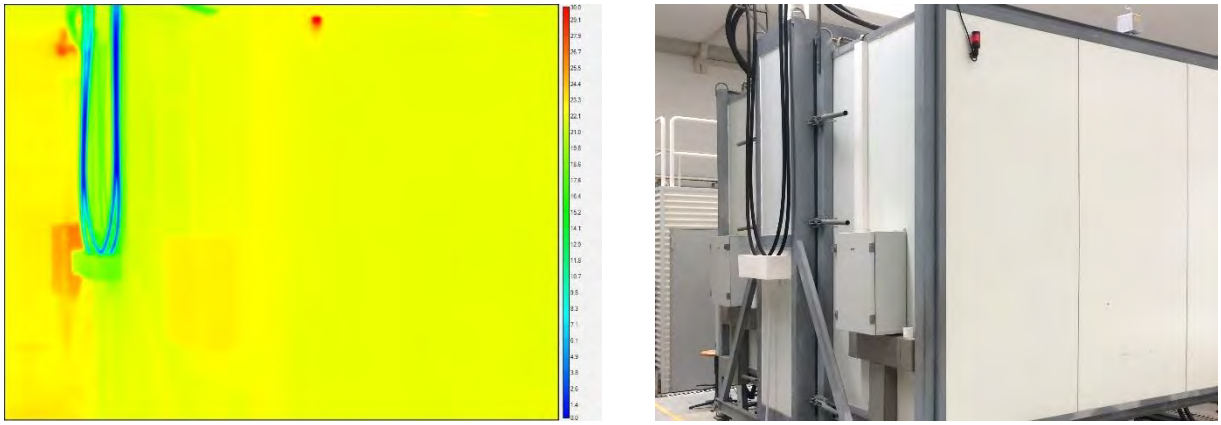

a) b)

Figure 4.104 – HB apparatus exterior wall left and front side: a) infrared thermographic images; and b) photography.

Figure 4.105a illustrates the right side of the apparatus, being the red spot an external engine of the cooling fluid for recirculation of the refrigerating system. The cold zones of the image are the external pipes also from the refrigerating system. Figure 4.105a also shows the difference of temperatures between the CB, left part of the image, and the GB, right part of the image, being visible that the first is slightly colder, 0° C in the interior or CB *vs* 50° C in the GB. Figure 4.105b shows the typical view of the illustrated in the IR image.

Figure 4.106a shows the distribution of temperatures in the back and right side of the apparatus, which gives a view from another angle of the cooling pipes of the refrigerating system showed in the previous IR image. The coldest points, visible in the IR image, are the hydraulic valves of the piping system that do not have thermal insulation. In the upper right corner of the image, it is visible the hydraulic reservoir, which also has a lower temperature. Figure 4.106b shows regular photography of the showed in the IR image.

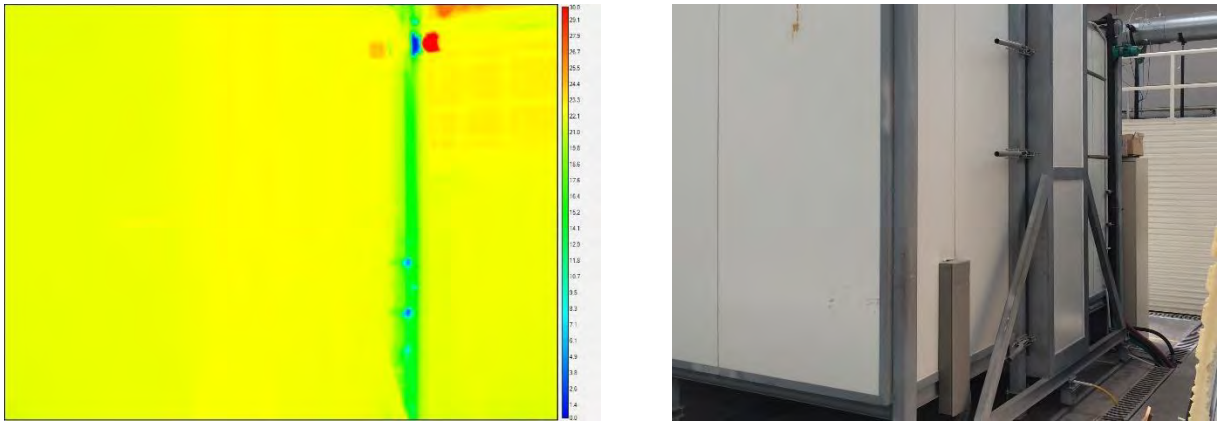

a) b)

Figure 4.105 – HB apparatus exterior wall right side: a) infrared thermographic images; and b) photography.

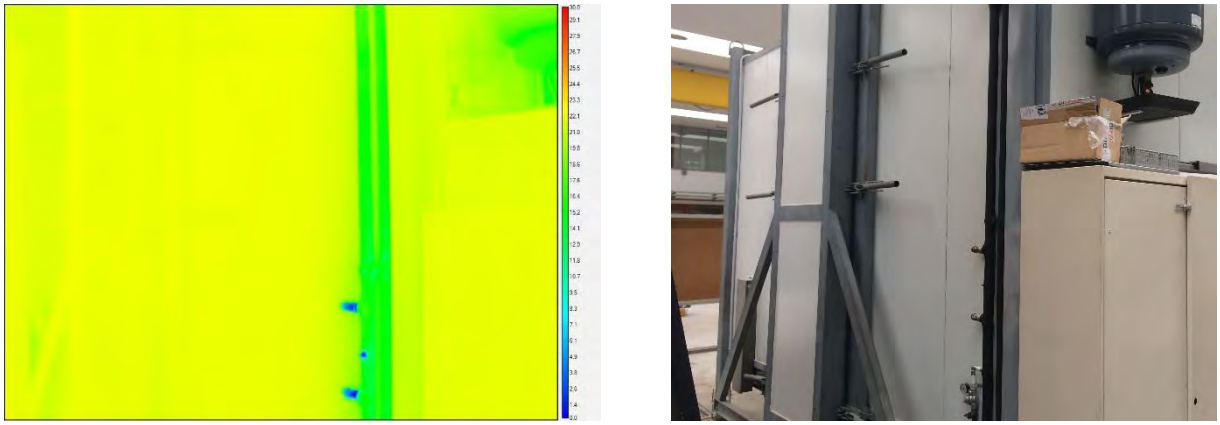

a) b)

Figure 4.106 – HB apparatus exterior wall back and right side: a) infrared thermographic images; and b) photography.

4.6.6. Calibration and verification discussion

The calibration process has been completed with good results, being performed 257 calibration tests on four different types of test specimens, in CHB and GHB modes. From the analysis and processing of data, it can be concluded that the values of losses by the periphery calculated numerically have high reliability since the data calibration parameter (C) used in all calibration processes was low.

The first specimen tested was 100 mm tick XPS panels. The tests were performed in both HB operating modes, CHB and GHB, respectively. In the CHB mode, the maximum thermal conductance difference obtained compared to the reference value was 2.7%, with an average difference of 0.6%. For the GHB, the maximum thermal conductance difference was -1.3%, with an average difference of -0.1%. Additionally, in both modes of operation of HB, tests were carried out by the HFM method, being obtained an average difference to the reference thermal conductance of 3% and 3.4%, using the CHB and GHB chambers configuration, respectively.

The second specimen analysed was made of calcium silicate plates, 24 mm thick. Like the previous calibration was used both configurations of the apparatus. For the CHB mode, the maximum thermal conductance difference compared to the reference value was 1.7%, with an average difference of -0.1%. For the GHB mode, the maximum thermal conductance difference compared to the reference value was 0.7%,

with an average difference of 0.4%. For the HFM method, the obtained average difference to the reference thermal conductance was 1.9% and 2.9%, using the CHB and GHB chambers configuration, respectively.

The third calibration test used EPS panels with 50 mm thickness. For the CHB mode, the maximum thermal conductance difference compared to the reference value was -1.7%, with an average difference of -0.4%. For the GHB mode, the maximum thermal conductance difference compared to the reference value was 1.2%, with an average difference of 0.2%. For the HFM method, the obtained average difference to the reference thermal conductance was 2.2% and 1.9%, using the CHB and GHB chambers configuration, respectively.

The fourth calibration test used EPS panels with 100 mm thickness. For the CHB mode, the maximum thermal conductance difference compared to the reference value was -1.1%, with an average difference of -0.04%. For the GHB mode, the maximum thermal conductance difference compared to the reference value was 1.7%, with an average difference of 0.1%. For the HFM method, the obtained average difference to the reference thermal conductance was 2.1% and 2.6%, using the CHB and GHB chambers configuration, respectively.

From the results presented for the four calibration specimens the average difference concerning the reference value is low, obtaining average differences of less than 1%, which takes into account the size of the equipment can be considered that the values are excellent. The results of the GHB mode are slightly better, which is due to the MB having in its surroundings a controlled environment, where there are no temperature fluctuations. It should be noted that in the CHB tests, where the envelope and MB temperatures are the same, several repetitions were made to achieve the objective of identical temperatures since the MB envelope has no controlled environment.

From the repeatability checks on the equipment, it can be concluded that it is reliable, a relative standard deviation of all tests was less than 1%.

The infrared image thermography checks show that the equipment has no leaks, and there is a uniform temperature on the exterior of the walls of the equipment.

A final note to remember that the calibration is done for the current needs, and desired thermal conductance ranges. For other ranges, it will be necessary to perform the calibration, as is standard for these types of equipment.

5. THERMAL PERFORMANCE OF LSF FRAMED WALLS

5.1. INTRODUCTION

The thermal characterization of LSF framed walls is difficult, as described in state of the art. This chapter presents the determination of the thermal transmittance of an LSF wall, with different configurations, using four different approaches: (*i*) an analytical estimation based on ISO 6946 [26]; (*ii*) experimental studies using the hot box method and (*iii*) the heat flow meter method; and (*iv*) 3D FEM numerical models; and the results are compared. Next is presented a parametric study that intends to find improvement strategies that allow reaching a better thermal performance of the wall, by implementing single and combined thermal bridges mitigation approaches and optimization of the U-value using different insulation materials.

The wall consists of modular elements 1.2 m wide by 2.50 m high and 0.249 m thick, with a structure of cold-formed steel studs, galvanised, with three different types of cross-sections illustrated schematically in Figure 5.1a. Figure 5.1b shows wall module layers, its materials and respective thicknesses. Table 5.1 presents the wall composition, from outer to the inner surface, including the thicknesses and thermal conductivities (λ) of each layer of material applied.

Table 5.1 – Wall materials and properties.

Material (from outer to the inner surface)	**Thickness** [mm]	λ [W/(m.K)]
ETICS Mortar	4	0.750
EPS	60	0.040
OSB	12	0.130
Steel frames	96	61.000
Stone wool	50	0.037
Wood	50	0.180
OSB	12	0.130
Gypsum board	15	0.250
PCM board	25	0.270

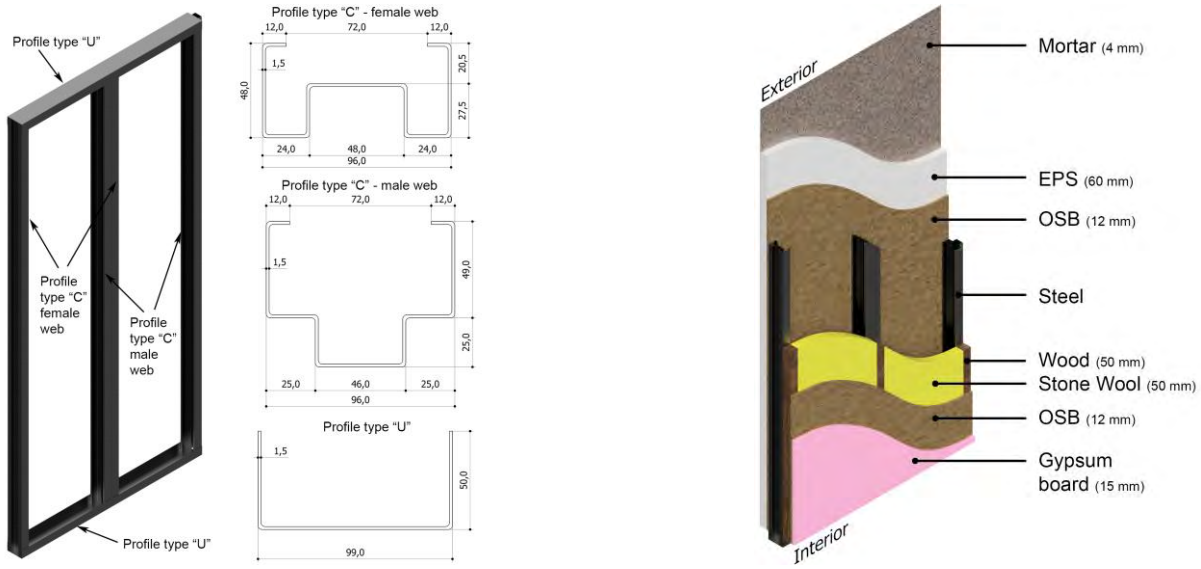

a) b)

Figure 5.1 – Wall module with LSF structure: a) steel profiles; b) wall composition.

5.2. WALL ANALYSIS

The evaluation of the thermal behaviour of the wall was carried out with four different arrangements of materials in the wall, in order to allow the comparison between the existence (or non-existence) of thermal insulation and checking the advantage of placing PCM boards, namely: (*i*) type 1 - wall without insulation, Figure 5.2a; (*ii*) type 2 - wall with stone wool in the air-cavity, Figure 5.2b; (*iii*) type 3 - a complete wall, with stone wool in the air-cavity and ETICS, Figure 5.2c; and (*iv*) type 4 - a complete wall with PCM boards, instead of gypsum boards, Figure 5.2d.

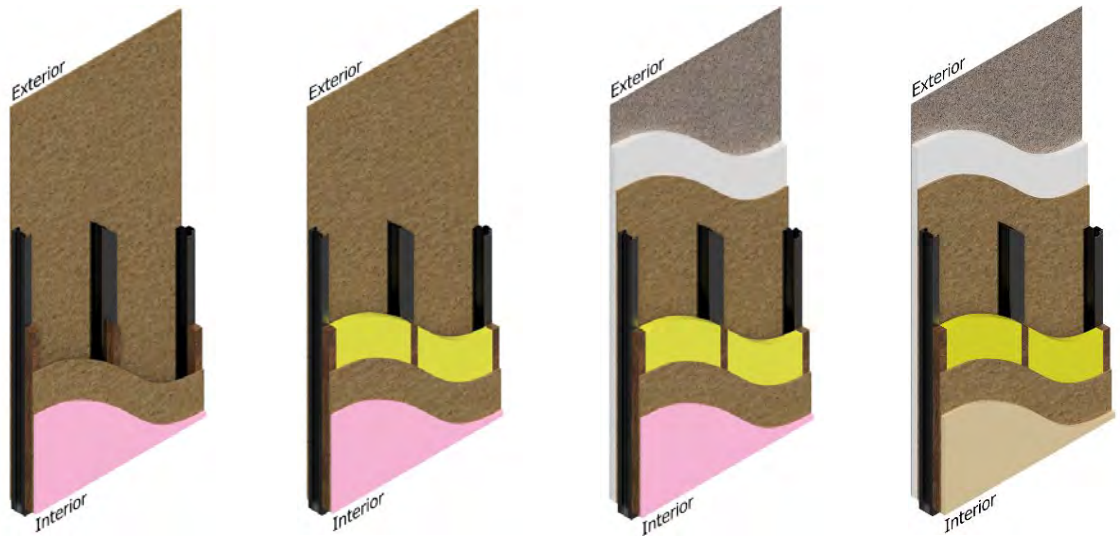

a) b) c) d)

Figure 5.2 – Tested LSF framed walls: a) Type 1 - without thermal insulation; b) Type 2 - with stone wool in the air-cavity; c) Type 3 - with stone wool in the air-cavity and ETICS; and d) Type 4 – With PCMs.

The LSF wall, type 1 configuration, Figure 5.2a, has no thermal insulation. From the inner side, there is gypsum plasterboard and OSB panels attached to the wood frame, being this fastened to the steel structure.

On the exterior side, the OSB panel is directly connected to the steel frame. In the second LSF wall, type 2 configuration, Figure 5.2b, a layer of mineral wool with 50mm tick fulfils the space between the wood frames. The third LSF wall, type 3 configuration, Figure 5.2c, has an additional external thermal insulation composite system (ETICS), made of an EPS thermal insulation layer and a mortar finishing layer.

The bolts used to assemble the steel structure, and that attach all the wall module, are not taken in account, due to their influence on the thermal transmittance be negligible, when compared with the thermal bridges caused by metal studs [290–292].

5.2.1. Analytical approach

The analytical determination of the thermal transmittance of the LSF framed wall presented in Figure 5.1 is possible with the methodology of ISO 6946 [26], described in subsection 2.1.1.6, using the approach for non-homogeneous walls. This procedure is applicable to warm frame construction, in which metallic elements never bridges the insulation layers. The methodology gives the total thermal resistance of the wall with the average of the upper and lower limits of thermal resistance. For calculating the thermal resistances limits, the cross-section of the wall is divided into sections and layers, parallel and perpendicular to the surfaces of the wall, respectively. Two simplifications have been introduced to reduce the number of sections and layers: (*i*) neglected the flanges of the steel studs; and (*ii*) ignored the male/female web deformations of the studs. Figure 5.3 illustrates the five horizontal sections of the walls, understudy, with the following configurations: (*i*) Type 1, without thermal insulation; (*ii*) Type 2, with stone wool in the air-cavity; (*iii*) Type 3, with stone wool in the air-cavity and ETICS; (*iv*) Type 4, with PCMs; and (*v*) Type 5, without steel profiles, to assess how much the steel structure affects the thermal performance of the wall.

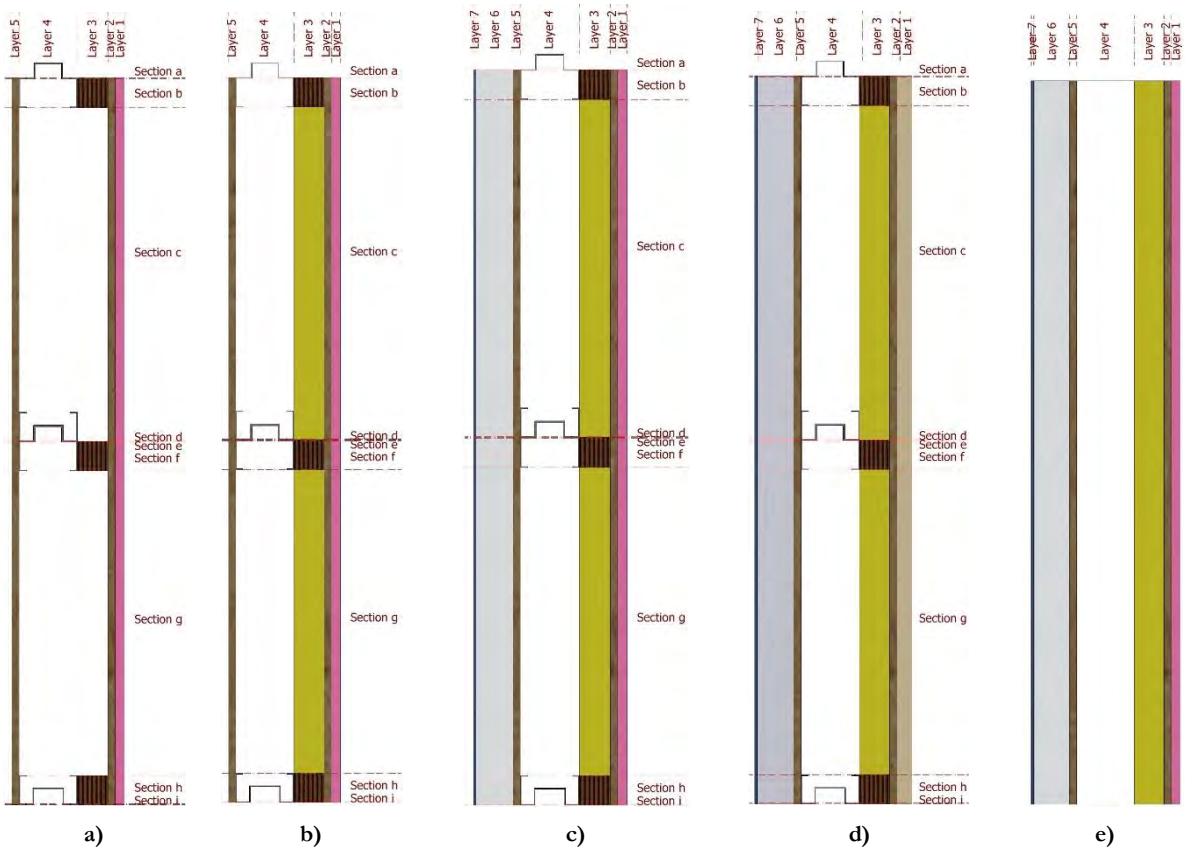

Figure 5.3 – LSF framed wall sections and layers for ISO 6946 approach: a) Type 1 - without thermal insulation; b) Type 2 - with stone wool in the air-cavity; c) Type 3 - with stone wool in the air-cavity and ETICS; d) Type 4 – with PCMs; and e) Type 5 – without steel profiles.

The approach gives the upper limit of the total thermal resistance by assuming one-dimensional heat flow perpendicular to the surfaces of the wall, and the lower limit taking on isothermal surfaces within all planes parallel to the surfaces of the wall. According to the standard, the difference between the upper and lower limit, divided by two times the total thermal resistance of the wall, gives the maximum relative error of the method.

Table 5.2 presents the *U*-values obtained using the ISO 6946 [26] analytical approach for inhomogeneous layers, as well as the differences between walls types, and the maximum relative errors of the methodology. The results show that the addition of insulation allows very significant improvements in thermal performance. The addition of stone wool decreases the *U*-value by 54.2%, and by adding ETICS further decreases in 76.3%. Comparing wall type 3 with wall type 5 (without steel) it is possible to verify that the metallic structure induces a 6.9% increase in the U value.

Table 5.2 – Analytical *U*-value of LSF framed wall by ISO 6946 approach.

Wall Type	**1**	**2**	**3**	**4**	**5**
***U*-value** [W/(m².K)]	**1.318**	**0.603**	**0.313**	**0.310**	**0.290**
Absolute difference	---	-0.714	-1.005	-1.008	-1.028
Percentage difference	---	-54.2%	-76.3%	-76.5%	-78.0%
Maximum relative error	±6.5%	±7.6%	±5.0%	±5.0%	---

5.2.2. Experimental tests

The experimental tests were done in two phases. The performing of the first set of tests was during software development of the HB, being tested the first three wall types, with three repetitions each. These tests were carried out in CHB mode, using the HFM methodology, and the data was obtained using an independent alternative logging system and sensors. In the second phase was used the HB apparatus, repeating the tests of wall type 3 and tested the fourth type, with three repetitions each.

The experimental tests were performed in a steady-state regime, with average ambient temperatures of 40° C and 10° C in the hot and cold chambers, respectively, and the air velocity in both chambers was 0.5 m/s. The convergence interval of each test was 24 hours.

For the first phase set of tests, the wall was instrumented with: (*i*) fifty-four thermocouples type K with ± 2.2° C accuracy, twenty-one for ; (*ii*) twelve heat flux sensors Hukseflux type HFP01 with ± 3 % accuracy; (*iii*) two thermo-hygrometers with ± 3 % accuracy; and (*iv*) two air velocity sensors with ± 1 % accuracy, being the data registered in a data logger. Half of these sensors were placed on each side of the wall (hot and cold side) to have symmetry at the measuring points. For detecting possible stratification of the air inside the chambers, three thermocouples were placed at three different heights, inside each chamber. The second phase set of tests, performed after the equipment calibration phase, it was used the HB instrumentation.

The modular wall was assembled in the specimen frame of the HB, with 3.6 (W) by 2.7 (H) m², using three modules of 1.2 (W) by 2.50 (H) m², and was filled the top and bottom space with 100 mm of XPS.

Figure 5.4a shows the location of the sensors, being the thermocouples and the heat flux meters placed between and in the vicinity of the vertical steel profiles, at different heights and on both wall surfaces, interior and exterior, at same locations. Figure 5.4b illustrates the interior of the wall, during the placement of the stone wool. Figure 5.5a shows the wall type 1, exterior side, which from an outside view is equal to

type 2, not having these configurations the exterior insulation system. Figure 5.5b shows wall type 3 with stone wool in the air-cavity and ETICS in the outer side. Figure 5.5c illustrates wall type 4, with PCMs boards in the interior face, which replaces the gypsum boards used in the other typologies under study.

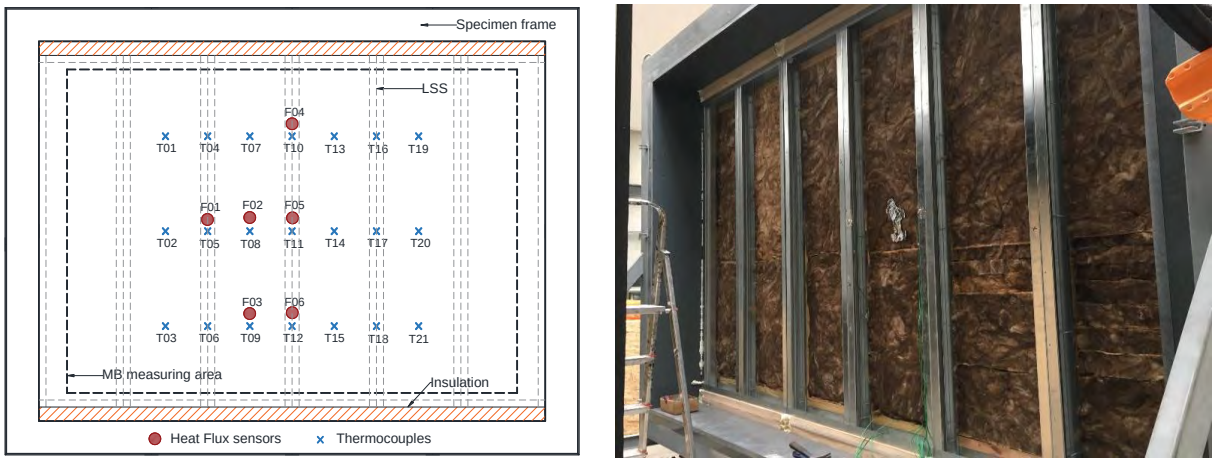

a) b)

Figure 5.4 – LSF framed wall: a) sketch with the location of temperature and heat flux sensors placed on the CHB hot side; and b) interior being assembled stone wool in the air-cavity.

a) b) c)

Figure 5.5 – LSF frame wall: a) Type 1 - without thermal insulation; b) Type 3 - with stone wool in the air-cavity and ETICS; and c) Type 4 – With PCMs.

Table 5.3 summarises the results of the four types of LSF frame walls tested. The first conclusion to be drawn is that the tests carried out with the HFM method, in the first and second phases, obtained identical results. The maximum difference was 0.6%, which shows good repeatability of results. It is noteworthy that between test phases, the same test conditions are the same, being only changed the type of sensors and data acquisition system.

From the results of Table 5.3, when comparing the two experimental methodologies CHB and HFM, the values are similar, being the difference more pronounced in-wall type 1. This is due to the fact that the wall type 1 has no insulation and in these situations, the HFM method can present a more significant error, due to the calculation of the area of influence heat flux sensor, something that the insulation attenuates.

The wall type 2, with stone wool in the air-cavity, presents results more similar between methods, being the difference of 3%. This improvement is due to the addition of insulation.

The differences in results, of the two approaches, for type 3 and 4 walls are similar, being reduced to 2%, which is less than the other walls configurations. This shows that the HFM method achieves better results when the elements with higher conductivity, which provides thermal bridges, are better insulated.

Table 5.3 – Results of the 24h test duration of CHB and HFM method for the LSF framed walls.

		Test n.º	U_{CHB} [W/(m².K)]	$\overline{U}_{CHB}$ [W/(m².K)]	U_{HFM} [W/(m².K)]	$\overline{U}_{HFM}$ [W/(m².K)]	$\Delta\Lambda_{CHB\rightarrow HFM}$
Phase 1	Type 1	T01.C258			1.264		
		T01.C259			1.262	1.264 ±5%	
		T01.C260			1.265		
	Type 2	T02.C261			0.552		
		T02.C262			0.551	0.553 ±5%	
		T02.C263			0.556		
	Type 3	T03.C264			0.299		
		T03.C265			0.292	0.295 ±5%	
		T03.C266			0.295		
Phase 2	Type 1	T01.C267	1.194		1.266		6.0%
		T01.C268	1.205	1.201 ±5%	1.265	1.266 ±5%	5.0%
		T01.C269	1.204		1.267		5.2%
	Type 2	T02.C270	0.573		0.554		-3.3%
		T02.C271	0.571	0.572 ±5%	0.552	0.554 ±5%	-3.3%
		T02.C272	0.571		0.557		-2.5%
	Type 3	T03.C273	0.299		0.292		-2.3%
		T03.C274	0.302	0.301 ±5%	0.295	0.294 ±5%	-2.3%
		T03.C275	0.301		0.294		-2.3%
	Type 4	T04.C276	0.297		0.290		-2.4%
		T04.C277	0.296	0.297 ±5%	0.291	0.291 ±5%	-1.7%
		T04.C278	0.298		0.292		-2.0%

Where: U_{CHB} is the calibrated thermal transmittance obtain by the CHB method; U_{HFM} is the thermal transmittance obtained by the difference between the reference material value and the calibrated obtain value; $\overline{U}$ is the average thermal transmittance; and $\Delta U_{CHB\rightarrow HFM}$ is the thermal transmittance difference between CHB method and HFM method

Table 5.4 summarizes the results of the four LSF frame walls types obtained with the HFM method. The first set of measurements aims to characterise the wall without any insulation. It can be seen that in the area of vertical steel profiles there is a decrease in the *U*-value, about 0.35 W/(m².K), about the remaining areas of the wall (between steel profiles), i.e., -23 %. This is due to the existence of the wood frame that provides greater insulation and attenuates the thermal bridge caused by the steel profiles. The overall *U*-value of the wall is 1.264 W/(m².K).

The second set of tests intends to characterize the thermal performance of the wall with the thermal insulation in the air-cavity, filling with 50 mm of stone wool. From the results obtained it can be concluded that, as expected, the stone wool improves the thermal performance of the wall significantly, reducing the *U*-value between the metallic profiles (-63 %) and in the vicinity of the profiles (- 37 %). This improvement resulted in a decrease to about half (-56 %) of the overall *U*-value of the wall, 0.553 W/(m².K) relative to the original wall, that is, without any thermal insulation.

The third set of tests intends to characterise the thermal performance of the wall with the thermal insulation in the air-cavity, stone wool, and ETICS in the exterior. From the results obtained, it can be concluded that, as expected, using continuous exterior insulation reduces the overall U-value of the wall in 78 %, relative to the initial wall.

The fourth set of tests intends to characterise the thermal performance of the wall similar to the third set, being replaced the gypsum by plasterboards Alba balance 25 with 300 (W) by 300 (H) by 25 (D) mm³. This

material is made of gypsum building boards with PCM microcapsules, with thermal conductivity of 0.270 W/(m.K). As expected, this type of wall had an identical behaviour to the previous one, in terms of thermal transmittance, differing only by 1%. The advantage of this type of material, as presented in sub-section 2.3.2, is improving the thermal inertia of the element. For example, if the room temperature rises above 25° C, the excess heat is absorbed by the plates, and when the temperature drops again, the energy returns it to the environment. The study of this advantage is out of this work scope, being only the thermal transmittance determination intended to study.

Table 5.4 – *U*-value by zones obtained experimentally with HFM method for the LSF frame walls.

Type	Description of the wall	***U*-value** [W/(m².K)]				
		Between steel profiles (BP)	**Steel profiles zone (SP)**	**ΔU_{SP-BP}**	**Overall weighted value (OW)**	**ΔU_{OW-BP}**
1	LSF wall without thermal insulation	**1.331**	**0.983**	-0.35 -26%	**1.265**	-0.07 -5%
2	LSF wall with stone wool in the air gap	**0.486** (ΔU_{12} = -63%)	**0.624** (ΔU_{12} = -37%)	0.14 28%	**0.554** (ΔU_{12} = -56%)	0.07 14%
3	LSF wall with stone wool in the air gap and ETICS	**0.276** (ΔU_{13} = -79%) (ΔU_{23} = -43%)	**0.382** (ΔU_{13} = -61%) (ΔU_{23} = -39%)	0.11 38%	**0.295** (ΔU_{13} = -77%) (ΔU_{23} = -47%)	0.02 7%
4	LSF wall with stone wool in the air gap and ETICS and PCMs	**0.272** (ΔU_{14} = -80 %) (ΔU_{24} = -44 %) (ΔU_{34} = -1 %)	**0.379** (ΔU_{14} = -61 %) (ΔU_{24} = -39 %) (ΔU_{34} = -1 %)	0.10 39 %	**0.291** (ΔU_{14} = -77 %) (ΔU_{24} = -47 %) (ΔU_{34} = -1 %)	0.02 7%

Figure 5.6 shows a chart of the surface temperatures recorded in one of the tests, with a duration of 24 hours, for the wall type 3, being visible: (*i*) that there is no significant air temp heat stratification in each chamber; (*ii*) the steady-state was achieved; and (*iii*) the temperatures do not variate significantly in each chamber, showing excellent uniformity. The chart letters HT and CT refer to thermocouples placed on the hot side (hot thermocouple) and the cold side (cold thermocouple), respectively. Due to the air movement imposed inside the chambers, there is no significant thermal stratification, as the air temperatures recorded by the thermocouples placed at different heights in each chamber are very similar.

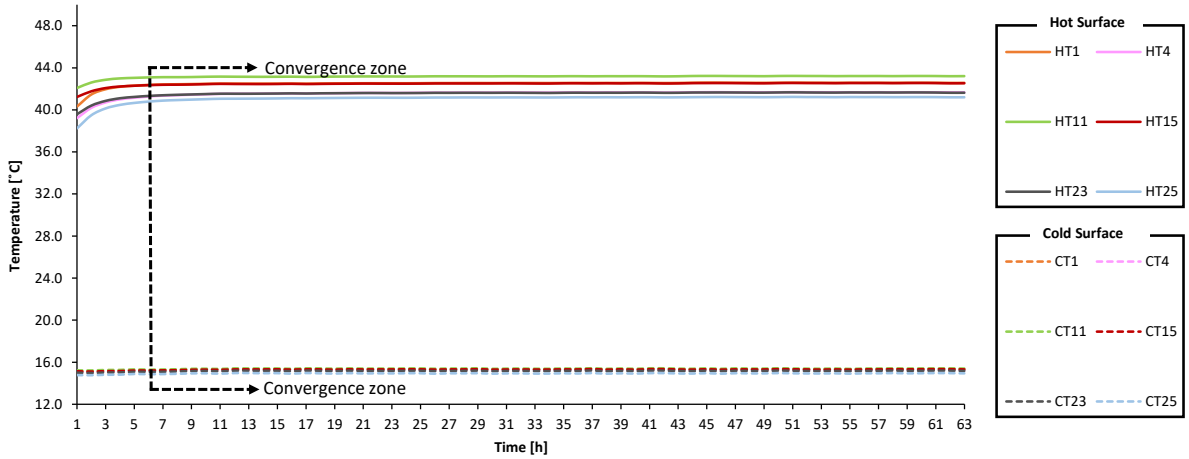

Figure 5.6 – Surface temperature on the LSF wall type 3: HT – hot thermocouple; CT – cold thermocouple.

Figure 5.7 graphically illustrates the distribution of the heat flows of the same test of the previous graphic. The letters HF and CF indicate whether the heat flux is measured on the hot or cold side. This chart shows the effect of continuous thermal insulation applied to the surface of the cold wall, and it is visible that the values of heat flow recorded on that face of the wall are much more similar than those recorded on the hot surface. The highest heat flux values are recorded by the HF1 sensor, placed in the vicinity of the steel frame on the joint between panels. The second highest heat flux values are in the vicinity of the steel frame but in the middle of the panel (HF4, HF5 and HF6). As expected, the lowest heat flux values are HF2 and HF3 sensors, placed between the steel frames, where there is no influence of the thermal bridges.

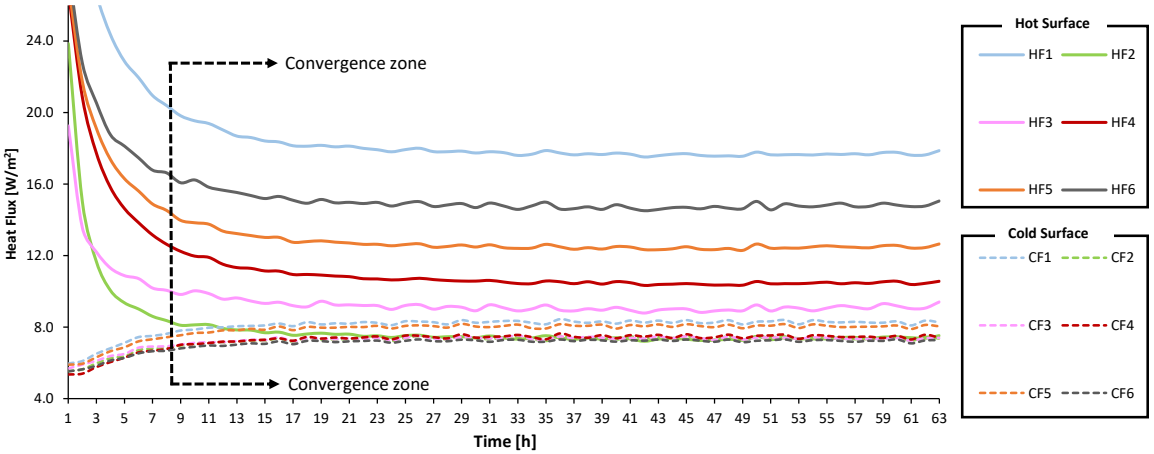

Figure 5.7 – Heat flux on the LSF wall type 3: HF – hot flux side; CF – cold flux side.

Figure 5.8a shows infrared thermal images (IRT) of the LSF wall without any thermal insulation (type 1), where it is possible to identify the location of the steel profiles with greater clarity since the wood frame allows to reduce the thermal bridge of the profiles. In this case, the heat flux is higher between them, causing a higher surface temperature. Figure 5.8b illustrates the solution with stone wool in the air-cavity, and although insulation has been placed, it does not minimise the thermal bridges caused by the steel profiles. This is justified by the fact that the insulation is not continuous, existing only between the profiles, which is why the temperature has decreased more significantly in the zones between profiles. Note that in this case, the temperature in the zone of the profiles is slightly higher. Figure 5.8c shows the complete wall, that is, with stone wool in the air-cavity and the ETICS system. In this case, due to the continuity of the outer thermal insulation, the steel profiles are no longer distinguishable, only being possible to see the place of the bolts that are fixing the EPS of the ETICS.

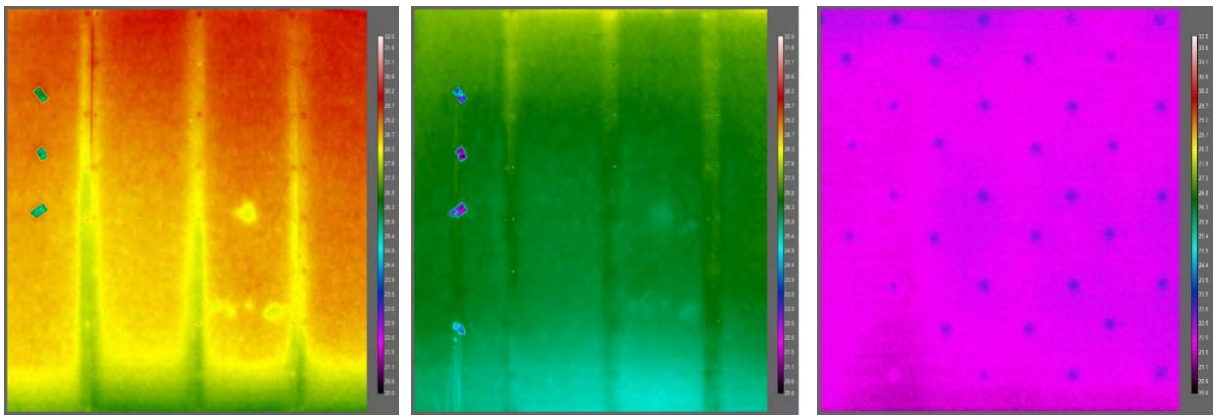

a) **b)** **c)**

Figure 5.8 – Infrared thermal images of the LSF walls cold side: a) LSF wall without thermal insulation; LSF wall with stone wool in the air gap; c) LSF wall with stone wool in the air gap and ETICS.

5.2.3. Numerical approach

A detailed model of the tested wall was obtained using Ansys CFX finite element software. The thermal boundary conditions used in the numerical model of the wall were: (*i*) Exterior ambient temperature of 15 °C; (*ii*) Interior ambient temperature of 45 °C; (*iii*) Exterior surface thermal resistance of 25 W/(m².K); (*iv*) Interior surface thermal resistance of 7.69 W/(m².K); and (*v*) adiabatic conditions in the edges of the modules.

Table 5.5 presents an overview of the obtained thermal transmittance values for the four walls types the thermal transmittance difference (ΔU) between the models. The walls type 3 and 4 achieve the best *U*-value, like the results obtained in the experimental tests. The *U*-value of the wall type 4 was reduced from 1.124 W/(m².K) to 0.295 W/(m².K), corresponding to a reduction of 73.7% in the *U*-value, which represents a good improvement in the thermal performance, showing the importance of the insulation.

Table 5.5 – *U*-value obtained numerically for the LSF frame walls.

Type	Description of the wall	***U*-value** [W/(m².K)]	***ΔU***
1	LSF wall without thermal insulation	**1.124**	
2	LSF wall with stone wool in the air gap	**0.562**	ΔU_{12} = -50.0%
3	LSF wall with stone wool in the air gap and ETICS	**0.299**	ΔU_{13} = -73.4% ΔU_{23} = -46.8%
4	LSF wall with stone wool in the air gap and ETICS and PCMs	**0.295**	ΔU_{14} = -73.7% ΔU_{24} = -47.5% ΔU_{34} = -1.2%

Figure 5.9 illustrates the temperature in the external surface of the wall, being clear the reduction of temperatures. Figure 5.10 shows the amount of heat flux that is coming out of the wall in the external side, where the minus sign of the values means that the heat flux is coming out of the wall.
In the first model, wall type 1 without insulation, was numerically obtained a *U*-value of 1.124 W/(m².K). Figure 5.9a shows the temperature on the outer face of the wall, where the increase in temperature is visible in the area of the steel profiles. Analogously to the temperature, it can be seen in Figure 5.10a the increase in heat flux in the areas of the metal profiles.

The second model, presented in Table 5.5, shows a reduction of 50% in the *U*-value, relatively to the previous model (wall type 1). The results of the 3D numerical model, in which the wall have insulation in the air gap, presents a reduction of temperature and heat flux in the outer face of the wall module, illustrated in Figure 5.9b and Figure 5.10b, respectively. The images show that in the zone of the steel profiles continues to be the place with the higher thermal bridge.

The third and fourth models show identical results, as measured in the experimental study presented in the previous subsection. They show a reduction of approximately 73% and 47% compared to the type 1 and 2 wall model, respectively. Figure 5.9c and Figure 5.9d present the temperature in the external surface of the walls, which are similar to the heat flux illustrated in Figure 5.10c and Figure 5.10d, of models type 3 and 4. The images show that the change in temperature and heat flow in the steel profiles area is much smaller and much less perceptible. This shows the importance of having continuous insulation, in the outside of the steel structure, allowing a clear improvement in the thermal performance of the element.

The last model of Table 5.5, in which the gypsum plasterboard give place to PCMs board, shows that this material only presents an improvement of 1.2% in the *U*-value. This is due to the similarity of thermal conductivity of the gypsum playboard and PCMs boards, 0.250 vs 0.270 W/(m.K).

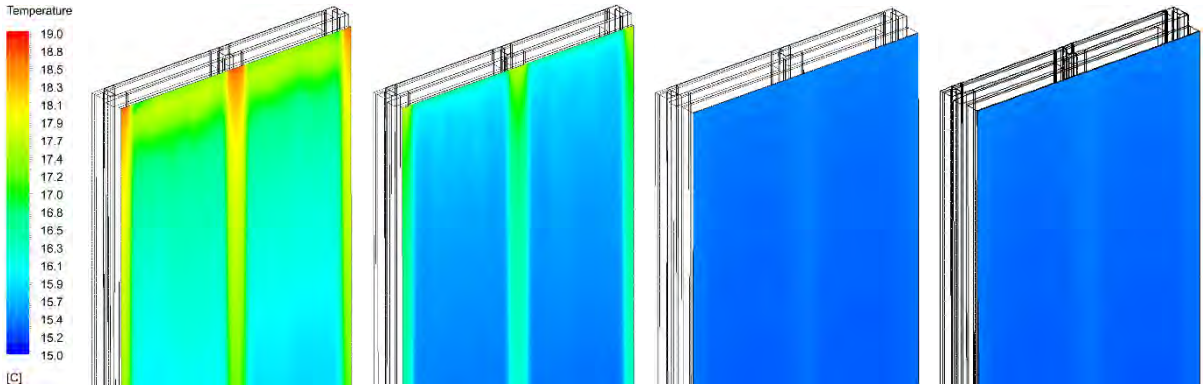

a) **b)** **c)** **d)**

Figure 5.9 – Temperature in the external surface of the wall: a) Type 1 - without thermal insulation; b) Type 2 - with stone wool in the air-cavity; c) Type 3 - with stone wool in the air-cavity and ETICS; and d) Type 4 – With PCMs.

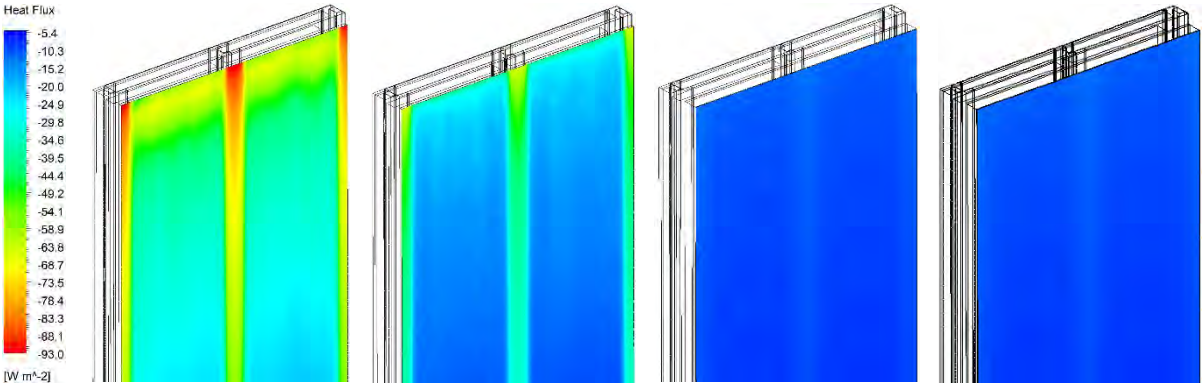

a) **b)** **c)** **d)**

Figure 5.10 – Heat flux in the external surface of the wall: a) Type 1 - without thermal insulation; b) Type 2 - with stone wool in the air-cavity; c) Type 3 - with stone wool in the air-cavity and ETICS; and d) Type 4 – With PCMs.

5.2.4. Results and discussion

Table 5.6 summarizes the results of the *U*-values obtained by the two experimental methodologies, CHB and HFM, from the 3D FEM numerical models, and by the ISO 6946 [26] analytical approach, for the four types of walls. Additionally, Table 5.6 presents numerical and analytical results of the *U*-value of a wall without a steel structure, and with the same layers and characteristics as the wall type 3.

The differences between CHB measurements and numerical predictions are small, less than -0.7% for wall type 3 and 4, having a higher value for wall type 1 and 2, 3.9% and -1.7%, respectively. The reason why the numerical model is less accurate on walls 1 and 2 is mostly due to the construction imperfections that were not introduced in the numerical models. The spacing between panels of the modules exists and is significant, creating a thermal bridge. This thermal bridge is attenuated and even cancelled by placing insulation on the external face, which is why the values of walls 3 and 4 are identical in both approaches.

The difference between the experimental methods in the walls type 1 and 2 is also due to the previous reason. In the two joints between the 1.2 m (W) panels, only one sensor was placed in the HFM method, extrapolating the value to the entire joints, which is found not to be rigorous. This event is interesting because it shows not only the various precautions to be taken with the HFM methodology but also shows why the HB method is more rigorous since it makes a global analysis rather than a local one.

For the other walls type 3 and 4, the difference in results between CHB and HFM are similar, only 2%. The HFM is less precise than then CHB methodology. However, under controlled environmental conditions and with known flanking loses, the model is much more reliable, obtaining more accurate results than *in situ* situations or with elements inhomogeneous that have zones of high thermal bridges.

The difference in results between the ISO 6946 analytical approach and the CHB experimental method is more significant than all other methodologies. For wall type 1 is more pronounced the difference, due to the wall not having insulation, which induces a higher thermal bridge that causes less accuracy of the methodology. As expected, when there is a continuous, homogenous thermal insulation layer, the analytical approach gives better results, and the *U*-values obtained for the LSF wall type 3, and 4 are more similar for both approaches.

The wall type 5, presented in Table 5.6, is similar to type 3, which has removed the steel structure. Analytically this element has a *U*-value of 0.29 W/(m².K), being obtained numerically the same value. This model intends to characterize the thermal bridge caused by the steel structure when compared with the other models. Comparing the theoretical *U*-value of wall type 5 with the experimental CHB value of wall type 3, it is possible to conclude that without the steel structure, there is a reduction of 3.9% of *U*-value. It is possible to draw a similar conclusion comparing the numerical *U*-values of wall 3 and 5, having, in this case, a reduction of 3.2%. Due to the differences in the wall type 3 between the reference value, CHB method, HFM method and theoretical analysis of ISO 6946, which are higher than the effect induced by the steel structure, a comparison between these methods and the theoretical value of the wall type 5 is not made, because it was going to be a mismatch of reality.

Table 5.6 – Results comparison between experimental, numerical and analytical approach for the LSF frame walls types.

Type	Description of the wall	CHB	HFM	3D FEM	ISO 6946
1	**LSF wall without thermal insulation**				
	U [W/(m².K)]	**1.201**	**1.265**	**1.3141**	**1.318**±6.5%
	Absolute difference		0.064	0.113	0.117
	Percentage difference		5.3%	3.9%	9.7%
2	**LSF wall with stone wool in the air gap**				
	U [W/(m².K)]	**0.572**	**0.554**	**0.562**	**0.603**±7.6%
	Absolute difference		-0.018	-0.010	0.031
	Percentage difference		-3.1%	-1.7%	5.5%
3	**LSF wall with stone wool in the air gap and ETICS**				
	U [W/(m².K)]	**0.301**	**0.295**	**0.2989**	**0.313**±5.0%
	Absolute difference		-0.006	-0.002	0.012
	Percentage difference		-2.0%	-0.7%	3.9%
4	**LSF wall with stone wool in the air gap and ETICS and PCMs**				
	U [W/(m².K)]	**0.297**	**0.291**	**0.2953**	**0.310**±5.0%
	Absolute difference		-0.006	-0.002	0.013
	Percentage difference		-2.0%	-0.6%	4.3%
5	**Without steel profiles**				
	U [W/(m².K)]	--	--	**0.290**	**0.290**

5.3. PARAMETRIC STUDY

In modular construction with LSF framed walls, the implementation of thermal bridges mitigation strategies and optimization of the wall module insulation layers to improve the thermal performance is essential to decrease the total energy demand for space heating and cooling.

In past work were presented some parametric studies of an LSF framed wall, which show the advantages of optimisation [50]. Figure 5.11 presents the 3D wall module used in the previous parametric study.

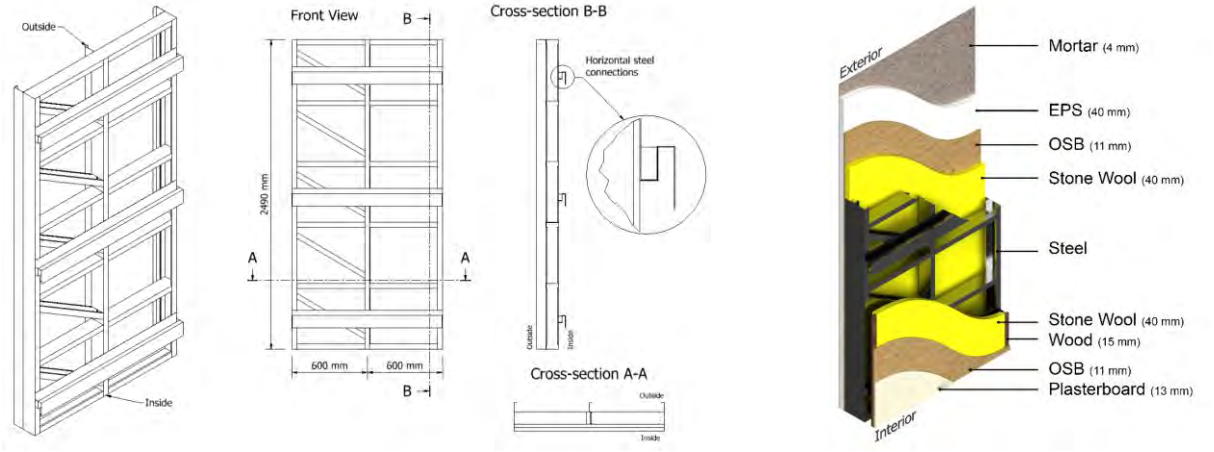

a) **b)**

Figure 5.11 – LSF wall model used in the previous parametric study: a) steel structure; and b) wall module materials [50].

The wall above was studied using tri-dimensional software Ansys CFX to evaluate the *U*-Value for different wall configurations. Several models for single thermal bridges mitigation strategies were developed: Model A was the reference wall; Model B uses thermal break rubber strips; Model C uses vertical male or female studs; Model D has stotted steel studs; and model E uses fixing bolts instead of horizontal steel plate connection. For combined mitigation strategies were developed: Model F with the combination of the improvements introduced in Model B2 with 10mm rubber strips, Model D2 with vertical slotted steel profiles and Model E with bolted connections; and Model G is similar to Model F but with all the steel structure slotted in the web (Model D). In this study, it was concluded that the thermal transmittance of the wall could be reduced by up to 8.3% (Model G), which is around 75% of the total impact of the steel thermal bridges. Figure 5.12a illustrates the parametric study overview of thermal bridges mitigation results for the wall models presented.

The same research performed other parametric study for achieve a *U*-value improvement in the LSF modular wall, with many alternatives tried, like: Model H replaces the air gap and stone wool by polyurethane foam; Model I change the air gap and interior stone wool by polyurethane foam and replaces the exterior stone wool by an air gap; Model J places an aerogel insulation on the internal side, between the internal stone wool and the air gap; Model K introduce aerogel on the external side, between the external stone wool and the air gap; Model L is the combined approach of Model J and K, with silica aerogel insulation blanket in both sides; Models M, N and O introduced VIPs 30 mm thick, with the same strategies used for the aerogel insulation blankets; Model P combined improvements of Model B2, D2, E and H; Model Q combined improvements of Model B2, D2, E and I; Models R and S have the solution as previous, changing the type of steel structure, full slotted; Model T combined the improvements of Models B2, D2, E and L; and Model U combined the improvements of Models B2, D2, E and O. In this study it was conclude that the air gap crossed by steel influences its thermal performance and filling the air gap space with insulation allows a significant improvement. The parametric study shows that the wall U-value can be reduced by near

three times with quite simple solutions, corresponding a reduction of 68%. Figure 5.12b illustrates the parametric study overview of *U*-value improvement results for the wall models presented.

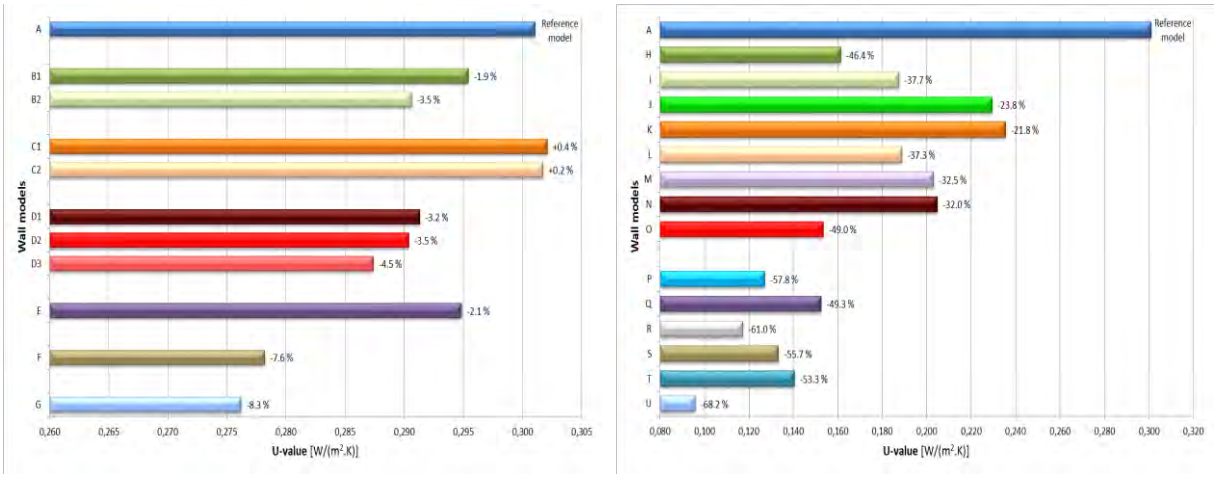

a) **b)**

Figure 5.12 – Parametric study overview of results for the wall models example: a) thermal bridges mitigation; and b) *U*-value improvement [50].

This subsection presents a set of parametric studies that aim to analyse the wall module. The wall module presented in subsection 5.1 has an acceptable thermal resistance. However, it can be improved significantly. By implementing strategies that allow to mitigate the thermal bridges and improve the thermal behaviour of the wall, it is possible to reduce the thermal transmission of this wall module significantly. For this purpose, two parametric studies are carried out for testing mitigation of thermal bridges and for implementing measures that improve thermal behaviour, namely: (*i*) analyses of single improvement strategies; and (*ii*) analyses of combined improvement strategies.

The modular LSF framed wall understudy, illustrated in Figure 5.1, was developed in the project ModCons, whose main objective for this element was to evaluate the connection between steel-to-OSB board. The behaviour of cold-formed steel structure screw connections with OSB panels subjected to lateral loading was investigated experimentally, numerically and with an analytical approach. Taking into account the structural research of the ModCons project, it should be noted that, for this parametric study, some characteristics of the wall must be maintained, namely: (*i*) type of steel structure; (*ii*) wooden frame; and (*iii*) OSB panel.

5.3.1. Single improvement strategies

To improve the thermal performance of the wall module presented in Figure 5.1, several strategies, of thermal bridges mitigation and *U*-value improvement, were implemented based on the validated model. The various models and results are described in the following sub-sections.

As mentioned before, the reference wall module, model A (Figure 5.1), presents adiabatic conditions in the edges, which are common conditions for all models analysed in this parametric study and are ideal conditions prescribed for experimental laboratory setups.

5.3.1.1. Thermal break rubber strip

The first improvement strategy consists of a thermal break rubber strip (λ = 0.037 W/(m.K)) with the thickness of 10 mm, inserted between the steel stud and the OSB panel on the outer surface, and placed in

between the steel stud and wood frame in the inner side. Figure 5.13a illustrates the wall with rubber strips, Model B.

Models B lead to a decrease of 11.7% in the *U*-value, respectively, corresponding to 0.264 W/(m².K) for the *U*-value. This solution provides small thermal performance improvement. However, this can be a good option, since this upgrading is easy and affordable to implement. Figure 5.13b and Figure 5.13c shows the heat flux in the exterior face of models A and B, respectively, where it is perceptible the reduction of the heat flux, mainly in the zone of the vertical profiles.

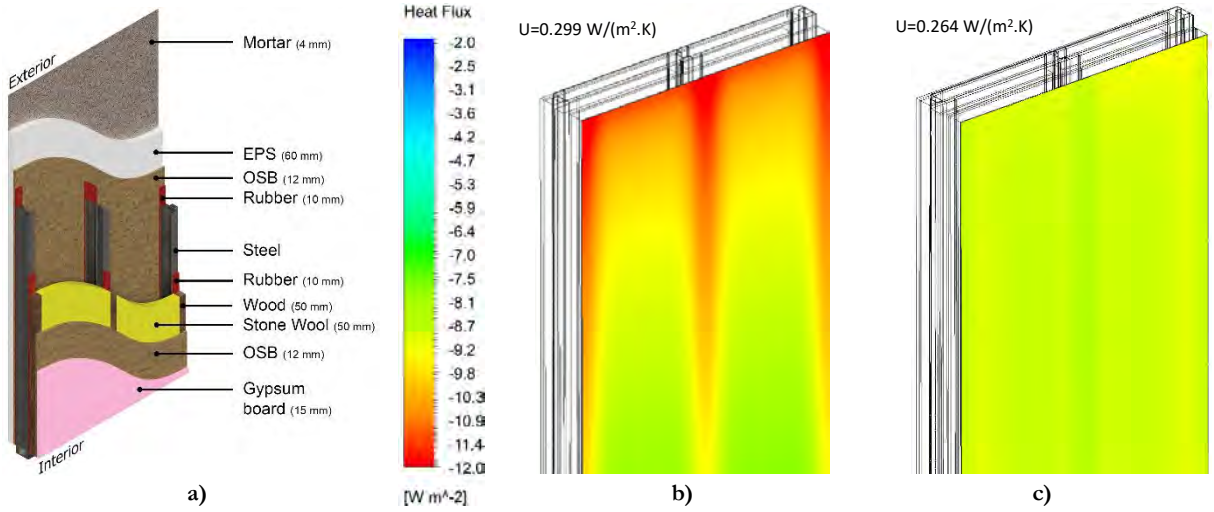

Figure 5.13 – Model B with rubber strips: a) Wall sketch; b) model A; and c) Heat flux in the external.

5.3.1.2. Stone wool between steel profiles

As individual strategies to improve the *U*-value, model C replaces the air gap between the steel profiles by stone wool. Like this, all inside of the wall has insulation, as illustrated in Figure 5.14a.

Model C achieved a significant improvement, reducing the *U*-value by 21.0%, with the adding of more insulation in the air cavity, corresponding to a *U*-value of 0.236 W/(m².K). In Figure 5.14b, it is possible to see the decrease of the heat flux compared to the previous models.

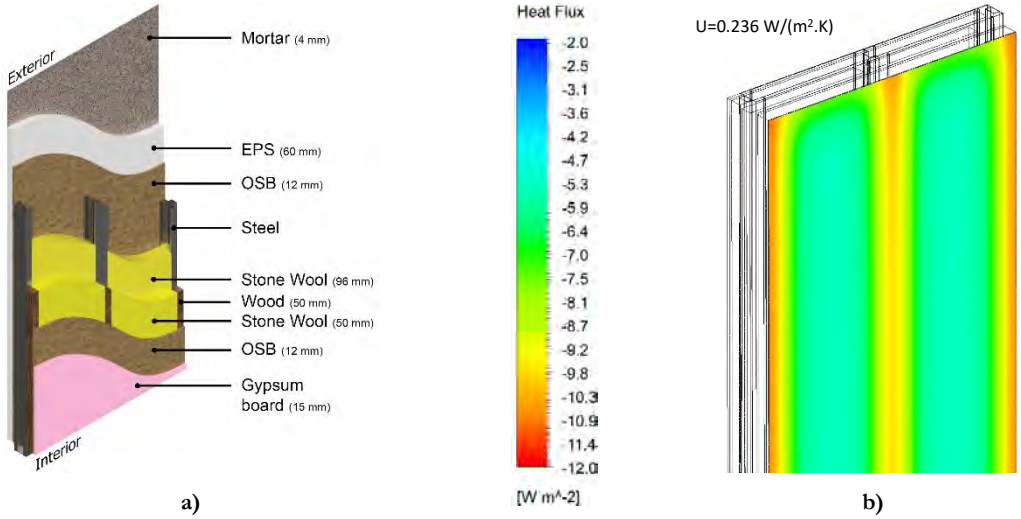

Figure 5.14 – Model C with stone wool: a) Wall sketch; and b) Heat flux in the external surface of the wall.

Figure 5.14b shows a good decrease in heat flux in the zone between profiles due to the increase of insulation. Nevertheless, there is an increase in heat flux in the zone of steel profiles, comparing with model B, due to not having the rubber strips. Although this is an excellent thermal performance improvement, this solution may have a functional drawback related to the lack of an air gap, if and whenever there is moisture infiltration or condensation.

5.3.1.3. Polyurethane foam

Model D presents an individual strategy of placing polyurethane foam (λ = 0.028 W/(m.K)) in the air cavity, replacing the air gap and stone wool of Model A by polyurethane foam, illustrated in Figure 5.15a.

Model D achieved a better improvement, reducing the *U*-value by 28.7%, corresponding to a *U*-value of 0.213 W/(m².K). In Figure 5.15b, it is possible to see the decrease of the heat flux, being similar to the previous model. Due to the lower thermal conductivity of the polyurethane foam, comparing to model C, the decrease of heat flux is visible in the zone between steel profiles. It also arises a slight reduction in the profiles zone.

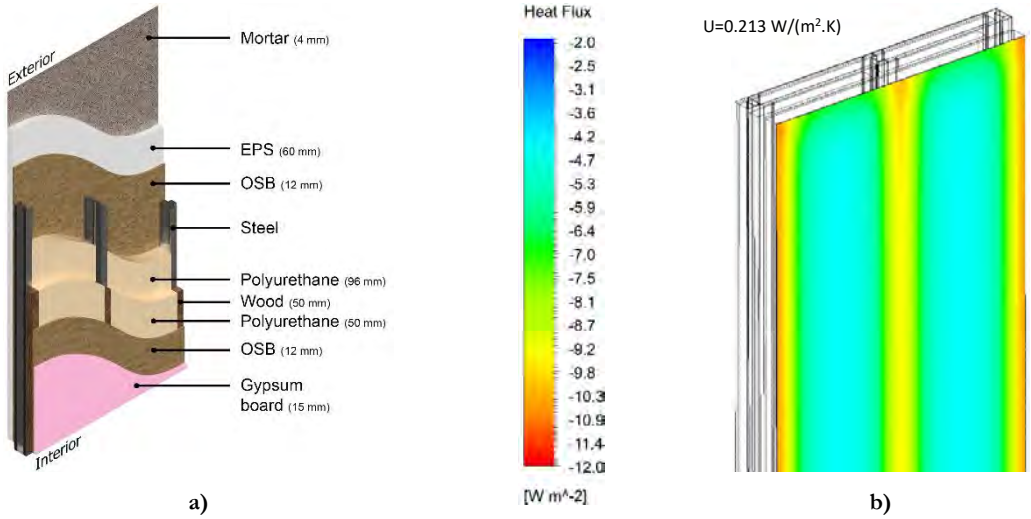

Figure 5.15 – Model D with polyurethane foam: a) Wall sketch; and b) Heat flux in the external surface of the wall.

5.3.1.4. Extruded polystyrene replacing expanded polystyrene

In model E the ETICS insulation of EPS is replaced by XPS (λ = 0.036 W/(m.K)). This material has the advantage of lower thermal conductivity and high mechanical strength than EPS. Figure 5.16a illustrates the model composition.

Model E presents a good improvement compared to model A, presenting a reduction of 5.3%, corresponding to a *U*-value of 0.283 W/(m².K). This simple measure has the advantage of being simple to implement with lower cost.

Figure 5.16b shows the reduction of heat flux when compared with model A. The reduction of heat flux, when compared with model C and D, is lower. However, due to the improvement of external insulation, the steel profiles have a small improvement of the thermal performance, showing the importance of continuous thermal insulation. This solution, combined with external rubber strips is interesting for reducing the thermal bridge effect of the steel profiles.

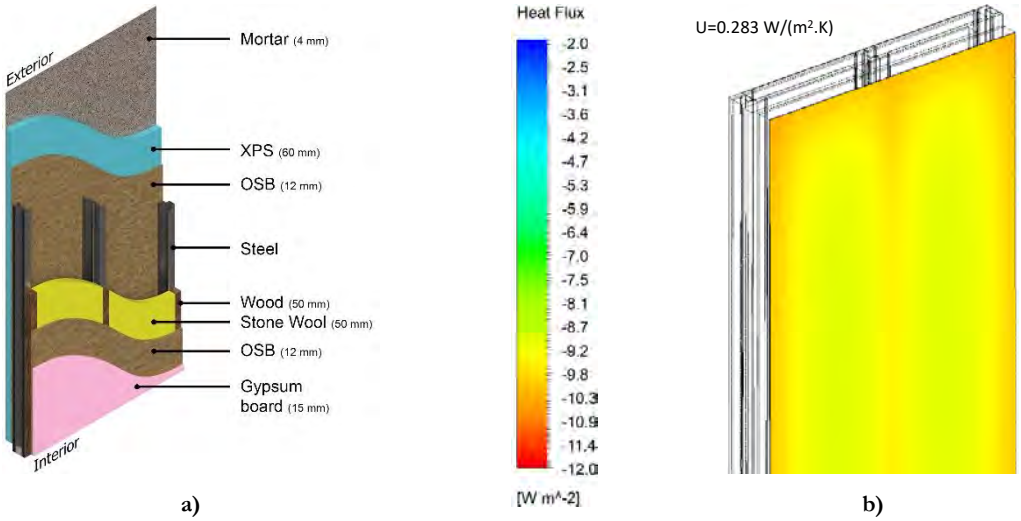

a) b)

Figure 5.16 – Model E with XPS: a) Wall sketch; and b) Heat flux in the external surface of the wall.

5.3.1.5. Silica aerogel insulation blanket

Model F introduces silica aerogel insulation blankets (λ = 0.015 W/(m.K)), that have a dual function by improving both fire protection and thermal performance. In this approach, the silica aerogel replaces the inner insulation of model A. In Figure 5.17a illustrates the aerogel blanket with 50 mm thickness.

The main difference between this model and previous is the low thermal conductivity of the material that allows achieving an excellent reduction of 18.0%, corresponding to a *U*-value of 0.245 W/(m².K). Figure 5.17b shows a clear better performance, having a better thermal performance behaviour than model C and D, which also have all the air cavity fulfilled of insulation.

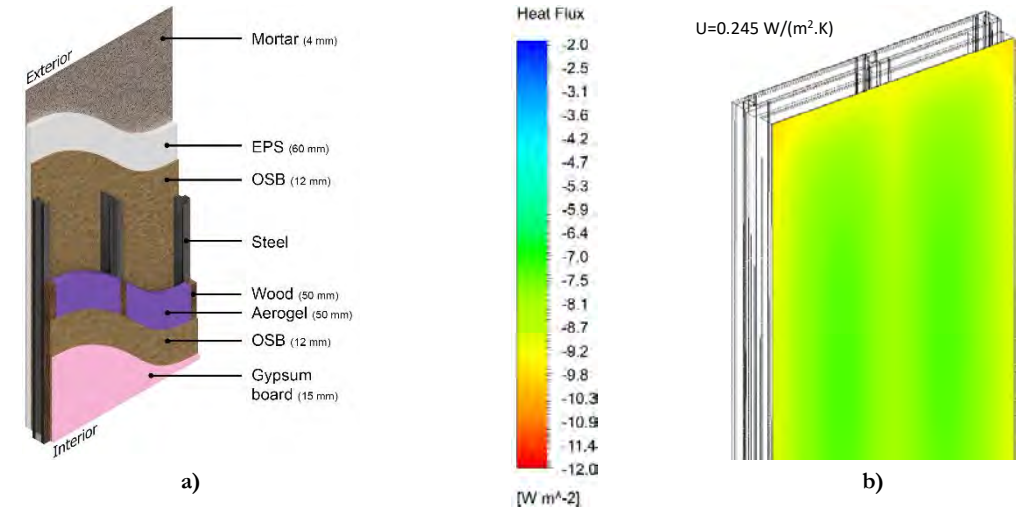

a) b)

Figure 5.17 – Model F with silica aerogel insulation: a) Wall sketch; and b) Heat flux in the external surface of the wall.

5.3.1.6. Vacuum insulation panels

Model G has a similar approach to the strategy used for the aerogel insulation blankets, placing in the same position vacuum insulation panels with 50 mm thickness, illustrated in Figure 5.18a.

The numerical model with VIPs gives the best result for the thermal performance, due to the low thermal conductivity of this material (λ = 0.007 W/(m.K)). Model G gives a good *U*-value, 0.212 W/(m².K), which represents an improvement of 29.1% concerning the reference model. Figure 5.18b shows the decrease in heat flux and shows that this solution is better for achieving a better thermal performance.

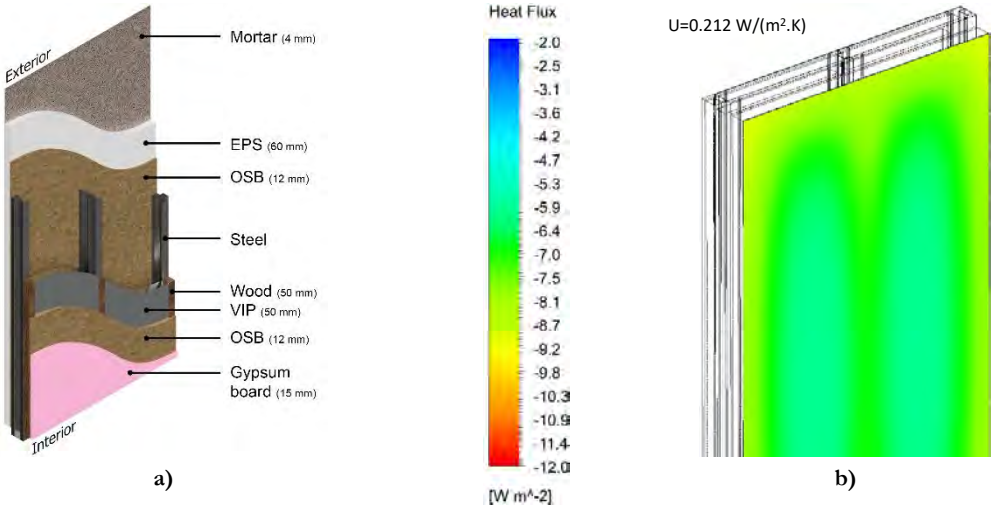

Figure 5.18 – Model G with VIPs: a) Wall sketch; and b) Heat flux in the external surface of the wall.

5.3.2. Combined improvement strategies

Combining the presented thermal bridge mitigation and *U*-value improvement strategies, a better *U*-value is reached. Four models were created that combine the best solutions presented earlier.

Model H presents the combination of placing thermal break rubber strips (model B), putting stone wool between the steel profiles (model C), and replacing EPS by XPS (model E), illustrated in Figure 5.19a. The model I is similar to the previous, being changed the stone wool by polyurethane foam (models B+D+E), showed in Figure 5.19b. The third, model J, presents the combination of thermal break rubber strips (model B), stone wool between profiles (model C), replacing EPS by XPS (Model E), and changing the inner stone wool by silica aerogel blankets (model F). Figure 5.19c illustrates model J. The last combined strategy is similar to the previous, being the aerogel replaced by VIPs (model B+C+E+G), illustrated in Figure 5.19d.

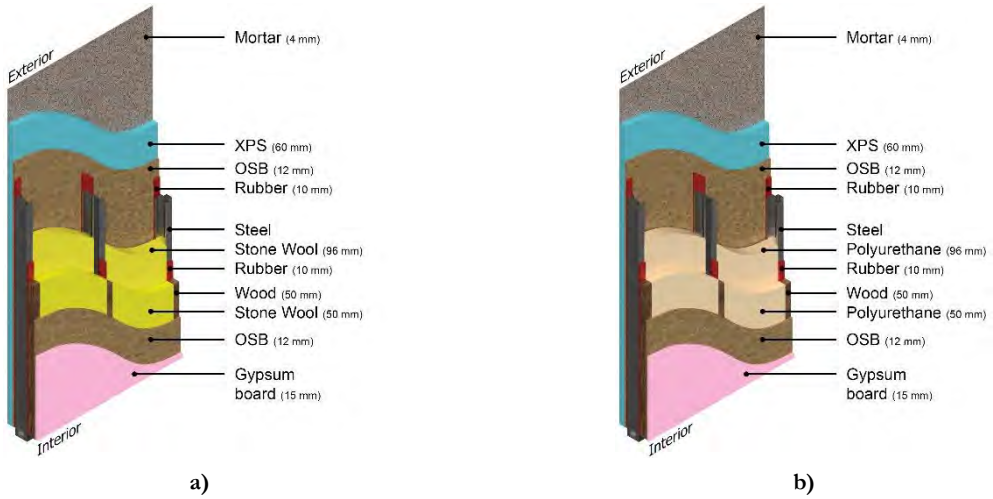

Figure 5.19 – Models with the combined improvement strategies: a) Model H; b) Model I; c) Model J; and d) Model K.

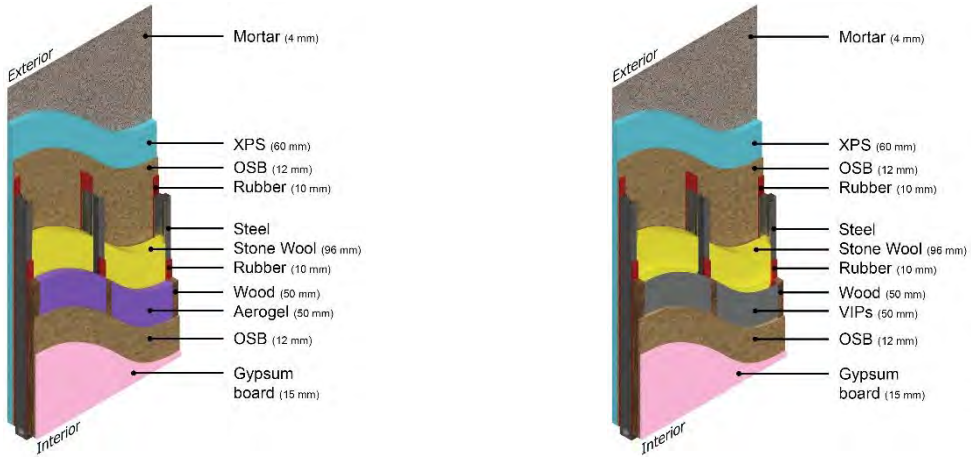

c) **d)**

Figure 5.19 – Models with the combined improvement strategies: a) Model H; b) Model I; c) Model J; and d) Model K.

Model H leads to a reduction of 35.1% in the *U*-value, corresponding to 0.194 W/(m².K). An apparent reduction of the heat flux is visible in Figure 5.20a.

The model I results in a reduction of 42.1% in the *U*-value, 0.173 W/(m².K). Figure 5.20b shows the heat flux in the external face, being visible a slight heat flux reduction in relation to the previous model. However, this solution is more complicated in the making and will not allow easy access to the inside of the wall module.

Model J shows a good improvement of the wall, a reduction of 45.1% in the *U*-value, corresponding to 0.164 W/(m².K). Figure 5.20c shows the heat flux in the external face, being clear the reduction of heat flux in the zone between the steel profiles.

These last model, model K, provide a good result for the U-value, being the best one obtained, with a thermal transmittance value of 0.140 W/(m².K). This model improves by 53.2% the *U*-value relatively to the reference model A. Figure 5.20d illustrates the better behaviour of the heat flux distribution along the external surface of the wall, being visible a substantial improvement of the thermal performance in the zone between the steel profiles.

From the analysis of the four models, it is possible to conclude that only a more significant reduction in the heat flow in the area of the steel profiles is possible using continuous external insulation or increasing the thickness of the rubber strips, or both combined.

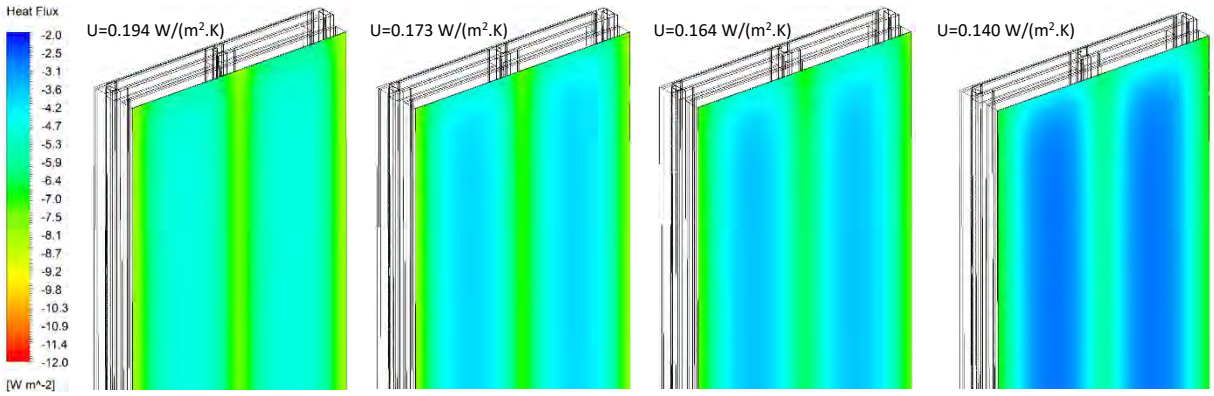

a) **b)** **c)** **d)**

Figure 5.20 – Heat flux in the external surface of the models with the combined improvement strategies: a) Model H; b) Model I; c) Model J; and d) Model K.

5.3.3. Results and discussion

Table 7 presents a summary of the thermal transmittance values for the improvements of the LSF modular walls and the thermal transmittance differences (ΔU) between each model and the reference one (Model A).

Table 7 – Parametric study for *U*-value improvement: an overview of models and results.

	Model	Rubber	Stone Wool between profiles	Polyurethane foam	XPS	Aerogel	VIPs	*U* [W/(m².K)]	*ΔU*
Single strategies	**A***							**0.299**	---
	B	✓						**0.264**	-11.7%
	C		✓					**0.236**	-21.0%
	D			✓				**0.213**	-28.7%
	E				✓			**0.283**	-5.3%
	F					✓		**0.245**	-18.0%
	G						✓	**0.212**	-29.1%
Combined strategies	**H**	✓	✓		✓			**0.194**	-35.1%
	I	✓		✓	✓			**0.173**	-42.1%
	J	✓	✓		✓	✓		**0.164**	-45.1%
	K	✓	✓		✓		✓	**0.140**	-53.2%

*Reference model

Figure 5.21 illustrates in a graphic the overview results of the parametric study for the wall thermal performance improvement presented.

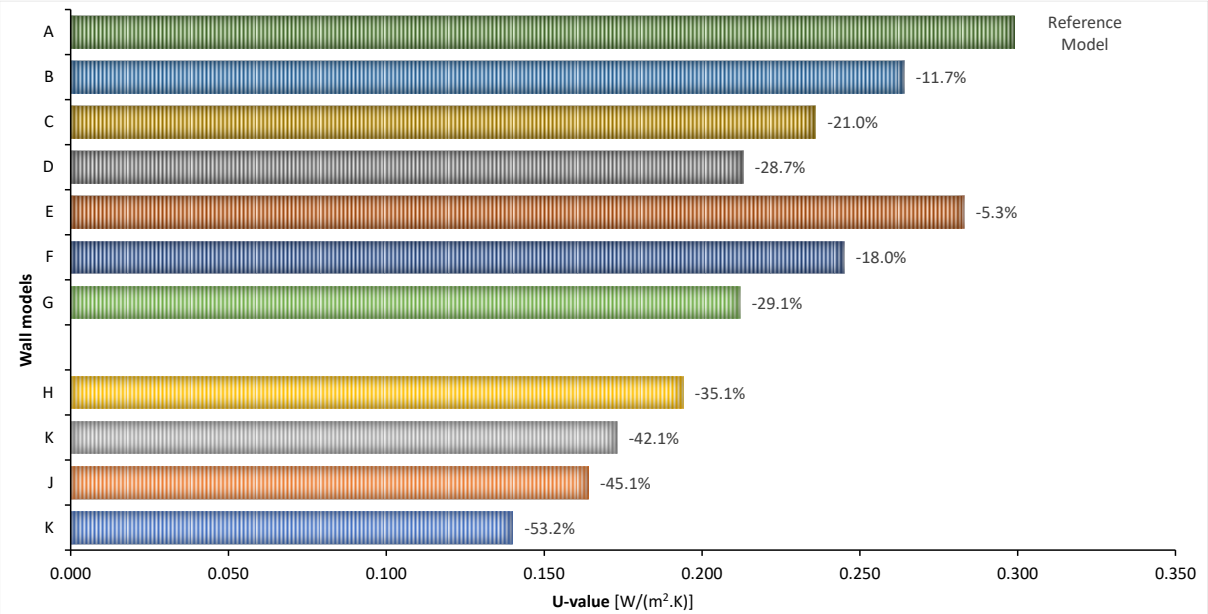

Figure 5.21 –Parametric study for wall thermal performance improvement.

The best single strategy for U-value improvement is model G, which adds VIPs in replacement of the stone wool. The *U*-value was reduced by 29.1%, to 0.212 W/(m².K), which represents a good improvement in the wall module thermal performance, considering that was only replaced a layer of insulation with 50 mm.

The single mitigation strategy with the inclusion of rubber strips, model B, allows obtaining a thermal transmittance reduction of 11.7%, to 0.264 W/(m².K). Additionally, this strategy allows entirely cancel the

thermal bridge caused by the steel structure, namely the wall without steel and wooden frame have a *U*-value of 0.290 W/(m².K), that is, this strategy reduces the *U*-value by 9%, and it cancels by 100% the thermal bridge. This can be considered a good thermal performance improvement since it has a small cost impact. Additionally, for this solution can be used a eco-friendly and cost-effective insulation composite material, as recycled tyre rubber [293].

From the numerical simulations, for the combined strategies, it is concluded that the best solution is the one that combines: (*i*) adding thermal break rubber strips (model B), (*ii*) stone wool between profiles (model C), (*iii*) replacing EPS by XPS replacing (model E), and (*iv*) changing the inner stone wool by VIPs (model G), identified as model K. The *U*-value was reduced from 0.299 W/(m².K), in the reference Model A, to 0.140 W/(m².K), which represents a reduction of 53.2%.

Model J, with Aerogel instead VIPs, presents a similar improvement, decreasing to 0.164 W/(m².K) the *U*-value, which represents less 45.1%. Although this model does not present the best result, is also a good solution because the placement of aerogel insulation blankets in the wall not only decreases the *U*-value but also increases the fire resistance of the wall.

The model I, which places polyurethane in the air gap, also present an excellent performance, reducing to 0.173 W/(m².K) the *U*-value, which represents less 42.1%. This solution has the advantage of being an economical solution, with a low cost and quick application. It has the disadvantage of not being possible to access the interior of the wall, something that is easier, for example, with stone wool.

Although the combine solutions present the drawback of not having an air gap, which in case of water infiltration can be a problem, this disadvantage can be mitigated by using a wind tight and water-resistant membrane, placed between the ETICS and the OSB.

The most efficient combined solution is the one that adds to the wall the VIPs material, improving by 53.2% the thermal performance. However, due to the difference in price between this solution and the polyurethane foam, that allows a reduction in the *U*-value of 42.1%, this second solution may also be considered a good option.

6. CONCLUSIONS AND OUTLOOK

6.1. CONCLUSIONS

This thesis aims the development of a hot box apparatus, its design and construction for the determination of the thermal performance of building elements. The choice of the theme was motivated by previous research and consultancy work developed in the last decade in the ISISE laboratory. In these works, it was felt the need to have a piece of equipment that allows testing the thermal performance of LSF framed walls. These types of elements have been developed and tested in the laboratory by the HFM method, which can induce errors in the results and provides only local characterization. Given the need for more rigorous results and doing better work, it was studied, planned, built, tested, verified, and calibrated a hot box apparatus. The secondary objective was to study the thermal performance of lightweight steel-framed walls using two experimental approaches: hot box method and heat flow meter methodology.

To achieve the primary objective of this work, creating a hot box apparatus that provide means for quantifying the thermal transmittance of vertical building elements, was performed an exhaustive study of state of the art, related with: (*i*) methods for determining the thermal transmittance of buildings envelope, namely, analytical, experimental and numerical; (*ii*) hot box history; and (*iii*) lightweight construction systems.

From the bibliographic review, it was concluded that the best experimental approach for testing heterogeneous buildings envelopes is the hot box method. Due to this fact and to study, researching, and develop new constructions system for buildings, was evident the need of having an HB apparatus. Having into consideration, the considerable price of the apparatus was concluded that the best option was the self-construction.

A research study was carried out on the construction and development of other hot box devices in many countries, which allowed to conclude that the best HB device for real and future work needs is to have flexible equipment that allows an extensive range of testing possibilities. For achieving this goal, it was decided to build a hybrid hot box, which allows it to be the two existing types, namely a calibrated hot box and a guarded hot box.

The study of the history of equipment development over time was very important, allowing to assess what should not be done, the best design and construction options for the equipment, as well as modes of control

and operation of the equipment. The study of other hot boxes also made it possible to assess the best dimensions of the equipment according to the elements that are intended to be tested. It also allows assessing the needs of the equipment thermal insulation according to the ranges to be tested. In resume, the contribution of the work developed for the construction of other hot boxes was an essential role in the choices made in the construction of the presented hot box.

With the objective of building a versatile and innovative equipment, this work contributes scientifically to the creation of a hybrid equipment that is in accordance with European, American and Russian standards, namely: (*i*) ISO 8990:1994 [17]; (*ii*) ASTM C1363-11 [18]; (*iii*) GOST 26602.1-99 [209] and GOST 26254-84 [276]; (*iv*) BS 874-3.1:1987 [277]; and (*v*) BS 874-3.2:1990 [87]. This approach was intended to be able to carry out tests following all existing standards for the equipment, as well as to have equipment that allows for great rigour, taking into account that each standard has different degrees of demand in certain aspects. For example, the American standard is more demanding in terms of quantities of sensors for temperature measurement. The Russian standard demands additionally to make local measurements of the heat flux with heat flux sensors, thus making global and local characterization, having this standard an intrinsic use of the heat flow meter method. Thus, the equipment performs an analysis of the thermal performance of vertical elements by the hot box method and by the heat flow meter method simultaneously. In chapter three, were presented the requirements of all the standards presented above, having been all the requirements in the construction and instrumentation of the equipment fulfilled.

The dimensions of the equipment were carried out according to the most important needs of tests to be carried out, namely, modular LSF framed walls. The built equipment innovates in the type of specimen frame, which allows testing specimens with different thicknesses that can go up to 800mm. Additionally, the specimen frame allows testing specimens with inner dimensions of 3.60 (W) by 2.70 (H) m^2. The equipment insulation solution, in particular the type of walls, allows a very generous operational range, with an operational thermal conductance range of 0.1 W/(m^2.K) to 15 W/(m^2.K).

The control and data logging system used in the equipment is extremely versatile, allowing for high acquisition rates and high control accuracy. The control hardware was carefully chosen, considering the quality, reliability, and the easy expandability of the system. Also, the control system implemented is managed by an application developed for this purpose, which allows great flexibility and can be evolved and improved whenever necessary. Although the data logging equipment has a quality certificate and proven reliability, tests were presented in which the results measured by the system were compared with those obtained by a dedicated data logger from another brand, being concluded high accuracy of recorded readings.

During the development phase of the control software, approximately four hundred tests were carried out that allowed to perfect the control algorithm and to fine-tune the control PID of the three chambers. The results of the parameterization of the system are very satisfactory, as shown by the stability of the system. Also, the low differences between the setpoints and the achieved system values, which differ by less than 1%, both for temperatures and air velocity, show that a proper control system configuration was achieved.

The equipment calibration and verification process were performed with success. For the eight calibration matrix, results identical to the reference values were achieved, with the maximum average difference being less than 0.6%. Additionally, 324 numerical 3D FEM models were made for understanding and quantifying the flaking losses by the equipment envelope. This numerical study was essential for the correct calibration of the equipment, which allowed to obtain the calibration coefficients. For the calibration and repeatability verification of the HB apparatus, 257 tests were carried out, all with at least eight hours of temperature stability in steady-state, which took eight months of continuous operation of the equipment. From the achieved results of calibration and repeatability analyses, it can be concluded that the equipment is working well. Additionally, it is possible to state that it has achieved the objective of having fully rigorous equipment,

perfectly functional, with several possibilities for studying new constructive solutions and validate the development of new constructive solutions.

For the heat flow meter method, good results were archived, being the maximum average difference less than 3.4%, which is an excellent result having in account that this method usually has elevated error. The low error is due to the control environment and insulated boundary conditions provided by the apparatus, instead of an *in situ* test.

The excellent performance of the apparatus envelope was also demonstrated with infrared image thermography, which shows that the equipment has no leaks, and there is a uniform temperature on the exterior of the walls of the equipment.

The second objective of this work was to test the thermal performance of LSF framed wall using two experimental approaches, hot box method and heat flow meter methodology, which was performed with success. Additionally, the LSF wall was studied with analytical and numerical approaches. From the experimental test was concluded that for the LSF wall, in its standard configuration (wall type 3), the CHB and HFM methods obtained similar results, differing only 2%, being the HB method more precise. The CHB method has higher accuracy because it makes a global assessment, instead of the local assessment performed by the HFM method. In the used apparatus, the HFM method uses twelve heat flux sensors, six placed on each side of the wall, and the accuracy can be increased by increasing the number of analysis points, that is, increasing the number of sensors.

The LSF wall numerical model was validated, having a small difference from the CHB measurements, less than 0.7%. The ISO 6946 analytical approach difference in results with CHB experimental method is more significant than all other methodologies, with a discrepancy of 3.9%, which shows the difficulty of the analytical approach in characterizing this type of elements.

The thermal performance of the wall shows that it is crucial to study the thermal behaviour and improve it, to obtain high energy efficiency, allowing a reduction in operating energy. The experimental study was essential for allowing further research and product development, allowing the calibration to confirm the accuracy of numerical models that allowed making parametric studies of optimization of the product. After having the validated numerical model, a parametric study was carried out in order to reduce the thermal bridges and improve the thermal performance of the LSF framed wall. The mitigation strategy implemented, in model B, that intends to reduce the impact of having the steel structure, in which was introduced rubber strips, allowed to obtain a thermal transmittance reduction of 11.7%, and 100% annulation of the thermal bridge caused by the steel structure. The parametric study with a combined solution of improvement strategies, model K, obtained a *U*-value reduction of 53.2%, which is considered an excellent improvement.

The parametric study results show that, after the numerical models validated, they have the advantage of being much faster and cheaper than the experimental tests. Allowing to perform various materials changings in the elements under study, enabling finding thermal bridges arising from, e.g. the steel structure, making possible the implementation of improvement measures of the thermal behaviour, and introduce mitigating effects of the thermal bridges. It also permits to perform an optimization of the insulation layers of these walls (e.g. making use of new insulation materials: aerogel and vacuum insulation panels), which combined with mitigation approaches give a significant reduction in heat transfer coefficient.

A final remark, the equipment is working as a top of the art apparatus, being a piece of unique equipment in the Portuguese research, with this high measuring area size. It allows a great valorisation, of the ISISE research centre laboratory, of the Department of Civil Engineering and will allow the University of Coimbra continues to have cutting-edge research. On a personal level, it was an exciting challenge, with much brainstorming to solve the various challenges that were appearing. It was an enriching work, which allowed to learn a lot.

6.2. OUTLOOK ON FURTHER WORK

A commercial product, such as the purchased hot boxes apparatus, are pieces of equipment with decades of development and have already been optimized. It has the great advantage of being ready to work and has the disadvantage of being limited to a certain range of operation and specific tests.

Although the research, development, construction, and calibration work on the Hot Box apparatus has achieved the established purposes, there is still room for several future developments, namely:

- Assembly of an air dehumidification system, which will allow to operate in temperature ranges closer to zero, or to go to negative temperatures since the equipment has the capacity of achieving it. This equipment is essential to avoid the process of ice formation inside of the apparatus;
- Placing a pressurization system to check the tightness of building elements;
- Equip the apparatus with rotation system, which allows testing of horizontal elements. Although it seems a complicated task, in the reality steel structure of the specimen frame and chambers, are calculated for this purpose. It is only necessary to implement a more robust fixing system between gantry and chambers and mount the rotation system;
- Implement post-processing results modules in the software;
- Insert a software module with an algorithm for checking the proper functioning of each sensor. Additionally, the algorithm must not include in the calculation of averages the damaged sensors during a test, and for which there is redundancy;
- Testing LSF framed walls with thermal break rubber strips of recycled tyre rubber from the project Tyre4BuildIns [293].

6.3. SCIENTIFIC PRODUCTION

The work done for this thesis gave rise to the following documents.

Journal papers:

- **Thermal performance of lightweight steel framed construction system** (Metallurgical Research & Technology) [294]. This paper presents:
  (*i*) LSF walls types, advantages and drawbacks (presented in subsection 2.1 and 2.3); (*ii*) presents mitigation techniques for thermal bridges (presented in subsection 2.3); and (*iii*) strategies to increase thermal mass (presented in subsection 2.3.1 and 2.3.2).
- **Laboratory and in-situ non-destructive methods to evaluate the thermal transmittance and behaviour of walls, windows, and construction elements with innovative materials: a review** (Journal of Energy and Buildings) [59], This paper presents:
  (*i*) experimental methods (presented in subsection 2.1.2); and (*ii*) lightweight construction systems (presented in subsection 2.3.1 and 2.3.2).
- **Thermal Transmittance of Lightweight Steel Framed Walls: Experimental Versus Numerical and Analytical Approaches** (Journal of Building Physics) [295]. This paper presents:
  (*i*) HFM methodology for measuring the thermal performance of LSF framed wall (presented in

subsection 2.1.2.1 and 5.2.2); (*ii*) numerical approach (presented in subsection 5.2.3); and (*iii*) analytical approach (presented in subsection 2.1.1).

- **Hot Box Station: State of the art**, (submitted to Journal of Building Engineering). This paper presents the state of the art of hot box apparatus (presented in subsection 2.2).

Papers in conference proceedings

- **Lightweight Steel Framed Construction System** (Portugal SB13) [296]. This paper presents a revision of the state of the art of LSF walls (presented in subsection 2.1 and 2.3);
- **Thermal performance of Lightweight Steel Framed Construction System** (8th International Conference on Society & Materials, SAM8) [297]. This paper presents a revision of the state of the art of LSF walls (presented in subsection 2.1 and 2.3);
- ***Edifícios com Estrutura Leve em Aço Enformado a Frio (LSF): Vantagens e Desvantagens do Sistema*** (XI Congr. Construção Metálica e Mista) [298]. This paper presents a revision of the state of the art of LSF walls (presented in subsection 2.1 and 2.3);
- ***Determinação experimental do coeficiente de transmissão térmica de uma parede com estrutura leve em aço enformado a frio*** (XI Congr. Construção Metálica e Mista) [299]. This paper presents: (i) Verification of the heat flow meter methodology using the apparatus in climatic chamber configuration (presented in subsection 4.6.1.1); and (ii) thermal performance of LSF framed walls (presented in subsection 5.2.2 and 5.2.3);
- ***Desenvolvimento de um protocolo experimental para medir o desempenho térmico de paredes em LSF*** (3o Congr. Luso-Brasileiro, Mater. Construção Sustentáveis) [300]. This paper presents HFM methodology for measuring the thermal performance of LSF framed wall (presented in subsection 5.2.2 and 5.2.3);
- **Phase change materials for improving the thermal performance of LSF construction** (Semin. PCMs4Buildings – PCMs Thermophys) [301]. This paper presents: (i) CHB apparatus (presented in subsection 2.3.2); (ii) experimental tests (presented in subsection 5.2.2);
- **Systems with PCM-filled rectangular cavities for the storage of solar thermal energy for buildings: the case of the PCMs4Buildings project** (Semin. PCMs4Buildings – PCMs Thermophys) [302]. This paper presents systems with PCM-filled rectangular cavities for the storage of solar thermal energy for buildings (presented in subsection 2.3.2);
- ***Construção de um equipamento para medição do coeficiente de transmissão térmica: especial foco paredes com estrutura em aço*** (XII Congr. Construção Metálica e Mista) [303]. This paper presents: (*i*) CHB and GHB apparatus (presented in chapter 4); (*ii*) experimental tests (presented in subsection 5.2.2);

Posters in scientific events

- *Apresentação do projeto* PCMs4Buildings;
- Phase change materials for improving the thermal performance of LSF construction;
- Systems with PCM-filled rectangular cavities for the storage of solar thermal energy for buildings: the case of the PCMs4Buildings project.

BIBLIOGRAPHY

[1] F. Chen, S.K. Wittkopf, Summer condition thermal transmittance measurement of fenestration systems using calorimetric hot box, Energy Build. 53 (2012) 47–56. doi:10.1016/j.enbuild.2012.07.005.

[2] European Parliament, Directive 2010/31/EU of the European Parliament and of the Council of 19 May 2010 on the energy performance of buildings (recast), Off. J. Eur. Union. (2010) 13–35. doi:10.3000/17252555.L_2010.153.eng.

[3] P. Santos, L. Simões da Silva, V. Ungureanu, Energy Efficiency of Light-weight Steel-framed Buildings, European Convention for Constructional Steelwork (ECCS), Technical Committee 14 - Sustainability & Eco-Efficiency of Steel Construction, ISBN 978-92-9147-105-8, N. 129, 1st edition, 2012.

[4] European Parliament, Directive (EU) 2018/844 amending Directive 2010/31/EU on the energy performance of buildings and Directive 2012/27/EU on energy efficiency, Off. J. Eur. Union. (2018). http://data.europa.eu/eli/dir/2018/844/oj.

[5] European Commission, Clean Energy For All Europeans, Off. J. Eur. Union. (2016) 1–13. http://eur-lex.europa.eu/legal-content/EN/ALL/?uri=CELEX:52016DC0860.

[6] European Commission, Annex 1 of Clean Energy for all Europeans - accelerating clean energy in buildings, Off. J. Eur. Union. (2016) 1–10. http://eur-lex.europa.eu/legal-content/EN/ALL/?uri=CELEX:52016DC0860.

[7] L.M. Al-Hadhrami, A. Ahmad, Assessment of thermal performance of different types of masonry bricks used in Saudi Arabia, Appl. Therm. Eng. 29 (2009) 1123–1130. doi:10.1016/j.applthermaleng.2008.06.003.

[8] A. de Gracia, A. Castell, M. Medrano, L.F. Cabeza, Dynamic thermal performance of alveolar brick construction system, Energy Convers. Manag. 52 (2011) 2495–2500. doi:10.1016/j.enconman.2011.01.022.

[9] H. Gervásio, P. SANTOS, L. Simões da Silva, A.M.G.M.G. LOPES, L.S. DA SILVA, A.M.G.M.G. LOPES, Influence of Thermal Insulation on the Energy Balance for Cold-Formed Buildings, Int. J. Adv. Steel Constr. (ISSN 1816-112X). 6 (2010) 742–766.

[10] F. Aldawi, F. Alam, A. Date, M. Alghamdi, F. Aldhawi, A new house wall system for residential buildings, Energy Build. 67 (2013) 403–418. doi:10.1016/j.enbuild.2013.08.019.

[11] S.A. Al-Sanea, M.F. Zedan, Improving thermal performance of building walls by optimizing

insulation layer distribution and thickness for same thermal mass, Appl. Energy. 88 (2011) 3113–3124.

[12] F. Stazi, F. Tomassoni, A. Vegliò, C. Di Perna, Experimental evaluation of ventilated walls with an external clay cladding, Renew. Energy. 36 (2011) 3373–3385. doi:10.1016/j.renene.2011.05.016.

[13] E. Sassine, A practical method for in-situ thermal characterization of walls, Case Stud. Therm. Eng. 8 (2016) 84–93. doi:10.1016/J.CSITE.2016.03.006.

[14] S. Schiavoni, F. D'Alessandro, F. Bianchi, F. Asdrubali, Insulation materials for the building sector: A review and comparative analysis, Renew. Sustain. Energy Rev. 62 (2016) 988–1011. doi:10.1016/J.RSER.2016.05.045.

[15] O. Kaynakli, A review of the economical and optimum thermal insulation thickness for building applications, Renew. Sustain. Energy Rev. 16 (2012) 415–425. doi:10.1016/J.RSER.2011.08.006.

[16] E. Rodrigues, N. Soares, M.S. Fernandes, A.R. Gaspar, Á. Gomes, J.J. Costa, An integrated energy performance-driven generative design methodology to foster modular lightweight steel framed dwellings in hot climates, Energy Sustain. Dev. 44 (2018) 21–36. doi:10.1016/J.ESD.2018.02.006.

[17] ISO 8990, Thermal insulation - Determination of steady-state thermal transmission properties - Calibrated and guarded hot box, (1994). https://www.iso.org/standard/16519.html.

[18] ASTM C1363-11, Standard Test Method for the Thermal Performance of Building Assemblies by Means of a Hot Box Apparatus, (2011). doi:10.1520/C1363-11.

[19] E. Lucchi, Thermal transmittance of historical brick masonries: A comparison among standard data, analytical calculation procedures, and in situ heat flow meter measurements, Energy Build. 134 (2017) 171–184. doi:10.1016/J.ENBUILD.2016.10.045.

[20] ISO 13370, Thermal performance of buildings - Heat transfer via the ground - Calculation methods, (2017). https://www.iso.org/standard/65706.html.

[21] ISO 13786, Thermal performance of building components - Dynamic thermal characteristics - Calculation methods, (2017). https://www.iso.org/standard/65711.html.

[22] ISO 10077-1, Thermal performance of windows, doors and shutters - Calculation of thermal transmittance - Part 1: General, (2017).

[23] ISO 10077-2, Thermal performance of windows, doors and shutters - Calculation of thermal transmittance - Part 2: Numerical method for frames, (2017).

[24] ISO 7345, Thermal insulation - Physical quantities and definitions, (1987).

[25] B. Anderson, Conventions for U-value calculations, Bre 4432006. (2006) 2 to 3.

[26] ISO 6946, Building components and building elements - Thermal resistance and thermal transmittance - Calculation method, (2017).

[27] ISO 10211, Thermal bridges in building construction - Heat flows and surface temperatures - Detailed calculations, (2017) 55. https://www.iso.org/standard/65710.html.

[28] F.B. Rowley, Transmission of Heat Through Building Materials, Minnesota, 1923.

[29] C.E. Barbour, J. Goodrow, J. Kośny, J.E. Christian, Thermal performance of steel-framed walls, in: ASHRAE Trans., 1995: pp. 766–777. doi:10.2172/111848.

[30] Y.A. Cengel, M.A. Boles, Thermodynamics: An Engineering Approach, 8th ed., McGraw-Hill Education Learning Technology Specialist, 2015. doi:10.1093/jac/dks274.

[31] J. Kośny, D.W. Yarbrough, Thermal Bridges In Building Structures, in: Raj P. Chhabra (Ed.), CRC Handb. Therm. Eng., Taylor & Francis Ltd, United Kingdom, 2017: pp. 800–817.

[32] ASHRAE, 2001 ASHRAE Handbook: Fundamentals, American Society of Heating Refrigerating and Air-conditioning Engineers, 2001.

[33] ASHRAE, 1993 ASHRAE Handbook: Fundamentals, American Society of Heating Refrigerating

and Air-conditioning Engineers, 1993. https://books.google.pt/books?id=dQJFAQAAIAAJ.

[34] J. Kośny, J.E. Christian, Reducing the uncertainties associated with using the ASHRAE zone method for R-value calculations of metal frame walls, in: American Society of Heating, Refrigerating and Air-Conditioning Engineers, Inc., Atlanta, GA (United States), United States, 1995. https://www.osti.gov/servlets/purl/211841.

[35] ASHRAE, 1997 ASHRAE Handbook: Fundamentals, American Society of Heating Refrigerating and Air-conditioning Engineers, 1997. https://books.google.pt/books?id=HMnoNAAACAAJ.

[36] J. Kośny, A.O. Desjarlais, J.E. Christian, Thermal performance of "energy efficient" metal stud wall systems, in: ASHRAE, BETEC, U.S.DOE VI Thermal Envelope Conference, Clearwater, 1995: pp. 717–726. https://web.ornl.gov/sci/buildings/conf-archive/1995 B6 papers/084_Kosny.pdf.

[37] J. Kośny, A.O. Desjarlais, Influence of Architectural Details on the Overall Thermal Performance of Residential Wall Systems, J. Therm. Insul. Build. Envel. 18 (1994) 53–69. doi:10.1177/109719639401800104.

[38] A.G. McGowan, A.O. Desjarlais, An investigation of common thermal bridges in walls, in: American Society of Heating, Refrigerating and Air-Conditioning Engineers, Inc., Atlanta, GA (United States), United States, 1997. https://www.osti.gov/servlets/purl/345256.

[39] S.M. Doran, M.T. Gorgolewski, U-values for light steel-frame construction, Building Research Establishment, 2002. www.bre.co.uk.

[40] M. Gorgolewski, Developing a simplified method of calculating U-values in light steel framing, Build. Environ. 42 (2007) 230–236. doi:10.1016/j.buildenv.2006.07.001.

[41] V. Gori, V. Marincioni, P. Biddulph, C.A. Elwell, Inferring the thermal resistance and effective thermal mass distribution of a wall from in situ measurements to characterise heat transfer at both the interior and exterior surfaces, Energy Build. 135 (2017) 398–409. doi:10.1016/J.ENBUILD.2016.10.043.

[42] greenTEG, gSKIN ® Application Note : U-Value Measurement Case Study, 2015.

[43] ISO 9869-1, Thermal insulation - Building elements - In-situ measurement of thermal resistance and thermal transmittance - Part 1: Heat flow meter method, (2014).

[44] C. Guattari, L. Evangelisti, P. Gori, F. Asdrubali, Influence of internal heat sources on thermal resistance evaluation through the heat flow meter method, Energy Build. 135 (2017) 187–200. doi:10.1016/j.enbuild.2016.11.045.

[45] X. Meng, T. Luo, Y. Gao, L. Zhang, Q. Shen, E. Long, A new simple method to measure wall thermal transmittance in situ and its adaptability analysis, Appl. Therm. Eng. 122 (2017) 747–757. doi:10.1016/j.applthermaleng.2017.05.074.

[46] G. Desogus, S. Mura, R. Ricciu, Comparing different approaches to in situ measurement of building components thermal resistance, Energy Build. 43 (2011) 2613–2620. doi:10.1016/J.ENBUILD.2011.05.025.

[47] P. Santos, C. Martins, L. Simões da Silva, L. Braganca, Thermal performance of lightweight steel framed wall: The importance of flanking thermal losses, J. Build. Phys. 38(1) (2014) 81–98. doi:10.1177/1744259113499212.

[48] ASTM C1155-95, Standard Practice for Determining Thermal Resistance of Building Envelope Components from the In-Situ Data, i (2013) 1–8. doi:10.1520/C1155-95R13.2.

[49] I. Nardi, S. Sfarra, D. Ambrosini, Quantitative thermography for the estimation of the U-value: State of the art and a case study, J. Phys. Conf. Ser. 547 (2014). doi:10.1088/1742-6596/547/1/012016.

[50] C. Martins, P. Santos, L.S. da Silva, L. Simões da Silva, Lightweight steel-framed thermal bridges mitigation strategies: A parametric study, J. Build. Phys. 39 (2015) 342–372. doi:10.1177/1744259115572130.

[51] M.T. Bomberg, K.R. Solcason, Discussion of Heat Flow Meter Apparatus and Transfer Standards Used for Error Analysis, ASTM Spec. Tech. Publ. 879 (1985) 140–153.

[52] P.L. Jankovic A, Antunovic B, Alternative method for on site evaluation of thermal transmittance, Facta Univ. Ser. Mech. Eng. 15 (2017) 341–351. doi:10.22190/FUME170419017J.

[53] ASTM C1046-95, Standard Practice for In-Situ Measurement of Heat Flux and Temperature on Building Envelope Components, 95 (2013). doi:10.1520/C1046.

[54] ASTM C518-17, Standard Test Method for Steady-State Thermal Transmission Properties, Astm. (2017). doi:10.1520/C0518-17.

[55] ISO 8301, Thermal insulation - Determination of steady-state thermal resistance and related properties - Heat flux meter apparatus, (1991). https://www.iso.org/standard/15421.html.

[56] ISO 10293, Glass in building - Determination of steady-state U values (thermal transmittance) of multiple glazing - Heat flux meter method, (1997). https://www.iso.org/standard/18335.html.

[57] ASTM C1784-14, Standard Test Method for Using a Heat flux Meter Apparatus for Measuring Thermal Storage Properties of Phase Change Materials and Products, (2014). doi:10.1520/C1784-14.

[58] ASTM C1667-15, Standard Test Method for Using Heat flux Meter Apparatus to Measure the Centre-of-Panel Thermal Transmission Properties of Vacuum Insulation Panels, (2015). doi:10.1520/C1667-15.

[59] N. Soares, C. Martins, M. Gonçalves, P. Santos, L. Simões da Silva, J.J. Costa, Laboratory and in-situ non-destructive methods to evaluate the thermal transmittance and behaviour of walls, windows, and construction elements with innovative materials: a review, (n.d.).

[60] I.A. Atsonios, I.D. Mandilaras, D.A. Kontogeorgos, M.A. Founti, A comparative assessment of the standardized methods for the in–situ measurement of the thermal resistance of building walls, Energy Build. 154 (2017) 198–206. doi:10.1016/J.ENBUILD.2017.08.064.

[61] K. Gaspar, M. Casals, M. Gangolells, A comparison of standardized calculation methods for in situ measurements of façades U-value, Energy Build. 130 (2016) 592–599. doi:10.1016/J.ENBUILD.2016.08.072.

[62] A.-H. Deconinck, S. Roels, Comparison of characterisation methods determining the thermal resistance of building components from onsite measurements, Energy Build. 130 (2016) 309–320. doi:10.1016/J.ENBUILD.2016.08.061.

[63] S.N. Flanders, A.O. Desjarlais, T.J. Kunz, A comparison of two techniques for R-value calculcation, using winter in-situ data, Therm. Envel. VI/Heat Transf. Walls. VI (1995) 151–161.

[64] O. Gutschker, Parameter identification with the software package LORD, Build. Environ. 43 (2008) 163–169. doi:10.1016/j.buildenv.2006.10.010.

[65] M.J. Jiménez, B. Porcar, M.R. Heras, Application of different dynamic analysis approaches to the estimation of the building component U value, Build. Environ. 44 (2009) 361–367. doi:10.1016/j.buildenv.2008.03.010.

[66] N. Yüksel, The Review of Some Commonly Used Methods and Techniques to Measure the Thermal Conductivity of Insulation Materials, in: Insul. Mater. Context Sustain., 2016: pp. 113–140. doi:10.5772/64157.

[67] ASTM C177-13, Standard test method for steady-state heat flux measurements and thermal transmission properties by means of the guarded-hot-plate apparatus, American Society for Testing and Materials, West Conshohocken, EUA, 2013. doi:10.1520/C0177-13.

[68] C.F. Eithun, Development of a thermal conductivity apparatus : Analysis and design, Norwegian University of Science and Technology, 2012. http://hdl.handle.net/11250/234764.

[69] C.J. Shirtliffe, R.P. Tye, Guarded Hot Plate and Heat Flow Meter Methodology: A Symposium, ASTM STP 8, AMERICAN SOCIETY FOR TESTING AND MATERIALS, 1985.

doi:10.1520/STP879-EB.

[70] D. Salmon, Thermal conductivity of insulations using guarded hot plates, including recent developments and sources of reference materials, Meas. Sci. Technol. 12 (2001) R89–R98. doi:10.1088/0957-0233/12/12/201.

[71] ISO 8302, Thermal insulation - Determination of steady-state thermal resistance and related properties - Guarded hot plate apparatus, (1991) 47. https://www.iso.org/standard/15422.html.

[72] J. Xamán, L. Lira, J. Arce, Analysis of the temperature distribution in a guarded hot plate apparatus for measuring thermal conductivity, Appl. Therm. Eng. 29 (2009) 617–623. doi:10.1016/j.applthermaleng.2008.03.033.

[73] R.R. Zarr, A History of Testing Heat Insulators at the National Institute of Standards and Technology, in: Annu. Meet. Am. Soc. Heating, Refrig. Air-Conditioning Eng., American Society of Heating, Refrigerating and Air-Conditioning Engineers, 2001: p. 11. http://ws680.nist.gov/publication/get_pdf.cfm?pub_id=860832.

[74] ISO 10291, Glass in building – Determination of steady-state U values (thermal transmittance) of multiple glazing – Guarded Hot Plate method, (1994). https://www.iso.org/standard/18333.html.

[75] G. Labudová, V. Vozárová, Hot wire and hot plate apparatuses for the measurement of the thermophysical properties, Вестник ТГТУТ - Trans. TSTU. 8 (2002) 85–96. http://vestnik.tstu.ru/rus/t_8/pdf/8_1_008.pdf.

[76] W.C. Thomas, R.R. Zarr, Transient Thermal Response of a Guarded-Hot-Plate Apparatus for Operation Over an Extended Temperature Range, J. Res. Natl. Inst. Stand. Technol. 123 (2018) 1–24. doi:10.6028/jres.123.001.

[77] F. Asdrubali, G. Baldinelli, Thermal transmittance measurements with the hot box method: Calibration, experimental procedures, and uncertainty analyses of three different approaches, Energy Build. 43 (2011) 1618–1626. doi:10.1016/j.enbuild.2011.03.005.

[78] R. Miller, E. Perrine, P. Linehan, A Calibrated/Guarded Hot-Box Test Facility, in: Therm. Transm. Meas. Insul., ASTM International, West Conshohocken, USA, 1978: pp. 329–341. doi:10.1520/STP35752S.

[79] A.E. Fiorato, Laboratory Tests of Thermal Performance of Exterior Walls, in: Therm. Perform. Exter. Envel. Build., American Society of Heating Refrigerating and Air-conditioning Engineers and US. Department of Energy Office of Energy Conservation and solar Energy Buildings and Community Systems Division, Kissimmee, Florida, USA, 1979: pp. 221–236. https://web.ornl.gov/sci/buildings/conf-archive/1979 B1 papers/015.pdf.

[80] W.P. Brown, K.R. Solvason, A.G. Wilson, A unique hot-box cold-room facility, ASHRAE Trans. 67 (1961) 561–577.

[81] C.J. Schumacher, J.F. Straube, D.G. Ober, A.P. Grin, Development of a New Hot Box Apparatus to Measure Building Enclosure Thermal Performance, in: Therm. Perform. Exter. Envel. Whole Build. XII Int. Conf., 2013. https://web.ornl.gov/sci/buildings/conf-archive/2013 B12 papers/212-Schumacher.pdf.

[82] K.E. Wilkes, R.L. Wendt, A. Delmas, P.W. Childs, Thermal Performance of One Loose-Fill Fiberglass Attic Insulation, in: R.S. Graves, D.C. Wysocki (Eds.), Insul. Mater. Test. Appl. ASTM STP 1116, American Society for Testing and Materials, West Conshohocken, USA, 1991: pp. 275–291. doi:10.1520/STP16352S.

[83] S. Seitz, C. Macdougall, Design of an Affordable Hot Box Testing Apparatus, NOCMAT 2015 - Constr. Sustain. - Green Mater. Technol. (2015). https://umanitoba.ca/faculties/engineering/departments/ce2p2e/alternative_village/media/16th_NOCMAT_2015_submission_143.pdf.

[84] R. Miller, W. Goss, Hot Box Instrumentation, Calibration and Error Estimation — A Survey, in: Insul. Mater. Test. Appl. 2nd Vol., ASTM International, 100 Barr Harbor Drive, PO Box C700, West Conshohocken, PA 19428-2959, 1991: pp. 326-326–29. doi:10.1520/STP16355S.

[85] J. Kosny, P. Childs, Accuracy of hot box testing of steel stud walls, ASTM Spec. Tech. Publ. (2002) 147–158. doi:10.1520/STP1426-EB.

[86] K.R. Solvason, Large-scale wall heat-flow measuring apparatus, ASHRAE Trans. 65 (1959) 541–550. https://nparc.nrc-cnrc.gc.ca/eng/view/accepted/?id=75a1f6cf-f5a1-42e7-97f2-764b87ec08c3.

[87] BS 874-3.2, Methods for determining thermal insulating properties Part 3: Tests for thermal transmittance and conductance - Section 3.2 Calibrated hot-box method, British Standards Institution, 1990.

[88] A. Lavine, J. Rucker, K. Wilkes, Flanking Loss Calibration for a Calibrated Hot Box, in: Therm. Insul. Mater. Syst. Energy Conserv. '80s, ASTM International, 100 Barr Harbor Drive, PO Box C700, West Conshohocken, PA 19428-2959, 1983: pp. 234-234–14. doi:10.1520/STP29449S.

[89] D. Burch, R. Zarr, B. Licitra, A Dynamic Test Method for Determining Transfer Function Coefficients for a Wall Specimen Using Calibrated Hot Box, ASTM Symp. Insul. Mater. Test. Appl. ASTM STP 1030. (1990) 345–361. doi:10.1520/STP23317S.

[90] ASTM C1199-14, Standard Test Method for Measuring the Steady-State Thermal Transmittance of Fenestration Systems Using Hot Box Methods, (2014) 1–23. doi:10.1520/C1199-12.2.

[91] ISO 12567-1, Thermal performance of windows and doors - Determination of thermal transmittance by the hot-box method - Part 1: Complete windows and doors, (2010). https://www.iso.org/standard/50327.html.

[92] ISO 12567-2, Thermal performance of windows and doors – Determination of thermal transmittance by the hot-box method - Part 2: Roof windows and other projecting windows, (2005). https://www.iso.org/standard/40053.html.

[93] E. Lucchi, Applications of the infrared thermography in the energy audit of buildings: A review, Renew. Sustain. Energy Rev. 82 (2018) 3077–3090. https://www.sciencedirect.com/science/article/pii/S1364032117314119 (accessed July 14, 2018).

[94] C.A. Balaras, A.A. Argiriou, Infrared thermography for building diagnostics, Energy Build. 34 (2002) 171–183. doi:10.1016/S0378-7788(01)00105-0.

[95] T. Taylor, J. Counsell, S. Gill, Energy efficiency is more than skin deep: Improving construction quality control in new-build housing using thermography, Energy Build. 66 (2013) 222–231. doi:10.1016/J.ENBUILD.2013.07.051.

[96] P.A. Fokaides, S.A. Kalogirou, Application of infrared thermography for the determination of the overall heat transfer coefficient (U-Value) in building envelopes, Appl. Energy. 88 (2011) 4358–4365. https://www.sciencedirect.com/science/article/pii/S0306261911003059 (accessed July 14, 2018).

[97] D.J. Titman, Applications of thermography in non-destructive testing of structures, NDT E Int. 34 (2001) 149–154. doi:10.1016/S0963-8695(00)00039-6.

[98] M. Rahim, O. Douzane, A.D. Tran Le, G. Promis, T. Langlet, Experimental investigation of hygrothermal behavior of two bio-based building envelopes, Energy Build. 139 (2017) 608–615. doi:10.1016/J.ENBUILD.2017.01.058.

[99] M.. Clark, D.. McCann, M.. Forde, Application of infrared thermography to the non-destructive testing of concrete and masonry bridges, NDT E Int. 36 (2003) 265–275. doi:10.1016/S0963-8695(02)00060-9.

[100] P. Battalwar, J. Gokhale, U. Bansod, Infrared Thermography and IR Camera, Internatio Nal J. Res. Sci. (2015) 9–14. https://pdfs.semanticscholar.org/2a24/b0240376c3c5a1dfd213284ff8fdaf647674.pdf.

[101] I. Nardi, D. Ambrosini, T. de Rubeis, S. Sfarra, S. Perilli, G. Pasqualoni, A comparison between thermographic and flow-meter methods for the evaluation of thermal transmittance of different wall constructions, J. Phys. Conf. Ser. 655 (2015). doi:10.1088/1742-6596/655/1/012007.

[102] J.R.R. Riachos, Avaliação da Determinação Experimental do Coeficiente de Transmissão Térmica com Recurso à Termografia, University of Coimbra, 2014. https://estudogeral.sib.uc.pt/handle/10316/38676.

[103] X.P. V Maldague, Introduction to NDT by active infrared thermography, Mater. Eval. 60 (2002) 1060–1073.

[104] F. Asdrubali, G. Baldinelli, F. Bianchi, A quantitative methodology to evaluate thermal bridges in buildings, Appl. Energy. 97 (2012) 365–373. doi:10.1016/j.apenergy.2011.12.054.

[105] M. O'Grady, A.A. Lechowska, A.M. Harte, Infrared thermography technique as an in-situ method of assessing heat loss through thermal bridging, Energy Build. 135 (2017) 20–32. doi:10.1016/J.ENBUILD.2016.11.039.

[106] F. Asdrubali, C. Buratti, F. Cotana, G. Baldinelli, M. Goretti, E. Moretti, C. Baldassarri, E. Belloni, F. Bianchi, A. Rotili, M. Vergoni, D. Palladino, D. Bevilacqua, Evaluation of green buildings' overall performance through in situ monitoring and simulations, Energies. 6 (2013) 6525–6547. doi:10.3390/en6126525.

[107] L. Evangelisti, C. Guattari, P. Gori, R. Vollaro, In Situ Thermal Transmittance Measurements for Investigating Differences between Wall Models and Actual Building Performance, Sustainability. 7 (2015) 10388–10398. doi:10.3390/su70810388.

[108] F. Asdrubali, F. D'Alessandro, G. Baldinelli, F. Bianchi, Evaluating in situ thermal transmittance of green buildings masonries - A case study, Case Stud. Constr. Mater. 1 (2014) 53–59. doi:10.1016/J.CSCM.2014.04.004.

[109] ISO 9869-2, Thermal insulation - Building elements - In-situ measurement of thermal resistance and thermal transmittance - Part 2: Infrared method for frame structure dwelling, International Standard Organization, Geneva, Switzerland, 2018. https://www.iso.org/standard/67673.html.

[110] ASTM C1060-11a, Standard practice for thermographic inspection of insulation installations in envelope cavities of frame buildings, (2015). doi:10.1520/C1060-11AR15.

[111] ISO 6781, Thermal insulation - Qualitative detection of thermal irregularities in building envelopes - Infrared method, (1983). https://www.iso.org/standard/13277.html.

[112] ASTM E1316-18a, Standard Terminology for Non-destructive Examinations, (2018). doi:10.1520/E1316-18A.

[113] ISO 10878, Non-destructive testing - Infrared thermography – Vocabulary, (2013). https://www.iso.org/standard/46265.html.

[114] ISO 10880, Non-destructive testing - Infrared thermographic testing - General principles, (2017). https://www.iso.org/standard/61881.html.

[115] ASTM E1213-14, Standard Practice for Minimum Resolvable Temperature Difference for Thermal Imaging Systems, (2014). doi:10.1520/E1213-14.

[116] ASTM E1311-14, Standard Practice for Minimum Detectable Temperature Difference for Thermal Imaging Systems, (2014). doi:10.1520/E1311-14.

[117] ISO 18251-1, Non-destructive testing - Infrared thermography - Part 1: Characteristics of system and equipment, (2017). https://www.iso.org/standard/61882.html.

[118] ASTM E1862-14, Standard Practice for Measuring and Compensating for Reflected Temperature Using Infrared Imaging Radiometers, (2014). doi:10.1520/E1862-14.

[119] ASTM E1933-14, Standard Practice for Measuring and Compensating for Emissivity Using Infrared Imaging Radiometers, (2014). doi:10.1520/E1933-14.

[120] R. Albatici, A.M. Tonelli, Infrared thermovision technique for the assessment of thermal transmittance value of opaque building elements on site, Energy Build. 42 (2010) 2177–2183. doi:10.1016/J.ENBUILD.2010.07.010.

[121] R. Albatici, A.M. Tonelli, M. Chiogna, A comprehensive experimental approach for the validation

of quantitative infrared thermography in the evaluation of building thermal transmittance, Appl. Energy. 141 (2015) 218–228. doi:10.1016/J.APENERGY.2014.12.035.

[122] I. Nardi, D. Paoletti, D. Ambrosini, T. de Rubeis, S. Sfarra, Validation of quantitative IR thermography for estimating the U-value by a hot box apparatus, J. Phys. Conf. Ser. 655 (2015) 012006. doi:10.1088/1742-6596/655/1/012006.

[123] B. Tejedor, M. Casals, M. Gangolells, X. Roca, Quantitative internal infrared thermography for determining in-situ thermal behaviour of façades, Energy Build. 151 (2017) 187–197. doi:10.1016/J.ENBUILD.2017.06.040.

[124] M. O'Grady, A.A. Lechowska, A.M. Harte, Application of infrared thermography technique to the thermal assessment of multiple thermal bridges and windows, Energy Build. 168 (2018) 347–362. doi:10.1016/J.ENBUILD.2018.03.034.

[125] F. Bianchi, A. Pisello, G. Baldinelli, F. Asdrubali, Infrared Thermography Assessment of Thermal Bridges in Building Envelope: Experimental Validation in a Test Room Setup, Sustainability. 6 (2014) 7107–7120. doi:10.3390/su6107107.

[126] F. Ascione, N. Bianco, R.F. De Masi, G.M. Mauro, M. Musto, G.P. Vanoli, Experimental validation of a numerical code by thin film heat flux sensors for the resolution of thermal bridges in dynamic conditions, Appl. Energy. 124 (2014) 213–222. doi:10.1016/J.APENERGY.2014.03.014.

[127] J. Quinten, V. Feldheim, Dynamic modelling of multidimensional thermal bridges in building envelopes: Review of existing methods, application and new mixed method, Energy Build. 110 (2016) 284–293. doi:10.1016/J.ENBUILD.2015.11.003.

[128] P. Aversa, D. Palumbo, A. Donatelli, R. Tamborrino, F. Ancona, U. Galietti, V.A.M. Luprano, Infrared thermography for the investigation of dynamic thermal behaviour of opaque building elements: Comparison between empty and filled with hemp fibres prototype walls, Energy Build. 152 (2017) 264–272. https://www.sciencedirect.com/science/article/pii/S0378778817308174 (accessed July 15, 2018).

[129] S.E. Gustafsson, Transient plane source techniques for thermal conductivity and thermal diffusivity measurements of solid materials, Rev. Sci. Instrum. (1991). doi:10.1063/1.1142087.

[130] ISO 22007-2, Plastics - Determination of thermal conductivity and thermal diffusivity - Part 2: Transient plane heat source (hot disc) method, International Organization for Standardization, Geneva, Switzerland, 2015.

[131] H. Zhang, Y.M. Li, W.Q. Tao, Theoretical accuracy of anisotropic thermal conductivity determined by transient plane source method, Int. J. Heat Mass Transf. 108 (2017) 1634–1644. doi:10.1016/j.ijheatmasstransfer.2017.01.025.

[132] W.Z. Fang, L. Chen, J.J. Gou, W.Q. Tao, Predictions of effective thermal conductivities for three-dimensional four-directional braided composites using the lattice Boltzmann method, Int. J. Heat Mass Transf. 92 (2016) 120–130. doi:10.1016/j.ijheatmasstransfer.2015.08.071.

[133] J.J. Gou, H. Zhang, Y.J. Dai, S. Li, W.Q. Tao, Numerical prediction of effective thermal conductivities of 3D four-directional braided composites, Compos. Struct. 125 (2015) 499–508. doi:10.1016/j.compstruct.2015.02.009.

[134] G. Kalaprasad, P. Pradeep, G. Mathew, C. Pavithran, S. Thomas, Thermal conductivity and thermal diffusivity analyses of low-density polyethylene composites reinforced with sisal, glass and intimately mixed sisal/glass fibres, Compos. Sci. Technol. 60 (2000) 2967–2977. doi:10.1016/S0266-3538(00)00162-7.

[135] M.G. Miller, J.M. Keith, J.A. King, B.J. Edwards, N. Klinkenberg, D.A. Schiraldi, Measuring thermal conductivities of anisotropic synthetic graphite-liquid crystal polymer composites, Polym. Compos. 27 (2006) 388–394. doi:10.1002/pc.20231.

[136] H. Zhang, Y.M. Li, W.Q. Tao, Theoretical accuracy of anisotropic thermal conductivity determined by transient plane source method, Int. J. Heat Mass Transf. 108 (2017) 1634–1644.

doi:10.1016/j.ijheatmasstransfer.2017.01.025.

[137] Hot Disk TPS - Transient Plane Source Method | Thermtest Inc., (n.d.). https://thermtest.com/tps (accessed May 13, 2020).

[138] Hot Disk TPS - Transient Plane Source Method | Thermtest Inc., (n.d.).

[139] O. Almanza, M.A. Rodri, G. Rez, J.A. De Saja, Applicability of the Transient Plane Source Method To Measure the Thermal Conductivity of Low-Density Polyethylene Foams, 2004.

[140] Y. Li, C. Shi, J. Liu, E. Liu, J. Shao, Z. Chen, D.J. Dorantes-Gonzalez, X. Hu, Improving the accuracy of the transient plane source method by correcting probe heat capacity and resistance influences, Meas. Sci. Technol. 25 (2014) 015006. doi:10.1088/0957-0233/25/1/015006.

[141] Q. Zheng, S. Kaur, C. Dames, R.S. Prasher, Analysis and improvement of the hot disk transient plane source method for low thermal conductivity materials, Int. J. Heat Mass Transf. 151 (2020) 119331. doi:10.1016/j.ijheatmasstransfer.2020.119331.

[142] LBNL, THERM, (2010). https://windows.lbl.gov/software/therm.

[143] A. Tilmans, D. Van Orshoven, Software and atlases for evaluating thermal bridges, Assess. Improv. EPBD Impact. P198 (2010).

[144] ANSYS CFX, ANSYS Inc., (2018). https://www.ansys.com.

[145] M.S. Van Dusen, J.L. Finck, Heat transfer through building walls, Bur. Stand. J. Res. 6 (1930) 493–522. doi:10.6028/jres.006.033.

[146] F.B. Rowley, A.B. Algren, Heat Transmission Through Building Materials, Minneapolis, USA, 1932.

[147] F. Rowley, A. Algren, Thermal Conductivity of Building Materials, Minneapolis, USA, 1937.

[148] H.L. Whittemore, A.H. Stang, V.B. Phelan, R.S. Dill, Structural and Heat-Transfer Properties of "U.S.S. Panelbilt" Prefabricated Sheet-Steel Constructions tor Walls, Partitions, and Roofs Sponsored by the Tennessee Coal, Iron & Railroad Co., Washington D.C., USA, 1941.

[149] H.L. Whittemore, V.B. Phelan, R.S. Dill, Structural and Heat-Transfer Properties of "Multiple Box-Girder Plywood Panels" for Walls, Floors, and Roots, Washington D.C., USA, 1943. http://www.ntia.doc.gov/files/ntia/publications/comments_of_c_tec_3-13-17.pdf.

[150] H.E. Robinson, F.J. Powlitch, The Thermal Insulating Value of Air Spaces, Washington D.C., USA, 1954.

[151] G. Christensen, W. Brown, A. Wilson, Thermal performance of idealized double windows, unvented, Am. Soc. Heating, Refrig. Air-Conditioning Eng. 71St Annu. Meet. 223 (1964) 13.

[152] G. Lorentzen, E. Brendeng, P. Frivik, On the Development of Methods for Measuring Heat Leakage of insulated Walls with Internal Convection, in: D.R. Flynn, B.A. Peavy (Eds.), Therm. Conduct. Proc., U.S. Dept. of Commerce, National Bureau of Standards, Washington D.C., USA, 1967: pp. 495–506. https://books.google.pt/books?id=xulMAQAAIAAJ&printsec=frontcover&hl=pt-PT&source=gbs_ge_summary_r&cad=0#v=onepage&q&f=false.

[153] P. Bondi, C. Codegone, V. Ferro, A. Sacchi, Experiments on Stationary and Oscillating Heat Transfer in Large Walls, in: Y. Zhou (Ed.), Heat Transf. Non-Stationary Heat Transf. Through Walls, Meas. Therm. Conduct. Heat Transf. with Two Phase Refrig., Elsevier Science, 1971: pp. 217–229. https://books.google.pt/books?id=Ps8gBQAAQBAJ.

[154] P. Di Filippo, M. Sovrano, G. Zorzini, Thermal Behavior of Composite Walls Under Transient Conditions. Their Characterization by Two Parameters. Simplified Calculation Method, in: Y. Zhou (Ed.), Heat Transf. Non-Stationary Heat Transf. Through Walls, Meas. Therm. Conduct. Heat Transf. with Two Phase Refrig., Elsevier Science, 1971: pp. 47–58. https://books.google.pt/books?id=Ps8gBQAAQBAJ.

[155] J. Mumaw, Calibrated hot box: an effective means for measuring thermal conductance in large wall

sections, Heat Transm. Meas. Therm. Insul. ASTM STP 544. (1974) 193–211. http://books.google.com/books?hl=en&lr=&id=OUlFzdi4elQC&oi=fnd&pg=PA193&dq=Calibrated+Hot+Box+:+An+Effective+Means+for+Measuring+Thermal+Conductance+In+Large+Wall+Sections&ots=BmI8IYGSPx&sig=1Wk0bYZEujeN1D4r3PA4XZmexAo.

[156] E. Brendeng, P. Frivik, New Development in Design of Equipment for Measuring Thermal Conductivity and Heat Flow, in: T. R.P. (Ed.), Heat Transm. Meas. Therm. Insul., ASTM International, 100 Barr Harbor Drive, PO Box C700, West Conshohocken, PA 19428-2959, 1974: pp. 147–166. doi:10.1520/STP34777S.

[157] W.R. Hunley, Design description of the large scale climate simulator, United States, 1989. https://www.osti.gov/servlets/purl/6297252.

[158] K. Hake, Oak ridge national laboratory, (1998). https://www.slideserve.com/saki/energy-transfer-and-the-building-envelope.

[159] H.J. Sabine, M.B. Lacher, D.R. Flynn, T.L. Quindry, Acoustical and thermal performance of exterior residential walls, doors and windows, Washington, DC, USA, 1975. https://www.gpo.gov/fdsys/pkg/GOVPUB-C13-d95f552291f2e2f8b266486c656ef991/content-detail.html.

[160] T.L. Lauvray, A Calibrated Hot-Box Approach for Measurements in Air Duct Systems, in: R.P. Tye (Ed.), Therm. Transm. Meas. Insul. ASTM STP 660, American Society for Testing and Materials, 1978: pp. 357–373. https://books.google.pt/books?id=Hsi61hBE9kkC.

[161] H. Wahle, D. Rausch, B. Allmon, New High-Temperature Guarded Hot-Box Facility for Reflective Insulation, in: R.P. Tye (Ed.), Therm. Transm. Meas. Insul. ASTM STP 660, ASTM International, West Conshohocken, USA, 1978: pp. 342–356. doi:10.1520/STP35753S.

[162] J.H. Klems, A Calibrated Hotbox for Testing Window Systems - Construction, Calibration, and Measurements on Prototype High-Performance Windows, in: ASHRAE/DOE Conf. Therm. Perform. Exter. Envel. Build., 1979. https://www.ntis.gov/Search/Home/titleDetail/?ABBR=LBL9803.

[163] J.L. Rucker, J.R. Mumaw, Calibration Procedures and Results for a Large Calibrated Hot Box, in: Therm. Perform. Exter. Envel. Build. ASHRAE STP 28, American Society of Heating Refrigerating and Air-conditioning Engineers, 1979: pp. 237–249. https://web.ornl.gov/sci/buildings/conf-archive/1979 B1 papers/016.pdf.

[164] E.L. Perrine, P.W. Linehan, J.W. Howanski, L.S. Shu, The Design and Construction of a Calibrated/Guarded Hot Box Facility, in: ASHRAE/DOE Conf. SP28, American Society of Heating Refrigerating and Air-conditioning Engineers, 1979: pp. 299–307. https://web.ornl.gov/sci/buildings/conf-archive/1979 B1 papers/021.pdf.

[165] A.J. Palfey, Thermal Performance of Low Emittance Building Sheathing, J. Therm. Insul. 3 (1980) 129–141. doi:10.1177/109719638000300301.

[166] J.. Mumaw, Thermal Research Facility — A Large Calibrated Hot Box for Horizontal Building Elements, Therm. Insul. Perform. ASTMSTP 718. (1980) 195–207.

[167] J.H. Klems, S.E. Selkowitz, S. Horowitz, A Mobile Facility for Measuring Net Energy Performance of Windows and Skylights, in: 3rd Int. CIB Symp. Energy Conserv. Built Environ., Dublin, Ireland, 1982. https://windows.lbl.gov/publications/mobile-facility-measuring-net-energy-performance-windows-and-skylights.

[168] J.H. Klems, U-Values, Solar Heat Gain, and Thermal Performance: Recent Studies Using the MoWiTT, in: ASHRAE Trans. Winter Meet. Fenestration U-Value Symp., Chicago, IL, 1989.

[169] P.W. Griffiths, An examination of the thermophysical nature of solar-control films using an illuminated hot box and computer based simulation modelling techniques, Cranfield University, 1994.

[170] W. Goss, A. Olpak, Design and Calibration of a Rotatable Thermal Test Facility, in: Therm. Insul. Mater. Syst. Energy Conserv. '80s, ASTM STP 789, 1983: pp. 215–233.

http://books.google.com/books?hl=en&lr=&id=p-vsLBXS0FAC&oi=fnd&pg=PA215&dq=Design+and+Calibration+of+a+Rotatable+Thermal+Test+Facility&ots=_EulHdiu1j&sig=WWUa_toUpfWBaQ8foL6pKTrbDO0.

[171] R. Orlandi, J. Howanski, G. Derderian, L. Shu, Development of a Testing Procedure for a Guarded Hot Box Facility, in: Francis A. Govan, D.M. Greason, J.D. McAllister (Eds.), Therm. Insul. Mater. Syst. Energy Conserv. '80s, ASTM STP 789, American Society for Testing and Materials, 1983: pp. 205–214. http://books.google.com/books?hl=en&lr=&id=-tSxl3q2HwQC&oi=fnd&pg=PA205&dq=Development+of+a+Testing+Procedure+for+a+Guarded+Hot+Box+Facility&ots=5Iz7MNQfZp&sig=0OmECXkm8mPmquQ4Geq2oRJXLEg.

[172] R.P. Bowen, National Research Council Canada, DBR's approach for determining the heat transmission characteristics of windows, Ottawa, Canada, 1985. https://trove.nla.gov.au/work/38337719?q&versionId=50806018.

[173] R.J. Onega, P.J. Burns, Thermal Flanking Loss Calculations for the National Bureau of Standards Calibrated Hot Box, 1985. https://www.gpo.gov/fdsys/pkg/GOVPUB-C13-ec6cd322daa93d50502f5bf1c3951315/content-detail.html.

[174] R. Bowen, K. Solvason, A Calorimeter for Determining Heat Transmission Characteristics of Windows, in: F.J. Powell, S.L. Matthews (Eds.), Therm. Insul. Mater. Syst. ASTM STP 922, ASTM International, West Conshohocken, USA, 1987: pp. 567–581. doi:10.1520/STP18504S.

[175] R.R. Zarr, D.M. Burch, T.K. Faison, C.E. Arnold, Thermal Resistance Measurements of a Well-Insulated Wall Using a Calibrated Hot Box, J. Therm. Insul. 10 (1986) 54–75. doi:10.1177/109719638601000108.

[176] A.G. Guy, J.A. Nixon, A Detailed Verification Procedure for a Guarded Hot Box, in: F.J. Powell, S.L. Matthews (Eds.), Therm. Insul. Mater. Syst. ASTM STP 922, American Society for Testing and Materials, Philadelphia, USA, 1987: pp. 297–309. https://books.google.pt/books?id=OQKgJEsq5YwC&printsec=frontcover&hl=pt-PT#v=onepage&q&f=false.

[177] M.G. Van Geem, Heat Transfer Characteristics of a Masonry Cavity Wall, in: F.J. Powell, S.L. Matthews (Eds.), Therm. Insul. Mater. Syst. ASTM STP 922, ASTM International, West Conshohocken, USA, 1987: pp. 367–374. doi:10.1520/STP18504S.

[178] F. De Ponte, Design Considerations on Guarded and Calibrated Hot Box Apparatus, in: F.J. Powell, S.L. Matthews (Eds.), Therm. Insul. Mater. Syst. ASTM STP 922, ASTM International, West Conshohocken, USA, 1987: pp. 345–359. doi:10.1520/STP18504S.

[179] A.H. Elmahdy, R.P. Bowen, Laboratory determination of the thermal resistance of glazing units, ASHRAE Trans. 94 (1988) 1301–1316. http://nparc.nrc-cnrc.gc.ca/eng/view/object/?id=81122659-3b88-4c08-8004-d426178ca62a.

[180] D.G. Stephenson, K. Ouyang, W.C. Brown, A procedure for deriving thermal transfer functions for walls from hot-box test results, National Research Council Canada, 1988. doi:10.4224/20377633.

[181] J.R. Hagan, R.G. Miller, R. Hagan, T. Testing, Long-Term R-Values and Thermal Testing Requirements for Rigid Insulating Foams, in: D.L. McElroy, J.F. Kimpflen (Eds.), Insul. Mater. Testing, Appl. ASTM STP 1030, American Society for Testing and Materials, Philadelphia, 1990: pp. 205–217. doi:10.1520/STP1030-EB.

[182] W.C. Brown, D.G. Stephenson, A guarded hot box procedure for determining the dynamic response of full-scale wall specimens - Part I, ASHRAE Trans. 99 (1993) 632–642. https://nparc.nrc-cnrc.gc.ca/eng/view/object/?id=43772b59-1fb6-4bc4-bd58-df0106bde486.

[183] W.C. Brown, D.G. Stephenson, Guarded hot box measurements of the dynamic heat transmission characteristics of seven wall specimens - Part II, ASHRAE Trans. 99 (1993) 643–660. https://nparc.nrc-cnrc.gc.ca/eng/view/object/?id=6e891a9c-4ac0-44c2-81b4-3ee63532df81.

[184] E.A. Adam, P.J. Jones, Thermophysical properties of stabilised soil building blocks, Build.

Environ. 30 (1995) 245–253. doi:10.1016/0360-1323(94)00041-P.

[185] S.D. Gatland, W.P. Goss, R.L. Baumgardner, R.G. Williams, R.G. Miller, A wall and edge Guarded Hot Box for thermal transmittance measurements, in: R.S. Graves, R.R. Zarr (Eds.), Insul. Mater. Test. Appl. ASTM STP 1320, American Society for Testing and Materials, 1997: pp. 46–59. https://books.google.pt/books?id=gn4mMnMVUlsC&pg=PA46&lpg=PA46&dq=a+wall+and+edge+guarded+hot+box+for+fenestration+testing&source=bl&ots=fKWmU9qGa6&sig=xskodHCjPkze7Vf-i9-oui0BRVM&hl=pt-PT&sa=X&ved=0ahUKEwjD7sf1vdvSAhWs5IMKHVVwCIAQ6AEIKjAC#v=onepage&q=aw.

[186] S.D. Gatland, W.P. Goss, D. Curcija, Design and Fabrication of a Second Generation Research Calibrated Hot Box, in: R.. . Graves, R.R. Zarr (Eds.), Insul. Mater. Te Sting Appl. Third Vol. ASTM STP 1320, American Society for Testing and Materials, 1997. https://books.google.pt/books?id=gn4mMnMVUlsC&printsec=frontcover&hl=pt-PT&source=gbs_ge_summary_r&cad=0#v=onepage&q&f=false.

[187] D. Derome, P. Fazio, A. Athienitis, J. Rao, Use of an environmental chamber to investigate large-scale envelope specimen hygrothermal performance, in: ICBEST '97, Int. Conf., Centre for Window and Cladding Technology, 1997: pp. 423–428. https://www.tib.eu/en/search/id/BLCP%3ACN031728582/Use-of-an-environmental-chamber-to-investigate/.

[188] A.H. Elmahdy, K. Haddad, Experimental procedure and uncertainty analysis of a guarded hotbox method to determine the thermal transmission coefficient of skylights and sloped glazing, in: ASHRAE Trans., NRC Institute for Research in Construction; National Research Council Canada, 2000: pp. 601–613. doi:NRCC-43378.

[189] J. Kosny, P. Childs, Validation of Heating 7.2 Simulations Using Hot Box Test Data for RASTRA Wall Form System with Expanded Polystyrene–Beads, (2000). http://citeseerx.ist.psu.edu/viewdoc/download?doi=10.1.1.622.5933&rep=rep1&type=pdf.

[190] D.P. Aviram, A.N. Fried, J.J. Roberts, Thermal properties of a variable cavity wall, Build. Environ. 36 (2001) 1057–1072. doi:10.1016/S0360-1323(00)00042-1.

[191] S. Yuan, S. Gatland, W. Goss, Calibration Procedures for Hot Boxes, in: A. 0. Desjarlais, R.R. Zarr (Eds.), Insul. Mater. Test. Appl. ASTM STP 1426, ASTM International, West Conshohocken, USA, 2002: pp. 221–238. doi:10.1520/STP11015S.

[192] S. Yuan, G.A. Russell, W.P. Goss, Uncertainty Analysis of a Calibrated Hot Box, in: A.O. Desjarlais, R.R. Zarr (Eds.), Insul. Mater. Test. Appl. ASTM STP 1420, American Society for Testing and Materials, West Conshohocken, USA, 2002: pp. 189–202. https://books.google.pt/books?id=zqoH5-XPmcEC&dq=Effect+of+Steel+Framing+in+Attic+Ceiling+Assemblies+on+Overall+Thermal+Resistance&hl=pt-PT&source=gbs_navlinks_s.

[193] T.W. Petrie, J. Kosny, J.A. Atchley, A.O. Desjarlais, Effect of Steel Faming in Attic/Ceiling Assemblies on Overall Thermal Resistance, in: A. 0. Desjarlais, R.R. Zarr (Eds.), Insul. Mater. Test. Appl. ASTM STP 1426, ASTM International, West Conshohocken, USA, 2002: pp. 159–175. https://books.google.pt/books?id=zqoH5-XPmcEC&dq=Effect+of+Steel+Framing+in+Attic+Ceiling+Assemblies+on+Overall+Thermal+Resistance&hl=pt-PT&source=gbs_navlinks_s.

[194] K.G. Wakili, C. Tanner, U-value of a dried wall made of perforated porous clay bricks Hot box measurement versus numerical analysis, Energy Build. 35 (2003) 675–680. doi:10.1016/S0378-7788(02)00209-8.

[195] I. NAHB Research Center, Development of Cost- Effective, Energy Efficient Steel Framing: Thermal Performance of Slit-Web Steel Wall Studs, Washington, DC, USA, 2002.

[196] Y. Gao, J.J. Roux, C. Teodosiu, L.H. Zhao, Reduced linear state model of hollow blocks walls, validation using hot box measurements, Energy Build. 36 (2004) 1107–1115.

doi:10.1016/j.enbuild.2004.03.008.

[197] J. Rose, S. Svendsen, Validating Numerical Calculations against Guarded Hot Box Measurements, Nord. J. Build. Phys. 4 (2004) 1–9.

[198] T. Blomberg, HEAT2, (1998). https://buildingphysics.com/.

[199] T. Blomberg, HEAT3, (1998). https://buildingphysics.com/.

[200] ISO 10211-1, Thermal bridges in building construction - Heat flows and surface temperatures - Part 1: General calculation methods, (1995). https://www.iso.org/standard/2541.html.

[201] T. Nussbaumer, K.G. Wakili, C. Tanner, Experimental and numerical investigation of the thermal performance of a protected vacuum-insulation system applied to a concrete wall, Appl. Energy. 83 (2006) 841–855. doi:10.1016/J.APENERGY.2005.08.004.

[202] J.M.M. Sala, A. Urresti, K. Martín, I. Flores, A. Apaolaza, Static and dynamic thermal characterisation of a hollow brick wall: Tests and numerical analysis, Energy Build. 40 (2008) 1513–1520. https://www.sciencedirect.com/science/article/pii/S0378778808000388 (accessed August 2, 2018).

[203] P. Baker, Thermal performance of traditional windows, 2008. www.historic-scotland.gov.uk/technicalpapers.

[204] F. Geoola, Y. Kashti, a. Levi, R. Brickman, A study of the overall heat transfer coefficient of greenhouse cladding materials with thermal screens using the hot box method, Polym. Test. 28 (2009) 470–474. doi:10.1016/j.polymertesting.2009.02.006.

[205] F. Asdrubali, G. Baldinelli, F. Bianchi, A. Libbra, A. Muscio, Comparative analysis of different methods to evaluate the thermal conductivity of homogenous materials, in: ASME-ATI-UIT 2010 Conf. Therm. Environ. Issues Energy Syst., Sorrento, Italy, 2010. http://www.crbnet.it/File/Pubblicazioni/pdf/1519.pdf.

[206] G. Baldinelli, A methodology for experimental evaluations of low-e barriers thermal properties: Field tests and comparison with theoretical models, Build. Environ. 45 (2010) 1016–1024. doi:10.1016/j.buildenv.2009.10.009.

[207] S. Cao, A. Gustavsen, S. Uvsløkk, B.P. Jelle, J. Gilbert, J. Maunuksela, The Effect of Wall-Integrated Phase Change Material Panels on the Indoor Air and Wall Temperature – Hot box Experiments, in: Renew. Energy Conf. 2010, Trondheim, Norway The, 2010: pp. 15–26.

[208] ASTM C1363-05, Standard Test Method for Thermal Performance of Building Materials and Envelope Assemblies by Means of a Hot Box Apparatus, (2005). doi:10.1520/C1363-05.

[209] GOST 26602.1-99, Windows and doors. Methods of determination of resistance of thermal transmission, (1999).

[210] K. Martin, A. Campos-Celador, C. Escudero, I. Gómez, J.M. Sala, Analysis of a thermal bridge in a guarded hot box testing facility, Energy Build. 50 (2012) 139–149. doi:10.1016/j.enbuild.2012.03.028.

[211] M.K. Choudhary, C.P. Kasprzak, D.E. Musick, M.J. Henry, N.D. Fast, ASHRAE / IES Standard 90 . 1 Metal Building U-factors - Part 5 : Mathematical Modeling of Wall Assemblies and Validation by Calibrated Hot Box Measurements, American Society of Heating, Refrigerating, and Air-Conditioning Engineers, 2012.

[212] H. Kus, E. Özkan, Ö. Göcer, E. Edis, Hot box measurements of pumice aggregate concrete hollow block walls, Constr. Build. Mater. 38 (2013) 837–845. doi:10.1016/j.conbuildmat.2012.09.053.

[213] F. Chen, S.K. Wittkopf, P. Khai Ng, H. Du, Solar heat gain coefficient measurement of semi-transparent photovoltaic modules with indoor calorimetric hot box and solar simulator, Energy Build. 53 (2012) 74–84. doi:10.1016/j.enbuild.2012.06.005.

[214] LBNL, WINDOW, (2010). https://windows.lbl.gov/software/window.

[215] A. Ghosh, S. Ghosh, S. Neogi, Performance Evaluation of a Guarded Hot Box U-value Measurement Facility under Different Software based Temperature Control Strategies, Energy Procedia. 54 (2013) 448–454. doi:10.1016/J.EGYPRO.2014.07.287.

[216] A.J. Holstein, D.R. Bohnhoff, The Design and Fabrication of a Rotatable Guarded Hot Box (RGHB) Capable of Static Pressure Application, in: 2013 ASABE Annu. Int. Meet., American Society of Agricultural and Biological Engineers, Kansas City, Missouri, 2013: p. 22. doi:10.13031/aim.20131578832.

[217] S. Shrestha, W. Miller, A. Desjarlais, Thermal Performance Evaluation of Attic Radiant Barrier Systems Using the Large Scale Climate Simulator (LSCS), ASHRAE Trans. (2013).

[218] A. Amundarain, J.L. Torero, A. Usmani, A.M. Al-remal, Light Steel Framing: Improving the Integral Design, in: Glob. Built Environ. Towar. an Integr. Approach Sustain., Lancashire, UK, 2014: pp. 1–8. http://hdl.handle.net/1842/1409.

[219] S.S. Shrestha, A.O. Desjarlais, J.A. Atchley, Thermal Performance Evaluation of Walls with Gas Filled Panel Insulation, Oak Ridge, TN (United States), 2014. doi:10.2172/1185731.

[220] C. Baldwin, C.A. Cruickshank, M. Schiedel, B. Conley, Comparison of Steady-state and In-situ Testing of High Thermal Resistance Walls Incorporating Vacuum Insulation Panels, Energy Procedia. 78 (2015) 3246–3251. doi:10.1016/j.egypro.2015.11.690.

[221] X. Meng, Y. Gao, Y. Wang, B. Yan, W. Zhang, E. Long, Feasibility experiment on the simple hot box-heat flow meter method and the optimization based on simulation reproduction, Appl. Therm. Eng. 83 (2015) 48–56. doi:10.1016/j.applthermaleng.2015.03.010.

[222] C. Buratti, E. Belloni, L. Lunghi, A. Borri, G. Castori, M. Corradi, Mechanical characterization and thermal conductivity measurements using of a new "small hot-box" apparatus: Innovative insulating reinforced coatings analysis, J. Build. Eng. 7 (2016) 63–70. doi:10.1016/j.jobe.2016.05.005.

[223] C. Buratti, E. Belloni, L. Lunghi, M. Barbanera, Thermal Conductivity Measurements By Means of a New 'Small Hot-Box' Apparatus: Manufacturing, Calibration and Preliminary Experimental Tests on Different Materials, Int. J. Thermophys. 37 (2016) 1–23. doi:10.1007/s10765-016-2052-2.

[224] I. Nardi, D. Paoletti, D. Ambrosini, T. de Rubeis, S. Sfarra, U-value assessment by infrared thermography: A comparison of different calculation methods in a Guarded Hot Box, Energy Build. 122 (2016) 211–221. doi:10.1016/j.enbuild.2016.04.017.

[225] P. Modi, R. Bushehri, C. Georgantopoulou, L. Mavromatidis, Design and development of a mini scale hot box for thermal efficiency evaluation of an insulation building block prototype used in Bahrain, Adv. Build. Energy Res. 11 (2017) 130–151. doi:10.1080/17512549.2016.1161545.

[226] E. Lucchi, F. Roberti, T. Alexandra, Definition of an experimental procedure with the hot box method for the thermal performance evaluation of inhomogeneous walls, Energy Build. 179 (2018) 99–111. doi:10.1016/j.enbuild.2018.08.049.

[227] EURAC research, (n.d.). http://www.eurac.edu/en/Pages/default.aspx (accessed May 17, 2020).

[228] BS EN 1934:1998 - Thermal performance of buildings. Determination of thermal resistance by hot box method using heat flow meter. Masonry, (n.d.). https://shop.bsigroup.com/ProductDetail?pid=000000000001340024 (accessed May 17, 2020).

[229] Photo, (n.d.). http://www.eurac.edu/en/news/photo/Pages/photogallery.aspx?entryid=110830 (accessed May 17, 2020).

[230] E. Lucchi, F. Roberti, T. Alexandra, Definition of an experimental procedure with the hot box method for the thermal performance evaluation of inhomogeneous walls, Energy Build. 179 (2018) 99–111. doi:10.1016/j.enbuild.2018.08.049.

[231] D. Chowdhury, S. Neogi, Thermal performance evaluation of traditional walls and roof used in tropical climate using guarded hot box, Constr. Build. Mater. 218 (2019) 73–89. doi:10.1016/j.conbuildmat.2019.05.032.

[232] X. Zhao, S.A. Mofid, M.R.A. Hulayel, G.W. Saxe, B.P. Jelle, R. Yang, Reduced-scale hot box method for thermal characterization of window insulation materials, Appl. Therm. Eng. 160 (2019) 114026. doi:10.1016/j.applthermaleng.2019.114026.

[233] K. Trgala, M. Pavelek, R. Wimmer, Energy performance of five different building envelope structures using a modified Guarded Hot Box apparatus—Comparative analysis, Energy Build. 195 (2019) 116–125. doi:10.1016/j.enbuild.2019.04.036.

[234] A. Pourghorban, B.M. Kari, Evaluation of reflective insulation systems in wall application by guarded hot box apparatus, and comparative investigation with ASHRAE and ISO 15099, Constr. Build. Mater. 207 (2019) 84–97. doi:10.1016/j.conbuildmat.2019.02.097.

[235] M. Andreotti, M. Calzolari, P. Davoli, L. Dias Pereira, E. Lucchi, R. Malaguti, Design and Construction of a New Metering Hot Box for the In Situ Hygrothermal Measurement in Dynamic Conditions of Historic Masonries, Energies. 13 (2020) 2950. doi:10.3390/en13112950.

[236] N. Soares, P. Santos, H. Gervásio, J.J. Costa, L. Simões da Silva, Energy efficiency and thermal performance of lightweight steel-framed (LSF) construction: A review, Renew. Sustain. Energy Rev. 78 (2017) 194–209.

[237] J. Kosny, J.E. Christian, E. Barbour, J. Goodrow, Thermal performance of steel-framed walls - CRADA Final Report for CRADA Number ORNL93-0235, 1994.

[238] N. Soares, A.R. Gaspar, P. Santos, J.J. Costa, Multi-dimensional optimization of the incorporation of PCM-drywalls in lightweight steel-framed residential buildings in different climates, Energy Build. 70 (2014) 411–421. doi:10.1016/j.enbuild.2013.11.072.

[239] P. Santos, C. Martins, L. Simões da Silva, Thermal performance of lightweight steel-framed construction systems, Metall. Res. Technol. 111 (2014) 329–338. doi:10.1051/metal/2014035.

[240] J. Kosny, J.E. Christian, Thermal evaluation of several configurations of insulation and structural materials for some metal stud walls, Energy Build. 22 (1995) 157–163. doi:10.1016/0378-7788(94)00913-5.

[241] T. Höglund, H. Burstrandb, H. Burstrand, Slotted steel studs to reduce thermal bridges in insulated walls, Thin-Walled Struct. 32 (1998) 81–109.

[242] T.R. Blomberg, J. Claesson, Heat Transmission Through Walls with Slotted Steel Studs, in: Therm. Envel. VII, 1998: pp. 621–628.

[243] L. Zalewski, S. Lassue, D. Rousse, K. Boukhalfa, Experimental and numerical characterization of thermal bridges in prefabricated building walls, Energy Convers. Manag. 51 (2010) 2869–2877. doi:10.1016/j.enconman.2010.06.026.

[244] N. Soares, C. Martins, M. Gonçalves, P. Santos, L. Simões da Silva, J.J. Costa, Laboratory and in-situ non-destructive methods to evaluate the thermal transmittance and behaviour of walls, windows, and construction elements with innovative materials: a review, J. Energy Build. (n.d.).

[245] R. Mayer, E. Enache-Pommer, G. Parsons, M. Mazor, J. Hansbro, J. Lastovica, C. Buck, M. Maurer, Finite element thermal modeling and correlation of various building wall assembly systems, Energy Build. 75 (2014) 410–418. doi:10.1016/j.enbuild.2013.11.034.

[246] G.M. Soret, D. Lázaro, J. Carrascal, D. Alvear, M. Aitchison, J.L. Torero, Thermal characterization of building assemblies by means of transient data assimilation, Energy Build. 155 (2017) 128–142. doi:10.1016/j.enbuild.2017.08.073.

[247] A. Amundarain, Assessment of the thermal efficiency, structure and fire resistance of lightweight building systems for optimised deign, University of Edinburgh, 2007.

[248] M. O'Grady, A.A. Lechowska, A.M. Harte, Infrared thermography technique as an in-situ method of assessing heat loss through thermal bridging, Energy Build. 135 (2017) 20–32. doi:10.1016/j.enbuild.2016.11.039.

[249] I.A. Atsonios, I.D. Mandilaras, D.A. Kontogeorgos, M.A. Founti, Two new methods for the in-situ measurement of the overall thermal transmittance of cold frame lightweight steel-framed walls,

Energy Build. 170 (2018) 183–194. doi:10.1016/j.enbuild.2018.03.069.

[250] Y. Li, J. Yao, R. Li, Z. Zhang, J. Zhang, Thermal and energy performance of a steel-bamboo composite wall structure, Energy Build. 156 (2017) 225–237. doi:10.1016/j.enbuild.2017.09.083.

[251] R. Baetens, B.P. Jelle, A. Gustavsen, Aerogel insulation for building applications: A state-of-the-art review, Energy Build. 43 (2011) 761–769. doi:10.1016/j.enbuild.2010.12.012.

[252] Á. Lakatos, Comprehensive thermal transmittance investigations carried out on opaque aerogel insulation blanket, Mater. Struct. Constr. 50 (2017). doi:10.1617/s11527-016-0876-7.

[253] K.G. Wakili, B. Binder, M. Zimmermann, C. Tanner, Efficiency verification of a combination of high performance and conventional insulation layers in retrofitting a 130-year old building, Energy Build. 82 (2014) 237–242. doi:10.1016/j.enbuild.2014.06.050.

[254] R. Walker, S. Pavía, Thermal performance of a selection of insulation materials suitable for historic buildings, Build. Environ. 94 (2015) 155–165. doi:10.1016/j.buildenv.2015.07.033.

[255] M. Alam, H. Singh, M.C. Limbachiya, Vacuum insulation panels (vips) for building construction industry - a review of the contemporary developments and future directions, Appl. Energy. 88 (2011) 3592–3602. doi:10.1016/j.apenergy.2011.04.040.

[256] K. Ghazi Wakili, R. Bundi, B. Binder, Effective thermal conductivity of vacuum insulation panels, Build. Res. Inf. 32 (2004) 293–299. doi:10.1080/0961321042000189644.

[257] T. Nussbaumer, K. Ghazi Wakili, C. Tanner, Experimental and numerical investigation of the thermal performance of a protected vacuum-insulation system applied to a concrete wall, Appl. Energy. 83 (2006) 841–855. doi:10.1016/j.apenergy.2005.08.004.

[258] A. Capozzoli, S. Fantucci, F. Favoino, M. Perino, Vacuum insulation panels: Analysis of the thermal performance of both single panel and multilayer boards, Energies. 8 (2015) 2528–2547. doi:10.3390/en8042528.

[259] I. Mandilaras, I. Atsonios, G. Zannis, M. Founti, Thermal performance of a building envelope incorporating ETICS with vacuum insulation panels and EPS, Energy Build. 85 (2014) 654–665. doi:10.1016/j.enbuild.2014.06.053.

[260] L.E. Mavromatidis, P. Michel, M. El Mankibi, M. Santamouris, Study on transient heat transfer through multilayer thermal insulation: numerical analysis and experimental investigation, Build. Simul. 3 (2010) 279–294. doi:10.1007/s12273-010-0018-z.

[261] Z. Ye, C.M. Wells, C.G. Carrington, N.J. Hewitt, Thermal conductivity of wool and wool-hemp insulation, Int. J. Energy Res. 30 (2006) 37–49. doi:10.1002/er.1123.

[262] A. Shea, K. Wall, P. Walker, Evaluation of the thermal performance of an innovative prefabricated natural plant fibre building system, Build. Serv. Eng. Res. Technol. 34 (2012) 369–380. doi:10.1177/0143624412450023.

[263] S.W. Lee, C.H. Lim, E.@ I. Bin Salleh, Reflective thermal insulation systems in building: a review on radiant barrier and reflective insulation, Renew. Sustain. Energy Rev. 65 (2016) 643–661. doi:10.1016/j.rser.2016.07.002.

[264] C. Escudero, K. Martin, A. Erkoreka, I. Flores, J.M. Sala, Experimental thermal characterization of radiant barriers for building insulation, Energy Build. 59 (2013) 62–72. doi:10.1016/j.enbuild.2012.12.043.

[265] N. Soares, J.J. Costa, A.R. Gaspar, P. Santos, Review of passive PCM latent heat thermal energy storage systems towards buildings ' energy efficiency, Energy Build. 59 (2013) 82–103. doi:10.1016/j.enbuild.2012.12.042.

[266] L.F. Cabeza, C. Barreneche, I. Martorell, L. Miró, S. Sari-bey, M. Fois, H.O. Paksoy, N. Sahan, R. Weber, M. Constantinescu, E. Maria, M. Malikova, I. Krupa, M. Delgado, P. Dolado, P. Furmanski, M. Jaworski, T. Haussmann, S. Gschwander, A.I. Fernández, Unconventional experimental technologies available for phase change materials (PCM) characterization. Part 1. Thermophysical properties, Renew. Sustain. Energy Rev. 43 (2015) 1399–1414.

doi:10.1016/j.rser.2014.07.191.

[267] Y. Dutil, D. Rousse, S. Lassue, L. Zalewski, A. Joulin, J. Virgone, F. Kuznik, K. Johannes, J.-P. Dumas, J.-P. Bédécarrats, A. Castell, L.F. Cabeza, Modeling phase change materials behavior in building applications: comments on material characterization and model validation, Renew. Energy. 61 (2014) 132–135. doi:10.1016/j.renene.2012.10.027.

[268] M. Lachheb, Z. Younsi, H. Naji, M. Karkri, S. Ben, Thermal behavior of a hybrid PCM/plaster: a numerical and experimental investigation, Appl. Therm. Eng. 111 (2017) 49–59. doi:10.1016/j.applthermaleng.2016.09.083.

[269] C. Amaral, R. Vicente, V.M. Ferreira, T. Silva, Polyurethane foams with microencapsulated phase change material: Comparative analysis of thermal conductivity characterization approaches, Energy Build. 153 (2017) 392–402. doi:10.1016/j.enbuild.2017.08.019.

[270] N. Shukla, A. Fallahi, J. Kosny, Performance characterization of PCM impregnated gypsum board for building applications, Energy Procedia. 30 (2012) 370–379. doi:10.1016/j.egypro.2012.11.044.

[271] J. Kosny, E. Kossecka, A. Brzezinski, A. Tleoubaev, D. Yarbrough, Dynamic thermal performance analysis of fiber insulations containing bio-based phase change materials (PCMs), Energy Build. 52 (2012) 122–131. doi:10.1016/j.enbuild.2012.05.021.

[272] I.D. Mandilaras, D.A. Kontogeorgos, M.A. Founti, A hybrid methodology for the determination of the effective heat capacity of PCM enhanced building components, Renew. Energy. 76 (2015) 790–804. doi:10.1016/j.renene.2014.11.078.

[273] P. Principi, R. Fioretti, Thermal analysis of the application of pcm and low emissivity coating in hollow bricks, Energy Build. 51 (2012) 131–142.

[274] T. Silva, R. Vicente, N. Soares, V. Ferreira, Experimental testing and numerical modelling of masonry wall solution with PCM incorporation: A passive construction solution, Energy Build. 49 (2012) 235–245. doi:10.1016/j.enbuild.2012.02.010.

[275] R. Vicente, T. Silva, Brick masonry walls with PCM macrocapsules: An experimental approach, Appl. Therm. Eng. 67 (2014) 24–34. doi:10.1016/j.applthermaleng.2014.02.069.

[276] GOST 26254-84, Methods for determination of thermal resistance of enclosing structures, (1984).

[277] BS 874-3.1, Methods for determining thermal insulating properties Part 3. Tests for thermal transmittance and conductance. Section 3.1 Guarded hot-box method., Br. Stand. (1987).

[278] ISO 9869, Thermal insulation – Building elements - In-situ measurement of thermal resistance and thermal transmittance, International Organization for Standardization, 1994.

[279] ASTM C 1155 – 95 (Reapproved 2001), Standard Practice for Determining Thermal Resistance of Building Envelope Components from the In-Situ Data, American Society for Testing and Materials, (2001).

[280] ASTM C1046-95, Standard Practice for In-Situ Measurement of Heat Flux and Temperature on Building Envelope Components, 2001.

[281] Hukseflux, HFP01 heat flux sensor, (2018). https://www.hukseflux.com/products/heat-flux-sensors/heat-flux-meters/hfp01-heat-flux-sensor (accessed August 20, 2008).

[282] E+E Elektronik, EE75, (2018). https://www.instrumart.com/assets/EplusE-EE75-Datasheet.pdf (accessed August 20, 2008).

[283] KPLAY, FKC X 22, (2018). https://www.klay-instruments.com/downloads/brochures/FKC_dP_Eng.pdf (accessed August 20, 2008).

[284] Comet model T3111-4, (2020). https://www.cometsystem.com/products/sensors/reg-t3111-4https://www.cometsystem.com/products/sensors/reg-t3111-4 (accessed March 7, 2020).

[285] Sfere, Diva 11, (2018). https://ardetem-sfere.com/en/peca-11-dc-diva-11-dc/ (accessed August 20, 2008).

[286] Sfere, Diva 5, (2018). https://ardetem-sfere.com/en/peca-5-diva-5/ (accessed August 20, 2008).

[287] ISO 10456, Building materials and products — Hygrothermal properties — Tabulated design values and procedures for determining declared and design thermal values, (2007). https://www.iso.org/standard/40966.html.

[288] JCGM, Evaluation of measurement data-Guide to the expression of uncertainty in measurement Évaluation des données de mesure-Guide pour l'expression de l'incertitude de mesure, 2008. www.bipm.org (accessed June 13, 2020).

[289] IPAC- Instituto Português Acreditação, Avaliação Da Incerteza De Medição Em Calibração, Lisbon, 2015. http://www.ipac.pt/docs/publicdocs/requisitos/OGC010.pdf (accessed June 21, 2020).

[290] I.A. Atsonios, I.D. Mandilaras, D.A. Kontogeorgos, M.A. Founti, Two new methods for the in-situ measurement of the overall thermal transmittance of cold frame lightweight steel-framed walls, Energy Build. 170 (2018) 183–194. doi:10.1016/j.enbuild.2018.03.069.

[291] E. Roque, P. Santos, The effectiveness of thermal insulation in lightweight steel-framedwalls with respect to its position, Buildings. 7 (2017) 1–13. doi:10.3390/buildings7010013.

[292] Santos, Lemes, Mateus, Thermal Transmittance of Internal Partition and External Facade LSF Walls: A Parametric Study, Energies. 12 (2019) 2671. doi:10.3390/en12142671.

[293] Tyre4BuildIns, Research project Tyre4BuildIns - "Recycled tyre rubber resin-bonded for building insulation systems towards energy efficiency", funded by FEDER European and FCT National funds. Reference: POCI-01-0145-FEDER-032061. University of Coimbra, Portugal, (n.d.). https://www.tyre4buildins.dec.uc.pt/ (accessed May 9, 2020).

[294] P. Santos, C. Martins, L. Simões da Silva, Thermal performance of lightweight steel-framed construction systems, Metall. Res. Technol. 111 (2014) 329–338. doi:10.1051/metal/2014035.

[295] P. Santos, M. Gonçalves, C. Martins, N. Soares, J.J. Costa, Thermal Transmittance of Lightweight Steel Framed Walls: Experimental Versus Numerical and Analytical Approaches, J. Build. Phys. (2018).

[296] C. Martins, P. Santos, L. Simões da Silva, Lightweight Steel Framed Construction System, in: Port. SB13 Contrib. Sustain. Build. to Meet EU 20-20-20 Targets, Portugal SB13, Guimarães, 2013: pp. 395–402.

[297] P. Santos, C. Martins, L. Simões da Silva, Thermal performance of Lightweight Steel Framed Construction System, in: Therm. Perform. Light. Steel Fram. Constr. Syst. 8th Int. Conf. Soc. Mater. SAM8, Liège, 2014.

[298] C. Martins, N. Rosa, P. Santos, L. Simões da Silva, Edifícios com Estrutura Leve em Aço Enformado a Frio (LSF): Vantagens e Desvantagens do Sistema, in: XI Congr. Construção Metálica e Mista, CMM, 2017: p. 10.

[299] C. Martins, M. Gonçalves, P. Santos, J. Costa, N. Soares, L. Simões da Silva, Determinação experimental do coeficiente de transmissão térmica de uma parede com estrutura leve em aço enformado a frio, in: XI Congr. Construção Metálica e Mista, CMM, 2017: p. 10.

[300] M. Gonçalves, C. Martins, N. Soares, P. Santos, J. Costa, Desenvolvimento de um protocolo experimental para medir o desempenho térmico de paredes em LSF, in: CLB-MCS 2018, 3º Congr. Luso-Brasileiro, Mater. Construção Sustentáveis, 2018: p. 12.

[301] P. Santos, M.G. Gonçalves, C. Martins, N. Soares, J.J. Costa, Phase change materials for improving the thermal performance of LSF construction, in: Semin. PCMs4Buildings – PCMs Thermophys. Charact. Build. Appl., 2018. http://hdl.handle.net/10316/79980.

[302] N. Soares, A.G. Lopes, M. Gonçalves, A.R. Gaspar, C. Martins, T. Matias, P. Santos, P.N. Simões, L. Durães, J.J. Costa, No TitleSystems with PCM-filled rectangular cavities for the storage of solar thermal energy for buildings: the case of the PCMs4Buildings project, in: Semin. PCMs4Buildings – PCMs Thermophys. Charact. Build. Appl., 2018. http://hdl.handle.net/10316/79976.

[303] P.S. Cláudio Martins, Nuno Rosa, Luís Simões da Silva, Construção de um equipamento para medição do coeficiente de transmissão térmica: especial foco paredes com estrutura em aço, in: XII Congr. Construção Metálica e Mista (Ed.), 2019.

ANNEXES

ANNEX A - TEMPERATURE SENSORS

I. Specimen surface temperature sensors

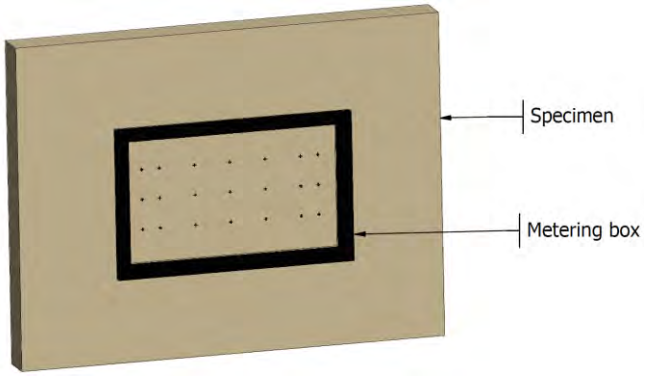

Table A.1 – Thermocouples

Location	Number of sensors
Metering box (GHB)	21
Cold box	21
Total	42

Figure A.1 – Specimen surface temperature sensors inside the metering box.

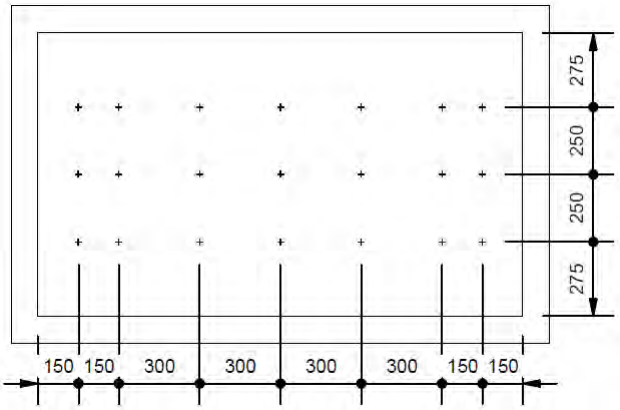

Figure A.2 – Specimen surface temperature sensors inside the metering and cold box – front view.

II. Air temperature sensors in the metering box (GHB), between specimen and baffle

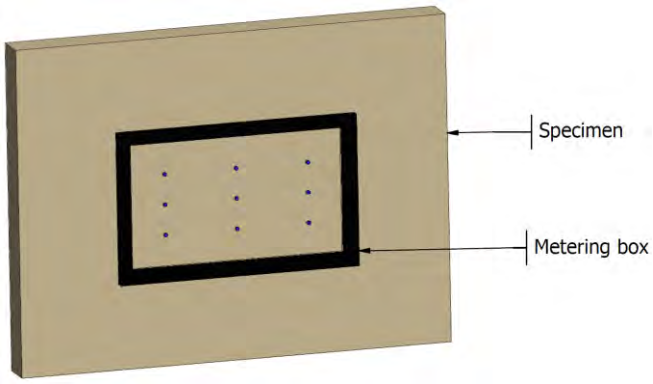

Table A.2 – Thermocouples

Location	Number of sensors
Metering box (GHB)	9
Total	9

Figure A.3 – Air temperature sensors in metering box (GHB).

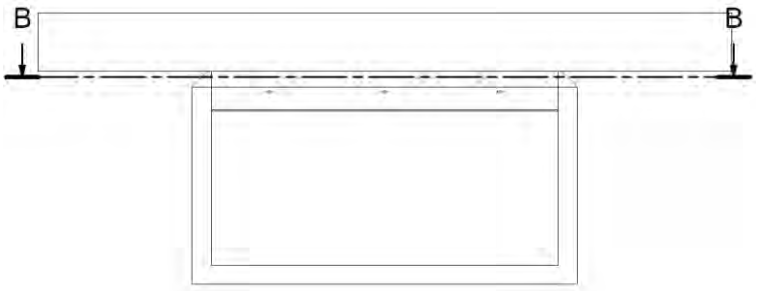

Figure A.4 – Air temperature sensors in metering box (GHB) top view.

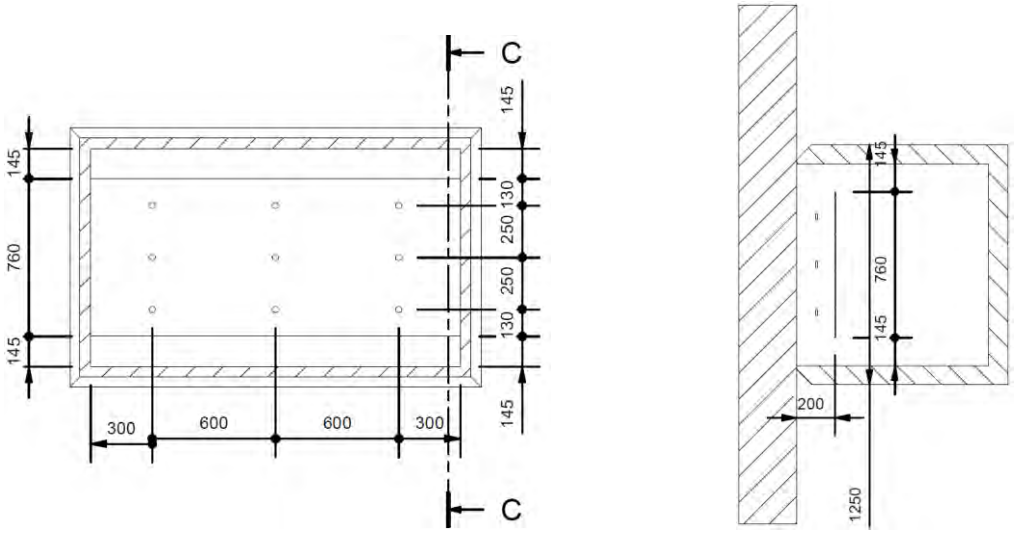

a) **b)**

Figure A.5 – Metering box (GHB): a) Cross-section B-B; b) Cross-section C-C.

III. Surface temperature sensors in the baffle of the GHB metering box

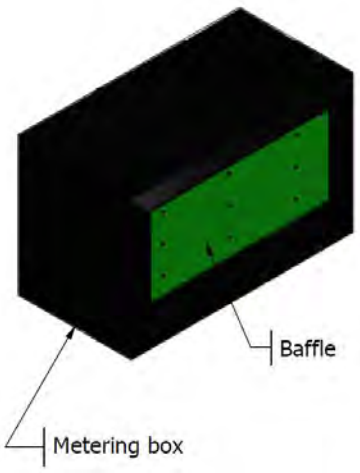

Figure A.6 – Surface temperature sensors in the baffle of the metering box (GHB).

Table A.3 – Thermocouples

Location	Number of sensors
Baffle	9
Total	9

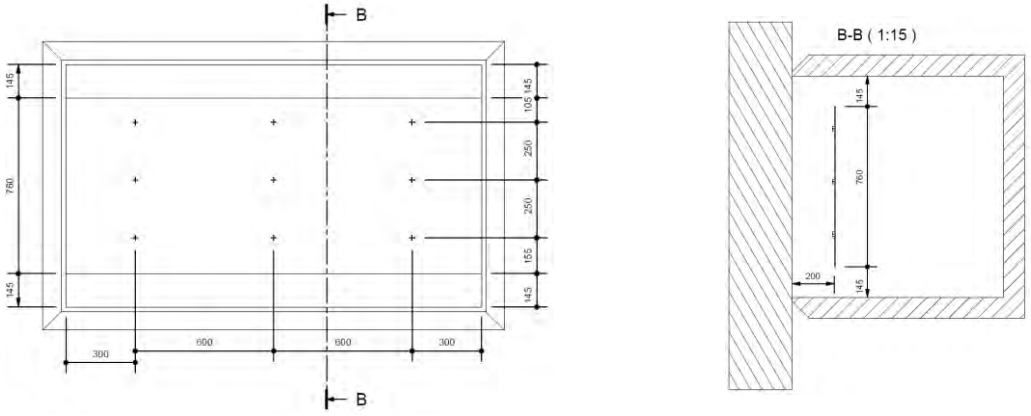

a) b)

Figure A.7 – Surface temperature sensors in the baffle of the metering box (GHB): a) Front view; b) Cross-section B-B.

IV. Surface temperature sensors in the baffle of the cold box

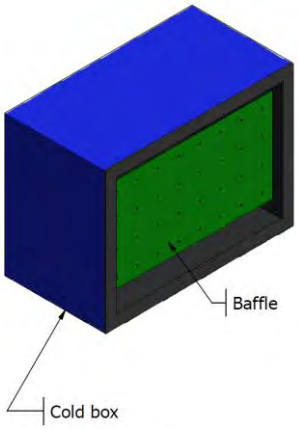

Figure A.8 – Surface temperature sensors in the baffle of the cold box.

Table A.4 – Thermocouples

Location	Number of sensors
Baffle	32
Total	32

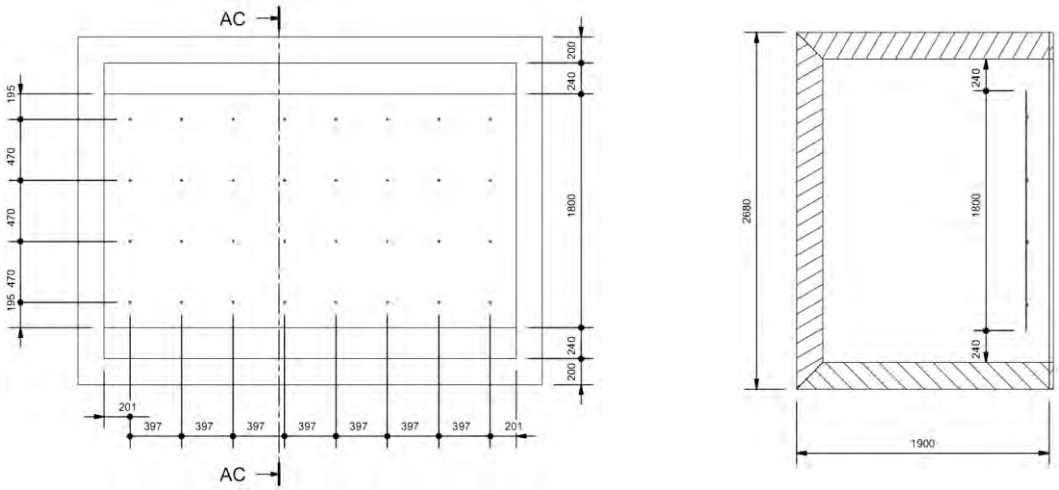

a) b)

Figure A.9 – Surface temperature sensors in the baffle of the cold box: a) Front view; b) Cross-section AC-AC.

V. Air temperature sensors in cold box, between specimen and baffle

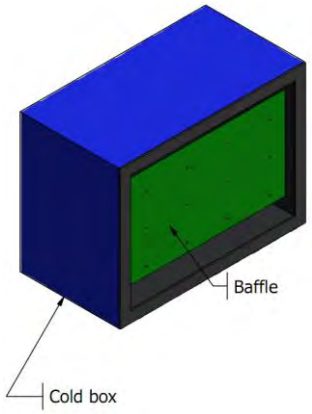

Figure A.10 – Air temperature sensors in cold box, between specimen and baffle.

Table A.5 – Thermocouples

Location	Number of sensors
Between specimen and baffle	12
Total	12

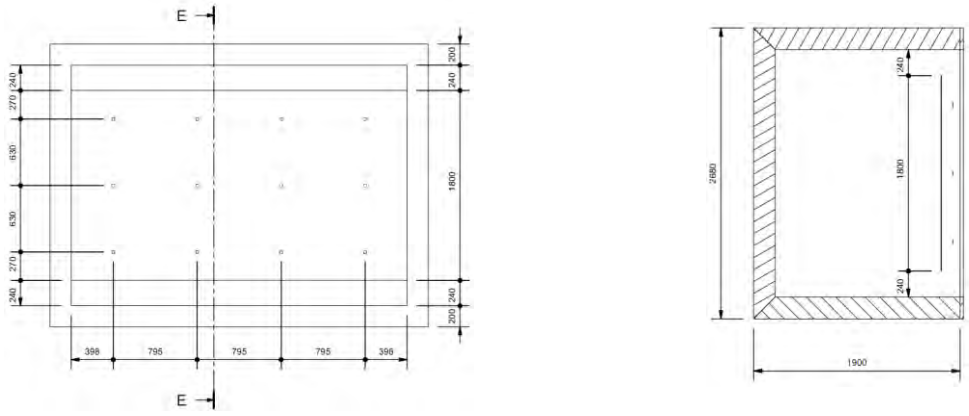

a) **b)**

Figure A.11 – Air temperature sensors in cold box, between specimen and baffle: a) front view; b) cross-section E-E.

VI. External air temperature sensors

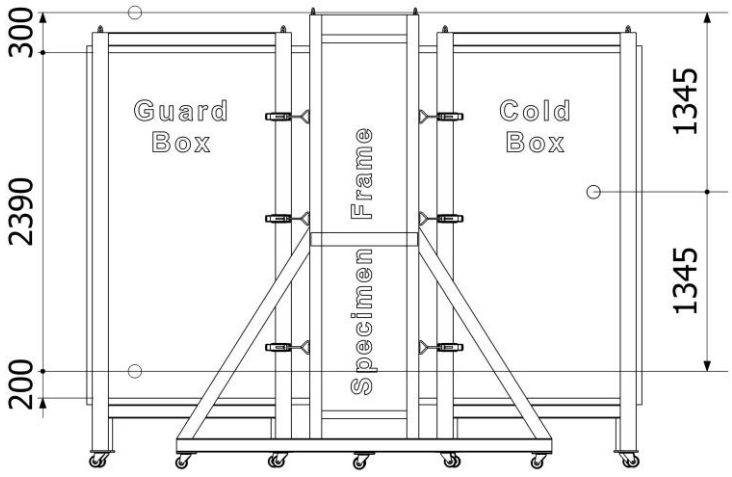

Figure A.12 – External air temperature sensors.

Table A.6 – Thermocouples

Location	Number of sensors
Guard box	2
Cold box	1
Total	3

VII. Air temperature sensors inside the guard box

Figure A.13 – Air temperature sensors in guard box.

Table A.7 – Thermocouples

Location	Number of sensors
Guard box	9
Total	9

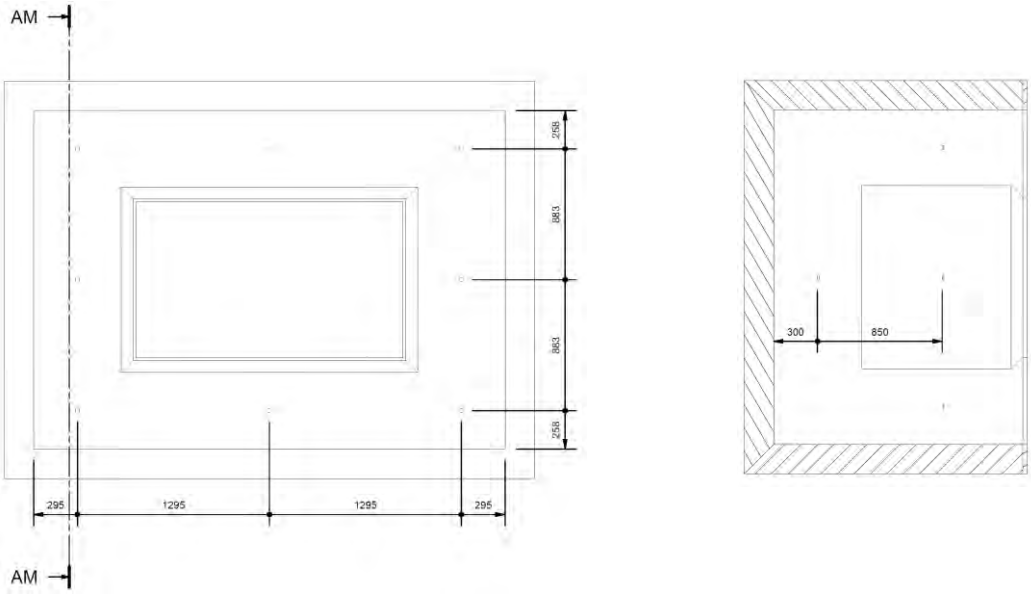

a) **b)**

Figure A.14 – Air temperature sensors in guard box: a) Front view; b) Cross-section AM-AM.

ANNEX B - THERMOPILES

I. Thermopile of GHB metering box

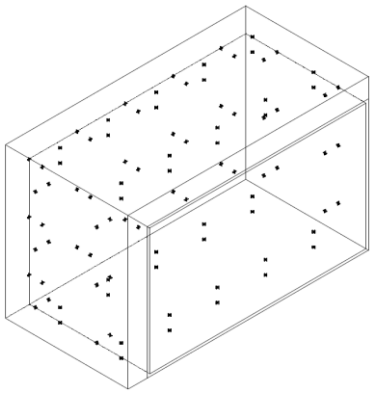

Figure B.1 – Thermopile of GHB metering box.

Table B.1 – Thermocouples

Location	Number of contacts
Interior	47
Exterior	47
Total	94

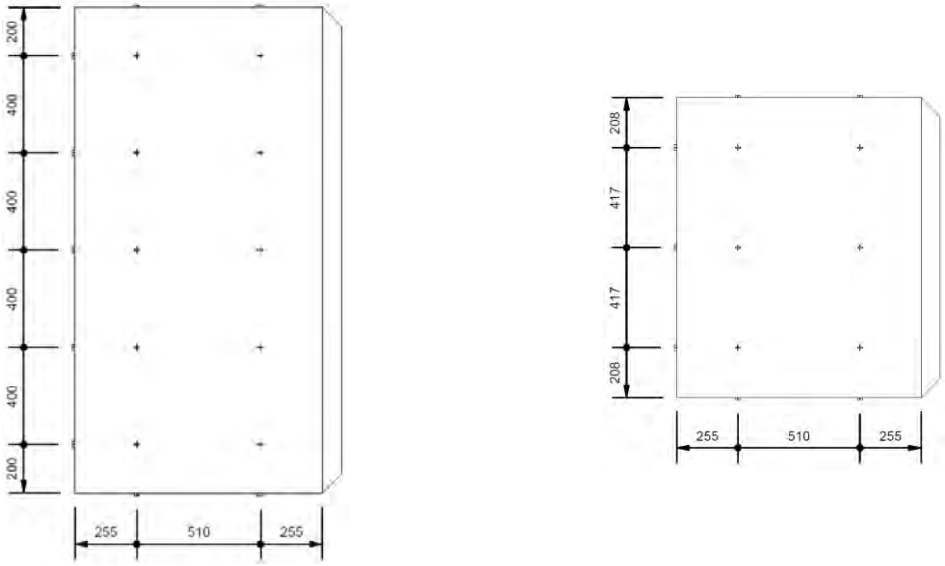

a) **b)**

Figure B.2 – Thermopile of GHB metering box: a) Top view; b) Front view.

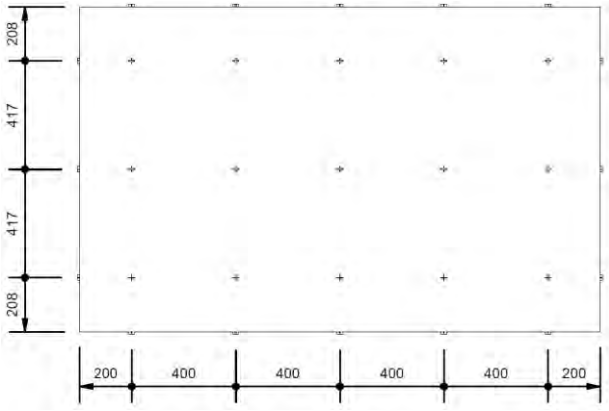

Figure B.3 – Thermopile of GHB metering box back view.

II. Thermopile of GHB metering box perimeter seal

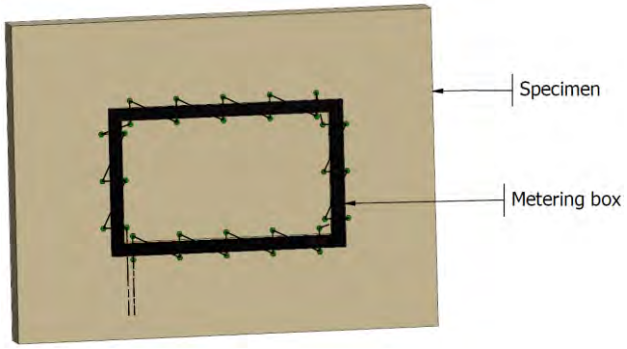

Table B.2 – Points of surface sensors contacts

Location	Number of contacts
Interior	16
Exterior	16
Total	32

Figure B.4 – Thermopile of GHB metering box perimeter seal.

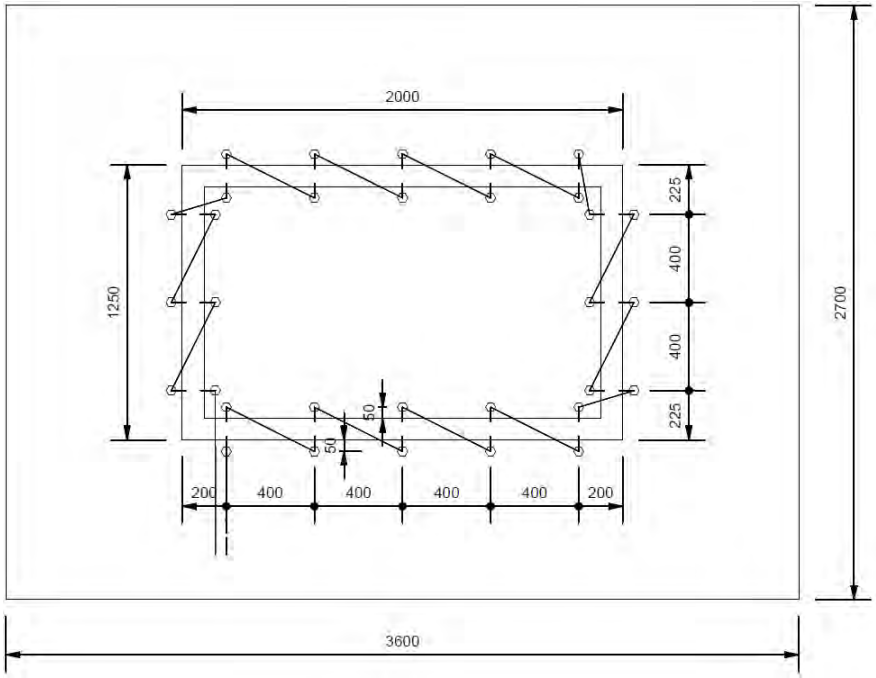

Figure B.5 – Thermopile of GHB metering box perimeter seal.

ANNEX C - AIR VELOCITY SENSORS

I. Air velocity sensors of guard box

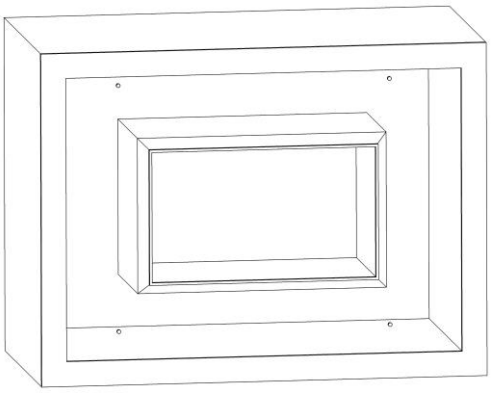

Figure C.1 – Air velocity sensors of guard box.

Table C.1 – Air velocity sensors

Location	Number of sensors
Guard box	4
Total	4

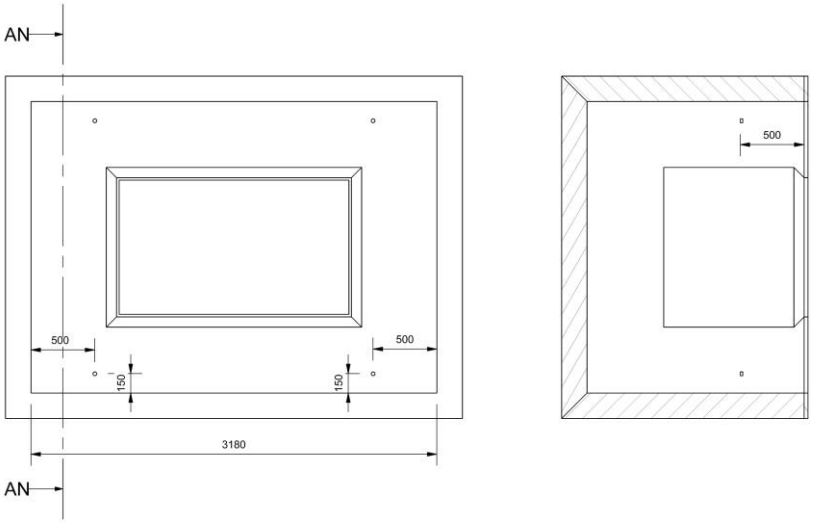

a) b)

Figure C.2 – Air velocity sensors of guard box: a) Front view; b) Cross-section AN-AN.

II. Air velocity sensors of GHB metering box

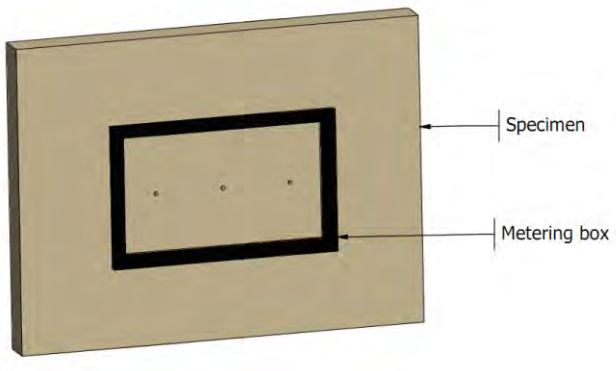

Figure C.3 – Air velocity sensors of metering box (GHB).

Table C.2 – Air velocity sensors

Location	Number of sensors
Metering box (GHB)	3
Total	3

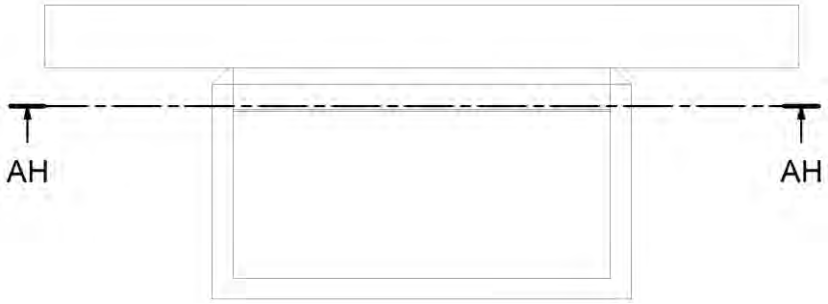

Figure C.4 – Air velocity sensors of metering box (GHB) top view.

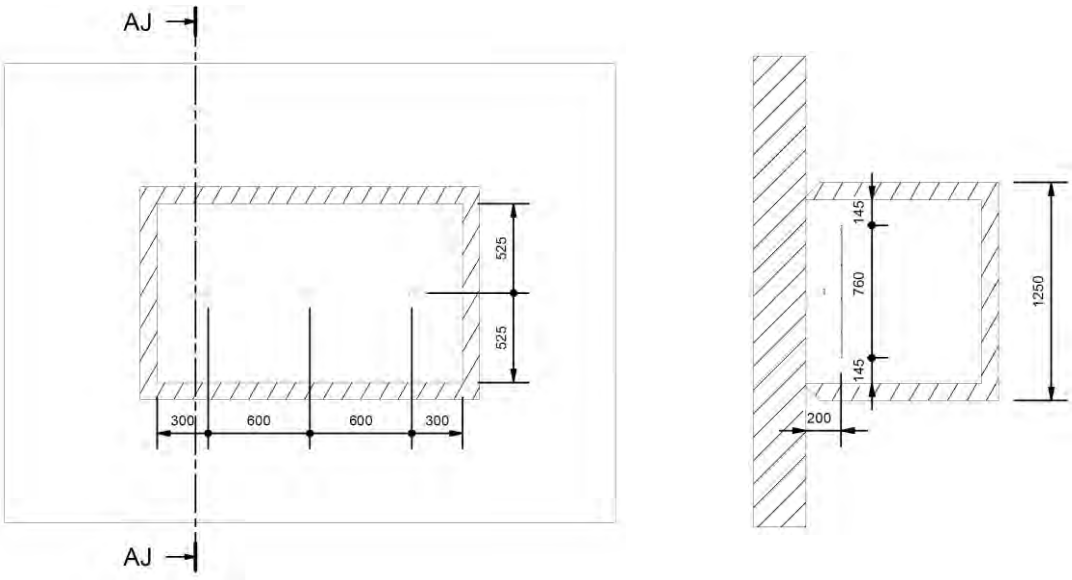

a) **b)**

Figure C.5 – Air velocity sensors of metering box (GHB): a) Cross-section AH-AH; b) Cross-section AJ-AJ.

III. Air velocity sensors of CHB metering box and cold box

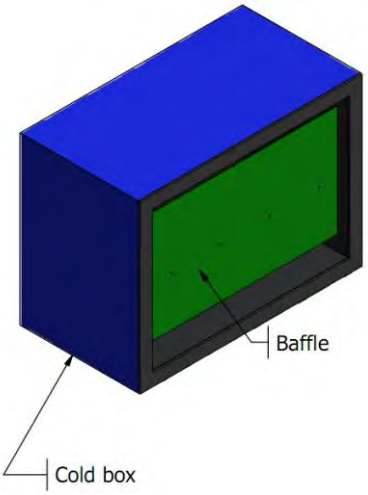

Table C.3 – Air velocity sensors

Location	Number of sensors
CHB metering box and cold box	4
Total	4

Figure C.6 – Air velocity sensors of CHB metering box and cold box.

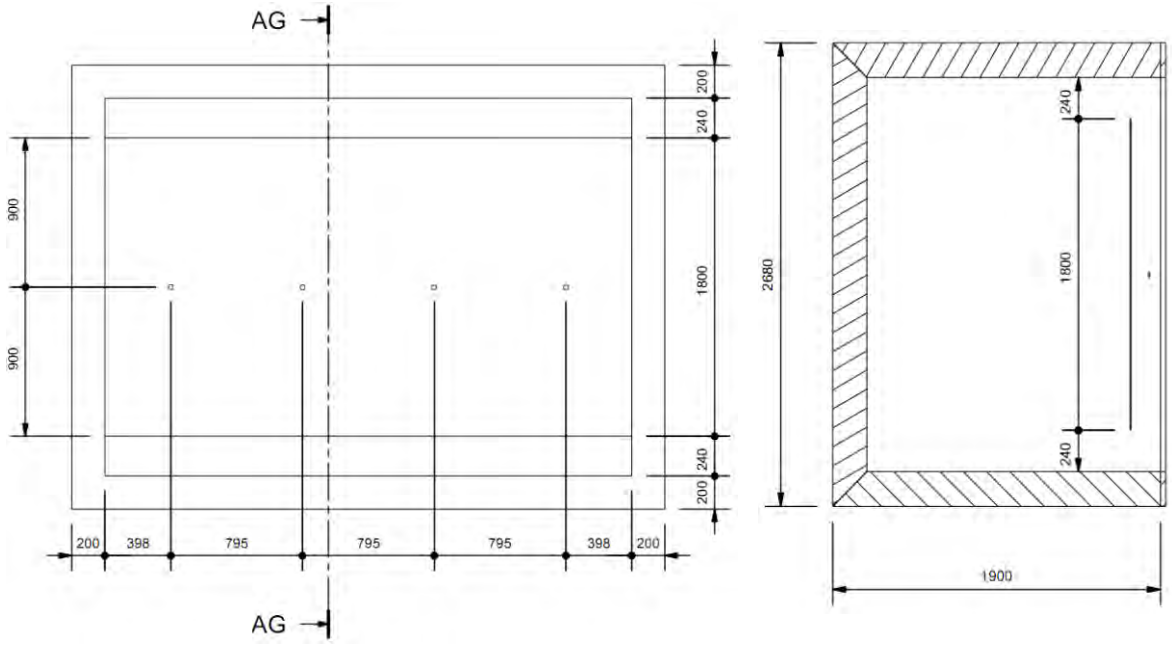

a) b)

Figure C.7 – Air velocity sensors of CHB metering box and cold box: a) Front view; b) Cross-section AG-AG.

ANNEX D - HYDRAULIC COOLING SYSTEM DESIGN

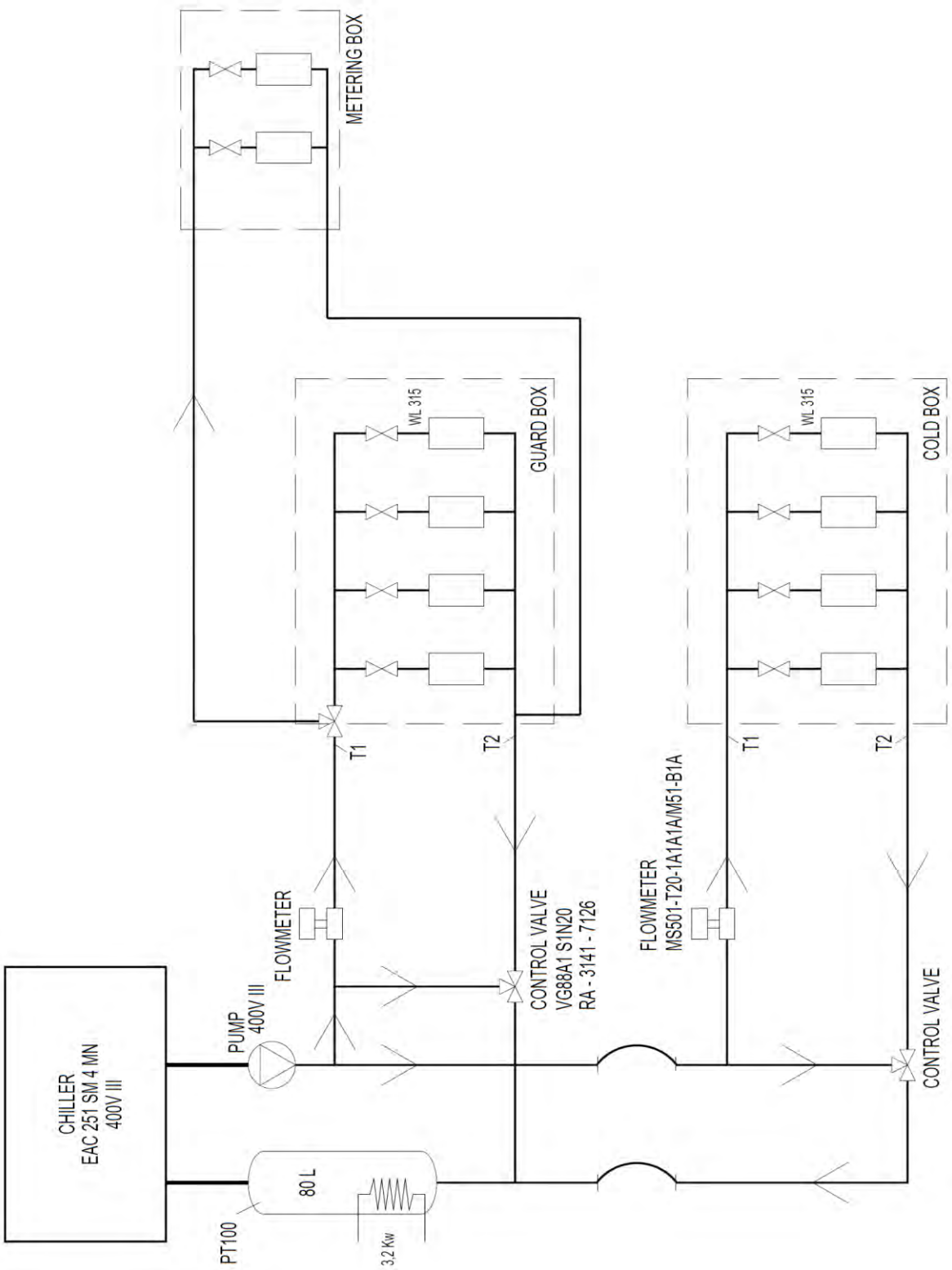

Figure D.1 – Hydraulic cooling system design.